NATIONAL TECHNICAL UNIVERSITY OF ATHENS
SCHOOL OF MECHANICAL ENGINEERING
MECHANICAL DESIGN AND CONTROL SYSTEMS SECTION

THREE-DIMENSIONAL MICROMECHANICAL MODELS OF TEXTILE FABRICS

PhD Dissertation

by
Argyro Kallivretaki

Advisor:
Professor Christopher Provatidis

May 2010
Athens

NATIONAL TECHNICAL UNIVERSITY OF ATHENS
SCHOOL OF MECHANICAL ENGINEERING
MECHANICAL DESIGN AND CONTROL SYSTEMS SECTION

THREE-DIMENSIONAL MICROMECHANICAL MODELS OF TEXTILE FABRICS

A dissertation submitted to the School of Mechanical Engineering of National Technical University of Athens in partial fulfilment of the requirements for the degree of Doctor of Philosophy

by
Argyro Kallivretaki

PhD Consultative Committee:
Professor Ch. Provatidis
Assoc. Professor I. Antoniadis
Assist. Professor S. Diplaris

PhD Examination Committee:
Professor Ch. Provatidis
Professor D. Manolakos
Professor G. Tsamasphyros
Assoc. Professor I. Antoniadis
Assoc. Professor N. Tsouvalis
Assist. Professor S. Diplaris
Assist. Professor S. Vassiliadis

May 2010
Athens

Table of Contents

List of Figures

List of Tables

Preface

The current dissertation was elaborated during the period September 2005 to March 2010 at the laboratory of Dynamics and Constructions, Mechanical Design and Control Systems Section, School of Mechanical Engineering of the National Technical University of Athens.

My incentive for postgraduate studies was raised from my contact with the laboratory during the elaboration of the undergraduate thesis owing to the constructive collaboration and my occupation with the research subject. The implementation of computational methods in the textile mechanics attracted my research interest. The long successful process of the researching team leaded by Prof. Provatidis in the field of the textile structures confirmed with under- and postgraduate theses and the research conducted previously in the laboratory, provided accumulated experience and massive literature references.

I would like to express my sincere gratitude to my supervisor Mr. Christopher Provatidis, Professor of Mechanical Engineering at N.T.U.A., for his guidance in each stage of the dissertation under excellent collaboration conditions. I particularly appreciate the creative balance achieved under his supervision, between the guidance and the freedom of initiatives. I also thank him for the continuous support in terms of consultation and encouragement.

I would like also to thank the members of the consultative committee Mr. Ioannis Antoniadis, Assoc. Professor of Mechanical Engineering, and Mr. Stefanos Diplaris, Assist. Professor of Mechanical Engineering, for the opportunity of graduate studies and the support of my efforts.

I would like to thank in particular Dr. Savvas Vassiliadis, Assist. Professor at the School of Technological Applications of T.E.I. of Piraeus, for my initiation in the field of textile mechanics and the motivation to postgraduate studies. His valuable knowledge and the indemnity of experimental measurements were determinant for the regular process of the thesis. I acknowledge also his substantial contribution in my personal progress and sociability, supporting many actions, as the participation in international conferences and the collaboration with researchers of universities abroad.

I would like also to thank the management of Clothing Textile & Fibre Technology Development Company (CLOTEFI) giving me the access in the laboratorial equipment for the experimental tests. In particular I would like to thank Dr. Konstantinos Mpoutris, chemical engineer, devoting his valuable time for my training in the operation of the Kawabata Evaluation System for Fabrics.

I also thank the laboratory members, Dimitrios Venetsanos, Vasilis Georgiopoulos, Ioannis Koukoulis, Clio Vossou, Evangelos Theodorou for the pleasant moments.

Finally I would like to dedicate this doctoral thesis to my parents and my brother for their continuous support and their sympathy.

Abstract

The current thesis aims at the development of an integrated method for the mechanical analysis of the textile structures based on their microstructure. The request for reliable textile mechanical design was intensified by their introduction in technical applications, mainly in composite materials, and their expansion in aerospace and shipping industry (composite propellers, composite aircraft & hovercraft panels), in civil constructions (composite framework, drainage), in sports equipment (protective equipment, breathable waterproofs), in land transportation (seat belts, tyre cord, air filters, airbags) etc. Despite the long-lasting attempts of the research community to develop a thorough technique for the prediction of the fabric performance, the used design procedure is still in evolution.

The effect of the structural elements of the fabrics, the fibres, in their mechanical analysis constituted the basic principle for the modelling approach, in contradiction to the existing mechanical two-dimensional models of the fabrics considered as simple sheets or membranes. Thus the discrete structure of the fabric, known as microstructure due to the small dimensions of the structural elements, was considered. This is exactly reflected in the title of the thesis.

In the **first chapter** of the thesis, the literature review of the developed methods for the mechanical analysis of the textile structures is conducted. From the first analytical approach for the 2D geometrical representation of the plain woven up to the advanced 3D computational models of composite materials, numerous approaches were recorded regarding the problem designing, the mechanical analysis method, the modelling scale and the considered assumptions. The current chapter presents the evolutionary process of the research and exposes the technological attempts, perspectives and limitations resulted from the mechanical analysis of the textile structures.

The production hierarchy of the textile structures (fibre – yarn – fabric) is correlated with the high level of complexity presented in the modelling procedure and the mechanical analysis of them. The difficulties are increased due to the high divergence of the dimensions corresponding to the fabric sheet (10^{-1} to 10^{0} m) and the structural elements (fibre diameter, 10^{-5} m). Thus the realistic representation of the fabric structure, including the level of the fibres representation, for the macromechanical modelling is computationally impractical. The structural singularity of the fabrics incurs their particular flexibility. Thereby the macromechanical behaviour of fabrics is characterized by the large displacements of the constituting fibres even under low loading conditions. The modelling difficulties resulted from the structural hierarchy of the textiles were faced adopting a relative modelling hierarchy. Thus three basic modelling scales were developed: the micromechanical modelling of yarns, the mesomechanical modelling of the fabric unit cell and the macromechanical modelling of the fabric sheet, that are described in the next chapters.

The **second chapter** focuses on the stage of the micromechanical modelling. The typical yarn structure was studied in the micro-scale (fibre level) that constitutes the structural element for

the production of textile products. The physical and the geometrical properties of the filaments and the ideal yarn geometrical structure are considered for the mechanical modelling of the multifilament twisted yarn. The FEM applying the beam theory enhanced with advanced solution algorithms supporting large deformation effects was implemented for the mechanical analysis. The proposed method offers a fast and flexible design in terms of modelling, meshing and analysis. Thus the difficulties resulted from the high structural complexity of the yarn models (e.g. yarn made of 100 filaments) are faced. The current stage of modelling aims at the calculation of the apparent yarn properties, mainly the elastic modulus and the bending rigidity. The respective deformations were simulated. For the evaluation of the proposed method, a set of 2- to 1200-filament twisted yarns were produced in the laboratory and tested in tensile and bending deformations. The comparison of the computational and the experimental data assured the reliability of the modelling approach. The effect of the major structural parameters as the filament radius and the yarn twist in the elastic properties and the bending rigidity was also examined.

The **third chapter** presents the mesomechanical modelling stage focusing on the apparent mechanical properties of the fabric unit cell. In the current stage of modelling the representation of the filaments constituting the yarns is omitted for the reduction of the computational cost and the yarns are represented as homogenous structures (their apparent properties were calculated in the above stage). Thus the attribution of the yarn properties constitutes the basic factor for the modelling reliability due to the homogenization of the yarns. Moreover the yarns interactions in the fabric structure are determinant for the structural stability of the fabrics subjected to deformations. Three approaches, the solid, the shell and the beam modelling, are investigated for the mesomechanical analysis of the plain woven structure. The beam modelling was proved the appropriate approach for the reliable attribution of the modelled yarns. Aim of the mesomechanical modelling stage is the calculation of the performance of the unit cell in the tensile, shear and bending deformation. The models of the basic woven and knitted structures were also presented. Especially the modelling approach of the knitted structures produced by cotton yarns was based on the proposed principle of the minimum loop length and it was confirmed by the experimental data.

In the **fourth chapter**, the macromechanical modelling stage of textile structures is presented. The macromechanical analysis refers to the mechanical performance of the fabric sheet in complex deformations. The reduction of the computational cost demands the omitting of the representation of the structural unit cells. Thus the discrete structure of the fabric is replaced by a continuum model. It is obvious that the evaluation of the apparent properties of the discrete model and the generation of an equivalent continuum model (homogenization) is essential for the reliability of the macromechanical analysis. Three methods were implemented for the generation of a continuum model of FE presenting equivalent performance with the discrete woven structure:

a. Two shell meshes of coincident nodes presenting different stiffness

b. Two shell meshes of coincident nodes of different material properties

c. 3-layer continuum structure (meshed using shells or solid-shell elements)

The reliability of the macromechanical models was evaluated using experimental data received by the literature. In particular, the computational prediction of the macromechanical performance was based on the generation of the mesomechanical model of the unit cell, the calculation of the apparent properties, the implementation of the homogenization approaches and the simulation of the mechanical tests using the continuum macromechanical model.

The **fifth chapter** of the thesis focuses on the simulation of the fabric drape test. The fabric drape corresponds to an extremely complex deformation given that the fabric is bent in several planes forming the folds. The drapeability of the fabric reinforcement offers the advantage of bending around double-curvature mould producing complex shaped composite parts. The fabric drape is a nonlinear problem that undergoes large displacements and rotations. The 3-layer homogenization method was proved adequate for the drape simulation. The 8-node solid-shell finite elements with 3 translational degrees of freedom in each node were used for the analysis. The success of the analysis was evaluated experimentally.

In the **sixth chapter**, the proposed textile modelling approach is implemented for the study of the compression performance of a spacer fabric. The warp-knitted spacer fabrics are successfully introduced in building constructions as thin sheet component reinforcement for wall panels, exterior siding, roofing tiles, flooring tiles, pressure pipes etc. Their structural advantages support an armature system of highly oriented yarns and the easily cement embodiment for the production of the composite. The compression resistance of the spacer fabric provides a major advantage for the performance and the composite manufacturing process. The mesomechanical models of the constitutive layers were generated and the apparent properties were calculated. Then the simulation of the compression test was performed using the macromechanical model.

Finally the conclusions of the thesis are presented in the **seventh chapter**. The adequacy of the proposed approach of textile design, the limitations of the method and the perspectives for further work are discussed.

Περίληψη

Στόχο της διδακτορικής διατριβής αποτελεί η ανάπτυξη μιας ολοκληρωμένης μεθόδου μηχανικής ανάλυσης των κλωστοϋφαντουργικών (κ/υ) προϊόντων βασισμένη στην μικροδομή τους. Η ανάγκη για ακριβή πρόβλεψη της μηχανικής απόδοσης των κ/υ δομών προέκυψε από την εισαγωγή τους σε τεχνικές εφαρμογές, κυρίως υπό την μορφή σύνθετων υλικών, και την ενσωμάτωσή τους στην αεροπορική βιομηχανία και ναυπηγική (προπέλες και πλαίσια σκαφών από σύνθετα υλικά), στην πολιτική μηχανική (ελαφριά πλαίσια σύνθετων υλικών, αποστράγγιση εδάφους), στον αθλητικό εξοπλισμό (προστατευτική ένδυση και ένδυση υψηλών επιδόσεων), στον τομέα των επίγειων μεταφορών (αερόσακοι, ζώνες ασφαλείας, ελαστικά οχημάτων) κ.α. Παρά τις μακροχρόνιες προσπάθειες της ερευνητικής κοινότητας για την ανάπτυξη μιας αξιόπιστης μεθοδολογίας για την πρόβλεψη της μηχανικής συμπεριφοράς των κ/υ δομών, η σχεδιαστική τους διαδικασία βρίσκεται ακόμα σε εξέλιξη.

Η επίδραση των δομικών στοιχείων (των ινών) των υφασμάτων στην μηχανική ανάλυση αυτών αποτέλεσε βασική αρχή για την προτεινόμενη προσέγγιση μοντελοποίησης, σε αντιδιαστολή με τα υπάρχοντα διδιάστατα μηχανικά μοντέλα των υφασμάτων τύπου ελάσματος ή μεμβράνης. Θεωρήθηκε επομένως η διακριτή δομή των υφασμάτων, γνωστή ως μικροδομή λόγω των μικρών διαστάσεων των δομικών στοιχείων. Αυτό ακριβώς εκφράζει ο τίτλος της διατριβής.

Στο **πρώτο κεφάλαιο** της διατριβής παρουσιάζεται η βιβλιογραφική επισκόπηση των μεθόδων που έχουν αναπτυχθεί για την μηχανική ανάλυση των κ/υ δομών. Από την πρώτη αναλυτική προσέγγιση για την δισδιάστατη γεωμετρική απεικόνιση της απλής ύφανσης μέχρι τα σύγχρονα τριδιάστατα υπολογιστικά μοντέλα σύνθετων υλικών σημειώθηκε πλήθος προσεγγίσεων όσον αφορά τον σχεδιασμό του προβλήματος, την μέθοδο μηχανικής ανάλυσης, το επίπεδο της μοντελοποίησης και τις θεωρούμενες παραδοχές. Καταγράφηκε, λοιπόν, η εξελικτική πορεία των σχετικών ερευνών, οι προοπτικές και οι περιορισμοί για την μηχανική ανάλυση των κ/υ δομών.

Το υψηλό επίπεδο δομικής πολυπλοκότητας που προκύπτει από την ιεραρχία ίνα – νήμα – ύφασμα επιφέρει σημαντικές δυσκολίες στην μοντελοποίηση και την μηχανική ανάλυση των κ/υ προϊόντων. Ενδεικτική είναι η απόκλιση που παρουσιάζουν οι διαστάσεις τυπικού μεγέθους υφάσματος (10^{-1} έως 10^{0} m) και των δομικών στοιχείων που το συνιστούν (διάμετρος ίνας, 10^{-5} m). Η πολυπλοκότητα που συναντάται στην μοντελοποίηση και μηχανική ανάλυση των κ/υ δομών λόγω της δομικής ιεραρχίας αντιμετωπίστηκε υιοθετώντας ανάλογη ιεραρχία στην διαδικασία μοντελοποίησης. Μ' αυτόν τον τρόπο αναπτύχθηκαν τρία επίπεδα μοντελοποίησης: η μικρομηχανική μοντελοποίηση των νημάτων, η μεσομηχανική μοντελοποίηση της δομικής μονάδας του υφάσματος και η μακρομηχανική μοντελοποίηση ευρύτερου τμήματος του υφάσματος. Κατ΄ επέκταση η προτεινόμενη μεθοδολογία για την μηχανική ανάλυση των κ/υ δομών περιλαμβάνει τρία κυρίως στάδια, τα οποία αναπτύσσονται στα επόμενα κεφάλαια.

Το **δεύτερο κεφάλαιο** εστιάζει στο στάδιο της μικρομηχανικής μοντελοποίησης. Μελετήθηκαν σε μικροκλίμακα (σε επίπεδο ίνας) νήματα τυπικής δομής τα οποία συνιστούν

το δομικό στοιχείο για την παραγωγή των κ/υ προϊόντων. Για την ανάπτυξη του μηχανικού μοντέλου πολυινικού στριμμένου νήματος θεωρήθηκαν οι ελαστικές και διαστατικές ιδιότητες των ινών και η δομή του ιδανικού νήματος. Για την μοντελοποίηση και μηχανική ανάλυση εφαρμόστηκε η μέθοδος των πεπερασμένων στοιχείων (ΠΣ) με στοιχεία δοκών συζευγμένη με προηγμένους αλγορίθμους επίλυσης για την πρόβλεψη μεγάλων παραμορφώσεων. Η ευχρηστία της προτεινόμενης μεθόδου στην γεωμετρική απεικόνιση και την ανάπτυξη του πλέγματος την καθιστούν κατάλληλη για την αντιμετώπιση των δυσκολιών που απορρέουν από την υψηλή δομική πολυπλοκότητα των μοντέλων των νημάτων (π.χ. νήμα 100 ινών). Σκοπός του τρέχοντος σταδίου είναι ο υπολογισμός των φαινόμενων ιδιοτήτων του νήματος, κυρίως του αξονικού μέτρου ελαστικότητας και της δυσκαμψίας. Για τον υπολογισμό τους πραγματοποιείται η προσομοίωση των αντίστοιχων δοκιμών. Για την αξιολόγηση της προτεινόμενης μεθόδου παράχθηκε εργαστηριακά μια σειρά νημάτων από 2 μέχρι 1200 ίνες, τα οποία υποβλήθηκαν σε δοκιμές εφελκυσμού και κάμψης. Από την σύγκριση των πειραματικών και υπολογιστικών δεδομένων επιβεβαιώθηκε η αξιοπιστία της μοντελοποίησης. Επιπλέον ακολούθησε παραμετρική ανάλυση του μοντέλου του νήματος που αποτυπώνει την επίδραση των κύριων δομικών χαρακτηριστικών των νημάτων στο φαινόμενο μέτρο ελαστικότητας και την δυσκαμψία του νήματος.

Στο **τρίτο κεφάλαιο** παρουσιάζεται το στάδιο της μεσομηχανικής μοντελοποίησης που εστιάζει στην μελέτη των μηχανικών ιδιοτήτων της δομικής μονάδας του υφάσματος. Στο τρέχον στάδιο μοντελοποίησης παραλήφθηκε η απεικόνιση των ινών που συνιστούν τα νήματα για την μείωση του υπολογιστικού κόστους και τα νήματα μοντελοποιήθηκαν ως ομογενείς δομές (οι φαινόμενες ιδιότητες τους υπολογίστηκαν στο πρώτο στάδιο). Επομένως η επιτυχής απόδοση των ιδιοτήτων στα μοντελοποιημένα νήματα αποτελεί βασικό παράγοντα για την αξιοπιστία των μεσομηχανικών μοντέλων. Επιπλέον η αλληλεπίδραση των νημάτων που συνιστούν την δομή του υφάσματος είναι καθοριστική για την δομική σταθερότητα του υφάσματος κατά την υποβολή του σε μηχανικά φορτία. Τρεις προσεγγίσεις, η μοντελοποίηση με ογκικά ΠΣ, ΠΣ κελύφους και ΠΣ δοκού, αναπτύχθηκαν για την μεσομηχανική ανάλυση της δομικής μονάδας του απλού υφαντού. Από την σύγκριση των προσεγγίσεων, η μοντελοποίηση με ΠΣ κελύφους αποδείχθηκε καταλληλότερη με πολλά σημεία υπεροχής, κυριότερο των οποίων είναι η επιτυχής απόδοση των φαινόμενων ιδιοτήτων στα ομογενοποιημένα νήματα. Σκοπός της μεσομηχανικής ανάλυσης είναι ο υπολογισμός της φαινόμενης συμπεριφοράς της δομικής μονάδας του υφάσματος σε εφελκυσμό, διάτμηση και κάμψη από την προσομοίωση των αντίστοιχων δοκιμών. Μελετήθηκε επίσης η γεωμετρία των βασικότερων δομών υφαντών και πλεκτών υφασμάτων και αναπτύχθηκαν τα αντίστοιχα μοντέλα. Ιδιαίτερα για τα μοντέλα των πλεκτών υφασμάτων από βαμβακερά νήματα αναπτύχθηκε μεθοδολογία σχεδιασμού που στηρίζεται στο ελάχιστο μήκος νήματος θηλιάς και επιβεβαιώθηκε από εργαστηριακά αποτελέσματα.

Στο **τέταρτο κεφάλαιο** παρουσιάζεται η μακρομηχανική μοντελοποίηση των κ/υ δομών. Η μακρομηχανική ανάλυση εστιάζει στην μηχανική συμπεριφορά μεγάλου τμήματος του υφάσματος σε σύνθετες καταπονήσεις. Για την μείωση του υπολογιστικού κόστους η απεικόνιση της δομικής μονάδας του υφάσματος παραλείπεται και η διακριτή δομή του

υφάσματος αντικαθίσταται από συνεχές μοντέλο. Προφανώς η απόδοση των φαινόμενων ιδιοτήτων του διακριτού μοντέλου στο ισοδύναμο συνεχές μοντέλο (μέθοδος ομογενοποίησης) είναι καθοριστική για την αξιοπιστία της μακρομηχανικής ανάλυσης. Αναπτύχθηκαν τρεις προσεγγίσεις για την ανάπτυξη συνεχούς μοντέλου ΠΣ που παρουσιάζει ισοδύναμη μηχανική συμπεριφορά με την διακριτή δομή του απλού υφαντού:

α. Μοντέλο από δύο πλέγματα κελύφους, με συμπίπτοντες κόμβους, που παρουσιάζουν διαφορετικό είδος δυσκαμψίας (ελαστική – καμπτική).

β. Μοντέλο από δύο πλέγματα κελύφους, με συμπίπτοντες κόμβους, από διαφορετικό υλικό.

γ. Μοντέλο τριών στρωμάτων συμμετρικής διατομής (πλεγματοποίηση με ΠΣ κελύφους, ογκικά ΠΣ ή solid-shell ΠΣ).

Η αξιοπιστία των μακρομηχανικών μοντέλων εκτιμήθηκε από πειραματικά αποτελέσματα που ελήφθησαν από βιβλιογραφικές πηγές. Συγκεκριμένα για την υπολογιστική πρόβλεψη της μακρομηχανικής συμπεριφοράς αναπτύχθηκε το μεσομηχανικό μοντέλο της δομικής μονάδας, υπολογίστηκαν οι φαινόμενες ιδιότητες, εφαρμόστηκαν οι μέθοδοι ομογενοποίησης και η προσομοίωση των μηχανικών καταπονήσεων στο συνεχές μακρομηχανικό μοντέλο. Αποτελεί επομένως επιβεβαίωση της ορθότητας των σταδίων μεσο- και μακρο-μηχανικής μοντελοποίησης.

Το **πέμπτο κεφάλαιο** της διατριβής εστιάζει στην προσομοίωση του πεσίματος του υφάσματος υπό την επίδραση του βάρους του σε βάθρο στήριξης (drape test). Πρόκειται για ιδιαίτερα σύνθετη καταπόνηση δεδομένου ότι το ύφασμα κάμπτεται σε πολλά επίπεδα σχηματίζοντας πτυχώσεις. Η δυνατότητα των υφασμάτων να κάμπτονται σε πολλά επίπεδα επιτρέπει την διαμόρφωσή τους σε μήτρες και την παραγωγή σύνθετων κομματιών πολύπλοκων σχημάτων. Η δοκιμή drape αποτελεί μη-γραμμικό πρόβλημα που διέπεται από μεγάλες μετατοπίσεις και στροφές. Η μέθοδος ομογενοποίησης με συνεχή δομή τριών στρωμάτων αποδείχτηκε κατάλληλη για την προσομοίωση της δοκιμής drape. Για την μοντελοποίηση χρησιμοποιήθηκαν τα 8-κομβικά solid-shell ΠΣ με 3 βαθμούς ελευθερίας ανά κόμβο. Η αξιοπιστία της προσομοίωσης αξιολογήθηκε πειραματικά.

Στο **έκτο κεφάλαιο** επιχειρείται η εφαρμογή της προτεινόμενης μεθόδου μοντελοποίησης για την μελέτη της συμπεριφοράς τριδιάστατης κ/υ δομής σε δοκιμή συμπίεσης. Πρόκειται για στημονοπλεκτά υφάσματα με σημαντικό πάχος που παρουσιάζουν υψηλή αντίσταση σε συμπίεση και χρησιμοποιούνται σε οικοδομικές κατασκευές ως δομές ενίσχυσης σκυροδέματος για την παραγωγή πλαισίων τοίχου, επένδυση οροφής κ.α. Η αντίσταση του υφάσματος σε συμπίεση αποτελεί πλεονέκτημα για την παραγωγή του σύνθετου υλικού (εύκολη ενσωμάτωση του σκυροδέματος στην κ/υ δομή) και την λειτουργικότητά του. Παράχθηκαν τα μεσομηχανικά μοντέλα των στρωμάτων της δομής από τα οποία υπολογίστηκαν οι φαινόμενες ιδιότητες. Στη συνέχεια το μακρομηχανικό μοντέλο υποβλήθηκε σε δοκιμή συμπίεσης προσομοιώνοντας την πειραματική δοκιμή.

Τέλος στο **έβδομο κεφάλαιο** παρουσιάζονται τα συμπεράσματα της διατριβής, διερευνάται η επάρκεια της προτεινόμενης μεθόδου μηχανικής ανάλυσης των κ/υ δομών και οι δυνατότητες εξέλιξής της καθώς και οι αδυναμίες της μεθόδου και οι προοπτικές για περαιτέρω έρευνα.

Chapter 1
Mechanical Analysis of Textile Structures: The State of the Art

Abstract

The textile sector presents remarkable delay concerning the adoption of a complete computational design procedure for the textile products. Despite the long-lasting attempts of the research community to develop a thorough technique for the prediction of the fabric performance, the used design procedure is still based on traditional methods. Thorough analytical investigations were carried out for the study of the mechanical properties of the textile structures. The inadequacy of these methods arose mainly from the consideration of simplified models for lower complexity. Unavoidably, these models ignore essential structural and mechanical features of the textiles. The evolution in computer programming and the related available power turned the researchers' interest to numerical approaches. The advanced computer based engineering tools are proved gradually suitable for the simulation of complex deformations of multi-body geometrical structures, such as the textile fabrics. The current chapter presents the evolutionary process of the research and exposes the technological attempts, perspectives and limitations resulted from the mechanical analysis of the textile structures. Moreover the proposed procedure for the integrated textile design based on a Computer Aided Engineering environment is discussed. The proposed textile design is based on the subdivision of the modelling procedure in three stages corresponding to the hierarchy levels of textile structures. Thus three basic modelling scales were developed: the micromechanical modelling of the yarns, the mesomechanical modelling of the fabric unit cell and the macromechanical modelling of the fabric sheet.

1.1 Introduction

The engineering design is the procedure of definition of the dimensional and physical characteristics of a product for the achievement of the desirable performance. The concept of the product performance corresponds to a synthesis of functional specifications, mechanical properties, aesthetic effects, resource limitations etc, depending on the application. Most of the engineering sectors have developed advanced computational design techniques in order to increase the quality, safety, reliability and operability of the designed structures while providing enhanced functionality. The evolutions in software programming and in the computer hardware performance have allowed more versatile applications of computers in design activities. The Computer Aided Design (CAD) serves the geometrical representation of the objects and the Computer Aided Engineering (CAE), among other functions, supports the

analysis of the performance and the prediction of properties. CAD and CAE software products, nowadays, are available in the market and they offer plethora of design capabilities, advanced numerical techniques and special facilities for the solution of the engineering problems.

The modern industries adopted the computer based design techniques in order to face the high competitiveness of the global liberated market. The maintenance of competitiveness demands the fast response to the continuously increased and abruptly changing requirements of the market, the achievement of the optimum relation of quality – cost and design innovations. Thus the fast processing speed supported by the computer based systems provides essential capabilities to the industries. A modern design culture was adopted by several engineering sectors as mechanical, civil, electrical and electronic engineering etc, as it is presented below.

The mechanical engineering field adopted advanced CAD and CAE software packages for the evolution of consumer products, heavy equipment, industrial components, machinery manufacturing, micro electromechanical systems as well as medical products. The computer based tools improve the aesthetics and ergonomics of product designs by generating advanced shapes, complex surfaces, and patterns. They allow fast design and performance prediction of large scale component assemblies. Static and dynamic structural analysis as well as thermal, fluid and acoustic analysis, support the solution of the mechanical problems. In the fast moving automotive industry sub-sector requirements, the state-of-the-art technology is combined with a high level of safety. Advanced specialized CAD and CAE systems are implemented providing the real-time simulation for power-train and vehicle dynamics. The automotive software packages support the simulation of the gasoline engine, the diesel engine, the vehicle behaviour, the brake hydraulics, the turbocharger etc. The structural and acoustic analysis in terms of frequency response, accomplished by the vehicle dynamics, provide vital evolutions in the balance of safety, ergonomic issues, noise and vibration performance of the vehicles (sourse: *dSPACE*). Accordingly, the demands in the aerospace sector imposed the rapidly adoption of the computer based engineering design. The products must provide the highest performance with indisputable reliability in an environment of continuously reduced costs and shortened times. A variety of physical phenomena acting on the aircrafts are approached by the simulation of flights using advanced software codes. Enhanced libraries are provided to model the rigid body equations of motion, aero forces and moments, aero derivative look-up tables, wind models, control systems and sensors, and control surface actuation saving both time and money for the engineers (source: *DELCAM*).

Civil engineering software is used to design, simulate and analyze structures such as buildings, bridges etc. Some types of civil engineering software are suitable for managing the administrative aspects of engineering projects, such as scheduling, costing, budgeting, materials acquisition, resource allocation, and the overall management of the projects. Typically, however, civil engineering software focuses on the physical components and requirements for actual construction of the structures. Engineers can also use civil engineering design software in road building to visualize highways, predict traffic flow, produce traffic and street-lighting schematics, and determine lane requirements. Civil engineering and

architectural software is used in building to visualize the structures designed, to determine the dimensions and offsets of residential versus commercial construction projects, and drape satellite or aerial photos over terrain models. Building design software is also used for predictive analysis on individual structural elements. Especially the architects focus on tools to design buildings, visualize the design proposals, display measurements and they are also supported by the respective structural analysis data. In general, the use of the civil engineering CAD and CAE software is exploited in such an extent, that they dominate today in the design and structural analysis of a building (source: *Graphisoft*).

In the field of electrical and electronics engineering the CAD and CAE software is an extremely useful tool. Specific CAD software packages are available for the particular applications such as electrical installations, electronic circuit design, electronic printed board design, integrated circuits design etc. CAE software is used for the simulation and analysis of the circuits and the prediction of their operational behaviour. Highly advanced systems are available providing absolutely realistic results. They eliminate the necessity of prototyping and they provide the only reliable method in use for the design and analysis of the circuits. In other words CAD and CAE tools provide a well established environment for the development of new electrical and electronic products.

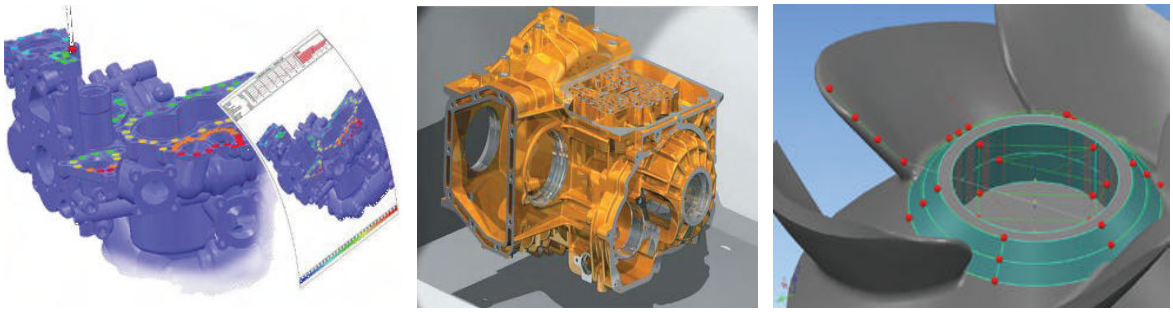

Figure 1-1: source: www.delcam.com

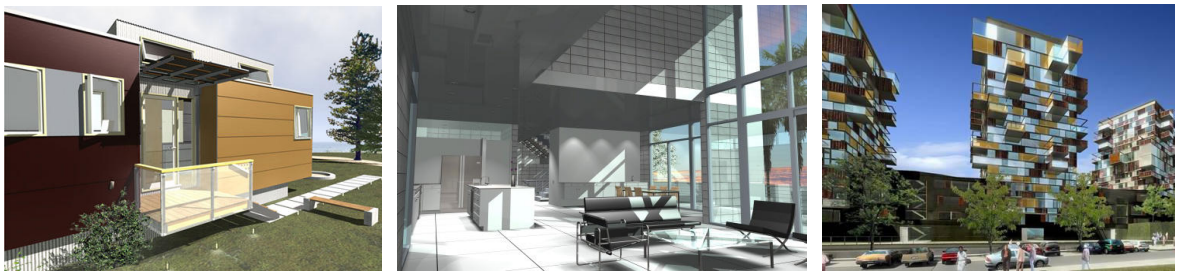

Figure 1-2: source: www.graphisoft.com

On the contrary to the above, an absence of a respective global CAD and CAE structural design tool is presented in the textile sector. A possible reason is that the exclusive aim of the textile products to fulfil simple functional clothing attributes, for thousands of years, undermined the significance of the structural engineering design. It is worth to mention that

the aesthetic design dominated over the whole period of the use of the textiles in clothing applications and consequently mainly artistic design tools have been developed. To mention some of them, *Textronics CAD/CAM*, *Optitex 2D/3D CAD*, *DesignScope Victor*, *Grafixoft*, *Evolution Textile Design Software*, *JacqCAD MASTERS*, *Lectra*, *Textile Vision* and *Triadem* are textile design tools. Some are specified in the visualization of textile patterns in two-dimensional sheets. Some advanced software packages provide the three-dimensional representation of weave structures. Some support also solutions from pattern design to manufacturing and retailing process. There are also design tools focusing on the mapping of textile patterns in three-dimensional structures.

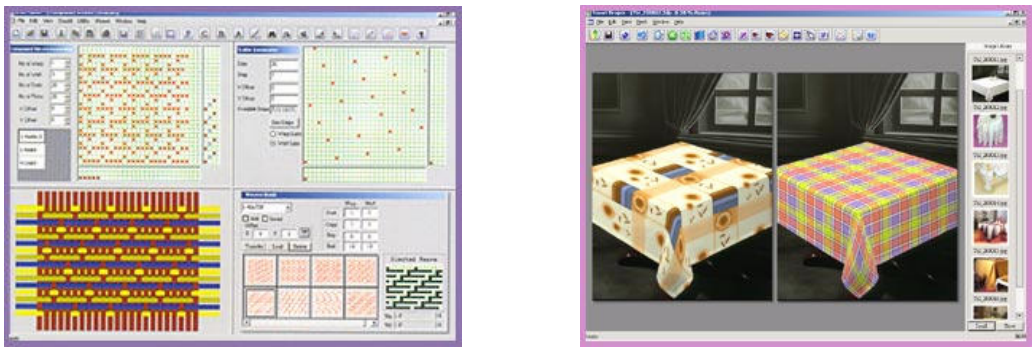

Figure 1-3: Artistic design tools for weave creation and 3D texture mapping (source: *Textronics CAD/CAM*).

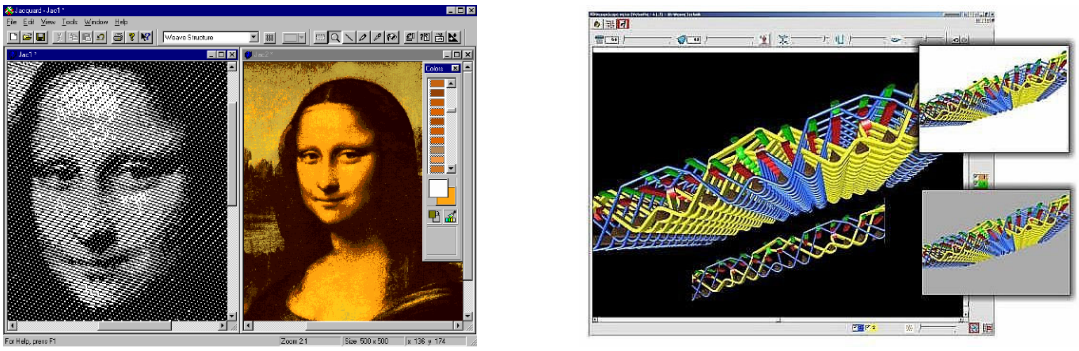

Figure 1-4: Jacquard design (*Grafixoft*) and 3D weave (*DesignScope Victor*)

However, the development of the textile industry and its recent dynamic expansion in advanced technical applications converted the design of the textile structures to a complex engineering operation. Thus the performance of a textile structure is specified by the mechanical, thermal, electrical, comfort and aesthetic properties. Consequently, the design parameters are the series of the material properties of the fibres and the structural characteristics of the fibres, the yarns and the textile fabrics. The current thesis focuses mainly on the mechanical design, but the concept methodology can be generalized over the total textile engineering field.

Despite the wide spread of the computer based design in the most of the engineering sectors and the unprecedented development of the textile machinery technology, the textile engineering still maintains the traditional methods of design (see Figure 1-5). These methods usually include iterative production of samples, tests for the definition of their properties, comparison with the desirable properties and change of the initial parameters for the production of new samples until the achievement of the desirable product (Hearle 2004). This procedure extends significantly the fabric production period. The cost also is kept high especially when the evaluation of the product properties is an expensive procedure. In addition the innovative character of some products precludes the use of accumulated experience for the production of the first sample increasing the number of the repetitions. Thus it is expected that the implementation of CAD and CAE tools would reduce the design phase duration and the cost of production. Hearle in his work (Hearle 2006) exposed the obstacles in the adoption of a modern engineering design culture by the textile industry. The conservatism of the textile community is referred as significant reason. The low necessity for the modification of the current design methodology in the partial case of the clothing products, resulted from the small scale and low cost of the textile products, is also discussed. But the fundamental reason, according to his report, is the important distinctions of the science of fibre assemblies related to the mainstream 20^{th} century development of applied mechanics. The anisotropic visco-elastic properties of textile structures, the flexibility, the structural porosity and discontinuity, the buckling phenomena and the relative large displacements are some of the mentioned distinctions.

In this chapter an extended review of the modelling attempts of the textile structures is presented. The technological review point out the difficulties and the bottle-necks towards a global textile structures modelling. The thorough overview of the related research activities indicates the specific structural character of the textile products, which is the main drag force in the progress of the modelling of the textile products. Taking into account the existent work, the complex structural character of the textile products and the current technological situation, in terms of numerical methods and computational power, we discuss the possible research directions in order to achieve a CAE environment similar to that already used in other engineering sectors.

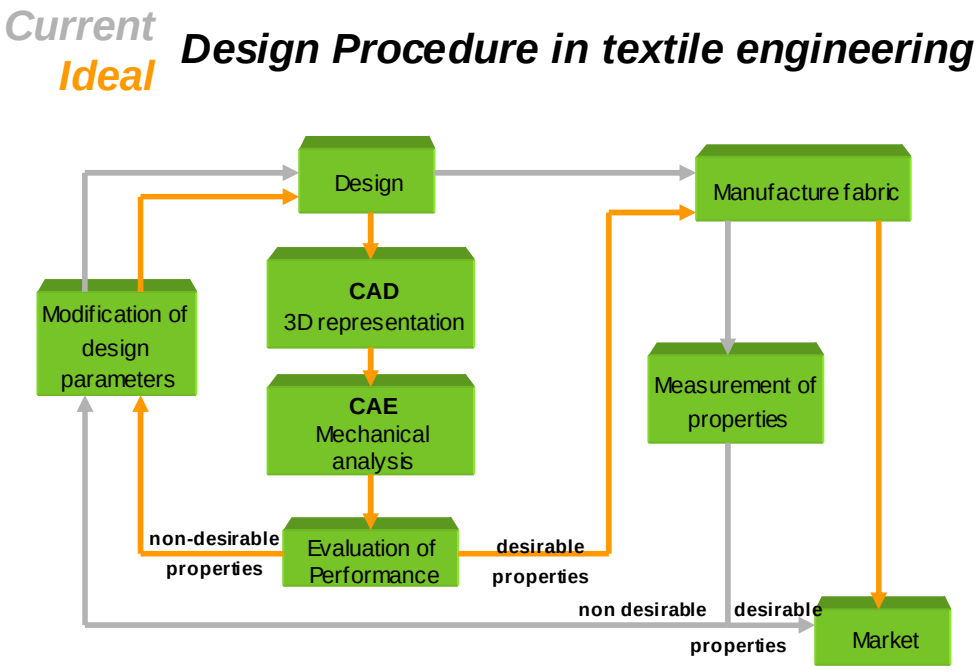

Figure 1-5: Traditional and ideal design procedure in textile engineering.

1.2 Overview of the textile structures

This overview is essential for the comprehension of the structural characteristics of the textile products considering the production hierarchy fibre – yarn – fabric. Moreover it introduces the underlying concepts that govern the mechanical performance of these structures.

1.2.1 Fibers

A fibre is defined as a flexible, macroscopically homogeneous body presenting a high length / width ratio and a small cross-section. The fibres constitute the raw material for the production of textile structures. The mechanical, physical and chemical properties of fibres substantially vary depending on their material and structure. Thus a wide range of applications is remarked in textile and manufacturing industry. Textile fibres are traditionally classified according to their origin as shown in the Table 1-1 (Hsieh).

Most man made fibres, i.e., regenerated and synthetic, are obtained in continuous form or filaments. Frequently, it is desired to obtain fibres in finite lengths. In this case, thousands of continuous filaments are collected together into a continuous rope of parallelized filaments called a tow. The tow is converted into staple length fibre by simply cutting it into specified lengths. The staple length produced in this conversion process depends on the system of yarn manufacture to be used. The staple fibres may be either natural fibres, such as cotton or wool, or any of a number of synthetic fibres.

Table 1-1: Classification of fibres according to their origin.

Natural fibres	Plant: based on cellulose, e.g., cotton, flax, hemp, jute, and ramie Animal: based on proteins, e.g., silk, wool, mohair, vicuna, other animal hairs Mineral: e.g., asbestos
Regenerated fibres (Based on natural cellulose and proteins)	Rayon: regenerated cellulose Acetate: partially acetylated cellulose derivative Triacetate: fully acetylated cellulose derivative Azlon: regenerated protein
Synthetic fibres (Based on synthesized organic polymers)	Acrylic: polyacrylonitrile (also modacrylic) Aramid: aromatic polyamides Nylon: aliphatic polyamides Olefin: polyolefins Polyester: polyesters of an aromatic dicarboxylic acid and a dihydric alcohol Spandex: segmented polyurethane Vinyon: poly(vinyl chloride) Vinal (or vinylon): poly(vinyl alcohol) Specialty fibres: poly(phenylene sulfide) and polyetheretherketone
Inorganic fibres	Carbon/graphite: derived from polyacrylonitrile, rayon Glass, metallic, ceramic

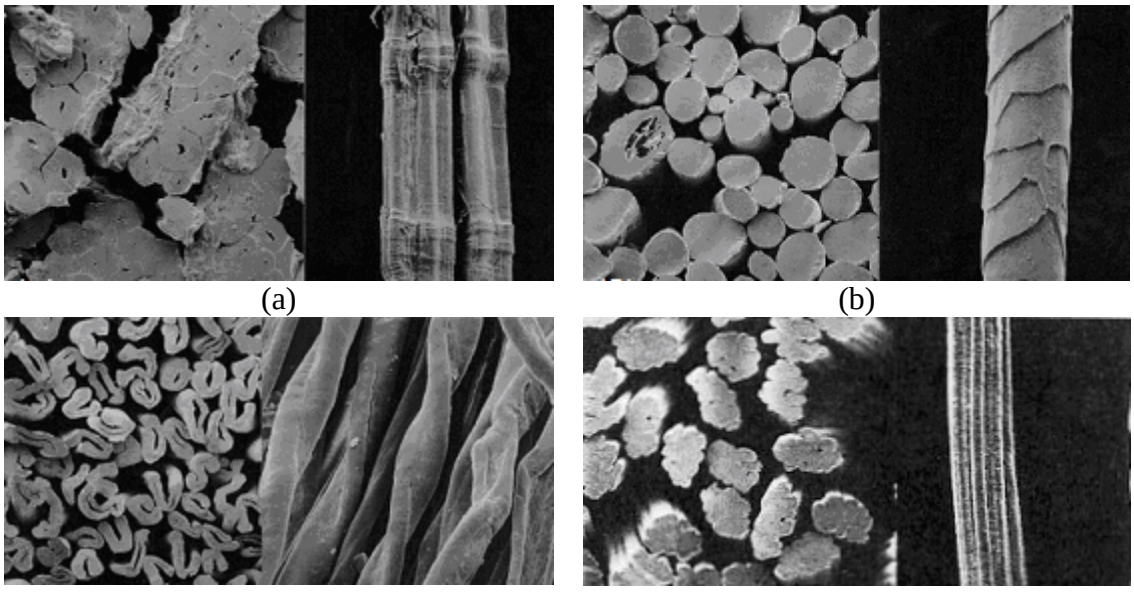

(a) (b) (c) (d)

Figure 1-6: Fibres from (a) flux, (b) wool, (c) cotton, (d) viscose**.**

1.2.2 Yarns

Generally, the manner by which fibres are processed into yarns is largely determined by the aspect ratio (length/width ratio) of the fibres. Various yarn spinning technologies are available

to physically align, bind, and twist fibres into yarns. Yarn spinning typically requires fibres with higher aspect ratios, e.g., 1000 or higher. Basic characteristics for the yarn structure are:

Filaments (continuous) or staple (finite length) fibres

Monofilament or multifilament

Twisted or flat (tows)

One-ply or two-ply or multi-ply yarns.

The textile yarns are produced from staple (finite length) fibres by a combination of processing steps referred to collectively as yarn spinning. After preliminary fibre alignment, the fibres are locked together by twisting the structure to form the spun yarn that is continuous in length and uniform. Textile yarns are also produced from continuous filament synthetic fibres. When several such filaments are combined together and slightly twisted to maintain unity, the product so obtained is called a multifilament yarn. The degree of twist introduced into a multifilament yarn is usually quite low and just adequate to produce some level of interfilament cohesion. A variety of processes have been developed to introduce bulk and texture in multifilament yarns. Individual filaments, considerably larger in cross-section than those used in multifilament yarns, may also be used in certain applications as monofilaments.

Figure 1-7: Flat yarn (left) and twisted multifilament yarn (right).

1.2.3 Two-dimensional structures

Two-dimensional woven fabrics

Weaving is the most widely used textile manufacturing technique and accounts for the majority of the two-dimensional (2-D) fabric produced. Conventional woven fabrics consist of two sets of yarns mutually interlaced into a textile fabric structure. The threads that run along the length of the fabric are called warp, while the threads that run along the width of the fabric from selvedge to selvedge are referred to as weft. Warp and weft yarns are mutually positioned at an angle of 90°. The number of warp and weft yarns per unit length is called the warp and weft density. The warp and weft yarns in a woven fabric can be interlaced in various ways, called a weave structure. The structure in which warp yarns alternately lift and go over across one weft yarn and vice versa is the simplest woven structure, called plain weave. Other common structures are twill and satin weave. Twill is a weave that produces diagonal lines on

the face of a fabric. A weave in which the binding places are arranged to produce a smooth fabric surface free from twill lines is called satin. The distribution of interlacing points must be as random as possible to avoid twill lines. The smallest repeat of satin weave is 5, while the most popular weaves are satins of 5 and 8 repeats. The 5-ends satin is most frequently used for technical applications for providing firm fabric, although having a moderate cover factor (Demboski, Bogoeva-Gaseva 2005).

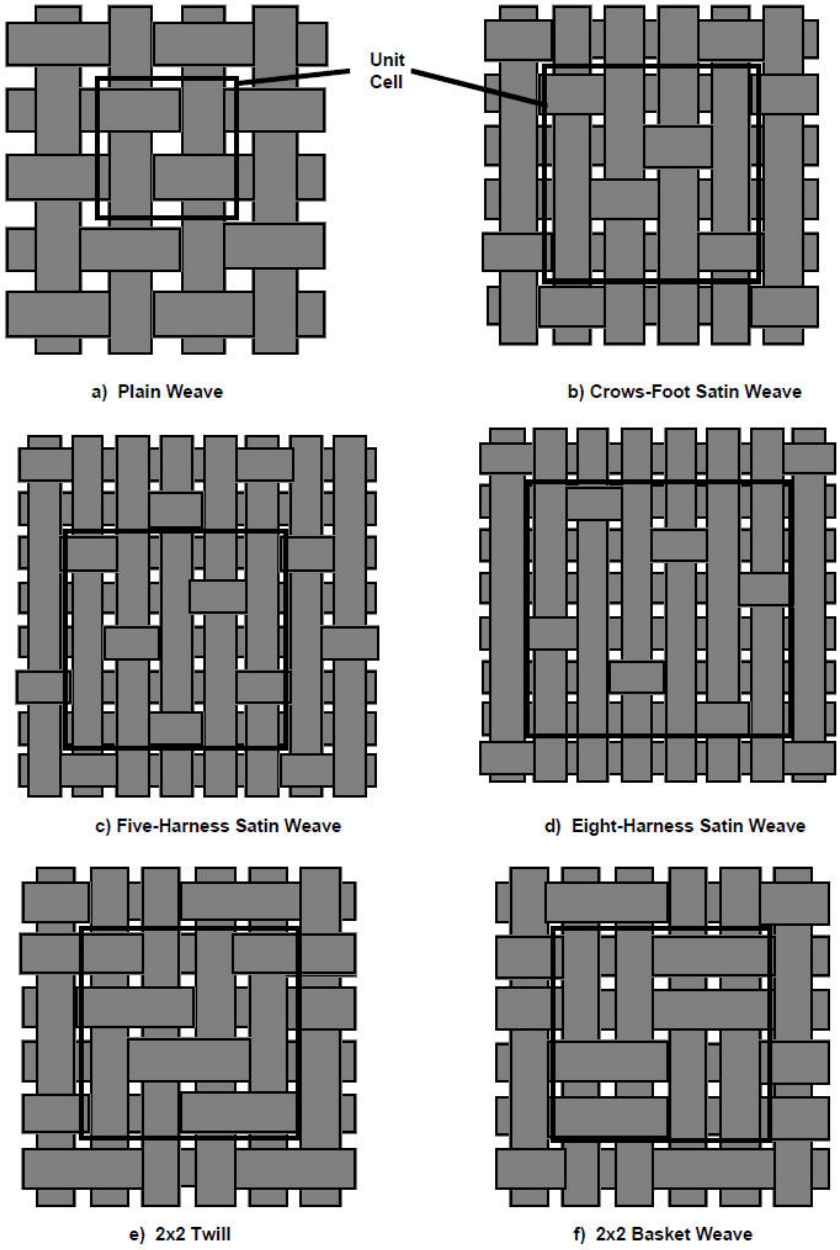

Figure 1-8: Commonly used 2D weave structures (Cox, Flanagan 1997).

Triaxial woven fabrics

A triaxial woven structure (Figure 1-9) consists of three systems of threads: one system for weft and two systems for warp. This fabric has three layers of material at any point, and is

thus stronger than a rectangular woven fabric made using the same elements. Warp threads in a basic triaxial fabric are interlaced at 60° and the structure is fairly open with a diamond-shaped centre. Since the interlacing points are fixed into the fabric structure, these fabrics exhibit high shear resistance (Hu 2008).

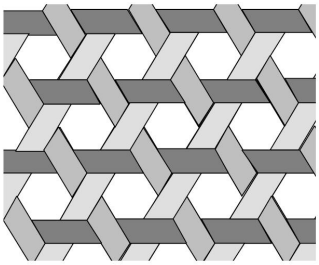

Figure 1-9: Basic triaxial weave.

Two-dimensional knitted fabrics

The knitted fabrics are textile structures assembled from basic construction units called loops. Two basic technologies exist for manufacturing knitted structures: weft and warp-knitted technology.

Weft-knitted fabric

The repeating unit of the knitted fabric is called the loop. The feature of weft-knitted fabric (Figure 1-10) is that the loops of one row of fabric are formed from the same yarn. A horizontal row of loops in a knitted fabric is called a course, and a vertical row of loops is called a wale. In weft-knitted fabrics the loops are formed successively along the fabric width. The simplest weft knit structure produced by the needles of one needle-bed machine is called plain knit or single jersey. Plain knit has a different appearance on each side of the fabric. A structure produced by the needles of both needle beds is called a rib structure or double jersey and has the same appearance on both sides of the fabric (Hu 2008).

Warp-knitted fabric

In warp-knitted technology every loop in the fabric structure is formed from a separate yarn called the warp, introduced mainly in the longitudinal fabric direction. The most characteristic feature of warp-knitted fabric (Figure 1-11) is that neighbouring loops of one course are not created from the same yarn. While weft-knitted technology is most commonly used in clothing manufacture, warp-knitted technology is substantially engaged in manufacturing structures for technical applications. Of special interest for technical applications are structures with inserted weft yarns, called weft-inserted warp-knitted fabric, and a multibar weft-knitted fabric (Demboski, Bogoeva-Gaseva 2005, Hu 2008).

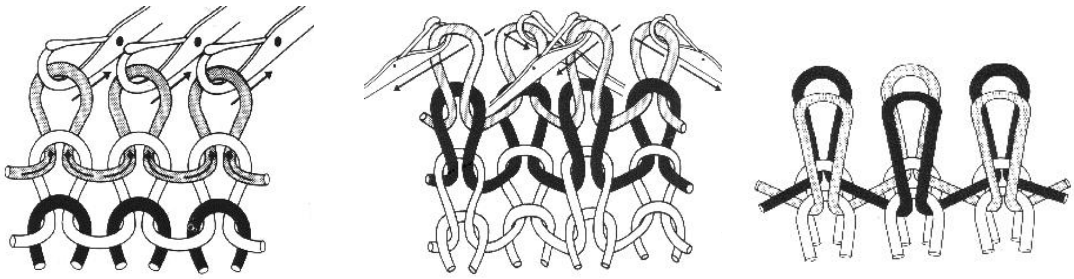

(a) (b) (c)

Figure 1-10: Weft-knitted structures, (a) single jersey, (b) rib 1x1, (c) interlock.

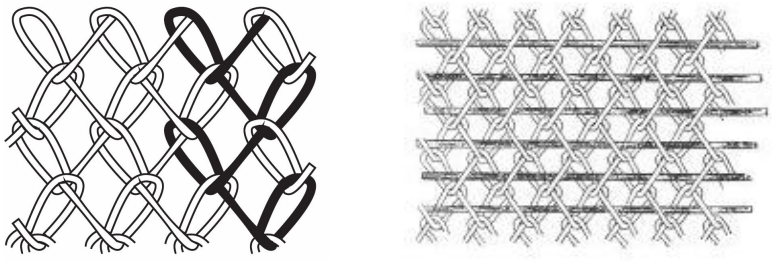

(a) (b)

Figure 1-11: (a) Basic warp-knit structure (b) Multibar weft-inserted warp-knit.

Two-dimensional non-wovens

The non-woven fabrics (Figure 1-12) are broadly defined as a sheet or web structure bonded together by entangling fibre or filaments either mechanically, thermally or chemically. They form a sheet, web or batt of directionally or randomly oriented fibres, bonded by friction and/or cohesion and/or adhesion. The fibres may be of natural or artificial origin. They may form staple or continuous filaments. They are engineered to provide specific properties such as absorbency, liquid repellency, resilience, stretch, softness, strength, flame retardancy, washability, cushioning, filtering, bacterial barrier and sterility. A basic non-woven structure is shown in Figure 1-12 (Hu 2008).

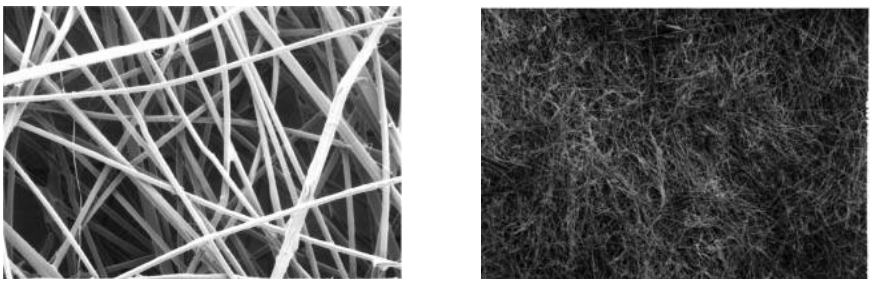

Figure 1-12: Non-woven fabric (Hsieh).

1.2.4 Three-dimensional structures

The three-dimensional woven or knitted structures are textile architectures having fibres oriented so that both the in-plane and transverse yarns are interlocked to form an integrated structure that has a unit cell with comparable dimensions in all three orthogonal directions. These materials offer particular properties, such as interlaminar shear force, mechanical and thermal stability along all three spatial axes. This integrated architecture provides improved stiffness and strength in the transverse direction and impedes the separation of in-plane layers in comparison to traditional 2-D fabrics. Because of their high transverse strength, high shear stiffness, low delamination tendency and near-net-shape manufacture, textile composites from weaving and knitting have received enormous attention recently (Hu 2008).

Classification of three-dimensional woven fabrics

The three-dimensional woven fabrics are produced principally by the multiple-warp weaving method, which has long been used for the manufacture of double and triple cloths for bags, waddings and carpets. The 3-D woven fabrics produced by using either multiwarp weaving technology or conventional weaving technology can be broadly classified as follows:

• 3-D solid (multilayer, orthogonal, angle interlock)

• 3-D hollow (flat surface, uneven surface)

• 3-D shell (by weave combination, by differential take-up, by moulding)

• 3-D nodal

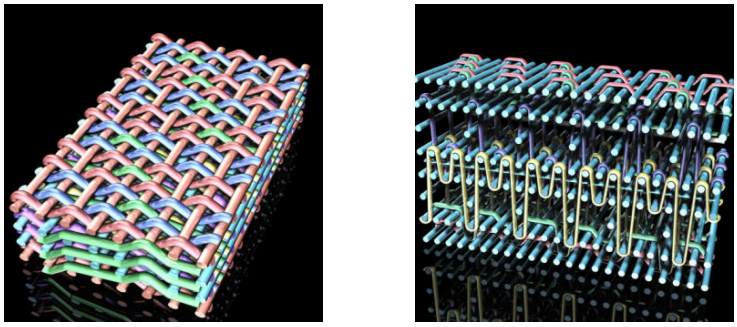

Figure 1-13: Geometrical models of 3-D multilayer interlaced weave (source: www.scotweave.com).

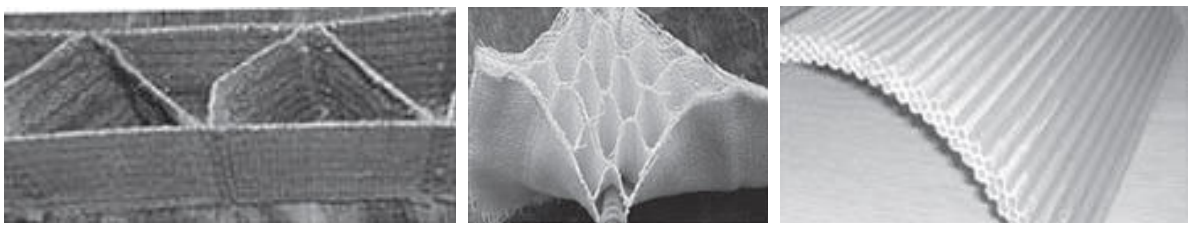

Figure 1-14: 3-D hollow woven structures.

Three-dimensional knitted fabrics

Knitting is the interlocking of one or more yarns through a series of loops. The knitted fabrics are considered 3-D due to their nonplanar configuration of the loops in the structure. They are also known as multiaxial–multilayer structures and are fabrics bonded by a loop system, consisting of one or several yarn layers stretched in parallel. Multilayers of linear yarns are assembled in warp (0°), weft (90°) and bias ($\pm\theta$) directions to provide structural integrity and through-thickness reinforcement.

The three-dimensional knitted fabrics are produced by weft or warp knitting. An example of a weft knit is the near-net-shape structure knitted under computer control by the pressure foot process. In a collapsed form this preform has been used for carbon–carbon aircraft brakes. While weft knitted structures have applications in limited areas, multiaxial warp knit (MWK) 3-D structures are more promising and have undergone a great deal of development in recent years. MWK fabrics generally possess up to four different load-bearing yarn systems arranged so that each can take on stress and strain virtually in all directions. Multiaxial–multilayer warp knits (MWK) are also termed non-crimp structures since the presence of knitted loops is to perform the function of holding layers of uncrimped inlay yarns. These yarn layers may have different orientation and different yarn densities of single ends. MWK fabrics are used to reinforce different matrices, since the combination of multidirectional fibre layers and matrices has proved capable of absorbing and distributing extraordinarily high strain forces.

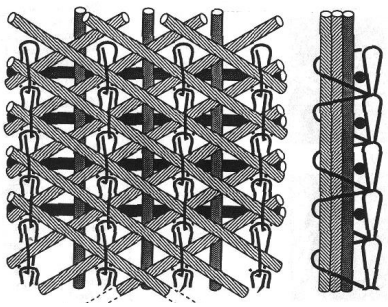

Figure 1-15: Multiaxial warp knitted fabric having inserted oriented yarns in warp, waft and diagonal directions.

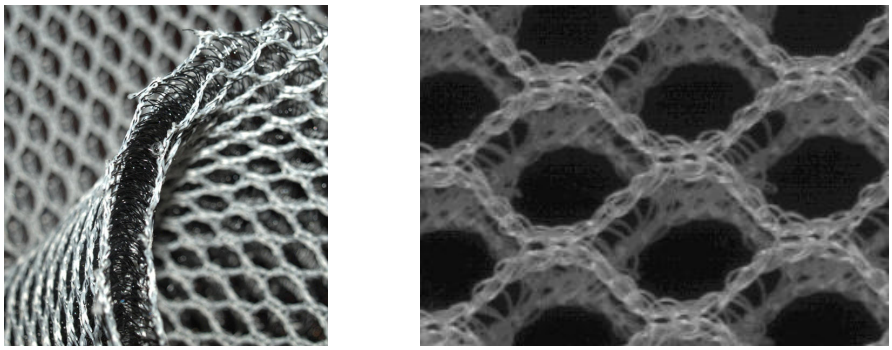

Figure 1-16: 3-D warp knitted structures.

Three-dimensional non-woven fabrics

The non-wovens are widely used in technical applications such as fitted filters, preforms for composites and geotechnical equipment. The three-dimensional shaped non-woven products are currently constructed from flat webs. In addition to the high cost of the conversion processes, irregularity is inevitably introduced into the final product because of joints. There is a long history of 3-D non-woven reinforcements, primarily in carbon–carbon composites. Orthogonal 3-D materials are fabricated by fixing a series of yarns in one direction (or rods which will later be withdrawn and replaced by yarns) and then inserting planar yarns in the two orthogonal directions around the fixed yarns.

1.2.5 Technical applications of Textiles

The great advantages of textiles manufacturing process considering the variety of constituent fibres (raw material), dimensions, shape and structure were essential for their spread in technical applications. Nowadays there are endless new applications of fibrous structures in most industrial sectors and constructions, summarized in the following.

Building: composite framework, Inflatable structures, awnings
Civil constructions: road stabilization, drainage
Aerospace: composite propellers, composite aircraft structural parts, parachute fabrics
Shipping: fibre composite hulls, hovercraft skirts, ropes
Land transportation: seat belts, tyre cord, air filters, airbags, seat covers
Packaging: wrapping, nets
Security: uniforms, bullet-proofs, camouflage fabrics
Sports and leisure: protective equipment, breathable waterproofs
Medical: sutures, antibandages, healthcare monitoring cloths

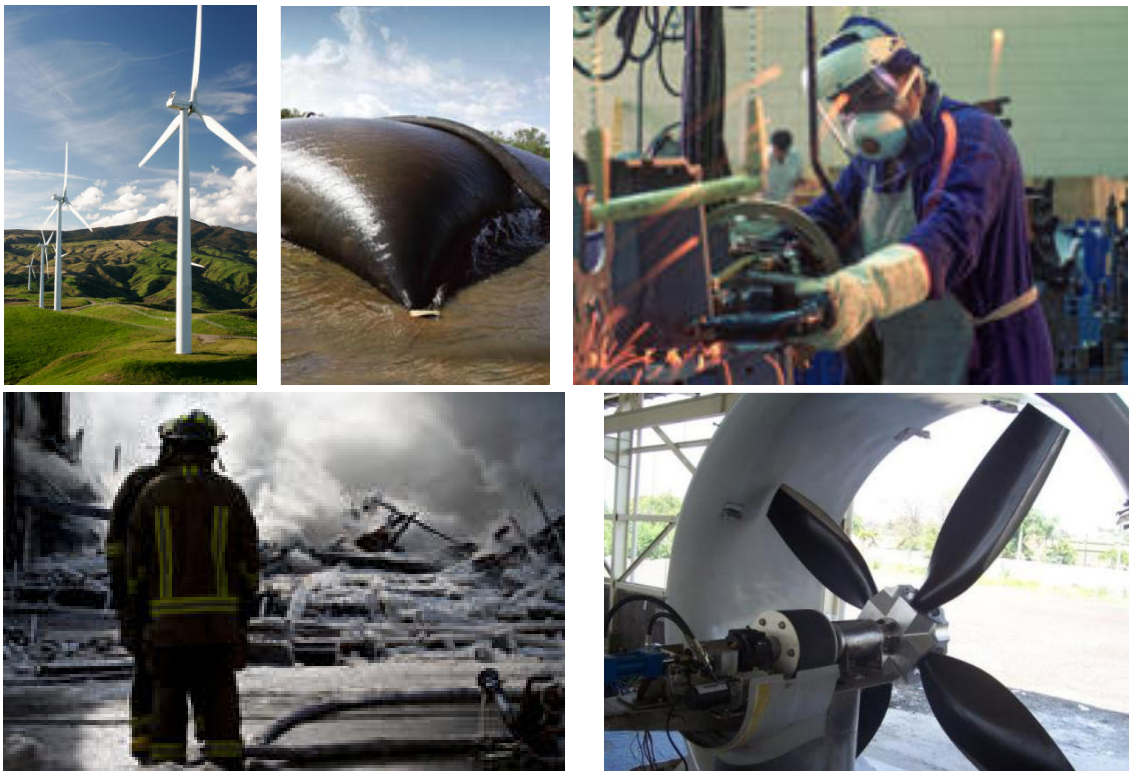

Figure 1-17: Technical application of textiles.

The smart or intelligent textiles correspond to the new generation textile products that sense and react to environmental conditions and stimuli, such as mechanical, thermal, electrical, magnetic or chemical sources. Thus sensors, actuators and controlling units are incorporated in smart textiles. The advanced coupling of traditional textile technology with material science, structural mechanics, sensor and actuator technology, artificial intelligence etc drives to innovative textile products (heat-storage and thermo-regulated clothing, wearable technology for snow clothing, vital signal recording clothing etc).

(a) (b) (c)

Figure 1-18: (a) Emotion sensitive apparel by Philips, (b) Pneuma dress by Fraunhofer IZM (c) Vital Jacket by Biodivices.

The new concept of fabric engineering was conceived during the evolution of technical textiles as a natural development of the trial and error methods. The commercially available fabrics failed in many cases to satisfy the specifications set by the producer and the designers and textile engineers were called upon to create entirely new structures. The properties in this case have to be "built-in" or applied to specific areas of the fabric at the correct orientation so as to withstand expected forces while maintaining economical production cost (Raz 2000).

1.2.6 The mechanical behaviour of textile structures

The geometrical complexity of the yarns as well as of the woven and knitted fabric patterns is an obstacle for the computational representation of the textile structures even in a simplified form. The complex geometry in continue results in a complicated deformation procedure of the textile structures even in the cases of simple loading. For example, the tensile deformation of a spun yarn corresponds to the superposition of bending, tensile and compression of the constituent helically arranged fibres. Contact phenomena, as sticking and sliding interaction, are also included in the deformation procedure increasing the complexity of the analysis. Accordingly, the mechanical analysis of the radial compression and axial bending of yarns include also complex deformations. Given that the deformation of a fabric results from the superposition of the tensile and bending deformations of the constituent yarns and their interactions at the crossing areas, the expected complexity of the mechanical analysis of a fabric is obviously very high.

The increased complexity of the representation and mechanical analysis of the fabrics often imposes the introduction of certain simplifying assumptions. Thus usually the yarns are considered as the basic structural unit of the fabrics. Additionally the yarn itself is assumed to be a homogeneous material. The elastic properties of the homogeneous yarn result from the elastic properties of the fibres and include the non-linear structural synergy of them within the yarn body. For example, the Young modulus of the homogenous yarn along its main axis direction must express the results of the reduction of the radius, the sliding of the fibres and their reorientation during the yarn elongation. Since the displacement of the fibres is related to frictional effects, an amount of energy is lost during the deformation of the yarn. This attribute is correlated with plasticity and hysteresis phenomena in the macroscopic examination of the properties of the yarns. Consequently, nonlinear elastic, plastic, viscoelastic anisotropic properties characterize the yarn macroscopic behaviour.

Even if the yarns are assumed as made of homogeneous material, the contact phenomena dominate in the deformation procedure of the fabrics. Actually, the friction effects support the stability of the textile structures. The contact phenomena have also a great significance for the stress and strain distribution in a fabric subjected to deformation. The friction energy losses appear during the load transferring along threads. Thus, very often, uneven load distribution appears within the textile structures.

The large deflection effects and the nonlinearity appearing in the deformation procedure of the textile structures presuppose special approaches for the mechanical analysis. The relative large deformation of the fabrics arises from the flexibility of the textile fibres and yarns as well as from the structural details and the way of load application. The yarns present high deformability which results from the low values of packing factor (the ratio of the fibres volume to the total volume of the yarn). The air trapped between the fibres is easily removed during the axial loading imposing the approach of the fibres, the reduction of the apparent yarn cross sections and consequently the high deformation of the yarns. This characteristic of the yarns is obviously transferred to the fabrics. Moreover the pattern of the fabrics itself and especially the structure of the knitted fabrics, supports the development of high deformations. From the structural point of view the fabric pattern can be considered as a multi-body system of yarns. The tensile deformation of the fabric corresponds to the synthesis of two processes, the straightening of the bent yarns and the subsequent elongation of them. The first process dominates in the lower loading stage and the second process appears upon the increase of the load. Thus the load-deflection curves of a textile structure subjected to tensile deformation is strongly nonlinear. The nonlinearity is supported also from the change of the contact status between the yarns, the large deflection effects observed even within the unit cell of the fabric and finally the material nonlinearities.

1.3 Mechanical modelling of the textile structures

1.3.1 Classification of the modelling approaches

The production hierarchy of the textile structures (fibre – yarn – fabric) is correlated with the high level of complexity presented in the modelling procedure and the mechanical analysis of them. The difficulties are increased due to the high divergence of the dimensions corresponding to the fabric sheet (10^{-1} to 10^{0} m) and the structural elements (fibre diameter, 10^{-5} m). Thus the realistic representation of the fabric structure, including the fibres representation, for the macromechanical modelling is computationally impractical. The structural singularity of the fabrics incurs their particular flexibility. Thereby the macromechanical performance of fabrics is characterized by large displacements of the constituting fibres even in low loading conditions. The textile society faced the modelling difficulties resulted from the structural hierarchy of textiles adopting a relative modelling hierarchy (Takano et al. 1999, Lomov et al. 2004, Bogdanovich 2006). Thus three basic modelling scales were developed: the micromechanical modelling of yarns, the mesomechanical modelling of the fabric unit cell and the macromechanical modelling of the fabric sheet.

The micromechanical modelling of yarns consists in the geometrical representation of the fibres and the mechanical analysis of the model for the evaluation of the apparent yarn properties. The yarn structure (fibre number, fibre geometry) and the fibre properties (elasticity) correspond to the input parameters in the current stage of modelling. The mesomechanical modelling of the fabric unit cell is based on the representation of the yarn as

homogenous structure. The 3D structure of the fabric is generated considering the central axes of the constituent yarns. Thus the fabric structure and the apparent yarn properties constitute the input parameters in the current stage of modelling, while the unit cell properties are calculated by the analysis. The macromechanical modelling stage of fabrics is based on the generation of simplified structure (usually continuum material) presenting equivalent performance with the discrete fabric structure. Thus the apparent properties of the fabric unit cells are considered for the generation of the equivalent sheet. The macromechanical modelling is required for the mechanical analysis of extended fabric pieces in complex deformations. Each individual modelling procedure such as their interface presents significant obstacles.

During the last decades, several methods were adopted for the mechanical modelling and analysis of the textile structures. A basic classification, according to the modelling method used, divides them into the analytical and numerical or computational approaches. The dominant engineering design culture played important role for the development and the succession of these approaches. Classical modelling methods find in textiles an attractive application field.

1.3.2 Classification of the deformations

For the mechanical analysis of the textile structures either on experimental or on modelling basis, the materials are subjected to deformations and the behaviour of the material is described by the correlation of the cause and effect principle. These deformations can be simple or complex. In the case of the simple deformations, a series of elementary tests as tensile, shearing, bending, compression, surface etc. are carried out. The mechanical behaviour of the fabrics is assessed through the synthesis of the partial responses to the various deformation modes. However, interesting from the design point of view is the mechanical analysis of the complex deformation of the textile structures. The complex deformations, as mainly the drape is, are even related to the aesthetic performance and quality of fabrics. Drape, along with colour, luster, and texture, is an important factor that affects the aesthetics and dynamic functionality of the fabrics. The fabrics have the ability to undergo large, recoverable draping deformations by bending in single and double curvature providing a sense of fullness and a graceful appearance. Especially when the fabrics are used as reinforcement materials for the construction of composites, drape is very important since it influences dramatically the formability of the fabric in the matrix. The formability is a unique characteristic distinguishing fabrics from other sheet materials like paper, leather, plastic etc**.** Hence, fabric drape modelling is a complex mechanical problem involving large displacements under the influence of relatively low stresses.

1.4 Analytical modelling

The first mechanical modelling and analysis attempts of the textile structures started about a hundred years ago. The earliest publication is said to be from R. Haas in a German Journal at about 1917. However the pioneering work of Peirce (Peirce 1937) is considered as the starting reference for the analytical mechanical modelling of the textile structures. The researchers focused on the application of the existent analytical methods already used in other sectors of engineering. The main characteristic is the balance between the simplifications introduced and the precision of the modelling. The energy methods and the elastica theory are dominating in these attempts.

1.4.1 Micromechanical modelling of simple deformations

In the field of the analytical modelling of the textile yarns, several investigations focused on multi-filament twisted yarns. Purpose of these investigations was the prediction of the response of a twisted yarn when subjected to a certain deformation. It was supposed that the mechanical parameters such as the load-elongation curve of the constituent fibres, the twist density, the initial specific volume etc are given. The analysis focused on the correlation of the macroscopic distortion of the yarn with the microscopic response of the constituent fibres. A basic challenge in the modelling of the yarns is the balance between the realistic formulation and the idealization required for a theoretically treatable model. In the most cases the yarn was considered as being made of continuous filaments of circular cross-sections and constant linear density along their length. All the fibres were assumed to have identical properties and to be perfectly elastic. The cylindrical-helix model of Hearle *et al.* (Hearle, El-Behery & Thakur 1959), the conical-helix model of Önder and Başer (Önder, Bacer 1996) and the statistical model of Komori (Komori 2001) approached the yarn mechanical modelling from different points of view, depending on the considered alignment of the fibres. The tensile, bending and torsional behaviour of the yarns were approached using the force, the stress-analysis and the energy methods (Backer 1952, Platt, Klein & Hamburger 1959, Freeston, Schoppee 1975, Choi, Tandon 2006, Park, Oh 2006).

1.4.2 Mesomechanical modelling of simple deformations

Starting point for the analytical modelling of woven fabrics was the uniaxial/biaxial deformation of the plain woven structure. The proposed approaches were based on three principal underlying geometrical models of plain weave (Dastoor et al. 1994). The “flexible thread” model of Peirce (Peirce 1937) assumed the yarns infinitely flexible, incompressible and inextensible, without bending rigidity and having circular cross-sections. The analytical transcendental equations proposed by Peirce for the systematic description of his model cannot easily give a solution. Thus graphical and nomographic tools were presented in order to support the users. Peirce’s model has been modified later towards a better representation of the real fabric structure. Thus the assumptions of the race-track or elliptical yarn cross-

sections (Kemp 1958, Olofsson 1964b) were adopted for the fabric modelling. The concept of the elastica model (Peirce 1937), in continue, introduced the yarn bending rigidity in the analysis. According to this model the shape of yarn axis can be obtained by treating the yarns as elastic slender rods subjected to transverse point forces, equidistant but alternating in direction. In general, the mentioned models and their later modifications used the equilibrium, energy or elastica method for the mechanical analysis.

An approach including the effect of crimp and yarn extension, based on a flexible thread model was proposed by Freeston *et al*. (Freeston, Platt & Schoppee 1967). The yarns were assumed as homogenous, linear elastic materials with linear work-hardening. An elastica model declining from the assumption of the standard shape yarn cross-section was published by Olofsson (Olofsson 1964a). The shape of the cross-section of the yarns was considered as a function of the forces acting on them and the degree of set. The mathematical analysis was given on equilibrium conditions, on stress-strain relationships in extension and compression and on energy in bending. The effect of fabric set was included, also, in the work of Grosberg and Kedia (Grosberg, Kedia 1966, Grosberg 1966). They adopted an energy method on small deformation for the investigation of the initial load extension modulus of completely relaxed woven fabrics, while the yarns were assumed inextensible and incompressible. Another approach based on the elastica theory including linear extensibility of the yarns was given by Dastoor *et al*. (Dastoor et al. 1994). They assumed the yarns to be homogeneous, weightless slender rods, frictionless and undeformed by shear forces. In addition the yarns were considered as having circular section which does not deform under external forces. A computational implementation was adopted for the solution of the equilibrium equations. The large biaxial deformation of partially and completely set plain woven fabrics was presented by Huang (Huang 1979b, Huang 1979a). His approach was based on the elastica model of yarns in the undeformed fabric and the combined action of extension and bending was considered for the fabric deformation. The introduction of bilinear moment-curvature relation (due to the sliding of the fibres within the yarn) in combination to the contact deformation of the yarns increases the reliability of the study. The “sawtooth” geometrical model was proposed by Kawabata *et al*. (Kawabata, Niwa & Kawai 1973). The mechanical analysis was based on the force equilibrium and the displacement of the warp and weft yarns in the thickness direction of the fabrics at the contact point of the crossing threads. Although the geometrical representation of the unit cell was approximant, the deformation effect at the cross-over points was taken into account.

Due to their complex structure the mechanical analysis of the knitted fabrics is very challenging. Most of the existing works focused on the mechanical analysis of tensile deformation of the plain weft knitted fabrics. Even in this simplest case of the fabric microstructure the proposed modelling approaches vary significantly. The geometrical complexity of the knitted fabrics was the first obstacle for the researchers. The independence between the loop configuration i.e. the geometrical characteristics of the unit cell and the yarn properties in the fully relaxed state was a basic assumption for many approaches. The consideration of the ideal yarn in terms of shape and mechanical behaviour was also often

applied. The first attempts for the representation of the loop configuration were based on the combination of straight lines and circular arcs (Chamberlain 1926, Peirce 1947, Shinn 1955, Leaf, Glaskin 1955, Munden 1959). Some researchers (Postle, Munden 1967, Shanahan, Postle 1970) considered the loop configuration of the plain knit using the elastica theory. For example Postle and Munden (Postle, Munden 1967) in their approach assumed a symmetrical yarn structure that behaves as a uniform homogeneous elastic rod that is straight in its stress-free configuration. The mechanical analysis of the plain weft knitted fabrics focused initially on the tensile deformation of the unit cell assuming negligible yarn extension, yarn slippage at the interlocking points and frictional effects. The yarn compression was introduced in the analysis by Shanahan and Postle (Shanahan, Postle 1970). McRory's model (McRory, McCraith & McNamara 1975) included the effect of slippage between the loops. Hepworth's model (Hepworth 1978) focused on the effect of yarn jamming occurring in tight structures. The approach of Kawabata (Kawabata 1989a) was based on the superposition of straightening of the bent yarns and their elongation during the tensile deformation of the fabric. This approach also included the slippage and the deformation of the yarns at the link points.

1.4.3 Mesomechanical modelling of complex deformations

The concept of the complex deformations on a mesomechanical scale is extremely marginal. It is almost impossible to simulate on the scale of the unit cell the effects occurring during the drape of a fabric. The so called mesomechanical models for the complex deformation of the fabrics mainly refer to the bending behaviour of the fabrics. The first study in complex deformations of fabrics was conducted by Peirce (Peirce 1937). He proposed an energy method for the analysis of 2D fabric bending. The analysis was based on the calculation of the change of the strain energy of the unit cell after the bending deformation. For the analysis the yarns were assumed to be of circular cross-section and incompressible and distributed forces were considered at the cross-sections of the yarns. Many researchers (Behre 1961)(Dahlberg 1961)(Lindberg, Behre & Dahlberg 1961)(Abbott, Grossberg & Leaf 1971)(Abbott, Grosberg & Leaf 1973) studied and reported the nonlinear nature of bending and shear properties. The approach adopted by Grosberg (Grosberg 1966) incorporated the effects of friction into the strip 2D bending analysis. Many relative research actions were carried out in continue contributing to the understanding of drape to some extent. But the 2D drape assessment cannot fully reflect the more complex 3D double curvature deformations of drape (Lo, Hu & Li 2002).

Shanahan *et al*. (Shanahan, Lloyd & Hearle 1978) accented the necessity of the complete drape treatment based on the structural mechanics shell theory. They also defended the consideration of anisotropic constitutive laws for the fabric sheet. Amirbayat and Hearle (Amirbayat, Hearle 1989) used aspects of the shell theory in their theoretical investigation of the complex buckling. They correlated the drape shape with the bending, membrane and potential energies. From their investigation they concluded that drape is also influenced by

other parameters such us the full set of anisotropic in-plane membrane, out-of-plane bending, cross term elastic constants, and the nonlinearity of the materials behaviour.

1.4.4 Macromechanical modelling of complex deformations

Many publications appeared in the past dealing with the macromechanical modelling of the complex deformations of the fabrics. For many years this specific area has concentrated the interest of many very important researchers. The most representative of them are referenced below.

An approach of the elastica theory for the analysis of complex deformations of fibres and fibre assemblies has been proposed by Konopasek (Konopasek 1980a, Konopasek 1980b, Konopasek 1980c). It was based on the concept of planar and spatial elastica as developed respectively by Euler and Kirchhoff. Phenomena corresponding to the nonlinear behaviour of material, friction-elasticity, elastic-plasticity, and visco-elasticity were introduced in the analysis. The planar elastica theory was applied for the analysis of the large deflections of a yarn in a plane and the cylindrical bending of a fabric treated as sheet material. The spatial elastica was applied in the analysis of fibre buckling and crimp. The solution of the system of the resulted nonlinear differential equations was supported by computational tools.

An alternative approach to the theoretical mechanics of static drape of fabrics based on the differential geometry of surfaces was published by Lloyd *et al.* (Lloyd, Mete & Hussain 1996). They developed a computationally convenient implementation of the theoretical mechanics of fabrics. The fabrics themselves were treated as 2D continua represented by a surface without considerable thickness embedded in the 3D Euclidean space. The mechanical properties of the fabric were assigned to the model. The shape of the surface was described for both the deformed and the undeformed state by the means of the differential geometry of the surface. The strain values were deduced from the differences in the differential geometry expressions for the two extreme states. The strain values were correlated to the applied forces by the constitutive equations that express the mechanical properties of the material.

The differential geometry of surfaces for the dynamical modelling of fabric deformations was used for the approach of the problem by J. and R. Postle (Postle, Postle 1996). The surface was considered as a series of twisted curves generated into the 3D Euclidean space. The differential geometry parameters incorporated the mechanical properties of the material (fabric) relating these mechanical properties to the changes in curvature as the surface was transformed into another surface. The deformation of the surface from the initial state to the final was mathematically modelled using the concept of homotopy. Bäcklund transformations were chosen for the solution of the nonlinear partial differential equations of the dynamic system.

Trying to combine the theoretical study to the experimental knowledge, Stump and Fraser (Stump, Fraser 1996) analyzed the drape of a circular fabric sample over the circular disk of the drapemeter. They proposed an elastic ring-theory model of the draped fabric and used an

energy analysis associated with the various large post-buckled deformations of the ring. Aim of their investigation was the study of the ability of the fabrics to present different configurations when they are draped under exactly the same conditions. The explanation of this ability was based on the calculation of the energy that corresponds to the various symmetric configurations.

1.4.5 Evaluation of the analytical approaches

The review of the literature of the analytical methods for the mechanical analysis of textile structures demonstrates the absence of a successful globally accepted technique suitable for the textile design. The various research attempts indicate exactly that the modelling problem is extremely complex and no existing method can be directly successfully applied.

Regardless the different approaches proposed by the researchers, some basic assumptions were applied for the mesomechanical analysis of fabrics. These assumptions and specific goals are mainly the following: The use of one unit cell corresponding to the repeated geometrical unit is suitable for the analysis of simple loading states as tensile, shear and compression of the fabric. The assumption of the ideal yarn simplifies the mechanical analysis of fabrics. In parallel, the introduction of contact effects as the compression deformation and the sliding at the linking points of the yarns is essential for the approach of the realistic behaviour of the fabrics subjected to deformation. Equally significant is the consideration of the tensile deformation of a fabric as a superposition of straightening and elongation of the yarns.

Since more factors are taken into account, the complexity of the analytical expression increases dramatically, in such an extent that they can not easily be used. If the simplified forms are used, the error of the predicted values is considerable. Exactly these omissions of the existent analytical methods determine the targets for the future research. Firstly an accurate technique suitable for the representation of the complex textile microstructures is required. Thus the use of approximate empirical equations corresponding to specific ranges of fabrics reduces the desirable accuracy. The consideration of the elastic yarn is not realistic since the deformation of the yarns results in the appearance of residual strains corresponding to plasticity effects. The prediction of the complex deformation procedure of the fibres within the yarn and of the yarns within the fabric is essential target for the accuracy of the mechanical analysis. Special effects as the reduction of the yarn cross-section due to tensile stresses, the yarn flattening at the linking points, the contact phenomena as sticking and sliding areas and the appearance of friction are also significant for the prediction of the nonlinear response of the textile structures. A more realistic modelling results in a huge number of complex equations. Then higher computational power is required for the analytical approaches. In addition, in some cases the lack of analytical solutions imposes an excess number of assumptions and simplifications that allow mainly qualitative results.

In general, it seems that the analytical modelling cannot guarantee the integration to a global technique necessary for the achievement of a complete design method. Such a design

environment should be based on the collaboration of a number of secondary tools carrying out different subtasks. The secondary tools should correspond to specific procedures. A typical example is the geometrical design module for yarns, woven and knitted fabrics. Another secondary tool could undertake the mechanical analysis, which could also be divided into many modules corresponding to the loading and deformation modes (tensile, shear, compression or bending). The lack of the integrated design tool based on analytical modelling has inspired the research activities in the field of the numerical modelling.

1.5 Numerical modelling

The enormous computational power arose from the development of the computer systems and the expansion of advanced commercial software codes for the analysis of mechanical problems guiding the textile design towards the numerical approaches. Mainly the Finite Element (FEM) and Boundary Element Method (BEM) were used for the mechanical modelling of the textile structures (Hu, Teng 1996).

1.5.1 Micro- and mesomechanical modelling of simple deformations

The first attempts in the computer based mesomechanics of textiles dealt with the 2D and 3D representation of the plain woven structure. The geometry proposed by Peirce was the starting point for the solid geometrical modelling since the numerical techniques succeed the solution of the complex system of equations. Keefe *et al.* (Keefe, Edwards & Yang 1992) based on Peirce's geometry presented the solid model of the plain woven fabric. They also extended the model for various compactions and fabric angles. Later comparative studies examined the accuracy of the geometrical models for use in the numerical modelling of fabrics (Provatidis, Vassiliadis 2002)(Provatidis, Vassiliadis 2004)(Provatidis, Vassiliadis & Anastasiadou 2005).

The initial application was the support of the load – deformation simulation of a textile structure. The computers provided numerical solutions to complex analytical expressions. The computational power at the earlier time was enough for the fast solution of the large number of equations required for the analysis. The use of numerical methods, as FEM, BEM etc, for the achievement of a rigorous approach for the textile micro- and mesomechanical analysis appeared in a later stage. Obstacles for the successful use of numerical methods were mainly the large displacement effects and the nonlinearity related with the deformations of textiles and the convergence problems arose. Munro *et al.* (Munro et al. 1997a) proposed a new approach for the application of FEM to the aligned fibre assembly problem. Three dimensional 8-node elements with cuboid shape in the neutral configuration and 6 degrees of freedom (DOF) per node employed for the investigation. The approach attempted to separate the various energy contributions to the element stiffness, allowing the user to specify their properties individually. This technique was successful in the easy introduction of nonlinear material properties in the solid model. The approach of Munro et al. (Munro et al. 1997b) was verified qualitatively by modelling realistic yarn situations. The yarn models were meshed by

dividing them into layers where the layer interfaces were surfaces perpendicular to the yarn axis. Each layer was split into a number of finite elements ranging from 1 to 22. Initial configurations were arranged so that the fibres within the elements followed idealized helical-yarn geometry. A multi-layer yarn model consisting of 9 elements per layer was subjected to axial extension and axial compression. The model presented the expected, in terms of quality, deformation behaviour. Thus the necking of the yarn piece was caused by the helical winding of the fibres appeared during extension. Moreover the elements of the model were opened significantly during the axial compressing test since the fibres were buckled to avoid compression of the fibre material.

The advance and easy manipulation of CAD tools, the last few years, allowed the construction of 3D solid models of textile structures based on the profits of these tools, as numerical interpolations, mirroring abilities etc. An approach for a 3D representation of the plain knitted fabrics using the cubic-spline method has been presented by Demiroz and Dias (Demiroz, Dias 2000a, Demiroz, Dias 2000b). Parametric solid modelling software packages are currently available allowing the construction of complex woven structures. The complete design flexibility provides the selection of weave pattern, yarn size or spacing. The yarn representation is still based on the assumption of the homogenous material for the simplification of modelling and the computational time saving (Toney 2000). The advance moreover of the FEA codes allowed the mechanical simulation of the unit cells of the modelled textile structures. The mesomechanical modelling of textile structures was improved by the employment of advanced finite elements types and libraries of material properties including linear, nonlinear, elastic, plastic, viscoelastic, isotropic, orthotropic, anisotropic options etc. Additionally the introduction of contact algorithms and large strain effects was essential for the realistic results of the simulated tests.

Significant progress noticed in the modelling of complex structures of fabrics. Tarfaoui and Akesbi (Tarfaoui, Akesbi 2001) presented the model of the twill woven fabric and the mechanical simulation using the FEM. The unit cell is composed by three warp yarns that intersect with three weft yarns, presenting a different type of crimp. Goktepe and Harlock (Goktepe, Harlock 2002) developed a 3D software code for solid modelling and visual simulation of warp knitted structures using non-uniform rational B-spline (NURBS) surfaces. Innovative was the work of Araújo *et al.* (de Araújo, Fangueiro & Hong 2004) for the modelling of plain weft knitted fabrics. Using a Mechanical Event Simulation method the final geometry of the plain weft knitted structure was produced. This approach was based on the interaction of a loop with the adjacent loops predicted by a finite element nonlinear simulation involving large displacements and contact without friction between yarns.

The research in the field of woven fabrics composites demonstrates intensive and continuous progress in computational mesomechanical analysis. The more advanced approaches were based on the prediction of the homogenized elastic properties of fabric composites using the unit cell of the composite structure. The geometrical representation of the model generated using certain assumptions for the geometry of tows in the knitted or woven form and the geometrical characteristics of the produced fabrics. The used tows (usually made of glass or

carbon fibres) were assumed as transverse isotropic material and the matrix (usually resin) as isotropic material. The homogenized elastic properties of the unit cell resulted from the micromechanical analysis using FEM. A relative approach proposed by Ng *et al.* (Ng, Tse & Lau 1998) for the prediction of the elastic properties of 2/2 twill weave fabric composites. The used model corresponds to the entire unit cell of the fabric structure. The 3D solid model for both the warp and weft yarn volumes were developed, while the matrix pocket was created by subtracting the yarn volumes from a rectangular block, the unit cell of the composite material. The contact areas generated during the subtracting operation are assigned to be shared entities for both the fibre and the matrix volumes, to ensure the transmission of loading. Choi and Tamma (Choi, Tamma 2001) dealt with the prediction of the elastic properties of a plain woven fabric composite. The predicted elastic properties were used in continue for the mesomechanical damage analysis of woven fabric composites.

Innovative research in the field of fabric composites was conducted in the K.U. Leuven, initially focusing on the generalized description of the internal structure of the textile reinforcement. Lomov developed a model for the internal geometry of 2D- and 3D-weaves based on a minimum number of topological data and yarn mechanical properties. The mechanical model applies a yarn deformation energy minimization algorithm to predict the internal geometry of any 2D- and 3D-weave. This approach was systematically extended to 2D- and 3D-woven, two- and three-axial braided, weft knitted and non-crimp warp-knit stitched fabrics and laminates (Verpoest, Lomov 2005, Lomov et al. 2000, Lomov et al. 2001).

1.5.2 Macromechanical modelling of complex deformations

The macromechanical modelling of fabrics or cloth modelling, as usually referred, attracted the interest of the textile community in the last decades. Many investigators attempted to approach computationally the macromechanical performance of fabrics for several purposes from the prediction of the drape behaviour of the fabric up to the virtual mode show (Gray 1998). Depending on the purpose served and the application field different techniques were developed. The basic classification of the developed techniques is divided into computer animation models (graphic models) and the engineering design models. Many numerical techniques including the particle-based model, the deformable node-bar model and the FEM were developed for the engineering design of fabrics. Most of the efforts were focused on the prediction of the drapeability of fabrics.

The used FEM for the drape simulation were based on a variety of element types from simple rods to complex shell elements. Collier (Collier et al. 1991) studied the drape behaviour of fabrics using a nonlinear FEM based on the classical nonlinear plate theory. The fabric was assumed to be two dimensional. It was considered as a linear elastic material with orthotropic anisotropy, where the symmetry lines are aligned in the warp and weft directions. Many corrective actions were assigned the following years by the researchers in the classical finite element techniques in order the realistic performance of fabrics to be approached.

The FEM and flexible thin shell theory was employed by Chen and Govindaraj (Chen, Govindaraj 1995) to simulate the fabric drape. Their approach provides nonlinear solution since large displacements appear during drape test. Thus the loads are applied incrementally to the system, and at each step, the equilibrium equation system is solved by a Newton-Raphson method. The nonlinearity was handled by calculating the stiffness matrix in each step as a function of the displacement vector. The fabric was considered continuous orthotropic material. A 9-node, doubly curved shell element with 5 DOF per node was used for the simulation.

The simulation of the 3D drape test based on the FEM was also approached by Kang and Yu (Kang, Yu 1995). The woven fabric was assumed to be an elastic material with orthotropic anisotropy. The fabric was considered as a thin flexible plate under the plane stress condition, and the transverse shear strain was included in the formulation. Since large displacements and large rotations are developed during draping, the drape phenomenon was considered as geometrically nonlinear and respectively the nonlinear analysis was adopted for the simulation. The Green-Lagrangian strains and the second Piolar-Kirchhoff stresses were used for the analysis. The formulation of the FEM was based on a total Lagrangian approach. 4-node quadrilateral elements were used with 5 DOF in each node. In order to avoid the shear locking phenomenon which is commonly observed in the thin plane analysis, a transverse shear strain interpolation method was applied. Almost the same approach was proposed by Gan *et al.* (Gan, Ly & Steven 1995). In their analysis 8-node shell elements were used with 5 DOF per node. The adopted technique in this approach for the elimination of locking was a reduced integration with zero energy mode control.

For the minimization of the computational power required for the simulation of fabric drape, a FEM using simple beam elements with 6 DOF per node was proposed by Ascough *et al.* (Ascough, Bez & Bricis 1996). The used beam elements include mass and stiffness properties and can represent iso- or orthotropic cloth properties. The large displacement effects were achieved with the addition of a geometric or initial stress matrix to the elastic stiffness matrix to form the element characteristic matrix. Newmark's method was used to allow a time-stepping approach to the solution, with the advantage that the mesh geometry can be updated at each step. The proposed analysis includes also interaction of the cloth with the body form. Checks for a collision detection of material elements with the body model are made following each time step of the drape simulation. An iterative calculation process is executed until contact rather than penetration of cloth element with the body model occurs.

Araújo *et al.* (de Araújo, Fangueiro & Hong 2004) proposed a finite element approach for the modelling of the plain weft knitted fabrics using truss elements. According to this approach the simple loop structure was simplified and represented by a 2D hexagonal structure constructed by nonlinear truss elements. In order to perform the simulation, the geometrical parameters and tensile properties of the knitted fabric must be converted to the truss elements parameters.

An approach for the drape simulation of woven fabrics quite different from the traditional macromechanical methods was proposed by Breen *et al.* (Breen, House & Wozny 1994). The cloth was modelled as a collection of particles that conceptually represent the crossing points of warp and wefts threads in a plain weave. Important mechanical interactions that determine the behaviour of woven fabric are discretized and lumped at these crossing points. The various yarn-level structural constraints are represented with energy functions that capture simple geometric relationships between the particles. These energy functions account for the four basic mechanical interactions of yarn collision, yarn stretching, out of plane bending, and trellising. The simulation was implemented as a three-phase process operating over a series of discrete time steps. The first phase for a single time step calculates the dynamics of each particle and accounts the collisions between particles and surrounding geometry. The second phase performs an energy minimization to enforce inter-particle constraints. The third phase corrects the velocity of each particle to account for particle motion during the second phase.

Stylios *et al.* (Stylios, Wan & Powell 1995)(Stylios, Wan & Powell 1996) proposed a node-bar model for the drape modelling of fabrics. The deformable elements were defined as consisting of one deformable node with a number of rigid bars. Thus the patch of cloth is divided into a grid (the patch is divided as a series of elements, which can be of equal or unequal sizes). The material properties of the continuum in all elements are lumped together at these deformable nodes by integrating all the energies within those elements. The total energy density was considered as the sum of strain, kinetic energy density, and the energy density introduced by external and boundary forces. Viscoelastic terms were added in the energy equation. The cloth motion in continue was determined using the Euler-Lagrange equations.

The finite volume method employed by Hu *et al.* (Hu, Chen & Teng 2000) for the drape modelling of fabrics. The mesh lines were aligned along the warp and weft direction producing rectangular internal volumes and triangular or quadrilateral boundary volumes in a circular fabric sheet. The equilibrium equations of the fabric sheet derived using the principle of stationary total potential energy. Geometric nonlinearity and linear elastic orthotropic material properties of the fabric were considered in the formulation. The full Newton-Raphson iteration method with line searches was adopted for the solution of the resulting nonlinear algebraic equations.

1.5.3 Evaluation of the numerical methods

The adoption of computational techniques in textile mechanics is essential to face and overcome the objective difficulties, as the geometrical representation, the complex deformations, the particular material properties, the contact phenomena and the large deflection effects. Moreover, the advanced computer based tools are suitable for the virtual representation of a product performance under loading. That is a significant facility for the textile designers since a realistic sense from the mechanical up to the aesthetic attributes can be provided.

Most of the mesomechanical modeling approaches implemented the finite element method using solid FE. The yarns were assumed as homogenous material with transverse isotropic elastic properties. The attribution of the yarn properties constitutes basic factor for the accuracy of the mesomechanical modelling stage. Thus the equivalent performance of the homogenous yarn, considering the discrete structure, in the tensile and bending deformation is required at least for the reliable attribution of yarn models. It is remarkable that most of the proposed models omitted the calculation of the real value of the yarn bending rigidity and its attribution at the modelled yarn.

The macromechanical modelling approaches are grouped in two basic categories. The first corresponds to the investigations based on the experimental measurement of the mechanical properties of fabrics and the generation of equivalent models describing their bending performance and drapeability (de Araújo, Fangueiro & Hong 2004, Collier et al. 1991, Ascough, Bez & Bricis 1996, Stylios, Wan & Powell 1995, Hu, Chen & Teng 2000). The second category focused on the computational analysis of fabrics in the mesoscopic level and the generation of models presenting equivalent in-plane elastic properties (Ng, Tse & Lau 1998, Choi, Tamma 2001, Lomov et al. 2007).

The basic drawback encountered in the existing modelling approaches concerns the collaboration of the different modelling stages (micro, meso, macro) for the development of an integrated design procedure of the textile structures. Thus the modelling of the structure in the mesoscopic level should incorporate the micromechanical performance of the yarns. Whereas the modelling of the structure in the macroscopic level should incorporate the mesoscopic performance of the unit cells and therefore the microscopic performance of the yarns. Consequently the collaboration of the discrete modelling stages is attainable generating realistic models and attributing the equivalent properties.

1.6 Experimental methods

The success and the efficiency of the theoretical work in the fields of analytical and numerical modelling must be evaluated by experimental data. The analytical models after certain calculations give the deformed state prediction of the fabric. In the case of the numerical models an existing fabric is represented structurally in the computer and it is analyzed from the mechanical point of view for the prediction of its behaviour. The fabric samples are subjected to laboratory tests for the measurement of their actual mechanical behaviour. The predicted data from either the analytical or the numerical modelling are compared to the actual ones taken from the laboratory tests. If the performance of the modelling is not the desired, a reengineering circle starts and a new more accurate model is expected for the better representation of the real fabrics. Thus the experimental part of the measurement of the mechanical properties of the fabrics is absolutely essential for the accurate modelling. The main interest of the mechanical analysis is focused on the area of the low stress testing. The low stress deformation mode corresponds to the nonlinear part of the stress-strain curve of the materials. This fact imposes a further complexity of the analysis of the mechanical behaviour

of the fabrics. The laboratory methods for the measurement of the low stress mechanical behaviour of the fabrics require special equipments with the respective sensitivity, accuracy and precision since the standard instruments can not reach easily the range of the measurements required. The special laboratory equipment for the low stress measurements supports also the textile character of the specimens in terms of dimensions, clamps, pretension requirements etc. In the following paragraphs the mostly used laboratory systems are presented.

1.6.1 Systems for the measurement of the mechanical properties

Innovative was the work of Hand Evaluation and Standardization Committee (HESK) established in 1972 by Kawabata in Japan. Main objective of Kawabata was the standardization of the hand evaluation methods and the development of an objective evaluation system (Kawabata, Niwa & Yamashita 2002). The first step supported the development of a method that provides numerical expression of the Total Hand Value (THV). Total Hand Value is a function of the Primary Hand Values which in turn are assessed subjectively and it is based on the comparison of the sample to a palette of standard samples. The hand of the fabric is considered as the superposition of the partial mechanical properties. So the hand can be viewed as the human perception of the response of a fabric subjected to a complex deformation. The second step was the development of the homonymous Kawabata Evaluation System for Fabrics (KES-F) for the objective evaluation of fabric hand based on the measurements of a defined range of mechanical and surface properties of the fabrics. KES-F has supported the passing from the empirical to the engineering textile design. Conceptually Kawabata has contributed to the overcoming of the main difficulty of the textile design: the correlation of a sensual term, the hand, with measurable objective values, the vector of the sixteen mechanical, surface and structural parameters. These parameters result from the low deformation tensile, shear, compression, bending test of the sample, the surface properties and the fabric thickness and weight, hence refer to the objective measurements. The experimental data resulting from KES-F were correlated in a following work with the fabric tailorability and the Total Appearance Value (TAV) used for the estimation of the suit appearance (Kawabata et al. 1990)(Kawabata, Niwa 1998)(Shishoo 1990)((Ganssauge, Lehmann & Augenadel 1998)(PavlinicÂ, GerÅ¡ak 2003). Today Kawabata Evaluation System for Fabrics is a reference system with a significant acceptance in the research communities. The majority of the textile numerical modelling attempts are evaluated with reference to the KES-F results.

The Fabric Assurance by Simple Testing (FAST) is a system developed by CSIRO in Australia. It serves also the measurement of the mechanical properties of the fabrics with the aim to be used for the fabric objective measurement technology and the prediction of final appearance (Minazio 1995). The innovation introduced is the addition of a new property named Pressing Performance (PP). Fabric PP can be estimated by forming a crease in a sample of fabric and measuring the recovery of the crease angle under a standard atmosphere.

Compared to KES-F is simpler in use, although it is usually considered as less precise. In any case it is a considerable alternative to the expensive installation of KES-F. The correlation of the results of the KES-F and the FAST has been the subject of thorough studies (Haiqing, Yanling 2000)(Yick et al. 1996)(Barndt et al. 1990). The main aim is the establishment of conversion methods between the results of the two systems so that the measurement could be independent of the specific system in use. The correlation proposed is not easy, safe and globally applicable.

Just for the sake of completeness we refer the research project initiated by Kawabata on the measurement of the mechanical properties of fibres, as an important step towards the engineering textile design (Kawabata, Niwa & Yamashita 2002). The practical difficulties resulting from the micro-scale of the fibre size increase the significance of this attempt. Kawabata stressed the need of knowledge of the full data of the anisotropy in mechanical properties of the fibre for the textile design. He has proposed the single-fibre measurement technique called “micro-measurement” based on a system suitable for the measurement of the mechanical properties which describe the fibre anisotropy. However the dedicated equipment for the high accuracy measurements of the mechanical properties of the fibres is not yet available in an integrated system.

Recently a new system for the objective measurement of the low-stress mechanical properties of the fabrics was presented, although it is not yet available in the market. The system was designed with the aim of the simplification of the handling of the specimens during the measurements procedure. It presents significant advantages comparing to the KES-F operation that is time consuming and requires specialized and skilled personnel. FAMOUS, the acronym of the full name “Fabric Automatic Measurement and Optimisation Universal System” promises extremely simplified handling of the specimens and fast execution of the tests. The main difference between the KES-F and FAMOUS is the measurement of the bending rigidity, which is performed in the second one via the buckling test. The other measurements are similar to those of the KES-F and thus directly comparable (Stylios 2003, Stylios 2005).

1.6.2 Measurements of complex mechanical properties

Several laboratory instruments were invented for the quantitative assessment of fabric drape. The study of the objective evaluation of fabric drape was started with Peirce (Peirce 1930). He used the fabric bending properties resulting from the cantilever test in order to assess the 2D drape. This test can be performed on the commercially available Shirley stiffness tester. A rectangular strip of fabric is allowed to bend under its own weight to a fixed angle when projected as a cantilever. The flexural rigidity and the bending modulus are calculated from the bending length. More cantilever and loop methods were proposed the following years for the measurement of the bending properties of the fabrics (Cassidy et al. 1991).

The 3D drape assessment was supported later by the development of the drapemeters of Fabric Research Laboratories (F.R.L) (Chu, Cummings & Teixeira 1950) and Cusick (Cusick

1968). A circular fabric sample (of standard diameter) is placed on the circular disk (of standard diameter) of the drapemeter. The unsupported area of the fabric produces the drape configuration. The measurement of the area corresponding to the transverse projection of the drape configuration on the horizontal plane is used for the calculation of the drape coefficient. An advanced tester was developed by Stylios *et al* for the study of the dynamic drape of the fabrics (Stylios, Zhu 1997).

Many researchers (Morooka, Niwa 1976)(Gaucher, King & Johnston 1983) (Niwa, Seto 1986)(Collier et al. 1991)(Okur, Cihan 2002) carried out investigations for the prediction of fabric drapeability from the respective mechanical properties. These investigations were based on the correlation of the drape coefficient with the mechanical properties resulted from KES-F or FAST.

1.7 Towards a computer-aided integrated design procedure

In the previous paragraphs an extended review was conducted over the textile mechanical modelling area. It is obvious that despite the about 70 years of actual research it's not possible to conclude in an Integrated Computer Aided Engineering Environment. The absence of a global tool was remarked, that aggravates the textile design procedure in terms of time and cost.

The production hierarchy of the textile structures (fibre – yarn – fabric) is correlated with the high level of complexity presented in the modelling procedure and the mechanical analysis of them. The difficulties are increased due to the high divergence of the dimensions corresponding to the fabric sheet (10^{-1} to 10^{0} m) and the structural elements (fibre diameter, 10^{-5} m). The modelling difficulties resulted from the structural hierarchy of textiles are faced adopting a relative modelling hierarchy. Thus three basic modelling scales were developed: the micromechanical modelling of yarns, the mesomechanical modelling of the fabric unit cell and the macromechanical modelling of the fabric sheet, that are described in the next chapters **(Vassiliadis, S., Kallivretaki, A. & Provatidis, C. 2006c)**.

The micromechanical modelling focuses on the study of the yarn structure in the micro-scale (fibre level) that constitutes the structural element for the production of textile products. The physical and the geometrical properties of the filaments and the ideal yarn geometrical structure are considered for the mechanical modelling of the multifilament twisted yarn. The current stage of modelling aims at the calculation of the apparent yarn properties, mainly the elastic modulus and the bending rigidity.

The mesomechanical modelling stage focuses on the apparent mechanical properties of the fabric unit cell. In the current stage of modelling the representation of the filaments constituting the yarns is omitted for the reduction of the computational cost and the yarns are represented as homogenous structures (their apparent properties were calculated in the above stage). Thus the attribution of the yarn properties constitutes the basic factor for the modelling reliability due to the homogenization of the yarns. Moreover the yarns interactions in the

fabric structure are determinant for the structural stability of the fabrics subjected to deformations. Aim of the mesomechanical modelling stage is the calculation of the performance of the unit cell in the tensile, shear and bending deformation.

The macromechanical analysis refers to the mechanical performance of the fabric sheet in complex deformations. The reduction of the computational cost demands the omitting of the representation of the structural unit cells. Thus the discrete structure of the fabric is replaced by a continuum model. It is obvious that the evaluation of the apparent properties of the discrete model and the generation of an equivalent continuum model (homogenization) is essential for the reliability of the macromechanical analysis.

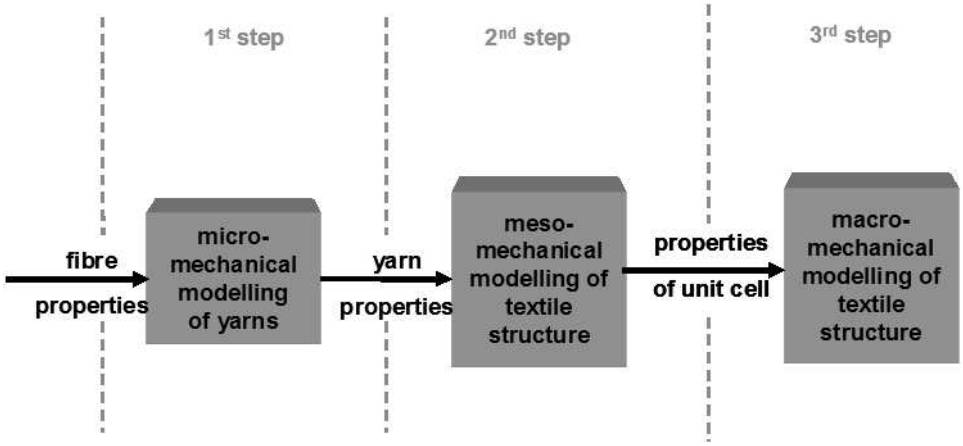

Figure 1-19: Schematic representation of the complete computational mechanical modelling of a textile structure.

This three-scale modelling seems logically complete, structurally robust and it could be successful. The design is supported using as input parameters the mechanical properties of the raw material (fibres) and the structural details of the final product (fabric). The major drawback of the existent modelling approaches is presented in the progressive transition of the modelling stages, i.e. the introduction of the yarn properties in the mesomechanical model and the introduction of the unit cell properties in the macromechanical model. The proposed textile design procedure is attempted in the current thesis implementing the FEM. The implementation of the FEM in each modelling stage raises certain difficulties, hence the FE algorithm and the considered assumptions are thoroughly selected and evaluated.

1.8 Conclusions

Despite the wide spread of the computer based design in the most of the engineering sectors and the unprecedented development of the textile machinery technology, the textile engineering maintained the traditional methods of design until the recent years. The technological advantages from the increased power provided by the computers hardware and

the advanced numerical techniques developed for the engineering design changed progressively the dominant textile culture. Massive efforts focus on the implementation of numerical methods in the textile design procedure.

The first attempts used the numerical methods for the solution of the analytical expressions proposed for the mechanical analysis of textiles based on significant simplification assumptions. The researchers, in continue, developed special algorithms based on FEM adequate to describe the nonlinear performance of textile structures when implemented in continuum bodies (yarn or fabric). Thus a qualitatively satisfactory approach was resulted. Nowadays a plethora of computational approaches, regarding the problem designing, the mechanical analysis method, the modelling scale and the considered assumptions, are proposed for the mechanical analysis of textiles. However the absence of an Integrated Computer Aided Engineering tool is insufficiency of the textile sector. The current study proposes a three-scale modelling approach for the integrated mechanical design of textile structures.

Chapter 2
The Micromechanical Modelling of Yarns

Abstract

The current chapter focuses on the stage of the micromechanical modelling. The typical yarn structure was studied in the micro-scale (fibre level) that constitutes the structural element for the production of textile products. The physical and the geometrical properties of the filaments and the ideal yarn geometrical structure were considered for the mechanical modelling of the multifilament twisted yarn. The FEM applying the beam theory enhanced with advanced solution algorithms supporting large deformation effects was implemented for the mechanical analysis. The proposed method offers a fast and flexible design in terms of modelling, meshing and analysis. Thus the difficulties resulted from the high structural complexity of yarn models (e.g. 100 filaments) are faced. The current stage of modelling aims at the calculation of the apparent yarn properties, mainly the elastic modulus and the bending rigidity. The respective deformations were simulated. Besides the comparison to an existing analytical model, a set of 2- to 1200-filament twisted yarns were produced in the laboratory and tested in tensile and bending, for the evaluation of the proposed approach. The comparison of the computational and the experimental data assured the reliability of the modelling approach. The effect of the major structural parameters as the filament radius and the yarn twist in the elastic properties and the bending rigidity was also examined.

2.1 Introduction

The mechanical properties of the yarns have a great effect on the mechanical performance and the processing characteristics of the produced fabrics such as the physical and aesthetic properties, the formability, drapeability and tailorability. The elastic stiffness and the bending rigidity constitute the basic mechanical properties of the yarns considering the usual deformations of the textile structures. Both properties are defined by the elastic and the geometrical properties of the fibres and their geometrical arrangement within the yarn structure. The complex architecture of the twisted yarns, related with the complex deformations of a large amount of fibres is the main obstacle for the mechanical analysis.

Several theoretical models were developed for the prediction of the tensile and bending properties of the twisted yarns. The idealized model of the yarn, proposed by Gegauff (Gegauff 1907), offered the standard groundwork for the later researches. The idealized model assumes a circular yarn cross-section and helical path of the filaments forming concentric cylinders around the yarn axis in the undeformed state. Therefore the elementary

study of a single helix in typical deformations is essential for the mechanical analysis of the twisted yarn.

The interactions of the filaments during the yarn deformation were studied in some researches (Batra 1973, Batra, Tayebi & Backer 1973). However most of the developed force and energy methods were based on simplifying mechanical assumptions for the reduction of the complexity of the problem. The negligence of the interactions between filaments, precluding lateral forces, friction and filament flattening, became a common consideration. Nevertheless the force methods (Park, Oh 2006, Platt 1950) induce significant computational cost and additional simplifications are required for the solution (approximated solutions). Moreover the nonlinear elastic properties are usually omitted for the reduction of the complication of the constitutive equations. Regarding to the analysis type, the linear small-strain is mainly selected, since the nonlinear large-strain analysis demands an iterative solution process with increased computational complexity. The energy methods (Freeston, Schoppee 1975, Choi, Tandon 2006, Liu, Choi & Li 2007) reduce the complexity of the analysis since the energy is a scalar quantity. The shortest-path hypothesis and the individual fibre contribution principle are applied. The success of the energy methods is strongly affected by the geometrical representation of the fibres in the deformed yarn. A rotating vector principle supports the natural generation of the fibre path in a curved yarn (Backer 1952).

The single helix mechanics (Göktepe, Lawrence & Leaf 2000, Leaf 1979a, Leaf 1979b) gave the basis for the analysis of the twisted yarns. Leaf studied the modifications in the cross-section of a single helix subjected to large-scale bending deformation. It was concluded that the initial circular cross section became elliptical. Despite the fundamental impact of the analytical approaches in the generation of the geometrical models of yarns and the conception of the deformation mechanism, the raised limitations disable the development of a rigorous integrated analytical method for the mechanical analysis of fibrous assemblies.

The first attempts for the implementation of computational methods for the mechanical analysis of yarns were presented in the 80’s. However those approaches adopted the FEM for the numerical solution of the analytical equations systems developed for the yarn mechanics. The substantial implementation of the FEM in yarn mechanics resulted some years later. Munro et al in 1997 (Munro et al. 1997a, Munro et al. 1997b) developed a three-dimensional Finite Element for the aligned fibre assemblies. The elastic stiffness matrix was defined by two linear elastic stiffness matrices, corresponding to the two stages of the yarn extension. Thereby they attempted to overcome certain difficulties, such as the definition of complex material properties and the presentation of small and large scales of deformations.

Nowadays the FEM prospects are promising for the development of an integrated approach for the mechanical analysis of fibrous assemblies based directly on the definition of the realistic properties of fibres and the structural characteristics of the assembly. The useful features of the FEM commercial software codes including powerful design tools and advanced solution algorithms offer great advantages in yarn modelling. Cartraud (Cartraud, Messager 2006) developed a realistic model for the analysis of 1+6 fibrous structures in

tensile deformations. The solid FE were selected for the analysis of the model and a relatively coarse mesh was generated (12 FE per wire section) probably for lower computational cost. The modelling of the pitch (one full turn of the filaments) leads to a total of 7056 FE and 52049 degrees of freedom (DOF). Thus the current approach would incur a huge computational cost, approximately 100000 FE and 744000 DOF, for the modelling of a 100-filament twisted yarn.

An integrated thorough method for the mechanical analysis of fibrous assemblies should fulfil certain requirements. Firstly the rapid generation of the yarn model based on the structural characteristics of the yarn and the constituting filaments (filament diameter, number of filaments per yarn cross-section, yarn twist density) is determinant for the handiness of the method. The realistic definition of the fibres' properties as nonlinear elasticity, even visco-elasticity is demanded for the realistic approach of the yarn performance. The analysis of the large scale displacements and strains presented in the fibres during the yarn deformations presupposes advanced iterative solution algorithms for the reliable and fast solution procedure. A flexible design procedure for the modelling of complex fibrous assemblies consisting of numerous fibres varying in the arrangement, the material properties and the structural characteristics is also useful. Furthermore the numerical analysis of fibrous assemblies should be able to implement interdisciplinary analysis of yarns recording the mechanical, electrical and thermal performance.

The proposed approach constitutes a fast model generation and mechanical analysis of fibrous assemblies in tensile and bending deformation implementing the FEM using beam elements. The evaluation of the method is based on the comparison with an existing analytical method and the implementation in a set of twisted yarns. In parallel to the experimental data, the analytical approach of Park and Oh (Park, Oh 2006) was selected for the evaluation as a recent and thorough reference presenting flexibility in application.

2.2 The proposed FEM for the mechanical modelling of multifilament twisted yarns

The geometry of the yarn used in the current approach (**Kallivretaki, Vassiliadis & Provatidis 2008**) meets the basic assumptions of the ideal structure. Circular cross-sections are considered for the undeformed yarn and the constituent fibres. Each fibre follows a uniform helical path retaining constant distance from the yarn axis. The distance between the adjacent fibres is nullified forming a close packing arrangement. The geometry of a filament within the yarn structure and the related structural parameters are given in Figure 2-1. The cross-section of a multifilament twisted yarn is presented in Figure 2-2.

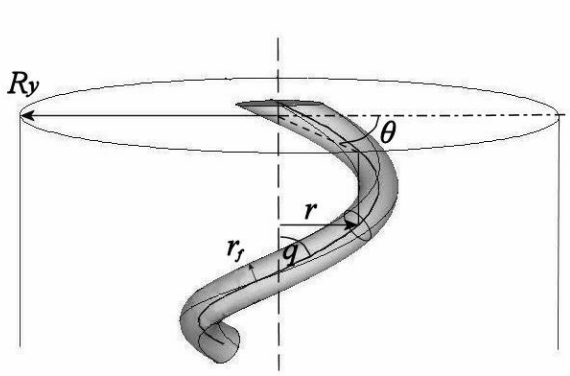

Figure 2-1: The configuration of a filament within the yarn.

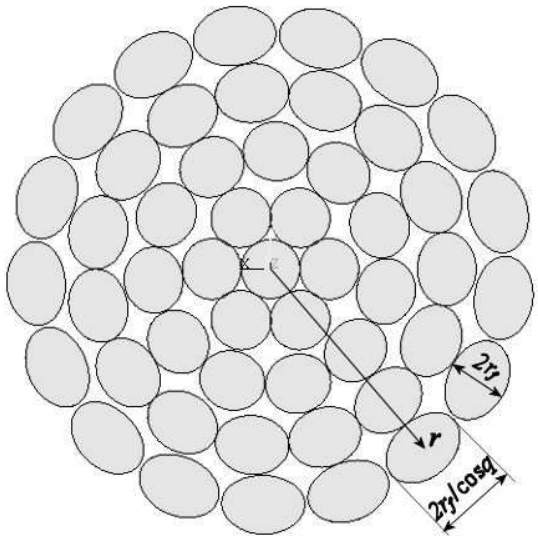

Figure 2-2: Cross-section of a multifilament twisted yarn

The structural parameters are the following:

r_f : fibre radius

t : turns per yarn unit length

sp : the length of one pitch

r : distance between fibre axis and yarn axis

R_y : yarn radius

q : helix angle with distance r

θ : rotational angle

nul : number of the layers of filament around the central filament

N : number of filaments

The basic geometrical equations describing the ideal yarn structure are the following:

$$sp=1/t \quad \text{(Eq. 2-1)}$$

$$q=\text{atan}(2\pi \cdot r \cdot t) \quad \text{(Eq. 2-2)}$$

$$R_y=r_f \cdot (2nul+1) \quad \text{(Eq. 2-3)}$$

$$LF(\text{i})= \text{LINT}(2\pi \cdot \text{i} \cdot \cos q) \quad \text{(Eq. 2-4)}$$

where LF(i) is the number of filaments constituting the i layer (i=0,1,..,nul) and the function LINT approximates to the lower integer number.

The mechanical characteristics are the following:

E : elastic modulus of a straight filament

G : shear modulus of a straight filament

E_{eff} : effective tensile modulus of yarn

B_y: bending rigidity of yarn

The FEM using beam elements was implemented for the mechanical analysis of the multifilament twisted yarns (see also Appendix II: Yarn Modelling Using Solid FE). The beam model is considered adequate to describe the yarn deformations given that the elongation and bending of filaments are dominant. Moreover the modelling with beam elements presents explicit advantages. Regarding the modelling and meshing phase, it is an extremely fast method since only the central lines of the filaments are required to be defined. The definition of the moment of inertia of the cross-section of the beam as an input parameter is beneficial for the analysis of specific cross-sections (irregular, open, hollow etc). In terms of analysis procedure, the beam models demand a relatively low computational power since a low number of beam elements is required, reducing the total DOF of the model. For example 3200 FE, 3300 nodes and 19800 DOF (maximum value) are required for the mechanical analysis of a 100-filament yarn model. The geometrical models for 2, 4, 8, 12, 50 and 1200 filaments are presented in the Figure 2-3. Nonlinear elasticity was considered for the model material according to the stress – strain curve of the fibre.

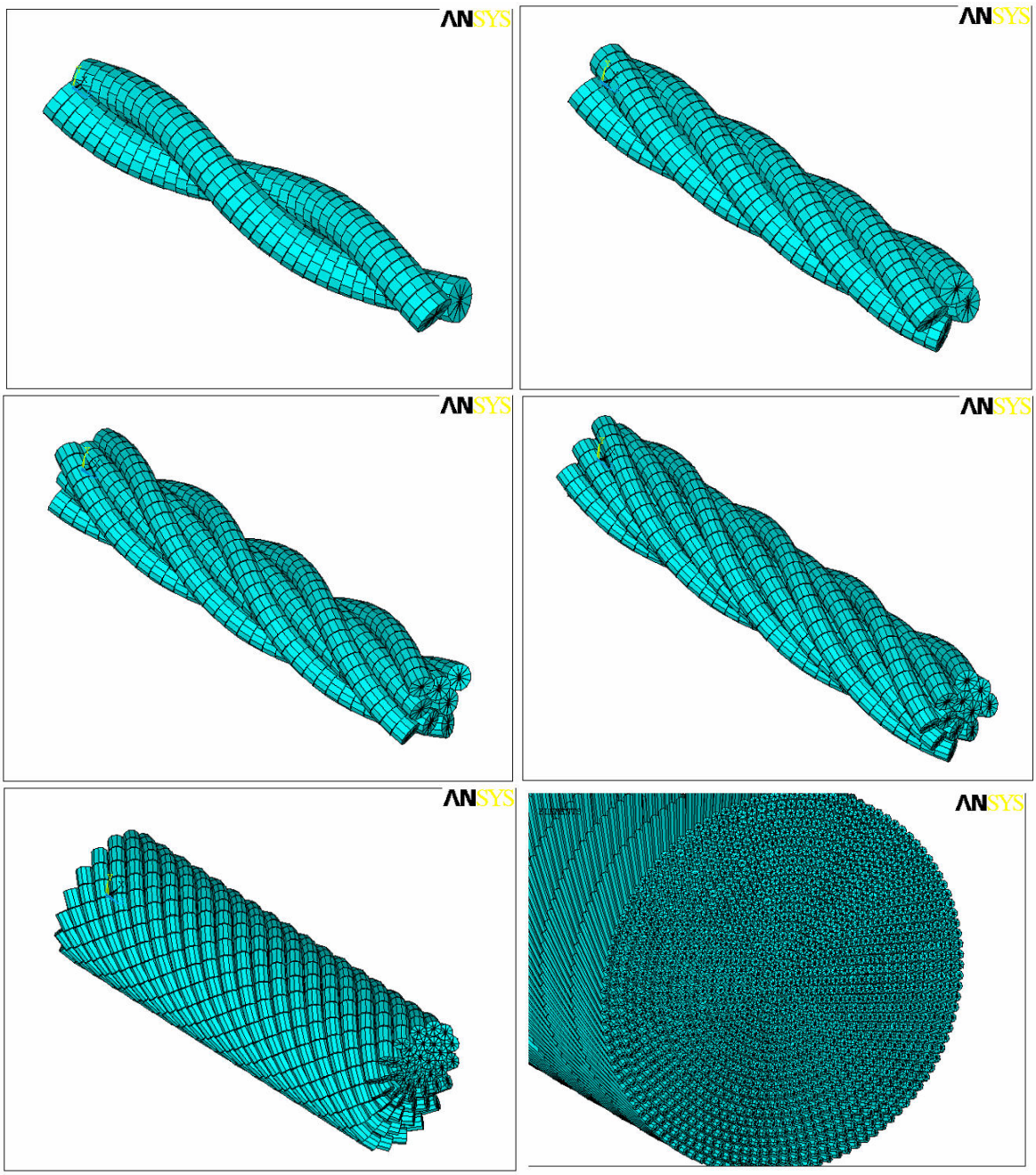

Figure 2-3: Generated models for a yarn of 2, 4, 8, 12, 50 and 1200 filaments.

The yarn models constituted from 50 and 1200 filaments were generated according to the configuration given in the Figure 2-2. In this approach the filaments are wrapped around the central straight filament and the helix radius of the i layer is given by:

$$r(i)=r(i-1)+2r_f \qquad \text{(Eq. 2-5)}$$

The current approach is not applicable for the yarn models consisting of 2, 4, 8 and 12 filaments. Thus the helix radius is $r= r_f$ for the case of 2-filament yarn, while for the cases of 4, 8 and 12 filaments consisting of 1, 2 and 3 layers the radii are:

$$r(1)= r_f/\cos(\pi/4) \qquad \text{(Eq. 2-6)}$$

$$r(2)= r_f(1+\sqrt{3}) \quad \text{(Eq. 2-7)}$$

$$r(3)= r(1)+r_f \quad \text{(Eq. 2-8)}$$

An extremely fast method was developed for the generation of the yarn models even for hundred of filaments. The modelling is based on the generation of the central axes of the filaments. The central straight filament is generated first. The helical path of one filament of the first layer is then generated in polar coordinate system. The helix is copied in radial direction with angular distance $2\pi/ LF(i)$. Similarly the outer layer is generated in continue.

For the simulation of the tensile test the one end of the modelled yarn was considered clamped. On the other end uniform displacement was imposed along the yarn axis. The reaction developed in the clamped edge was calculated for the definition of the load – displacement or the stress – strain curve of the yarn. The nodes of the total model were restricted with zero radial displacement (see also Appendix III: Contact Analysis vs CE in Beam Modelling of Yarns). This constraint precludes the reduction of the helix radius and the appearance of penetration between the filaments. Given that the tensile of a single helix corresponds basically to the reduction of the helix radius, the proposed constraint is essential for the simulation. Thus a realistic deformed shape is derived.

For the simulation of the bending test the one end of the model was considered clamped. On the other edge, a vertical displacement (to the yarn axis) was imposed. The reaction developed in the clamped edge deriving from the simulation was considered for the definition of the bending rigidity of yarn. The penetration effects presented in the bending test are narrow thus there isn't requirement for additional constraints.

The modelling and the mechanical analysis of the yarn structures were performed using the ANSYS commercial software code. A full Newton-Raphson solution algorithm was implemented to support large-scale deformations. The advantage of the current algorithm is the update of the stiffness matrix in every computational iteration. Two options were activated in order to control the number of iterations and to accelerate the convergence achievement. The prediction option extrapolates the DOF solution using the previous history for an improved prediction of the next solution. The line search option improves the Newton-Raphson solution by scaling the solution vector by a scalar value.

The deformed shapes of a 30-filament model resulting from the tensile and bending simulation are given in Figure 2-4. The contour plots of the axial stresses developed in the filaments are also presented in Figure 2-5. A significant divergence is presented in the axial stresses depending on the helix radius of the filament in the tensile test. Thus in a given tensile deformation of the yarn, the filaments are governed by discrete points of the nonlinear stress-strain curve (depending on the helix radius). This fact increases the complexity of the calculations in an analytical approach. On the contrary, the axial stresses developed in the bending deformation present values within a narrow range close to zero. Thus the assumption of a linear elastic modulus corresponding to the first part of the stress – strain curve is acceptable for the bending deformation models. Actually the bending test of the yarn

corresponds to the bending of the curved filaments. Thus the resultant force in the cross section of the filament is approximately zero. The tensile test of the yarn, on the other hand, corresponds to the superposition of filament straightening (bending) and elongation, and the proportion of straightening and bending varies with the filament position. Obviously the inner filaments are mainly subjected to elongation, while the outer filaments are mainly subjected to straightening.

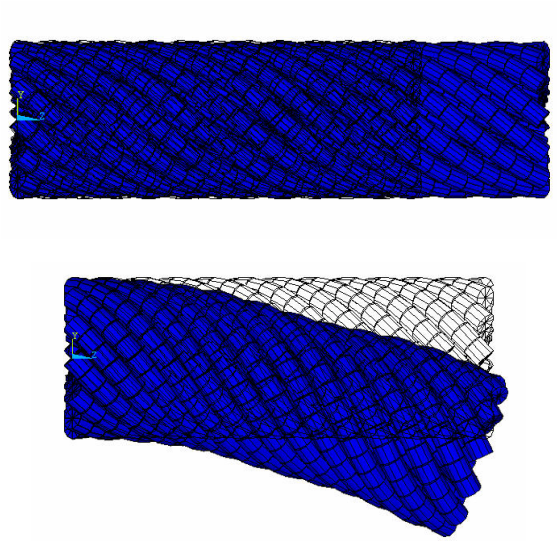

Figure 2-4: Deformed shapes resulting from the simulation of the tensile and bending test of a 30-filament twisted yarn.

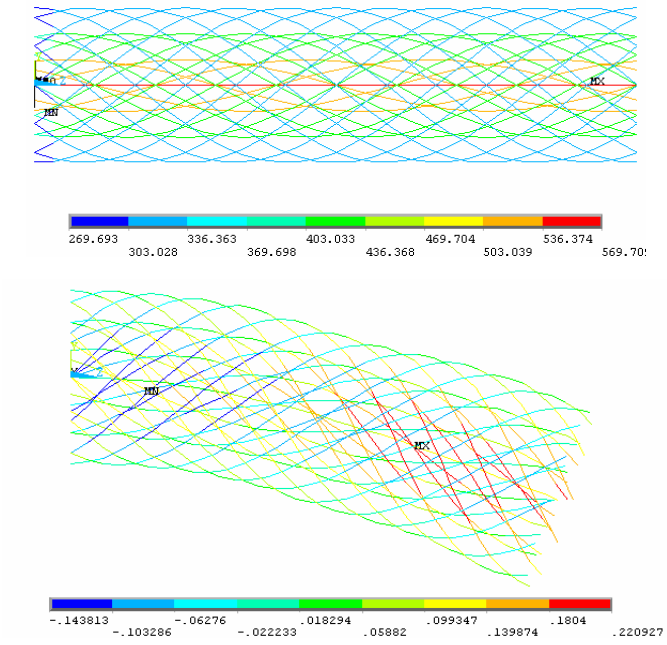

Figure 2-5: Axial stresses developed in the filaments from the simulation of the tensile (270…570 N/mm²) and bending test (-0.14…0.22 N/mm²) of a 30-filament twisted yarn.

2.3 The analytical approach

The analytical approach of Park and Oh (Park, Oh 2006) for the prediction of the bending rigidity of multifilament twisted yarn was compared to the proposed computational method. The selection of the approach was based on certain requirements. Firstly it is a recently presented method applying realistic assumptions and a thorough mechanical analysis. Secondly it presents flexibility in the application in terms of fibre material and yarn structure. Moreover the authors (Park, Oh 2006) compared the calculated dimensionless bending rigidity with the ones resulting from the analytical approaches of Zurek, Platt and Owens. The dimensionless bending rigidity was defined as the value of $B_y \cdot \frac{4}{E\pi R_y^4}$ (considering the bending rigidity of the homogeneous yarn). The four models presented similar tendency relatively to the material characteristics (the ratio $K=E/G$ was considered) and the yarn twist. The dimensionless bending rigidity was calculated for a wide range of material characteristics and the yarn twist varied between the values 0.25 and 1. Actually the curves resulted from the model of Park and Oh correspond to an intermediate performance. Thus the approach of Park and Oh was selected as a representative analytical method.

According to their model the tensile modulus E_f of a filament embodied in the yarn structure considering the contribution of a filament in the tensile deformation of the yarn is:

$$E_f = \frac{E\cos^2 q}{\cos^2 q + \frac{E}{G}\sin^2 q} = \frac{E}{1+K\tan^2 q} \qquad \text{(Eq. 2-9)}$$

The inertia moment of a filament having a helical path to the yarn axis is:

$$I_f = (r\sin\theta)^2 \frac{\pi r_f^2}{\cos q} \qquad \text{(Eq. 2-10)}$$

Thus the bending rigidity of a filament B_f was considered as:

$$B_f = E_f I_f = \frac{E(r\sin\theta)^2 \pi r_f^2}{(1+K\tan^2 q)\cos q} \qquad \text{(Eq. 2-11)}$$

The yarn bending rigidity was considered equal to the summation of the bending rigidity of the constitutive filaments. The integration given in the Eq. 2-12 was proposed to simplify the calculations. A very large yarn diameter compared with the fibre diameter was assumed for the implementation of the integration.

$$\begin{aligned} B_y = \sum B_f = \int_{\theta=0}^{\theta=2\pi}\int_{r=0}^{r=R} \frac{E\pi r_f^2 \cos q (r\sin\theta)^2 r}{\pi r_f^2 \cos q(1+K\tan^2 q)} dr\cdot d\theta = \\ = \frac{E\pi R^4}{4}\cdot\frac{2}{K^2\tan^2 Q}\cdot\left\{K+\frac{1}{\tan^2 Q}\ln\left(\frac{1}{1+K\tan^2 Q}\right)\right\} \end{aligned} \qquad \text{(Eq. 2-12)}$$

where $\tan Q = 2\pi R_y t$. It is worth to mention that the bending rigidity of the yarn is presented independent from the filament radius and number.

2.4 Experimental data

2.4.1 Preparation of samples

The multifilament yarns are unavailable as end product in the market since their use in common clothing applications is unusual. Thus the production of multifilament yarns was demanded for the measurement of their mechanical performance. Major significance for the selection of the monofilament material was the capability of structural stabilization after the spinning (introduction of twist) implementing a thermosetting process. On this account the polyamide monofilaments were selected that are traded in the market basically as fishing-lines.

Although the nominal characteristics of the monofilament (diameter, weight and strength) are provided by the producer, their values were examined and additional measurements were held. The relaxing and conditioning of the filaments forewent the examination of the filament and the yarn production. This procedure is demanded for the elimination of the remaining strains, developed in the filament material through the long period packing. Thus the monofilament was removed from the package case and it was wrapped forming skeins. The skeins were conditioned at 20 ± 2^{o} C temperature and 65±5% relative humidity for 2 days.

Five specimens of each filament type were used for the measurement of the filament diameter and the linear density. The mean values were used in all cases. A microscope was used for the measurement of the diameter. Specimens of 1 m length were weighted in electronic assay balance for the calculation of the linear density. Ten specimens were subjected to the tensile test using the Tensile Tester SDL (described before). The mean stress-strain curve was considered for the evaluation of the elastic properties.

A set of continuous filament twisted yarns was then produced for the evaluation of the proposed and the examined model. A wide range of filament number was used, from 2 to 1200, for the generalisation of the results. Moreover three types of polyamide (PA6) filaments were selected for the yarn production corresponding to 170, 110 and 20 μm filament diameter. The measured properties are given in the Table 2-1. The elasticity of the filaments is described by the mean stress-strain curve resulted from the tensile test of the ten specimens. The nonlinear stress-strain curve was approached by a multi-linear curve for the computational implementation (Figure 2-8). Increasing the desirable filament number of the yarns the filament diameter was reduced for the easier handling of the samples in terms of production (stabilization) and measurement (measurable deflection in bending). Thus three series of yarns were produced: the 2, 4, 8, 12-filament yarn of 170 μm filament diameter, the 50-filament yarn of 110 μm filament diameter and the 1200-filament yarn of 20 μm filament diameter.

The Twist Tester D314 of Zweigle (shown in the Figure 2-6) was used for the introduction of the desirable twist density. The apparatus is suitable for determining the twist level of twisted yarns produced by a spinning process. The sample is clamped in the stationary and rotary clamping heads of the apparatus. The maximum free clamping length is 50 cm. The clamped-in sample is twisted by a motor drive in the direction contrary to the original twist until the fibres are parallel with each other. The speed of the rotary clamping head is infinitely variable. The turns of twist are obtained from the counter. The value read off the counter represents the turns of twist per 1 m if the original test length was 0.5 m. A preload equivalent to the weight of 500 m of yarn is demanded for the measurements. When the thread tension meter is preloaded, the pointer should settle on zero after clamping.

In the current study the apparatus was used for the reverse procedure, that is the introduction of twist in parallel filaments. Thus the filaments of the desired number were fixed in the clamping heads and the desirable twists were imposed forming multifilament twisted yarns. The initial distance of the clamping heads is longer than the final distance (sample shrinkage) due to the elliptical formulation of the filaments. Thus for the calculation of the initial distance corresponding to final distance of 30 cm, a preliminary test was conducted. The parallel filaments (of particular diameter and number) were fixed for a clamps distance of 35 cm and the twists are introduced gradually. The clamps distance was recorded in every 10 twists. Thus the sample shrinkage was calculated for each twist level. If we consider as Nt(=10, 20, 30…) the number of twists, L_{in} =35 cm the initial distance and L_f the final distance resulted from the preliminary test, then the twist level is $t=Nt/L_f$ and the sample shrinkage $\delta= L_{in} - L_f$. The production of a sample length of 30 cm demands initial clamps distance 30 cm × L_{in} / L_f.

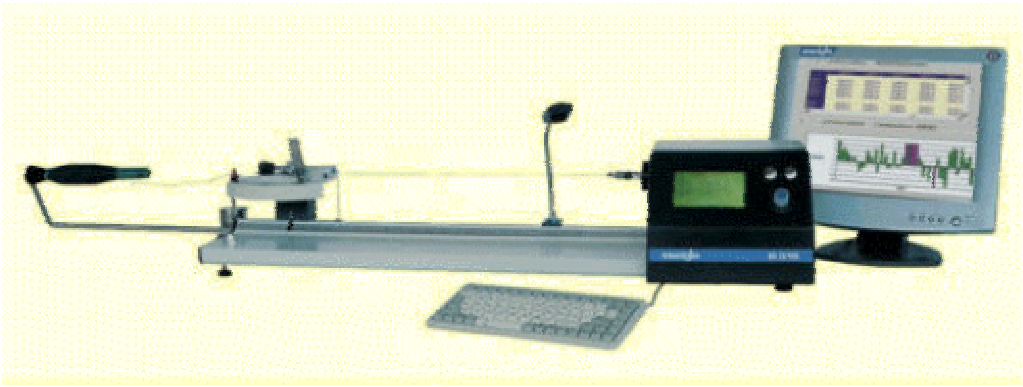

Figure 2-6: Twist Tester Zweigle

The produced samples were carefully removed from the twist tester and fixed in a horizontal board in order to retain the imposed twist. Then the twist was stabilized after thermosetting. The samples were subjected to a thermal procedure using a device of warm air flow for 5 min keeping a distance of 5 cm.

Two levels of twist densities were introduced for each combination of filament diameter – filament number. The nomenclature of the yarns corresponds to: filament diameter (μm) /

filament number / yarn twist (turns/mm). Ten specimens were prepared for each yarn structure for the measurement of their mechanical properties. The linear density of the samples was calculated by the corresponding computational models by the filaments length within the yarn pitch and the linear density of the filament.

Table 2-1: Physical properties of filaments constituting the yarns.

Diameter (μm)	Linear density (Tex)	Material density (kg/mm^3)
170	29.5	5.763E-09
110	10.5	1.048E-08
20	0.37	5.455E-08

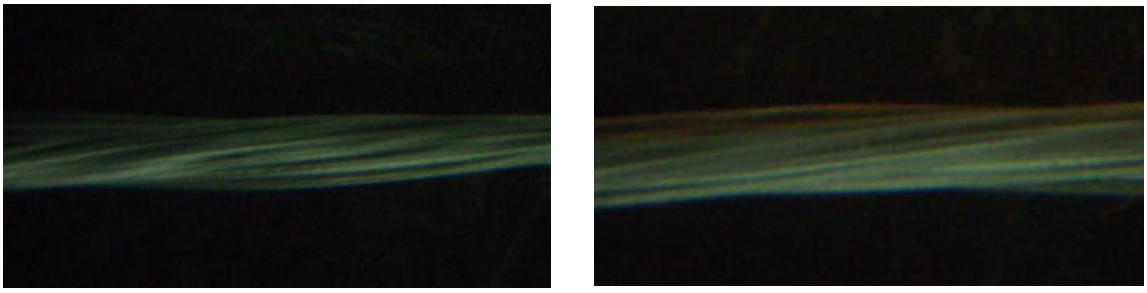

8-filament yarn 12-filament yarn

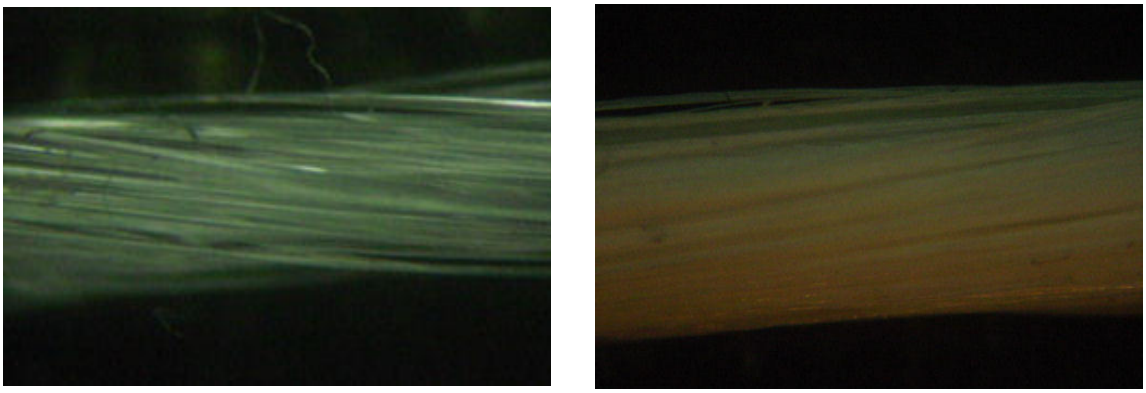

50-filament yarn 1200-filament yarn

Figure 2-7: Microscopic view of prepared yarn samples.

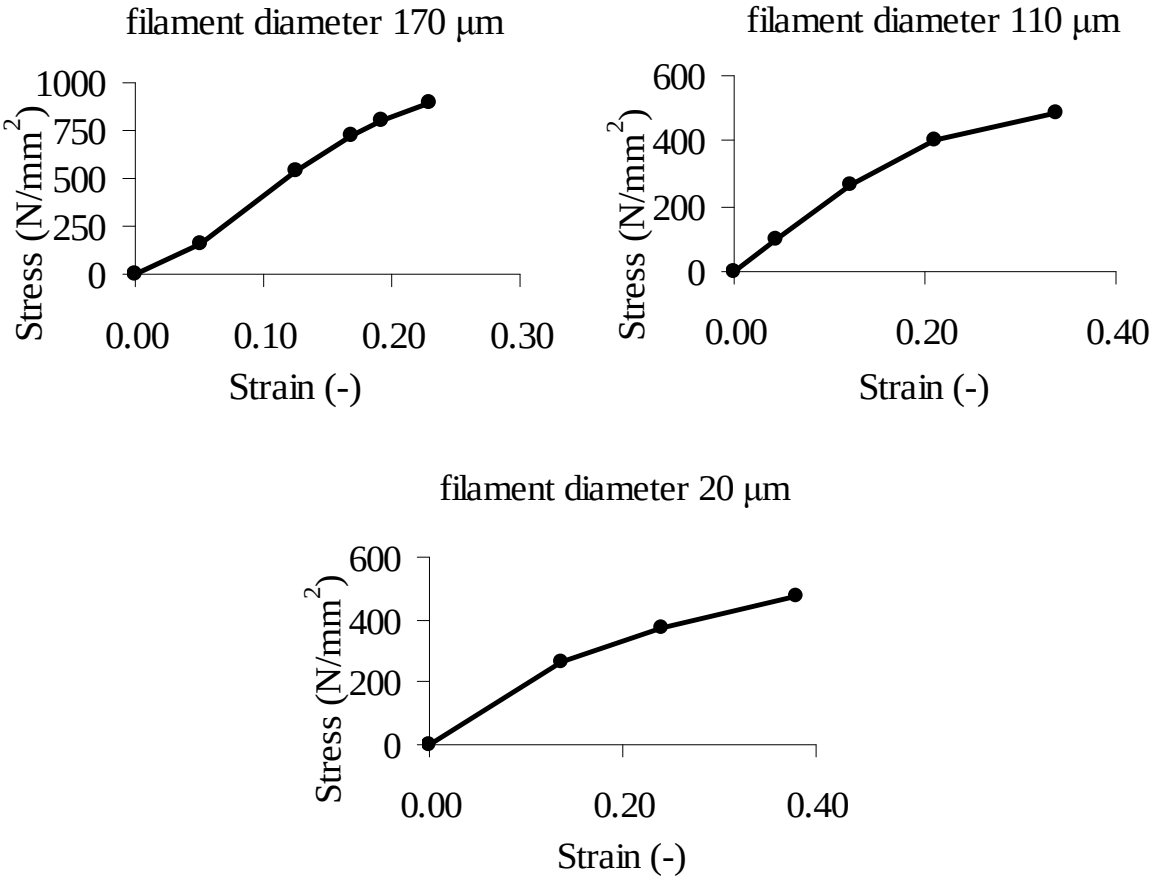

Figure 2-8: Multi-linear elastic curve of filaments constituting the yarns.

2.4.2 Tensile test of the samples

The Tensile Tester of SDL (shown in Figure 2-9) was used for the measurement of the tensile properties of the produced samples. The Tensile Tester comprises a stationary and a driving clamp that moves with constant speed imposing the elongation in the specimen. The load and breaking load is measured by high precision load cell. The linear density (Tex) is introduced as an input parameter for the calculation of the pre-tension (about 0.5cN/Tex) and the breaking strength. Moreover the specimen length is introduced for the adjustment of the testing speed. The specimen length and the test speed were defined at 50 mm and 50 mm/min for the tensile test.

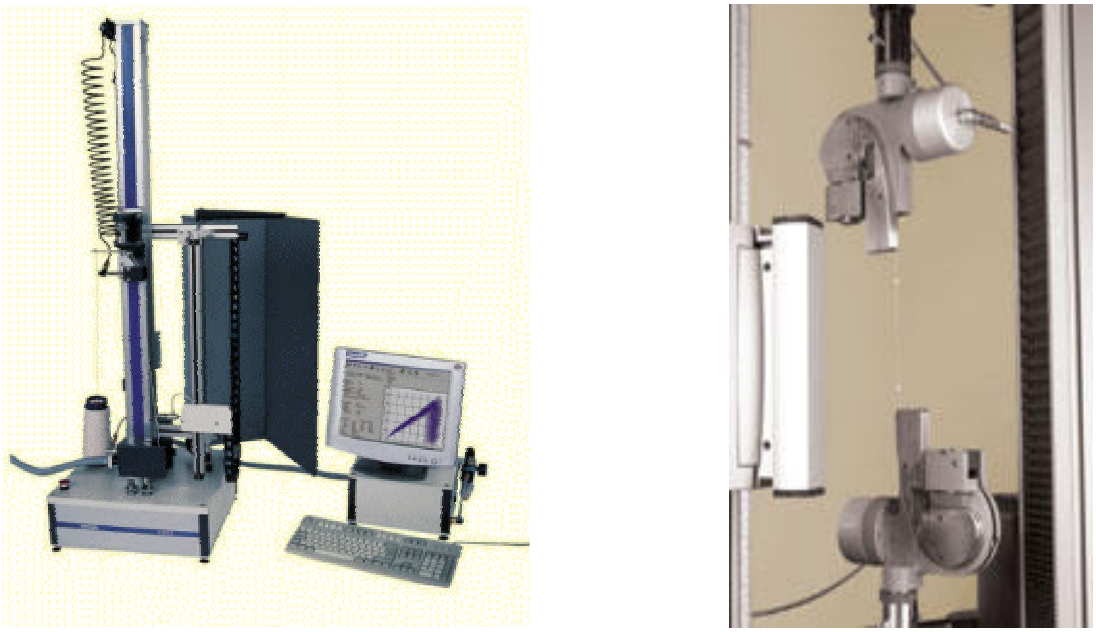

(a) (b)

Figure 2-9: (a) Tensile Tester SDL, (b) Clamp heads.

2.4.3 Bending test of the samples

The bending properties were measured according to the cantilever principle. The specimen was laid on a smooth surface and a rule was placed above it. The edge of the specimen and the 0 cm of the rule coincide with the edge of the surface. Moving the rule and the specimen forward to the free edge of the surface, the free length of the specimen bends under its own weight. The length of the specimen (rule indication in the surface edge) and the vertical deflection were recorded. A vertical rule and a vertical mirror were used for the recording of the deflection. Actually the considered indication of the rule corresponds to the one received when the specimen and its idol coincide. The considered indication is then received on the horizontal view.

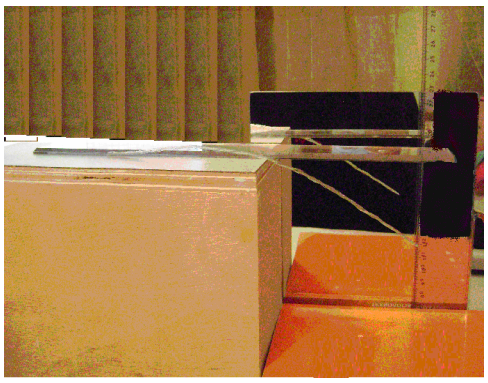

Figure 2-10: Yarn specimen subjected to bending test.

2.5 Results

2.5.1 Evaluation of the approaches using the experimental data

The analytical and computational approaches were adopted for the calculation of the elastic stiffness and the bending rigidity of the prepared samples (**Vassiliadis, Kallivretaki & Provatidis 2010**). Although the approach of Park and Oh dealt with the yarn bending rigidity, the yarn elastic modulus can be calculated by the elastic modulus of the helical filaments E_{fi} (i=1…N) considering the effective cross-section area of the filaments (A_i) and the yarn ($A_{eff} = \sum_{i=1}^{N} A_i = \sum_{i=1}^{N} \frac{\pi r_f^2}{\cos q_i}$).

$$E_{eff} = \frac{\sum_{i=1}^{N} E_{fi} A_i}{A_{eff}} \qquad \text{(Eq. 2-13)}$$

Since the computational complexity precludes the introduction of nonlinear elastic properties a mean value of the elastic modulus of fibres was considered for the analytical approach. The multi-linear curves given in Figure 2-8 were introduced in the computational model for the definition of the fibre properties. Ten samples of each structure were prepared for the tensile test. Thus the experimental curve was defined as the multi-linear mean curve. A good agreement is observed between the analytical, computational and experimental stress – strain curves (Figure 2-11). The computational model presents a more realistic performance owing to the nonlinear elastic properties. A small divergence is observed between the experimental and the predicted curves corresponding to the slippage of the filaments between the clamps.

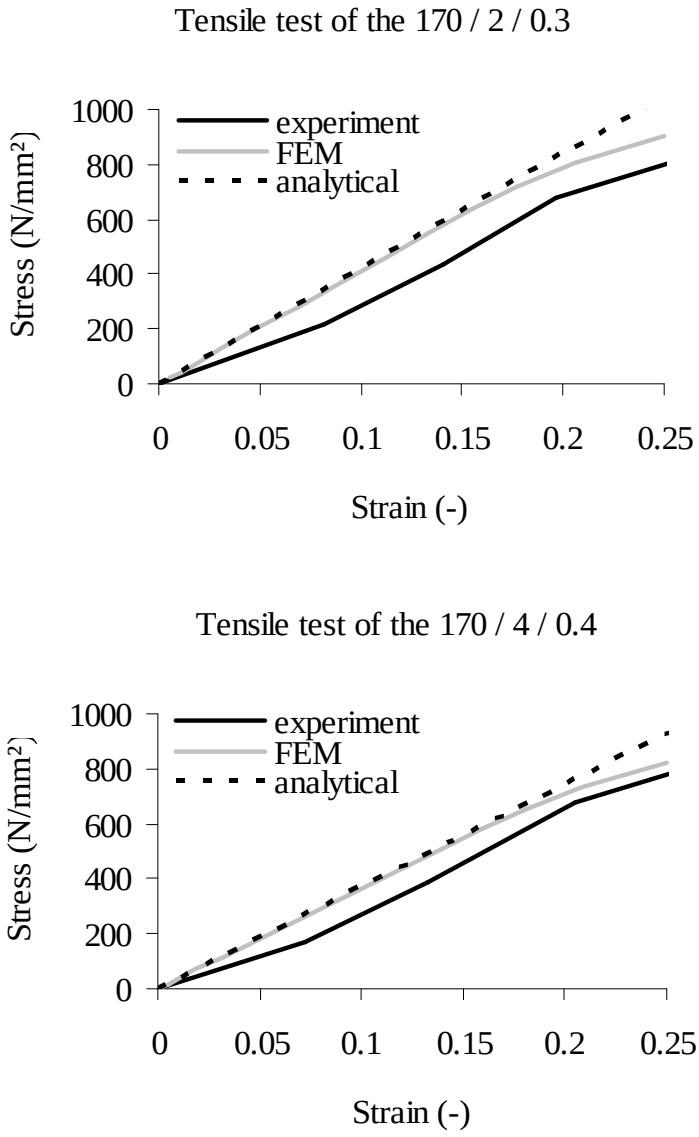

Figure 2-11: Experimental and predicted curves from tensile test of yarn samples.

Ten samples of each yarn structure were prepared for the calculation of the bending rigidity. Several specimen lengths were used (see Table 2-2) for the measurement of the vertical deflection.

The average value and the standard deviation (stdev) were calculated for each length. When the ratio of stdev/average resulted higher than 20 % the current average value was omitted. Moreover the ratio of deflection / length (y/L) was calculated. When the ratio y/L resulted higher than 0.125 the large deformation theory was implemented for the calculation of the bending rigidity of the yarn. The normalized deflection of a cantilever beam loaded with uniform distributed load (w) was calculated implementing the FEM for large deformation analysis (see Appendix IV: The Elastica of a Cantilever Beam).

The curve of normalized deflection (y/L) – normalised load (wL^3/B) is given in the Figure 2-12. Thus for the normalized deflection resulted from the experiment the normalized load is calculated and, in continue, the bending rigidity of the yarn (since the distributed load w, and the specimen length L are known). The distributed load of the specimen was calculated computationally by the length of the filaments constituting a yarn pitch and the filament density (filaments length × cross-section × density / length of pitch). At least the bending rigidity of the structure was defined by the average value of the bending rigidity resulted from the acceptable specimen lengths.

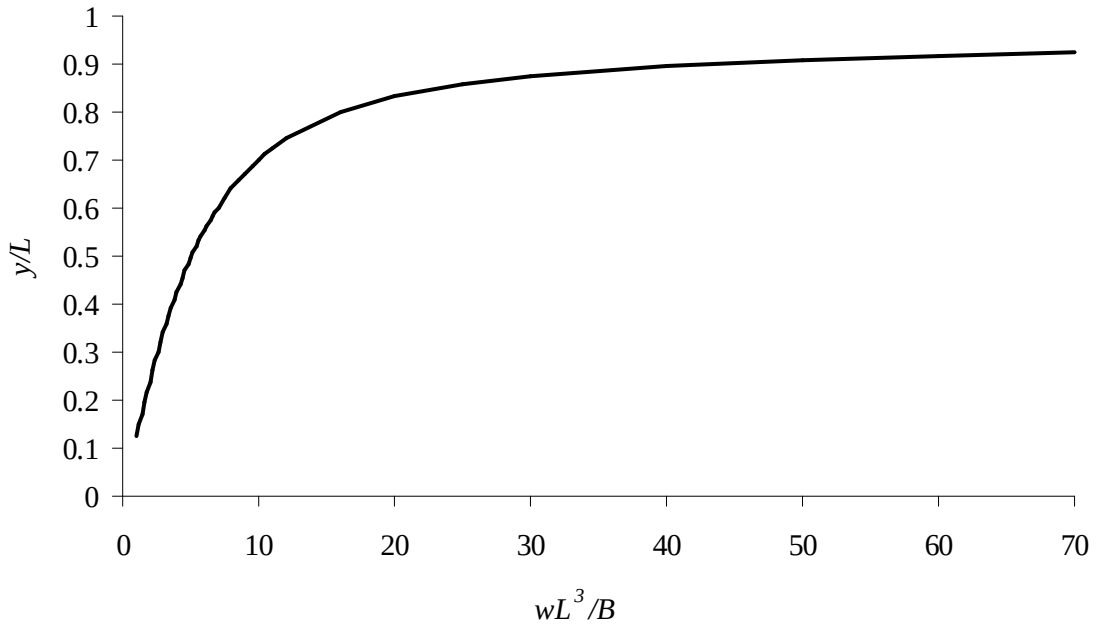

Figure 2-12: Normalized deflection of the cantilever beam loaded by uniform distributed load as a function of the normalized load.

Table 2-2: Experimental data from the bending test.

	Yarn 170 / 2 / 0.3							
	specimen length L (mm)	120	110	100	90	80	70	60
ttttvertical deflection (mm)	sample 1	58.0	44.0	32.0	29.0	23.0	15.0	10.0
	sample 2	54.0	39.5	28.0	21.0	12.0	7.0	5.0
	sample 3	52.0	38.0	28.0	18.0	11.0	7.0	3.0
	sample 4	54.0	44.0	27.0	29.0	20.0	9.0	7.0
	sample 5	56.0	38.0	31.0	20.5	10.0	11.0	5.0
	average value (mm)	54.8	40.7	29.2	23.5	15.2	9.8	6.0
	standard deviation (mm)	2.28	3.07	2.17	5.15	5.89	3.35	2.65
	stdev / average (%)	4.16	7.55	7.42	21.91	38.75	34.15	44.10
	y/L	0.46	0.37	0.29	0.26	0.19	0.14	0.10
	wL^3/B	4.41	3.33	2.50	2.19	1.55	1.16	
	w (N/mm)	5.858E-07						
	B (N·mm²)	0.230	0.234	0.234	0.195	0.194	0.173	0.158
	average B (N·mm²)							0.233

	Yarn 170 / 2 / 0.5							
	specimen length *L* (mm)	120	110	100	90	80	70	60
vertical deflection (mm)	sample 1	57.0	43.5	32.0	22.0	14.0	9.0	4.0
	sample 2	60.0	49.0	36.0	24.0	18.5	11.0	4.0
	sample 3	60.0	41.0	31.0	21.0	16.0	10.0	5.0
	sample 4	62.0	44.0	30.0	19.0	13.0	7.0	4.0
	sample 5	56.0	41.5	30.0	21.0	12.0	6.0	4.0
	sample 6	59.0	47.0	34.0	23.0	16.0	8.0	4.0
	sample 7	53.0	38.0	27.0	16.0	12.0	5.0	4.0
	sample 8	51.0	38.0	28.0	19.5	13.0	11.0	3.0
	average value (mm)	57.3	42.8	31.0	20.7	14.3	8.4	4.0
	standard deviation (mm)	3.77	3.95	2.98	2.52	2.31	2.26	0.53
	stdev / average (%)	6.59	9.23	9.60	12.18	16.16	27.03	13.36
	y/L	0.48	0.39	0.31	0.23	0.18	0.12	0.07
	wL^3/B	4.70	3.55	2.69	1.90	1.46		
	w (N/mm)	5.971E-07						
	B (N·mm²)	0.220	0.224	0.222	0.229	0.210	~~0.214~~	0.242
	average B (N·mm²)							0.225

	Yarn 170 / 4 / 0.2							
	specimen length *L* (mm)	120	110	100	90	80	70	60
vertical deflection (mm)	sample 1	51.0	38.0	28.0	18.0	12.0	7.0	3.5
	sample 2	51.5	39.0	27.0	19.0	2.0	8.0	3.0
	sample 3	50.0	36.0	25.0	18.0	11.5	7.0	5.0
	sample 4	51.0	39.0	27.0	19.0	12.0	7.0	3.0
	sample 5	50.0	36.0	26.0	18.0	10.0	8.0	4.0
	sample 6	49.0	36.0	28.0	20.0	12.0	7.0	5.0
	average value (mm)	50.4	37.3	26.8	18.7	9.9	7.3	3.9
	standard deviation (mm)	0.92	1.51	1.17	0.82	3.95	0.52	0.92
	stdev / average (%)	1.82	4.03	4.36	4.37	39.88	7.04	23.42
	y/L	0.42	0.34	0.27	0.21	0.12	0.10	0.07
	wL^3/B	3.93	3.00	2.27	1.70			
	w (N/mm)	1.170E-06						
	B (N·mm²)	0.515	0.520	0.517	0.503	~~0.604~~	0.479	~~0.484~~
	average B (N·mm²)							0.507

	Yarn 170 / 4 / 0.4							
	specimen length *L* (mm)	120	110	100	90	80	70	60
vertical deflection (mm)	sample 1	57.0	45.0	34.0	24.0	15.0	9.0	4.0
	sample 2	53.0	43.0	30.0	20.0	13.0	8.0	4.0
	sample 3	52.0	41.0	29.0	19.0	13.0	8.5	4.0
	sample 4	52.0	42.0	31.0	22.0	11.0	6.0	4.0
	sample 5	55.0	43.0	29.0	21.0	14.0	9.0	4.0
	sample 6	56.0	44.0	32.0	20.0	14.0	9.5	5.0
	sample 7	52.0	40.0	28.0	19.0	12.0	8.0	4.0
	sample 8	57.0	45.0	33.0	25.0	15.0	9.0	5.0
	sample 9	55.0	42.0	31.0	22.0	13.0	8.5	4.0
	average value (mm)	54.3	42.8	30.8	21.3	13.3	8.4	4.2
	standard deviation (mm)	2.12	1.72	1.99	2.12	1.32	1.02	0.44
	stdev / average (%)	3.90	4.01	6.45	9.94	9.92	12.21	10.44
	y/L	0.45	0.39	0.31	0.24	0.17	0.12	0.07
	wL^3/B	4.35	3.55	2.66	1.97	1.36		
	w (N/mm)	1.205E-06						
	B (N·mm²)	0.478	0.452	0.453	0.447	0.455	0.431	0.462
	average B (N·mm²)							0.454

	Yarn 170 / 8 / 0.1							
	specimen length *L* (mm)	120	110	100	90	80	70	60
vertical deflection (mm)	sample 1	60.0	46.0	33.0	22.0	14.0	8.5	4.5
	sample 2	60.0	45.5	33.0	25.0	14.0	9.0	6.0
	sample 3	59.0	43.0	31.0	23.0	14.0	9.0	4.5
	sample 4	60.0	45.0	32.5	25.0	15.0	9.0	5.0
	sample 5	60.0	48.0	32.0	21.0	15.0	7.0	4.0
	sample 6	59.0	46.0	33.0	23.0	15.0	8.5	4.0
	sample 7	60.0	44.0	32.0	23.0	14.0	8.0	4.0
	sample 8	60.0	47.0	33.0	22.0	14.0	8.5	4.0
	sample 9	60.0	46.0	33.0	23.0	15.0	9.0	5.0
	sample 10	60.0	44.0	30.0	23.0	17.0	11.5	6.0
	average value (mm)	59.8	45.5	32.3	23.0	14.7	8.8	4.7
	standard deviation (mm)	0.42	1.50	1.03	1.25	0.95	1.14	0.79
	stdev / average (%)	0.71	3.30	3.21	5.42	6.45	12.90	16.78
	y/L	0.50	0.41	0.32	0.26	0.18	0.13	0.08
	wL^3/B	5.02	3.84	2.82	2.14	1.50	1.06	
	w (N/mm)	2.320E-06						
	B (N·mm²)	0.799	0.804	0.824	0.790	0.795	0.747	0.800
	average B (N·mm²)							0.794

	Yarn 170 / 8 / 0.15							
	specimen length L (mm)	120	110	100	90	80	70	60
vertical deflection (mm)	sample 1	54.0	42.0	30.0	22.0	13.0	8.5	5.0
	sample 2	54.0	39.0	28.0	19.5	13.0	7.0	3.5
	sample 3	54.5	42.0	31.0	20.0	12.0	7.0	3.5
	sample 4	54.0	38.0	30.0	21.0	12.5	7.0	4.0
	sample 5	53.0	40.0	29.0	20.0	13.0	8.0	5.0
	sample 6	52.0	39.0	28.0	20.0	14.0	7.0	4.0
	sample 7	55.0	39.0	28.5	19.5	12.0	8.0	4.0
	sample 8	52.0	37.0	28.0	19.0	13.0	7.0	4.0
	sample 9	54.0	39.0	30.0	20.0	13.0	7.0	4.0
	sample 10	53.0	38.0	28.0	19.0	12.5	7.5	3.5
	average value (mm)	53.6	39.3	29.1	20.0	12.8	7.4	4.1
	standard deviation (mm)	1.01	1.64	1.12	0.91	0.59	0.57	0.55
	stdev / average (%)	1.89	4.16	3.84	4.56	4.59	7.67	13.59
	y/L	0.45	0.36	0.29	0.22	0.16	0.11	0.07
	wL^3/B	4.27	3.19	2.49	1.83	1.31		
	w (N/mm)	2.329E-06						
	B (N·mm²)	0.943	0.971	0.937	0.928	0.913	0.944	0.932
	average B (N·mm²)							0.938

	Yarn 170 / 12 / 0.1							
	specimen length *L* (mm)	120	110	100	90	80	70	60
vertical deflection (mm)	sample 1	63.0	48.0	37.0	26.0	18.0	11.0	7.5
	sample 2	64.0	42.0	33.0	23.0	14.5	8.0	4.5
	sample 3	64.0	48.0	35.0	24.0	12.0	8.5	5.0
	sample 4	59.0	47.0	33.0	22.5	15.0	9.0	5.0
	sample 5	61.0	45.0	34.0	21.0	13.0	7.0	4.0
	sample 6	63.0	47.0	33.0	22.5	14.0	9.0	5.0
	sample 7	61.5	47.0	34.0	24.0	14.5	9.0	5.0
	sample 8	62.0	45.0	33.0	25.0	15.0	9.5	4.0
	sample 9	61.0	44.0	33.0	25.0	14.5	10.0	4.0
	sample 10	64.0	48.0	34.5	26.0	15.0	11.0	4.0
	average value (mm)	62.3	46.1	34.0	23.9	14.6	9.2	4.8
	standard deviation (mm)	1.65	2.02	1.30	1.65	1.55	1.25	1.06
	stdev / average (%)	2.66	4.39	3.83	6.89	10.68	13.61	22.07
	y/L	0.52	0.42	0.34	0.27	0.18	0.13	0.08
	wL^3/B	5.35	3.92	3.00	2.24	1.48	1.10	
	w (N/mm)	3.508E-06						
	B (N·mm²)	1.133	1.193	1.171	1.143	1.214	1.092	~~1.184~~
	average B (N·mm²)							1.157

	Yarn 170 / 12 / 0.15							
	specimen length *L* (mm)	120	110	100	90	80	70	60
vertical deflection (mm)	sample 1	50.0	35.0	25.0	15.0	10.0	5.5	2.0
	sample 2	49.0	37.0	27.0	19.0	11.0	6.0	3.0
	sample 3	54.0	39.0	28.0	19.0	11.5	7.0	4.0
	sample 4	51.0	36.0	26.0	18.5	12.0	8.0	4.5
	sample 5	51.5	40.0	30.0	19.0	12.0	8.0	3.5
	sample 6	57.5	45.0	33.0	23.0	14.0	8.0	4.0
	sample 7	52.5	37.0	27.5	18.5	12.0	7.5	4.0
	sample 8	54.5	41.5	31.0	20.0	11.0	5.0	3.0
	sample 9	55.0	40.5	30.0	21.0	13.0	7.0	3.0
	average value (mm)	52.8	39.0	28.6	19.2	11.8	6.9	3.4
	standard deviation (mm)	2.71	3.13	2.57	2.15	1.17	1.14	0.77
	stdev / average (%)	5.13	8.03	8.99	11.20	9.91	16.54	22.31
	y/L	0.44	0.35	0.29	0.21	0.15	0.10	0.06
	wL^3/B	4.18	3.16	2.44	1.75	1.22		
	w (N/mm)	3.553E-06						
	B (N·mm²)	1.469	1.496	1.455	1.479	1.495	1.548	~~1.671~~
	average B (N·mm²)							1.490

	Yarn 110 / 50 / 0.1										
	specimen length *L* (mm)	160	150	140	130	120	110	100	90	80	70	60
vertical deflection (mm)	sample 1	142.0	130.0	119.0	106.0	94.0	80.0	65.0	51.0	35.0	25.0	12.0
	sample 2	140.0	128.0	117.0	103.5	93.0	79.0	67.0	51.0	38.0	22.0	12.0
	sample 3	143.0	131.0	120.0	107.0	98.0	84.0	68.0	52.0	38.0	23.0	12.0
	sample 4	145.0	131.0	120.0	108.0	94.0	79.0	65.0	51.0	35.0	23.0	12.0
	sample 5	143.0	131.0	120.0	108.0	95.0	83.0	68.0	49.0	36.0	23.0	13.0
	sample 6	142.0	130.0	119.0	106.0	94.0	79.0	65.0	48.0	35.0	23.0	14.0
	sample 7	143.0	131.0	120.0	108.0	96.0	85.0	68.0	52.0	40.0	23.0	12.0
	sample 8	141.0	129.0	116.0	106.0	90.0	77.0	63.0	47.0	35.0	23.0	13.0
	sample 9	141.0	131.0	120.0	108.0	95.0	85.0	63.0	52.0	37.0	22.0	13.0
	average value (mm)	142.2	130.2	119.0	106.7	94.3	81.2	65.8	50.3	36.6	23.0	12.6
	standard deviation (mm)	1.48	1.09	1.50	1.52	2.18	3.03	2.05	1.87	1.81	0.87	0.73
	stdev / average (%)	1.04	0.84	1.26	1.43	2.31	3.73	3.11	3.72	4.95	3.77	5.79
	y/L	0.89	0.87	0.85	0.82	0.79	0.74	0.66	0.56	0.46	0.33	0.21
	wL^3/B	36.00	28.50	23.00	18.00	15.00	12.00	8.54	6.09	4.41	2.88	1.71
	w (N/mm)	5.039E-06										
	B (N·mm²)	0.573	0.597	0.601	0.615	0.581	0.559	0.590	0.603	0.585	0.600	0.635
	average B (N·mm²)											0.594

	Yarn 110 / 50 / 0.16										
	specimen length *L* (mm)	150	140	130	120	110	100	90	80	70	60
vertical deflection (mm)	sample 1	136.0	122.0	109.0	98.0	87.0	77.0	63.0	49.0	29.0	11.0
	sample 2	129.0	120.0	106.0	95.0	84.0	67.0	58.0	38.0	23.0	14.0
	sample 3	133.0	119.0	106.0	98.0	81.0	65.0	54.0	37.0	24.0	15.0
	sample 4	127.0	118.0	106.0	93.0	80.0	75.0	53.0	39.0	26.0	15.0
	sample 5	128.0	121.0	106.0	93.0	81.0	66.0	54.0	37.0	21.0	12.0
	sample 6	134.0	122.0	109.0	94.0	82.0	65.0	52.0	37.0	23.0	15.0
	sample 7	132.0	120.0	110.0	97.0	84.0	67.0	54.0	37.0	21.0	12.0
	sample 8	130.0	118.0	107.0	97.0	82.0	65.0	52.0	36.0	22.0	13.0
	sample 9	132.0	122.0	105.0	94.0	80.0	67.0	53.0	40.0	24.0	13.0
	average value (mm)	131.2	120.2	107.1	95.4	82.3	68.2	54.8	38.9	23.7	13.3
	standard deviation (mm)	2.95	1.64	1.76	2.07	2.29	4.52	3.56	3.98	2.55	1.50
	stdev / average (%)	2.25	1.37	1.65	2.17	2.78	6.63	6.50	10.24	10.77	11.25
	y/L	0.87	0.86	0.82	0.80	0.75	0.68	0.61	0.49	0.34	0.22
	wL^3/B	28.50	25.50	18.50	16.00	12.50	9.34	7.19	4.83	2.98	1.83
	w (N/mm)	5.523E-06									
	B ($N \cdot mm^2$)	0.654	0.594	0.656	0.597	0.588	0.591	0.560	0.585	0.635	0.652
	average B ($N \cdot mm^2$)										0.611

	Yarn 20 / 1200 / 0.1						
	specimen length *L* (mm)	80	70	60	50	40	30
vertical deflection (mm)	sample 1	75.0	63.0	55.0	40.0	30.0	10.0
	sample 2	75.0	64.0	56.0	38.0	30.0	16.0
	sample 3	74.0	65.0	57.0	38.0	31.0	
	sample 4	80.0	70.0	61.0	44.0	34.0	
	sample 5	77.0	66.0	60.0	42.0	32.0	
	sample 6	76.0	64.0	54.0	42.0	29.0	
	sample 7	70.0	58.0	52.0	36.0	26.0	
	sample 8	73.0	62.0	53.0	40.0	30.0	
	average value (mm)	75.0	64.0	56.0	40.0	30.3	13.0
	standard deviation (mm)	2.14	2.50	2.79	2.42	1.79	4.24
	stdev / average (%)	2.85	3.91	4.98	6.06	5.91	32.64
	y/L	0.94	0.91	0.93	0.80	0.76	0.43
	wL^3/B		57.00	70.00	16.00	11.50	4.15
	w (N/mm)	4.38434E-06					
	B (N·mm²)		0.026	0.014	0.034	0.024	~~0.034~~
	average B (N·mm²)						0.025

	Yarn 20 / 1200 / 0.16						
	specimen length *L* (mm)	80	70	60	50	40	30
vertical deflection (mm)	sample 1	77.0	67.0	60.0	41.0	34.0	11.0
	sample 2	76.0	63.0	59.0	40.0	35.0	15.0
	sample 3	74.0	66.0	58.0	39.0	32.0	9.5
	sample 4	77.0	63.0	57.0	44.0	35.0	
	sample 5	79.0	67.0	58.0	42.0	34.0	
	sample 6	75.0	65.0	60.0	38.0	33.0	
	sample 7	71.0	59.0	50.0	37.0	37.0	
	sample 8	74.0	60.0	54.0	41.0	34.0	
	average value (mm)	76.3	65.2	58.7	40.7	34.3	11.8
	standard deviation (mm)	1.75	1.83	1.21	2.16	1.17	2.84
	stdev / average (%)	2.29	2.82	2.06	5.31	3.41	24.03
	y/L	0.95	0.93	0.98	0.81	0.86	0.39
	wL^3/B		60.50	47.00	19.00	14.50	5.2
	w (N/mm)	4.48709E-06					
	B (N·mm²)		0.025	0.021	0.030	0.020	~~0.038~~
	average B (N·mm²)						0.024

The Eq. 2-12 proposed by Park and Oh was implemented for the analytical calculation of the bending rigidity of the produced yarn structures. Since the integration presupposes a very large yarn diameter compared to the fibre diameter the current solution was implemented only for the 1200-filament yarns. In reverse the summation was used in the cases of 2 to 50-filaments yarns. The geometry of the models corresponds to the one presented in the Figure 2-3.

The bending rigidity resulted from the models, analytical and computational, and the experiment are given in the Table 2-3. A good agreement is presented between the computational and the experimental results. Actually the divergence varies between -28 and +36 %. The presented divergence can be imputed to laboratorial errors during the sample production and measurement. The divergence range, moreover, eliminates the prospect of a systematic error introduced by the considered assumptions or the analysis method. Thus the reliability of the proposed computational method is proved by the experimental data.

Table 2-3: The bending rigidity of yarns resulted from the models and the experiment.

	Experiment	Analytical		FEM	
structure	*Bexp* (N·mm²)	*Ban* (N·mm²)	ratio *Ban*/*Bexp*	*Bc* (N·mm²)	ratio *Bc*/*Bexp*
170 / 2 / 0.3	0.233	1.012	4.34	0.261	1.12
171 / 2 / 0.5	0.225	0.931	4.14	0.251	1.12
170 / 4 / 0.2	0.507	2.035	4.02	0.525	1.04
170 / 4 / 0.4	0.454	1.800	3.96	0.498	1.10
170 / 8 / 0.1	0.797	9.726	12.20	1.056	1.33
170 / 8 / 0.15	0.938	9.319	9.93	1.043	1.11
170 / 12 / 0.1	1.157	21.351	18.45	1.576	1.36
170 / 12 / 0.15	1.490	20.103	13.49	1.548	1.04
110 / 50 / 0.1	0.594	48.557	81.68	0.594	1.00
110 / 50 / 0.16	0.611	46.860	76.65	0.591	0.97
20 / 1200 / 0.1	0.025	38.866	1552.94	0.018	0.72
20 / 1200 / 0.16	0.024	33.662	1385.28	0.018	0.72

The analytical approach, on the other hand, presents a significant divergence from the experimental data. It is remarkable that for increasing filament number the divergence is also increased. The ratio of the values of bending rigidity resulted from the analytical approach to the experimental ones (*Ban*/*Bexp*) is indicative for the evaluation of the divergence. Thus the analytical prediction of the yarn performance is adequate in the tensile deformation (the mean linear elastic properties are calculated) and deficient in the bending deformation. The error was evidently introduced by the assumption of the Eq. 2-11 ($B_f=E_f \cdot I_f$), since the E_f was

sufficiently defined. Actually the Eq. 2-11 is valid for a series of conditions as the continuity and homogeneity of the structure, the constant cross-section of the beam, the perpendicular cross-section of the bent beam etc. In the examined approach the E_f was defined for the helical filament embodied in the yarn structure i.e. a non-continuum structure. Consequently the predicted yarn bending performance corresponds to a bonded filament assembly precluding the slippage between the filaments. It could be realistic for high friction conditions between the filaments.

2.5.2 The dependence of the bending rigidity of the yarns from the number of the filaments

The considerable differences appearing after the comparison of the analytical model results and the experimental data initiated a particular study indicating the effect of the filament number on the predicted yarn bending rigidity. The study was based on a typical yarn structure with constant radius R_y=1 mm and varying number of constituent filaments N. Consequently the radius of filament $r_f(N)$ is a function of the filament number. The yarn structure is formed by a central straight filament and layers of filaments wrapped around it, in a close packing configuration. Each wrapped filament forms a helical path of constant radius. Linear isotropic elastic properties were assumed for the filaments corresponding to E = 2000 N/mm^2 and G = 770 N/mm^2. Moreover the typical value t=0.1 turns/mm was selected. The bending rigidity of the yarn was calculated using first the analytical model. With the same data set the computational model gave a second group of values of the bending rigidity (Figure 2-13). The integration and the summation of the Eq. 2-12 were applied for the investigation of the analytical approach. Both operations lead to a constant value of bending rigidity independently from the filament number. Consequently, according to the analytical approach, the apparent radius of the yarn results more effective on the yarn bending rigidity than the radius of the constituent filaments. However the radius of the filaments is determinant for their individual bending rigidity. Thus the analytical model assumes a bonded structure of twisted filaments. In reverse, significant is the effect of the filament number in the yarn bending rigidity according to the computational approach. A high decrease of the bending rigidity results from the increase of the filament number, as it is normally expected.

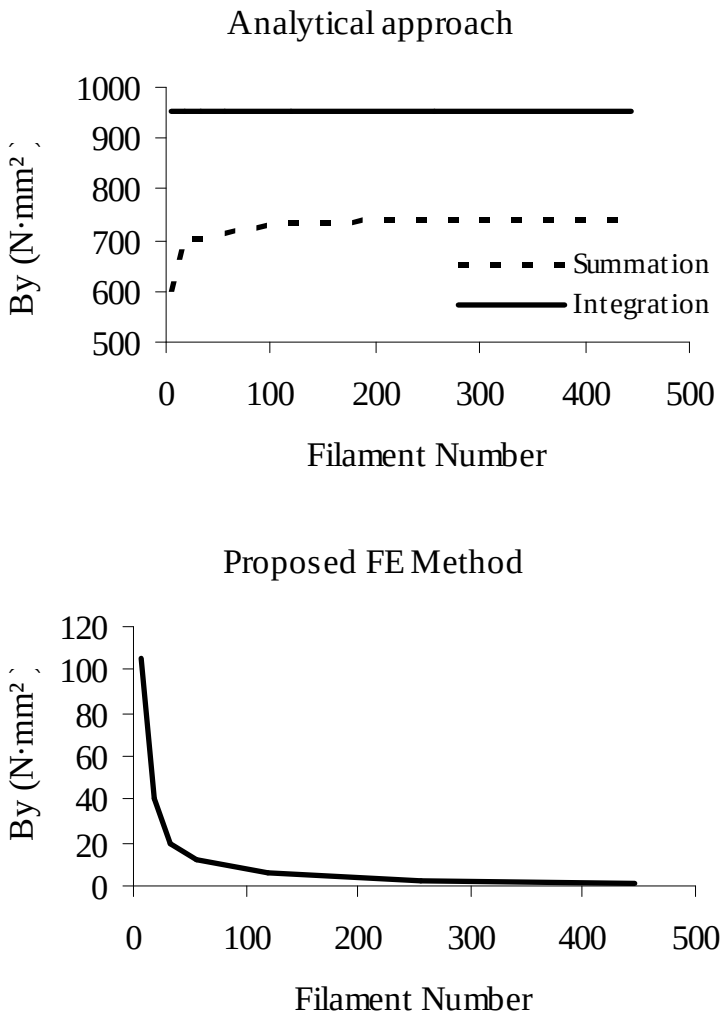

Figure 2-13: The effect of the filament number on the yarn bending rigidity (R_y=1 mm and t=0.1 turns/mm) by the analytical and the computational approach.

2.5.3 Parametric analysis using the proposed FE Method

The effect of the yarn structure on the yarn bending rigidity was investigated implementing the proposed approach. A series of models varying in the filament radius (r_f) , twist (t) and filament number (N) were generated and analyzed. Essential for the analysis was considered the product $t \cdot r_f$, since for constant values and constant filament number the generated yarn structures are similar. Evidently similar structures correspond to similar performance. The value of the product $t \cdot r_f$ ranges between 0 and 0.5, owing to geometrical constraints ($0 < 1/t < 2r_f$). The sum of the bending rigidity of the constitutive filaments in the straight formulation ($B_{fs} = N\frac{E\pi r_f^4}{4}$) was considered as the reference quantity for the calculation of the dimensionless bending rigidity of yarn B_y/B_{fs}. The effect of the product $t \cdot r_f$ on the dimensionless yarn bending rigidity B_y/B_{fs} is presented in the Figure 2-14. It is worth to mention that the presented curves apply to all cases of linear isotropic elastic filaments with Poisson ratio equal to 0.3, it is however indicative for other material properties.

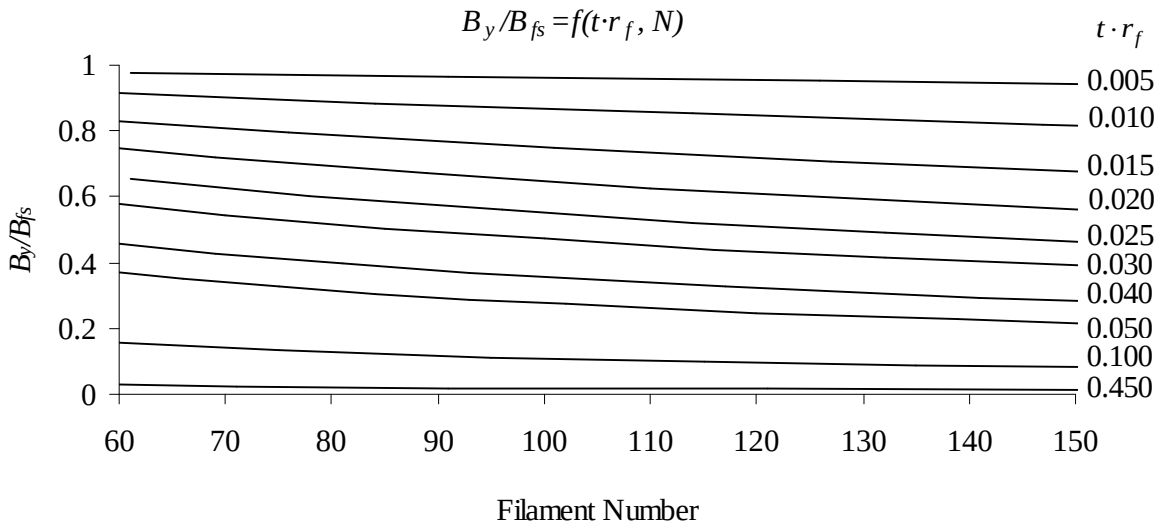

Figure 2-14: The effect of the product $t \cdot r_f$ on the dimensionless yarn bending rigidity B_y/B_{fs} for linear isotropic fibres.

The diagram of Figure 2-14 renders qualitatively the effect of each parameter in the yarn bending rigidity since it is independent from the value of the parameters (r_f, t, N, E). Thus the dimensionless yarn bending rigidity decreases for increasing filament number and by increasing the product $t \cdot r_f$. In particular the following conclusions were reached:

- The decrease of the twist level in a given yarn, of constant filament material and diameter and constant filament number, results in increase of the yarn bending rigidity. The upper limit of course is the value B_{fs} (sum of bending rigidity of the straight filaments) for zero twist.
- The increase of the filament diameter for a given yarn, of constant filament material, filament number and twist level, induces increase of the yarn bending rigidity. As mentioned before the dimensionless bending rigidity decreases in this case, whereas the value B_{fs} increases depending on the 4^{th} power of r_f. Since the decrease rate of the dimensionless bending rigidity is very low compared to the increase rate of the B_{fs} the yarn bending rigidity results increased.
- The increase of the filament number incurs decrease of the dimensionless bending rigidity and increase of the value B_{fs}. Since the decrease rate of the dimensionless bending rigidity is very low compared to the increase rate of the B_{fs} the yarn bending rigidity results increased.

Finally it is worth to mention that the normalization proposed in the diagram of Figure 2-14 is successful since the curves are independent from the values of the structural characteristics and the Young Modulus. Thus the bending rigidity for every multifilament yarn structure is obtained. For example if we consider the characteristics r_f = 0.05 mm, t = 2 turns/mm, N =

115 filaments, E = 2000 N/mm², then $t \cdot r_f = 0.1$ and $B_{fs} = 1.129$ N·mm². From the diagram we take $B_y/B_{fs} = 0.098$, thus the yarn bending rigidity results $B_y = 0.11$ N·mm².

2.6 Conclusions

A computational method was proposed for the mechanical analysis of multi-filament twisted yarns. The apparent yarn properties, elastic modulus and bending rigidity, were calculated considering the filaments characteristics and the yarn structure. The FEM using beam elements was implemented for the analysis. The proposed method presents basic advantages in modelling and analysis. Thus a fast and flexible design is offered in terms of geometrical representation and material properties. Moreover the implementation of the Newton-Raphson solution algorithms supports the nonlinear analysis with large deformations. The evaluation of the proposed method was based on experimental data. A series of twisted yarns consisting from 2 to 1200 filaments were produced and tested for the evaluation. Further on a rigorous analytical approach was selected for the comparison of the predicted performances and the resultant error. A good agreement was presented between the computational, analytical approach and the experimental data regarding the tensile test. High reliability was also presented in the proposed computational model in regard to the bending deformation. In reverse, the analytical method presented significant divergence in the prediction of the yarn bending rigidity increasing with the number of filaments. Finally the FEM was implemented for the parametric analysis of the yarn mechanical behaviour. The effect of the structural parameters on the yarn bending rigidity was presented qualitatively in a diagram.

Chapter 3
The Mesomechanical Modelling of Fabrics

Abstract

The current chapter presents the mesomechanical modelling stage focusing on the apparent mechanical properties of the fabric unit cell. In the current stage of modelling the representation of the fibres constituting the yarns is omitted for the reduction of the computational cost and the yarns are represented as homogenous structures (their apparent properties were calculated in the previous stage). Thus the attribution of the yarn properties constitutes the basic factor for the modelling reliability due to the homogenization of the yarns. Moreover the yarns interactions in the fabric structure are determinant for the structural stability of the fabrics subjected to deformations. Three approaches, the solid, the shell and the beam modelling, were investigated for the mesomechanical analysis of the plain woven structure. The beam modelling was proved the appropriate approach for the reliable attribution of the modelled yarns. Aim of the mesomechanical modelling stage is the calculation of the performance of the unit cell in the tensile, shear and bending deformation. The models of the basic woven and knitted structures were also presented. Especially the modelling approach of the knitted structures produced by cotton yarns was based on the proposed principle of the minimum loop length and it was confirmed by the experimental data.

3.1 Introduction

The mesomechanical modelling stage focuses on the evaluation of the mechanical performance of the fabric unit cell. The unit cell corresponds to the repetitive structural unit presented in the periodic fabric sheet. For computational cost reduction, the filaments are omitted in the generation of the mesomechanical model and the yarns are represented as homogeneous structures.

Several mesomechanical models of the basic woven structures were proposed mainly for the analysis of composite materials. The objective of these researches is the simulation of the deformation of the woven reinforcement unit cell. The mesoscopic properties are then considered for the evaluation of the macromechanical performance of the composite reinforcements (without the resin). The performance of the composite reinforcement is essential for the manufacturing of the composite part. The manufacturing process consists in the formulation of the dry textile and the injection of the resin within the preform. If a complex composite part is produced, the reinforcement is subjected to double curvature deformations. The meso-scale models are also demanded for the damage prediction of the

composite material and the permeability prediction of the deformed shape. The permeability of the deformed reinforcement defines the resin flow during the injection process (Badel et al. 2008).

Some of the proposed computational mesomechanical models were referred in the §1.5.1. Most of them implemented the finite element method using solid FE. The yarns were assumed as homogenous material with transverse isotropic elastic properties. The attribution of the yarn properties constitutes basic factor for the accuracy of the mesomechanical modelling stage. Thus the equivalent performance of the homogenous yarn, considering the discrete structure, in the tensile and bending deformation is required at least for the reliable attribution of yarn models. It is remarkable that most of the proposed models omitted the calculation of the real value of the yarn bending rigidity and its attribution at the modelled yarn. Badel *et al* considered a significantly low value for the longitudinal shear moduli in order to keep low the bending stiffness of the homogenous yarn (Badel et al. 2008).

3.2 The geometrical modelling of the fabric structure

3.2.1 The geometrical modelling of woven structures

Several studies were conducted focusing on the geometrical modelling of the plain woven structure. The prevailing analytical models correspond to the pioneering studies of Peirce (Peirce 1937), Kawabata (Kawabata 1989b), Leaf (Leaf 1979c) and Kemp (Kemp 1958). Today the initial 2D analytical models of the woven unit cell have been evolved to 3D computational models described by splines and NURBS surfaces. However, it is useful to present the analytical model proposed by Peirce for the definition of the basic geometrical parameters and their expression in analytical form.

Model of Peirce (Peirce 1937)

Peirce in his approach considered the net spatial requirements for the geometrical representation of the threads within the fabric structure. The yarns were assumed flexible circular cylinders. The cross sections were considered undistorted presenting a “just in touch” formulation in the cross points.

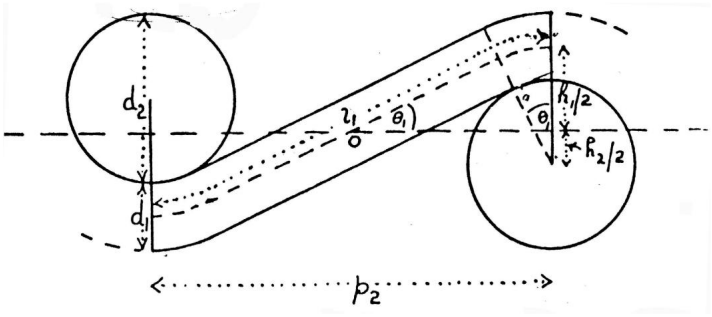

Figure 3-1: The geometrical model of plain woven structure proposed by Pierce.

In Figure 3-1 the section of the plane of the warp axis that is normal to the plane of the cloth is presented. Moreover the structural parameters used for the description of the model are given.

Nomenclature:

d_1 : diameter of warp (mm)

d_2 : diameter of weft (mm)

p_1 : warp spacing (mm)

p_2 : weft spacing (mm)

θ_1 : maximum angle of the warp axis to the plane of cloth (radians)

θ_2 : maximum angle of the weft axis to the plane of cloth (radians)

l_1 : length of warp between planes containing the axes of consecutive cross threads (mm)

l_2 : length of wefts between planes containing the axes of consecutive cross threads (mm)

h_1 : maximum displacement of the warp axis, normal to the plane of the cloth (mm)

h_2 : maximum displacement of the weft axis, normal to the plane of the cloth (mm)

c_1 : crimp of warp (fractional)

c_2 : crimp of weft (fractional)

To maintain general and symmetrical forms, the basic length determining the scale were defined to be the sum of the diameters,

$$D = d_1 + d_2 \qquad \text{(Eq. 3-1)}$$

By definition,

$$c_1 = \frac{l_1}{p_2} - 1 \qquad \text{(Eq. 3-2)}$$

$$c_2 = \frac{l_2}{p_1} - 1 \qquad \text{(Eq. 3-3)}$$

Applying the geometrical equations,

$$p_2 = (l_1 - D\theta_1)\cos\theta_1 + D\sin\theta_1 \qquad \text{(Eq. 3-4)}$$

$$p_1 = (l_2 - D\theta_2)\cos\theta_2 + D\sin\theta_2 \qquad \text{(Eq. 3-5)}$$

$$h_1 = (l_1 - D\theta_1)\sin\theta_1 + D(1 - \cos\theta_1) \qquad \text{(Eq. 3-6)}$$

$$h_2 = (l_2 - D\theta_2)\sin\theta_2 + D(1 - \cos\theta_2) \qquad \text{(Eq. 3-7)}$$

$$D = h_1 + h_2 = d_1 + d_2 \qquad \text{(Eq. 3-8)}$$

The model proposed by Peirce corresponds to a system of 7 nonlinear equations and 11 parameters.

3.2.2 The geometrical modelling of the plain weft-knitted structure

Several studies analyzed the dimensional properties of knitted structures, with prevalent the work of Chamberlain, Peirce, Leaf and Glaskin, Munden and Kawabata on the plain weft knitted structure (single jersey). These studies presented either formulated geometrical models consisting of curves of known analytical description, for example circular arcs and straight lines, or the results of measurements that were carried out on a series of knitted structures (Demiroz, Dias 2000a). The 2D proposed model (Chamberlain 1926) is inadequate to be used for the mechanical analysis of the fabrics, since the change in fabric thickness and the contact phenomena between yarns cannot be predicted. However, Chamberlain's model provides the fundamental geometrical principles for the 3D modelling of the knitted structure. The insufficient accuracy of the predicted dimensions of the existing 3D geometrical models of knitted structures, on the other hand, increases the need for the production of a more accurate model (Vassiliadis et al. 2005). A structural parameter of the knitted fabric used for the estimation of the accuracy of the various models is the loop length (l) since it is easy to be measured using standard laboratory equipment.

Model of Chamberlain

The first known 2D geometrical model of the plain knitted structure was reported by Chamberlain (Chamberlain 1926). This model represents the projection of the loop in the plain of the fabric and it is composed of circular arcs and straight lines. The limitation in the use of the model is due to the lower accuracy deriving from the 2D representation of the loop. The following equation gives the expression of the length of yarn in a loop:

$$l = w(3\pi + 2\sqrt{13})/4 \qquad \text{(Eq. 3-9)}$$

where l is the loop length in mm; and w, the wale spacing in mm.

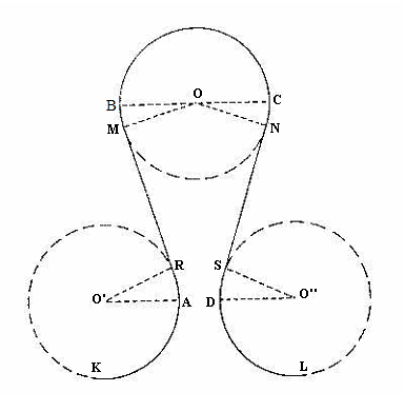

Figure 3-2: The model of Chamberlain for the plain weft knitted structure.

Model of Peirce

Peirce (Peirce 1947) generated a 3D model based on the assumption that the central axis of the yarn forming a course lies on a circular cylindrical surface whose central axis follows the line of the course. Further, he assumed that when the cylinder is projected on a plane, the axis of the yarn in the planar condition is composed of circular arcs and straight lines. Using the above modelling considerations, Peirce obtained the following equation for the calculation of loop length:

$$l = \frac{2}{C} + \frac{1}{W} + 5.94D \qquad \text{(Eq. 3-10)}$$

where l is the length of yarn in one loop in mm; C, the course density in courses/mm; W, the wale density in wales/mm; and D, the apparent diameter of the yarn in mm.

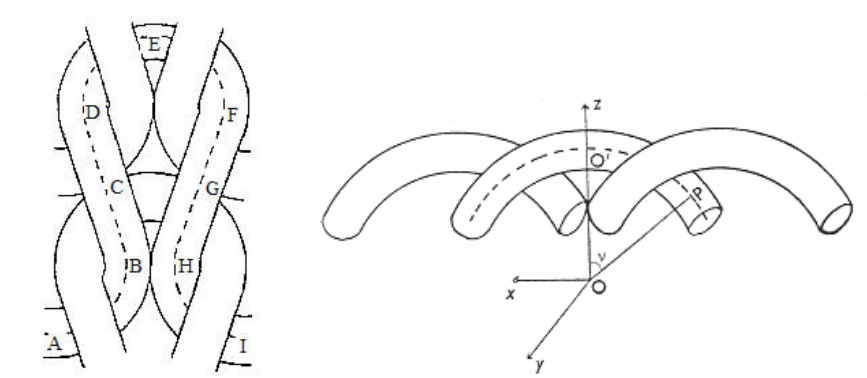

Figure 3-3: The model of Peirce for the plain weft knitted structure.

Model of Leaf and Glaskin

Leaf and Glaskin (Leaf, Glaskin 1955) assumed that the projection of central axis of yarn on the plane of the fabric is composed of circular arcs, i.e. the yarn forming a course lies on the surface of a series of circular cylinders whose central axes are perpendicular to the plane of the fabric. Leaf and Glaskin, using certain assumptions, obtained an approximation for the length of yarn in the loop. The approximate equations [Eq. 3-11, 3-12, 3-13] are more accurate, especially for the fabrics produced using cotton yarns than the initial equations, at least for the samples under consideration. The symbols C (courses/inch), W (wales/inch), D (inch), l (inch) of the following equations are corresponding to the parameters mentioned above:

$$l = 4a\varphi D \qquad \text{(Eq. 3-11)}$$

where:

$$\varphi = \pi + \sin^{-1}\left\{\frac{C^2 D}{\sqrt{C^2 + W^2\left(1 - C^2 D^2\right)^2}}\right\} - \tan^{-1}\left\{\frac{C}{W\left(1 - C^2 D^2\right)}\right\} \qquad \text{(Eq. 3-12)}$$

$$a = 1/(4WD\sin\varphi)\; l = \frac{2}{C} + \frac{1}{W} + 5.94D \qquad \text{(Eq. 3-13)}$$

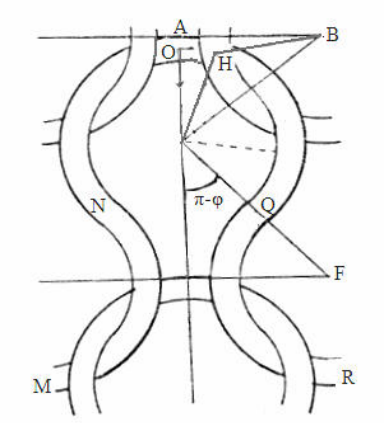

Figure 3-4: The model of Leaf & Glaskin for the plain weft knitted structure.

Model of Munden

Munden (Munden 1969) developed a model based on the forces which would result from the pressure of one loop on its neighbour. The direction of the forces was considered parallel to the course direction of the fabric corresponding to the directions of the resultant of all the pressures at the intersection region, if there is no resultant force on the fabric as a whole. The loop length l (mm) is given by the following equation, where the course spacing c (mm) and the apparent yarn thickness D (mm) are used. As it is shown, the loop length was considered independent of the wale spacing.

$$\frac{l}{c} = 1.088\frac{c}{D} + 2\left\{1 + \frac{9}{16}\left(\frac{D}{c}\right)^2\right\} \qquad \text{(Eq. 3-14)}$$

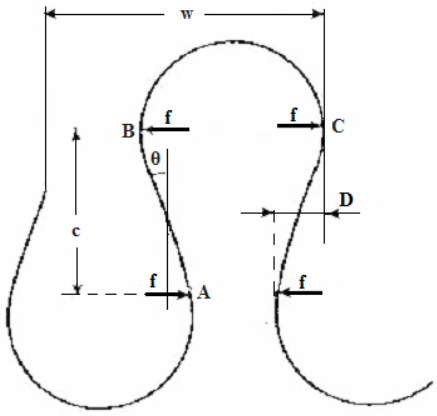

Figure 3-5: The model of Munden for the plain weft knitted structure.

Model of Kawabata

Kawabata (Kawabata 1989a) proposed a geometrical model of the single jersey knitted fabric structure in order to predict the tensile properties of the fabric on the basis of known fabric structure and yarn mechanical properties. The structural model was constructed considering the basic parameters (*c*, *w*), the yarn diameter (D_o) and the yarn diameter at the closest packing state of fibres (D_c). The unit structure that corresponds to the quarter of the loop consists of a circular arc and a straight line. Kawabata provides the loop length in the unit cell under deformation using the basic parameters and the stretch ratios of the unit cell as shown below:

$$\frac{l}{2}=\frac{1}{\lambda_{y1}}\left[\sqrt{\left(\lambda_1 c-\frac{\pi D}{2\sqrt{2}}\right)^2+\left(\frac{\pi D}{2\sqrt{2}}\right)^2}+\frac{\pi D}{\sqrt{2}}\right]+\frac{1}{\lambda_{y2}}\left(\lambda_2\frac{w}{2}+\frac{\pi D}{2\sqrt{2}}\right) \qquad \text{(Eq. 3-15)}$$

where parameters $\lambda_{y1}, \lambda_{y2}, \lambda_1, \lambda_2$ are the stretch ratios of the yarn and the fabric respectively (indices 1, 2 correspond to the wale and course directions); *D*, the yarn diameter in the deformed state. The parameters *c*, *w*, *D* and *l* of Eq. 3-15 can be expressed in mm. If we consider the unit cell without deformation ($\lambda_{y1}, \lambda_{y2}, \lambda_1, \lambda_2$ =1, $D = D_o$) the Eq. 3-16 results in the following equation:

$$\frac{l}{2}=\frac{w}{2}+\frac{3\pi D_o}{2\sqrt{2}}+\sqrt{\left(c-\frac{\pi D_o}{2\sqrt{2}}\right)^2+\left(\frac{\pi D_o}{2\sqrt{2}}\right)^2} \qquad \text{(Eq. 3-16)}$$

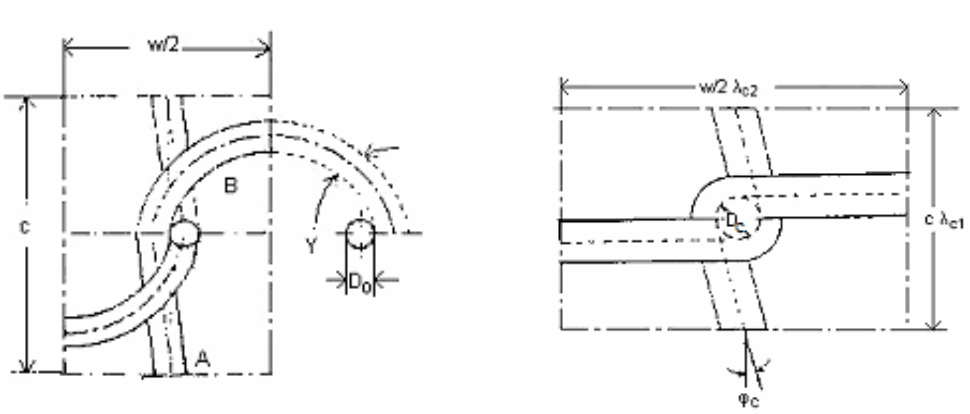

Figure 3-6: The model of Kawabata for the plain weft knitted structure.

Minimum loop length model **(Vassiliadis, Kallivretaki & Provatidis 2007a)**

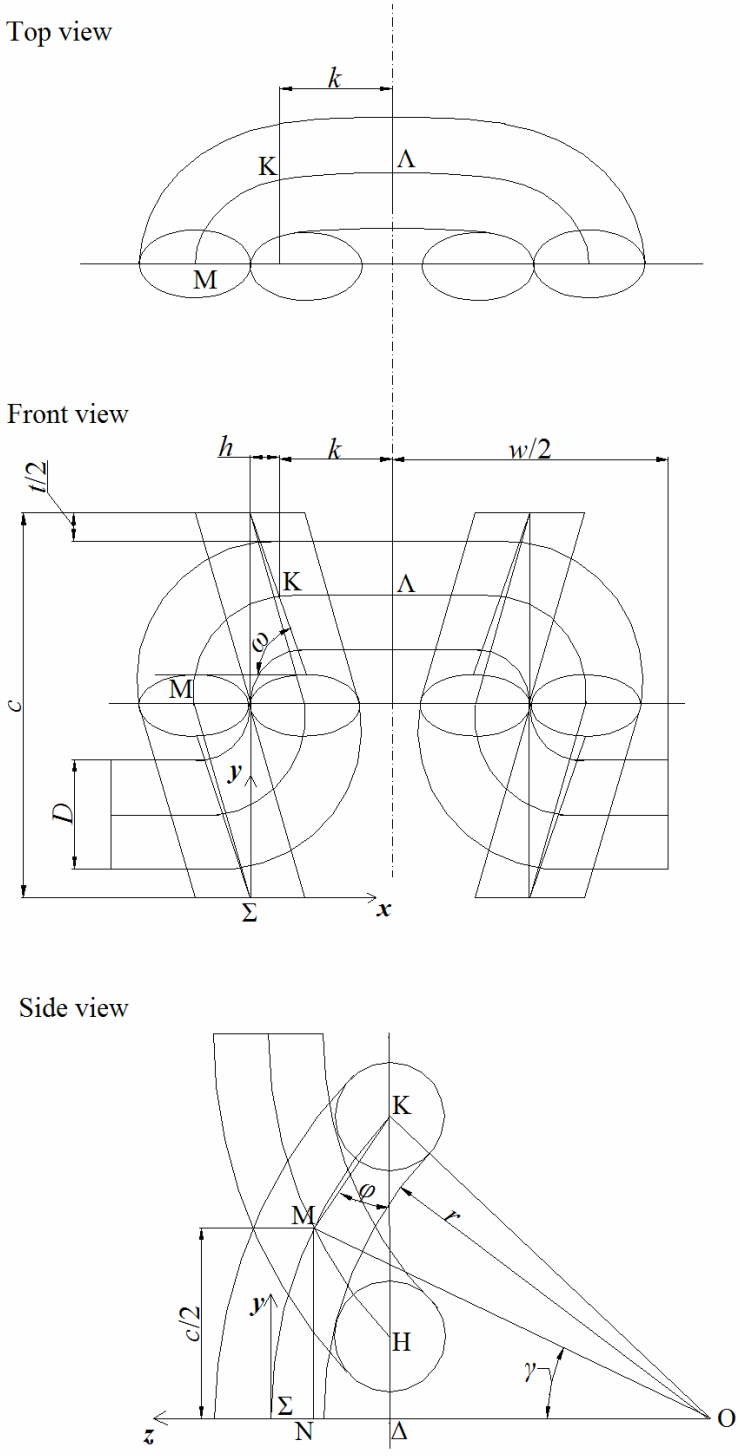

Figure 3-7: Proposed geometrical model of single jersey knitted fabric structure

[c – course spacing, w – wale spacing, D – yarn thickness, t, r, φ, γ, ω and h – geometrical parameters given in Eq. 3-17 – 3-24, Oxyz – Cartesian coordinate system, Σ, M, K and Λ – points of the central axis of the yarn used for the partition of the loop, N, Δ and H – points used for the geometric relationships]

Since the success of the mechanical simulation of the knitted fabrics depends significantly on the accuracy of the geometrical representation of its structure, the unit cell structure was investigated so that a new and more precise model will derive. The technological evolution in the field of computer technology changes the basic aspects of the modelling as well. In the past, with low calculation power available, a simplified model was accepted even with lower accuracy. Today, with the computational power provided by the computers, more precise models are considered even if they are more complex.

The new proposed model results from the improvement in a previously presented one, taking into account the variation in loop length value (Vassiliadis et al. 2005). The model is generated by using the main structural parameters of a single jersey fabric, the course spacing c (or the course density $C=1/c$), the wale spacing w (or the wale density $W=1/w$) and the thickness of the yarn D. The rest of the geometrical parameters required for the complete description of the structure derive analytically from them, either by getting the geometrical benefits of the ideal loop shape or by applying optimization criteria. The estimation of the geometrical parameters has been based on the assumption of the ideal elastic yarn. Thus, the yarns are represented as homogenous cylinders of constant diameter with restricted initial contact area between them.

In addition to the main structural parameters c, w and D, the distance t as observed in Figure 3-7, is initially being considered independent. The others parameters, derived from the geometric relationships, are mentioned below:

$$R = \frac{c}{2} - \frac{t}{2} - \frac{D}{2} \quad \text{, where } 0 \le t \le c - 2D \qquad \text{(Eq. 3-17)}$$

Thus, the parameter R corresponds to the projection of MK on the y-axis. The following Eq. 3-18 and 3-19 are derived from the triangles OΔK and OΔH (Figure 3-7) respectively:

$$(\mathrm{O\Delta})^2 + \left(c - \frac{D+t}{2}\right)^2 = \left(r + \frac{D}{2}\right)^2 \qquad \text{(Eq. 3-18)}$$

$$(\mathrm{O\Delta})^2 + \left(\frac{D+t}{2}\right)^2 = \left(r - \frac{D}{2}\right)^2 \qquad \text{(Eq. 3-19)}$$

The radius (r) is calculated from the Eq. 3-18 and 3-19:

$$r = \left\{\left(c - \frac{D}{2} - \frac{t}{2}\right)^2 - \left(\frac{D}{2} + \frac{t}{2}\right)^2\right\} \Big/ (2D) \qquad \text{(Eq. 3-20)}$$

$$\tan\varphi = \frac{(\mathrm{ON}) - (\mathrm{O\Delta})}{R} = \left(\sqrt{\left(r + \frac{D}{2}\right)^2 - \left(\frac{c}{2}\right)^2} - \sqrt{\left(r - \frac{D}{2}\right)^2 - \left(\frac{D+t}{2}\right)^2}\right) \Big/ R \qquad \text{(Eq. 3-21)}$$

$$\sin\gamma = \frac{0.5c}{r + 0.5D} \qquad \text{(Eq. 3-22)}$$

$$\tan\omega = \frac{c - D\sin\gamma}{D} \quad \text{(Eq. 3-23)}$$

$$k = \frac{w}{4} - \left(\frac{c}{2} - R\right)\cdot\tan\left(\frac{\pi}{2} - \omega\right) \quad \text{(Eq. 3-24)}$$

The total loop can be generated from a quarter of it using the symmetry of the ideal loop shape. Thus, only the central axis of a quarter of the loop (part ΣMKΛ) should be represented. The part ΣMKΛ can be divided into three parts of known mathematical expression curves. The part ΣM is considered as an elliptic arc in the 3D space that can be represented as a circular arc of radius $\left(r + \frac{D}{2}\right)$ in the *yz* plane and a straight line in the *xy* plane. The second part (MK) is also considered as an elliptic arc in 3 dimensions. It is also represented as an arc of the mentioned circle in the *yz* plane and a quarter of an ellipse of minor and major radius $a = \frac{D}{2} + h$ and $b = R$ in the *xy* plane. The third part (KΛ) has been considered as an arc of the same circle in the *yz* plane and a circular arc attached to the curve MK in the *xz* plane.

Thus, the coordinates of the part ΣMKΛ are derived from the following functions:

Part ΣM $\{0 < y < c/2\}$: $x(y) = -\frac{D}{c}y$ (Eq. 3-25)

$$z(y) = \sqrt{(r + D/2)^2 - y^2} - (r + D/2) \quad \text{(Eq. 3-26)}$$

Part MK $\{c/2 < y < c/2 + R\}$: $x(y) = h - a\sqrt{1 - \left(\frac{y - c/2}{b}\right)^2}$ (Eq. 3-27)

$$z(y) = \sqrt{(r + D/2)^2 - y^2} - (r + D/2) \quad \text{(Eq. 3-28)}$$

Part KΛ $\{x(y = c/2 + R) < x < w/4\}$:

$$z(x) = OZ - \sqrt{A^2 - (x - OX)^2} \quad \text{(Eq. 3-29)}$$

$$y(z) = \sqrt{(r + D/2)^2 - (z + r + D/2)^2} \quad \text{(Eq. 3-30)}$$

where

$$OX = w/4 \quad \text{(Eq. 3-31)}$$

$$OZ = \frac{(x_2 - OX)^2 - (x_1 - OX)^2 + z_2^2 - z_1^2}{2z_2 - 2z_1} \quad \text{(Eq. 3-32)}$$

$$A = \sqrt{(x_1 - OX)^2 + (z_1 + OZ)^2} \quad \text{(Eq. 3-33)}$$

The Eq. 3-29 represents the arc of a circle of center $(x, y)=(OX, OZ)$ and radius *A*, when two points of the circle (x_1, z_1) and (x_2, z_2) are known. This circle was considered attached to the

projection of the curve MK in the *xz* plane. Consequently, the two mentioned points have to be selected from the part of the curve MK, where circle is considered attached. Thus, the two points are derived from the Eqs 3-27 and 3-28 for $y_1 = c/2+R-0.001$, $y_2 = c/2+R$.

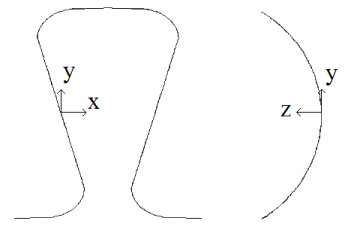

Figure 3-8: Proposed model, central axis of the loop

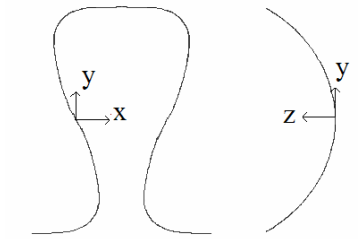

Figure 3-9: Central axis of the loop for the optimised model

The central axis of a loop formed according to the above model is shown in Figure 3-8 and an optimized model resulting from the replacement of the part ΣM of a B-Spline is given in Figure 3-9 for the same parameters (*c*, *w*, *D*, *t*). The B-Spline is generated trough the control points Σ, M, tangential to the vector $\left(\frac{D}{2}, -\frac{c}{2}, 0\right)$ at the point Σ and tangential to the vector $\left(0, \frac{c}{2}, -\frac{0.5c}{\tan(0.5\pi - \gamma)}\right)$ at the point M.

The value of the parameter *t*, temporarily considered as independent, results from a repeated calculation process. For every value of the parameter *t*, belonging in the field [0, (*c*-2*D*)], the central axis of the loop is generated and the loop length *l* is calculated. The calculations are performed using the related developed programming code within the ANSYS FEA software. By considering the elastic behaviour of the yarn while forming the loop, the selected value for the parameter *t* is the one that corresponds to the minimum loop length $l_{\min}$. For the calculation purposes, the values of the distance *t* start from zero and in steps of magnitude, depending on the accuracy required increases to its final value.

The method of modelling presented applies optimisation criteria by the assumption of the elastic energy minimization of the yarns composing the relaxed fabric. The relaxation of the yarns from the remaining stresses is accompanied by the minimization of the existing deformations. Thus, the elongation of the yarns imposed by the knitting machine during the fabric production is minimized. During relaxation the adjacent yarns slide over each other until the minimum elastic energy structure will appear.

The Table 3-1 contains only the main structural parameters, the dependant parameter *t* and the loop length *l* derived from the optimised model. As it can be seen there is only one value for the parameter *t* that corresponds to the minimum value of the loop length.

Table 3-1: Loop length as a function of distance *t*

[Course spacing= 0.50 mm; Wale spacing= 0.60 mm; Yarn thickness= 0.14 mm; and Maximum distance *t*= 0.22 mm]

Distance (t) mm	Loop length mm
0.00	2.550
0.02	2.513
0.04	2.479
0.06	2.446
0.08	2.416
0.10	2.388
0.12	2.365
0.14	2.346
0.16	**2.335**
0.18	2.337
0.20	2.366
0.21	2.407
0.22	2.624

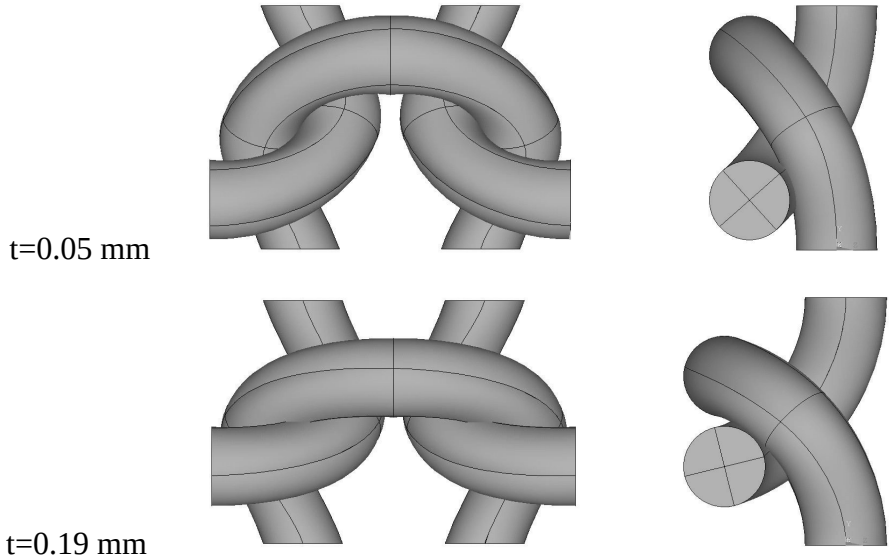

Figure 3-10: Solid models of a plain weft knitted structure for varying distance *t*.

Evaluation of the models

The proposed model was based on certain considerations such as the energy minimization. The application of the proposed model on the cotton grey fabrics is supported since the model was based on the assumption of the relaxation of the fabric in its grey state. The application on the finished fabrics is also acceptable assuming that the particular finishing does not introduce considerable strains and elongation in the fabrics yarns. For the evaluation of the geometrical model, the experimentally measured loop length of a given fabric was compared to the respective length calculated by the geometrical models generated for the same main parameters (*c*, *w*, *D*). As reference test set data, a part of the Fletcher and Roberts was chosen (Leaf, Glaskin 1955). The set data was also used by Leaf and Glaskin for the evaluation of their equations for loop length. The evaluation indicated the approximate equations [Eqs 3-19, 3-20] as the more accurate equations, especially for the fabrics produced using cotton yarns than the initial equations. The 46 selected samples produced by cotton yarns were selected in order the approximate equations of Leaf and Glaskin to be used. Since the yarn thickness was not given by them, it was calculated from the curve of the linear density versus thickness of the yarn. The related graph derived after extended laboratory measurements on ring-spun yarns manufactured under controlled conditions for the specific purpose. Figure 3-11 shows the experimental curves correlating the linear density and the thickness of a yarn for three values of twist multiplier (a_e=3, 3.5, 4). The mean curve was used for the particular estimation of the yarn thickness. Table 3-2 shows the data set of the 46 samples, constituted of cotton grey (samples 1 – 6) and finished (samples 7 – 46) fabrics.

The loop length of the 46 samples was calculated according to the methodology of six models and compared to the reference value of the laboratory measurements. The calculated values of loop lengths are presented in the Table 3-3. The difference between the calculated loop lengths and the measured ones, expressed as error (%), is considered as an indication of the accuracy of the geometrical models (Table 3-4). The knitted fabric loop length as the criterion of the accuracy of the models is convenient since it can be easily measured. The mean error, the maximum error and the standard deviation of the error values for each model were calculated and used for evaluation (Table 3-5). Although these three values have no direct physical meaning, they support the overall evaluation of the accuracy and the reliability of the models.

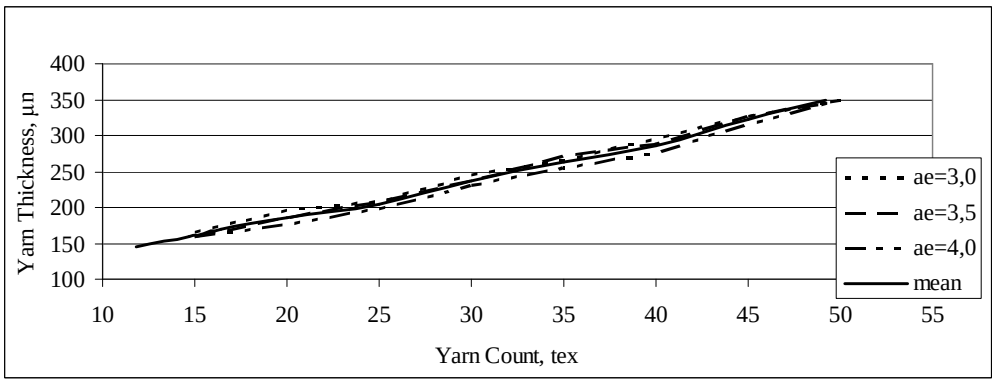

Figure 3-11: Experimental curves of yarn thickness vs. yarn linear density.

Table 3-2: Main parameters and measured loop lengths of the samples

Sample	Yarn count Ne	Course density courses/inch	Wale density wales/inch	Yarn thickness mm	Loop length mm
1	1/30	26.6	32.6	0.190	3.912
2		31.2	34.4		3.416
3		35.5	34.2		3.122
4		37.9	33.8		3.040
5		40.9	33.9		2.926
6		44.8	36.7		2.746
7		26.9	31.5		3.866
8		32.6	33.0		3.432
9		37.2	34.1		3.109
10		41.6	36.7		2.972
11		42.9	37.0		2.870
12		48.2	37.1		2.715
13	1/12	18.6	21.5	0.330	5.664
14		20.6	22.5		5.187
15		23.9	23.3		4.836
16		28.4	23.4		4.315
17	1/20	17.7	24.7	0.235	5.364
18		20.6	24.3		4.968
19		23.6	26.4		4.470
20		27.9	28.1		4.001
21		29.2	29.1		3.830
22	1/28	22.8	33.8	0.195	4.064
23		25.2	34.4		3.889
24		30.2	36.2		3.500
25		34.9	36.1		3.167
26		37.9	38.2		3.101
27		41.5	39.4		2.898
28	1/36	22.7	35.7	0.179	4.171
29		25.4	37.8		3.777
30		30.2	37.4		3.449
31		33.1	37.5		3.292
32		35.3	38.0		3.084
33		40.5	37.7		2.791
34	1/40	27.9	38.7	0.165	3.510
35		32.9	41.0		3.073
36		34.3	41.1		3.005
37		37.9	42.5		2.860
38		43.0	42.3		2.629
39		45.9	43.4		2.530
40	1/50	27.9	43.0	0.150	3.449
41		32.6	41.8		3.211
42		35.6	41.3		2.946
43		38.2	43.5		2.743
44		42.0	45.4		2.606
45		46.6	44.4		2.479
46		49.9	45.9		2.337

Table 3-3: Calculated loop lengths

Sample	Loop length, mm					
	Chamberlain	Peirce	Leaf & Glaskin	Munden	Kawabata	New model
1	3.240	3.818	3.677	7.174	3.592	3.710
2	3.071	3.495	3.309	5.473	3.282	3.373
3	3.089	3.302	3.104	4.419	3.103	3.172
4	3.125	3.220	3.027	3.973	3.028	3.087
5	3.116	3.120	2.936	3.516	2.938	2.984
6	2.878	2.955	2.766	3.046	2.786	2.816
7	3.354	3.823	3.677	7.037	3.599	3.713
8	3.201	3.457	3.267	5.087	3.248	3.331
9	3.098	3.239	3.042	4.095	3.045	3.107
10	2.878	3.042	2.839	3.422	2.862	2.905
11	2.855	2.999	2.799	3.260	2.824	2.862
12	2.847	2.867	2.696	2.721	2.711	2.728
13	4.913	5.873	5.534	8.969	5.509	5.611
14	4.695	5.555	5.183	7.578	5.210	5.328
15	4.534	5.176	4.787	5.965	4.863	4.939
16	4.514	4.834	4.493	4.563	4.570	4.591
17	4.277	5.294	5.231	12.447	5.000	5.183
18	4.347	4.907	4.747	9.555	4.624	4.776
19	4.001	4.511	4.301	7.573	4.240	4.365
20	3.759	4.121	3.873	5.726	3.870	3.962
21	3.630	4.008	3.753	5.314	3.764	3.847
22	3.125	4.138	4.070	9.191	3.897	4.038
23	3.071	3.913	3.790	7.727	3.679	3.802
24	2.918	3.542	3.353	5.680	3.323	3.417
25	2.926	3.317	3.102	4.470	3.114	3.184
26	2.765	3.164	2.938	3.910	2.970	3.026
27	2.681	3.027	2.799	3.384	2.846	2.886
28	2.959	4.013	4.003	9.880	3.787	3.935
29	2.795	3.735	3.665	8.114	3.516	3.641
30	2.825	3.425	3.274	6.025	3.217	3.316
31	2.817	3.275	3.100	5.161	3.075	3.160
32	2.780	3.171	2.984	4.636	2.976	3.052
33	2.802	2.991	2.799	3.703	2.811	2.866
34	2.730	3.457	3.376	7.320	3.256	3.369
35	2.577	3.144	3.004	5.514	2.952	3.043
36	2.570	3.079	2.928	5.138	2.891	2.976
37	2.486	2.918	2.746	4.348	2.738	2.809
38	2.497	2.762	2.579	3.534	2.594	2.647
39	2.434	2.672	2.487	3.181	2.511	2.555
40	2.457	3.302	3.279	7.860	3.115	3.255
41	2.527	3.057	2.957	5.994	2.877	2.995
42	2.558	2.933	2.807	5.155	2.758	2.843
43	2.428	2.805	2.664	4.575	2.634	2.710
44	2.327	2.660	2.503	3.904	2.497	2.560
45	2.379	2.553	2.393	3.291	2.399	2.449
46	2.301	2.462	2.300	2.947	2.315	2.356

Table 3-4: Error of calculated loop lengths

Sample	% error of loop length					
	Chamberlain	Peirce	Leaf & Glaskin	Munden	Kawabata	New model
1	17.16	2.41	6.01	83.39	8.18	5.15
2	10.11	2.31	3.13	60.21	3.92	1.27
3	1.05	5.79	0.58	41.57	0.61	1.62
4	2.80	5.92	0.45	30.67	0.40	1.55
5	6.50	6.62	0.35	20.16	0.40	1.98
6	4.83	7.61	0.73	10.95	1.46	2.57
7	13.25	1.10	4.89	82.03	6.92	3.96
8	6.71	0.73	4.78	48.23	5.35	2.92
9	0.36	4.18	2.15	31.71	2.07	0.07
10	3.14	2.36	4.48	15.16	3.69	2.23
11	0.53	4.50	2.49	13.58	1.61	0.29
12	4.87	5.59	0.72	0.22	0.17	0.46
13	13.26	3.68	2.29	58.35	2.74	0.94
14	9.48	7.10	0.07	46.10	0.44	2.73
15	6.25	7.02	1.01	23.33	0.55	2.12
16	4.61	12.03	4.11	5.73	5.90	6.39
17	20.27	1.31	2.49	132.04	6.80	3.39
18	12.50	1.23	4.46	92.32	6.92	3.87
19	10.49	0.90	3.80	69.41	5.15	2.36
20	6.03	3.00	3.17	43.14	3.27	0.97
21	5.23	4.65	2.02	38.74	1.74	0.42
22	23.10	1.82	0.16	126.16	4.10	0.64
23	21.03	0.61	2.54	98.69	5.40	2.22
24	16.63	1.20	4.22	62.27	5.06	2.37
25	7.61	4.74	2.06	41.12	1.70	0.51
26	10.83	2.01	5.28	26.08	4.24	2.44
27	7.49	4.45	3.41	16.77	1.80	0.42
28	29.05	3.79	4.02	136.90	9.20	5.66
29	26.01	1.11	2.95	114.83	6.91	3.60
30	18.11	0.72	5.09	74.66	6.74	3.88
31	14.42	0.50	5.84	56.78	6.59	4.00
32	9.85	2.83	3.24	50.35	3.48	1.03
33	0.38	7.16	0.28	32.64	0.70	2.66
34	22.24	1.51	3.82	108.52	7.25	4.01
35	16.17	2.29	2.26	79.41	3.94	0.99
36	14.46	2.47	2.57	71.00	3.79	0.97
37	13.09	2.03	4.00	52.02	4.27	1.79
38	5.00	5.06	1.88	34.43	1.34	0.68
39	3.79	5.62	1.69	25.75	0.75	0.98
40	28.78	4.26	4.94	127.88	9.70	5.63
41	21.28	4.78	7.89	86.70	10.39	6.71
42	13.19	0.46	4.73	74.95	6.39	3.52
43	11.47	2.24	2.89	66.77	3.97	1.20
44	10.71	2.07	3.94	49.81	4.20	1.75
45	4.03	2.99	3.46	32.77	3.24	1.20
46	1.51	5.38	1.58	26.12	0.95	0.83

Table 3-5: Evaluation of the models

Model	Mean error %	Maximum error %	Standard deviation
Chamberlain	11.08	29.05	7.72
Peirce	3.52	12.03	2.45
Leaf & Glaskin	3.02	7.89	1.78
Munden	56.97	136.90	35.77
Kawabata	4.01	10.39	2.75
proposed model	2.33	6.71	1.71

The new proposed model corresponds to the lower values of the error and hence it is considered as the more accurate one. Its accuracy guarantees the success of the mechanical simulation of the knitted fabrics. The computational load of the repeated process used for the loop representation is not important nowadays, even for a common personal computer. Under these conditions, the new proposed model can be considered as a successful approach to the computational representation of the single jersey knitted fabric structure. A precise computational representation of the structure guarantees the minimization of the error in the step of the mechanical analysis in the frame of computer aided engineering tools.

3.2.3 The geometrical modelling of weft knitted structures

The generality of the geometrical modelling method applied in the plain weft knitted structure was proved by the implementation in two more weft knitted structures produced by cotton yarns, rib 1×1 and interlock. The basic design parameters are demanded in the proposed technique for the generation of the 3D meso-scale model. Actually the technique comprises the generation of the possible geometrical models for the defined design parameters and the final selection of the optimum one. The minimum loop length model is assumed the minimum elastic energy model and thus it is selected as the optimum one.

The applied assumption was evaluated by the mechanical analysis of the generated models. The Finite Element Method was implemented for the mechanical analysis of the solid structural models. In continue the proposed technique was evaluated by the comparison of the values of the loop length of existing samples measured in the laboratory with the predicted values resulting from the proposed technique. The modelling and simulations were performed using the ANSYS software.

Representation of the 3D models

The design parameters of the proposed technique correspond to the main structural parameters of the knitted structures: the course-spacing (c) the wale-spacing (w) and the thickness

(apparent diameter) of the yarn (*D*). The main structural parameters and one (*t*, for plain weft and rib 1×1) or two (*t* and *dh*, for interlock) secondary parameters are adequate for the generation of the model. The range of values of the secondary parameters results from the principle geometric considerations of the unit cells. The other geometrical parameters required for the complete description of the structure derive analytically from them. The generated geometry was based on the assumption of the ideal elastic yarn. Thus the yarns are represented as homogenous cylinders of constant diameter, with initial restricted contact area between them. The geometrical models that correspond to the repeated structural unit of single jersey (a), double jersey (b) and interlock (c) are presented in the Figure 3-12. The main and the secondary parameter(s) are shown in these figures.

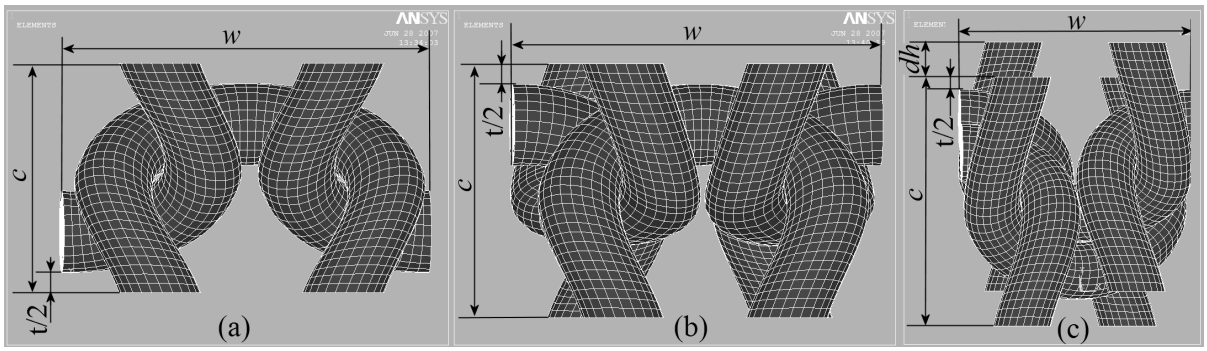

Figure 3-12: Unit cell of (a) plain weft knitted, (b) rib 1×1, (c) interlock.

Rib 1×1 (Vassiliadis, Kallivretaki & Provatidis 2006b)

The representation of the unit cell of the rib 1×1 considering the front view (1a), the side view (1b) and the top view (1c) are given in the Figure 3-13. The eq. 3-17, 3-20, 3-22, 3-23 and 3-24 given before are also used for the geometrical representation of the rib 1×1 structure. It is considered that the geometry of the unit cell consists of four repeated parts: $l_1 \equiv l_4, l_2, l_3$ and l_5. The part l_1 or l_4 defines a linear part projected in the *xy* plane and a circular arc of γ degrees and radius r projected in the *yz* plane. The part l_2 defines a part of ellipsis projected in the *xy* plane and circular arc of r radius projected in the *yz* plane. The part l_3 is linear and the part l_5 is represented by a spline. Essential assumption for the geometrical representation is the limited contact area at the point B. Thus before the representation of the spline, the parts l_1, l_2, l_3, l_4 are produced, the distance AB is calculated and the anti-symmetric parts derive. The spline l_5 connects the two l_4 parts. The slope of the spline at the starting and ending point in the *yz* plane is defined by the angle γ as shown in Figure 3-13.

The value of the parameter t, which was temporarily considered as independent, can be defined from a repeated calculation process. For every value of the parameter t, belonging in the field $[0,(c-2D)]$, the central axis of the loop is generated and the loop length l is calculated. The selected value for the parameter t is the one that corresponds to the minimum loop length $l_{\min}$.

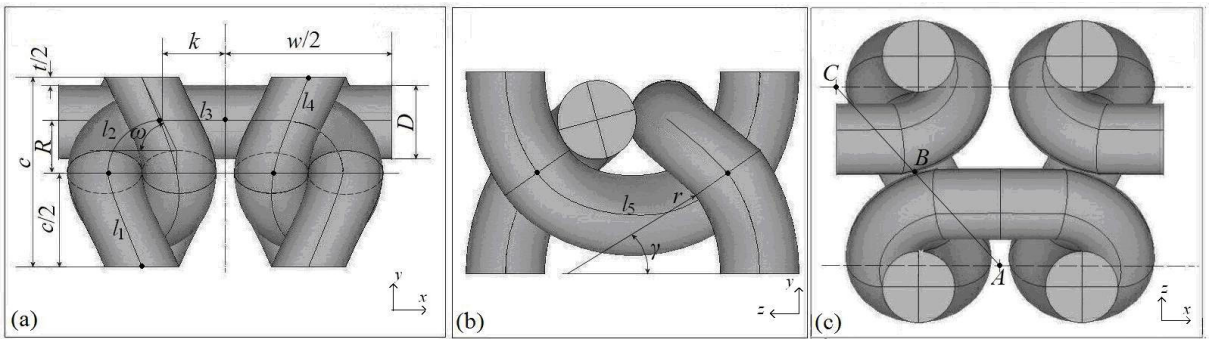

Figure 3-13: Representation of the unit cell of the rib 1×1 structure

***Interlock* (Vassiliadis, Kallivretaki & Provatidis 2006a)**

In Figure 3-14 are shown the front view (a), the side view (b) and the top view (c) of the geometrical model that corresponds to the half (due to symmetry) of the repeated structural unit of the interlock. The eq. 3-17, 3-20, 3-22, 3-23, 3-24 and 3-34 given before are also used for the geometrical representation of the rib 1×1 structure.

$$e = \sqrt{D^2 - dh^2} \qquad \text{(Eq. 3-34)}$$

It is considered that the geometrical structure of the unit cell consists of five repeated parts: l_1, l_2, l_3, l_4 and l_5. In the above figure are shown the parts l_1 (Figure 3-14e), l_2 and l_3 (Figure 3-14d) as well as l_4 and l_5 (Figure 3-14f). The part l_1 defines a linear part projected in the *xy* plane and a circular arc of γ radians and radius r projected in the *yz* plane. The part l_2 defines a part of ellipsis projected in the xy plane and circular arc of radius r projected in the *yz* plane. The part l_3 is linear and the parts l_4 and l_5 are represented by splines. The spline l_4 connects the l_1 parts. The slope of the spline at the starting and ending point in the yz plane is defined by the angle γ. The spline l_5 connects two l_1 parts and it is tangent to the l_4 part. The slope of the spline l_5 at the starting and ending point in the *yz* plane is defined by the angle γ.

The value of the parameters t and *dh* which were temporarily considered as independent, can be defined from a repeated calculation procedure. For every value of the parameter t and *dh* belonging in the fields $[0,(c-2D)]$ and [0, *D*] respectively, the central axis of the loop is generated and the loop length l is calculated. By considering the elastic behaviour of the yarn while forming the loop, the selected values for the parameter t, *dh* are those that correspond to the minimum loop length $l_{\min}$.

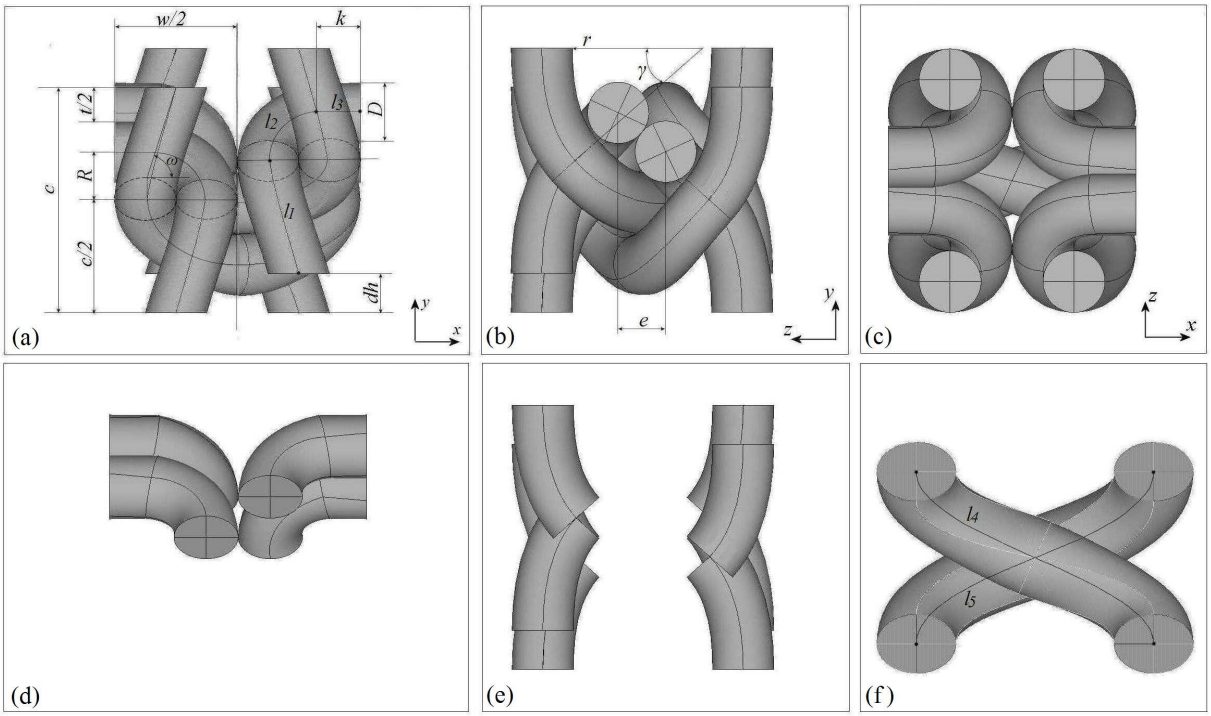

Figure 3-14: Representation of the half repeated structural unit of interlock.

An iterative calculation process was used for the generation of the final model. Several models are generated using the main structural parameters and stepped selected values in the defined range for the secondary parameters. The model corresponding to the minimum yarn length is selected as the final one.

Elastic Energy Minimization Assumption

The assumption applied for the selection of the minimum elastic energy structure was evaluated by the mechanical analysis of the generated structures **(Blaga, Kallivretaki, Vassiliadis & Provatidis 2007)**. Thus the identification of the minimum elastic energy model with the minimum loop length model was examined. The evaluation was based on the comparison of the energy absorbed by several structures for the same deformation of the unit cell. The biaxial tensile deformation up to a constant extension value of the unit cell of each structure was simulated in ANSYS software. The structure absorbs the higher value of energy corresponds to the minimum elastic energy structure.

The Finite Element Method with contact phenomena **(Vassiliadis, Kallivretaki & Provatidis 2007c)** was implemented for the mechanical analysis of the biaxial test. The yarns are represented as homogenous cylinders. Transverse isotropic properties were considered for the yarn material. The transverse isotropic properties describe the different elastic properties along the yarn axis direction and the radius direction approaching the non-homogenous behaviour of the yarn. Considering the local coordinate system *xyz* of the yarn where the *z* axis corresponds to the longitudinal yarn axis and the plane *xy* corresponds to the yarn cross-

section, the elastic parameters of the yarn are assumed as having the values: $E_x = E_y = 10$ N/mm^2, $E_z = 800$ N/mm^2, $\nu_{xy} = 0.30$, $\nu_{xz} = \nu_{yz} = 0.30$, $G_{yz} = G_{xz} = 5$ N/mm^2 and $G_{xy} = 0.5 \cdot E_{xy} / (1 + \nu_{xy})$. The considered boundary conditions serve mainly two requirements **(Kallivretaki, Blaga, Vassiliadis & Provatidis 2007)**. The symmetrical deformation that results from the geometrical symmetry is the first requirement. The continuity of the deformed unit cells, by their adjacency, is the second requirement.

The selected models for simulation derived from given values of main parameters and selected values of secondary parameters are shown in Figure 3-15. The Table 3-6 presents the energy absorbed for the biaxial tensile deformation of each unit cell. The higher amount of energy is absorbed by the minimum loop length model in each knitted structure. Thus the identification of minimum loop length and minimum elastic energy structure is proved assumption.

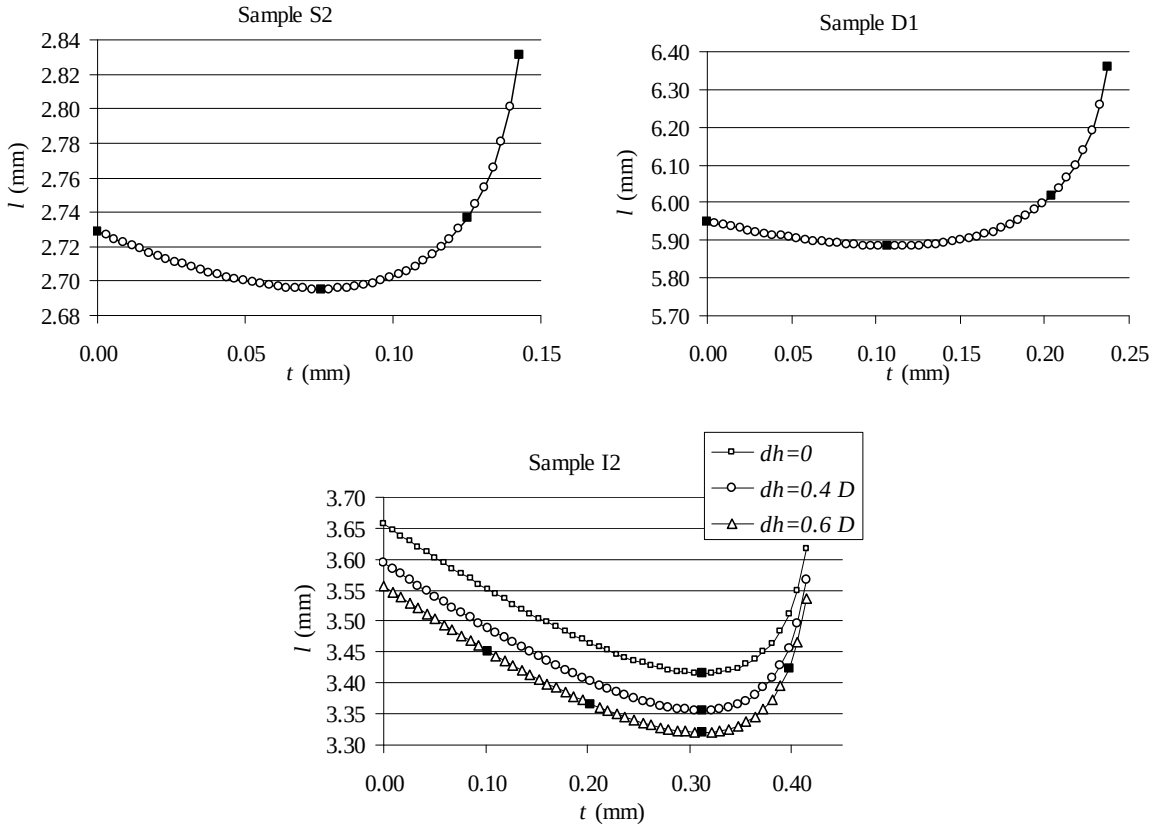

Figure 3-15: Models of weft knitted fabrics selected for the simulation of biaxial deformation.

Table 3-6: Energy absorbed for the biaxial tensile deformation of the unit cell of selected models.

	Model	*l* (mm)	Absorbed energy (N/mm)
S2	S2_1	2.729	1.79E-04
	S2_2	**2.695**	**9.37E-04**
	S2_3	2.737	7.98E-04
	S2_4	2.832	3.38E-04
D1	D1_1	5.950	1.98E-04
	D1_2	**5.884**	**8.56E-04**
	D1_3	6.016	6.55E-04
	D1_4	6.361	4.17E-04
I2	I2_1	3.415	1.54E-03
	I2_2	3.355	1.77E-03
	I2_3	**3.321**	**1.96E-03**
	I2_4	3.452	1.40E-03
	I2_5	3.366	6.73E-04
	I2_6	3.423	9.41E-04

For the evaluation of the proposed technique, 3 samples per knitted structure produced by cotton yarns were used. The structural parameters of the selected samples are shown in Table 3-7. The evaluation was based on the comparison of the values of the loop length measured in laboratory with the predicted values according to the proposed technique. The mean value of the absolute error of the predicted values represents an indication of the accuracy of the geometrical model.

A generic technique was proposed for the definition of the geometrical characteristics of the typical knitted structures produced by cotton yarns. The proposed technique comprises the generation of a series of models and the selection of the one that corresponds to the minimum loop length. The correlation of the loop length with the initial energy is proved by the mechanical analysis of representative models belonging in the generated series. The modelling technique was evaluated by the comparison of the structural characteristics (loop length) of the models with the experimental values. The proposed modelling demonstrates satisfying accuracy according to the estimated error in the resulted value of the loop length.

Table 3-7: Evaluation of the proposed meso-scale models of weft knitted fabrics.

sample	fabric type	course density (courses per cm)	wale density (wales per cm)	loop density CxW (loops/cm²)	yarn thickness (mm)	measured loop length (mm)	calculated loop length (mm)	absolute error (%)
S1	single jersey	16.29	10.35	168.6	0.241	3.473	3.288	5.33
S2		19.40	11.98	232.4	0.185	2.795	2.695	3.58
S3		20.30	14.01	284.4	0.177	2.634	2.503	4.97
D1	double jersey	14.65	10.00	146.5	0.220	5.824	5.885	1.05
D2		16.32	11.00	179.6	0.227	5.742	5.680	1.08
D3		19.02	10.60	201.6	0.236	5.690	5.505	3.25
I1	interlock	10.42	13.60	141.7	0.183	3.904	3.671	5.99
I2		12.65	13.60	172.0	0.184	3.368	3.321	1.42
I3		15.05	14.80	222.7	0.168	3.121	2.852	8.65
				Mean error of calculated loop length:				3.93

3.2.4 The geometrical modelling of warp knitted structures

In the warp knitting technology, warp yarn is introduced in the longitudinal fabric direction. The characteristic feature of the warp knitted structure is the formation of adjacent loops in the course direction by the separate warp. Usually the basic lapping structures are used in combination producing more than one warp sheet. The considered structure, Charmeuse or Locknit, is a combination of tricot and 2×1 plain stitches. Thus two guide bars are used for the manufacturing of the structure under consideration.

Warp knitted fabrics have a limited range of applications in apparel fabrics and household textiles. However, their continuously widespread use in technical applications attracts increasing research interest. The technological advantages of warp knitted fabrics as formability, contourability, dynamic mechanical properties along with easy and rapid manufacturability are essential reasons for their establishment in composite manufacturing. Nowadays the warp knitted structures produced by high performance fibres made from glass or carbon are used for composite reinforcement. The increasing requirements of the industry for high performance technical textiles demand an accurate definition of their properties. Thus realistic modelling and mechanical analyses of warp knitted structures are of great importance.

Several research studies were reported concerning the mesomechanical analysis of the basic warp knitted structures. The geometrical representation of the structure comprised obviously the starting point for the researchers. The representations were based mainly on the division of the loop configuration into discernible parts as loop’s head and arms, root of the loop and

underlapping sections. Depending on the approach and complexity, two- and three-dimensional models were proposed including or ignoring the loop inclination. Convenient geometrical shapes as straight lines and circular parts and in some cases complicated geometries based on empirical assumptions were used for the representation of the defined partitions (Dalidovici 1940, Allison 1958, Grosberg 1964, Korlinski 1981, Raz 1987, Vékássy 1960). There was a different approach proposed by Grosberg based on the elastica theory. According to his approach, the loop configuration results from the forces applied to the yarn at the base of the loop (Grosberg 1964). Some authors proposed algebraic equations for the calculation of the yarn loop length according to the proposed geometrical models. A relative accurate equation for the yarn consumption was proposed by Dalidovici for the two guide bars warp knitted structures (Dalidovici 1940).

The difficulties of applying the analytical methods in textile modelling in conjunction to the introduced simplifications and the continuous development of the computer technology led to the numerical modelling and simulation (Goktepe, Harlock 2002, Goktepe 2001). The geometrical complexity of the multiple guide bar warp knitted structures impedes the accurate representation using analytical geometrical equations. In contrast, the interpolation techniques for areal and spatial representations provided by the modern CAD software codes are special facilities for the realistic design of complex structures. Several numerical methods were developed for the representation of the freeform curves and surfaces. These methods use piecewise polynomial curves (splines), including interpolating spline, rational and non-uniform rational basis-spline (NURBS) and Bézier curves. Modelling advantages as flexibility in smooth freeform representations, numerical stability, algorithm accuracy and memory sparing in storing shapes support and impose the use of splines in CAD systems. The proposed modeling approach was carried out using the ANSYS software.

Used samples

Twelve samples of Charmeuse structure were examined for this research activity **(Kallivretaki, Vassiliadis, Blaga & Provatidis 2007a,b,c)**. They were produced by a 12-filament polyamide flat yarn: PA6 44/12 dtex. The samples are of different structural parameters in order a generalized geometrical modelling to be achieved. The single fibre thickness was calculated by the microscopic observation equal to 12 μm. The structural characteristics of the samples are given in the Table 3-8.

Table 3-8: Structural data of the samples

Knitting Machine	Sample	Course Density (courses/cm)	Wale Density (wales/cm)	Yarn consumption Bar 1 (mm/rack)	Yarn consumption Bar 2 (mm/rack)
	A1	20.69	14.79	1760	1360
	A2	21.69	15.48	1640	1240
HKS 28E	A3	23.42	16	1560	1160
K. Mayer	A4	25.7	16.44	1500	1100
	A5	26.97	18.09	1450	1050
	A6	28.49	17.11	1420	1020
	B1	18.92	14.9	1960	1480
	B2	22.58	12.55	1780	1300
Copcentra	B3	22.4	15.8	1640	1200
32E Liba	B4	23.45	16.48	1580	1150
	B5	24.51	18	1500	1100
	B6	25.35	18.12	1460	1060

Image processing

The microscopic observation of the structure and the processing of the received digital images constituted the first stage for the modelling procedure. Main purpose of the current stage was the understanding and tracing of the yarns orientation within the structure. The projection of the loop formation in the plane of the fabric resulted from the study of the corresponding images (Figure 3-16a). The cross-sectional images offered significant information for the 3D representation of the structure. Figure 3-18 b and 1c present the cross-section of a sample vertical to the courses and wales respectively.

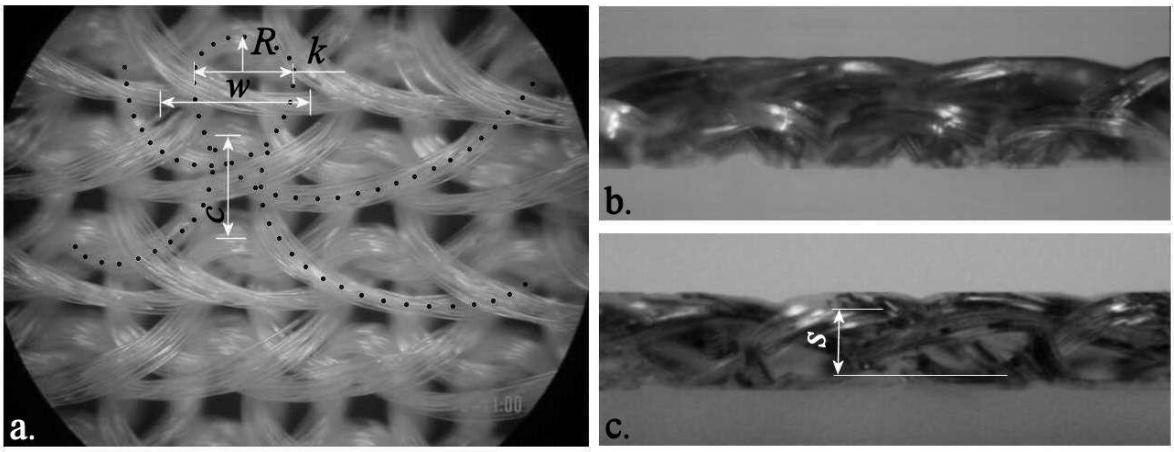

Figure 3-16: Microscopic observation and image processing of warp knitted samples.

The definition of the minimum number of the structural parameters required for the representation is essential. 9 parameters were defined for the preliminary 3D representation as follows:

c: course spacing

w: wale spacing

B_1: yarn consumption/2 rows of Bar 1

B_2: yarn consumption/2 rows of Bar 2

D_p: yarn thickness in the plane of the fabric

D_t: yarn thickness along the thickness of the fabric

k: maximum distance between the loop arms

R: minimum radius of the loop head

s: distance of projection of the loop along thickness

The above parameters are divided into two categories, the main and the secondary parameters. The parameters *c*, *w*, B_1, B_2 resulted from the structural data given in Table 3-8 (macroscopically defined) and thus they are considered as main parameters. The yarn thicknesses were also considered as main parameters since they resulted from the structural characteristics of the yarn (yarn type, number of filaments and filament thickness). The parameters *k*, *R* and *s* constitute the secondary parameters set since their values resulted from the microscopic observation of the structure.

For the predictive modelling of the fabric microstructure is desirable the representation to be based on the main structural parameters. Thus it is essential to estimate the values of the secondary parameters using certain assumptions or functions. The influence of the secondary parameters in the microstructure formation was studied by the correlation of the main – secondary parameters. The values of the main and the secondary parameters were recorded for the 12 samples and their geometrical correlation was expressed as ratios useful for the geometrical representation of the loop. The value of the thickness D_p was calculated for the samples belonging to the range 0.10 – 0.14 mm. The variance is prospective for the type of the yarn. Thus the value 0.12 mm was assumed for D_p. The ratio D_p/D_t resulted approximately equal to 2. Thus the value 0.06 mm was assumed for D_t. Table 3-9 presents the noticeable investigated ratios.

Table 3-9: Correlation of secondary – main parameters.

Sample	Parameters					Ratios		
	w (mm)	c (mm)	R (mm)	k (mm)	s (mm)	$\frac{c/2}{R+D_p/2}$	$\frac{k+2\cdot D_p}{w}$	s/c
A1	0.6762	0.4834	0.167	0.421	0.160	1.067	0.978	0.331
A2	0.6461	0.4610	0.157	0.387	0.236	1.061	0.971	0.511
A3	0.6250	0.4270	0.145	0.385	0.172	1.043	1.000	0.402
A4	0.6084	0.3892	0.111	0.334	0.176	1.135	0.944	0.452
A5	0.5529	0.3708	0.115	0.281	0.178	1.059	0.942	0.480
A6	0.5844	0.3510	0.128	0.338	0.140	0.932	0.989	0.398
B1	0.6711	0.5285	0.204	0.539	0.200	1.003	1.161	0.379
B2	0.7969	0.4429	0.182	0.638	0.154	0.915	1.101	0.348
B3	0.6329	0.4464	0.140	0.401	0.173	1.115	1.012	0.388
B4	0.6068	0.4264	0.144	0.389	0.175	1.045	1.037	0.409
B5	0.5556	0.4080	0.138	0.359	0.198	1.030	1.079	0.486
B6	0.5519	0.3945	0.112	0.342	0.124	1.149	1.055	0.315

The investigated ratios introduced certain assumptions for the representation of the warp knitted structure.

$$R = c/2 - D_p/2 \quad \text{(Eq. 3-35)}$$

$$k = w - 2D_p \quad \text{(Eq. 3-36)}$$

$$s/c = 0.3\sim0.5 \quad \text{(Eq. 3-37)}$$

3D Geometrical Representation

Six main structural parameters were used: the wale spacing w (mm), the course spacing c (mm), the yarn loop length of the front B_1 (mm/2 rows) and the back guide bar B_2 (mm/2 rows) and two values of the yarn thickness along the fabric plane D_p (mm) and the fabric thickness D_t (mm). The values of B_1 and B_2 resulted from the measurement of the yarn consumption. The values of c, w, D_p and D_t resulted from the microscopic observation of the samples and the respective image processing. One secondary parameter was also defined, the distance s (mm).

The total loop formation is represented by two sections. The first section, defined as main loop corresponds to the model shown in Figure 3-17a. The parameter l_m is used for the length of the main loop (Figure 3-17a). The second section, defined as connecting part, corresponds to the underlap and the inclined part of the loop's arms. The parameters l_{c1}, l_{c2} are used for

the lengths of the connecting parts of the front and the back bar yarn respectively (Figure 3-17c,d,f,g).

An iterative procedure was used for the generation of the geometrical model using the main structural parameters. The front and the back loop were firstly designed. The structural characteristics of the double loop are shown in Figure 3-17a. Elliptical shape was supposed for the yarn cross-sections (with D_p and D_t the major and the minor ellipsis diameters respectively).

The central axis of each loop is formed by a cubic Spline defined by the control points 1,2,3,4,5. The cubic Spline interpolation is a piecewise continuous curve passing through each of the control points. The orientation of the starting and the ending point are defined by the vectors $\lfloor D_p/2, -c/2, 0 \rfloor$ and $\lfloor -D_p/2, -c/2, 0 \rfloor$ respectively.

A value was assumed for the parameter *s* in the range [*c*/4, 3*c*/4]. The double loop was then drawn for 3 courses × 3 wales as shown in Figure 3-17b. The length of the formed loops was calculated (l_m) and subtracted from the total yarn length (B_1, B_2 for the front and the back bar respectively) for the calculation of the yarn length corresponding to the connecting parts: $l_{c1} = \frac{B_1 - 2 \cdot l_m}{2}$, $l_{c2} = \frac{B_2 - 2 \cdot l_m}{2}$. The connecting parts were designed with Splines defined by four control points and the direction of the Splines at the control points. The Spline direction at the first and forth point resulted from the double loops. The Spline direction at the other two control points resulted from an iterative procedure based on the generation of Splines and the selection of the one with appropriate orientation and length. The appropriate orientation supports the just in touch contact of the yarn precluding the penetration. A mean value of the yarn thickness was used for the calculations at this stage. The appropriate length corresponds to the calculated one (l_{c1} or l_{c2}). This procedure is used for the design of the connecting parts of the front (Figure 3-17c, Figure 3-17d) and the back yarn (Figure 3-17f, Figure 3-17g). If there is no feasible design constraint for the current value of *s*, the value *s* will be changed and the procedure will be repeated. The control points used for the definition of the Splines are shown with the numbers 1,2,3,4 in Figure 3-17c,d,f,g.

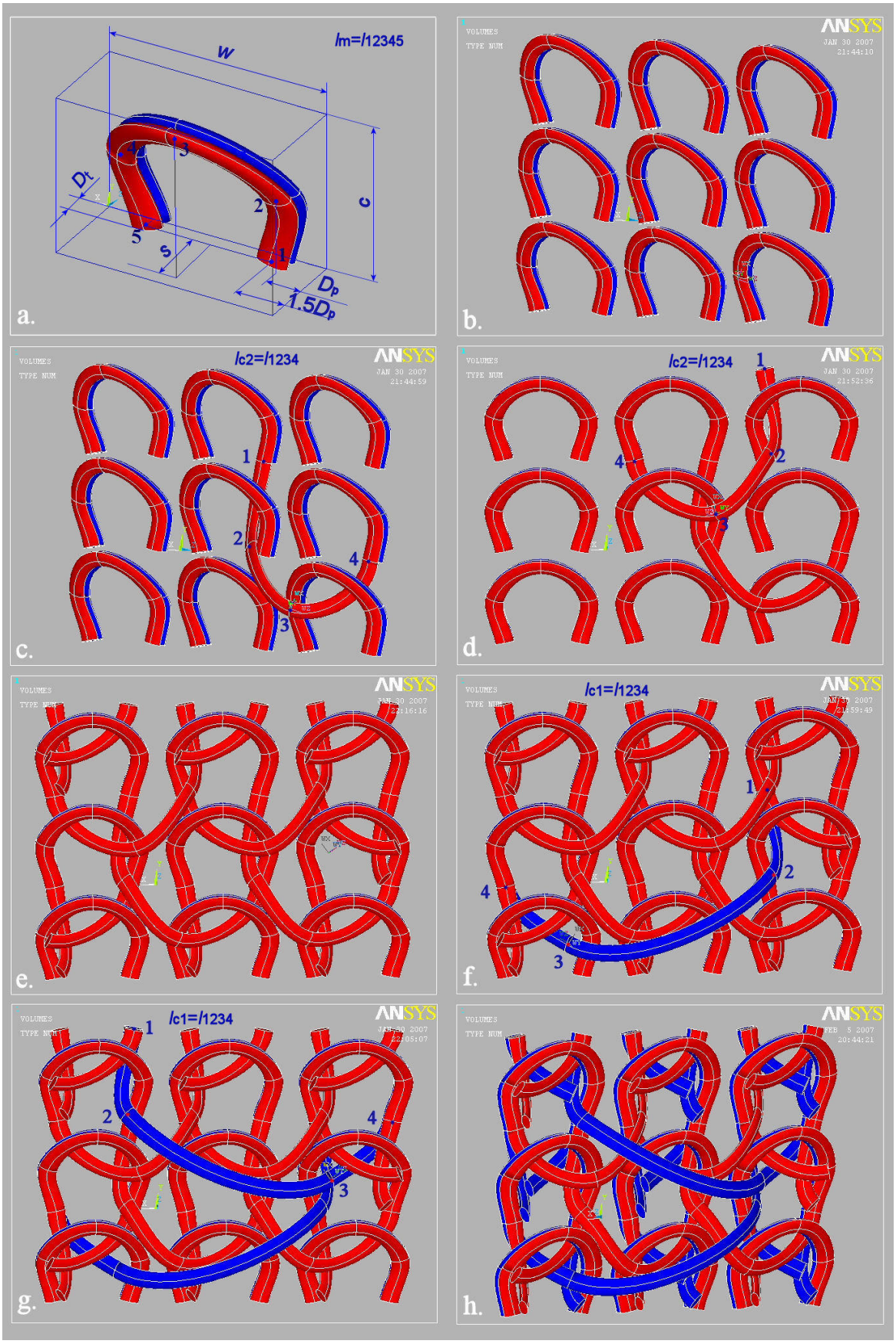

Figure 3-17: Generation of the 3D structural unit of Charmeuse.

3.3 The mechanical modelling of the plain woven unit cell

Three approaches, the solid, shell and beam modelling, were investigated for their implementation in the mesomechanical analysis of the fabrics. The three approaches were evaluated regarding the attribution of the yarn properties, the convenience in the application of the boundary conditions (BC), the computational cost, the convergence success in the solution procedure and the reliability of the results **(Vassiliadis, Kallivretaki & Provatidis 2009)**. The evaluation of the three approaches was based on the simulation of the tensile deformation of a woven unit cell. The plain woven structure corresponding to the simplest fabric structure was selected for the study. The tensile test of the woven fabric corresponds to the superposition of tensile and bending of the constituent yarns, such as compression and sliding between them. Thus the tensile test was considered adequate for the evaluation of the implemented modelling approaches, examining different yarn deformations.

The yarns constituting the plain woven structures under investigation were based on the ideal yarn structure. Thus considering the structural characteristics of the monofilament and the multifilament twisted yarn and the filament properties given in the Table 3-10, the yarn properties were calculated by the beam micro-scale modelling (§ 2.2). The apparent elastic modulus and the apparent bending rigidity of the yarn were considered adequate to describe the mechanical performance of the yarn.

Table 3-10: The structural and mechanical properties of the yarns constituting the considered fabrics.

yarn characteristics		yarn properties calculated using beam modelling of yarns	
	filament number	E_{app} (N/mm^2)	B_y (N·mm^2)
R_y=1 mm, E=5000 N/mm^2, v=0.3, t=0.1 turns/mm	1	5000	3927
	2	2075	454
	12	2454	113
	85	2649	20

The parameters used in the Table 3-10 are:

R_y : apparent yarn radius (mm)

E : elastic modulus of filament (N/mm^2)

v : Poisson ratio of filament (-)

t : yarn twist (turns/mm)

E_{app} : apparent elastic modulus of yarn (N/mm^2)

B_y : apparent bending rigidity of yarn ($N \cdot mm^2$)

3.3.1 The solid modelling approach

The meshed model of the unit cell used for the analysis of the plain woven structure is presented in the Figure 3-18. The yarns are represented as homogenous cylinders of constant radius equal to the apparent radius of yarn (R_y). The 8-node hexahedron solid elements (solid45) of 3 DOF (translations) per node were used for the solid modelling of the unit cell. The generated mesh corresponds to 25920 FE, 29524 nodes and 88572 DOFs. The high computational cost is further increased by the generated contact pairs. The contact and target elements are placed as an overlay on the solid elements in the defined areas (contact pair) around the crossing points of warps – wefts (Figure 3-19). Thus the appropriate mesh of the bodies in these areas increases the convergence achievement during the solution procedure. A mesh including coincident nodes (Figure 3-18) generated in the contact-target area is practically approved as well-defined mesh. The geometrical modelling and meshing were performed using the commercial ANSYS software **(Vassiliadis, Kallivretaki, Grancaric, Giannakis & Provatidis 2008)**.

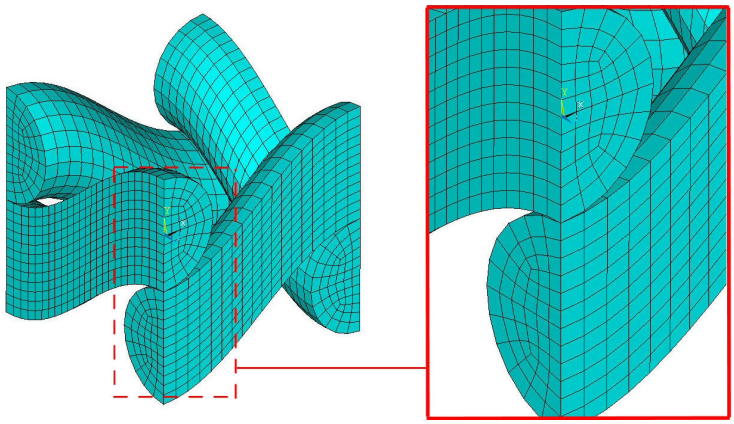

Figure 3-18: The solid mesh of the plain woven unit cell and zoom in the contact points.

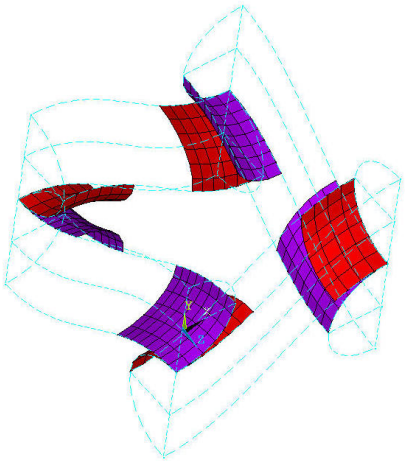

Figure 3-19: The contact pairs generated for the solid modelling of the unit cell.

The selection of the appropriate contact algorithm is determinant for the regular solution procedure in terms of computational power and time. The current approach adopted the surface-to-surface contact, offered by ANSYS software. The Augmented Lagrangian algorithm was adopted for the analysis. Furthermore the initial gap closing and the initial penetration reduction of the defined contact pairs were activated for a faster convergence achievement.

The material properties of the cylinder constitute the input parameter in the solid model. Thus the elastic properties (elastic modulus, E_{cyl}) of the modelled yarn is defined and the bending rigidity (B_{cyl}) is calculated based on the moment of inertia (I_{cyl}) of the cylinder cross section. For the modelled yarn of elastic modulus, E_{cyl}, and radius, R_y, the bending rigidity results by:

$$B_{cyl} = E_{cyl} \cdot I_{cyl} = E_{cyl} \cdot \pi R_y^4 / 4 \qquad \text{(Eq. 3-38)}$$

where:

E_{cyl} : elastic modulus of the solid cylinder (N/mm^2)

I_{cyl} : moment of inertia of the cross section of the solid cylinder (mm^4)

B_{cyl} : bending rigidity of the solid cylinder (N$\cdot$mm^2)

Since the individual definition of the apparent properties of yarn (elastic modulus and bending rigidity) is impossible in the solid modelling approach, two cases were studied.

The apparent elastic modulus of yarn was considered in the first case. The mechanical properties of the modelled yarn correspond to:

Elastic modulus: E_{app}

Bending Rigidity: $B_{e1} = E_{app} \cdot I_{cyl} = E_{cyl} \cdot \pi R_y^4 / 4 > B_{app}$

In the second case the apparent bending rigidity of the yarn was considered. The mechanical properties of the modelled yarn correspond to:

Elastic modulus: $E_{b1} = 4B_y / (\pi R_y^4) < E_{app}$

Bending Rigidity: B_y

The two cases are identical when monofilament yarn of isotropic material is modelled. The effect of the improper attribution of the homogenised yarns in the tensile deformation of the fabric unit cell was evaluated. The results are given in the Table 3-13.

The coordinate system given in the Figure 3-20 was considered for the definition of the BC, with the *x*, *z*, *y* axes corresponding to the weft direction, the warp direction and the vertical direction to the plane of the fabric respectively. The BC and constraint equations (CE) imposed for the simulation of tensile deformation along warp direction correspond to:

- Opposite displacement along the Z direction was applied on the outer areas of the unit cell z=0 and z=-p_2 {UZ(z=0) = - UZ(z=-p_2)}.

- Zero displacement along the X direction was applied on the outer areas of the unit cell x=0 and x=p_1 {UX(x=0) = UX(x=p_1) = 0}.
- The condition of opposite displacement (equal value) along the y direction was imposed on the central nodes of the yarns corresponding to the sections of crossing points (arrows in the Figure 3-20).

The BC imposed for the simulation of tensile deformation along weft direction correspond to:

- Opposite displacement along the x direction was applied on the outer areas of the unit cell x =0 and x =p_1 {UX(x =0) = - UX(x =p_1)}.
- Zero displacement along the z direction was applied on the outer areas of the unit cell z=0 and z =-p_2 { UZ(z =0) = UZ(z =-p_2)0}.
- The condition of opposite displacement (equal value) along the y direction was imposed on the central nodes of the yarns corresponding to the sections of crossing points (arrows in the Figure 3-20).

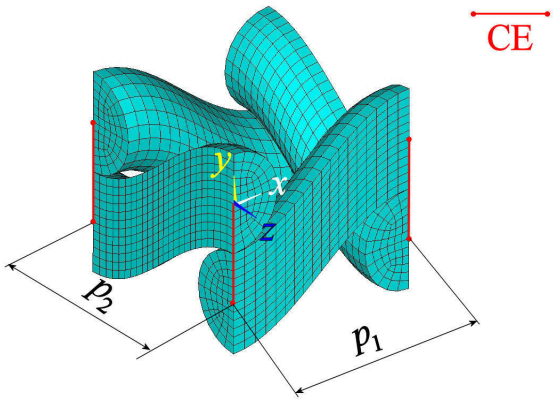

Figure 3-20: Nodes constrained along the vertical direction to the plane of the fabric (solid model).

The change of contact status, the sliding between the yarns and the flattening of the yarn cross-sections during the deformation of the models induce a highly nonlinear procedure of analysis. Thus a full Newton-Raphson solution procedure was implemented for faster convergence. The update of stiffness matrix in every iteration step is the great advantage of the selected algorithm. The control of the iteration number is important for the convergence of the solution procedure under the minimum CPU time required. Two options were activated to support the reduction of the iterations, the predictor option and the line search option.

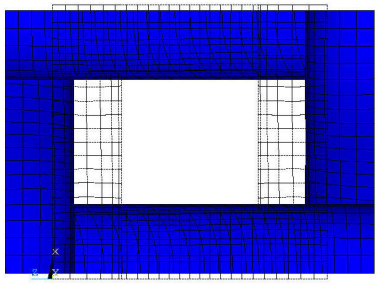

Figure 3-21: Deformed and undeformed shape of the solid unit cell in tensile test (deformation = 0.35).

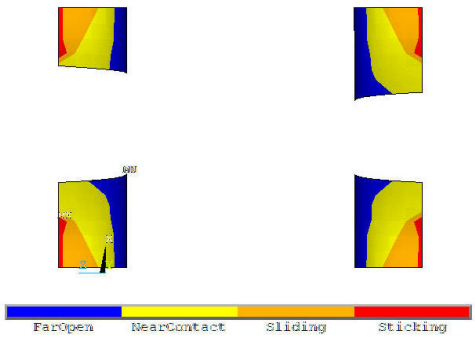

Figure 3-22: Contact status of the solid unit cell in tensile test (deformation = 0.35).

Thus the solid modelling approach is beneficial considering the evaluation of the contact effects, since the contact pressure, the yarn flattening and the sliding or sticking states are evaluated. Regarding the attribution of the modelled yarn, the option of transverse isotropic elasticity is quite realistic considering the elastic behaviour of multifilament yarns. The current option is essential for the compression performance of the multifilament yarns (yarn flattening). On the other hand, the attribution of the yarn properties, considering the apparent elastic modulus and bending rigidity, is problematic. Actually the elastic modulus of the modelled yarn is the input parameter for the attribution of the yarn model and the bending rigidity is calculated considering the model cross-section. Thus two cases were studied, considering the apparent elastic modulus or the bending rigidity, and the reliability of the two cases was evaluated. Moreover, the application of the boundary conditions and the high computational cost are correlated with the complexity of the current approach.

Yarns Interactions using surface-to-surface contact

The surface-to-surface contact, offered by ANSYS software, was implemented for the calculations of the interactions presented between the modelled yarns. The surface-to-surface contact is suitable for the mechanical contact analysis of equally deformable bodies (with similar elastic properties). Moreover the large scale sliding between the bodies is supported by the selected contact mode (see Appendix I: Surface-to-surface contact analysis)

The Augmented Lagrangian algorithm was adopted for the analysis. It belongs to the algorithms based on an iterative series of penalty methods. The resulting contact tractions (pressure and frictional stresses) are augmented during iterations with equilibrium criterion so that the final penetration will be less than the allowable tolerance. Furthermore the initial gap closing and the initial penetration reduction of the defined contact pairs were activated for a faster convergence achievement.

3.3.2 The shell modelling approach

The shell modelling approach was based on the representation of the yarns with hollow cylinders. Thus the shell modelling demands lower computational power comparing to the solid modelling, since only the external areas of the yarns are meshed. The 8-node shell elements (shell93) of 6 DOF per node were used for the shell modelling of the unit cell. The generated mesh, shown in the Figure 3-23, corresponds to a mesh of 1712 FE, 4660 nodes and 27960 DOFs. The standard contact conditions are also supported in the shell modelling approach. The surface-to-surface contact was implemented for the analysis. The contact pairs are presented in the Figure 3-24. The Augmented Lagrangian contact algorithm was adopted for the contact analysis (see Appendix I: Surface-to-surface contact analysis).

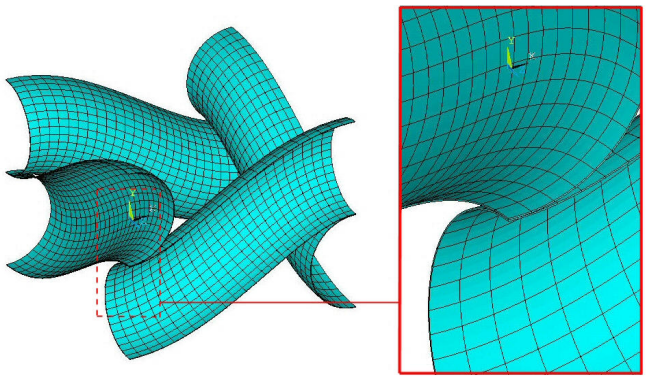

Figure 3-23: The shell mesh of the plain woven unit cell and zoom in the contact points.

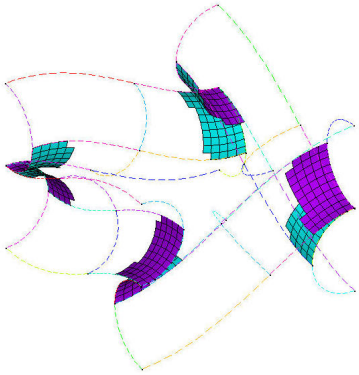

Figure 3-24: The contact pairs generated for the shell modelling of the unit cell.

The elastic modulus (E_{hc}) of the shell elements and the shell thickness (th=R_y-R_i) are the input parameters in shell modelling. Thus the elastic modulus and the bending rigidity of the modelled yarn are individually defined. The bending rigidity (B_{hc}) of the modelled yarn is defined by the following equation:

$$B_{hc} = E_{hc} \cdot I_{hc} = E_{hc} \frac{\pi \cdot (R_y^4 - R_i^4)}{4} \qquad \text{(Eq. 3-39)}$$

where:

E_{hc} : elastic modulus of the hollow cylinder (N/mm^2)

th : shell thickness (mm)

R_y : yarn radius and outer radius of the hollow cylinder (mm)

R_i : inner radius of the hollow cylinder (mm)

I_{hc} : moment of inertia of the cross section of the hollow cylinder (mm^4)

E_{app} : apparent elastic modulus of yarn (N/mm^2)

B_y : apparent bending rigidity of yarn (N·mm^2)

For the appropriate attribution of the hollow cylinders, that is equivalent performance with the yarn, the E_{hc} and R_i should fulfil the following equation:

$$E_{app} = E_{hc} \frac{R_y^2 - R_i^2}{R_y^2} \qquad \text{(Eq. 3-40)}$$

$$B_y = E_{hc} \cdot I_{hc} = E_{hc} \frac{\pi \cdot (R_y^4 - R_i^4)}{4} \qquad \text{(Eq. 3-41)}$$

The E_{hc} is replaced in the Eq. 3-41 considering the Eq. 3-40:

$$B_y = E_{app} \cdot \frac{R_y^2}{R_y^2 - R_i^2} \cdot \frac{\pi \cdot (R_y^4 - R_i^4)}{4} = E_{app} \cdot \frac{R_y^2}{R_y^2 - R_i^2} \cdot \frac{\pi \cdot (R_y^2 - R_i^2)(R_y^2 + R_i^2)}{4} \Rightarrow$$

$$B_y = E_{app} \cdot \frac{\pi \cdot R_y^2 \cdot (R_y^2 + R_i^2)}{4} = E_{app} \cdot \frac{\pi \cdot R_y^4}{4} + E_{app} \cdot \frac{\pi \cdot R_y^2 \cdot R_i^2}{4} \Rightarrow$$

$$B_y - E_{app} \cdot \frac{\pi \cdot R_y^4}{4} = E_{app} \cdot \frac{\pi \cdot R_y^2 \cdot R_i^2}{4} > 0 \Rightarrow B_y > E_{app} \cdot \frac{\pi \cdot R_y^4}{4} \qquad \text{(Eq. 3-42)}$$

The system of equations (Eq. 3-40, Eq. 3-41) has no solution since the resultant inequality (Eq. 3-42) is infeasible.

Since the generation of a shell model presenting equivalent performance with the considered yarn is impossible, two cases were studied.

The apparent elastic modulus of yarn was considered in the first case. The mechanical properties of the modelled yarn correspond to:

Elastic modulus: E_{app} , $\left(E_{hc} = E_{app} \frac{R_y^2}{R_y^2 - R_i^2} \right)$

Bending Rigidity: $B_{e2} = E_{app} \cdot \frac{\pi \cdot R_y^4}{4} + E_{app} \cdot \frac{\pi \cdot R_y^2 \cdot R_i^2}{4} > B_{e1} > B_y$

In the second case the apparent bending rigidity of the yarn was considered. The mechanical properties of the modelled yarn correspond to:

Elastic modulus: $E_{b2} = \frac{4B_y}{\pi(R_y^4 - R_i^4)} \cdot \frac{R_y^2 - R_i^2}{R_y^2} = \frac{4B_y}{\pi R_y^4 + \pi R_y^2 R_i^2} < E_{b1} < E_{app}$

Bending Rigidity: B_y

Thus the shell modelling of yarn presents higher divergence considering the mechanical properties (B_{e2}, E_{b2}) comparing to the respective properties of the solid model (B_{e1}, E_{b1}).

The coordinate system given in the Figure 3-25 was considered for the definition of the BC, with the *x*, *z*, *y* axes corresponding to the weft direction, the warp direction and the vertical direction to the plane of the fabric respectively. The BC imposed for the simulation of tensile deformation along warp direction correspond to:

- Opposite displacement along the Z direction was applied on the outer areas of the unit cell z=0 and z=-p_2 {UZ(z=0) = - UZ(z=-p_2)}.
- Zero displacement along the X direction was applied on the outer areas of the unit cell x=0 and x=p_1 {UX(x=0) = UX(x=p_1) = 0}.
- The condition of opposite displacement (equal value) along the *y* direction was imposed on the central nodes of the yarns corresponding to the sections of crossing points (arrows in the Figure 3-25).

The BC imposed for the simulation of tensile deformation along weft direction correspond to:

- Opposite displacement along the *x* direction was applied on the outer areas of the unit cell x =0 and x =p_1 {UX(x =0) = - UX(x =p_1)}.
- Zero displacement along the *z* direction was applied on the outer areas of the unit cell z=0 and z =-p_2 { UZ(z =0) = UZ(z =-p_2)0}.
- The condition of opposite displacement (equal value) along the *y* direction was imposed on the central nodes of the yarns corresponding to the sections of crossing points (arrows in the Figure 3-25).

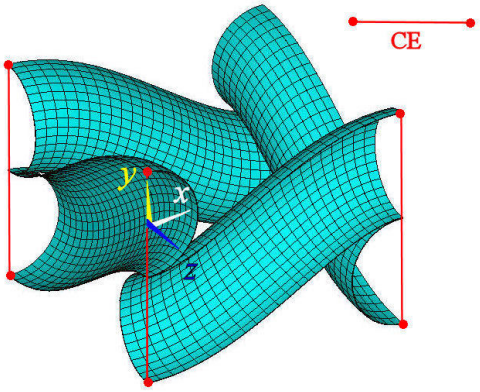

Figure 3-25: Nodes constrained along the vertical direction to the plane of the fabric (shell model).

The full Newton-Raphson solution procedure was implemented. The predictor option and the line search option were activated to support the reduction of the iterations. Convergence difficulties were presented in the solution procedure of the shell model, despite the low DOF number. The deformed shape of the unit cell model resulted from the simulation of the tensile test are given in the Figure 3-26. The folds presented in the thin walls of the modelled yarns correspond to modelling drawback since they are not presented in the real tensile test of fabrics. Moreover the yarn flattening is increased in the current approach, as shown in the figure. Thus the shell modelling approach is rejected for the mesomechanical modelling of fabrics for three basic reasons:

- the improper definition of the yarn properties
- the convergence difficulties in the solution procedure
- the non-realistic deformed shapes resulting from the analysis.

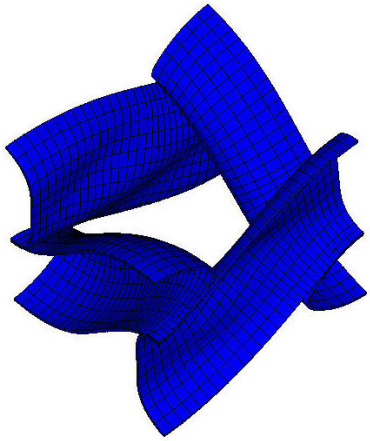

Figure 3-26: Deformed shape of the shell model of the unit cell in tensile test (deformation = 0.07).

3.3.3 The beam modelling approach

The beam modelling is preferential approach for the mechanical analysis of the unit cell for certain reasons. Firstly the individual definition of the elastic modulus and the bending stiffness (defining the moment of inertia) offered using beam elements is beneficial option for the analysis of yarns. Secondly the principle deformations of yarns (elongation and bending) resulting from the woven fabric loading are sufficiently predicted using the beam elements. Moreover the low computational cost required in the modelling (generation of central lines), meshing and analysis procedure is essential for the computational modelling of flexible structures. The mesh of the unit cell consists of 80 beam elements, 84 nodes and 504 DOFs. The Figure 3-27 presents the unit cell of the structure, the considered Cartesian coordinate system and the nodes designation. The warp and weft direction correspond to z and x axis respectively.

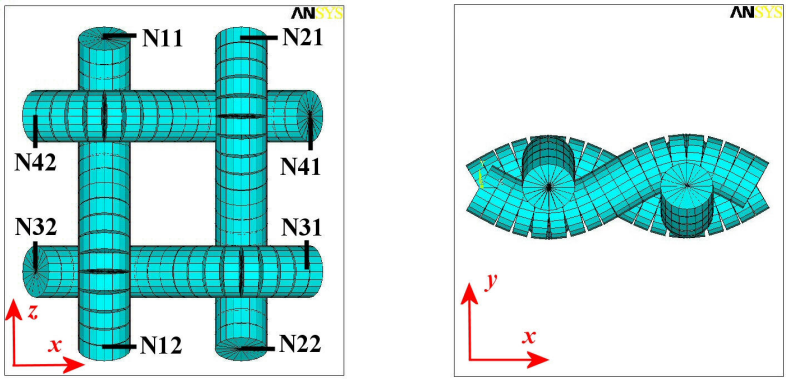

Figure 3-27: The beam mesh of the plain woven unit cell.

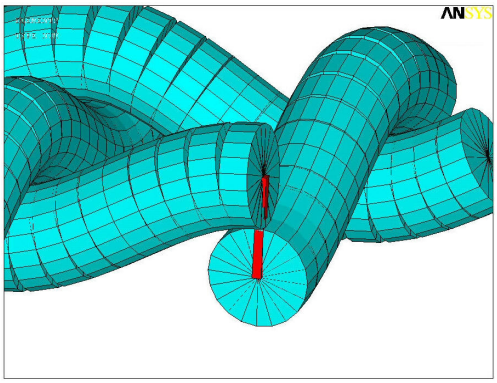

Figure 3-28: Link elements in the contact points of the beam model of the plain woven unit cell.

The structural stability of the woven fabrics subjected to deformations is mainly obtained by the interactions of the constituent yarns at the linking points. The forces resulted from these interactions are essential for the mechanical analysis of the structure. Especially in the tensile deformation, the straightening of the constituent yarns incurs the approach of the yarn axes at the contact points, the compression of the yarns and in some cases the sliding between them. The yarns interactions presented in the tensile deformation of the fabric were accounted in the

beam model. Two methods are proposed based on the generation of linking elements that connect the yarn axes in the contact points (shown in the Figure 3-28). Link elements of the appropriate properties were generated in the first method. In the second method the point-to-point contact was implemented. Both methods are described in the respective paragraphs.

The apparent mechanical properties of the yarn were introduced as input parameters in the yarn model. Actually the apparent elastic modulus of yarn, E_{app}, and the moment of inertia $I=B_y/E_{app}$ were used. Thus the homogenization of the yarns is successfully achieved when beam modelling is implemented.

Table 3-11: BC, CE and displacement applied for the simulation of the tensile test. {UW(Ni): displacement of node Ni along W axis, (w=x,y,z)}

Tensile Test	
Along Warp Direction	Along Weft Direction
UY(N11,N12,N21,N22,N31,N32,N41,N42)=0	UY(N11,N12,N21,N22,N31,N32,N41,N42)=0
UZ(N11,N21)=u	UX(N31,N41)=u
UZ(N12,N22)=-u	UX(N32,N42)=-u
UX(N31,N41)=-UX(N32,N42)	UZ(N11,N21)=-UZ(N12,N22)
UZ(N31)=UZ(N32)	UX(N11)=UX(N12)
UZ(N41)=UZ(N42)	UX(N21)=UX(N22)

The BC, CE and displacement applied for the simulation of the tensile test along warp or weft direction are given in the Table 3-11. The load - displacement curve derives by the imposed displacement and the resultant reactions. A full Newton-Raphson solution procedure was implemented since nonlinear analysis is recommended due to the resultant large deformations.

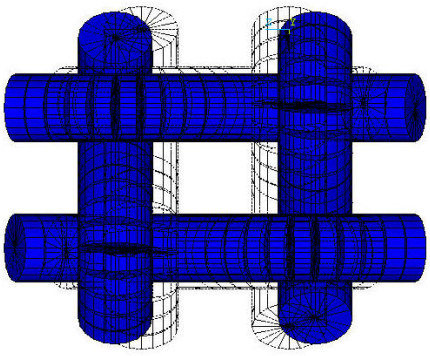

Figure 3-29: Deformed and undeformed shape of the beam unit cell in tensile test (deformation = 0.35).

Yarns Interactions using Link Elements

The link elements (LINK10) are generated between the nodes of the central axes of the modelled yarns corresponding to the contact points. The link elements have 3 DOF (translations) and the compression only (gap) option is selected. Thus the link elements are activated when compression loads are developed due to the approach of the yarn axes. The characteristics of the link elements (elastic modulus and cross-section) are evaluated by the yarns compression, considering the vertical placement of the yarns. The performance of monofilament yarns in compression can be estimated computationally.

The solid modelling was selected for the simulation of the monofilament yarn compression. The mesh was generated using hexahedral 8-node solid elements having 3 DOF (translations) at each node. A simplified model representing the half of the cylindrical yarns close to the contact point was developed. The surface-to-surface mode and the Augmented Lagrangian contact algorithm were selected for the analysis of the contact effects. Displacement was applied on the upper area of the model, while the lower area was fully constrained, and the reaction force was calculated. The deformed shape of the model is given in the Figure 3-30. The elastic performance corresponding to the curve of load – displacement determines the elastic properties of the link elements used in the model of the unit cell.

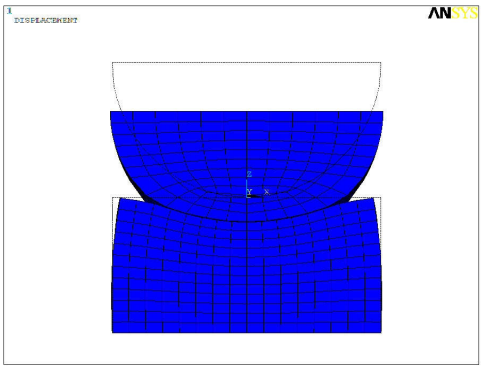

Figure 3-30: Deformed model from the simulation of yarn compression.

In the case of multifilament yarn compression the solid modelling proposed above is improper. Actually the yarn compressibility corresponds to the homogenised elastic modulus in the radius direction and it is calculated in the micromechanical analysis of yarns. Thus the representation of the filaments is required for the evaluation of the compressive performance of the multifilament yarns. Then the link elements used in the contact points of the woven mesomechanical model support the compressive performance of two vertical yarns. The experimental evaluation of the yarn compression behaviour is still not available since an equipment of special sensitivity is required. Thus the woven fabric compression test is usually performed for the evaluation of yarn compression.

The use of link elements for the development of yarns interactions (only normal forces) in the mesomechanical modelling of fabrics is beneficial considering the range of values. Accordingly the current method is appropriate for monofilament of multifilament yarns of any

material and structure. Moreover the computational cost of the mesomechanical analysis is kept low. However the method is inadequate in the transferring of tangential forces. Thereby, the frictional forces and the sliding between the yarns are not considered in the current method.

Yarns Interactions using Point-to-Point Contact Elements

The point-to-point contact elements (CONTAC52) are generated between the nodes of the central axes of the modelled yarns close to the contact points (Release 11.0 Documentation for ANSYS). More than one contact elements are generated at each contact area in order the new contact points developed during the sliding of the yarns to be predicted. The contact elements represent two surfaces which may maintain or break physical contact and may slide relative to each other. They are capable to support only compression in the direction normal to the surfaces and shear (Coulomb friction) in the tangential direction. The elements have three DOF at each node: translations in the nodal x, y, and z directions. The element is defined by two nodes (I,J), two stiffnesses (KN and KS), an initial gap or interference (GAP), and an initial element status (START).

The orientation of the interface was defined by the node locations and the contact interface was assumed to be perpendicular to the I-J line. The normal stiffness, KN, is based upon the stiffness of the surfaces in contact. The sticking stiffness, KS, represents the stiffness in the tangential direction when elastic Coulomb friction is selected. The initial gap defines the gap size (if positive) or the displacement interference (if negative). The initial element status (START) is used to define the "previous" condition of the interface to be used at the start of the first substep.

The only material property used is the interface coefficient of friction μ. A zero value is used for frictionless surfaces. The force deflection relationships for the interface element can be separated into the normal and tangential (sliding) directions. The element condition at the beginning of the first substep is determined from the START parameter. If the interface is closed and sticking, KN is used in the gap resistance and KS is used for sticking resistance. If the interface is closed but sliding, KN is used in the gap resistance and the constant friction force μFN is used for the sliding resistance.

In the normal direction, when the normal force (FN) is negative, the interface remains in contact and responds as a linear spring. As the normal force becomes positive, contact is broken and no force is transmitted. In the tangential direction, for $FN < 0$ and the absolute value of the tangential force (FS) less than $\mu|FN|$, the interface sticks and responds as a linear spring. For $FN < 0$ and $FS = \mu|FN|$, sliding occurs. If contact is broken, $FS = 0$.

The current approach is beneficial for the transferring of yarns interactions since the tangential loads are evaluated. Thereby the frictional forces and the sliding between the modelled yarns are evaluated. The evaluation of the tangential forces is essential for the simulation of the shear deformation of the fabrics. Moreover the appropriate definition of the

stiffness values (KN, KS) supports the contact effects of any kind of modelled yarn (monofilament, multifilament).

3.4 Comparison of the implemented modelling approaches

The FE approaches under investigation were compared for their appropriateness considering their implementation in the mesomechanical modelling of fabrics. The features considered for the comparison of the approaches are: the definition of the homogenized yarn properties, the evaluation of contact effects, the computational cost of the analysis, the easy application of the analysis, the nonlinear solution, the convergence success and the reliability of the deformed shapes. The benefits and drawbacks of the approaches are presented using + and ─ respectively in the Table 3-12.

Table 3-12: Benefits and drawbacks of the studied modelling approaches for the mesomechanical stage.

	Modelling approach			
Special Features	Solid	Shell	Beam + Link (at contact points)	Beam + point-to-point contact
Definition of mechanical properties				
Individual definition of elastic and bending properties	–	–	+	+
Anisotropic Behaviour (orthotropy, transverse isotropy)	+	+	–	–
Nonlinear elasticity (bilinear, multilinear)	+	+	+	+
Plasticity, viscoelasticity	+	+	+	+
Contact effects				
Compressional forces between yarns	+	+	+	+
Sliding between yarns	+	+	–	+
Yarn flattenning	+	+	–	–
Computational cost (one unit cell)				
Number of FE	25920	1712	80	80
Number of nodes	29524	4660	84	84
Number of DOF	88572	27960	504	504
Easy application of load and BC	–	–	+	+
Nonlinear solution	+	+	+	+
Convergence success				
Tensile test	+	–	+	+
Shear Test	increased number of BC		not used	+
Bending Test	huge number of DOF		+	+
Compression Test	increased number of BC		+	+
Reliability of deformed shapes	+	–	+	+

The solid modelling approach corresponds to the common used method for the mesomechanical modelling of fabrics. The benefits of the method are correlated with the improved contact algorithm implemented in solid modelling. Thereby the evaluation of changing contact status from no-contact to contact (sticking and sliding) and the deformation of the contact pair due to the contact pressure (yarn flattening) increase the accuracy of the contact analysis. The increased accuracy, on the other hand, is associated with high

computational cost and convergence difficulties presented in the solution of the contact algorithm. Either way, the solid modelling of one unit cell of the plain woven corresponds to high computational power, 88572 DOF, excluding the contact elements. Thus the modelling of 5 unit cells for the simulation of the bending test corresponds to extremely high computational cost, approximately 440000 DOF. However the basic drawback of the solid modelling is the attribution of the modelled yarns since the individual definition of the elastic modulus and the bending rigidity is impossible.

The shell modelling was implemented to face the drawbacks presented in the solid models. The shell modelling is adequate in contact analysis since advanced contact algorithms are available, such as the solid model. The shell model presents lower computational cost (27960 DOF) compared to the solid modelling approach, since one layer of elements around the yarn cross-section is required. However unsolvable convergence difficulties are presented in the solution procedure. The convergence failure is probably correlated with the folds presented in the thin walls of the modelled yarns. Actually these folds and the increased flattening of the yarn cross-sections presented in the deformed shapes of the woven fabric in the tensile simulation are unrealistic. Moreover the shell modelling approach resulted impropriate in the attribution of the homogenised yarn properties in the shell models. Thus the current approach was totally rejected.

The beam modelling, on the other hand, is considered adequate for certain reasons. Firstly the offered option of individual definition of the elastic modulus (E_{app}) and the moment of inertia (I) is preferential for the attribution of yarn models. Secondly the principle deformations of yarns (elongation and bending) resulting from the woven fabric loading are sufficiently predicted using the beam elements. Moreover the modelling, the meshing and the analysis are fast procedures in beam modelling approach. The computational cost is extremely low (504 DOF). The soft spot of the approach corresponds to the simplifications in the yarns interactions. Although the normal and tangential (friction) loads are evaluated, the yarn flattening presented during the yarn compression is omitted.

The beam and solid approaches were implemented for the simulation of the tensile deformation of the plain woven unit cell. The yarn properties calculated by the beam micro-scale modelling were considered (Table 3-10). The apparent elastic modulus (E_{app}) and the moment of inertia of the yarn cross section ($I=B_y/E_{app}$) were introduced in the beam model. The elastic modulus of yarn constitutes the input parameter in the solid model. Thus two cases were studied. The apparent elastic modulus was considered in the first case corresponding to the tensile deformation of the yarn. In the second case the elastic modulus [$E_{b1} = 4B_y/(\pi R_y^4) < E_{app}$] was calculated considering the bending deformation of the yarn and the assumption of the homogenized yarn model. The two cases are identical when monofilament yarn of isotropic material is modelled.

The results of the solid and beam approach are given in the Table 3-13. A good agreement of solid and beam modelling is presented in the woven structure consisting of monofilament yarn. The reliability of the solid approach in the current model was assured since the

attribution of the yarns was accurate. The success of the beam approach in the current model ensures the reliability of the approach despite the simplified contact conditions (omitted yarn flattening). Thus the only soft spot of the beam modelling approach has a weak influence in the accuracy of the results.

The divergence of the elastic modulus calculated by the two approaches is increased when the number of the filaments constituting the yarns is increased. The attribution of multifilament yarn properties using solid models is inadequate since the elastic or bending performance of the yarn can be considered. The superposition of tensile, bending and compression of the yarns constituting the unit cell under deformation is achieved implementing the beam modelling.

Table 3-13: Apparent elastic properties of plain woven unit cell resulted from the beam and solid modelling.

yarn characteristics		unit cell properties		
			beam modelling	solid modelling
	filament number	density=2.5 threads/cm	elastic modulus (N/thread)	elastic modulus (N/thread) for E_{app}	elastic modulus (N/thread) for E_b
Ry=1 mm, E=5000 N/mm^2, v=0.3, t=0.1 turns/mm	1		7015	6959	6959
	2		1698	2910	806
	12		829	3418	200
	85		217	3698	36

3.5 The beam modelling of the woven structures

The beam modelling approach was implemented for the mechanical analysis of the unit cell of the basic woven structures. The plain weave, basket, 2/2 twill and 5-satin were selected for the investigation. The mechanical analysis aims at the evaluation of the apparent mechanical properties of the structures required for the homogenisation method (developed in continue). Thus the tensile and the (in-plane) shear test of the textile unit cell along the warp and weft directions were simulated. Moreover the bending rigidity of the structure considering the warp and weft direction was evaluated by the simulation of the bending deformation. More than one unit cells are required for the simulation of the bending deformation in order to eliminate the fixed end effects. The evaluation of the respective bending properties presupposes a number of unit cells to be added along the warp or weft direction. The modelling and simulation were performed using the ANSYS software.

The symmetry and the periodicity of the unit cells within the fabric structure were taken into account for the definition of the appropriate boundary conditions (BC) and constraint equations (CE). The load - displacement curve derives by the imposed displacement and the resultant reactions. The beam model of the unit cell, the considered Cartesian coordinate system and the nodes designation are given for each structure in the respective figures. The warp and weft direction correspond to Z and X axis respectively. The BC, CE and displacement applied for the simulations are given in the respective tables using UW(Ni) the displacement of node Ni along W axis, (W=X,Y,Z). The Ni corresponds to the node designations given in the figures. Thus the BC and CE for the simulation of the tensile, shear and bending test of the woven structures are given in the Table 3-14, Table 3-15 and Table 3-16 respectively. The deformed shapes of the unit cells are also presented in the respective figures.

The point-to-point contact elements for each unit cell are represented in the figures with the central axes of the beams. The contact elements are generated between the nodes of adjacent threads (warps or wefts) using an iterative procedure that evaluates the node distance. The different colour of the contact elements (red or blue-azure) indicates the different initial condition defined. The initial conditions used are:

- when, node distance ≤ yarn diameter

START=1, gap is initially closed and not sliding (red elements),

- when, yarn diameter < node distance < 1.2×yarn diameter

START=3, gap is initially open (blue-azure elements).

3.5.1 Plain woven structure

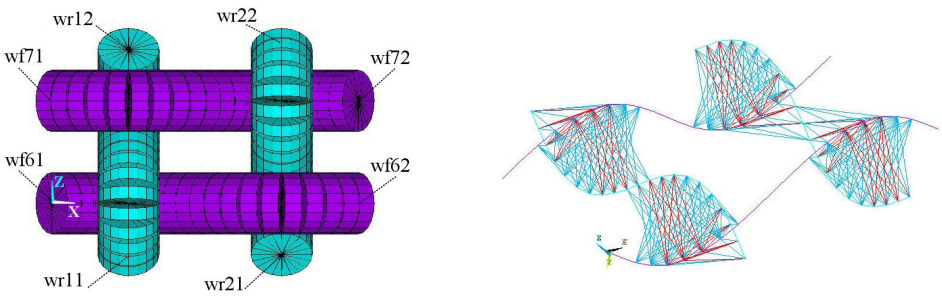

Figure 3-31: Beam model of the plain woven unit cell, realistic representation (left), central axes and contact elements (right). [BC tensile: Table 3-14, i=1~2, j=6~7], [BC shear: Table 3-15, i=1~2, j=6~7]

Table 3-14: BC, CE and displacement applied for the simulation of the woven unit cell in tensile test. {UW(Ni): displacement of node Ni along W axis, (W=X,Y,Z)}

Tensile Test	
Along Warp Direction	Along Weft Direction
UY(wr i1,wr i2, wf j1,wf j2)=0, i=1…5, j=6…10	UY(wr i1,wr i2, wf j1,wf j2)=0, i=1…5, j=6…10
UZ(wr i1)=-u , i=1…5 UZ(wr i2)=u , i=1…5	UX(wf i1)=-u , i=6…10 UX(wf i2)=u , i=6…10
UX(wf j1)=equal, UX(wf j2)=equal, j=6…10	UZ(wr i1)=equal, UZ(wr i2)=equal, i=1…5
UX(wf j1)=-UX(wf j2), j=6...10	UZ(wr i1)=-UZ(wr i2), i=1…5

Table 3-15: BC, CE and displacement applied for the simulation of the woven unit cell in shear test.

Shear Test	
Along Warp Direction	Along Weft Direction
UY(wr i1,wr i2, wf j1,wf j2)=0, i=1…5, j=6…10	UY(wr i1,wr i2, wf j1,wf j2)=0, i=1…5, j=6…10
UZ(wf i1)=u UZ(wf i2)=-u	UX(wr i1)=u , i=1…5 UX(wr i1)=-u , i=1…5
UX(wf j1)=equal, UX(wf j2)=equal, j=6…10	UZ(wr i1)=equal, UZ(wr i2)=equal, i=1…5
UX(wf j1)=-UX(wf j2), j=6...10	UZ(wr i1)=-UZ(wr i2), i=1…5
UZ(wr i1)=UZ(wr i2), i=1…5 UX(wr i1)=UX(wr i2), i=1…5	UZ(wf j1)=UZ(wf j2), j=6...10 UX(wf j1)=UX(wf j2), j=6...10

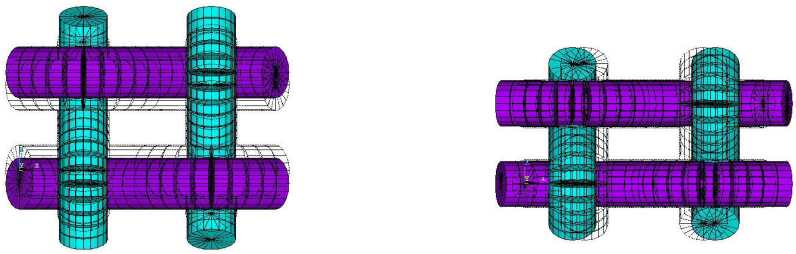

Figure 3-32: Deformed and undeformed shape of the plain woven unit cell in tensile test (deformation = 0.30) along warp (left) and weft direction (right).

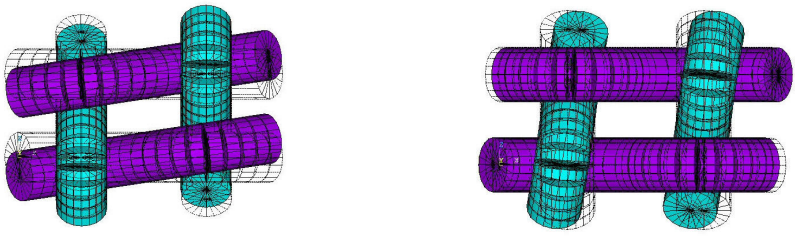

Figure 3-33: Deformed and undeformed shape of the plain woven unit cell in shear test (shear angle = 0.15) along warp (left) and weft direction (right).

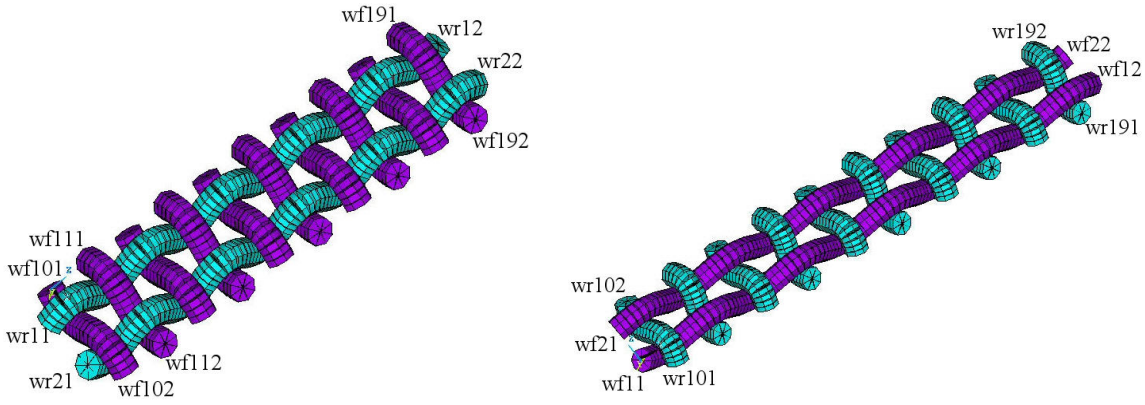

Figure 3-34: Mesh of 5 unit cells along warp (left) or weft (right) direction for the plain woven structure. [BC bending warp: Table 3-16, i=1…2, j=10…19], [BC bending weft: Table 3-16, j=1…2, i=10…19]

Table 3-16: BC, CE and displacement applied for the simulation of the woven model (5 units along warp or weft direction) in bending test.

Bending Test	
Along Warp Direction	Along Weft Direction
wr i1,i=1…5 fully supported	wf j1, j=1…5 fully supported
UY(wr i2)=u, i=1…5	UY(wf j2)=u, j=1…5
UZ(wf j1)=UZ(wf j2), j=10…34 UY(wf j1)=UY(wf j2), j=10…34	UX(wr i1)=UX(wr i2), i=10…34 UY(wr i1)=UY(wr i2), i=10…34

Figure 3-35: Deformed and undeformed shape of the plain woven model in bending test (y/L = 0.2).

3.5.2 Basket structure

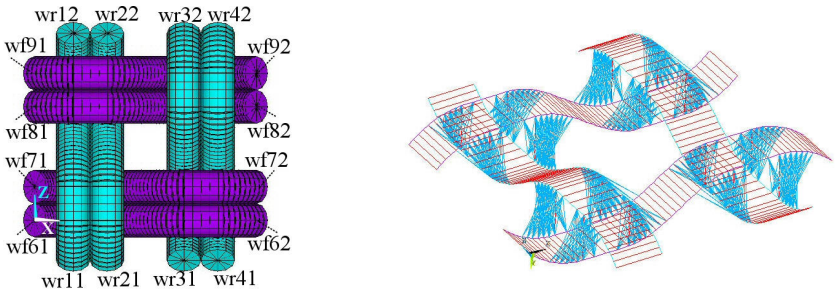

Figure 3-36: Beam model of the basket unit cell, realistic representation (left), central axes and contact elements (right). [BC tensile: Table 3-14, i=1…4, j=6…9], [BC shear: Table 3-15, i=1…4, j=6…9]

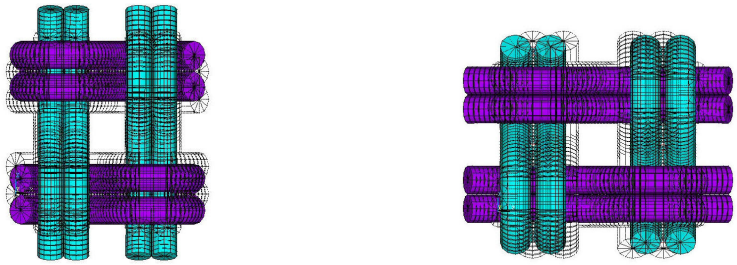

Figure 3-37: Deformed and undeformed shape of the basket unit cell in tensile test (deformation = 0.3) along warp (left) and weft direction (right).

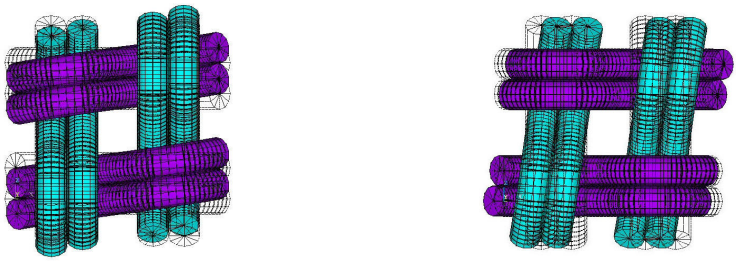

Figure 3-38: Deformed and undeformed shape of the basket unit cell in shear test (shear angle = 0.15) along warp (left) and weft direction (right).

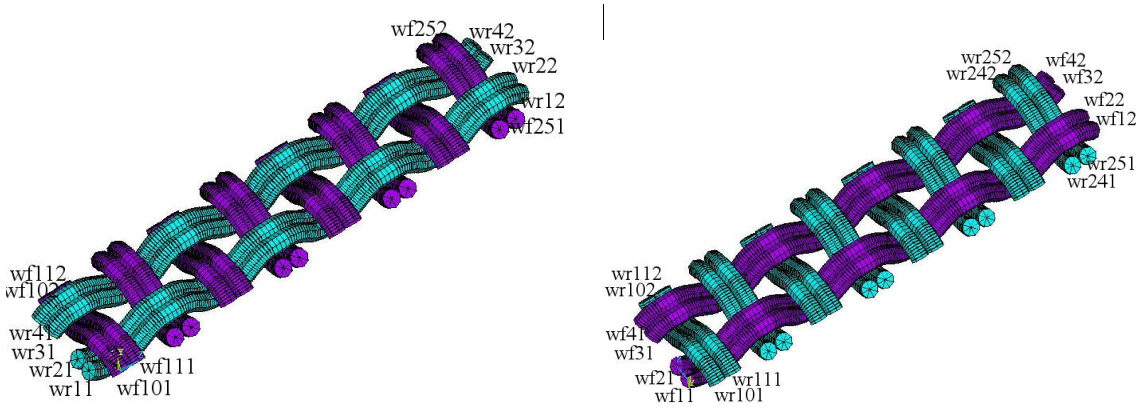

Figure 3-39: Mesh of 5 unit cells along warp (left) or weft (right) direction for the basket structure. [BC bending warp: Table 3-16, i=1…4, j=10…25], [BC bending weft: Table 3-16, j=1…4, i=10…25]

Figure 3-40: Deformed and undeformed shape of the basket model in bending test (y/L = 0.2).

3.5.3 Twill structure

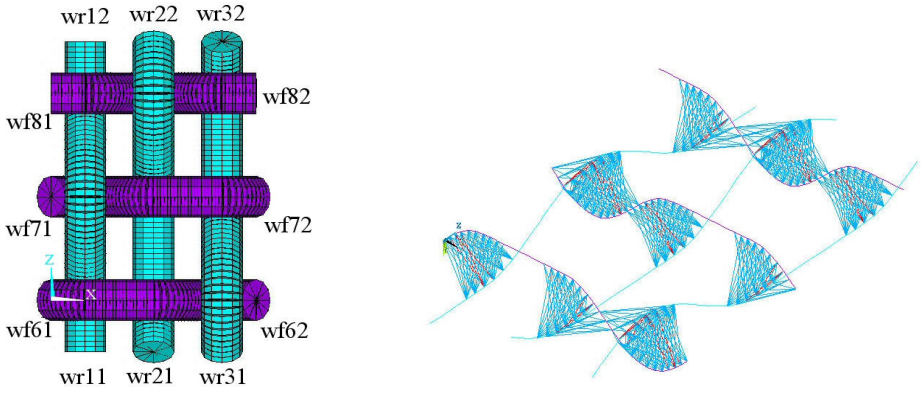

Figure 3-41: Beam model of the twill unit cell, realistic representation (left), central axes and contact elements (right). [BC tensile: Table 3-14, i=1…3, j=6…8], [BC shear: Table 3-15, i=1…3, j=6…8]

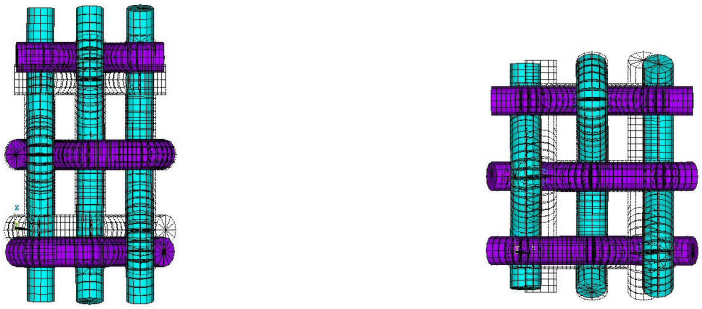

Figure 3-42: Deformed and undeformed shape of the twill unit cell in tensile test (deformation = 0.30) along warp (left) and weft direction (right).

Figure 3-43: Deformed and undeformed shape of the twill unit cell in shear test (shear angle = 0.15) along warp (left) and weft direction (right).

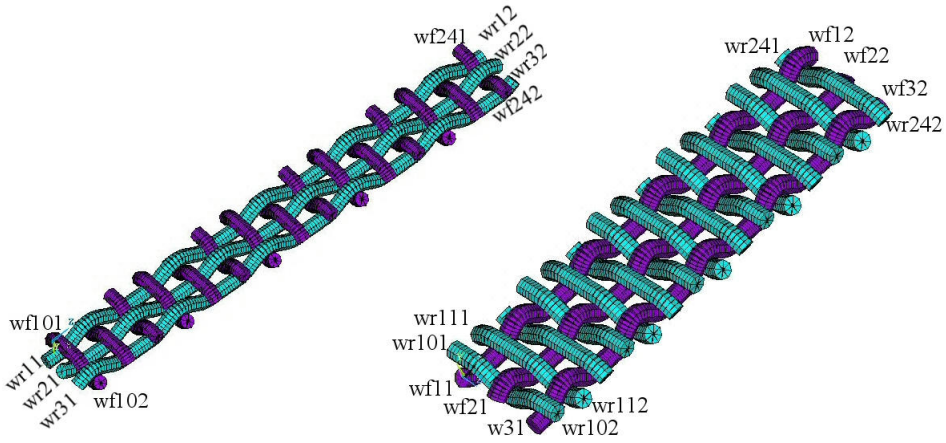

Figure 3-44: Mesh of 5 unit cells along warp (left) or weft (right) direction for the twill structure. [BC bending warp: Table 3-16, i=1…3, j=10…24], [BC bending weft: Table 3-16, j=1…3, i=10…24]

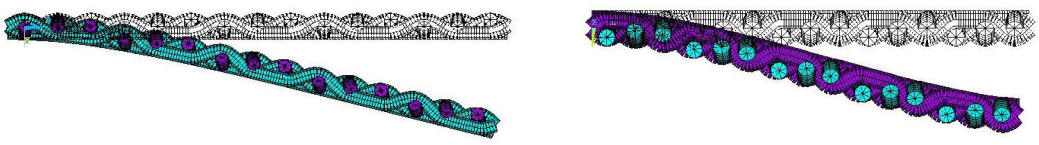

Figure 3-45: Deformed and undeformed shape of the twill model in bending test (y/L = 0.2).

3.5.4 Satin structure

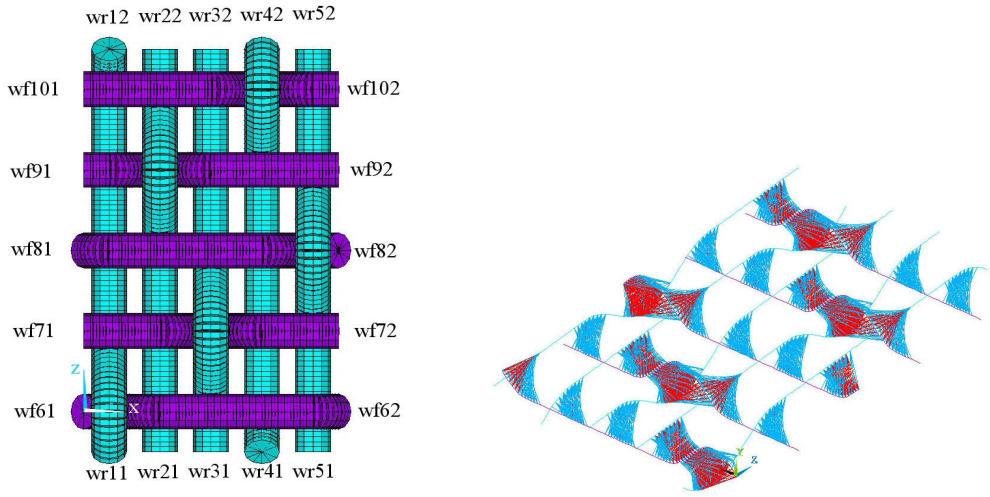

Figure 3-46: Beam model of the satin unit cell, realistic representation (left), central axes and contact elements (right). [BC tensile: Table 3-14, i=1…5, j=6…10], [BC shear: Table 3-15, i=1…5, j=6…10]

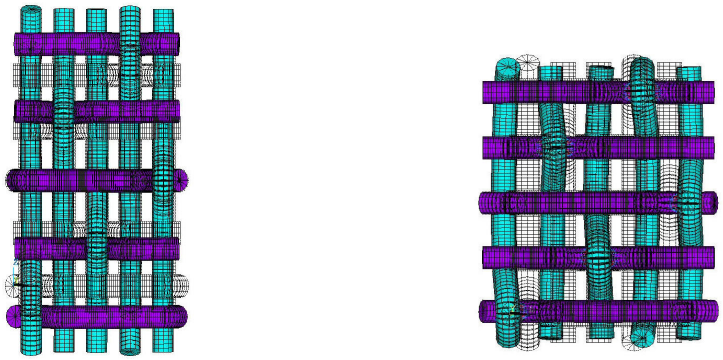

Figure 3-47: Deformed and undeformed shape of the satin unit cell in tensile test (deformation = 0.30) along warp (left) and weft direction (right).

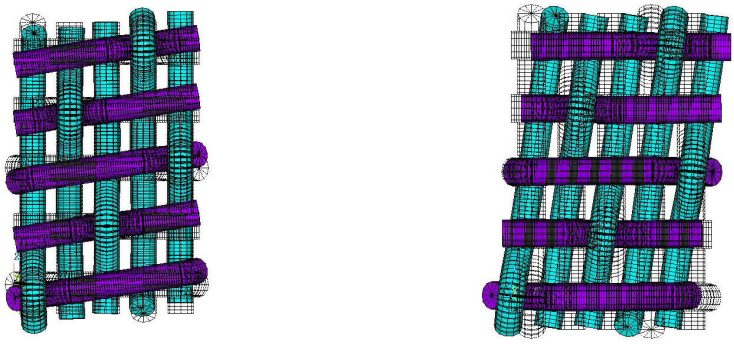

Figure 3-48: Deformed and undeformed shape of the satin unit cell in shear test (shear angle = 0.15) along warp (left) and weft direction (right).

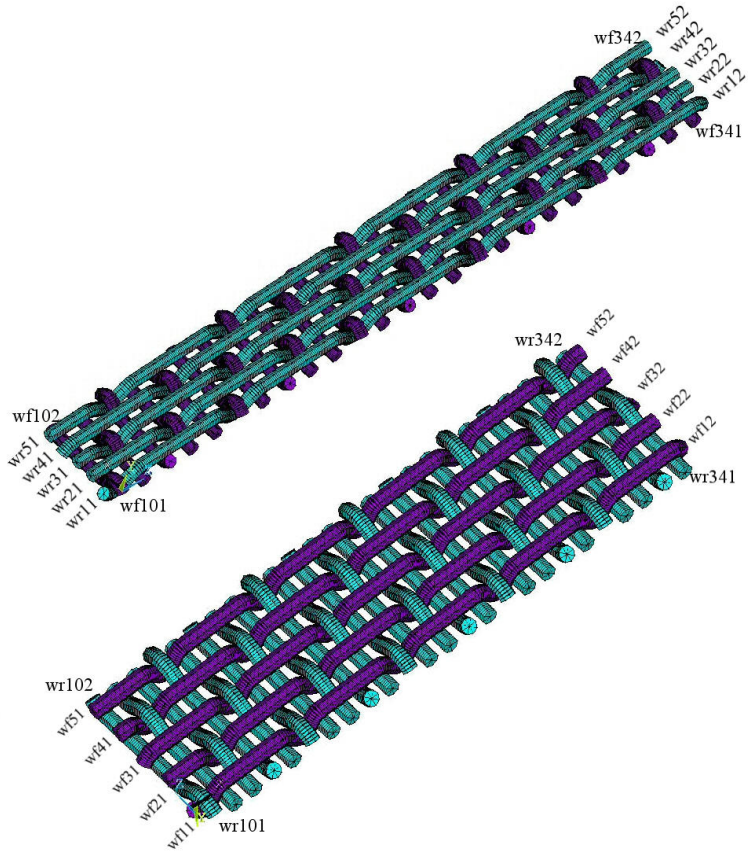

Figure 3-49: Mesh of 5 unit cells along warp (up) or weft (down) direction for the satin structure. [BC bending warp: Table 3-16, i=1…5, j=10…34], [BC bending weft: Table 3-16, j=1…5, i=10…34]

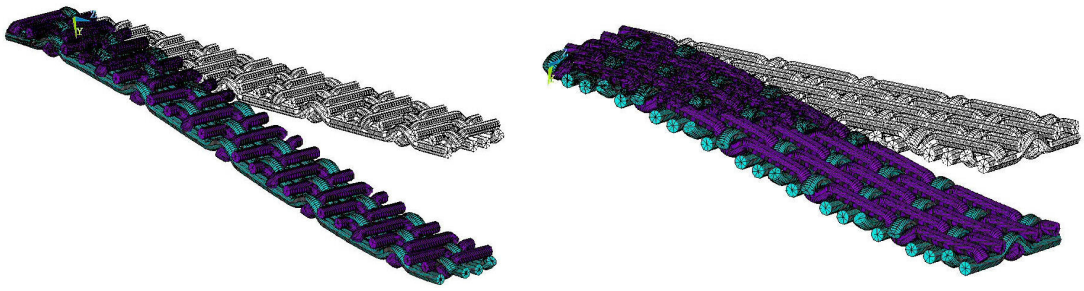

Figure 3-50: Deformed and undeformed shape of the satin model in bending test (y/L = 0.2).

3.6 The beam modelling of weft-knitted structures

The beam modelling approach was implemented for the mechanical analysis of the unit cell of the basic weft knitted structures. The plain weft knitted, the rib 1×1 and the interlock structures are presented. The tensile and the shear test of the textile unit cell along the wale and course directions were simulated. Moreover the bending rigidity of the structure considering the wale and course direction was evaluated by the simulation of the bending deformation. The modelling and simulation were performed using the ANSYS software.

The beam model of the unit cell, the considered Cartesian coordinate system and the nodes designation are given for each structure in the respective figures. The wale and course direction correspond to Y and X axis respectively. The BC, CE and displacement applied for the simulations are given in the respective tables using UW(Ni) the displacement of node Ni along W axis, (W=X,Y,Z). The Ni corresponds to the node designations given in the figures. Thus the BC and CE for the simulation of the tensile, shear and bending test of the woven structures are given in the tables below. The deformed shapes of the unit cells are also presented in the respective figures.

The point-to-point contact elements for each unit cell are represented in the figures with the central axes of the beams. The contact elements are generated between the adjacent parts of the knitting thread using an iterative procedure that evaluates the node distances. The different colour of the contact elements (red or blue-azure) indicates the different initial condition defined. The initial conditions used are:

- when, node distance ≤ yarn diameter

START=1, gap is initially closed and not sliding (red elements),

- when, yarn diameter < node distance < 1.2×yarn diameter

START=3, gap is initially open (blue-azure elements).

3.6.1 Plain weft knitted structure

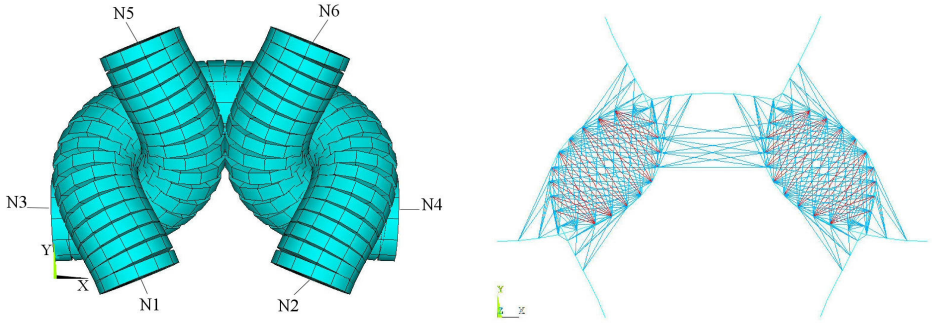

Figure 3-51: Beam model of the plain weft knitted unit cell, realistic representation (left), central axes and contact elements (right).

Table 3-17: BC, CE and displacement applied for the simulation of the plain weft knitted model in tensile test.

Tensile Test	
Along Wale Direction	Along Course Direction
UZ(N1, N2, N5, N6)=0	UZ(N1, N2, N5, N6)=0
UY(N1, N2)=-u UY(N5,N6)=u	UX(N3)=-u UX(N4)=u
UX(N1)=UX(N5) UX(N2)=UX(N6) UY(N3)=UY(N4)	UX(N1)=UX(N5) UX(N2)=UX(N6) UY(N3)=UY(N4)
UX(N3)=-UX(N4)	UY(N1)=UY(N2), UY(N5)=UY(N6) UY(N1,N2)=-UY(N5,N6)
ROTY(N3, N4)=0	ROTY(N3, N4)=0
ROTX(N1, N2, N5, N6)=0	ROTX(N1, N2, N5, N6)=0

Table 3-18: BC, CE and displacement applied for the simulation of the plain weft knitted model in shear test.

Shear Test	
Along Wale Direction	Along Course Direction
UZ(N1, N2, N5, N6)=0	UZ(N1, N2, N5, N6)=0
UY(N3)=u UY(N4)=-u	UX(N1, N2)=-u UX(N5, N6)=u
UX(N3)=-UX(N4)	UY(N1)=UY(N2), UY(N5)=UY(N6) UY(N1,N2)=-UY(N5,N6)
UX(N1)=UX(N5), UX(N2)=UX(N6) UY(N1)=UY(N5), UY(N2)=UY(N6)	UY(N3)=UY(N4) UX(N3)=UX(N4)
ROTY(N3)= ROTY(N4)	ROTY(N3)= ROTY(N4)
ROTX(N1)=ROTX(N5) ROTX(N2)=ROTX(N6)	ROTX(N1)=ROTX(N5) ROTX(N2)=ROTX(N6)

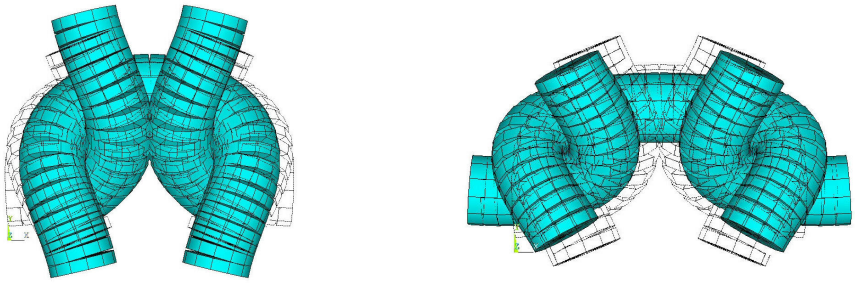

Figure 3-52: Deformed and undeformed shape of the plain weft knitted unit cell in tensile test (deformation = 0.3) along wale (left) and course direction (right).

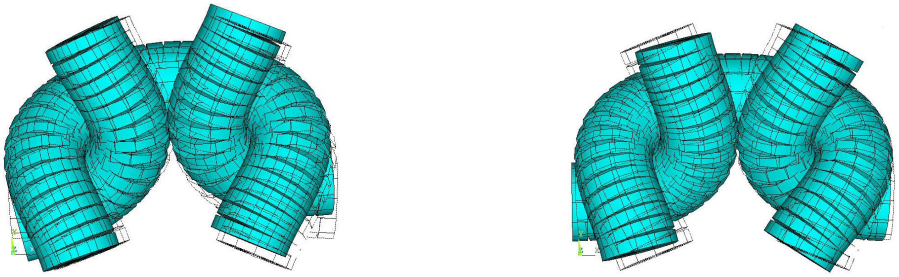

Figure 3-53: Deformed and undeformed shape of the plain weft knitted unit cell in shear test (shear angle = 0.15) along wale (left) and course direction (right).

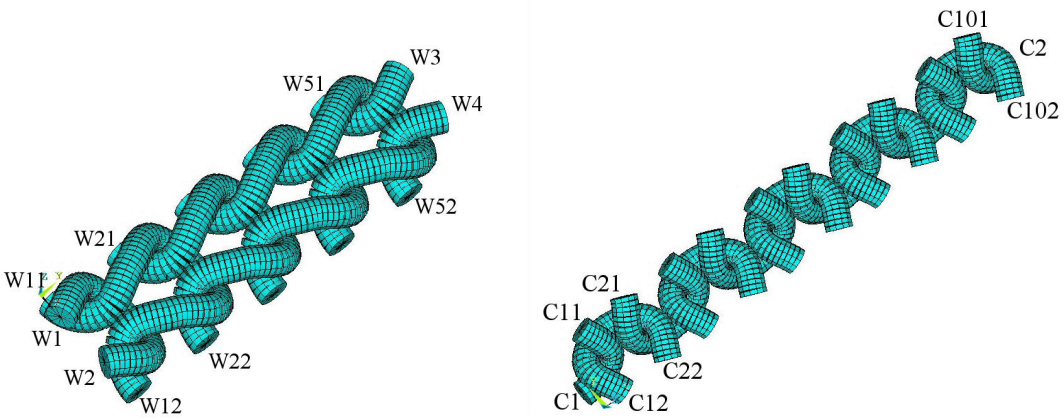

Figure 3-54: Mesh of 5 unit cells along wale (left) or course (right) direction for the plain weft knitted structure.

Table 3-19: BC, CE and displacement applied for the simulation of the plain weft knitted model in bending test.

Bending Test	
Along Wale Direction	Along Course Direction
W1, W2 fully supported	C1 fully supported
UZ(W3, W4)=u	UZ(C2)=u
UX(W j1)=UX(W j2), j=1…5 UY(W j1)=UY(W j2), j=1…5	UX(C i1)=UX(C i2), i=1…10 UY(C i1)=UY(C i2), i=1…10

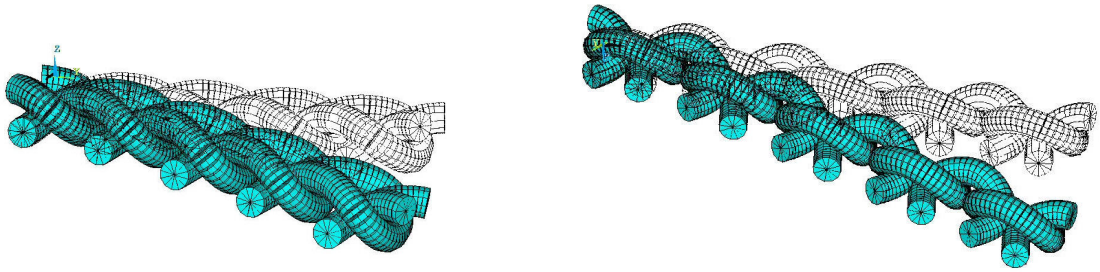

Figure 3-55: Deformed and undeformed shape of the plain weft knitted model in bending test (y/L = 0.2).

3.6.2 Rib 1x1 structure

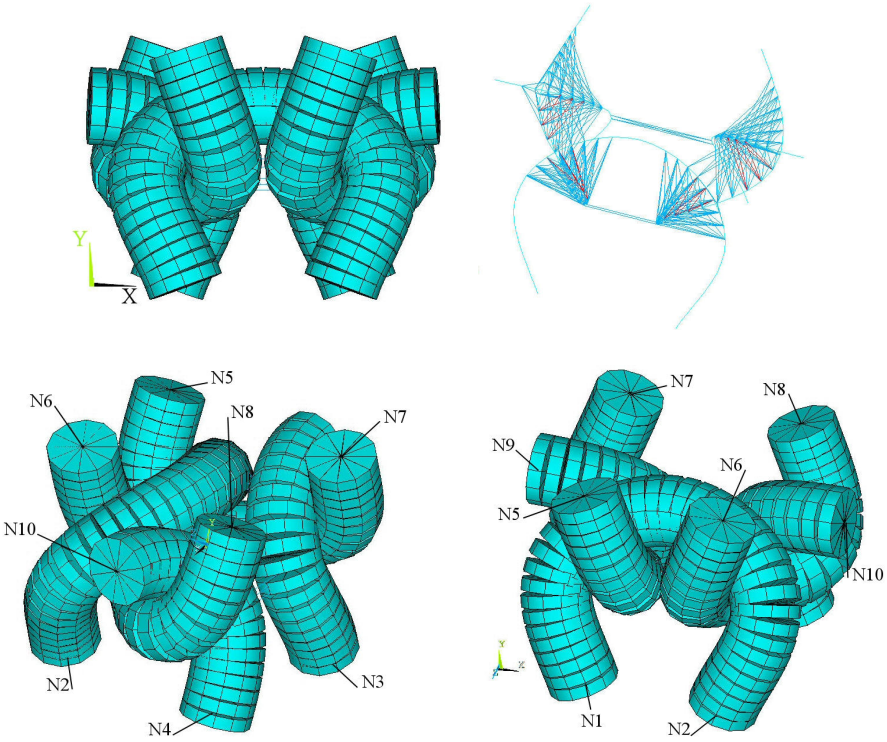

Figure 3-56: Beam model of the rib 1×1 unit cell, realistic representation (left), central axes and contact elements (right).

Table 3-20: BC, CE and displacement applied for the simulation of the rib 1×1 model in tensile test.

Tensile Test	
Along Wale Direction	Along Course Direction
UZ(N9, N10)=0	UZ(N9, N10)=0
UY(N1, N2, N3, N4)=-u UY(N5,N6, N7, N8)=u	UX(N9)=-u UX(N10)=u
UX(N1)=UX(N5) UX(N2)=UX(N6) UX(N3)=UX(N7) UX(N4)=UX(N8) UY(N9)=UY(N10)	UX(N1)=UX(N5) UX(N2)=UX(N6) UX(N3)=UX(N7) UX(N4)=UX(N8) UY(N9)=UY(N10)
UX(N9)=-UX(N10)	UY(N1, N2, N3, N4)=equal, UY(N5, N6, N7, N8)= equal UY(N1, N2, N3, N4)=-UY(N5, N6, N7, N8)
ROTY(N9, N10)=0	ROTY(N9, N10)=0
ROTX(N i)=0, i=1…8	ROTX(N i)=0, i=1…8

Table 3-21: BC, CE and displacement applied for the simulation of the rib 1×1 model in shear test.

Shear Test	
Along Wale Direction	Along Course Direction
UZ(N9, N10)=0	UZ(N9, N10)=0
UY(N9)=u UY(N10)=-u	UX(N1, N2, N3, N4)=-u UX(N5,N6, N7, N8)=u
UX(N9)=-UX(N10)	UY(N1, N2, N3, N4)=equal, UY(N5, N6, N7, N8)= equal UY(N1, N2, N3, N4)=-UY(N5, N6, N7, N8)
UX(N1)=UX(N5), UY(N1)=UY(N5) UX(N2)=UX(N6), UY(N2)=UY(N6) UX(N3)=UX(N7), UY(N3)=UY(N7) UX(N4)=UX(N8), UY(N4)=UY(N8)	UY(N9)=UY(N10) UX(N9)=UX(N10)
ROTY(N9)= ROTY(N10)	ROTY(N9)= ROTY(N10)
ROTX(N1)=ROTX(N5) ROTX(N2)=ROTX(N6) ROTX(N3)=ROTX(N7) ROTX(N4)=ROTX(N8)	ROTX(N1)=ROTX(N5) ROTX(N2)=ROTX(N6) ROTX(N3)=ROTX(N7) ROTX(N4)=ROTX(N8)

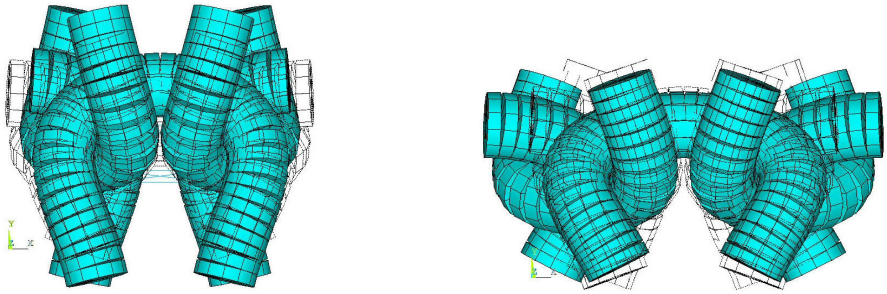

Figure 3-57: Deformed and undeformed shape of the rib 1×1 unit cell in tensile test (deformation = 0.30) along wale (left) and course direction (right).

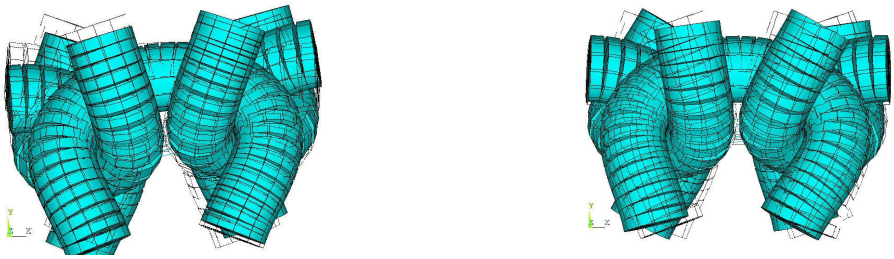

Figure 3-58: Deformed and undeformed shape of the rib 1×1 unit cell in shear test (shear angle = 0.15) along wale (left) and course direction (right).

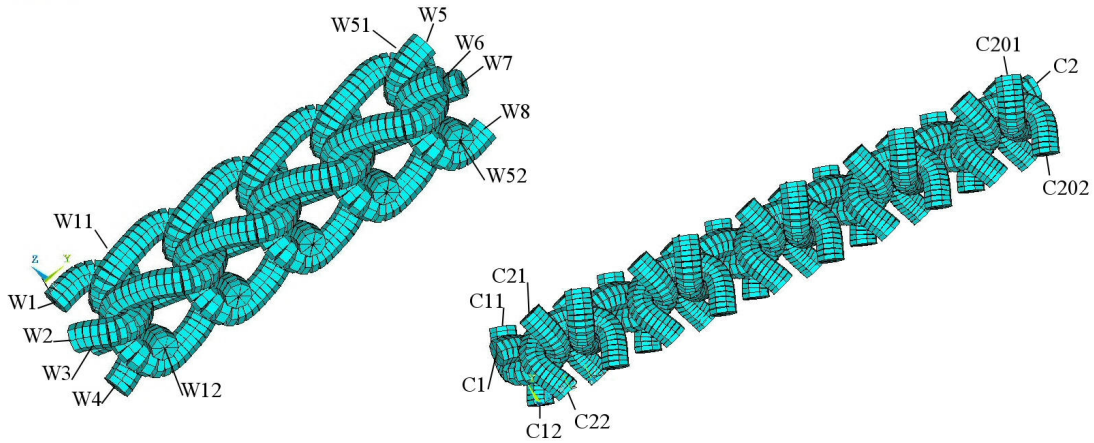

Figure 3-59: Mesh of 5 unit cells along wale (left) or course (right) direction for the rib 1×1 structure.

Table 3-22: BC, CE and displacement applied for the simulation of the rib 1×1 model in bending test.

Bending Test	
Along Wale Direction	Along Course Direction
W1, W2, W3, W4 fully supported	C1 fully supported
UZ(W5, W6, W7, W8)=u	UZ(C2)=u
UX(W j1)=UX(W j2), j=1…5 UY(W j1)=UY(W j2), j=1…5	UX(C i1)=UX(C i2), i=1…20 UY(C i1)=UY(C i2), i=1…20

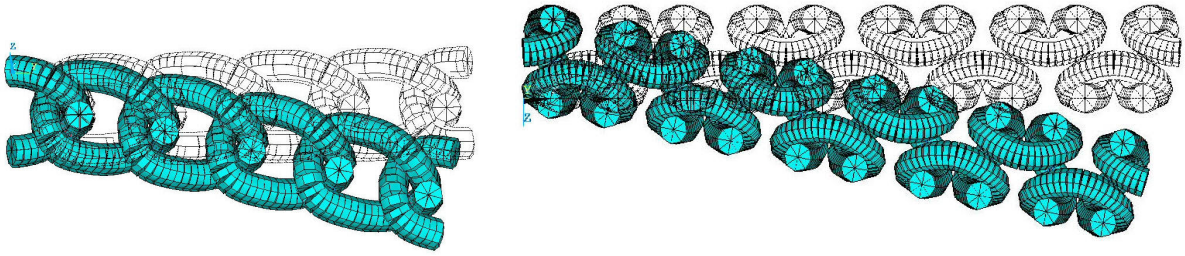

Figure 3-60: Deformed and undeformed shape of the rib 1×1 model in bending test (y/L = 0.2).

3.6.3 Interlock structure

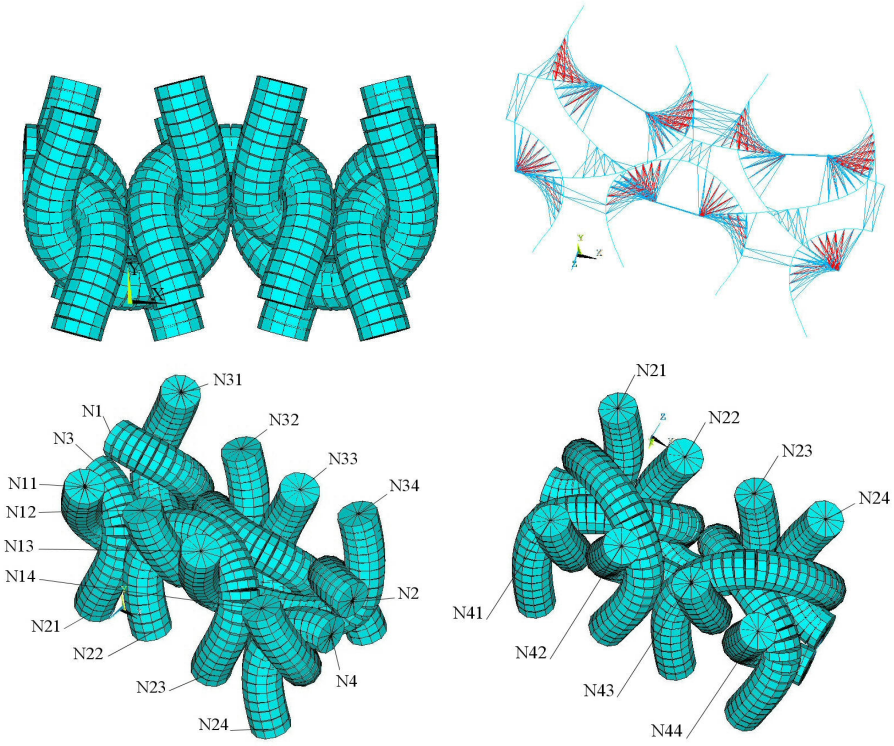

Figure 3-61: Beam model of the interlock unit cell, realistic representation (left), central axes and contact elements (right).

Table 3-23: BC, CE and displacement applied for the simulation of the interlock model in tensile test.

Tensile Test	
Along Wale Direction	Along Course Direction
UZ(N1, N2)=0	UZ(N1, N2)=0
UY(N2i, N4i)=-u, i=1…4 UY(N1i, N3i)=u, i=1…4	UX(N1,N3)=-u UX(N2,N4)=u
UX(N1i)=UX(N2i), i=1…4 UX(N3i)=UX(N4i), i=1…4 UY(N1)=UY(N2) UY(N3)=UY(N4)	UX(N1i)=UX(N2i), i=1…4 UX(N3i)=UX(N4i), i=1…4 UY(N1)=UY(N2) UY(N3)=UY(N4)
UX(N1)=UX(N3), UX(N2)=UX(N4) UX(N1,N3)=-UX(N2,N4)	UY(N1i, N3i)=equal, UY(N2i, N4i)= equal, i=1…4 UY(N1i, N3i)=-UY(N2i, N4i)
ROTY(N1, N2, N3, N4)=0	ROTY(N1, N2, N3, N4)=0
ROTX(N1i, N2i, N3i, N4i)=0, i=1…4	ROTX(N1i, N2i, N3i, N4i)=0, i=1…4

Table 3-24: BC, CE and displacement applied for the simulation of the interlock model in shear test.

Shear Test	
Along Wale Direction	Along Course Direction
UZ(N1, N2)=0	UZ(N1, N2)=0
UY(N1,N3)=-u UY(N2,N4)=u	UX(N2i, N4i)=-u, i=1…4 UX(N1i, N3i)=u, i=1…4
UX(N1)=UX(N3), UX(N2)=UX(N4) UX(N1,N3)=-UX(N2,N4)	UY(N1i, N3i)=equal, UY(N2i, N4i)= equal, i=1…4 UY(N1i, N3i)=-UY(N2i, N4i)
UX(N1i)=UX(N2i), i=1…4 UX(N3i)=UX(N4i), i=1…4 UY(N1i)=UY(N2i), i=1…4 UY(N3i)=UY(N4i), i=1…4	UX(N1)=UX(N2) UX(N3)=UX(N4) UY(N1)=UY(N2) UY(N3)=UY(N4)
ROTY(N1)= ROTY(N2), ROTY(N3)= ROTY(N4)	ROTY(N1)= ROTY(N2), ROTY(N3)= ROTY(N4)
ROTX(N1i)=ROTX(N2i), i=1…4 ROTX(N3i)=ROTX(N4i), i=1…4 ROTY(N1i)=ROTY(N2i), i=1…4 ROTY(N3i)=ROTY(N4i), i=1…4	ROTX(N1i)=ROTX(N2i), i=1…4 ROTX(N3i)=ROTX(N4i), i=1…4 ROTY(N1i)=ROTY(N2i), i=1…4 ROTY(N3i)=ROTY(N4i), i=1…4

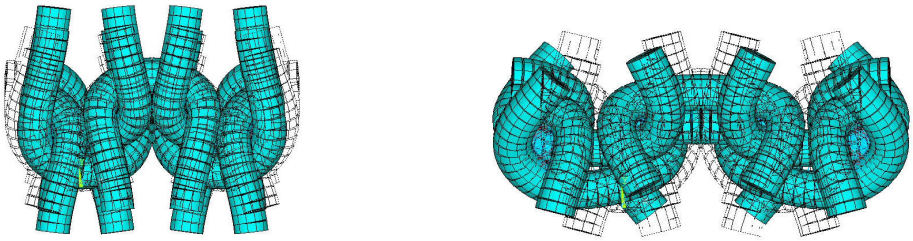

Figure 3-62: Deformed and undeformed shape of the interlock unit cell in tensile test (deformation = 0.30) along wale (left) and course direction (right).

Figure 3-63: Deformed and undeformed shape of the interlock unit cell in shear test (shear angle = 0.15) along wale (left) and course direction (right).

3.7 Conclusions

The typical structures of woven and knitted fabrics were studied for the generation of the respective geometrical models required for the mesomechanical analysis. Basic principle of the current stage is the representation of the yarns as homogenous structures. The uncompressed form of the yarns was assumed for the modelling of the initial conditions (undeformed state). Thereby the yarn cross sections, normal to the yarn axis, were considered circular through the yarn length. Under these considerations, the geometrical modelling of the fabric structure is fully defined by the three dimensional representation of the central axis of the yarn path and the definition of the cross section area. The advanced numerical design tools provided by the modern CAD software codes achieve the fast and easy geometrical modelling of complex textile structures.

Particular effort was given for the geometrical modelling of knitted structures. A generic technique was proposed for the definition of the geometrical characteristics of the typical knitted structures produced by cotton yarns. The proposed technique comprises the generation of a series of models and the selection of the one that corresponds to the minimum loop length. The correlation of the loop length with the initial energy was proved by the mechanical analysis of representative models belonging in the generated series. The modelling technique was also evaluated by the comparison of the structural characteristics (loop length) of the models with the real samples. The proposed modelling demonstrates satisfying accuracy according to the estimated error in the resulted value of the loop length.

Three FE approaches, the solid, shell and beam modelling, were implemented for the mesomechanical analysis of the fabrics. The three approaches were evaluated regarding the attribution of the yarn properties, the convenience in the application of the BC, the computational cost, the convergence success in the solution procedure and the reliability of the results. The evaluation of the three approaches was based on the simulation of the tensile deformation of the plain woven unit cell.

The beam modelling was proved adequate for certain reasons. Firstly the offered option of individual definition of the elastic modulus (E_{app}) and the moment of inertia (I) is preferential for the attribution of yarn models. Secondly the principle deformations of yarns (elongation and bending) resulting from the woven fabric loading are sufficiently predicted using the beam elements. Moreover the modelling, the meshing and the analysis are fast procedures in beam modelling approach. The computational cost is extremely low (504 DOF). The soft spot of the approach corresponds to the simplifications in the yarns interactions. Although the normal and tangential (friction) loads are evaluated, the yarn flattening presented during yarn compression is omitted.

The beam modelling approach was implemented for the mechanical analysis of the unit cell of typical fabric structures. The plain weave, basket, 2/2 twill and 5-satin were studied from the woven structures. The plain weft knitted, the rib 1×1 and the interlock structures were studied from the knitted structures. The tensile, shear and bending test of the textile mesoscopic model were simulated for the calculation of the respective properties. The symmetry and the periodicity of the unit cells within the fabric structure were taken into account for the definition of the appropriate boundary conditions (BC) and constraint equations (CE).

Chapter 4
The Macromechanical Modelling of Fabrics

Abstract

In the current chapter, the macromechanical modelling stage of textile structures is presented. The macromechanical analysis refers to the mechanical performance of the fabric sheet in complex deformations. The reduction of the computational cost demands the omitting of the representation of the structural unit cells. Thus the discrete structure of the fabric is replaced by a continuum model. It is obvious that the evaluation of the apparent properties of the discrete model and the generation of an equivalent continuum model (homogenization) is essential for the reliability of the macromechanical analysis. Three modelling approaches based on shell or solid-shell FE were adopted for the generation of the equivalent macromechanical model. The reliability of the macromechanical models was evaluated using experimental data received by the literature. In particular, the computational prediction of the macromechanical performance was based on the generation of the mesomechanical model of the unit cell, the calculation of the apparent properties, the implementation of the homogenization approaches and the simulation of the mechanical tests using the continuum macromechanical model.

4.1 Introduction

The mechanical performance of the textile structures is essential for their use in technical applications, as reinforcement in composite materials and face-sheets (resin impregnated woven fabrics) for sandwich structures. The bending and elastic characteristics have a great effect for the composite manufacturing process and the mechanical response of the composite structure. The evaluation of the performance of certain textile structures in complex deformations demands the mechanical analysis of them in the macro-scale. In general the structural architecture of textiles (fibres – yarns – fabrics) constitutes the basic obstacle for the macromechanical analysis of them, since the representation of the microstructure (constituent fibres) demands extremely high computational power for the modelling and the analysis of the structure in complex deformation states.

The mechanical analysis of these problems presenting complex microstructure and periodicity is faced implementing homogenization methods. Skeleton of the homogenization methods is the mechanical analysis of the unit cell in the micro- or meso-scale for the evaluation of the apparent properties and the generation of an equivalent macromechanical model presenting the performance of the structure. The homogenization was applied in biomechanics (Hollister et al. 1991), wood materials (Holmberg, Persson & Petersson 1999) and masonry panels (Lee

et al. 1996, Sacco 2009). Moreover a homogenization method was proposed for the prediction of the elastic properties of a composite structure consisting of a wire woven mesh imbedded in resin (Hübsch et al. 1996). This is a typical structure used for the construction of orthodontic brackets.

Several investigations were conducted focusing on the macromechanical performance of the fabrics, grouped in two basic categories. The first corresponds to the investigations based on the experimental measurement of the mechanical properties of fabrics and the generation of equivalent models describing their bending performance and drapeability (de Araújo, Fangueiro & Hong 2004, Collier et al. 1991, Ascough, Bez & Bricis 1996, Stylios, Wan & Powell 1995, Hu, Chen & Teng 2000). The second category focused on the computational analysis of fabrics in the mesoscopic level and the generation of models presenting equivalent in-plane elastic properties (Ng, Tse & Lau 1998, Choi, Tamma 2001, Lomov et al. 2007).

The current chapter focuses on the development of a homogenization method adequate for flexible structures, as textiles are. A sheet structure of simple geometry was firstly examined presenting similarities with woven structures (beam modelling, flexibility). A homogenization method was developed for the generation of equivalent continuum model with the simple discrete structure. The evaluation of the homogenization method was conducted computationally by the comparison of the macromechanical performance of the discrete and the continuum model.

Then the homogenization method was implemented in the plain-woven structure. The mechanical analysis of the structural unit cell for the definition of the mesoscopic properties was presented in the previous chapter. Three modelling approaches based on shell or solid-shell FE were adopted for the generation of the equivalent macromechanical model. The ANSYS software was used for the modelling and simulation. The evaluation of the homogenization method was based on the comparison of the mechanical performance of the continuum model with experimental data. A good approach between computational and experimental performance resulted. The major advantage of the proposed homogenization method is the generation of a continuum structure presenting simultaneously equivalent tensile, shear and bending performance with the discrete structure.

4.2 Homogenization method implemented in simple structure

The homogenization method was firstly implemented in a simple structure in order the macromechanical analysis of complex deformations using the discrete model to be practicable. Actually the simulation of the discrete structure in complex deformation is requisite for the evaluation of the implemented homogenization method. In general the homogenization of periodic structures is based on the study of the structural unit cell for the definition of the apparent properties and the generation of an equivalent model of continuum structure. The simulation of complex deformations demands the modelling of the structure in the macro-scale increasing significantly the computational cost or disabling the solution

achievement. Thus a simple structure was selected for the study, demanding low computational cost for the modelling, in order the simulation of complex deformations to be achievable using the discrete structure in the macro-scale (using a large part of the discrete structure). The homogenization method was evaluated computationally comparing the macromechanical performance of the discrete and the continuum structure. The ANSYS commercial code was used for the modelling and simulation in the meso- and macro-scale.

The model of the simple structure under investigation is given in the Figure 4-1. The structure consists of horizontal and vertical beams (type 2) jointed with diagonal supporting beams (type 1). The unit cell corresponds to the repeated unit of the structure (given also in the Figure 4-1). Every part of the unit cell (horizontal, vertical, diagonal) is modelled by a beam FE (BEAM188). Thus the unit cell consists of 6 beam elements and 4 nodes. The material and structural characteristics of the beam elements are given in the Table 4-1. The length of the horizontal beam (ℓ_x) and the vertical beam (ℓ_y) defines the geometry of the unit cell.

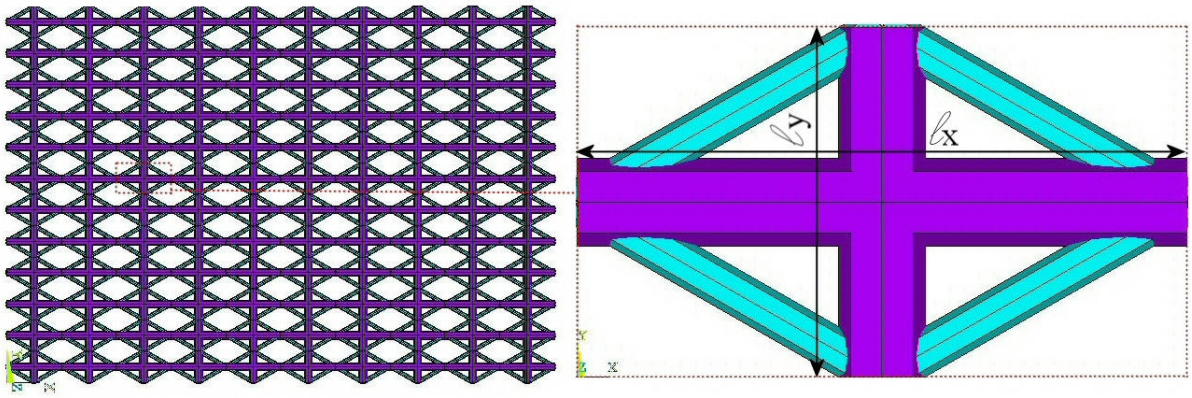

Figure 4-1: Model of the simple structure under investigation and the structural unit cell.

Table 4-1: Properties of the beam elements.

	material	section	moment of inertia
type 1	material 1 linear elastic isotropic E_1=142000 N/mm^2, ν=0.2	circular radius r_1=0.05 mm	$I_1 = \frac{\pi \cdot r_1^4}{4}$
type 2	material 2 linear elastic isotropic E_2=39000 N/mm^2, ν=0.2	circular radius r_2=0.1 mm	$I_2 = \frac{\pi \cdot r_2^4}{4}$

The apparent mechanical properties of the structure were calculated by the mechanical analysis of the unit cell considering the in-plane tensile and shear test. The innovation of the proposed homogenization method consists in the account of the bending stiffness of the discrete model. A model consisting of more than one unit cells (10 units ware used) was demanded for the simulation of the bending test for the elimination of the fixed end effect.

Thereafter the mechanical properties of the equivalent continuum model were calculated taking into account the in-plane tensile, in-plane shear and bending performance of the discrete structure. It was considered that the continuum model results from the replacement of the discrete unit cell by a shell FE of equal dimensions (in-plane). Thus the elastic properties of the shell FE and the thickness were demanded. Orthotropic elastic properties were introduced in the shell FE considering the symmetry presented in the discrete structure of the unit cell. The assumption of orthotropy will be evaluated comparing the mechanical performance of the discrete and the continuum structure. The elastic parameters of the orthotropic continuum model (E_x, E_y, G_{xy}, ν_{xy}) and the thickness (t) were calculated, as presented in continue.

Nomenclature:

E_x	: apparent elastic modulus of unit cell along x
E_y	: apparent elastic modulus of unit cell along y
G_{xy}, G_{yx}	: apparent shear moduli of the unit cell in xy plane
ν_{xy}, ν_{yx}	: apparent minor and major Poisson ratio of the unit cell in xy plane
A_x	: apparent section of the unit cell normal to x
A_y	: apparent section of the unit cell normal to y
I_x	: moment of inertia of the section of the continuum unit about x
I_y	: moment of inertia of the section of the continuum unit about y
B_1	: bending rigidity of the discrete structure about y (10 units along x)
B_2	: bending rigidity of the discrete structure about x (10 units along y)
t	: thickness of the continuum unit
ε_x, F_x	: imposed deformation and resultant reaction of the tensile of the unit cell along x
$\varepsilon_y^{'}$	: deformation of the unit cell along y axis resulted from the tensile along x
ε_y, F_y, σ_y	: imposed deformation and resultant reaction of the tensile of the unit cell along y
$\varepsilon_x^{'}$	: deformation of the unit cell along x axis resulted from the tensile along y
F_{z1}, u_{z1}	: reaction and displacement along z, the bending test of N units along x
F_{z2}, u_{z2}	: reaction and displacement along z, the bending test of N units along y
F_{sx}, u_{sx}	: reaction and imposed displacement of the unit cell, shear along x
F_{sy}, u_{sy}	: reaction and imposed displacement of the unit cell, shear along y

Table 4-2: Boundary conditions imposed for the deformation of the unit cell.

Tensile along *x*	Tensile along *x*
ux(1)=uy(1)=0	ux(2)=0, uy(2)=0
ux(3)=ux, uy(3)=0	uy(4)=uy, ux(4)=0
uy(2)=-uy(4)	ux(1)=-ux(3)
Shear along *x*	Shear along *y*
ux(4)=usx	ux(3)=usy
uy(1)=uy(3)=0	ux(2)=ux(4)=0
ux(2)=uy(2)=0	ux(1)=uy(1)=0

Tensile test along x axis

A displacement was applied corresponding to the deformation ε_x and the reaction force F_x was received. The apparent properties of the unit cell fulfil the following equation:

$$\frac{F_x}{t \cdot \ell_y} = E_x \cdot \varepsilon_x \Leftrightarrow E_x = \frac{F_x}{t \cdot \ell_y \cdot \varepsilon_x} \quad \text{(Eq. 4-1)}$$

$$\nu_{xy} = -\frac{\varepsilon'_y}{\varepsilon_x} \quad \text{(Eq. 4-2)}$$

Tensile test along y axis

A displacement was applied corresponding to the deformation ε_y and the reaction force F_y was received. Thus:

$$\frac{F_y}{t \cdot \ell_x} = E_y \cdot \varepsilon_y \Leftrightarrow E_y = \frac{F_y}{t \cdot \ell_x \cdot \varepsilon_y} \quad \text{(Eq. 4-3)}$$

$$\nu_{yx} = -\frac{\varepsilon'_x}{\varepsilon_y} \quad \text{(Eq. 4-4)}$$

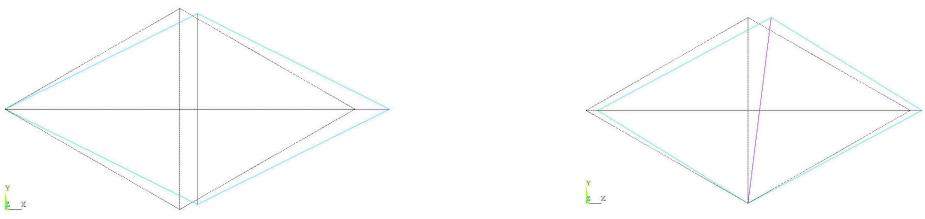

Figure 4-2: Deformed and undeformed model of the unit cell subjected to tensile and shear test.

Shear test in xy plane

A displacement u_{sy} was applied and the reaction F_{sy} was calculated. Thus:

$$G_{xy} = \frac{F_{sy} \cdot \ell_x}{u_{sy} \cdot A_x} = \frac{F_{sy} \cdot \ell_x}{u_{sy} \cdot t \cdot \ell_y} \qquad \text{(Eq. 4-5)}$$

Shear test along y

A displacement u_{sx} was applied and the reaction F_{sx} was calculated. Thus:

$$G_{yx} = \frac{F_{sx} \cdot \ell_y}{u_{sx} \cdot A_y} = \frac{F_{sx} \cdot \ell_y}{u_{sx} \cdot t \cdot \ell_x} \qquad \text{(Eq. 4-6)}$$

Bending test, moment about y

The model subjected in the bending test consists of *N* unit cells along the *x* axis, shown in the Figure 4-3. A vertical displacement, u_{z1}, was imposed and the reaction force was calculated, F_{z1}. The bending rigidity and the apparent elastic properties of the model fulfil the following equations:

$$\left.\begin{array}{l} B_1 = \dfrac{F_{z1} \cdot (N \cdot \ell_x)^3}{3u_{z1}} \\ B_1 = E_x \cdot I_y = E_x \cdot \dfrac{\ell_y \cdot t^3}{12} \end{array}\right\} \Rightarrow \frac{F_{z1} \cdot (N \cdot \ell_x)^3}{3u_{z1}} = E_x \cdot \frac{\ell_y \cdot t^3}{12} \qquad \text{(Eq. 4-7)}$$

Bending test, moment about x

The model subjected in the bending test consists of *N* unit cells along the y axis. A vertical displacement, u_{z2}, was imposed and the reaction force was calculated, F_{z2}. The bending rigidity and the apparent elastic properties of the model fulfil the following equations:

$$\left.\begin{array}{l} B_2 = \dfrac{F_{z2} \cdot (N \cdot \ell_y)^3}{3u_{z2}} \\ B_2 = E_y \cdot I_x = E_y \cdot \dfrac{\ell_x \cdot t^3}{12} \end{array}\right\} \Rightarrow \frac{F_{z2} \cdot (N \cdot \ell_y)^3}{3u_{z2}} = E_y \cdot \frac{\ell_x \cdot t^3}{12} \qquad \text{(Eq. 4-8)}$$

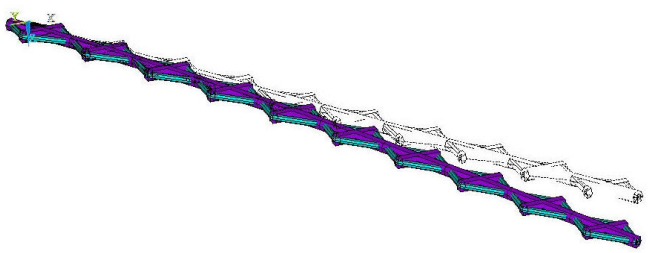

Figure 4-3: Deformed and undeformed model of 10 units along *x* resulted from the bending test.

The Eq. 4-1, 4-3, 4-7, 4-8 constitute a nonlinear equation system of 4 equation and 3 unknown parameters (E_x, E_y, t). The equation system has a solution when the Eq. 4-9 is fulfilled. This consideration corresponds to symmetric unit cell structure ($\ell_x = \ell_y$). Thus it is proved that the generation of a continuum orthotropic model (shell or solid-shell) presenting equivalent mechanical performance with an asymmetric discrete structure is impractical.

$$\frac{B_1}{B_2} = \frac{E_x \cdot \frac{\ell_y \cdot t^3}{12}}{E_y \cdot \frac{\ell_x \cdot t^3}{12}} \Leftrightarrow \frac{B_1}{B_2} = \frac{E_x}{E_y} \cdot \frac{\ell_y}{\ell_x} \qquad \text{(Eq. 4-9)}$$

4.2.1 Macromechanical modelling for symmetric unit cell

The symmetric unit cell was considered, with $\ell_x = \ell_y = 1$ mm, for the generation of the equivalent continuum model. The tensile, shear and bending test of the unit cell was performed along x axis (since it is symmetric) and the results are given below:

A deformation ε_x=0.1 was applied in the tensile test along x and the reaction force F_x =180.7 N and normal deformation $\varepsilon_y^{'}$=0.035 were received.

A displacement u_{sx} =0.1 mm was applied and the reaction F_{sx}=79.17 N was calculated.

The model subjected in the bending test consists of N=10 unit cells along the x axis. A vertical displacement, uz_1=0.1 mm, was imposed and the reaction force was calculated, F_{z1}=1.19E-03 N.

The system of Eq. 4-1, 4-2, 4-5, 4-7 gave: $E_x = E_y$ =11137 N/mm2, G_{xy} = 4880 N/mm2, v_{xy} = 0.355 and t=0.162 mm.

The evaluation of the homogenization method was based on the comparison of the macromechanical performance of the continuum and the discrete structure in two tests. Thus the discrete and the continuum model of the structure were generated for 30×30 units and their mechanical performance was compared. The continuum model corresponds to a shell mesh (SHELL63) of dimensions $30\ell_x \times 30\ell_y$. The linear elastic orthotropic material calculated above (Ex=Ey, Gxy, vxy) were introduced in the continuum model.

Firstly a complex deformation was examined. The model (discrete and continuum) was fully supported at the external nodes and a normal displacement, $3\times\ell_x$, was imposed in the central area of $6\ell_x \times 6\ell_y$. The deformed models are given in the Figure 4-4. The reactions (displacement direction) developed in both models were compared:

ΣFz (discrete) = 635.75 N

ΣFz (continuum) = 649.67 N

Ratio ΣFz (continuum/ discrete)= 1.022

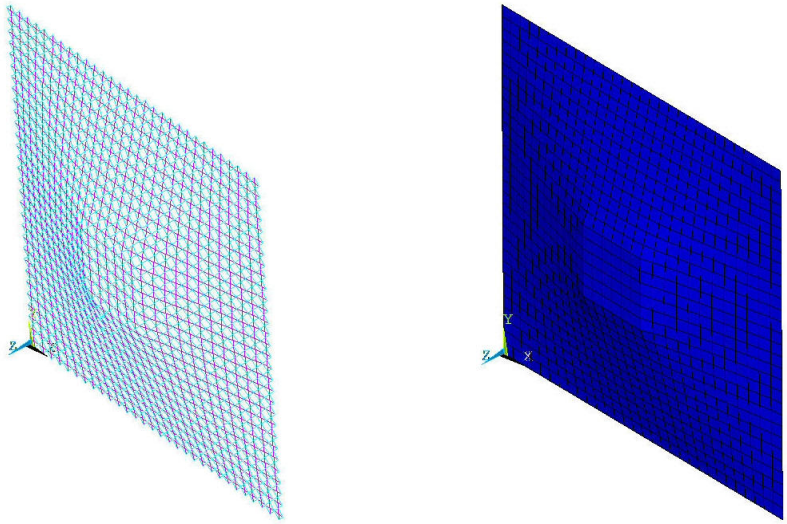

Figure 4-4: Deformed shape of the discrete and the continuum model resulted from the first deformation.

The second deformation corresponds to the bending test of the model applying a pressure=0.005 N/mm^2. A simple support was imposed in one edge of the model and a rolling support in the cross edge. The deformed shapes of the discrete and continuum model are given in the Figure 4-5. The vertical displacement (along z) resulted from the simulation was calculated for both models:

u_z (discrete) = 8.2238 mm

u_z (continuum) = 7.8433 mm

Ratio u_z (continuum/ discrete) = 0.954

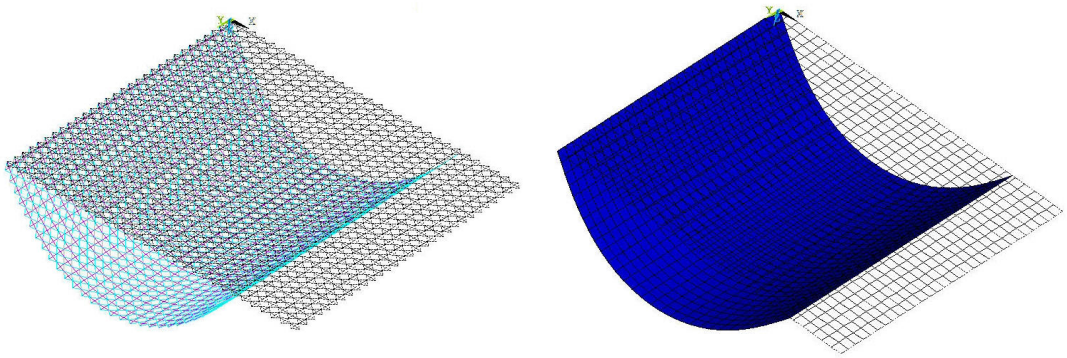

Figure 4-5: Deformed shape of the discrete and the continuum model resulted from the second deformation.

The low divergence presented in the mechanical performance of the discrete and the continuum model in the examined deformations ensures the reliability of the proposed homogenization method for symmetric unit cells.

4.2.2 Macromechanical modelling for asymmetric unit cell

The 3-layer continuum model was examined for the homogenization of the asymmetric structures. The considered 3-layer structure consists of two orthotropic continuum materials and symmetrical cross-section. Identical layers (material properties and thickness) were used for the outer layers.

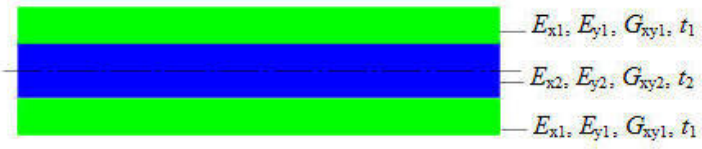

Figure 4-6: Cross-section of the 3-layer structure.

The elastic and shear moduli and the thickness of the outer layers E_{x1}, E_{y1}, G_{xy1}, t_1 and the respective parameters of the inner layer E_{x2}, E_{y2}, G_{xy2}, t_2 were considered for the formulation of the equilibrium equations.

Tensile test along x axis

$$F_x = 2F_{x1} + F_{x2} = \sigma_{x1} \cdot 2t_1 \cdot \ell_y + \sigma_{x2} \cdot 2t_2 \cdot \ell_y = \varepsilon_x \cdot E_{x1} \cdot 2t_1 \cdot \ell_y + \varepsilon_x \cdot E_{x2} \cdot t_2 \cdot \ell_y \Leftrightarrow$$

$$E_{x1} \cdot 2t_1 + E_{x2} \cdot t_2 = \frac{F_x}{\varepsilon_x \cdot \ell_y} \qquad \text{(Eq. 4-10)}$$

where F_{x1} and F_{x2} the hypothesized reaction force developed in the external and internal layer respectively.

Tensile test along y axis

$$F_y = 2F_{y1} + F_{y2} = \sigma_{y1} \cdot 2t_1 \cdot \ell_x + \sigma_{y2} \cdot 2t_2 \cdot \ell_x = \varepsilon_y \cdot E_{y1} \cdot 2t_1 \cdot \ell_x + \varepsilon_y \cdot E_{y2} \cdot t_2 \cdot \ell_x \Leftrightarrow$$

$$\Leftrightarrow E_{y1} \cdot 2t_1 + E_{y2} \cdot t_2 = \frac{F_y}{\varepsilon_y \cdot \ell_x} \qquad \text{(Eq. 4-11)}$$

where F_{y1} and F_{y2} the hypothesized reaction force developed in each external and internal layer respectively.

Shear test in xy plane

$$F_{sy} = 2\sigma_{xy1} \cdot (\ell_y \cdot t_1) + \sigma_{xy2} \cdot (\ell_y \cdot t_2) = 2 \cdot \frac{u_{sy}}{\ell_x} \cdot G_{xy1} \cdot \ell_y \cdot t_1 + \frac{u_{sy}}{\ell_x} \cdot G_{xy2} \cdot \ell_y \cdot t_2 \Leftrightarrow$$

$$\Rightarrow 2 \cdot G_{xy1} \cdot t_1 + G_{xy2} \cdot t_2 = \frac{F_y \cdot \ell_x}{u_{sy} \cdot \ell_y} \qquad \text{(Eq. 4-12)}$$

Shear test in yx plane

$$F_{sx} = 2\sigma_{yx1} \cdot (\ell_x \cdot t_1) + \sigma_{yx2} \cdot (\ell_x \cdot t_2) = 2 \cdot \frac{u_{sx}}{\ell_y} \cdot G_{yx1} \cdot \ell_x \cdot t_1 + \frac{u_{sx}}{\ell_y} \cdot G_{yx2} \cdot \ell_x \cdot t_2 \Leftrightarrow$$

$$\Rightarrow 2 \cdot G_{yx1} \cdot t_1 + G_{yx2} \cdot t_2 = \frac{F_x \cdot \ell_y}{u_{sx} \cdot \ell_x} \qquad \text{(Eq. 4-13)}$$

Bending test, moment about y

$$\left.\begin{aligned} B_1 &= 2E_{x1} \cdot I_{y1} + E_{x2} \cdot I_{y2} = 2E_{x1}\left[\frac{\ell_y \cdot t_1^{\,3}}{12} + \ell_y \cdot t_1 \cdot \left(\frac{t_1 + t_2}{2}\right)^2\right] + E_{x2}\frac{\ell_y \cdot t_1^{\,3}}{12} \\ B_1 &= \frac{F_{z1} \cdot (N \cdot \ell_x)^3}{3u_{z1}} \end{aligned}\right\} \Leftrightarrow$$

$$\frac{F_{z1} \cdot (N \cdot \ell_x)^3}{3u_{z1}} = \ell_y\left[2E_{x1}\left(\frac{t_1^{\,3}}{12} + t_1 \cdot \frac{(t_1 + t_2)^2}{4}\right) + E_{x2}\frac{t_2^{\,3}}{12}\right] \qquad \text{(Eq. 4-14)}$$

where I_{y1}, I_{y2} the bending rigidity and moment of inertia of each external and internal layer.

Bending test, moment about x

$$\left.\begin{aligned} B_2 &= 2E_{y1} \cdot I_{x1} + E_{y2} \cdot I_{x2} = 2E_{y1}\left[\frac{\ell_x \cdot t_1^{\,3}}{12} + \ell_x \cdot t_1 \cdot \left(\frac{t_1 + t_2}{2}\right)^2\right] + E_{y2}\frac{\ell_x \cdot t_1^{\,3}}{12} \\ B_2 &= \frac{F_{z2} \cdot (N \cdot \ell_y)^3}{3u_{z2}} \end{aligned}\right\} \Leftrightarrow$$

$$\frac{F_{z2} \cdot (N \cdot \ell_y)^3}{3u_{z2}} = \ell_x\left[2E_{y1}\left(\frac{t_1^{\,3}}{12} + t_1 \cdot \frac{(t_1 + t_2)^2}{4}\right) + E_{y2}\frac{t_2^{\,3}}{12}\right] \qquad \text{(Eq. 4-15)}$$

where I_{x1}, I_{x2} the bending rigidity and moment of inertia of each external and internal layer.

The Eq. 4-10, 4-11, 4-14, 4-15 constitute an equation system of 4 equations and 6 unknown parameters (E_{x1}, E_{x2}, E_{y1}, E_{y2}, t_1, t_2). The values of the thicknesses were considered, received from an acceptable field, and the equation system was solved for the calculation of the other 4 parameters. The feasible solutions (positive values) were selected from the infinite solutions

number. Moreover the mean value $E_{m2}=\frac{E_{x2}+E_{y2}}{2}$ was calculated and the shear modulus $G_{xy2}=\frac{E_{m2}}{2(1+\nu_{xy})}$, was considered for the inner layer. The shear modulus G_{xy1} of the outer layers was calculated by the Eq. 5-12. Similarly the G_{xy1}, G_{xy2} were calculated.

Firstly the effect of the layers thickness in the mechanical performance of the continuum model was evaluated. Thus considering the discrete structure for ℓ_x=1 mm, ℓ_y=1.2 mm, the solutions of the equation system for the defined values t_1, t_2 are given in the Table 4-3.

Table 4-3: Defined thickness and resultant parameters from the homogenization of the discrete structure ℓ_x=1 mm, ℓ_y=1.2 mm

model	t_1	t_2	E_{x1}	E_{x2}	E_{y1}	E_{y2}	E_{z1}	E_{z2}	G_{xy2}	G_{xy1}
1	**0.1**	**0.05**	**846.1**	**5040**	**2985.2**	**48683**	**1915.6**	**26862**	**1380.0**	**73.46**
2	0.1	0.06	734.8	4571	2490.6	42218	1612.7	23395	1243.9	70.64
3	0.1	0.07	636.2	4200	2042.7	37467	1339.4	20833	1133.7	68.27
4	0.1	0.08	548.0	3895	1634.8	33803	1091.4	18849	1041.7	66.29
5	**0.1**	**0.09**	**468.8**	**3639**	**1261.5**	**30877**	**865.1**	**17258**	**962.9**	**64.63**
6	0.1	0.1	397.2	3418	918.5	28475	657.8	15947	894.4	63.24
7	0.1	0.11	332.1	3226	602.1	26462	467.1	14844	834.0	62.08
8	0.1	0.12	272.7	3056	309.2	24745	290.9	13900	780.3	61.14
9	**0.1**	**0.13**	**218.2**	**2905**	**37.2**	**23260**	**127.7**	**13082**	**732.1**	**60.37**

The continuum models 1, 5 and 9 corresponding to 10×10 units were used for the simulation of the second complex deformation presented before for a pressure 0.1 N/mm^2 and the results are given in the Table 4-4. Thus equivalent mechanical performance is presented in the examined homogenous models.

Table 4-4: Results of the complex deformation for the models 1, 5, 9.

model	ΣU_z (mm) (discrete)	ΣU_z (mm) (continuum)	ratio $\Sigma U_{z,\text{continuum}}/\Sigma U_{z,\text{discrete}}$
1	3.610	3.618	1.002
5	3.610	3.617	1.002
9	3.610	3.617	1.002

The evaluation of the proposed homogenization method was conducted computationally comparing the macromechanical performance of the discrete and the continuum model in a complex deformation. The macromechanical discrete and the respective homogenized model were generated for 10×10 units. The values of the layers thickness were defined (t_1=0.1 mm, t_2=0.05 mm) and the elastic parameters were calculated by the solution of the equations system. The continuum model was meshed using layer shell elements (SHELL91). Both models were tested in the second complex deformation presented above. The reaction forces are presented in the Table 4-5.

Table 4-5: Reaction forces resulted from the simulation of the complex deformation for the discrete and the continuum model.

structure	Pressure (N/mm^2)	ΣU_z (mm) (discrete)	ΣU_z (mm) (continuum)	Ratio $\Sigma U_{z,\text{continuum}}/\Sigma U_{z,\text{discrete}}$
ℓ_x=1 mm, ℓ_y=1.2 mm	0.1	3.610	3.618	1.002
ℓ_x=1.4 mm, ℓ_y=0.8 mm	0.1	4.415	4.460	1.010
ℓ_x=1 mm, ℓ_y=3 mm	0.1	2.658	2.585	0.973

Concluding the proposed homogenization method results in reliable equivalent models accounting the tensile, shear and bending performance of the examined structure. The accuracy of the proposed method was evaluated computationally by the comparison of the mechanical performance of the discrete and the continuum models. The divergence of the models was less than 5 % for symmetric or asymmetric structures.

4.3 Homogenization method implemented in the plain woven structure

The proposed homogenization method was implemented for the macro-scale analysis of the plain woven structure. The modelling assumptions and the mechanical analysis of the unit cell of the woven structure for the evaluation of the apparent properties was presented in the previous chapter. Considering the tensile, shear and bending deformation of the discrete model the elastic parameters are calculated.

Nomenclature:

p_1 : warp spacing of woven structure (mm)

p_2 : weft spacing of woven structure (mm)

B_{rp} : bending rigidity of 5 units placed along warp, moment about weft (N·mm²/thread)

B_{ft} : bending rigidity of 5 units placed along weft, moment about warp

(N·mm²/thread)

E_{rp} : elastic modulus of unit cell along warp (N/thread)

E_{ft} : elastic modulus of unit cell along weft (N/thread)

G_{rp} : shear modulus of unit cell warpwise (N/thread)

G_{ft} : shear modulus of unit cell weftwise (N/thread)

ν_{rp} : Poisson ratio of the unit cell warpwise

ν_{ft} : Poisson ratio of the unit cell weftwise

E_{iz} : elastic modulus of the layer *i* along *Z* - warp (N/mm^2)

E_{ix} : elastic modulus of the layer *i* along *X* - weft (N/mm^2)

G_{ixz} : *XZ* shear modulus of the layer *i* (N/mm^2)

G_{izx} : *ZX* shear modulus of the layer *i* (N/mm^2)

ν_{ixz} : *XZ* Poisson ratio of the layer *i* (N/mm^2)

ν_{izx} : *ZX* Poisson ratio of the layer *i* (N/mm^2)

th_i : thickness of layer *i*

i (index) : *M*, 1, 2 for monolayer, layer 1, layer 2 respectively

Thus the continuum model of thickness th_M and mechanical parameters E_{Mx}, E_{Mz}, G_{Mxz}, G_{Mzx}, ν_{Mxz}, ν_{Mzx} should fulfil the following system of equations:

$$E_{Mz} = E_{rp} / (p_1 \cdot th_M) \quad \text{(Eq. 4-16)}$$

$$E_{Mx} = E_{ft} / (p_2 \cdot th_M) \quad \text{(Eq. 4-17)}$$

$$E_{Mz} = 12 \cdot B_{rp} / (p_1 \cdot th_M^3) \quad \text{(Eq. 4-18)}$$

$$E_{Mx} = 12 \cdot B_{ft} / (p_2 \cdot th_M^3) \quad \text{(Eq. 4-19)}$$

$$G_{Mxz} = \frac{G_{rp}}{th_M \cdot p_2} \quad \text{(Eq. 4-20)}$$

$$G_{Mzx} = \frac{G_{ft}}{th_M \cdot p_1} \quad \text{(Eq. 4-21)}$$

$$\nu_{Mxz} = \nu_{ft} \quad \text{(Eq. 4-22)}$$

$$\nu_{Mzx} = \nu_{rp} \quad \text{(Eq. 4-23)}$$

The system of equations 4-16, 4-17, 4-18, 4-19 (4 equations – 3 unknown parameters: E_{Mx}, E_{Mz}, th_M) has a solution when the Eq. 4-24 is fulfilled. This consideration corresponds to symmetric woven structure (equal warp and weft spacing, warp and weft diameter).

$$B_{rp} / B_{ft} = E_{rp} / E_{ft} \quad \text{(Eq. 4-24)}$$

The different elastic properties of the woven structure along warp and weft direction and the different bending properties (depending on the thread properties, the warp and weft density) preclude the generation of a continuum structure of equivalent performance (Vassiliadis et al. 2009, Kallivretaki, Vassiliadis & Provatidis 2009). Several methods were implemented for the generation of a sheet model presenting equivalent performance with the asymmetric woven structure:

a. Two shell meshes of coincident nodes presenting different stiffness (membrane or bending)

b. Two shell meshes of coincident nodes of different material properties

c. 3-layer continuum structure of symmetric cross-section (meshed using shells or solid-shell elements)

Orthotropic material was considered for each mesh to present different elastic properties along warp and weft direction.

4.3.1 Two shell meshes of different stiffness

Two shell meshes of coincident nodes were used in the first approach **(Kallivretaki, Vassiliadis & Provatidis 2009)**. The meshes individually support the elastic or the bending performance of the structure. Thus the first shell mesh (layer 1) provides the membrane stiffness (fulfilling the Eq. 4-16, 4-17) the second mesh (layer 2) provides the bending stiffness (fulfilling the Eq. 4-18, 4-19). Consequently the mechanical parameters E_{Mx}, E_{Mz} presented in the equations of the tensile and the bending deformation receive independent values (M=1, 2) and the equation system (4-16, 4-17, 4-18, 4-19) has infinite solutions (4 equations – 6 unknown parameters: E_{1x}, E_{1z}, th_1, E_{2x}, E_{2z}, th_2). Considering the thickness values, the mechanical parameters are calculated by the equation system solution.

Orthotropic material was considered for each mesh to present different elastic properties along warp and weft direction. The current homogenized model presents equivalent performance in tensile and bending with the discrete model. Drawback of the approach is the failure of the analysis in large deformation conditions that is essential for the simulation of the macromechanical tests.

4.3.2 Two shell meshes of different material

The second approach constitutes a development of the first one intending at the generation of an equivalent model supporting large scale deformations **(Kallivretaki, Vassiliadis & Provatidis 2009)**. This approach consists in the generation of two shell meshes of coincident nodes that present different material properties. Both shell meshes present membrane and bending stiffness in this case. The keypoint of the current approach is the superposition of the meshes to present the apparent performance of the discrete structure. The calculation of the material properties of the meshes result from the fulfilling of the following equations:

$$E_{1z} \cdot th_1 + E_{2z} \cdot th_2 = E_{rp} / p_1 \quad \text{(Eq. 4-25)}$$

$$E_{1x} \cdot th_1 + E_{2x} \cdot th_2 = E_{ft} / p_2 \quad \text{(Eq. 4-26)}$$

$$E_{1z\cdot} \cdot p_1 \cdot th_1^3 / 12 + E_{2z\cdot} \cdot p_1 \cdot th_2^3 / 12 = B_{rp} \quad \text{(Eq. 4-27)}$$

$$E_{1x\cdot} \cdot p_2 \cdot th_1^3 / 12 + E_{2x\cdot} \cdot p_2 \cdot th_2^3 / 12 = B_{ft} \quad \text{(Eq. 4-28)}$$

$$G_{1xz} \cdot th_1 + G_{2xz} \cdot th_2 = G_{rp} / p_2 \quad \text{(Eq. 4-29)}$$

$$G_{1zx} \cdot th_1 + G_{2zx} \cdot th_2 = G_{ft} / p_1 \quad \text{(Eq. 4-30)}$$

$$\nu_{1xz} = \nu_{2xz} = \nu_{ft} \quad \text{(Eq. 4-31)}$$

$$\nu_{1zx} = \nu_{2zx} = \nu_{rp} \quad \text{(Eq. 4-32)}$$

The equation system (4-25, 4-26, 4-27, 4-28) has infinite solutions (4 equations – 6 unknown parameters: E_{1x}, E_{1z}, th_1, E_{2x}, E_{2z}, th_2). Considering the thickness values, the mechanical parameters are calculated by the equations given below.

SYSTEM SOLUTION

th_1, th_2 are defined

$$E_{2z} = \left(12 \cdot B_{rp} - th_1^2 \cdot E_{rp}\right) / \left(p_1 \cdot th_2^3 - p_1 \cdot th_1^2 \cdot th_2\right) \quad \text{(Eq. 4-33)}$$

$$E_{1z} = \frac{1}{th_1}\left(\frac{E_{rp}}{p_1} - E_{2z} \cdot th_2\right) \quad \text{(Eq. 4-34)}$$

$$E_{2x} = \left(12 \cdot B_{ft} - th_1^2 \cdot E_{ft}\right) / \left(p_2 \cdot th_2^3 - p_2 \cdot th_1^2 \cdot th_2\right) \quad \text{(Eq. 4-35)}$$

$$E_{1x} = \frac{1}{th_1}\left(\frac{E_{ft}}{p_2} - E_{2x} \cdot th_2\right) \quad \text{(Eq. 4-36)}$$

The capability of nonlinear analysis of the proposed model is advantageous for the simulation of the fabric deformation in the macro-scale.

4.3.3 3-Layer continuum structure (meshed using shell or solid-shell elements)

The 3-layer structure consists of two orthotropic continuum materials and symmetrical cross-section **(Vassiliadis, Kallivretaki, Frantzeskakis & Provatidis 2009)**. Identical layers (material properties and thickness) were used for the outer layers. Considering E_{1x}, E_{1z}, G_{1xz}, G_{1zx}, ν_{1xz}, ν_{1zx} the mechanical properties and th_1 the thickness of the outer layers and E_{2x}, E_{2z}, G_{2xz}, G_{2zx}, ν_{2xz}, ν_{2zx} the mechanical properties and th_2 the thickness of the inner layer, the equivalent properties fulfil the following equation system:

$$2E_{1z} \cdot th_1 + E_{2z} \cdot th_2 = E_{rp} / p_1 \quad \text{(Eq. 4-37)}$$

$$2E_{1x} \cdot th_1 + E_{2xt} \cdot th_2 = E_{ft} / p_2 \quad \text{(Eq. 4-38)}$$

$$2E_{1z}\left(\frac{th_1^{\,3}}{12} + th_1 \cdot \frac{(th_1 + th_2)^2}{4}\right) + E_{2z}\frac{th_2^{\,3}}{12} = B_{rp} / p_1 \quad \text{(Eq. 4-39)}$$

$$2E_{1x}\left(\frac{th_1^{\,3}}{12} + th_1 \cdot \frac{(th_1 + th_2)^2}{4}\right) + E_{2x}\frac{th_2^{\,3}}{12} = B_{ft} / p_2 \quad \text{(Eq. 4-40)}$$

$$2G_{1xz} \cdot th_1 + G_{2xz} \cdot th_2 = G_{rp} / p_2 \quad \text{(Eq. 4-41)}$$

$$2G_{1zx} \cdot th_1 + G_{2zx} \cdot th_2 = G_{ft} / p_1 \quad \text{(Eq. 4-42)}$$

$$\nu_{1xz} = \nu_{2xz} = \nu_{ft} \quad \text{(Eq. 4-43)}$$

$$\nu_{1zx} = \nu_{2zx} = \nu_{rp} \quad \text{(Eq. 4-44)}$$

The equation system (4-37, 4-38, 4-39, 4-40) has infinite solutions (4 equations – 6 unknown parameters: E_{1x}, E_{1z}, th_1, E_{2x}, E_{2z}, th_2). Considering the thickness values, the mechanical parameters are calculated by the equations given below.

SYSTEM SOLUTION

th_1, th_2 are defined

$$C_A = \frac{th_1^3}{12} + \frac{1}{4} th_1 (th_1 + th_2)^2 \quad \text{(Eq. 4-45)}$$

$$C_B = \frac{th_2^3}{12} \quad \text{(Eq. 4-46)}$$

$$E_{1z} = \frac{1}{2th_1}\left(\frac{E_{rp}}{p_1} - E_{2z} \cdot th_2\right) \quad \text{(Eq. 4-47)}$$

$$E_{2z} = \frac{C_A \cdot E_{rp} - th_1 \cdot B_{rp}}{p_1 (C_A \cdot th_2 - C_B \cdot th_1)} \quad \text{(Eq. 4-48)}$$

$$E_{1x} = \frac{1}{2th_1}\left(\frac{E_{ft}}{p_2} - E_{2x} \cdot th_2\right) \quad \text{(Eq. 4-49)}$$

$$E_{2x} = \frac{C_A \cdot E_{ft} - th_1 \cdot B_{ft}}{p_2 (C_A \cdot th_2 - C_B \cdot th_1)} \quad \text{(Eq. 4-50)}$$

4.4 Experimental evaluation of the homogenization method

4.4.1 Case Study 1: The macromechanical simulation of the bending test

The proposed homogenization method was evaluated using experimental data received from the literature (Ghosh, Batra & Barker 1990). A set of plain woven fabrics was selected constituted by monofilament yarns. The yarn properties (material, diameter and bending rigidity) and the structural characteristics of the samples (warp and weft density) were given by the authors (Table 4-6). Moreover the researchers measured the bending performance of the samples using the KES-F. The bending properties of the samples (macromechanical performance) under examination are given in the Table 4-11.

Table 4-6: Properties of the examined samples.

Fabric	Threads/cm		Spacing		Yarn Properties			
	Warp	Weft	Warp (p_1,mm)	Weft (p_2,mm)	Type	Diameter (D, mm)	Bending Rigidity (B, N·mm²)	Elastic Modulus* (E, N/mm²)
MF2	19.3	16.9	0.5181	0.5917	nylon 6	0.1975	0.0902	1208.0
MF3	19.3	20.1	0.5181	0.4975				
MF4	24.4	24.0	0.4098	0.4167	nylon 6.6	0.1450	0.0363	1672.2
MF5	20.5	20.7	0.4878	0.4831				
MF6	24.4	23.6	0.4098	0.4237				

*The elastic modulus of the Nylon fibres was calculated by $E=64\cdot B/(\pi\cdot D^4)$.

The mesomechanical modelling was implemented for the evaluation of the apparent mechanical properties of the unit cells of each structure. The elastic properties and Poisson ratios were calculated by the nonlinear analysis of the unit cell in the tensile test for the tensile strain 0.1. The shear properties were calculated by the nonlinear analysis of the unit cell in the shear test for the shear angle 0.1 radians. The bending rigidity was calculated by the linear analysis of the bending test of the model consisting of 5 unit cells. The deflection equal to 5 % of the model length was imposed for the bending simulation. The resultant values are given in the Table 4-7.

Table 4-7: Results from the mesomechanical analysis of the unit cell.

Sample	Tensile properties (N/thread)		Poisson ratio	
	warp (E_{rp})	weft (E_{ft})	warp (ν_{rp})	weft (ν_{ft})
MF2	22.4	19.0	0.288	0.311
MF3	19.8	20.9	0.256	0.238
MF4	15.7	15.3	0.321	0.325
MF5	16.3	16.5	0.369	0.373
MF6	15.9	15.2	0.324	0.326
Sample	Bending rigidity (N·mm²/thread)		Shear properties (N/thread)	
	warp (B_{rp})	weft (B_{ft})	warp (G_{rp})	weft (G_{ft})
MF2	8.47E-02	8.33E-02	0.365	0.268
MF3	8.27E-02	8.33E-02	0.319	0.356
MF4	3.39E-02	3.28E-02	0.202	0.196
MF5	3.45E-02	3.45E-02	0.102	0.105
MF6	3.40E-02	3.38E-02	0.183	0.169

The mechanical properties of the continuum model were calculated by the solution of the respective equation system defining the thickness values. The calculation of the mechanical properties for each homogenization method is described in continue.

In the homogenisation approach based on the two shell meshes of different stiffnesses the mechanical properties were calculated independently for each mesh. The elastic properties of the homogenized model for the sample MF2 are presented as a function of the thickness of the shell meshes in the Figure 4-7. For example if we consider the thickness values th_1=th_2=0.2 mm the elastic properties E_{1z}=216.2 N/mm^2, E_{1x}=160.6 N/mm^2, E_{2z}=245.3 N/mm^2, E_{2x}=211.1 N/mm^2 derive. The divergence of the curves E_{1x}, E_{2x} and E_{1z}, E_{2z} for the condition th_1= th_2 ensures the absence of a shell sheet supporting sufficiently the tensile and bending performance of the sample. Since the thicknesses are independent values, there is also the option to select unequal thicknesses for the two shell meshes. The mechanical properties calculated for the samples under investigation, defining th_1=th_2=0.2 mm, are given in the Table 4-8.

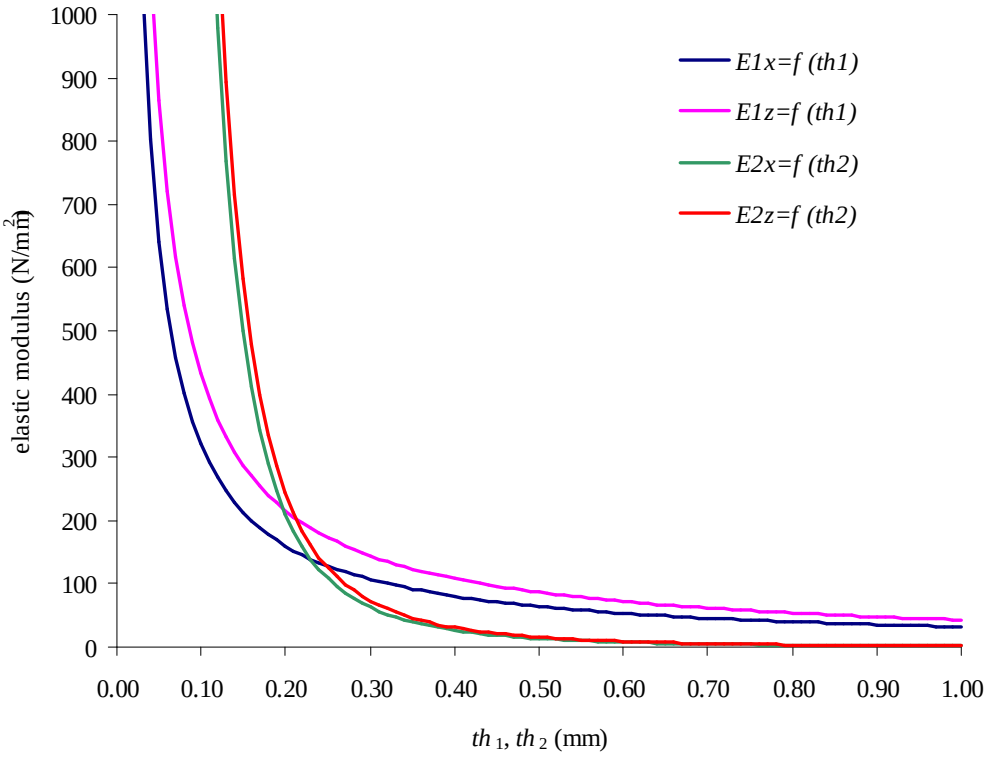

Figure 4-7: The relation of the elastic moduli of the continuum model and the thickness value resulting from the homogenization method of two shell meshes with different stiffness. The MF2 sample was considered.

Table 4-8: Properties of the shell meshes providing different stiffness.

Sample	shell mesh with membrane stiffness				shell mesh with bending stiffness			
	th_1 (mm)	E_{1x} (N/mm^2)	E_{1z} (N/mm^2)	G_{1xz} (N/mm^2)	th_2 (mm)	E_{2x} (N/mm^2)	E_{2z} (N/mm^2)	G_{2xz} (N/mm^2)
MF2	0.2	160.6	216.2	3.09	0.2	211.1	245.3	2.58
MF3	0.2	209.7	191.0	3.21	0.2	251.0	239.5	3.44
MF4	0.2	184.1	191.3	2.42	0.2	118.1	124.1	2.39
MF5	0.2	170.3	167.2	1.06	0.2	107.1	106.0	1.08
MF6	0.2	179.9	193.7	2.16	0.2	119.8	124.3	2.07

In the homogenisation approach based on the two shell meshes of different material the thicknesses and the mechanical properties of the two meshes are correlated. The elastic properties of the homogenized model for the sample MF2 are presented as a function of the thickness of the shell meshes in the Figure 4-8. Actually the thickness of the shell mesh 1 is considered constant in each graph and the thickness of the shell mesh 2 varies between the

values 0 and 1 mm. Thus the graphs for th_1=0.1, 0.2, 0.5 and 1 mm are given. The mechanical properties calculated for the samples under investigation, for the selected th_1 and th_2, are given in the Table 4-9.

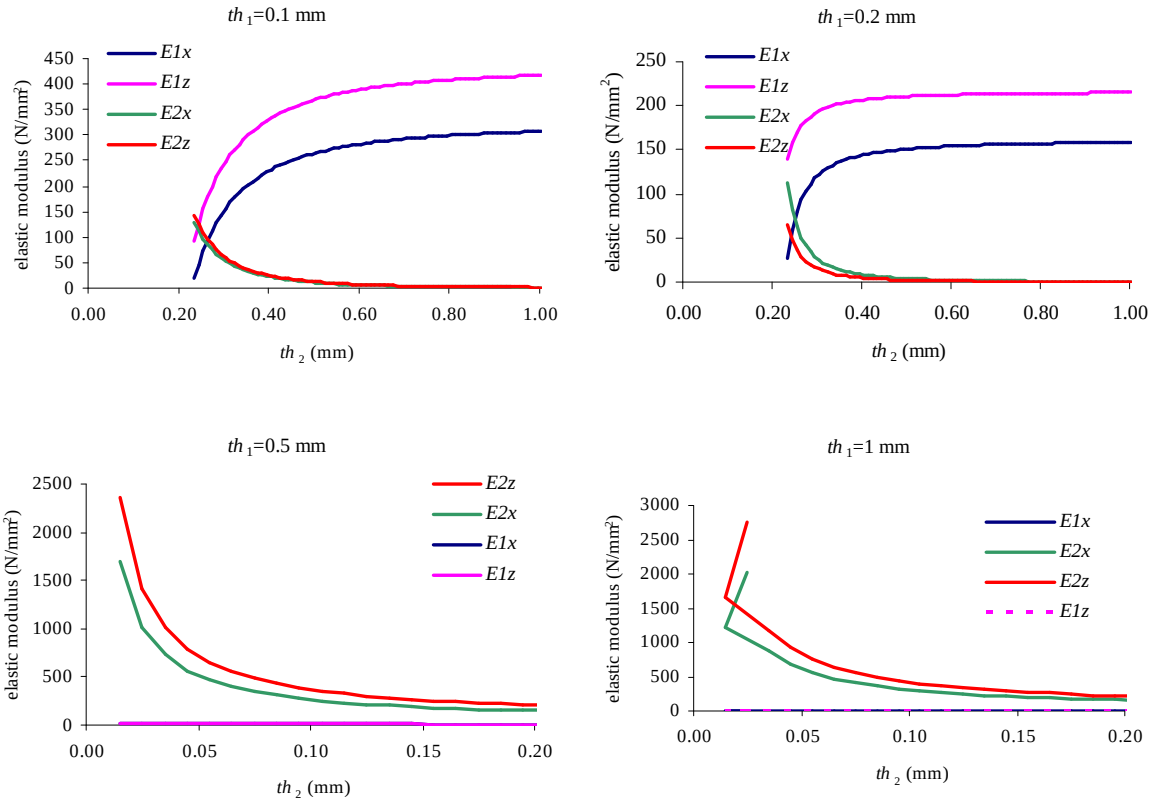

Figure 4-8: The relation of the elastic moduli of the continuum model and the thickness value resulting from the homogenization method of two shell meshes with different material. The MF2 sample was considered.

Table 4-9: Properties of the shell meshes of different material.

Sample	shell mesh 1				shell mesh 2			
	th_1 (mm)	E_{1x} (N/mm^2)	E_{1z} (N/mm^2)	G_{1xz} (N/mm^2)	th_2 (mm)	E_{2x} (N/mm^2)	E_{2z} (N/mm^2)	G_{2xz} (N/mm^2)
MF2	0.14	63.5	142.9	1.60	0.26	84.9	89.3	1.51
MF3	0.14	125.8	99.0	1.60	0.26	95.0	93.6	1.61
MF4	0.15	108.1	117.7	1.60	0.17	106.8	121.2	1.43
MF5	0.15	127.4	123.3	0.70	0.17	83.4	87.9	0.63
MF6	0.15	111.5	129.8	1.30	0.17	136.4	113.3	1.39

In the homogenisation approach based on the 3-layer sheet the selection of the layers' thicknesses is a more demanding procedure. Actually the convergence achievement during the macromechanical analysis of the homogenous model requires the definition of comparative

values of the elastic parameters. Convergence difficulties due to interlaminar shear derive when increased ratios of the elastic moduli are attributed to the different layers. Thus the appropriate values of the thicknesses are considered the ones that correspond to the ratios E_{1z}/E_{2z}, E_{1x}/E_{2x} approximately equal to 1. The calculation is an iterative procedure consisting of the selection of the thickness value, solution of the equation system and calculation of the ratios. The ratios E_{1z}/E_{2z}, E_{1x}/E_{2x} for varying thickness values, calculated for the sample MF2, are presented in the Figure 4-9. The thickness of the outer layers received the constant values th_1=0.01, 0.05, 0.1, 0.2, 0.05 and 1 mm and the thickness of the inner layer varied between the values 0 and 1 mm. Only the feasible solutions of the equation system are presented in the graphs. The ratios vary from 10^{-4} (for th_1=1 mm) to 60 (for th_1=0.05 mm). The appropriate thickness values were selected by the iterative procedure and the mechanical properties are given in the Table 4-10.

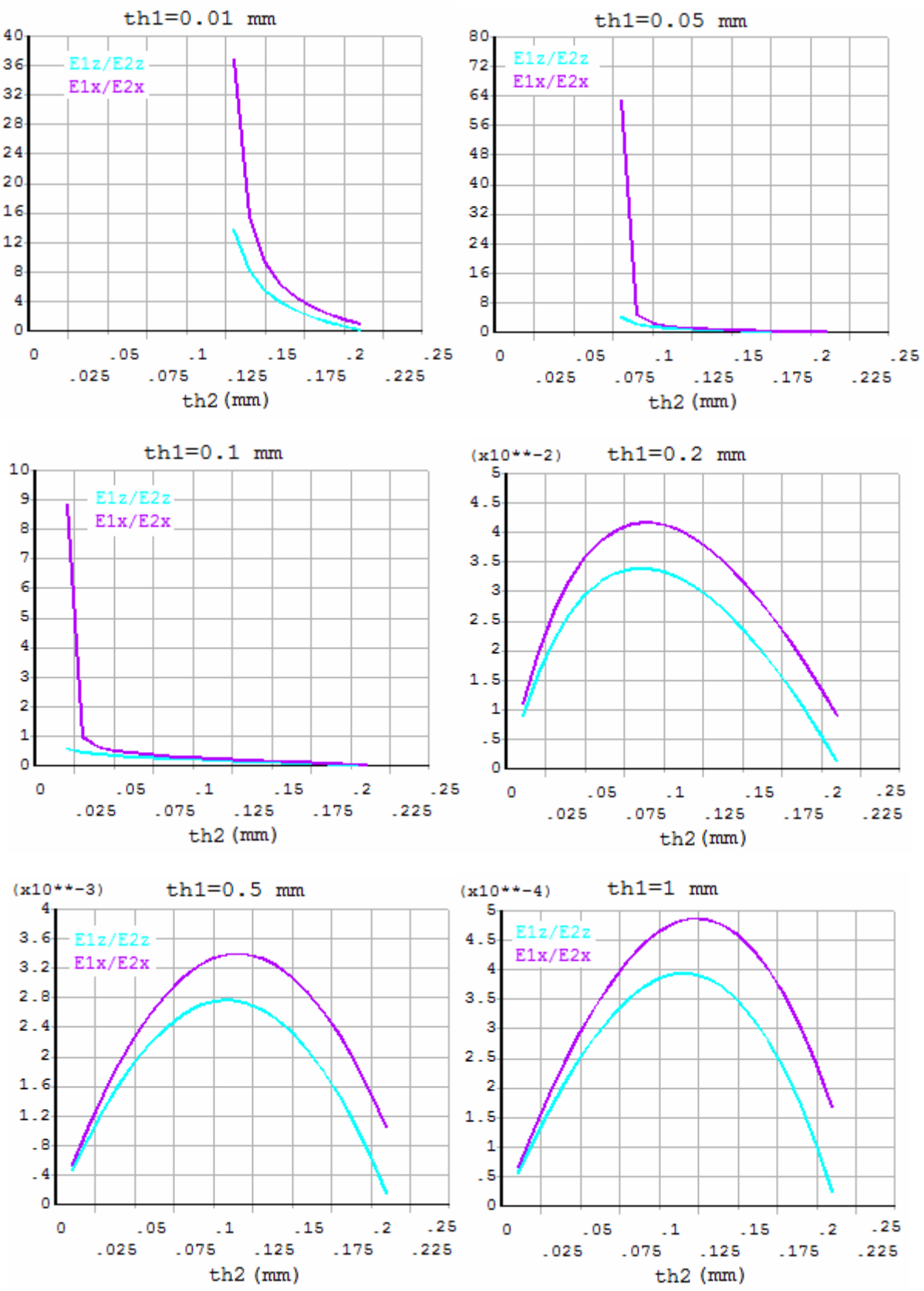

Figure 4-9: The relation of the ratios E_{1z}/E_{2z}, E_{1x}/E_{2x} of the continuum model and the thickness values resulting from the 3 layers homogenization method. The MF2 sample was considered.

Table 4-10: Properties of the shell mesh consisting of 3 layers.

Sample	Outer layers				Inner layer			
	th_1 (mm)	E_{1x} (N/mm^2)	E_{1z} (N/mm^2)	G_{1xz} (N/mm^2)	th_2 (mm)	E_{2x} (N/mm^2)	E_{2z} (N/mm^2)	G_{2xz} (N/mm^2)
MF2	0.07	160.5	182.4	2.80	0.08	120.6	221.2	2.82
MF3	0.07	188.3	180.9	2.90	0.08	194.8	160.8	2.95
MF4	0.04	230.8	243.4	3.00	0.08	229.4	234.8	3.05
MF5	0.04	208.0	206.3	1.30	0.08	217.6	211.6	1.35
MF6	0.04	236.9	243.1	2.70	0.08	212.9	241.0	2.69

The macromechanical analysis of fabric bending test as it is executed in the Kawabata Evaluation System for Fabrics (KES-F) was simulated (Appendix VII: Kawabata Evaluation System for Fabrics). According to the test principle, a sample area of 20 × 1 cm is subjected to the bending deformation along the short dimension. The sample is clamped between a fixed and a moving arm and then bent at a constant rate of a curvature K from -2.5 to 2.5 cm^{-1}. The track of the moving arm in the horizontal level x-y is described by the Eq. 4-51, 4-52. The angular moment is calculated during the test.

$$x = (1 - \cos K) / K \qquad \text{(Eq. 4-51)}$$

$$y = \sin K / K \qquad \text{(Eq. 4-52)}$$

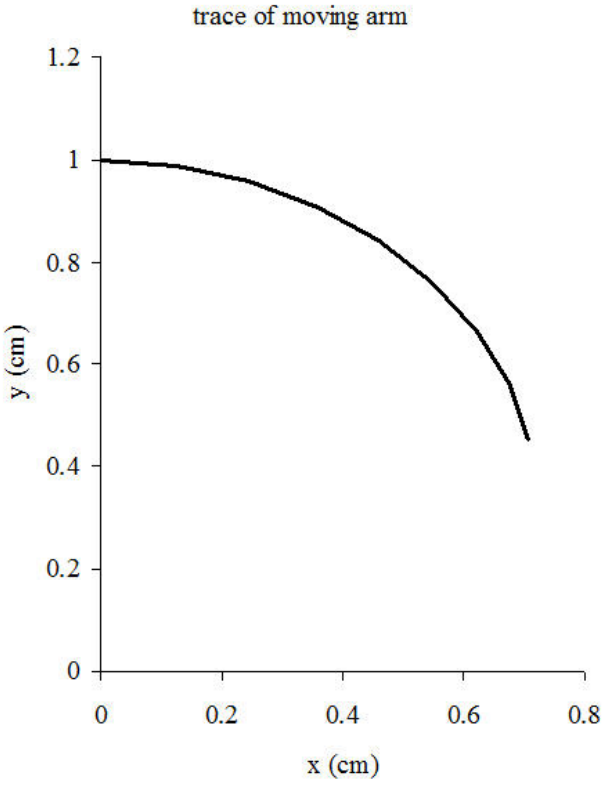

Figure 4-10: The track of the moving arm in the horizontal level x-y.

The macromechanical simulation was performed in ANSYS software. The real dimensions of the effective area (20 × 1 cm) of the sample were considered for the simulation. The fabric sheet was meshed using shell FE (SHELL63) for the continuum model of 2 shell meshes of different material and layered shell FE (SHELL91) for the 3-layer continuum model. The one edge of the model was fully supported while the displacement was applied on the other edge according to the arm track. The nonlinear analysis supporting large deformation effects was implemented for the solution. The deformed shape of the model during the imposition of the displacement is presented in the Figure 4-11. The curve of moment – curvature for the bending test of the sample MF2 is given in the Figure 4-12. For the comparison of the computational results with the experimental data the bending rigidity was calculated between the curvatures 0.5 and 1.5 cm^{-1}. The bending rigidity measured by the test of the samples is given in the Table 4-11. The respective computational results calculated by the macromechanical simulation and the divergence from the experimental data are given in the Table 4-12 and Table 4-13. The low values of the resultant divergence ensure the reliability of the proposed homogenization method for the evaluation of the bending performance.

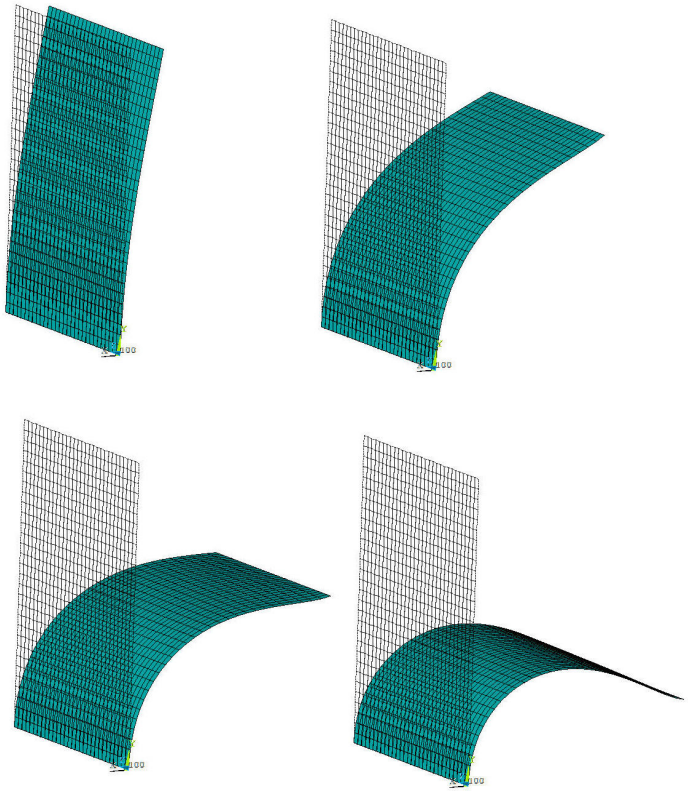

Figure 4-11: Deformed shape of the model subjected to the bending test.

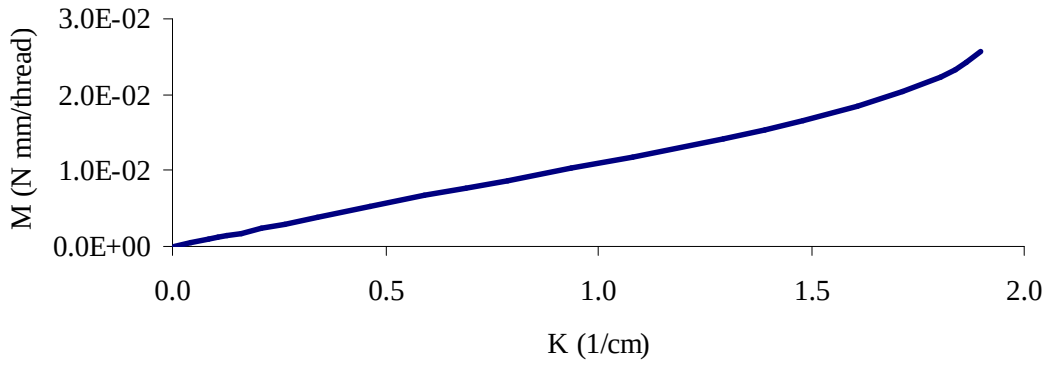

Figure 4-12: Moment - curvature of the model subjected to the bending test.

Table 4-11: Experimental data of the fabric bending test.

Sample	Experimental Fabric Bending Rigidity (gf·cm²/thread)		(N·mm²/thread)	
	Warp	Weft	Warp	Weft
MF2	0.112	0.121	0.1098	0.1187
MF3	0.115	0.118	0.1128	0.1157
MF4	0.049	0.050	0.0481	0.0490
MF5	0.043	0.045	0.0422	0.0441
MF6	0.046	0.048	0.0451	0.0471

Table 4-12: Bending rigidity resulted from the macromechanical model using the double shell mesh of different material and divergence from the experimental data.

Sample	Double shell mesh of different material Bending Rigidity (N·mm²/thread)		Divergence (%)	
	Warp	Weft	Warp	Weft
MF2	0.1044	0.1198	5.17	-0.94
MF3	0.1121	0.1084	0.56	6.73
MF4	0.0448	0.0447	7.35	9.58
MF5	0.0461	0.0458	-8.61	-3.72
MF6	0.0445	0.0459	1.32	2.55

Table 4-13: Bending rigidity resulted from the macromechanical model using the 3layer structure and divergence from the experimental data.

Sample	3-layer structure Bending Rigidity (N·mm²/thread)		Divergence (%)	
	Warp	Weft	Warp	Weft
MF2	0.1105	0.1188	-0.62	-0.14
MF3	0.1090	0.1185	3.43	-2.35
MF4	0.0460	0.0451	4.39	8.63
MF5	0.0473	0.0477	-10.81	-7.39
MF6	0.0465	0.0464	-2.93	1.34

4.4.2 Case Study 2: The macromechanical simulation of the tensile and shear test

The proposed homogenization method was also applied for the macromechanical simulation of tensile and shear test. The reliability of the method was evaluated using experimental data received from the literature (Carvelli, Corazza & Poggi 2008). A monofilament technical textile presenting the typical plain-weave geometry was investigated. The structural and mechanical characteristics of the polyester filaments were given by the researchers. Moreover the mechanical performance in tensile and shear test of the fabric was measured.

The characteristics of the yarn and the meso-scale geometry of fabric were considered for the mesomechanical modelling of the plain woven. The nominal diameter of the filament D_f = 0.034 mm was considered for the warp and weft thread. The linear elasticity was applied for the filament modelling considering the values E_{warp} = 3800 N/mm² and E_{weft} = 4400 N/mm² for the tensile modulus of warp and weft thread respectively and the Poisson ratio ν=0.2. The stress – strain curve of the tensile test of the warp and weft thread resulted from the experiment and the simulation for the considered values is presented in the Figure 4-14.

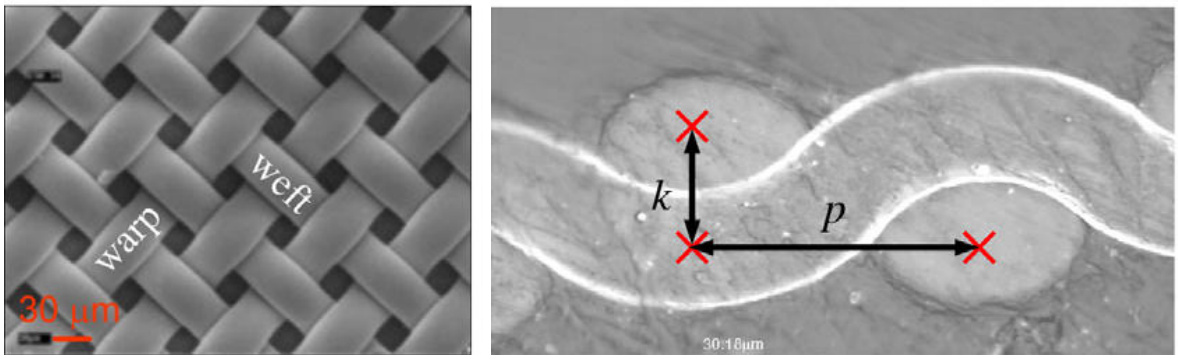

Figure 4-13: Frond view and cross section of Textile A. Source: (Carvelli, Corazza & Poggi 2008).

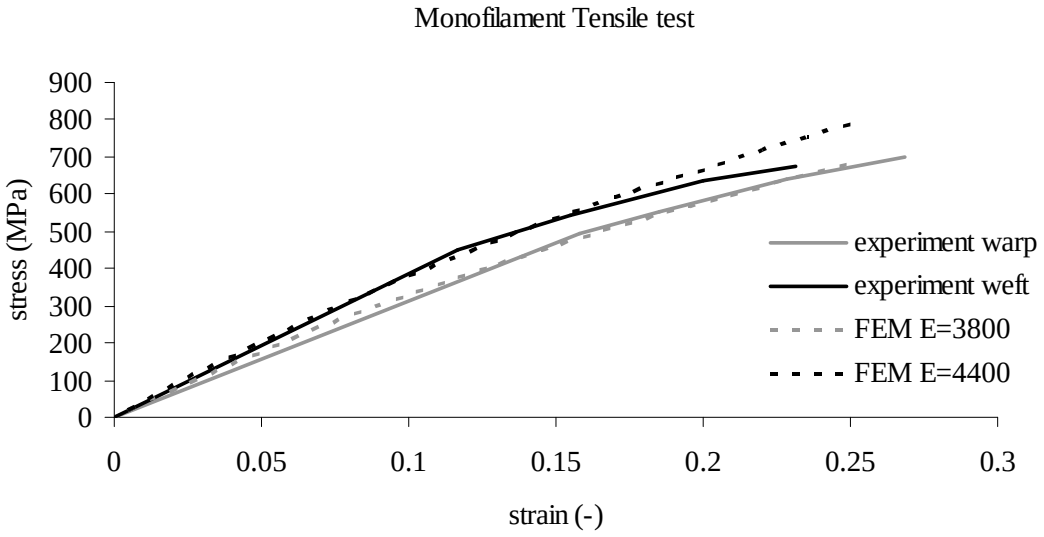

Figure 4-14: Stress – strain curve of the monofilament tensile test resulted experimentally and the respective curves assumed for the modelling approach.

It is worth to mention that the researchers (Carvelli *et al.*) presented the stress – strain curve of the tensile test of the filaments extracted from the textile. Thus the considered filaments were presenting permanent deformations resulting from the weaving and the thermosetting process. Moreover the overalization of the threads was evaluated measuring the minimum and the maximum diameter of the warp and weft threads:

(D_{warp})min = 34.01 mm

(D_{warp})max = 44.92 mm

(D_{weft})min = 37.97 mm

(D_{weft})max = 42.67 mm

In the implemented modelling approach the flattening of the threads in the woven structure was ignored.

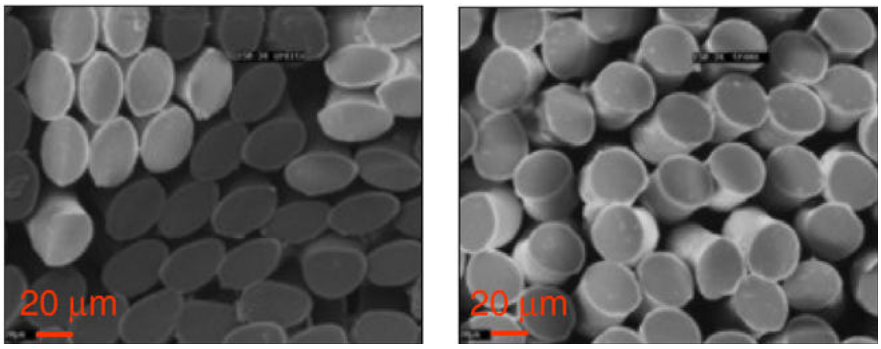

(a) (b)

Figure 4-15: Cross sections of the filaments in the warp (a) and the weft direction (b). Source: (Carvelli, Corazza & Poggi 2008).

The nominal warp and weft densities (150 threads / cm) were considered for the geometrical representation of the meso-scale model. Thus the warp and weft spacing received the values p_1=p_2=0.067 mm. The fibre-fibre friction coefficient (evaluated by Carvelli) was also introduced in the model:

fibre-fibre friction coef. = 0.112

The normal stiffness KN=2 and sticking stiffness KS=2 were considered for the implementation of the point-to-point contact. The mesomechanical analysis of the unit cell in tensile, shear and bending test was conducted and the mechanical characteristics were calculated:

B_{rp} = 2.17E-04 N·mm²/thread

B_{ft} = 2.51E-04 N·mm²/thread

E_{rp} = 1.47 N/thread

E_{ft} = 1.57 N/thread

G_{rp} = 0.076 N/thread

G_{ft} = 0.076 N/thread

ν_{rp} = 0.166

ν_{ft} = 0.155

The homogenization method based on the double shell meshes of different material was implemented for the generation of the macromechanical model. The mechanical characteristics of the continuum model are given below:

t_1 = 0.03 mm

t_2 = 0.05 mm

E_{1z} = 334.9 N/mm²

E_{1x} = 380.8 N/mm²

E_{2z} = 238.8 N/mm²

E_{2x} = 300.1 N/mm²

G_{1xz} = 14 N/mm²

G_{2xz} = 14.19 N/mm²

ν_{1xz} = ν_{2xz} = 0.155

ν_{1zx} = ν_{2zx} = 0.166

The uniaxial tensile test along warp and weft directions were carried out by Carvelli *et al.* according to the standards ASTM D 5035-95. Rectagular strips were cut parallel to the threads, 50 mm width and 300 mm length. The tensile force vs. strain was recorded during the tests. Moreover other specimens were cut with the fibres oriented ±45º to the load direction. In the current test the force vs. the shear strain were calculated.

The simulation of the mentioned tests was performed using the macromechanical model. The force - strain curves resulted by the simulation were compared to the respective experimental curves (Figure 4-17, Figure 4-18, Figure 4-19). The continuum model, original edge and deformed shape, resulted from the simulation of the tensile with the specimen threads oriented at ±45º to the load direction is given in the Figure 4-16. The asymmetric deformation presented accents the importance of the macromechanical modelling in the current deformation.

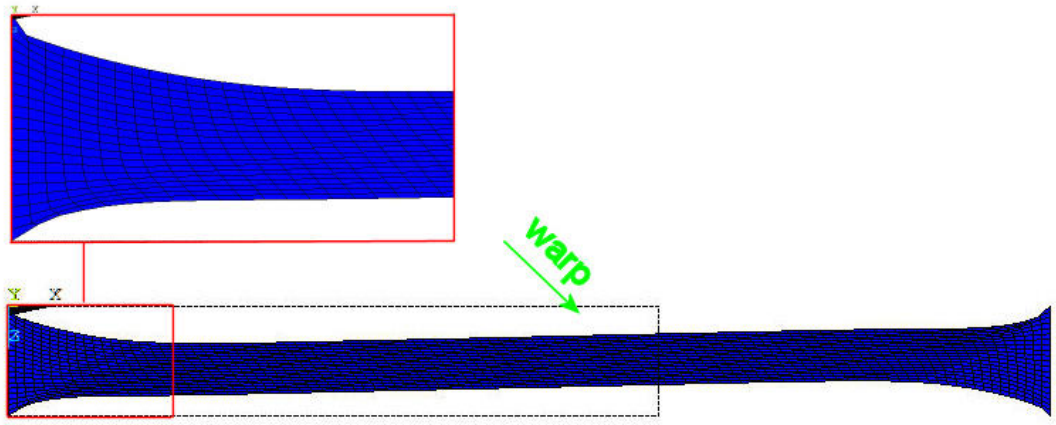

Figure 4-16: Simulation of the tensile test of the fabric with the fibres oriented at ±45 degrees.

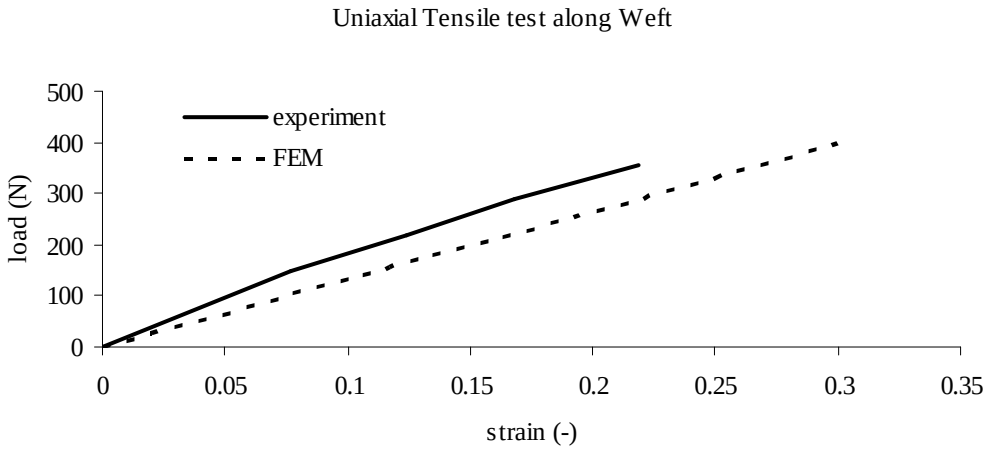

Figure 4-17: Experimental and computational curve of load – strain for the uniaxial tensile test along weft direction.

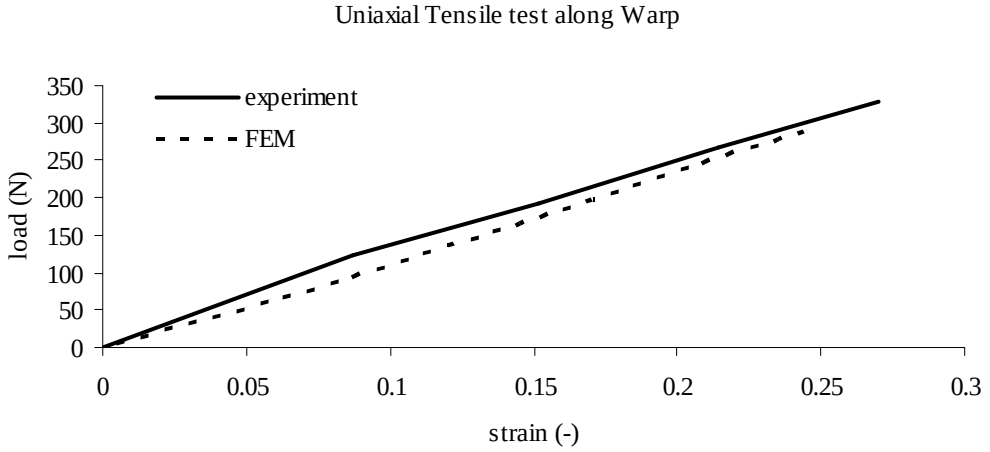

Figure 4-18: Experimental and computational curve of load – strain for the uniaxial tensile test along warp direction.

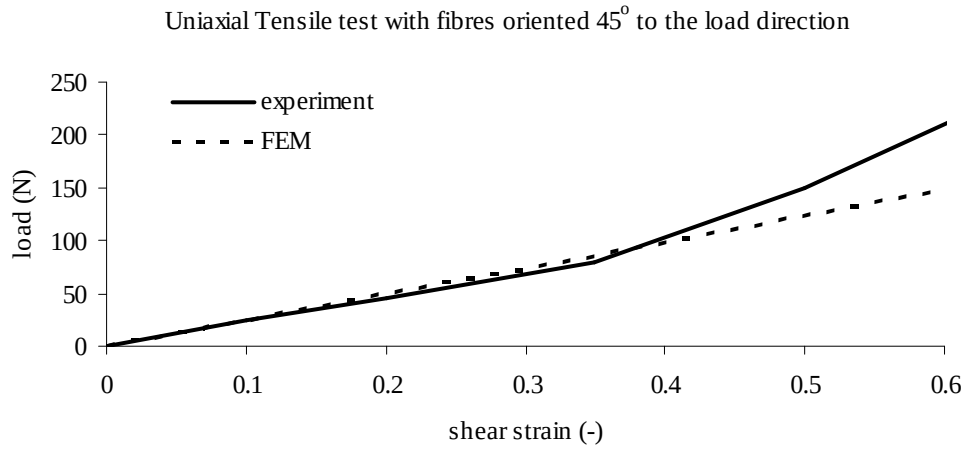

Figure 4-19: Experimental and computational curve of load – shear strain resulted from the uniaxial tensile test with fibres oriented at ±45º.

The adequate approximation of the computational and the experimental curves assures the reliability of the proposed homogenization method for the tensile and the shear performance. The small divergence presented in the uniaxial tensile test along warp and weft direction derives probably from the assumptions considered for the models (circular cross section of threads, nominal diameters, nominal thread density, linear elasticity etc). An interesting point is derived from the third test, since the experimental curve presents a turning point and the curve slope is increased. This probably derives in the real test from the flattening of the threads and the increase of the friction forces or the approach of the adjacent threads and the appearance of additional compression forces. The current mechanism is not predicted by the proposed model since the shear modulus was considered linear.

4.5 Conclusions

The homogenization is a thorough method for the mechanical analysis of periodic structures in complex deformations. The implementation of the homogenization in textile structures is requisite since the complexity of the structure and the large-scale deformations developed even in low loading conditions are prohibitive for the evaluation of the macromechanical performance using the micromechanical model. The accurate calculation of the apparent properties of the structural unit cell is determinant for the reliability of the homogenization method. In the proposed modelling approach the mechanical performance of the unit cell in tensile, shear and bending deformation were considered for the evaluation of the apparent properties.

Moreover the attribution of the apparent properties in the continuum model is of great importance for the definition of an equivalent model. Three methods were implemented for the generation of a sheet model presenting equivalent performance with the asymmetric woven structure. In the first approach (a), the meshes individually support the elastic or the bending performance of the structure. Thus the first shell mesh provides the membrane stiffness, while the second mesh provides the bending stiffness. The current homogenized model presents equivalent performance in tensile and bending with the discrete model. Drawback of the approach is the failure of the analysis in large deformation conditions that are essential for the simulation of the macromechanical tests. The second approach (b) consists in the generation of two shell meshes of coincident nodes that present different material properties. Both shell meshes present membrane and bending stiffness in this case. The keypoint of the current approach is the superposition of the meshes to present the apparent performance of the discrete structure. The 3-layer structure, proposed in the third (c) approach, consists of two orthotropic continuum materials and symmetrical cross-section. Thus identical layers (material properties and thickness) are used for the outer layers. Principle of the current approach is the generation of a homogenous structure that fulfil the constitutive equations of the discrete structure. Layered shell or solid-shell FE are appropriate for the generation of the homogenous structure. Basic drawback of the current approach is the presentation of convergence difficulties resulting from the high divergence of the layers elastic properties, due to interlaminar sliding. This difficulty is faced with the suitable definition of the layers properties (comparative elastic parameters). The capability of nonlinear analysis of the second (b) and the third (c) model is advantageous for the simulation of the fabric deformation in the macro-scale.

The reliability of the proposed methods was evaluated using experimental data. The used experimental data were received from the literature, since the production and measurement of the desired set of samples (monofilament woven structures) was impossible with the available resources. Thus two case studies were conducted for the evaluation of the out-of-plane performance (bending) and the in-plane performance (tensile and shear) of the proposed continuum models.

In the case study 1, the three proposed homogenization methods were implemented and the calculation of the equivalent properties was presented. A set of 5 samples produced from monofilament yarns was examined. The filament characteristics and the textile structure were considered for the mesomechanical analysis and the evaluation of the apparent properties. Then the macromechanical models were generated implementing the homogenization methods. The simulation of the macromechanical bending test as it is executed in the KES-F was performed using the continuum models. The bending rigidity was calculated considering the real deformation and the simulation. The low divergence presented between the experimental values and the computational results ensures the reliability of the proposed homogenization methods in the bending performance.

In the case study 2, the homogenization method based on the double shell meshes of different material was implemented for the generation of the macromechanical model. A sample produced from monofilament yarns was examined. The filament characteristics and the textile structure were considered for the mesomechanical analysis and the evaluation of the apparent properties. Then the macromechanical model was generated implementing the homogenization method. Three tensile tests were performed (a) along warp (b) along weft and (c) with filaments oriented at ±45º and the load – strain curves were recorded. The simulation of the macromechanical tests was conducted and the respective curves were calculated. The low divergence presented between the experimental and the computational curves ensures the reliability of the proposed homogenization method in the tensile and shear test.

Chapter 5
Simulation of the Drape Test

Abstract

The woven fabric reinforced composites were introduced in the aerospace and the automotive industry thanks to their special performance combining light-weight structure, high strength properties and easy formability. The drapeability of the fabric reinforcement offers the advantage of bending around double-curvature mould producing complex shaped composite parts. The current chapter focuses on the simulation of the fabric drape implementing the proposed homogenization method. The fabric drape is a nonlinear problem that undergoes large displacements and rotations. The 3-layer homogenization method was proved adequate for the drape simulation. The 8-node solid-shell finite elements with 3 translational degrees of freedom in each node were used for the analysis. The success of the analysis was evaluated experimentally. The bending and the in-plane apparent properties (tensile and shear) of the samples were measured using the Kawabata Evaluation System for fabrics. The drape configuration of the samples over a circular pedestal was captured. The 3-layered homogenous structure was generated and the drape simulation was performed. The reliability of the modelling approach was evaluated comparing the experimental and the computational drape feature. The comparison was based on the calculation of the area resulted from the projection of the draped fabric on the horizontal level. A good agreement was resulted between the experiment and the simulation.

5.1 Introduction

The woven fabric reinforced composites were introduced in the aerospace and the automotive industry thanks to their special performance combining light-weight structure, high strength properties and easy formability. The drapeability of the fabric reinforcement offers the advantage of bending around double-curvature mould producing complex shaped composite parts. The drape of a fabric refers to the configuration resulting when it falls with gravity on a pedestal or a human body (Hu, Chan 1998). Thus the prediction of the drape performance of a woven fabric is essential for the design and optimization of woven reinforced composite structures.

Many numerical techniques including the particle-based model (Breen, House & Wozny 1994), the deformable node-bar model (Stylios, Wan & Powell 1995) and the FEM have been developed for the simulation of the fabric drape. The used FE methods for the drape simulation are based on a variety of element types from simple rods to complex shell

elements. Collier (Collier et al. 1991) studied the drape behaviour of fabrics using a nonlinear FEM based on the classical nonlinear plate theory. The fabric was assumed two dimensional. It was considered as a linear elastic material with orthotropic anisotropy, where the symmetry lines are aligned in the warp and weft directions. Many corrective actions were assigned the following years by the researchers in the classical FE techniques in order the realistic performance of fabrics to be approached.

Chen and Govindaraj (Chen, Govindaraj 1995) implemented the flexible thin shell theory for the FE analysis of fabric drape. A 9-node, doubly curved shell element with 5 DOFs per node was used for the simulation. The Newton-Raphson method was applied for the nonlinear solution of the equilibrium equation system. The formulation of the FEM proposed by Kang and Yu (Kang, Yu 1995) was based on a total Lagrangian approach. 4-node quadrilateral elements were used with 5 DOFs in each node. In order to avoid the shear locking phenomenon which is commonly observed in the thin plane analysis, a transverse shear strain interpolation method was applied. A similar approach was proposed by Gan *et al.* (Gan, Ly & Steven 1995). In their analysis 8-node shell elements were used with 5 DOFs per node. The adopted technique in this approach for the elimination of locking was a reduced integration with zero energy mode control.

The basic obstacle in the drape simulation is the handling of the rotational nodal DOFs in long free-hanging length models. In these cases some nodal directors are reversed and thus the solution is non-physical. Sze and Liu proposed a solid-shell element partitioned into a surface, four line and four point sub-elements. The modelling using solid-shell elements with only translational DOFs tackles the complication of handling the nodal rotations (Sze, Liu 2007).

The current study proposes a FE model for the simulation of the fabric drape test using solid-shell elements. The 8-node solid-shell elements with 3 translational DOFs in each node were used for the analysis. The 3-layer homogenization method was implemented for the generation of the continuum model. The reliability of the simulation was evaluated using experimental data. Thus a set of 30 plain woven samples was used. Since the properties of the microstructure, the yarn elastic modulus and the yarn bending rigidity, were unknown, the mesomechanical modelling was omitted. The mesomechanical characteristics were assumed equal to the apparent properties of the samples resulted from the mechanical tests. The bending and the in-plane (tensile and shear) properties of the samples were measured using the Kawabata Evaluation System for fabrics (see also: Appendix VII: Kawabata Evaluation System for Fabrics). The drape configuration of the samples over a circular pedestal was captured. The drape coefficient was calculated by the experiment and the simulation for the evaluation of the proposed approach. A good agreement was resulted between the experiment and the simulation ensuring the reliability of the proposed drape simulation.

5.2 Experimental data

A set of 30 samples of plain woven structure was used for the estimation of the drape simulation reliability. The samples are prepared using constant characteristics and one varying structural parameter. Cotton yarns of 50 Ne and 40 Ne were used for the warps and wefts respectively. The warp and weft yarn (structure and properties) and the warp density constitute the constant structural parameters while the weft density corresponds to the varying parameter. Thus the effect of the thread density in the drapeability was also obtained. The bending rigidity, the in-plane shear stiffness, the elastic modulus and the apparent thickness of the produced samples were measured in the Kawabata Evaluation System for Fabrics (KES-F). Moreover the thread densities and the mass per unit area of the samples were measured. The structural characteristics and the measured properties of the samples are given in the Table 5-1. The dimensions of the unit cell (thread spacing) and the apparent mechanical properties of the unit cell are given in the Table 5-2.

Table 5-1: Structural characteristics of the samples and mechanical parameters resulted from KES-F.

Sample no	thread density (thread /cm)		Mass per unit area (gr/m^2)	exper. thick-ness (mm)	Bending rigidity ($g.cm^2/cm$)		shear stiffness (gf /cm·deg)		extension at 500 cN/cm specimen width, EMT (%)	
	weft	warp			weft	warp	weft	warp	weft	warp
1	20	54	101.5	0.41	0.0143	0.0421	0.50	0.59	5.98	4.95
2	25	54	112.2	0.54	0.0263	0.0459	1.07	1.11	5.90	6.17
3	30	54	121.9	0.40	0.0349	0.0538	2.03	2.05	4.86	5.98
4	35	54	130.6	0.43	0.0478	0.0505	2.63	2.58	4.15	7.17
5	40	54	140.9	0.40	0.0662	0.0579	3.64	3.47	3.95	6.64
6	45	54	151.6	0.49	0.0763	0.0591	4.30	4.26	4.27	6.78
7	20	57	106.9	0.47	0.0177	0.0397	0.50	0.60	4.59	6.27
8	25	57	112.5	0.42	0.0294	0.0450	1.11	1.18	4.07	5.73
9	30	57	125.1	0.50	0.0397	0.0564	1.94	1.97	3.49	6.20
10	35	57	135.9	0.44	0.0502	0.0500	2.98	2.85	3.27	6.81
11	40	57	142.6	0.57	0.0696	0.0734	4.19	4.14	2.83	6.20
12	45	57	153.3	0.46	0.0844	0.0638	4.34	4.43	3.39	7.17
13	20	60	110.9	0.49	0.0172	0.0440	0.60	0.71	4.39	5.93
14	25	60	120.1	0.44	0.0268	0.0476	1.32	1.41	3.93	6.44
15	30	60	133.3	0.57	0.0399	0.0454	2.22	2.14	3.86	7.30
16	35	60	142.3	0.48	0.0450	0.0493	3.41	3.21	3.34	6.78
17	40	60	148.2	0.45	0.0827	0.0588	4.19	4.23	3.05	6.98
18	42	60	155.7	0.54	0.0825	0.0655	4.07	3.94	3.37	7.12
19	20	63	113.4	0.48	0.0210	0.0505	0.64	0.71	4.05	5.20
20	25	63	125.2	0.47	0.0210	0.0445	1.20	1.27	3.44	6.73
21	30	63	132.6	0.57	0.0423	0.0514	2.36	2.19	3.10	6.32
22	35	63	146.0	0.48	0.0493	0.0507	3.15	3.04	3.03	6.76
23	40	63	157.4	0.50	0.0605	0.0693	4.07	3.94	3.20	7.15
24	42	63	159.7	0.46	0.0968	0.0732	4.54	4.21	2.88	7.22
25	20	66	116.4	0.50	0.0203	0.0488	0.66	0.74	3.17	5.22
26	25	66	128.4	0.43	0.0268	0.0481	1.36	1.45	3.61	6.42
27	30	66	138.8	0.42	0.0375	0.0524	2.61	2.36	2.68	7.00
28	35	66	146.5	0.42	0.0509	0.0636	3.64	3.50	2.76	5.73
29	40	66	156.9	0.52	0.0617	0.0677	4.51	4.41	2.32	5.73
30	42	66	160.1	0.60	0.0756	0.0619	4.96	4.52	2.15	5.78

Table 5-2: Structural characteristics of the samples and apparent properties of the unit cell.

Sample no	thread spacing (mm)		Mass per unit area (Kg/mm^2)	bending rigidity ($N.mm^2$/thread)		shear stiffness (N/thread)		elastic modulus (N/thread)	
	weft [p2]	warp [p1]		weft [Bft]	warp [Brp]	weft [Gft]	warp [Grp]	weft [Eft]	warp [Erp]
1	0.500	0.185	1.02E-07	7.01E-04	7.65E-04	0.0052	0.0166	0.410	0.184
2	0.400	0.185	1.12E-07	1.03E-03	8.34E-04	0.0111	0.0250	0.333	0.147
3	0.333	0.185	1.22E-07	1.14E-03	9.77E-04	0.0211	0.0384	0.336	0.152
4	0.286	0.185	1.31E-07	1.34E-03	9.17E-04	0.0274	0.0414	0.338	0.127
5	0.250	0.185	1.41E-07	1.62E-03	1.05E-03	0.0379	0.0488	0.310	0.137
6	0.222	0.185	1.52E-07	1.66E-03	1.07E-03	0.0448	0.0532	0.255	0.134
7	0.500	0.175	1.07E-07	8.68E-04	6.83E-04	0.0049	0.0169	0.534	0.137
8	0.400	0.175	1.12E-07	1.15E-03	7.74E-04	0.0109	0.0265	0.482	0.150
9	0.333	0.175	1.25E-07	1.30E-03	9.70E-04	0.0191	0.0369	0.468	0.139
10	0.286	0.175	1.36E-07	1.41E-03	8.60E-04	0.0294	0.0458	0.429	0.126
11	0.250	0.175	1.43E-07	1.71E-03	1.26E-03	0.0413	0.0582	0.433	0.139
12	0.222	0.175	1.53E-07	1.84E-03	1.10E-03	0.0428	0.0553	0.322	0.120
13	0.500	0.167	1.11E-07	8.43E-04	7.19E-04	0.0056	0.0200	0.559	0.138
14	0.400	0.167	1.20E-07	1.05E-03	7.78E-04	0.0124	0.0317	0.499	0.127
15	0.333	0.167	1.33E-07	1.30E-03	7.42E-04	0.0208	0.0401	0.424	0.112
16	0.286	0.167	1.42E-07	1.26E-03	8.06E-04	0.0319	0.0515	0.420	0.121
17	0.250	0.167	1.48E-07	2.03E-03	9.61E-04	0.0393	0.0594	0.402	0.117
18	0.238	0.167	1.56E-07	1.93E-03	1.07E-03	0.0381	0.0527	0.347	0.115
19	0.500	0.159	1.13E-07	1.03E-03	7.86E-04	0.0057	0.0200	0.606	0.150
20	0.400	0.159	1.25E-07	8.24E-04	6.93E-04	0.0107	0.0286	0.570	0.116
21	0.333	0.159	1.33E-07	1.38E-03	8.00E-04	0.0211	0.0410	0.527	0.123
22	0.286	0.159	1.46E-07	1.38E-03	7.89E-04	0.0281	0.0488	0.463	0.115
23	0.250	0.159	1.57E-07	1.48E-03	1.08E-03	0.0363	0.0554	0.383	0.109
24	0.238	0.159	1.60E-07	2.26E-03	1.14E-03	0.0405	0.0563	0.406	0.108
25	0.500	0.152	1.16E-07	9.95E-04	7.25E-04	0.0056	0.0208	0.774	0.142
26	0.400	0.152	1.28E-07	1.05E-03	7.15E-04	0.0116	0.0326	0.543	0.116
27	0.333	0.152	1.39E-07	1.23E-03	7.79E-04	0.0222	0.0442	0.610	0.106
28	0.286	0.152	1.46E-07	1.43E-03	9.45E-04	0.0310	0.0562	0.508	0.130
29	0.250	0.152	1.57E-07	1.51E-03	1.01E-03	0.0384	0.0620	0.529	0.130
30	0.238	0.152	1.60E-07	1.77E-03	9.20E-04	0.0422	0.0605	0.543	0.129

Orthogonal samples of dimensions 200×200 mm were cut parallel to the principal directions of warp and weft. The samples were mounted over a circular pedestal of 107 mm diameter and the top view of the drape configuration was captured for the evaluation of the drape performance. An image process was conducted thereinafter for the calculation of the defined drape coefficient. As drape coefficient was defined the percentage of the projection of the draped fabric area on the horizontal level subtracting the pedestal area divided by the undeformed fabric area subtracting the pedestal area:

$$DC(\%) = \frac{\text{projection of the draped fabric area on the horizontal level} - \text{pedestal area}}{\text{undeformed fabric area - pedestal area}} \cdot 100$$

(Eq. 5-1)

The boundary tracing of the images and the areas calculation were executed in Matlab software. The image process of a sample is given in the Figure 5-1 (see also Appendix VIII: Experimental data of samples drape).

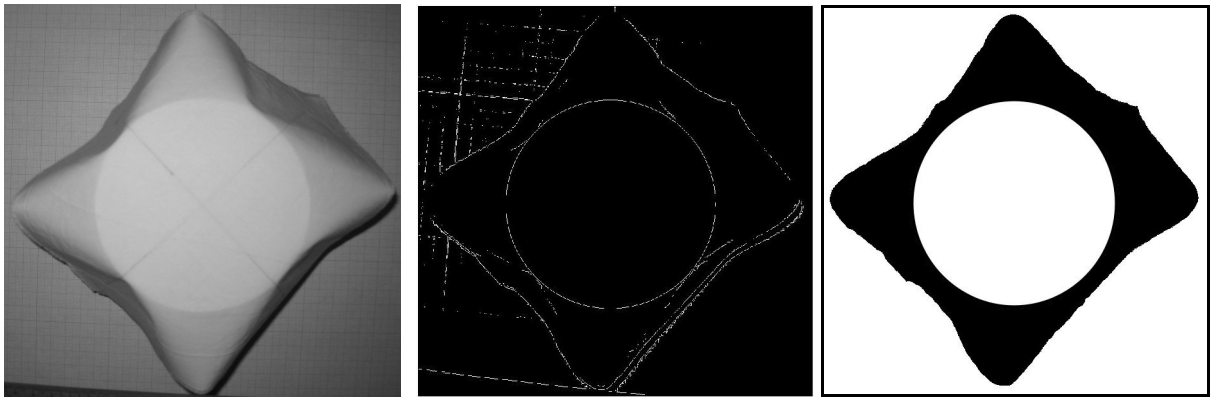

Figure 5-1: Image process for the calculation of the drape coefficient.

5.3 Finite element analysis of fabric drape

The Finite Element Analysis was implemented for the simulation of the fabric drape **(Provatidis, Kallivretaki & Vassiliadis 2009)**. The 3-layer homogenization was adopted for the generation of the continuum model. The mechanical properties of the 3-layered continuum structure for the 30 samples are given in the Table 5-3. The layered solid-shell (solsh190) elements consisting of 8 nodes with 3 DOFs (translational) per node were used for the analysis of the sheet in drape. Orthotropic material was assumed for the attribution of the mechanical properties. The principle axes of orthotropy correspond to the warp, weft and along thickness direction.

Table 5-3: Apparent properties of continuum models.

Sample no	layer thickness		density (kg/mm^3)	elastic properties of outer layers			elastic properties of inner layers		
	t_1 (mm)	t_2 (mm)		E_{1z}	E_{1x}	G_{1xz}	E_{2z}	E_{2x}	G_{2xz}
1	0.1	0.1	3.38E-07	1.65	0.36	0.11	6.61	7.48	0.11
2	0.1	0.1	3.74E-07	1.92	0.94	0.21	4.11	6.43	0.20
3	0.1	0.1	4.06E-07	2.30	1.29	0.38	3.61	7.51	0.39
4	0.1	0.1	4.35E-07	2.19	1.85	0.48	2.46	8.12	0.49
5	0.1	0.1	4.70E-07	2.53	2.73	0.65	2.32	6.96	0.65
6	0.1	0.1	5.05E-07	2.60	3.26	0.80	2.04	4.96	0.79
7	0.1	0.1	3.56E-07	1.62	0.42	0.11	4.58	9.84	0.11
8	0.1	0.1	3.75E-07	1.85	0.94	0.22	4.86	10.17	0.22
9	0.1	0.1	4.17E-07	2.44	1.36	0.37	3.04	11.33	0.37
10	0.1	0.1	4.53E-07	2.15	1.84	0.53	2.90	11.33	0.54
11	0.1	0.1	4.75E-07	3.27	2.69	0.78	1.37	11.95	0.77
12	0.1	0.1	5.11E-07	2.84	3.54	0.83	1.15	7.40	0.83
13	0.1	0.1	3.70E-07	1.81	0.38	0.13	4.65	10.42	0.13
14	0.1	0.1	4.00E-07	2.02	0.79	0.26	3.58	10.89	0.27
15	0.1	0.1	4.44E-07	1.95	1.43	0.40	2.83	9.85	0.40
16	0.1	0.1	4.74E-07	2.12	1.59	0.60	3.00	11.50	0.60
17	0.1	0.1	4.94E-07	2.59	3.38	0.79	1.85	9.31	0.80
18	0.1	0.1	5.19E-07	2.92	3.44	0.74	1.04	7.68	0.74
19	0.1	0.1	3.78E-07	2.08	0.53	0.13	5.27	11.06	0.13
20	0.1	0.1	4.17E-07	1.88	0.44	0.24	3.53	13.39	0.24
21	0.1	0.1	4.42E-07	2.20	1.41	0.41	3.37	12.99	0.41
22	0.1	0.1	4.87E-07	2.18	1.74	0.57	2.89	12.70	0.57
23	0.1	0.1	5.25E-07	3.11	2.33	0.74	0.64	10.67	0.74
24	0.1	0.1	5.32E-07	3.31	4.04	0.79	0.18	8.96	0.79
25	0.1	0.1	3.88E-07	2.00	0.35	0.14	5.39	14.77	0.14
26	0.1	0.1	4.28E-07	2.04	0.75	0.27	3.56	12.09	0.27
27	0.1	0.1	4.63E-07	2.28	1.08	0.44	2.45	16.15	0.44
28	0.1	0.1	4.88E-07	2.76	1.76	0.65	3.04	14.26	0.67
29	0.1	0.1	5.23E-07	2.96	2.14	0.83	2.63	16.85	0.83
30	0.1	0.1	5.34E-07	2.68	2.76	0.85	3.12	17.30	0.85

Geometrically the model consists of an orthogonal surface of the sample dimensions (200×200 mm) subtracting the surface of the circular pedestal. The part of the fabric supported by the table was subtracted by the model for computational simplification and the DOFs constraints (simple support) were applied in the lower nodes of the circumference. The load application consists in the definition of the apparent density (reflected value considering the model thickness) and the gravity acceleration (9.807 m/sec²). Thus the model was subjected to complex deformation (bending in double curvature) in low loading conditions (self-weight). The problem domain is highly nonlinear presenting large displacements and rotations. Additional constraints were applied in 4 nodes of the upper circumference to ensure the convergence achievement. These nodes correspond to the angles 0, 90, 180, 270 degrees of the circle. The modelling and the simulation were performed using the ANSYS commercial software code. A full Newton-Raphson solution algorithm was implemented to support the large-scale deformations. The advantage of the current algorithm is the update of the stiffness matrix in every computational iteration. Two options were activated in order to control the number of iterations and to accelerate the convergence achievement. The prediction option extrapolates the DOFs solution using the previous history for an improved prediction of the next solution. The line search option improves the Newton-Raphson solution by scaling the solution vector by a scalar value. Six states during the deformation procedure of a sample are given in the Figure 5-2.

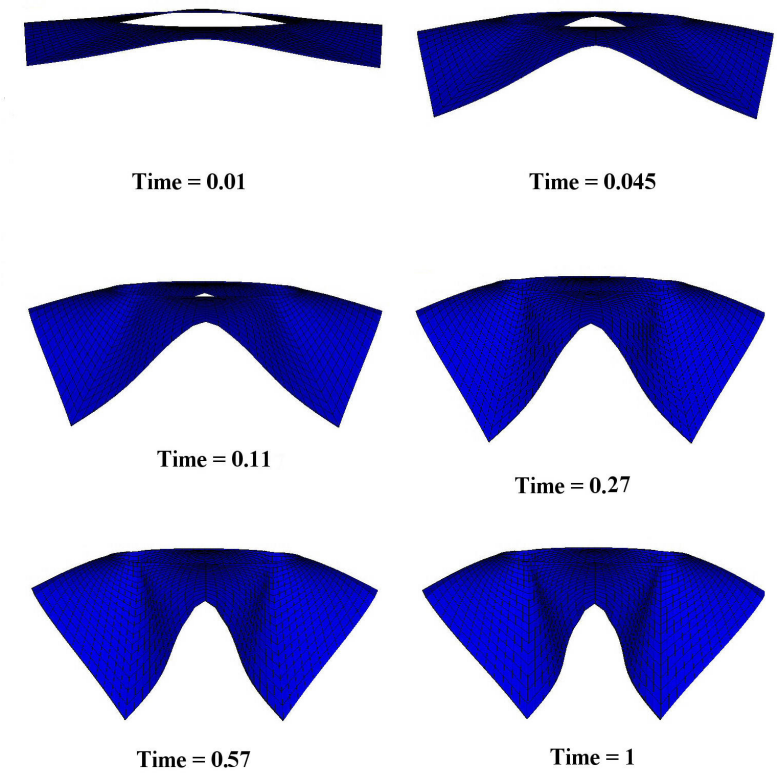

Figure 5-2: Drape configurations of a model during the deformation procedure.

5.4 Evaluation of the model

The comparison of the simulation results and the experimental data was based on the calculation of the drape coefficient as defined in the Eq. 5-1. The drape coefficients are given in the Table 5-4. A low divergence was presented between the computational and the experimental values confirming the reliability of the proposed drape simulation. The divergence range, moreover, eliminates the prospect of a systematic error introduced by the calculation of the properties or the simulation method. The drape configurations of the samples and the respective models are also given in the Figure 5-3, Figure 5-4, Figure 5-5, Figure 5-6 and Figure 5-7.

Table 5-4: Drape coefficient by the simulation and the experiment.

Sample no	Drape coefficient (%)		Divergence (%)
	fem	experiment	
1	24.2	20.6	17.7
2	26.1	24.0	9.1
3	29.6	26.5	11.7
4	31.0	30.3	2.1
5	34.7	34.3	1.0
6	35.1	32.9	6.6
7	23.9	21.5	11.5
8	26.2	22.3	17.3
9	29.8	27.1	9.9
10	31.3	31.4	-0.2
11	37.4	33.0	13.2
12	36.0	34.2	5.2
13	24.2	22.4	7.8
14	26.1	26.3	-0.6
15	28.1	28.8	-2.3
16	30.2	33.3	-9.5
17	36.2	34.4	5.1
18	35.4	35.2	0.4
19	24.7	23.9	3.7
20	24.7	25.5	-2.9
21	29.1	26.6	9.6
22	29.4	29.9	-1.4
23	33.6	35.0	-3.9
24	37.2	34.0	9.5
25	24.4	22.3	9.2
26	25.6	25.0	2.2
27	28.7	29.7	-3.2
28	32.3	32.3	0.3
29	34.5	34.1	1.2
30	35.8	32.6	9.7

Sample	Experiment	Simulation
1	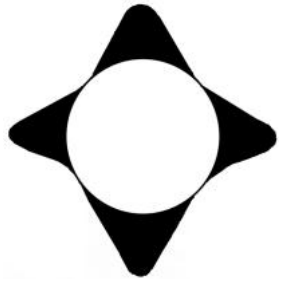	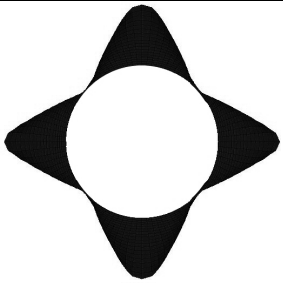
2	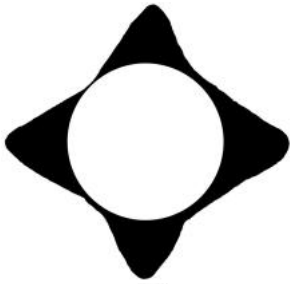	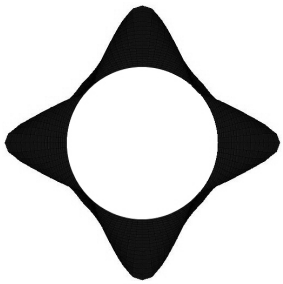
3		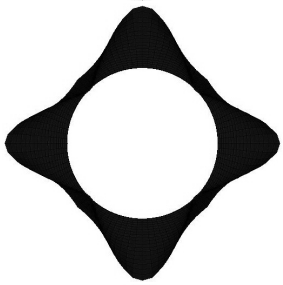
4	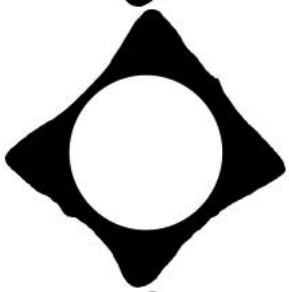	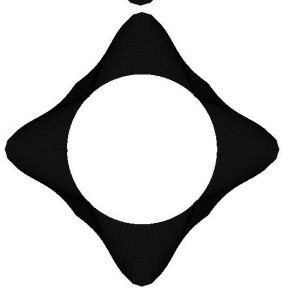
5	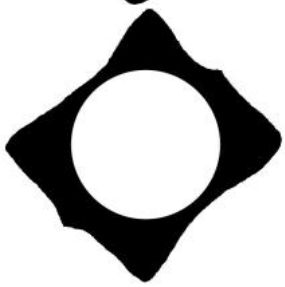	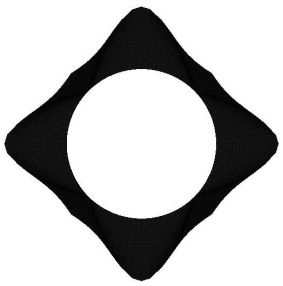
6	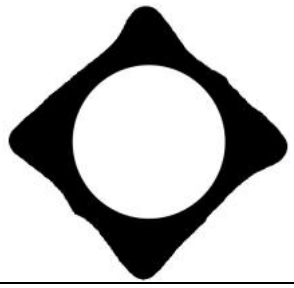	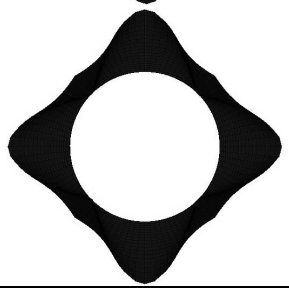

Figure 5-3: Drape configurations resulted from the experiment and the simulation (samples 1-6).

Sample	Experiment	Simulation
7	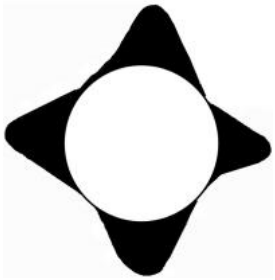	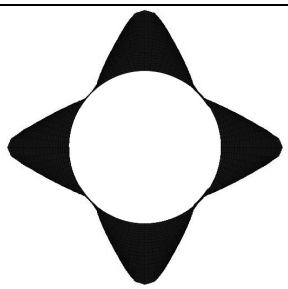
8	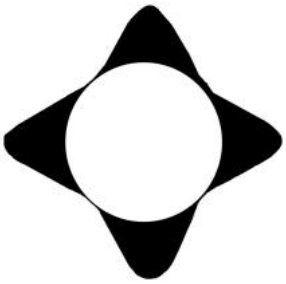	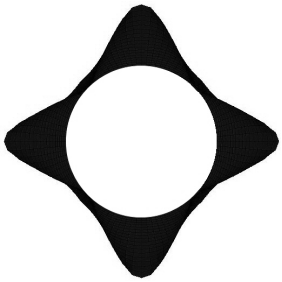
9	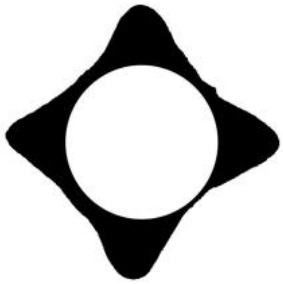	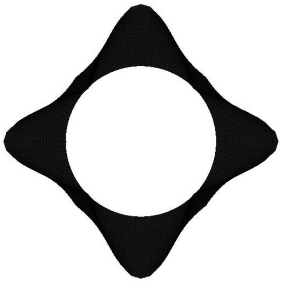
10	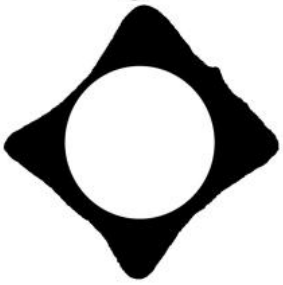	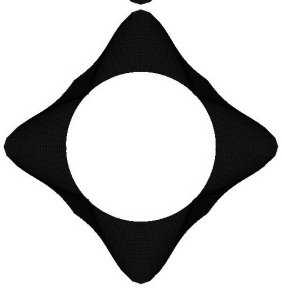
11		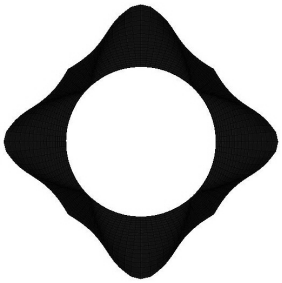
12	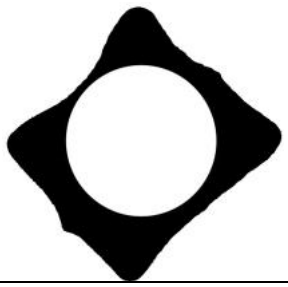	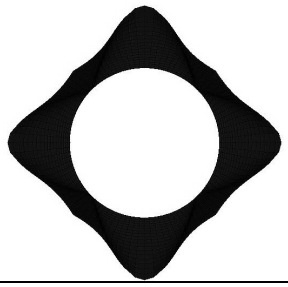

Figure 5-4: Drape configurations resulted from the experiment and the simulation (samples 7-12).

Sample	Experiment	Simulation
13	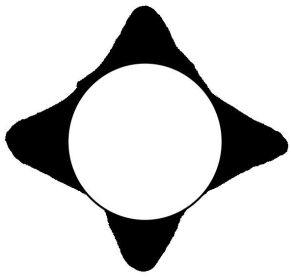	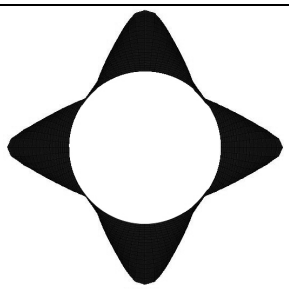
14	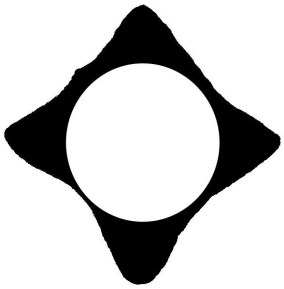	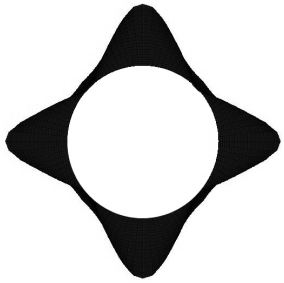
15	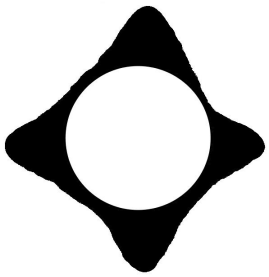	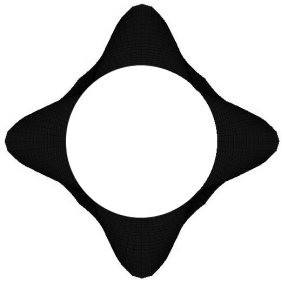
16	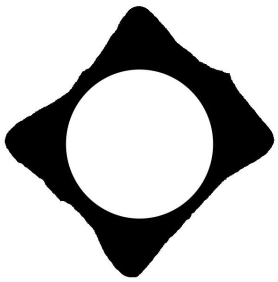	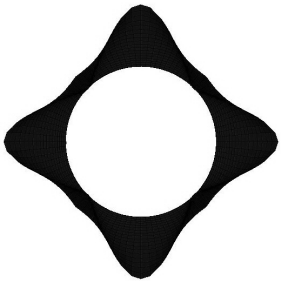
17	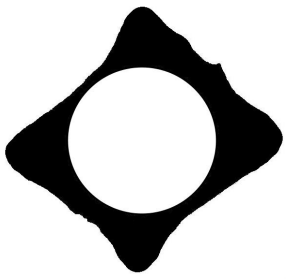	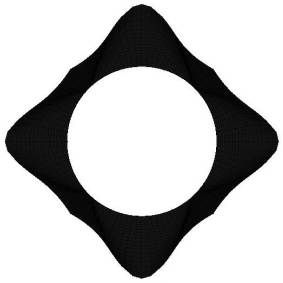
18	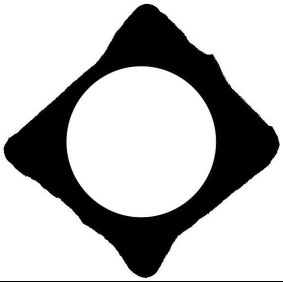	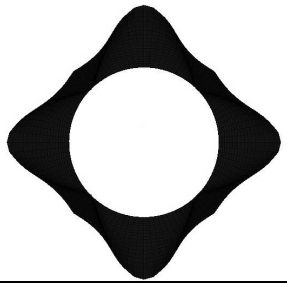

Figure 5-5: Drape configurations resulted from the experiment and the simulation (samples 13-18).

Sample	Experiment	Simulation
19	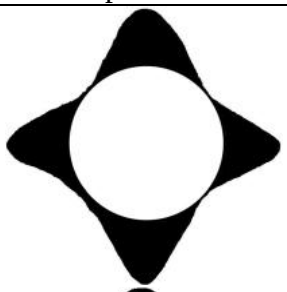	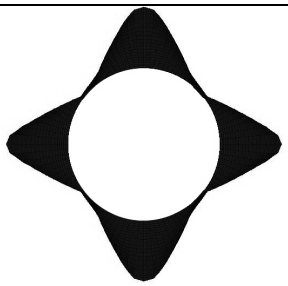
20		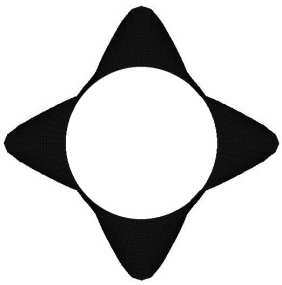
21	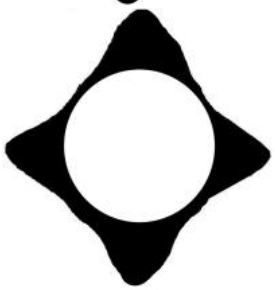	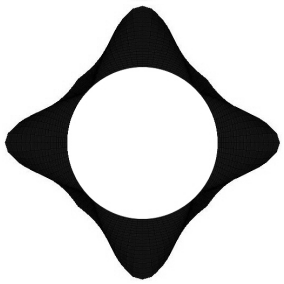
22	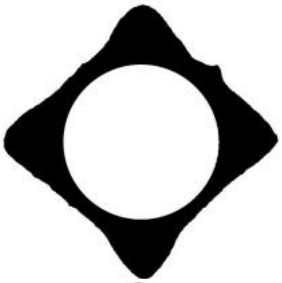	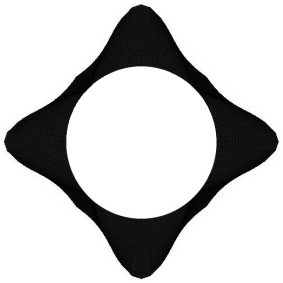
23		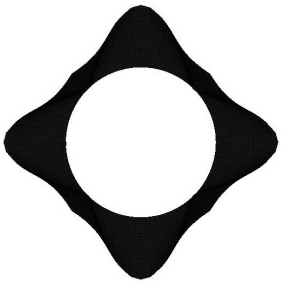
24	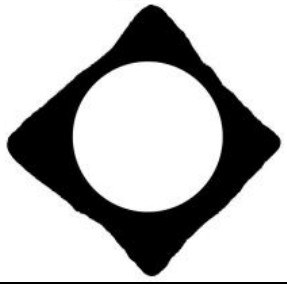	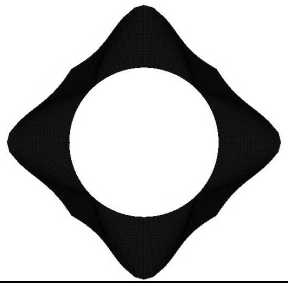

Figure 5-6: Drape configurations resulted from the experiment and the simulation (samples 19-24).

Sample	Experiment	Simulation
25	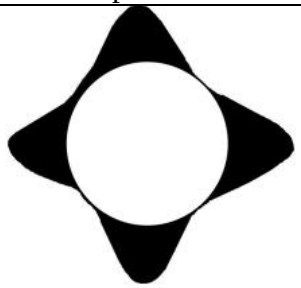	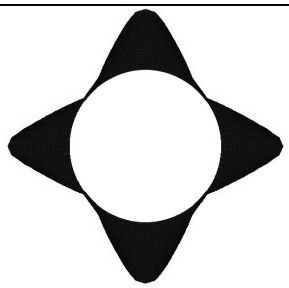
26	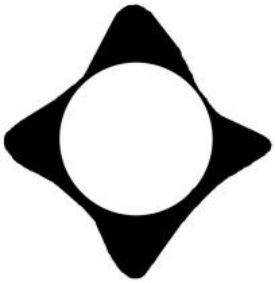	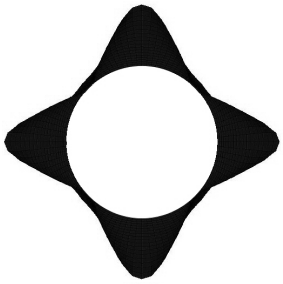
27	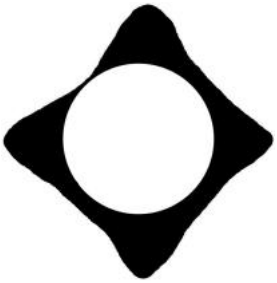	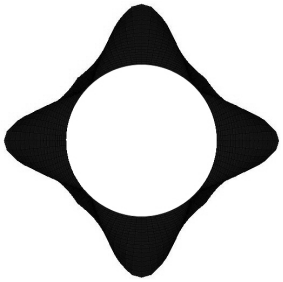
28		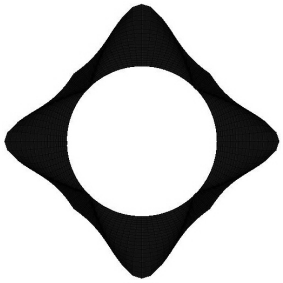
29		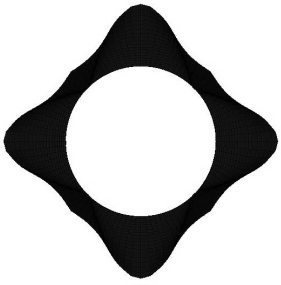
30	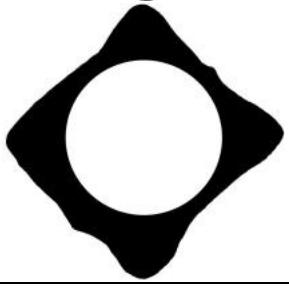	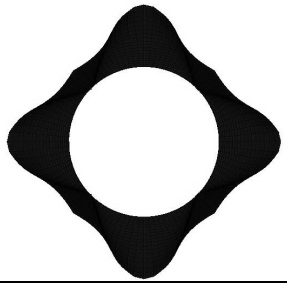

Figure 5-7: Drape configurations resulted from the experiment and the simulation (samples 25-30).

5.5 Conclusions

The drapeability of fabric structures is essential for their mechanical performance and their use in technical applications. The implementation of the FEM for the drape analysis imposes certain assumptions. Basic consideration is the attribution of the equivalent continuum model. The proposed approach implemented the 3-layer homogenization method for the generation of the continuum model. Moreover the mechanical analysis of the fabric drape is a nonlinear problem that undergoes large translations and rotations. The current approach proposed a FE model using solid-shell elements with translational DOFs. Thus the convergence difficulties resulting from the evaluation of the rotational nodal DOFs were omitted. The proposed approach was evaluated using experimental data. The drape configuration was captured for the models and the respective samples and an image process supported the calculation of the drape coefficient in both cases. The good agreement between the computational and the experimental values of the drape coefficient ensures the reliability of the structure.

Chapter 6
Technical Application: Compression behaviour of warp-knitted spacer fabrics

Abstract

In the current chapter, the proposed textile modelling approach is implemented for the study of the compression performance of a spacer fabric. The warp-knitted spacer fabrics were successfully introduced in building constructions as thin sheet component reinforcement for wall panels, exterior siding, roofing tiles, flooring tiles, pressure pipes etc. Their structural advantages support an armature system of highly oriented yarns and the easily cement embodiment for the production of the composite. The compression resistance of the spacer fabric provides a major advantage for the performance and the composite manufacturing process. The optimum compression performance of spacer fabrics varies according to the requirements of the specific application. The mesomechanical models of the constitutive layers were generated and the apparent properties were calculated. Then the simulation of the compression test was performed using the macromechanical model. The proposed computational method was evaluated by the comparison of the load – displacement curves resulted from the simulation and the experimental data of compression. Moreover the effect of structural and physical parameters of the sample in the compression resistance was investigated.

6.1 Introduction

The spacer fabrics are three-dimensional textile structures consisting of two outer textile surfaces connected by an inner layer (spacer layer) appropriate for the formation of space between the surfaces (Figure 6-1). Several techniques can be applied for the production of spacer fabrics as the woven, weft and warp knitting technology. The warp knitting is the most commonly used technology for the production of spacer fabrics providing several advantages. Among others the wide range in yarn type and fabric thickness such as the high production speed are supported by the warp knitting in two needle bars Raschel machines.

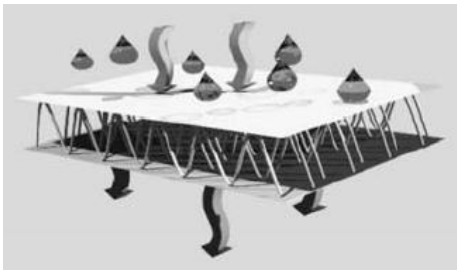

Figure 6-1: Air and moisture permeability of spacer fabrics.

The spacer fabrics present special characteristics compared to the conventional textiles due to their own structure. The compression resistance is beneficial for the structural stability of spacer fabrics suitable for permanent or instant loading and recovery. An even distribution of pressure or the respective even damping effect can be achieved by the selection of the appropriate yarns and patterns. The control of air permeability, heat and moisture transport between the environment and the outer layers offers a great advantage for special applications. The semi-permeability is also possible selecting outer layers of different attributes. The microclimatic quality in conjunction with the compression ability of the spacer fabrics offers a potential adequate physiological comfort (Figure 6-1). The low weight of spacer fabrics, moreover, is essential for their use as reinforcement elements for composites when light constructions are required. The ability, moreover, of spacer fabrics to embody functional components conveys the manufacturing of multifunctional products.

The wide range of materials and patterns used for the production of spacer fabrics and the subsequent range of resultant properties justify the extended application area of spacer fabrics. Actually the applications of spacer fabrics range from garment sector to reinforcement applications, including the areas of automotive, medicine, geotextiles and environmental protection, civil engineering, sports and leisure, safety and protection (Bruer, Powell & Smith 2005).

The warp-knitted spacer fabrics could be successfully used as reinforcement components for concrete applications due to their beneficial characteristics (Holler et al. 2004). The capability of manufacturing warp-knitted spacer fabrics using technical fibres (glass, carbon, aramid etc) is essential, as the well known advantages of the conventional “single layer” fabrics (high tensile resistance in oriented directions, durability against corrosion, low weight, etc (Kim 1995), (ACI Committee 1996) could be combined with the special characteristics of the specific product. In fact, the relatively high compression resistance offered by the spacer fabrics ensures stability of the product in the third direction (perpendicular to its surface), preventing the deformation of the outer layers. The spacer yarns are presented highly oriented in the total structure, forming “truss” elements and providing stiffness also in the third direction. It should be noted here, that the flexibility of the conventional “single layer” fabrics, constitutes one of their main properties making them particularly suitable for “external” repair of damaged concrete members (Triantafillou 1998). On the contrary, the warp-knitted spacer fabrics, thanks to their stiffness in the third direction, provide stability

during construction procedure and concreting under in-situ, but especially under precast quality controlled conditions. As a consequence, they could be easily used as “inner” reinforcement for concrete members, in the position where steel reinforcing bars were conventionally used. Moreover, thanks to the stability of the spacer fabric, the embodiment of the concrete is easily achieved (for example by injection molding), allowing the development of cohesion forces between the concrete and the spacer fabric and permitting the transfer of tensile forces along a crack. In addition, the online production of warp-knitted spacer fabrics in one production step is related to a profitable manufacturing procedure.

Figure 6-2: Textile reinforced concrete elements at RWTH Aachen University (Roye, Gries 2007)

Figure 6-3: Prototype and detail of the rhombic framework of textile reinforced concrete (Hegger, Voss 2008)

Due to their aforementioned beneficial characteristics, the warp-knitted spacer fabrics could consist an armature solution, profitable and competitive to the conventional reinforcing systems: a thin sheet component reinforcement capable to retain its position and to carry the

weight of net concrete during concreting, but also capable to carry high amount of tensile forces under service conditions by appropriate arrangement of the technical fibres of the outer layers (usually in two perpendicular directions). This could be extremely useful, especially for precast plane or shell concrete members i.e. load or non-load bearing precast concrete wall panels for precast industrial buildings and housing (ACI Committee 1993), industrial flooring tiles, precast concrete segments for underground structures, etc.

The compression resistance of the spacer fabrics is a critical factor for the performance and the composite manufacturing process, as well as for the embodiment of the spacer fabrics in concrete structures, as an innovative armature system. The optimum compression performance of spacer fabrics varies according to the specific application requirements. Modifications in the design parameters of the spacer fabric affect its structural characteristics and consequently the compression resistance of the sample. Purpose of the current investigation is the parametric analysis of the spacer fabric structure for the definition of the effect of certain parameters in the compression deformation.

6.2 Used samples

The warp knitted spacer fabrics under investigation were produced on a double needle bar Raschel machine type HDR 6-7 DPLM, Karl Mayer Textilmaschinenfabrik GmbH, Obertshausen, modified especially for concrete applications at the ITA, RWTH Aachen University, Germany (Roye, Gries 2007). The modifications comprise additional insertion yarn systems in warp and weft direction. Thus a grid net like structure is available for the outer surfaces increasing the facility of cement penetration within the yarns (Figure 6-5). The principle of production consists of the simultaneously production of the outer surfaces, each independently on each side of the machine. The spacer layer is also formed during the outer surfaces production by another set of needles. The length of the connecting yarns can be varied between 3 mm and 160 mm, resulting in a flexible range of spacer fabric thickness (Roye, Gries 2007).

Figure 6-4: Cross-sections of warp knitted spacer fabric in both directions.

Figure 6-5: The grid structure of the outer surfaces.

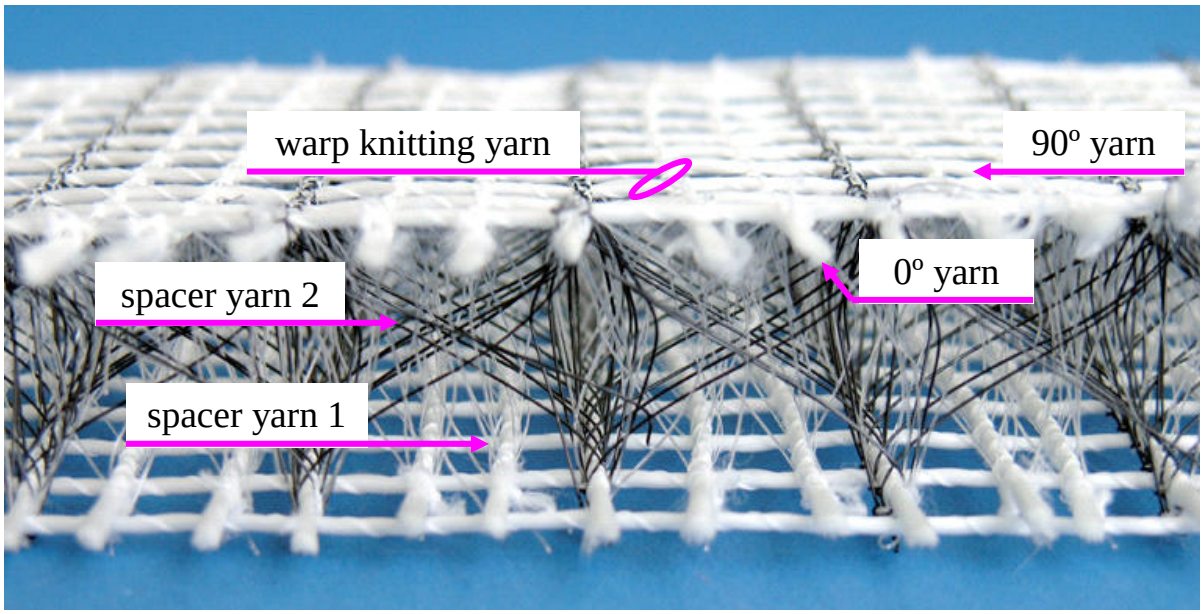

Figure 6-6: The spacer fabric components.

Table 6-1: Properties of spacer fabric components (X: Not used, N/A: Not applicable)

Component	Description	Elastic behaviour	E (N/mm²)	v	B (N·mm²)	σ (yield stress N/mm²)
warp knitting yarn	16 tex multifilament PP	X	X	X	X	X
0º yarn	2400 tex AR-Glass Roving	Linear Elastic	72000	0.3	24	N/A
90º yarn	2400 tex AR-Glass Roving cabled with PA twisted yarn	Linear Elastic	72000	0.3	24	N/A
spacer yarn 1	0,25 mm PES monofilament (white)	Bilinear elastic	E1=4876 E2=2252	0.3	0.94	167.2
spacer yarn 2	0,30 mm PES monofilament (black)	Bilinear elastic	E1=5141 E2=1792	0.3	2.04	151.7

The proposed study is focused on a group of warp-knitted spacer fabrics prepared in ITA, RWTH Aachen University. The properties of the spacer fabric components are given in the Table 6-1. The 0º and 90º yarns correspond to the warp and weft inserted yarns of the outer layers. The spacer yarns connect the two outer surfaces forming the spacer layer. The warp knitting yarns fulfil the binding of the structure through the knitting process (Figure 6-6). The group of samples was produced keeping constant the materials and the patterns used for the warp knitting yarn, the 0° and 90° yarn and the spacer yarn 1 and varying pattern of the spacer yarn 2. The patterns and the relevant set ups for the components of the examined samples are given in Table 6-2 and Table 6-3. The spacing of warp and wefts inserted yarns is 8 mm. The initial thickness of spacer fabrics is defined at 25 mm. The cross-sectional pictures of the samples are presented in Figure 6-7.

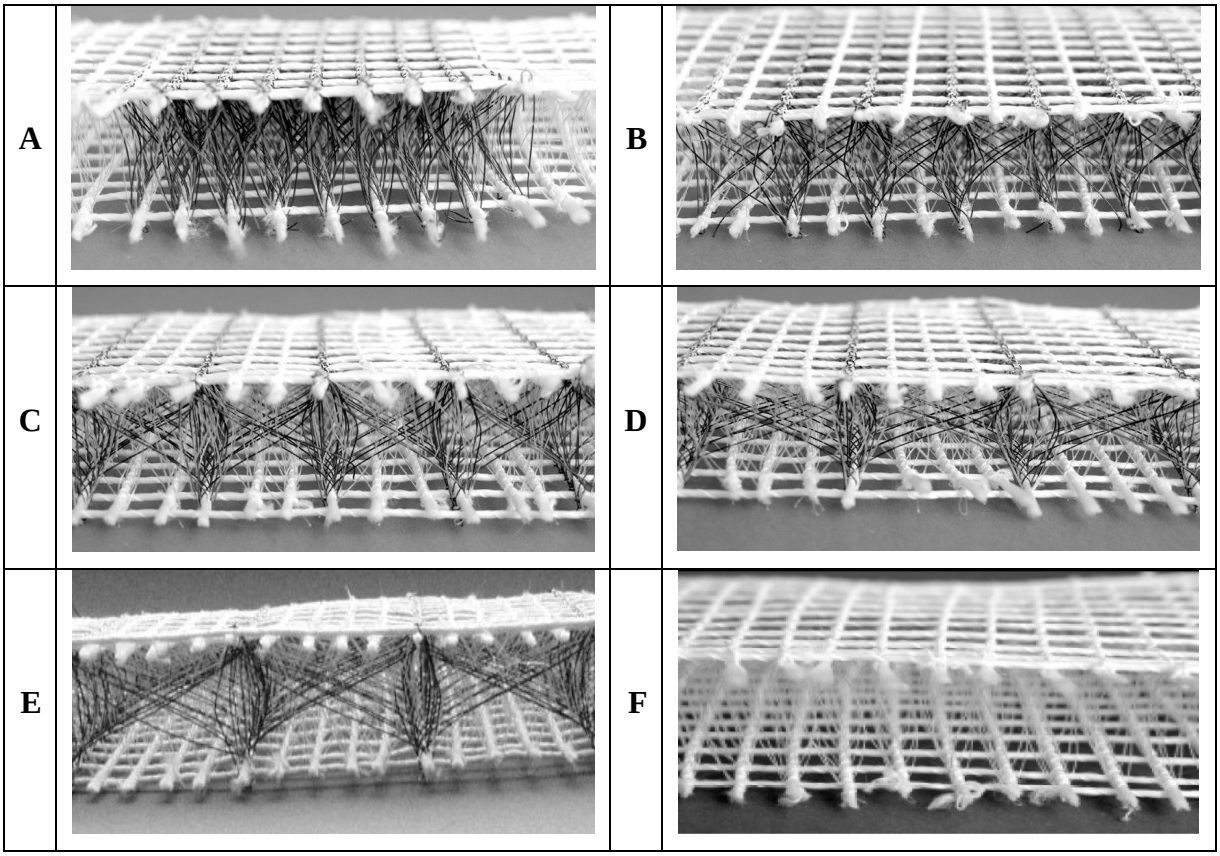

Figure 6-7: Group of samples of warp-knitted spacer fabrics.

Table 6-2: The patterns and relevant setups for warp knitting yarns, 0° and 90° yarn and spacer yarn 1.

Component	Number of the needles used	Threading	Pattern
0° yarn	42	1 full 1 empty	0000/1111
90° yarn	42	1 full 1 empty	Weft
Warp knitting yarn	42	1 full 1 empty	0101//
Spacer yarn 1	42	1 full 1 empty	0110//

Table 6-3: The patterns and relevant setups for the spacer yarn 2.

Component	Sample	Threading	Pattern
Spacer yarn 2	A	1 full 1 empty	1 2 3 4 / 4 3 2 1
	B	1 full 3 empty	1 2 5 6 / 6 5 2 1
	C	1 full 5 empty	1 2 7 8 / 8 7 2 1
	D	1 full 7 empty	1 2 9 10 / 10 9 2 1
	E	1 full 9 empty	1 2 11 12 / 12 11 2 1
	F	-	-

6.3 Experimental data

The Young modulus of the yarns was measured using the TEXTECHNO Testing Apparatus. The sample length was defined at 250 mm, the test speed at 250 mm/min and the pretension at 50 N/Tex (see also Appendix IV: Tensile Test of Spacer Yarn 1 and 2). However the bending rigidity of the single filaments was calculated based on the beam mechanics. Since the structural elements are synthetic filaments, they can be easily considered as beams of cylindrical structure. The bending rigidity of the glass roving cabled with PA twisted yarn was measured from a respective test.

The compression test of the samples was performed on the Zwick/Roell 2.5 testing equipment (Figure 6-8). The procedure for the compression test of the spacer fabrics was defined, since there was not a related standard in use available (Mecit 2005, Mecit, Roye 2006). According to this, the pressure stamp of a diameter 50 mm was mounted to the device. The samples were cut in a circular area of diameter about 200 mm. The test speed was set to 100 mm/min. The testing device measured the forces developed for the applied compression displacements. The experimental data were used for the evaluation of the accuracy of the proposed modelling method.

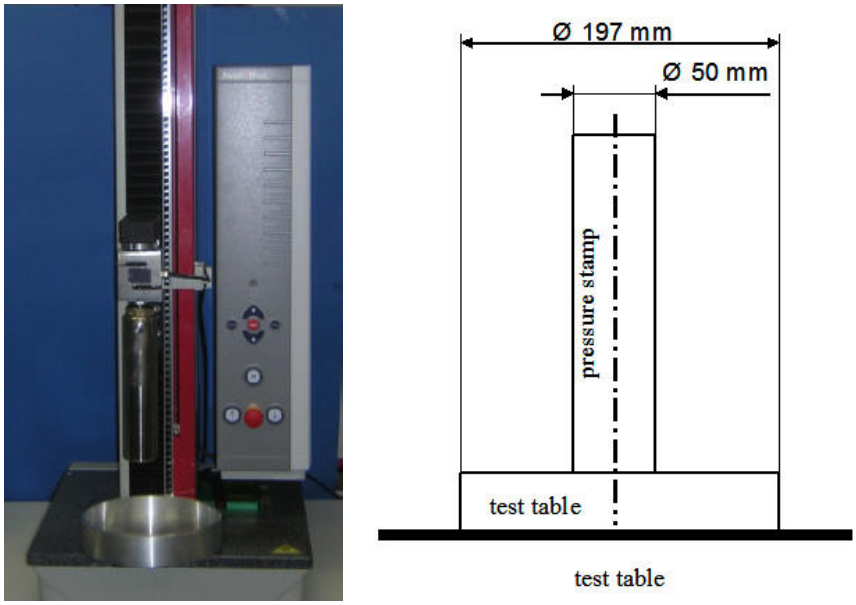

Figure 6-8: Zwick/Roell 2.5 testing equipment and testing principle.

6.4 Modelling and simulation

Two scales of modelling were adopted for the simulation of the compression test of the spacer fabric. The Finite Element Method was implemented in each modelling stage applying beam, solid and shell theory depending on the simulation requirements. The first scale corresponds to the mesomechanical analysis of the spacer and the outer layers individually for the definition of the apparent mechanical properties. The apparent properties thereinafter were introduced in the macromechanical model of the total sample developed in the second stage for the simulation of the compression test. Principle of the proposed methodology is the replacement of the discrete structure of each layer by a continuum structure presenting the identical mechanical performance. The replacement of the discrete models by continuum layers is signally beneficial for the reduction of the computational cost. Thus the simulation of the compression test of the total sample was possible in an acceptable time period. The ANSYS software was used fot the modelling and simulation of the considered structures.

6.4.1 Mesomechanical modelling of the spacer layer

The mesomechanical modelling of the spacer layer was conducted for the prediction and evaluation of the mechanical properties of the spacer layer considering the layer structure and the properties of the constituting spacer yarns (Table 6-1). The structural complexity of the spacer layer demands the generation of a short part of the considered structure for the reduction of the computational cost. Thus the modelling of the unit cell of the layer was decided. Since the compression test of the total sample induces compression in the spacer layer, the compression resistance was principally studied. Although the unit cell of the spacer layer is adequate for the current stage of modelling, the adjacent yarns of the outer layers are

also presented in the generated model for the precise representation of the structure. Two basic assumptions were introduced for the representation of the spacer yarns. Firstly, the spacer yarns were considered bonded at the warp yarns of the outer layers. The effect of the omitted loops of the spacer filaments (around the 0º yarns of the outer layers) and the omitted warp knitted yarn was assured implementing the appropriate constraint equations. The spacer filaments were represented fixed at the outer layers, since the loops of the spacer filaments are constantly connected with the outer layers (by the warp knitting yarn). Secondly, the length of the spacer yarns was assumed equal to the one obtained considering the straight formulation of them at the initial spacer fabric thickness. Therefore the length of the straight parts (spacer yarns) connecting the outer layers in the distance of 25 mm (distance of the two needle bars) was calculated. The removal of the fabric from the knitting machine incured the reduction of the outer layers distance (≈20 mm) and the curved form of the spacer yarns. According to the proposed technique the spacer yarns were represented by selected spline curves connecting the binding points and presenting the calculated length (**Vassiliadis, Kallivretaki, Kavagia, Provatidis, Mecit. and Roye 2008,** Kavagia 2008).

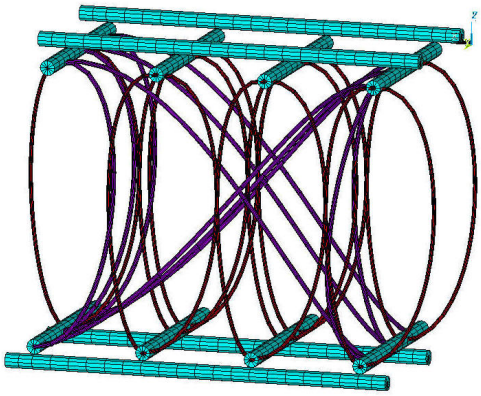

Figure 6-9: The discrete model of the unit cell (sample C).

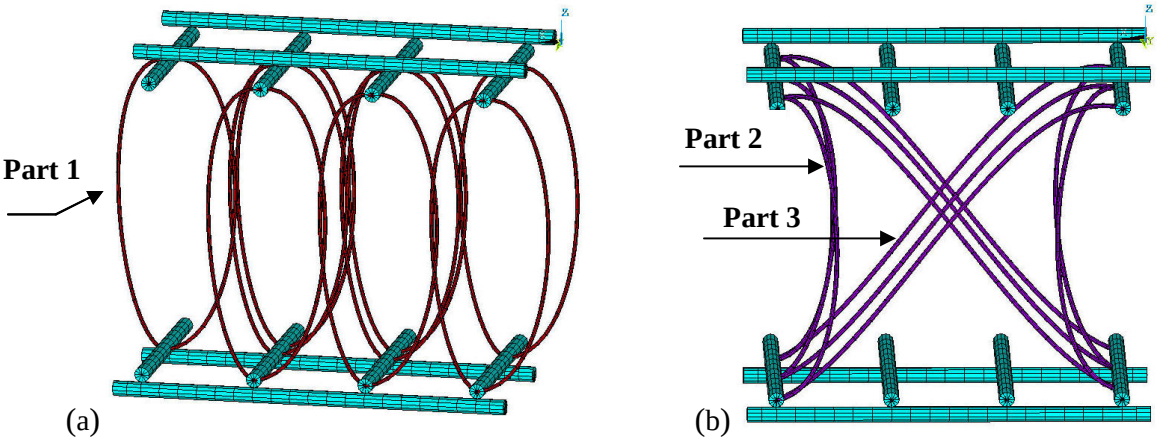

Figure 6-10: Representation of the unit cell (sample C) omitting (a) spacer yarn 2, (b) spacer yarn 1.

The configuration of the spacer yarns corresponds to spline curves generated for certain starting and ending points and line length. The starting and the ending vectors are required for the generation of a spline curve between two points (start, end). The vectors are easily expressed as functions of the angles formed with the axis of the coordinate system. A Cartesian coordinate system was defined considering the *x*, *y* and *z* axis identical to the direction of the weft inserted yarn, warp inserted yarn and fabric thickness respectively. Two angles a_{xz}, a_{yz} formed in the planes *xz*, *yz* were used for the definition of each vector. A range of values was defined for each angle according to the geometrical requirements. Thus four angles were required for the generation of a spline, two for each vector (the starting and the ending). A series of spline curves was generated for the defined range of angles. From the resultant curves the ones presenting the appropriate length, according to the assumption, were selected. Due to the iterative pattern of the spacer yarns in the fabric structure identical representation was assumed for the respective parts. Thus the definition of one geometrical element for the spacer yarn 1 and two for the spacer yarn 2 are adequate for the representation of the total unit cell. These geometrical parts are noted in the Figure 6-10.

The spline curves generated for each of the three geometrical parts (shown in Figure 6-11) were subjected to a compression deformation in order the divergences of their performance to be recorded. The boundary conditions applied for the simulation of the compression test correspond to the ones applied for the compression of the unit cell. A load was applied in the upper point of the spline and its displacement was derived. The Finite Element Method based on the beam theory was implemented for the analysis. The results of the analysis for the 3 groups of splines are given in the Table 7-4, Table 6-5 and Table 6-6.

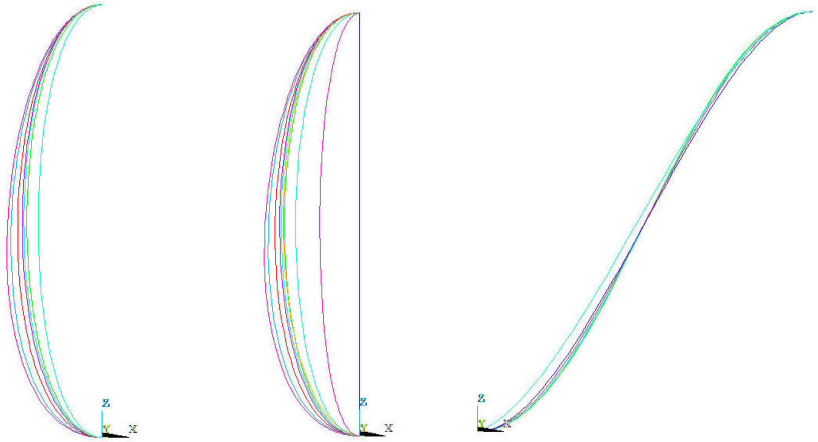

Figure 6-11: Generated splines for the geometrical part 1 (left), 2 (centre) and 3 (right).

The divergence of the strain resulted from the deformation of the splines generated for the geometrical part 1, 2, 3 corresponds to 3.9, 3.3, 15.1 % respectively. Thus the selection of the spline curve presenting a mean value of strain for each part reduces the error in 2, 1.7 and 7.1 %. Given that the real samples present divergences in the geometry of the considered parts the introduced error results lower.

Table 6-4: Results from compression for the geometrical part 1 of spacer yarn 1

Spline	Load (N)	Displacement (mm)	Strain
1	0.002	2.706	0.1424
2		2.711	0.1427
3		2.715	0.1429
4		2.667	0.1404
5		2.469	0.1299
6		2.704	0.1423
7		2.606	0.1372
8		2.480	0.1305
9		2.680	0.1414
10		2.434	0.1281
11		2.654	0.1397
12		2.635	0.1387
average			0.1380
standard deviation			0.0054

Table 6-5: Results from compression for the geometrical part 2 of spacer yarn 2

Spline	Load (N)	Displacement (mm)	Strain
1	0.002	2.134	0.1123
2		2.142	0.1127
3		2.159	0.1136
4		2.146	0.1129
5		2.009	0.1057
6		2.128	0.1120
7		2.032	0.1069
8		2.094	0.1120
9		2.037	0.1072
10		2.002	0.1053
Average			0.1010
standard deviation			0.0033

Table 6-6: Results from compression for the geometrical part 3 of spacer yarn 2 (sample C)

Spline	Load (N)	Displacement (mm)	Strain
1	0.0005	2.678	0.1409
2		2.738	0.1441
3		2.937	0.1546
4		3.320	0.1747
5		3.954	0.2080
6		3.311	0.1743
Average			0.1661
standard deviation			0.0251

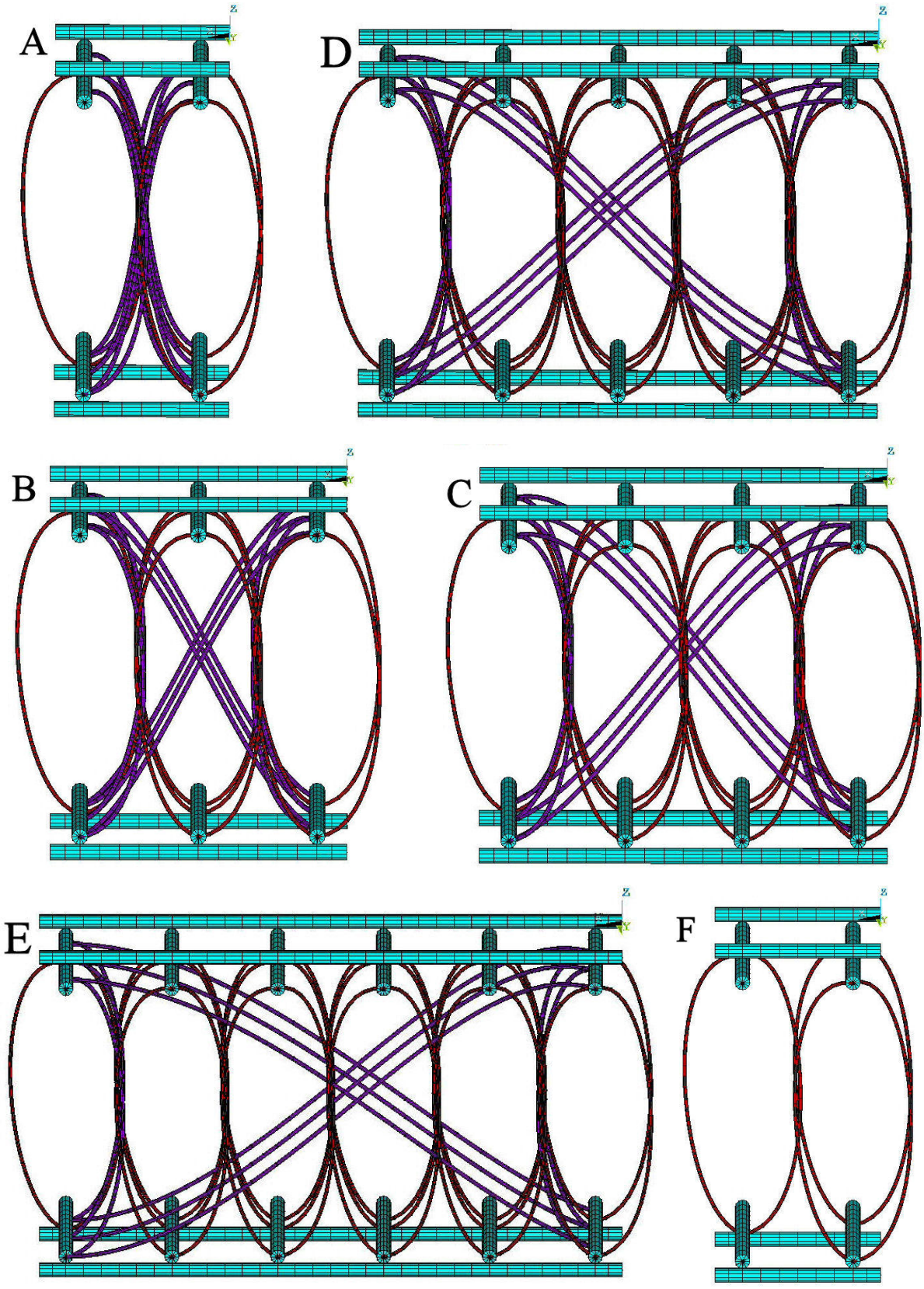

Figure 6-12: Models of unit cells of the warp-knitted spacer fabrics.

The FEM using beam elements was implemented for the simulation of the model compression. The beam theory is considered the appropriate method for the analysis given that the yarn bending constitutes the dominant deformation of the compression of the spacer layer. For the simulation of the compression of the unit cell the lower outer surface is simply supported while the upper surface moves vertically reducing the distance between them. The rotations of the nodes at the connection points are also restricted (around the warp and weft directions) in order the penetration of the outer layers by the spacer yarns to be prevented (Figure 6-13). A full Newton-Raphson algorithm supporting large strain effects was implemented for the nonlinear solution procedure.

The deformed models of the unit cells are presented in the Figure 6-14. Moreover the contour plots of the axial loads developed in the beam elements of the compressed unit cells are given in the Figure 6-15. The reaction developed by the applied displacement derived. The load – displacement curve resulted by the simulation was converted to the stress (load/area) – strain (displacement/initial thickness) curve, considering the apparent unit cell area. Therefore the compression resistance of the unit cell was reflected to the value of the elastic modulus for the continuum model of the spacer layer. The stress – strain curves corresponding to the six samples are given in the Figure 6-16. Thus a multilinear curve was considered to describe the elasticity of the spacer layer in each case.

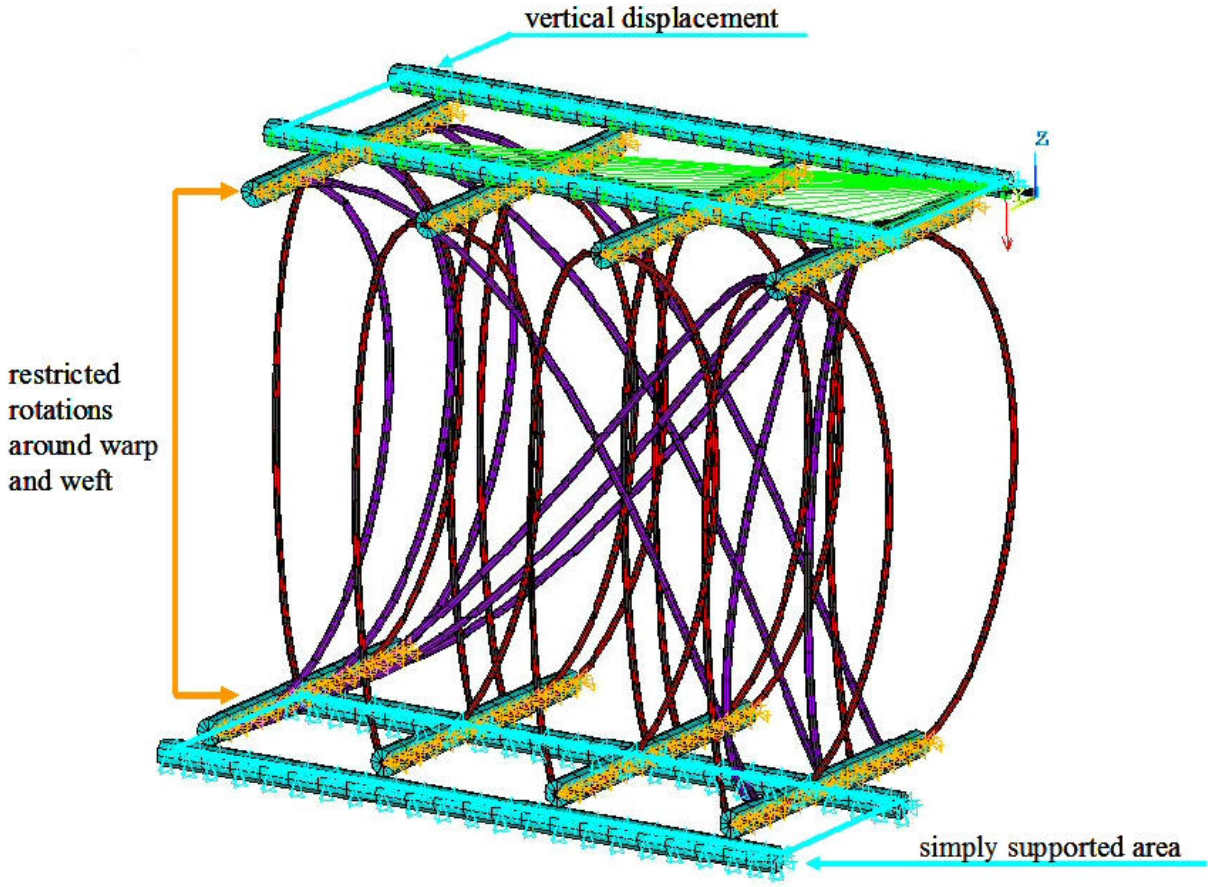

Figure 6-13: The BC for the compression of the unit cell (sample C).

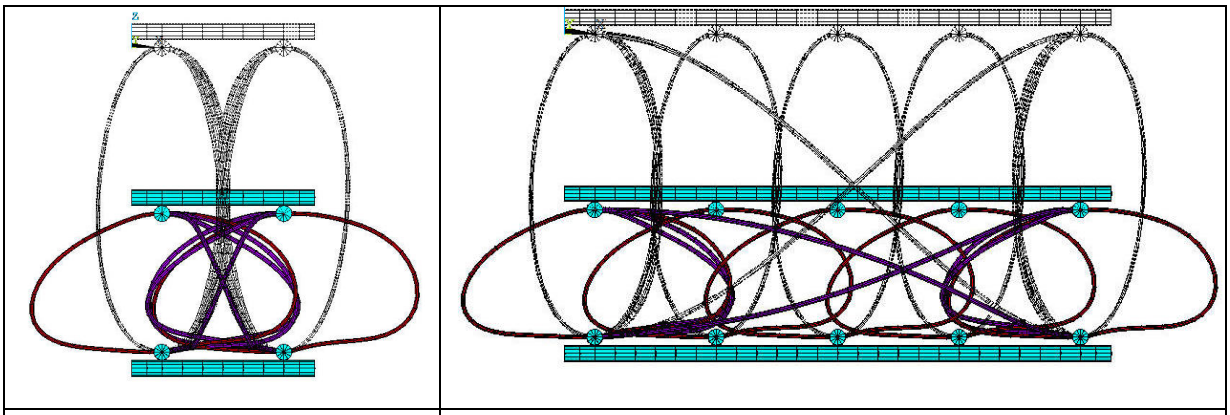

Sample A	Sample D

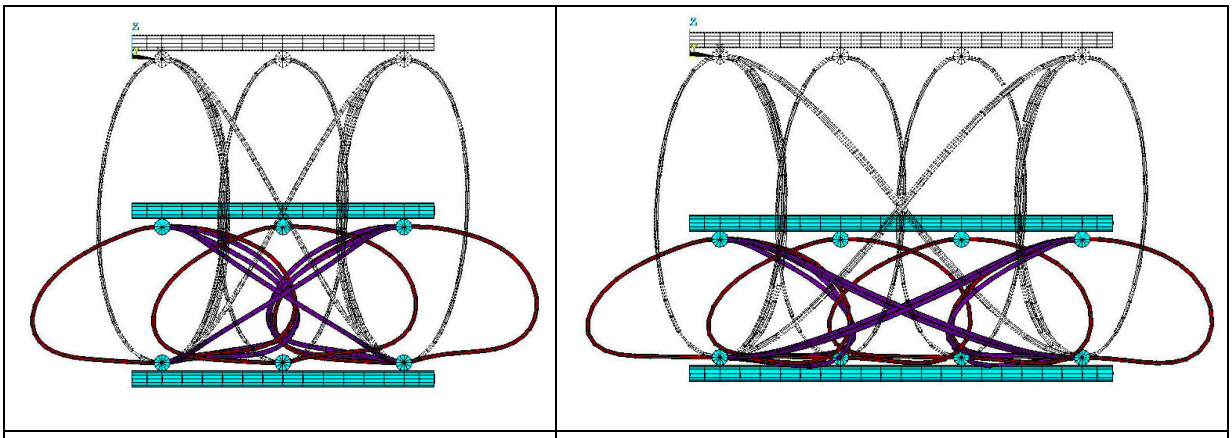

Sample B	Sample C

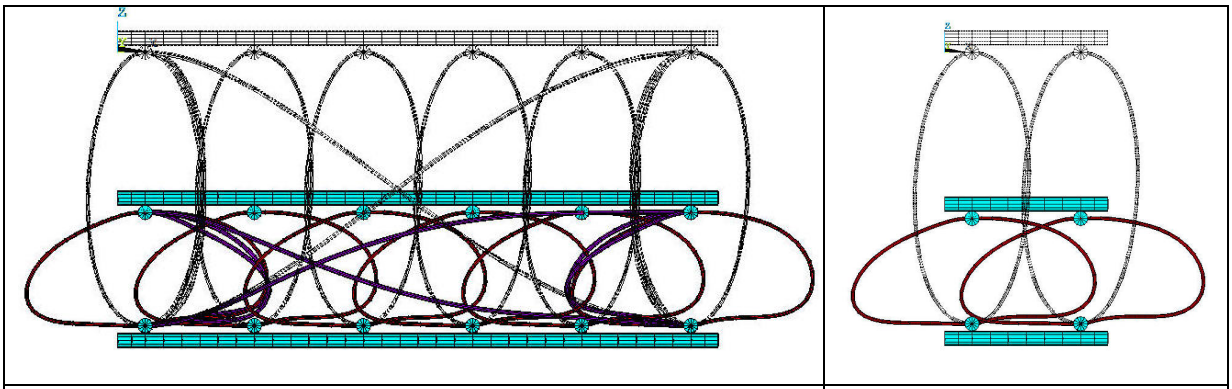

Sample E	Sample F

Figure 6-14: The deformed shape of the unit cells of spacer fabrics.

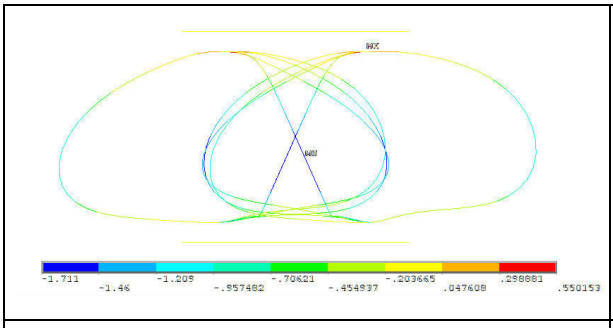

Sample A

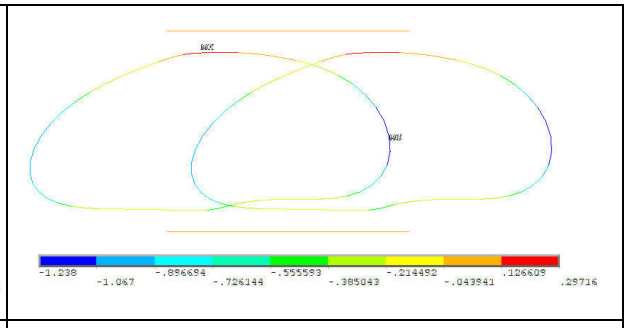

Sample F

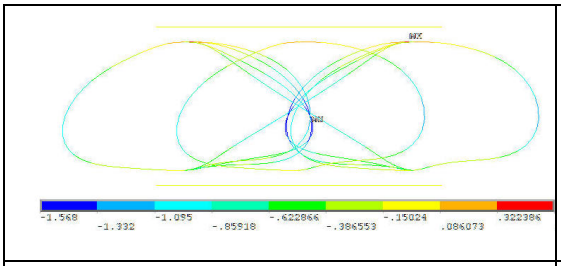

Sample B

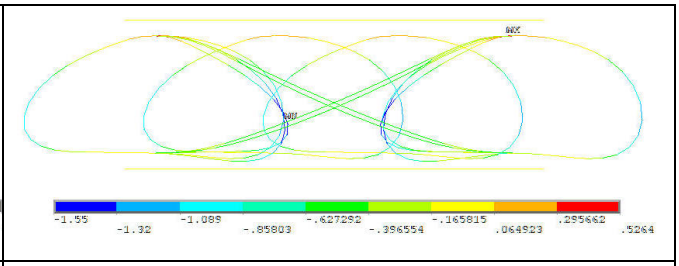

Sample C

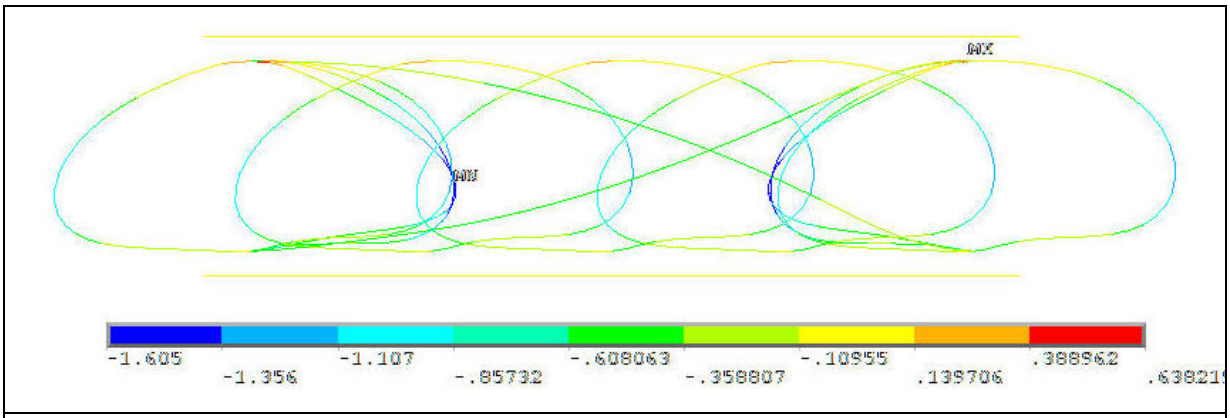

Sample D

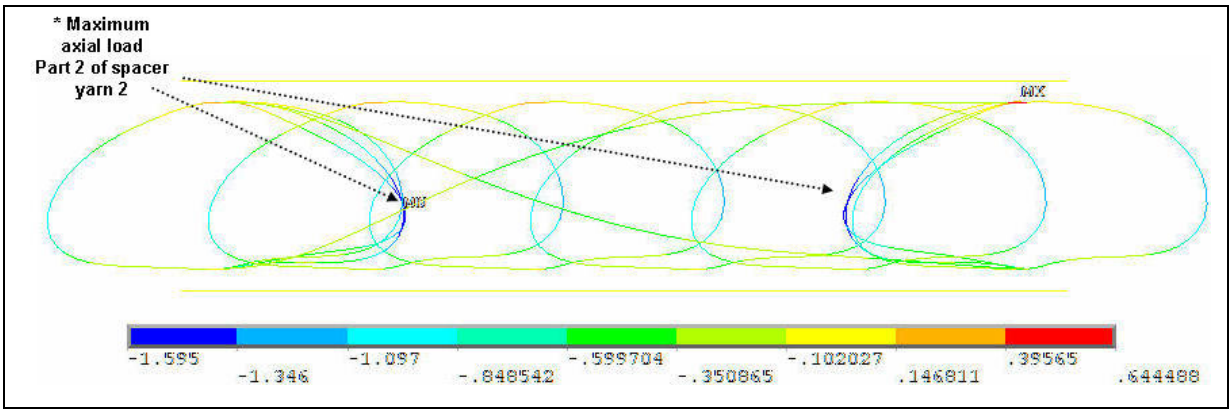

Sample E

Figure 6-15: The axial load developed in the compressed unit cells of spacer fabrics.

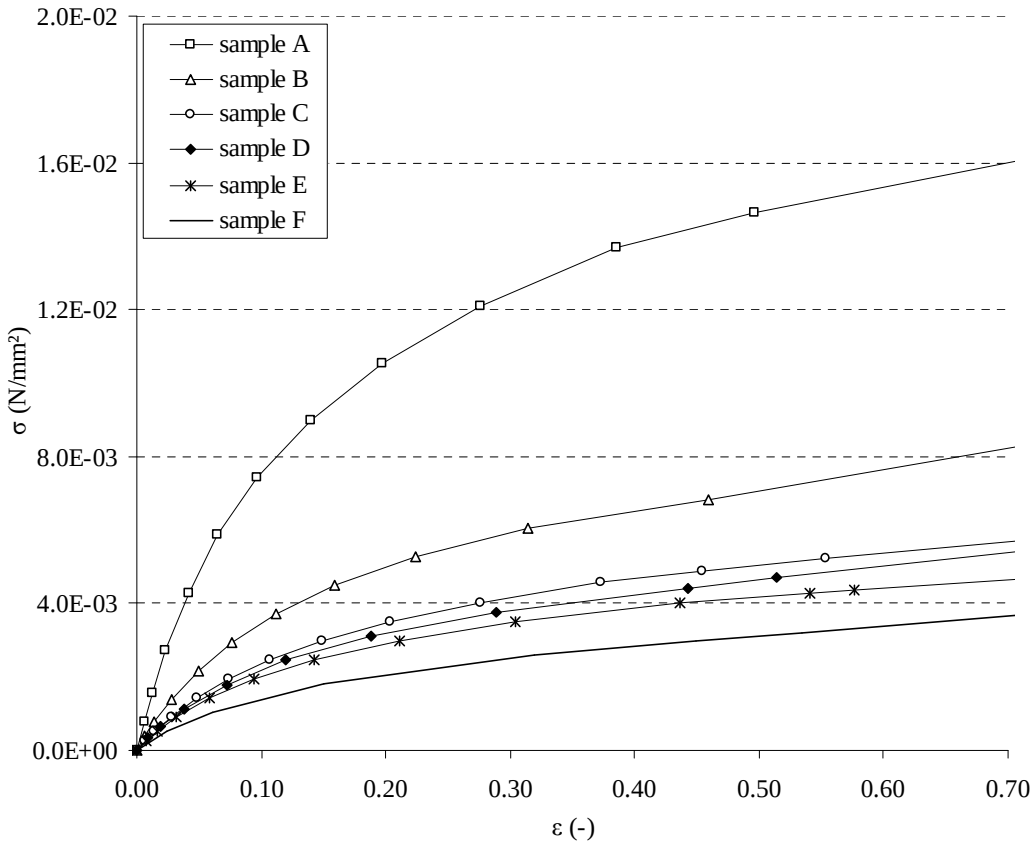

Figure 6-16: Stress – strain curves from the simulation of the compression test of the spacer layer.

The comparison of the stress – strain curves of the considered structures bring out the effect of the pattern of the spacer yarn 2. Thus the samples A – B – C – D – E – F present gradual decrease in the compression resistance since the density of the yarn 2 is decreased. The study of the axial loads developed in the spacer yarns during the unit cell compression (Figure 6-15) is determinant for the understanding of the deformation mechanism. The higher axial load is presented in the part 2 of the spacer yarn 2 due to structure (vertical yarn) and the properties (high bending rigidity of the yarn). Accordingly the compression resistance of the sample A presents high divergence in comparison to the rest patterns.

6.4.2 Mesomechanical modelling of the outer layer

The mesomechanical modelling of the outer layer was implemented for the evaluation of the mechanical properties of the outer surfaces considering the structural and the mechanical properties of the constituting yarns. The compression test of the total sample incurs a complex deformation of the outer surfaces including bending. Thus the bending rigidity and the elastic modulus were required for the replacement of the discrete by a continuum model. The FEM using beam elements was implemented for the mesomechanical analysis of the structure. Equal displacements were imposed for the nodes corresponding to the cross-points of warp-wefts in order the lacing of the yarns to be described. The deformed models resulting from the

tensile and bending are presented in the Figure 6-18 and Figure 6-18 respectively. Linear analysis was applied for the tensile deformation. Nonlinear analysis, in contrast, was implemented for the bending deformation. The apparent characteristics of the homogenised outer layer (t_o=0.0671 mm, E_o=124031 N/mm² and B_o=624 N·mm²) result from the following equations:

$$B_o = \frac{F_b \cdot D_o^3}{3dy} \quad \text{(Eq. 6-1)}$$

$$t_o = \frac{12B_o \cdot dx}{F_t \cdot D_0} \quad \text{(Eq. 6-2)}$$

$$E_o = \frac{F_t}{t_o \cdot dx} \quad \text{(Eq. 6-3)}$$

where:

D_o : the sample length (mm)

F_t : horizontal load applied in tensile deformation (N)

F_b : vertical load applied in bending deformation (N)

dx : deflection (mm) for tensile load F_t

dy : vertical deflection (mm) for bending load F_b

t_o : apparent thickness of the homogenised layer (mm)

E_o : equivalent elastic modulus of the homogenised layer (N/mm²)

B_o : equivalent bending rigidity of the homogenised layer (N·mm²)

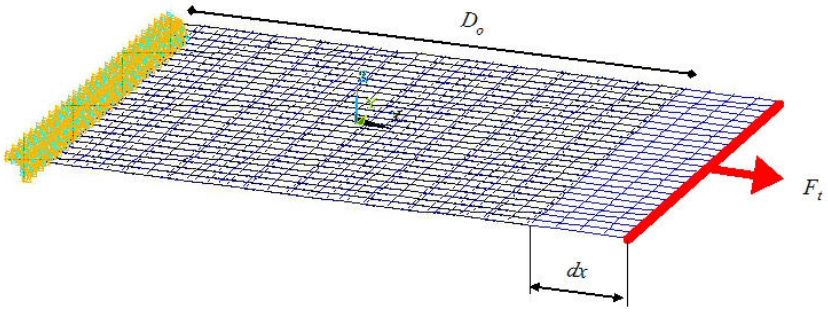

Figure 6-17: Tensile deformation of the outer layer model

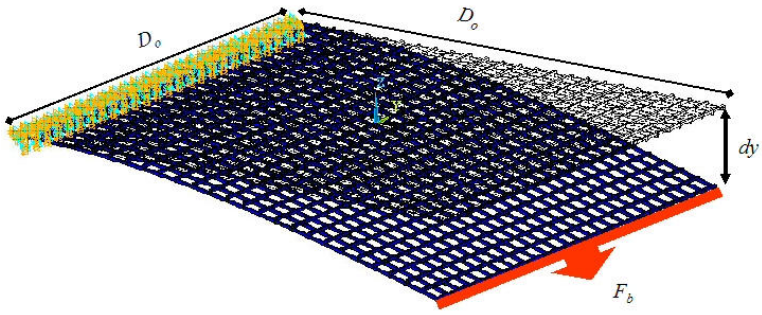

Figure 6-18: Bending deformation of the outer layer model

6.4.3 Macromechanical modelling of the total sample

In continue the derived apparent partial properties of the outer and the spacer layers were introduced in the macromechanical model of the total sample for the simulation of the complex deformation during the compression test. The macromechanical model consists of an internal volume and two overlaid surfaces corresponding to the spacer and the outer layers respectively. The volume was meshed by solid elements while shell elements were laid on the surfaces. The volume thickness was defined equal to the thickness of the spacer layer. Multilinear isotropic elasticity was considered for the internal volume. The stress-strain curves of the continuum material correspond to the ones given in the Figure 6-16. Linear orthotropic properties were introduced for the surface material. The shell thickness (t_o) and the elastic modulus (E_o) of the continuum surface model, given above, describe the tensile and bending behaviour of the discrete model. The boundary conditions applied for the simulation of the compression test of the total sample correspond to simple support of the lower outer surface and load of the upper outer surface. For the application of the load a node component was selected in the area corresponding to the stamp surface, constrained with equal vertical movement. Nonlinear solution was implemented for the analysis. The deformed model is presented in the Figure 6-19. The load – displacement curves resulted from the simulation of the compression test for the group of samples are given in the Figure 6-20 with the corresponding experimental curves.

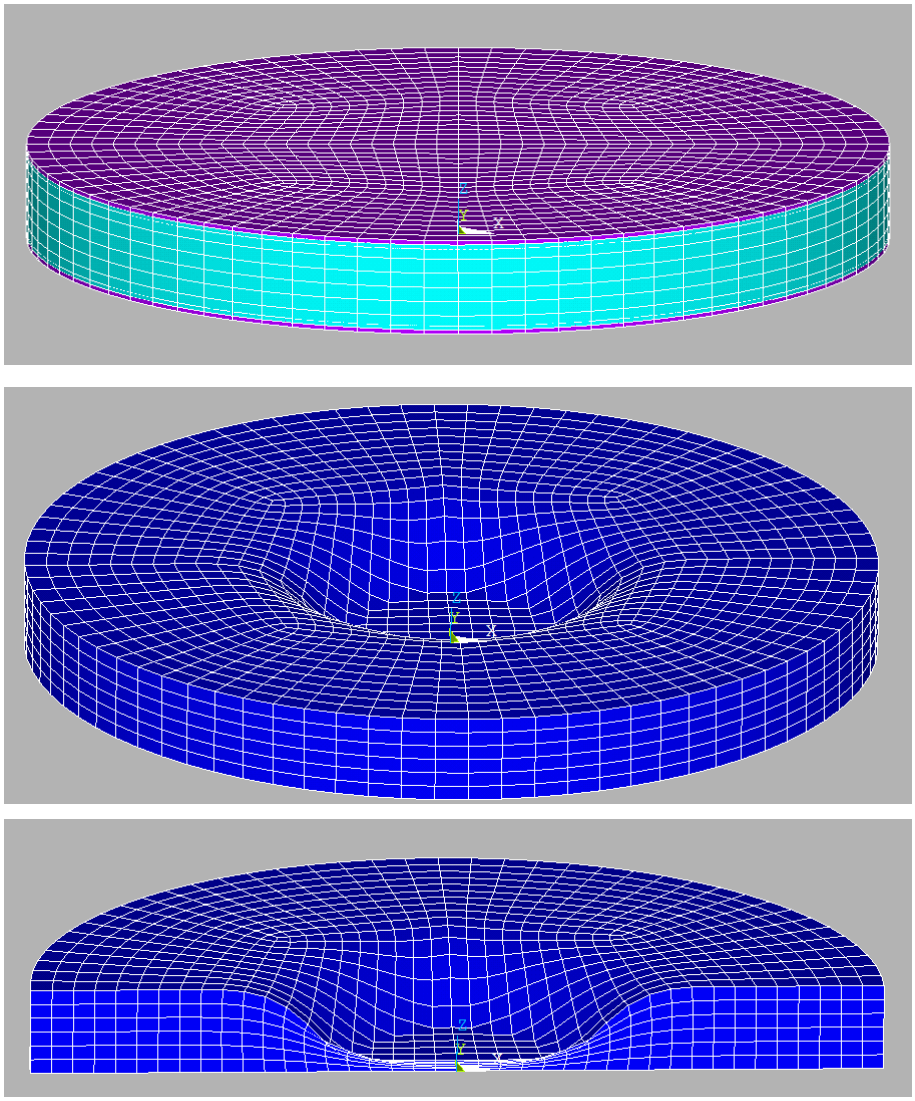

Figure 6-19: The macromechanical model in undeformed and deformed shape.

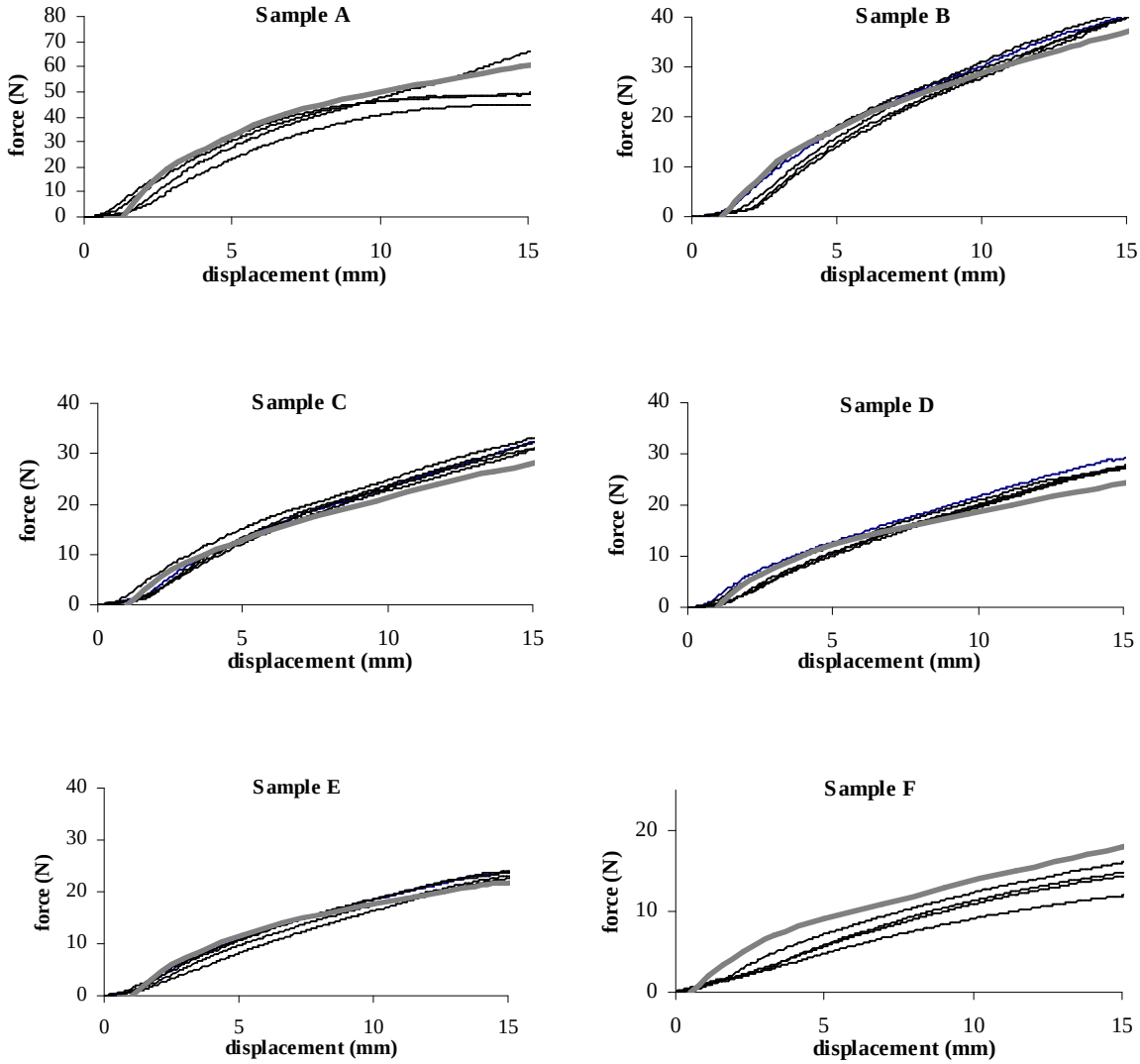

Figure 6-20: Load – displacement curves resulted from the compression test for the group of samples resulted from experiment (black) and simulation (grey).

6.5 Results and discussion

The satisfactory coincidence of the predicted and the experimental load – displacement curves of the compression test (Figure 6-20) ensures the reliability of the proposed computational modelling method. In continue the proposed method was implemented for the analysis of the effect of certain structural and physical parameters of the spacer fabric in its compression performance (**Vassiliadis, Kallivretaki, Psilla, Provatidis, Mecit, Roye 2009**). The pattern of spacer yarn 2 such as the mechanical properties of the yarns constituting the spacer and outer layers were considered substantial for the compression resistance of the specific type of spacer fabrics. Actually the effect of the pattern of the spacer yarn 2 arises by the comparison of the load – displacement curves of the studied samples (A, B, C, D, E, F). The curves are presented in Figure 6-21. The loose knitting of the spacer yarn 2 obviously leads to lower

compression resistance. The divergence of the compression resistance between the patterns A and B is remarkable. Moreover the samples with the patterns C, D, E present approximately the same compression performance. The sample F corresponds to the structure produced without the spacer yarn 2.

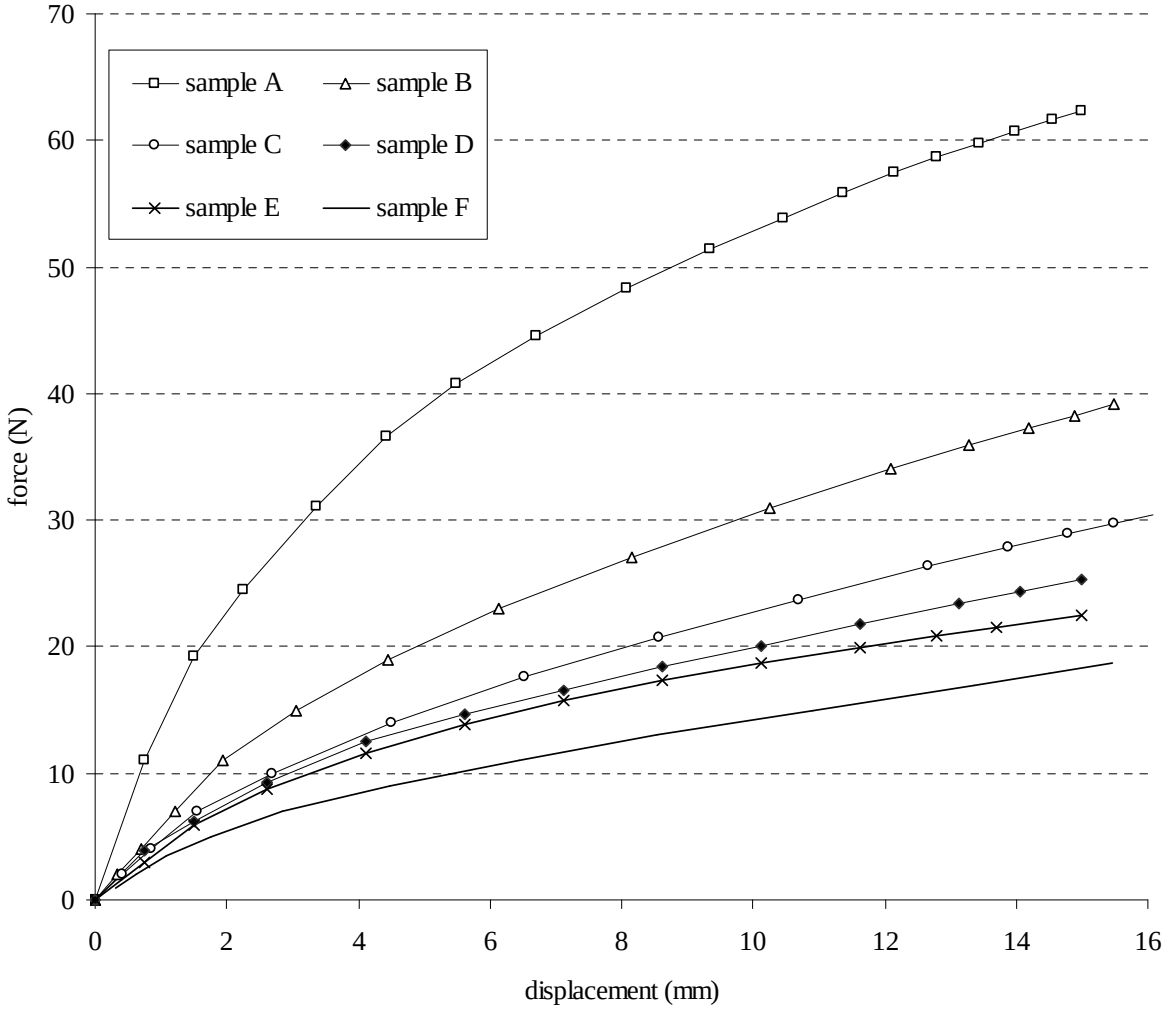

Figure 6-21: Predicted load – displacement curves resulted from the compression test for the group of samples.

The effect of the mechanical properties of the yarns constituting the spacer and outer layers in the compression performance of the spacer fabric was investigated in continue. The structure of sample F was considered as a representative one for the analysis. Linear elastic properties were assumed for the yarns as well. Given the domination of the yarns bending phenomenon in the deformation procedure during the compression test, the bending rigidity range of the yarns must be defined for the analysis. Thus ten values of bending rigidity were considered for the glass yarns (Bg=24 N·mm², 0.1·Bg, 0.5·Bg, 2·Bg, 5·Bg, 10·Bg, 15·Bg, 20·Bg, 25·Bg, 30·Bg) and the spacer yarn 1 (Bs=0.94 N·mm², 0.1·Bs, 0.5·Bs, 2·Bs, 5·Bs,10·Bs, 15·Bs,

20·Bs, 25·Bs, 30·Bs). The modification of the bending rigidity of the yarn can be achieved by changing the modulus of elasticity or the moment of inertia of the cross section. Both cases incur identical performance for the constituted layer. Thus two groups of samples were modelled for the analysis; the first corresponds to constant value of the glass yarn bending rigidity (Bg) and varying value of the spacer yarn rigidity, while the second corresponds to constant value of the spacer yarn bending rigidity (Bs) and varying value of the glass yarn rigidity. The load – displacement curves from the simulation of the compression test of the two groups are presented in Figure 6-22.

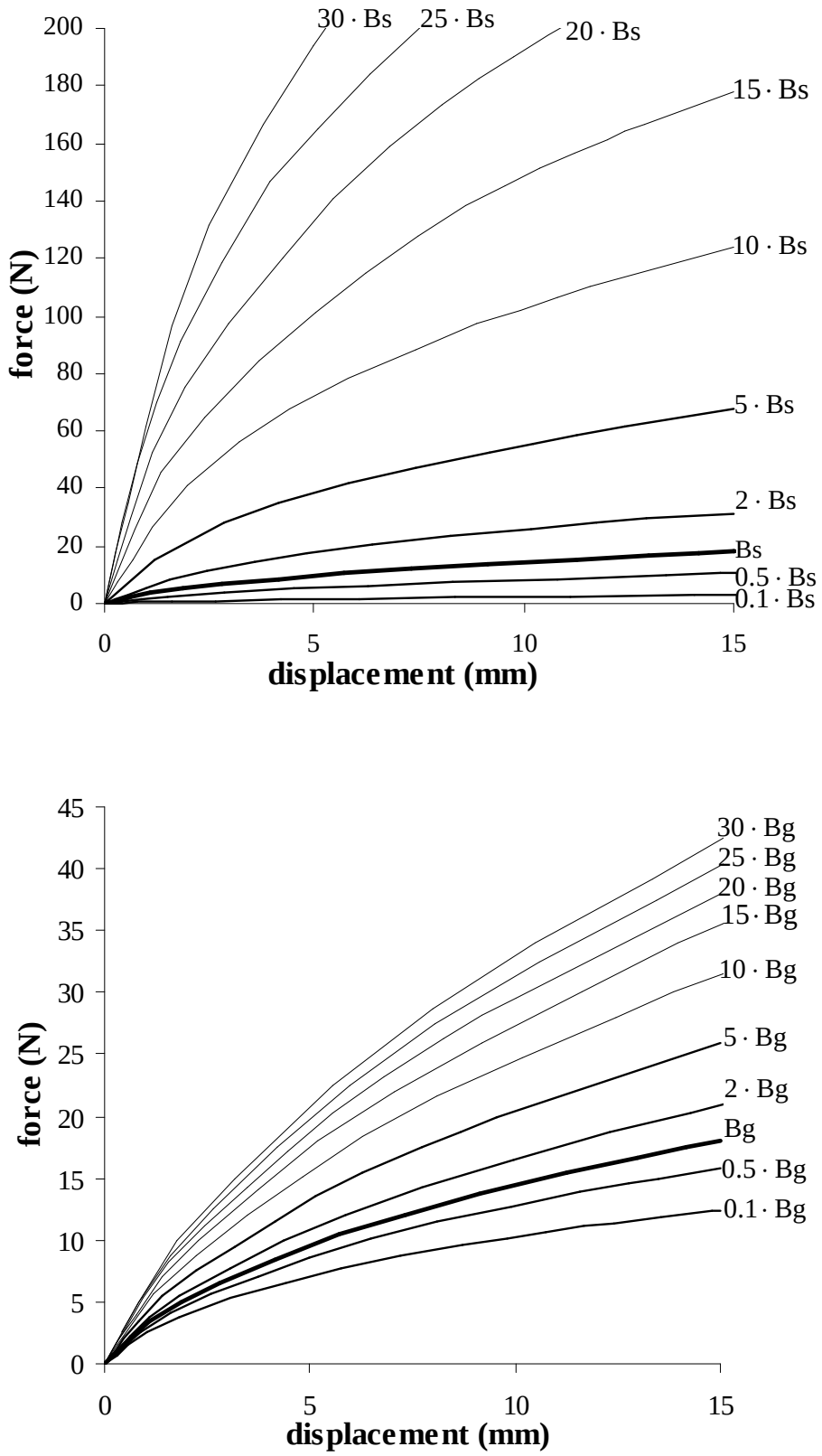

Figure 6-22: Predicted load – displacement curves resulted from the simulated compression test of the sample F with varying values of the yarn bending rigidity for the spacer layer (left) and the outer layer (right).

The load – displacement curves of Figure 6-22 support the qualitative assessment of the effect of the bending rigidity of the yarns constituting the spacer and the outer layers. The increase of the sample compression resistance due to the increase of the yarns bending rigidity is obvious. The higher impact of the bending rigidity of the spacer yarns is also raised comparing the graphs. The curve of the model developed for the basic values of Bg and Bs is presented with the bold line. For the quantitative comparison of the spacer and glass yarn impact in the sample compression performance the energy absorbed for a standard compressive deflection (10 mm) was calculated. The energy absorbed corresponds to the area formed between the load – displacement curve and the displacement axis up to the selected value of displacement (10 mm). The energy absorbed depending on the bending rigidity of the yarns is given in Figure 6-23. Consequently the multiplication by ten of the bending rigidity of the spacer yarn incurs increase of the absorbed energy 6 – 7.6 times while the same increase in the bending rigidity of the glass yarns incurs an increase of the absorbed energy 1.3 – 1.7 times.

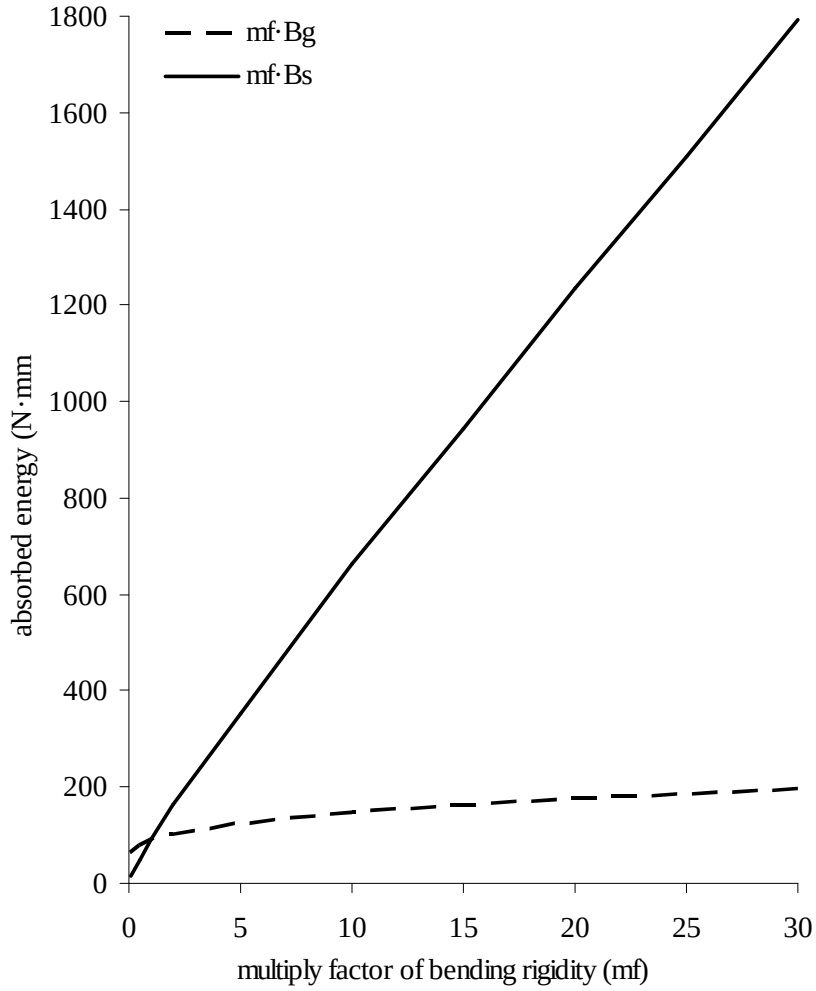

Figure 6-23: Effect of bending rigidity of yarns in the energy absorbed for compressive deflection 10 mm.

6.6 Conclusions

A simulation method was developed for the prediction of the compression performance of spacer fabrics for concrete applications. The proposed method comprises two stages of mechanical analysis in meso- and macroscopic levels. The Finite Element Analysis applying beam, solid and shell theory was implemented in each modelling stage. The mesomechanical analysis was conducted separately in the spacer and the outer layers of the fabric for the evaluation of their performance in compression and bending respectively. The results in continue were used for the calculation of the apparent properties of the continuum models. Principle of the proposed methodology was the replacement of the discrete structure of each layer by a continuum structure presenting the identical mechanical performance.

The accuracy of the proposed method was evaluated with experimental data for a group of six samples. The adequate fitting between the experimental and the predicted curves of load – displacement assures the reliability of the used method. Moreover the effect of the varying pattern of the spacer yarn 2 in the compression performance of the spacer fabric was investigated thoroughly. Finally the effect of the bending rigidity of the yarns constituting the spacer and the outer layers was examined, in order to complete the analysis of the structural parameters influencing the behaviour of the spacer fabrics.

Conclusions and suggestions for further work

The objective of the thesis is the conceptual development of an integrated mechanical design procedure for the textile structures. A systematic approach was proposed which integrates all the stages of textile modelling implementing the Finite Element Method. The production hierarchy of the textile structures (fibre – yarn – fabric) was considered for the subdivision of the design procedure in the respective modelling stages. Thus three basic modelling scales were developed: the micromechanical modelling of yarns, the mesomechanical modelling of the fabric unit cell and the macromechanical modelling of the fabric sheet. The major achievement of the proposed design procedure is referred to the progressive transition between the modelling stages, i.e. the attribution of the yarn properties in the mesomechanical model and the attribution of the unit cell properties in the macromechanical model. The definition of the basic mechanical parameters of a discrete model and the generation of an equivalent continuum model constituted the general principles for each transition mode within the modelling stages. Thereby the proposed design procedure faced the main drawback presented in the existent modelling approaches. The integrated design procedure provides the drape simulation of a fabric sheet when the filaments properties, the yarn structure and the fabric pattern are given.

Except from the successful integration of the modelling stages, substantial achievements were noticed in each modelling stage. Regarding the micromechanical modelling stage, a FEM using beam elements was proposed for the analysis of multi-filament twisted yarns. The proposed method presents significant advantages in modelling and analysis. Thus a fast and flexible design is offered in terms of geometrical representation and material properties. Moreover the low computational power demanded for the analysis is beneficial for the study of multifilament yarns. The reliability of the proposed method was proved using experimental data. Finally the proposed modelling approach was implemented for the parametric analysis of the yarn mechanical behaviour. The effect of the structural parameters on the yarn bending rigidity was presented quantitatively in a diagram.

Three FE approaches, the solid, shell and beam modelling, were implemented for the mesomechanical analysis of the fabric unit cell. The three approaches were evaluated regarding the attribution of the yarn properties, the convenience in the application of the boundary conditions, the computational cost, the convergence success in the solution procedure and the reliability of the results. The beam modelling was selected as the adequate modelling method for certain reasons. Main reason was the successful attribution of the yarn properties. Actually the realistic attribution of the yarn properties is essential for the accuracy of the mesomechanical modelling stage. Thus the equivalent performance of the homogenous

yarn, considering the discrete structure, in the tensile and bending deformation is required at least for the reliable attribution of yarn models. It is remarkable that most of the existent modelling approaches omitted the calculation of the real value of the yarn bending rigidity and its attribution at the modelled yarn.

The effectual attribution of the apparent properties of the unit cell discrete structure, calculated in the mesomechanical stage, in the continuum model of the fabric sheet is the keypoint for the reliability of the macromechanical modelling stage. In the proposed modelling approach the mechanical performance of the unit cell in tensile, shear and bending deformation along warp and weft direction were considered for the evaluation of the apparent properties of the unit cell. Three modelling methods were implemented for the generation of a sheet model presenting equivalent performance with the asymmetric woven structure. The reliability of the proposed methods was proved using experimental data from the tensile, shear and bending test of the fabrics. The used experimental data were received from the literature. Moreover the drape test was simulated implemented the 3-layer macromechanical modelling approach. The layered solid-shell elements with translational degrees of freedom were used for the FEA. Thus the convergence difficulties resulting from the evaluation of the rotational nodal degrees of freedom were omitted. The proposed approach was evaluated using experimental data.

The proposed design procedure was modified for the mechanical analysis of a three-dimensional technical textile. The compression performance of a group of warp knitted spacer fabrics, used in building constructions as thin sheet component reinforcement, was studied. The mesomechanical modelling stage was implemented separately for the evaluation of the apparent properties of the spacer and the outer layers. The effective apparent properties of the layers, related to the compression test of the total fabric, were calculated by the respective simulations. The macromechanical model of the structures under investigation was used for the simulation of the compression test. The reliability of the results was evaluated using experimental data. The successful implementation of the developed design procedure in the three-dimensional structures assures the universal validity of the proposed textile design.

The proposed design procedure focused on the static analysis of textile structures in low loading conditions. Thus the apparent properties of the unit cell were calculated at low loading tests and linear elasticity was considered for the equivalent macromechanical model. The developed macromechanical models predict sufficiently the mechanical performance of the fabrics in complex deformations with large displacements and rotations including bending in multiple planes, as drape test or molding of the textile sheet. They are also sufficient for the evaluation of the fabric performance in tensile and shear test at relatively low strains depending on the structure. Actually increasing the in-plane load the fabric sheet performance becomes highly nonlinear due to the flattening of the yarns at linking points, the increase of the contact pressure and friction and the reduction of the yarn cross-section. Accordingly the linear elastic macromechanical model is unable to predict the mentioned nonlinear performance of the fabric sheet. Some textile structures, basically knitted, present highly nonlinear performance even for low-loading conditions due to the structural changes during

the deformation procedure. Thereby the nonlinear performance of the discrete structure should be considered in a further improved macromechanical model.

Moreover two shear moduli are required for the definition of the in-plane shear performance of the fabric since different shear properties derive along warp and weft direction in an asymmetric structure. Since orthotropic properties were considered for the proposed macromechanical model the mean value of the two shear moduli was used. The mentioned assumption is probably related with the symmetric configuration of fabric drape resulted from the simulation. The resultant symmetry is unrealistic. Thereby two in-plane shear moduli should be considered in an improved macromechanical model.

Actually the textile design corresponds to an unlimited field, considering the materials, the structures and the applications. The current thesis presented a conceptual integrated textile design focusing in a specific range of structures and applications. Therefore massive effort is required for the expansion of the proposed design procedure in a wider field, considering the investigated structures (staple yarns, 3D fabrics, composite materials), the material properties (plasticity, viscoelasticity) and the analysis type (dymanic analysis).

Appendix I: Surface-to-surface contact analysis

The surface-to-surface contact is suitable for the mechanical contact analysis of equally deformable bodies (with similar elastic properties). Moreover the large scale sliding between the bodies is supported by the selected contact mode. In studying the contact between two bodies, the surface of one body is conventionally taken as a contact surface and the surface of the other body as a target surface. The contact and target surfaces constitute the contact pair.

The contact element (CONTA174) is associated with the 3-D target segment elements (TARGE170) using a shared real constant set number. The contact and target elements are located on the surface of the 3-D solid, shell elements (underlying element) and they have the same geometric characteristics as the underlying elements.

The contact detection points are the integration points and are located either at nodal points or Gauss points. The contact element is constrained against penetration into the target surface at its integration points. However, the target surface can, in principle, penetrate through into the contact surface. CONTA174 uses Gauss integration points as a default, which generally provides more accurate results than those using the nodes themselves as the integration points.

The penetration distance is measured along the normal direction of contact surface located at integration points to the target surface. It is uniquely defined even the geometry of the target surface is not smooth. Such discontinuities may be due to physical corners on the target surface, or may be introduced by a numerical discretization process (e.g. finite elements).

The position and the motion of a contact element relative to its associated target surface determine the contact element status. The program monitors each contact element and assigns a status:

STAT = 0 Open far-field contact

STAT = 1 Open near-field contact

STAT = 2 Sliding contact

STAT = 3 Sticking contact

A contact element is considered to be in near-field contact when the element enters a pinball region, which is centred on the integration point of the contact element. The computational cost of searching for contact depends on the size of the pinball region. Far-field contact element calculations are simple and add few computational demands. The near-field calculations (for contact elements that are nearly or actually in contact) are slower and more complex. The most complex calculations occur the elements are in actual contact.

In the basic Coulomb friction model, two contacting surfaces can carry shear stresses up to a certain magnitude across their interface before they start sliding relative to each other. The state is known as sticking. The Coulomb friction model is given in (Release 11.0 Documentation for ANSYS).

Once the equivalent shear stress exceeds, the contact and target surfaces will slide relative to each other. This state is known as sliding. The sticking/sliding calculations determine when a point transitions from sticking to sliding or vice versa. The contact cohesion provides sliding resistance even with zero normal pressure.

The augmented Lagrangian method is an iterative series of penalty updates to find the Lagrange multipliers (i.e., contact tractions). Compared to the penalty method, the augmented Lagrangian method usually leads to better conditioning and is less sensitive to the magnitude of the contact stiffness coefficient.

Appendix II: Yarn modelling using solid FE

The implementation of FEM using solid FE (solid modelling) for the mechanical analysis of fibrous assemblies was proved insufficient presenting three major drawbacks. Firstly the required computational power for the analysis even of a few-filament assembly is extremely high due to the huge number of the generated FE and nodes. Secondly the standard contact algorithm fails to converge. Thus the bonded contact algorithm is used for the convergence of the solution procedure, applying additional constraints. Finally the solid modelling fails to model the bending properties of irregular filament cross sections.

The modelling and simulation of the yarn was performed using the ANSYS commercial code. The 8-node hexahedron solid elements (SOLID45) of 3 DOF (translations) per node were used for the solid modelling of the yarn filaments. The model was based on the generation of a mesh with 48 FE in the filament cross-section that corresponds to 2304 FE, 2793 nodes, 8379 DOF per filament for the modelling of one pitch of yarn. Thus N×2304 solid FE are required for the modelling of one pitch of an N-filament yarn. Additional elements (contact and target) are generated increasing the computational cost of the model. The contact and target FE are responsible for the load transfer between the contact areas of the filaments, the friction forces application and the definition of the contact state (sticking or sliding). The contact and target elements were placed as an overlay on the solid elements in the areas defined as contact-target (contact pair). Thus the appropriate mesh of the filaments supported the convergence during solution. A mesh including coincident nodes generated in the contact-target area was practically approved as a well-defined mesh. The solid model of a 2-filament twisted yarn is represented in the Figure II-1. The mesh is generated by 2×2304 solid elements and 768 contact and target elements. A zoom in the filaments cross-section is also presented in the Figure II-1.

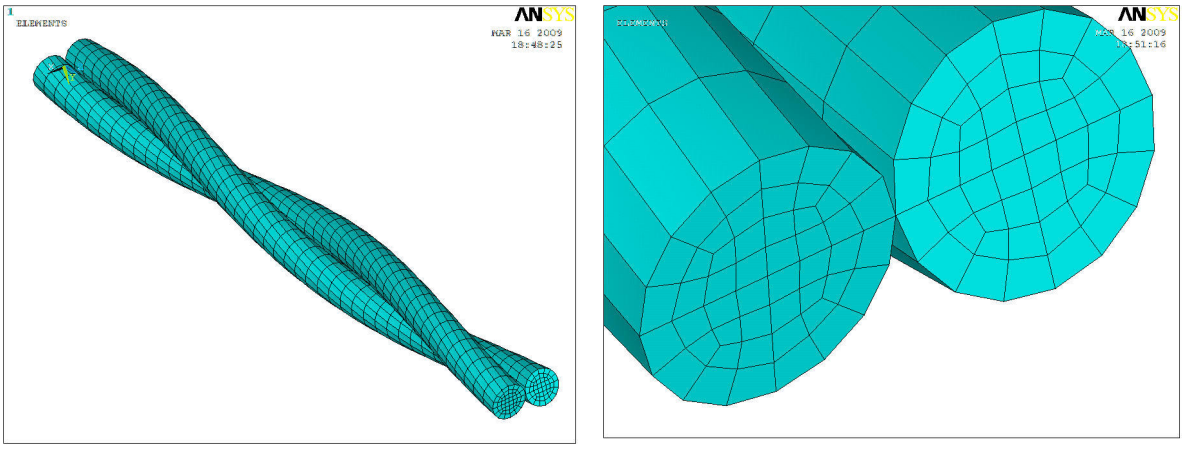

Figure II-1: Solid model of 2-filament twisted yarn.

The selection of the contact algorithm is essential for the reliability of the simulation. ANSYS FEM code provides several contact algorithms and specific options to support the different

contact conditions. For the current simulations, the surface-to-surface contact was selected. The selected one is suitable for the contact analysis of equally deformable bodies (with the same elastic properties). Two contact algorithms were implemented separately in the bending test of the N-filament twisted yarn for the evaluation of the deformation and the convergence procedure. The Augmented Lagrangian contact algorithm was used to describe the standard contact conditions. This algorithm ensures the free deformation procedure permitting also large scale sliding between the bodies. The Internal Multipoint Constraint (MPC) algorithm in conjunction with bonded contact was used to predict the deformation procedure under bonded contact conditions. In both simulations the adjustment of just touching contact pairs was achieved activating the appropriate options of the software. The yarn characteristics described in the 2.5.2 were considered for the evaluation of the implemented contact algorithms in the yarn bending simulation. Moreover the results of the beam modelling (presented in the 2.2) and the analytical approach (presented in the 2.3) are given for the comparison. The bending rigidity of the yarns calculated by the mentioned approaches is given in the Table II-1.

Noteworthy conclusions resulted by the comparison of the above approaches. Firstly, convergence failure was presented by the implementation of Lagrangian contact algorithm (standard contact conditions) for filament number higher than 2. The bending rigidity of the 2-filament yarn resulted from the solid modelling with standard contact conditions approximates the respective value corresponding to the beam model. Thus the proposed beam modelling approach represents the standard contact conditions. The values of yarn bending rigidity calculated from the solid modelling with bonded contact conditions present significant divergence comparing with the respective values resulted from the solid modelling with standard contact (for 2 filaments) or beam modelling and they approximate the analytical values. Thus the analytical approach represents the bonded contact conditions. By inference the solid modelling of multifilament yarns approved inadequate to predict the yarn bending performance considering the standard contact conditions.

Table II-1: The bending rigidity of yarns resulted from the beam modelling, solid modelling and the analytical approach.

	r_f (mm)	filament number, N	B_y (N·mm^2)			
			analytical approach	beam model	solid model	
					standard contact	bonded contact
R_y=1 mm, E=5000 N/mm^2, v=0.3, t=0.1 turns/mm	0.5000	2	1637.8	453.6	438.2	647.8
	0.4142	4	1457.5	419.8	not converged	1889.5
	0.3333	6	1492.3	263.3	not converged	1013.4
	0.2679	8	1148.5	147.9	not converged	1207.6
	0.2265	12	1292.8	112.8	not converged	1101.0

In addition the solid modelling presents a significant drawback comparing to the beam modelling in the definition of the moment of inertia. Actually in solid modelling the moment of inertia of a cross-section is calculated by the geometrical characteristics of the structure contrary to the beam modelling that the moment of inertia is introduced as parameter value. Thus the solid modelling of irregular (hollow, elliptical etc) cross-sections of filaments requires the geometrical representation of them, increasing the complexity of the modelling and meshing procedure.

Appendix III: Contact analysis vs. CE in beam modelling of yarns

Two beam modelling methods for the simulation of the yarn tensile are compared for the evaluation of the results and the convergence procedure. The approaches differ in the imposition of the constraints between the filaments during the yarn tensile deformation. Given that the tensile of a single helix corresponds basically to the reduction of the helix radius, the constraints are essential to preclude the appearance of penetration between the filaments.

In the approach proposed in the 2.2 the constraints were imposed as zero radial displacement in the nodes of the total model. In the second approach the constraints were imposed implementing the line-to-line contact algorithm. The contact pairs were defined between the adjacent filaments. For example 18 contact pairs were generated in the 12-filament structure shown in the Figure III-1. Practically the applied contact analysis retains a constant distance between the beam axes constituting the contact pairs (contact – target). The two approaches were applied in the 12-filament structure and identical load-elongation curves resulted from the tensile simulation. Moreover the same deformation mechanism constitutes both approaches presenting zero radial nodal displacement in the model. A zoom in selected elements constituting the yarn cross-section in the undeformed and the deformed state is presented in the Figure III-2. Since the two approaches incurs identical results, the approach imposing the CE (replacing the contact algorithm) was proposed as beneficial for the modelling simplicity (omits the generation of contact pairs), for the computational time saving and the fast convergence achievement.

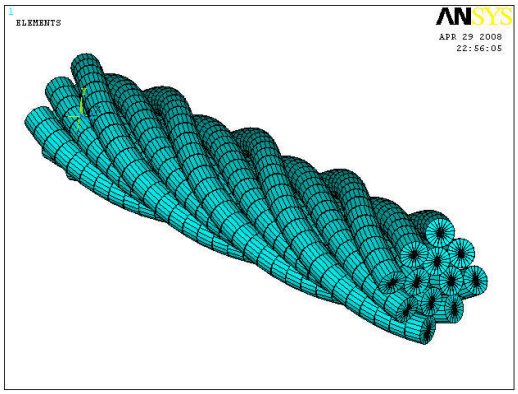

Figure III-1: Beam model of a 12-filament twisted yarn.

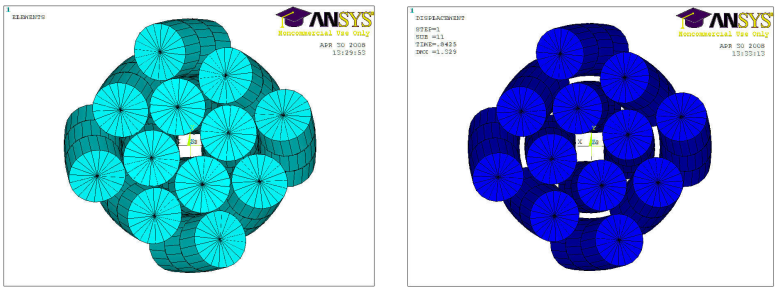

Figure III-2: Selected elements in undeformed and deformed state by tensile deformation.

Appendix IV: The elastica of a cantilever beam

The mathematical model describing the deflection curve of a flexible sheet or beam is called elastica. A cantilever beam is considered inextensible with a uniform cross-section such that the moment – curvature relationship obeys the Euler-Bernoulli theorem. The governing equation (Demiroz 2005) for the cantilever beam loaded as shown in the Figure IV-1 is:

$$M = EI\frac{d\theta}{ds} = P_y(L-\Delta x-x) + P_x(\Delta y - y) + \frac{w}{2}(L-s)^2\cos\theta \qquad \text{(Eq. IV-1)}$$

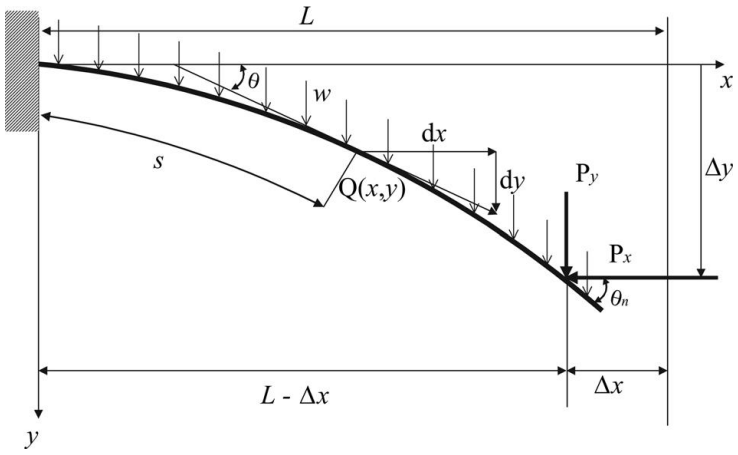

Figure IV-1: A cantilever beam under large deformation

The second-order differential equation can be obtained:

$$\frac{dx}{ds} = \cos\theta \qquad \text{(Eq. IV-2)}$$

$$\frac{dy}{ds} = \sin\theta \qquad \text{(Eq. IV-3)}$$

$$EI\frac{d^2\theta}{ds^2} = -P_y\cos\theta - P_x\sin\theta - w(L-s)\cos\theta - \frac{w}{2}(L-s)^2\sin\theta\frac{d\theta}{ds} \qquad \text{(Eq. IV-4)}$$

The dimensionless variable $\bar{s} = s/L \quad (0 < \bar{s} < 1)$ is introduced and defining $\overline{M} = \frac{ML}{EI}$, $\overline{P}_y = \frac{P_y L^2}{EI}$, $\overline{P}_x = \frac{P_x L^2}{EI}$, $\overline{w} = \frac{wL^3}{EI}$, then $\frac{d\theta}{d\bar{s}} = \overline{M}$ and the differential equation results:

$$\frac{d^2\theta}{d\bar{s}^2} = -\overline{P}_y\cos\theta - \overline{P}_x\sin\theta - \overline{w}(L-\bar{s})\cos\theta - \frac{\overline{w}}{2}(L-\bar{s})^2\sin\theta\frac{d\theta}{d\bar{s}} \qquad \text{(Eq. IV-5)}$$

Defining P_y=P_x=0, the above equation corresponds to the normalized deformation shape of a cantilever beam under normalized uniformly distributed load.

$$\frac{d^2\theta}{d\bar{s}^2} = -\bar{w}(L-\bar{s})\cos\theta - \frac{\bar{w}}{2}(L-\bar{s})^2 \sin\theta \frac{d\theta}{d\bar{s}} \qquad \text{(Eq. IV-6)}$$

The solution of the above differential equation was achieved using the Matlab software. The normalized deformation shapes of a cantilever beam under normalized uniformly distributed loads are given in the Figure IV-2.

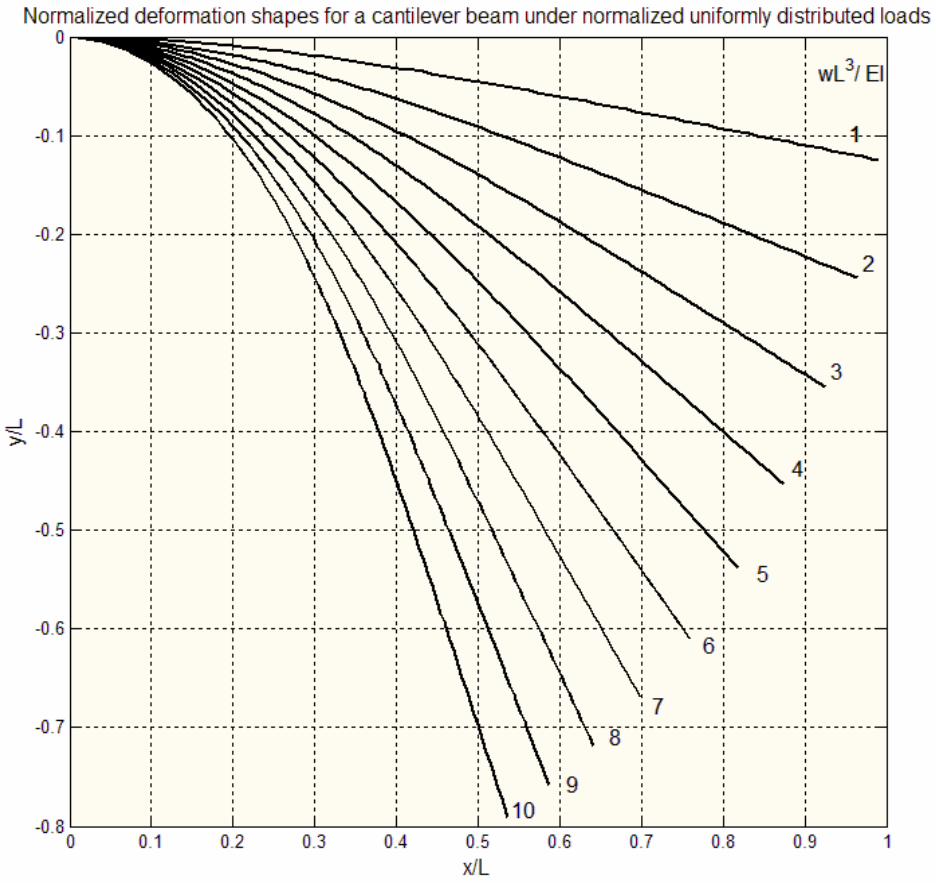

Figure IV-2: Normalized deformation shapes of a cantilever beam under normalized uniformly distributed loads.

Moreover the FEM was implemented for the definition of the elastica corresponding to the cantilever beam under uniformly distributed load. Beam FE were used for the modelling of the cantilever and the Newton-Raphson iteration method was applied for the nonlinear analysis taking into account the large deformation effects. The normalized vertical deflection of the cantilever beam under normalized uniformly distributed load and under normalized concentrated load is given in the Figure IV-3 and Figure IV-4 respectively.

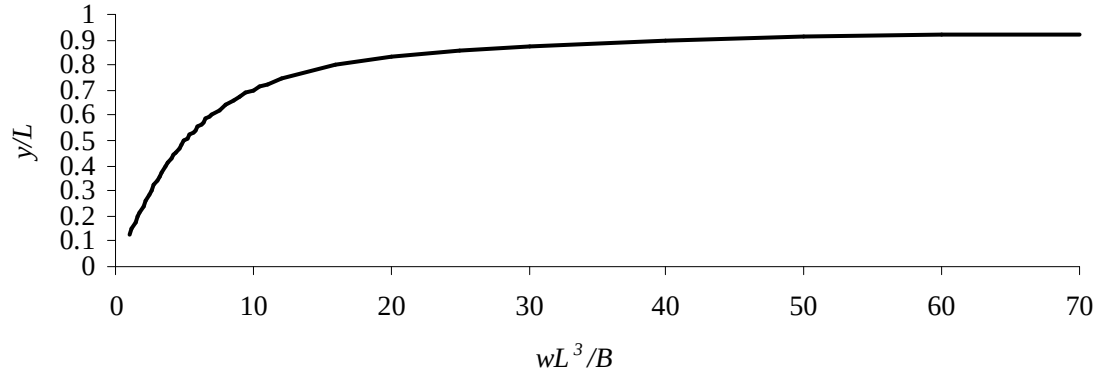

Figure IV-3: The normalized vertical deflection of a cantilever beam under normalized uniformly distributed loads calculated by the FEM.

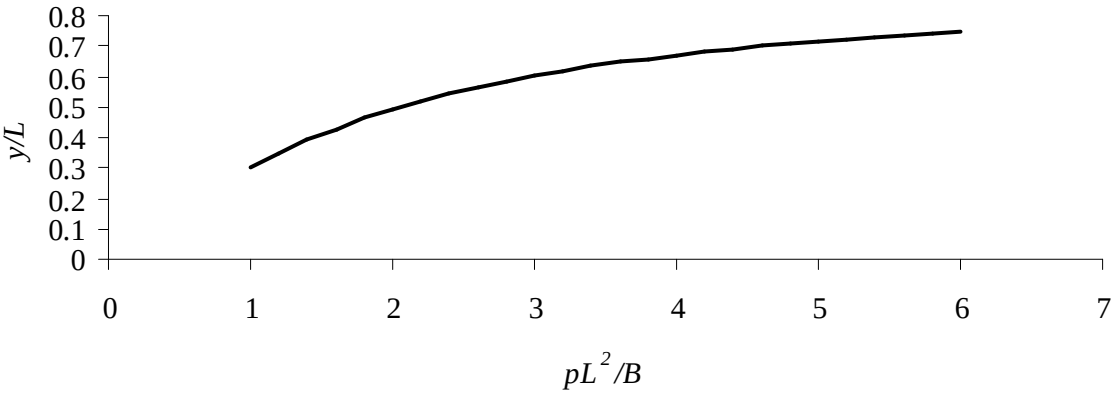

Figure IV-4: The normalized vertical deflection of a cantilever beam under normalized concentrated loads calculated by the FEM.

Appendix V: Tensile test of spacer yarn 1 and 2 (experimental data)

Spacer yarn 1: 0.25 mm PES

INSTITUT FÜR TEXTILTECHNIK
DER RWTH AACHEN

TEXTECHNO STATIMAT M TEST

DATUM / PRUEF-NR.	22-08-2005 / 1261	PRUEFER	J.Donhauser
VERSUCHSBEZ.	PES Monofil	PARTIE NR.	
BEMERKUNGEN	SFB 532		

CODE : techgarn

EINSPANNLAENGE	250 (mm)	PRUEFGESCHW.	250 (mm/min)
KRAFTAUFNEHMER	100 (N)	VORSPANNKRAFT	0.50 (cN/tex)

GRENZWERTE:

DEHNUNG:	MIN. E	0.0 %	MAX. E	100.0 %
KRAFT:	MIN. F	0.0 N	MAX. F	50.0 N

SPULE PES Monofil 0,25

VERSUCH		HOECHSTZUG-K.R.DEHNUNG %	HOECHSTZUG-KRAFT N	FEINH. H.Z.KRAFT cN/tex	HOECHSTZUG-KRAFTARBEIT cm*N
1	MAXIMUM	33.04	31.20	48.52	151.58
	E,0.02FMAX	33.33			
2	MAXIMUM	33.27	31.20	48.52	157.81
	E,0.02FMAX	33.40			
3	MAXIMUM	31.77	30.71	47.76	144.81
	E,0.02FMAX	31.95			
4	MAXIMUM	33.89	31.15	48.45	154.79
	E,0.02FMAX	34.05			
5	MAXIMUM	31.41	30.71	47.76	139.34
	E,0.02FMAX	31.66			
6	MAXIMUM	34.18	31.69	49.28	163.41
	E,0.02FMAX	34.47			
7	MAXIMUM	34.80	31.54	49.06	166.37
	E,0.02FMAX	35.04			
8	MAXIMUM	31.67	30.40	47.27	140.49
	E,0.02FMAX	31.83			
9	MAXIMUM	33.07	30.71	47.76	146.15
	E,0.02FMAX	33.27			
10	MAXIMUM	32.15	30.59	47.57	140.48
	E,0.02FMAX	32.41			

KRAFT: 100mm ≙ 50N DEHNUNG: 100mm ≙ 100.0%

STATISTIK	-N-	-X-	-S-	-CV-	q(95%)	MIN	MAX
H.Z.DEHNUNG	10	32.92%	1.15	3.50	0.83	31.41	34.80
E,0.02FMAX	10	33.14%	1.16	3.51	0.83	31.66	35.04
H.ZUGKRAFT	10	30.99N	0.43	1.38	0.31	30.40	31.69
ARBEIT	10	150.52N*cm	9.82	6.52	7.02	139.34	166.37
FEINH. H.Z.KRAFT	10	48.20cN/tex	0.67	1.38	0.48	47.27	49.28
FEINHEIT	1	643.00dtex					
REISSZEIT	10	19.79s					

Figure V-1: Data of the tensile test of spacer yarn 1 (0.25 mm).

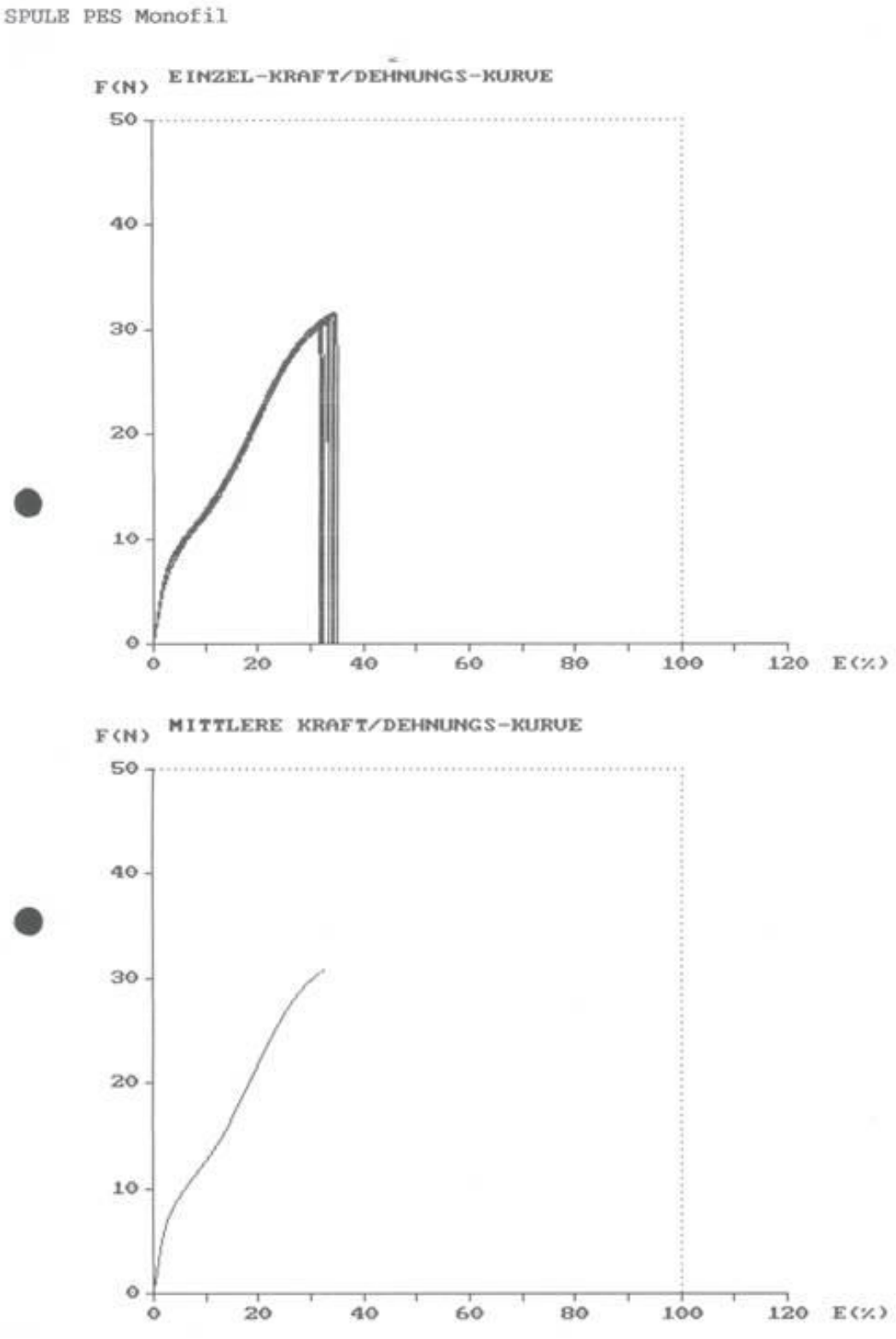

Figure V-2: Load – elongation curve from the tensile test of spacer yarn 1 (0.25 mm).

Spacer yarn 2: 0.30 mm PES

INSTITUT FÜR TEXTILTECHNIK
DER RWTH AACHEN

TEXTECHNO STATIMAT M TEST

DATUM / PRUEF-NR.	02-08-2005 / 1219	PRUEFER	J.Donhauser
VERSUCHSBEZ.	Monofil 0.30	PARTIE NR.	
BEMERKUNGEN	PES		

CODE : techgarn

EINSPANNLAENGE	250 (mm)	PRUEFGESCHW.	250 (mm/min)
KRAFTAUFNEHMER	100 (N)	VORSPANNKRAFT	0.50 (cN/tex)

GRENZWERTE:

DEHNUNG:	MIN. E	0.0 %	MAX. E	80.0 %
KRAFT:	MIN. F	0.0 N	MAX. F	80.0 N

SPULE Monofil 0.30 (PES)

KRAFT: 100mm ≙ 80N DEHNUNG: 100mm ≙ 80.0%

STATISTIK	-N-	-X-	-S-	-CV-	q(95%)	MIN	MAX
H.Z.DEHNUNG	10	50.46%	1.98	3.92	1.42	47.70	53.94
E.0.1FMAX	10	50.57%	2.00	3.96	1.43	47.73	54.02
H.ZUGKRAFT	10	46.90N	0.72	1.52	0.51	45.51	47.75
ARBEIT	10	382.38N*cm	21.40	5.60	15.31	351.42	414.48
FEINH. H.Z.KRAFT	10	41.10cN/tex	0.63	1.52	0.45	39.88	41.85
FEINHEIT	1	1141.00dtex					
REISSZEIT	10	30.32s					
E.1.FIL.BRUCH	10	50.26%	2.01	3.99	1.43	47.54	53.76
F.1.FIL.BRUCH	10	46.82N	0.71	1.52	0.51	45.40	47.64

Figure V-3: Data of the tensile test of spacer yarn 2 (0.30 mm).

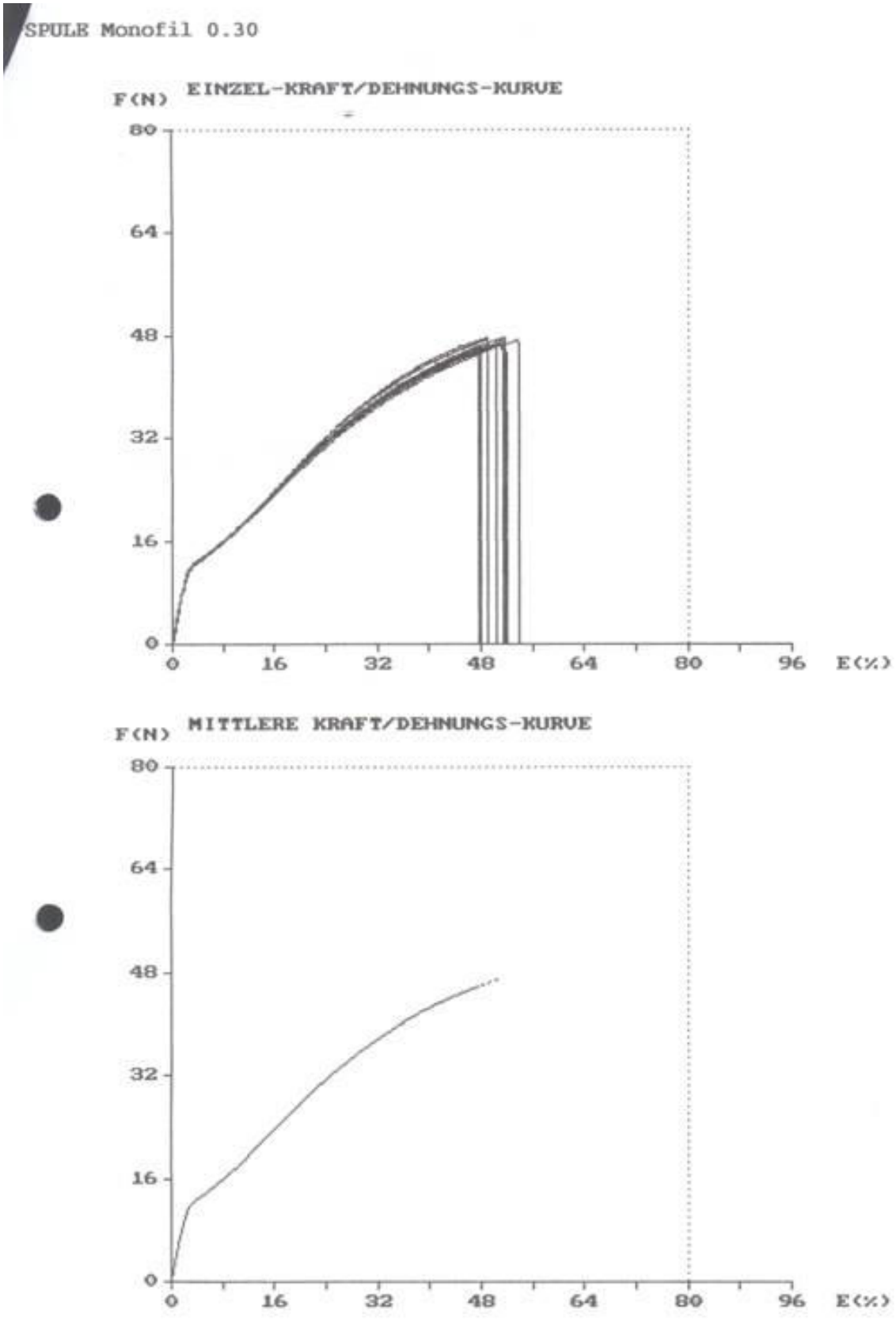

Figure V-4: Load – elongation curve from the tensile test of spacer yarn 2 (0.30 mm).

Appendix VI: Splines

Spline

A spline S is a piecewise polynomial function interpolating a set of knots or control points.

$$S(x)=\begin{cases} P_0(x) \text{ for } x\in\left[x_0,x_1\right] \\ P_1(x) \text{ for } x\in\left[x_1,x_2\right] \\ \quad\ldots \\ P_n(x) \text{ for } x\in\left[x_n,x_{n+1}\right] \end{cases}$$ where $\left[x_i, y_i\right]$ is the set of n+1 control points.

The vector $x=(x_0,x_1,...,x_n)$ is called the knot vector of the spline. The equidistant distribution of the knots in the interval $\left[x_0,x_n\right]$ corresponds to a uniform spline. Otherwise the spline is non-uniform.

Cubic Spline

The cubic Spline interpolation is a piecewise continuous curve passing through each of the control points. Each segment (between two control points) is described by a third-order polynomial. Let us define the n+1 control points $\left[x_i, y_i\right]$ for i=0,1,…,n. The cubic spline has the form:

$$S_i(x)=a_i(x-x_i)^3+b_i(x-x_i)^2+c_i(x-x_i)+d_i \text{ for } x\in\left[x_i,x_{i+1}\right]$$

Thus 4n parameters (4 coefficients × n segments) are required for the definition of the total Spline $S(x)$. The 4n-2 conditions are:

$$S_i(x_i)=y_i$$

$$S_i(x_{i+1})=y_{i+1}$$

$$S'_{i-1}(x_i)=S'_i(x_i)$$

$$S''_{i-1}(x_i)=S''_i(x_i)$$

Enforcing zero second derivatives at the endpoints, 2 more boundary conditions are defined and the natural cubic spline derives:

$$S''_0(x_0)=S''_n(x_{n+1})=0$$

Bernstein polynomial

The n + 1 Bernstein basis polynomials of degree n are defined as:

$$b_{v,n}(x) = \binom{n}{v} x^v (1-x)^{n-v},\ v = 0,...,n$$

Bernstein polynomial or polynomial in Bernstein form of degree *n* is a linear combination of Bernstein basis polynomials:

$$B(x) = \sum_{v=0}^{n} \beta_v b_{v,n}(x)$$

The coefficients β_v are called Bernstein coefficients or Bézier coefficients. The first few Bernstein basis polynomials are:

$$b_{0,0}(x) = 1$$
$$b_{0,1}(x) = 1-x\ , \qquad b_{1,1}(x) = x$$
$$b_{0,2}(x) = (1-x)^2,\ b_{1,2}(x) = 2x(1-x),\ \ b_{2,2}(x) = x^2$$
$$b_{0,3}(x) = (1-x)^3,\ b_{1,3}(x) = 3x(1-x)^2,\ b_{2,3}(x) = 3x^2(1-x),\ \ b_{3,3}(x) = x^3$$

Bézier Curve

Let us define a set of *n*+1 control points $\mathbf{P}_0$, $\mathbf{P}_1$, …, $\mathbf{P}_n$. The corresponding Bézier curve (or Bernstein-Bézier curve) is given by $C(t) = \sum_{i=0}^{n} \mathrm{P}_i\, B_{i,n}(t)$, where $B_{i,n}(t)$ is a Bernstein polynomial and $t \in [0,1]$. A Bézier curve of *n* degree results from *n* control points.

A rational Bézier curve is defined by $C(t) = \dfrac{\sum_{i=0}^{n} B_{i,p}(t)\ w_i\, \mathrm{P}_i}{\sum_{i=0}^{n} B_{i,p}(t)\ w_i}$, where *p* is the order, $B_{i,p}(t)$ are the Bernstein polynomials, and the weight w_i of $\mathbf{P}_i$ is the last ordinate of the homogeneous point P_i^w.

B-spline

A B-spline is simply a generalisation of a Bézier curve. Given *m* control points (real valued t_i) with $t_0 \le t_1 \le ... \le t_{m-1}$ a B-spline of degree *n* is defined:

$$S(t) = \sum_{i=0}^{m-n-2} \mathrm{P}_i\, b_{i,n}(t),\ \ t \in [t_n, t_{m-n-1}]$$

The *m-n-1* basis B-splines of degree *n* can be defined using the Cox-de Boor recursion formula:

$$b_{j,0(t)} = \begin{cases} 1 \text{ if } t_j \le t \le t_{j+1} \\ 0 \quad \text{otherwise} \end{cases}$$

$$b_{j,n(t)} = \frac{t - t_j}{t_{j+n} - t_j} b_{j,n-1}(t) + \frac{t_{j+n+1} - t}{t_{j+n+1} - t_{j+1}} b_{j+1,n-1}(t)$$

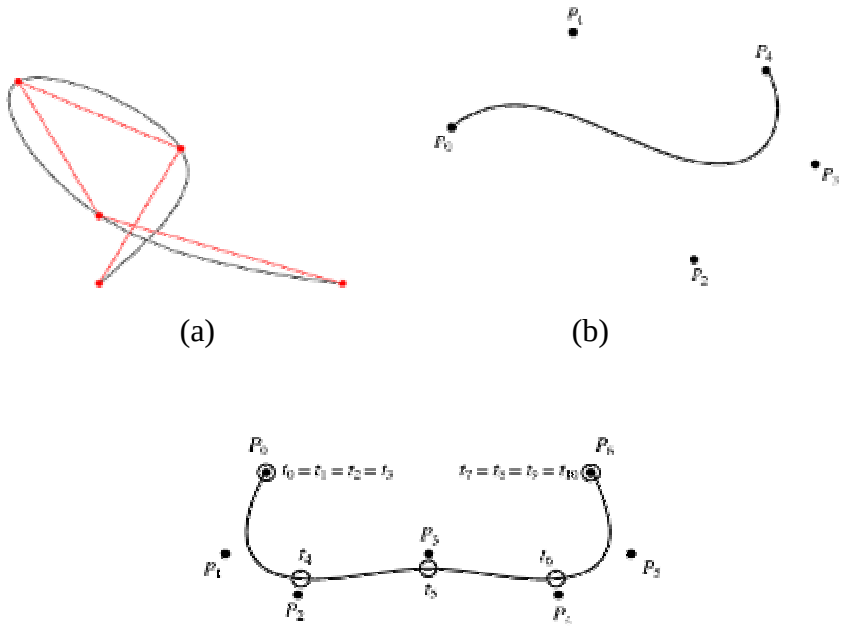

(a) (b)

(c)

Figure VI-1: (a) Cubic spline (b) cubic Bézier Curve (c) B-spline.

Appendix VII: Kawabata evaluation system for fabrics

Dr. Sueo Kawabata organised in 1972 the committee "Hand Evaluation and Standardization Committee" (HESC) working in the following research activities (Kawabata 1980):

- Selection of the important hand expressions from a series of expressions.
- Definition of the feelings with respect to each of these important expressions.
- Establishment of the standards samples which indicate the feeling with respect to each of the expressions and its intensity by numerical value.
- Analysis of the experts' hand feeling and establishment of the translation formulas which can translate the mechanical properties of fabrics into experts' hand.

On the other hand, Dr. Kawabata, based on his fundamental work on the mechanical properties of fabric, designed in 1972 the Kawabata Evaluation System for Fabrics (KES-F). The KES-F consists of four instruments, which were developed by Kato Tekko Co., Kyoto, Japan, in collaboration with Kawabata. The first KES-F instruments were produced in 1973. Some minor modifications were made to produce the four improved KES-FB instruments (Bishop 2003):

KES-FB1 tensile and shear tester

KES-FB2 bending tester

KES-FB3 compression tester

KES-FB4 surface-friction and geometrical-roughness tester

Later (1991) an automated version of KES-FB was produced presenting improved tensile and shear tester (KES-F1) and compression tester (KGS-G5). The instruments of the KES-FB, the measurement principles and the received characteristic values are presented in followings.

KES-FB1 for tensile and shear test (Anonymous)

The specimen is clamped between two chucks of 20 cm length. The distance of the chucks is 5 cm. Thus a rectangular shape of 20×5 cm corresponds to the effective area of the specimen. The front chuck (A) is fixed to a 4 cm drum while the back chuck (B) is fixed on a sliding base.

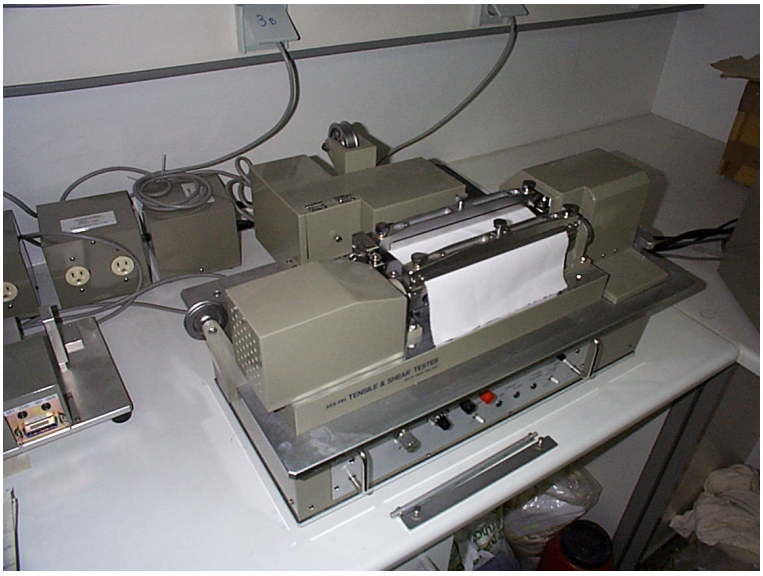

Figure VII-1: The instrument KES-FB1.

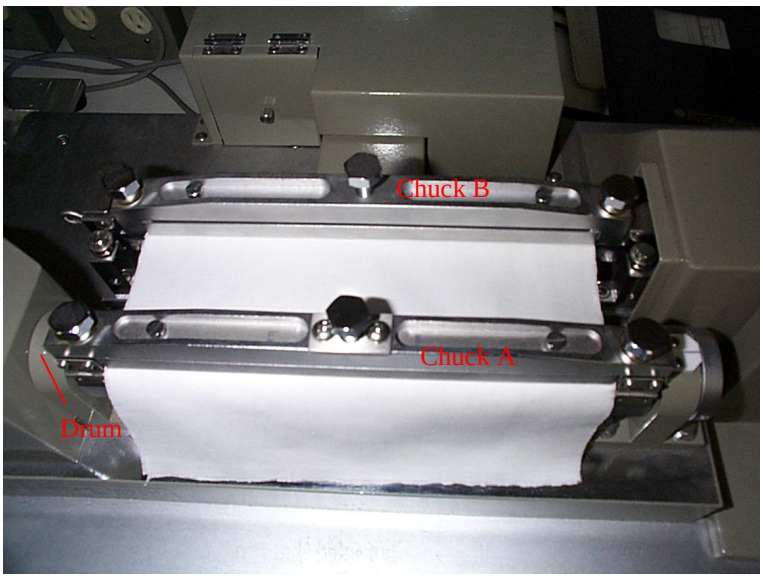

Figure VII-2: The placement of the specimen in the KES-FB1.

For the tensile test the clutch of the drum is activated keeping the chuck A constant and the chuck B is moving to backward direction imposing the tensile deformation. The tensile stress is detected by the torque meter using a strain gauge installed on the axis of the drum. The tensile strain is detected by a potentiometer recording the movement of the chuck B. The strain is proportional to the output voltage. Two tensile rates are available, 0.2 mm/sec and 0.1 mm/sec, changing the gear. When the output voltage of the tensile force receives the preset value the motor turns automatically to the inverse direction for the recording of the recovery curve. The deformation applied corresponds to strip biaxial deformation. The load - deformation curve recorded by the apparatus is shown in the Figure VII-3.

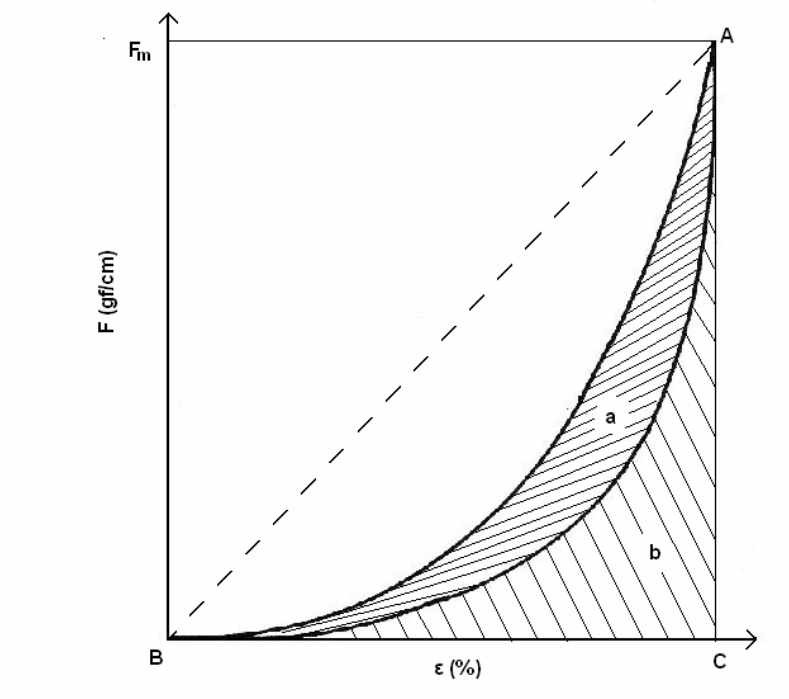

Figure VII-3: Load - deformation curve received from the tensile test.

The characteristic values defined are the following:

$LT=\frac{WT}{WOT}$, Linearity of load – extension curve

$WT=\int_0^{\varepsilon_m} F d\varepsilon$, Tensile energy

$RT=(WT'/WT)\cdot 100$, Tensile resilience

where:

$WOT=F_m\,\varepsilon_m/2$

F_m and ε_m maximum values of F and ε respectively

$WT'=\int_0^{\varepsilon_m} F' d\varepsilon$, recovering energy per unit area

F', tensile force in recovering process.

For the shear test a constant tension is applied on the specimen mounting a weight on the drum, which now rotates freely (the clutch is removed). The shear force is detected by a transducer connected with the chuck B along the shear direction. The chuck B moves parallel to its axis at a constant rate imposing the shear deformation. The shear strain is detected by a potentiometer. A maximum shear angle of 8 degrees is defined for the starting of the inverse

motion (recovery procedure). The load - deformation curve results from the test is shown in the Figure VII-4.

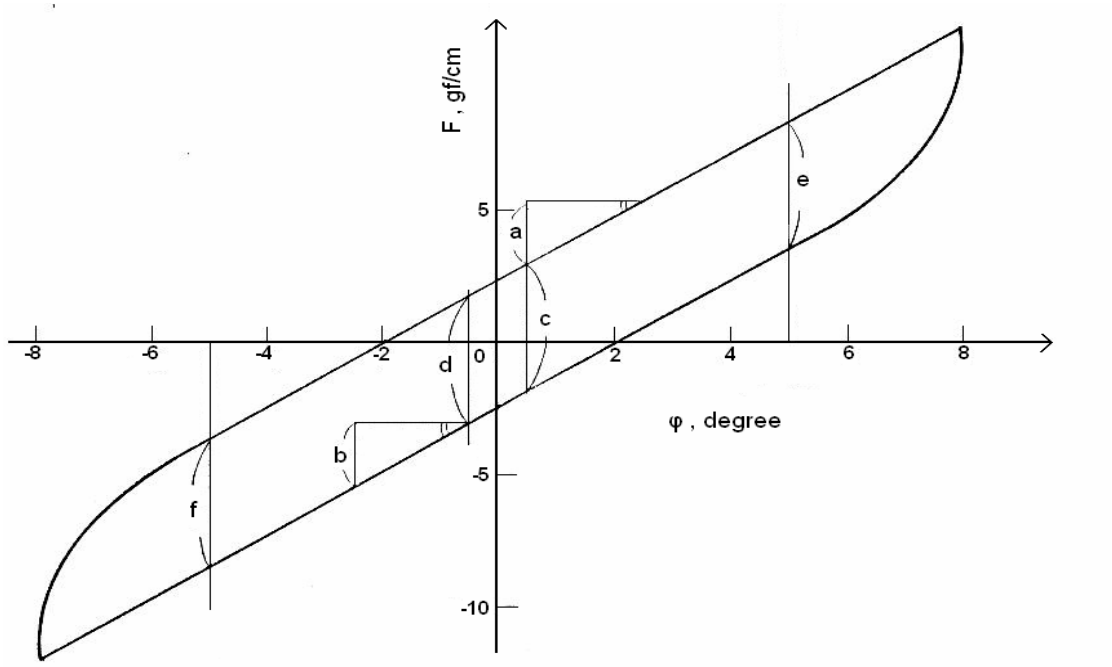

Figure VII-4: Load - angle curve received from the shear test.

The characteristic values defined are the following:

$G = \frac{a+b}{2 \cdot 2}$, Shear stiffness

$2HG = \frac{c+d}{2}$, Hysteresis at the shear angle φ=0.5 degree

$2HG5 = \frac{e+b}{2}$, Hysteresis at the shear angle φ=5 degree

KES-FB2 for pure bending (Anonymous)

Unlike the cantilever method, the current instrument has a special feature. The specimen is bent accurately in an arc of curvature which changes continuously. An effective area of 20 cm length and 1 cm width of the specimen is used for the test. One edge of the specimen is held by a fixed chuck, while the other is held by the moving chuck as shown in the Figure VII-5. The bending test is performed vertically to prevent the effect of the gravity. The moving chuck follows a fixed orbit turning the head at an angle, in order the specimen to present a uniform curvature. The pure bending is performed between the curvatures K=-2.5 and 2.5 cm^{-}

[1] with constant rate of curvature rate 0.5 cm^{-1}/sec. A torque meter and a potentiometer are used to record the torque and the angle θ respectively.

Figure VII-5: The instrument KES-FB2.

The drawing of the specimen deformation (top view) and the principle of the bending deformation are presented in the Figure VII-6. The coordinates of the orbit and the φ angle, considering the curvature K, result as follow.

$$X = (1 - \cos K) / K \qquad \text{(Eq. VII-1)}$$

$$Y = \sin K / K \qquad \text{(Eq. VII-2)}$$

$$K\ (cm^{-1}) = \varphi \qquad \text{(Eq. VII-3)}$$

when C=1 cm.

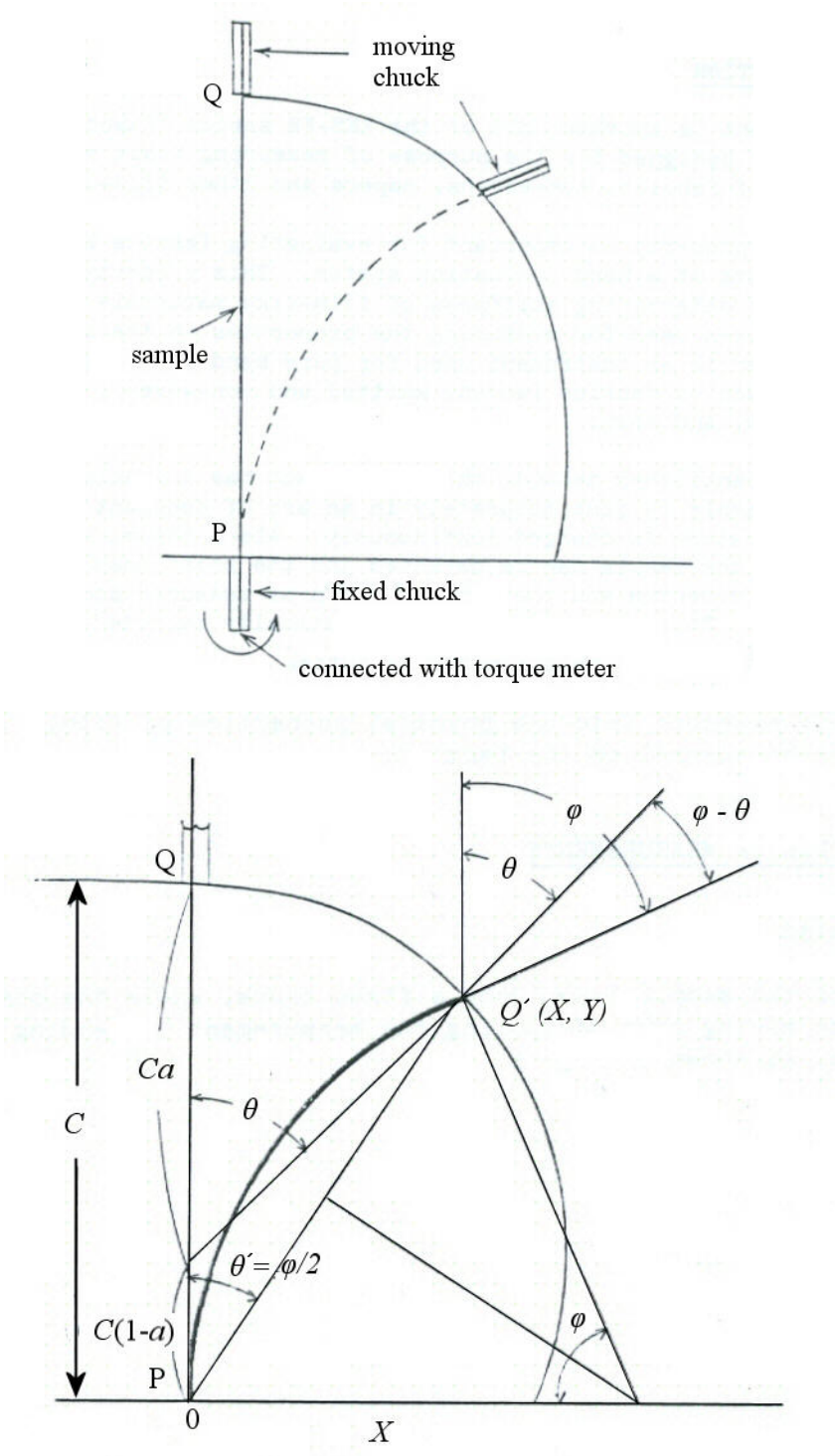

Figure VII-6: Principle of the pure bending deformation.

The load - deformation curve results from the test is shown in the Figure VII-7. The characteristic values defined are the following:

$B = B_f + B_b$, Bending rigidity per unit length

$2HB = 2HB_f + 2HB_b$, Hysteresis of the bending moment per unit length

where:

B_f = *a*, slope of the curve for K=0.5… 1.5 cm^{-1}

B_b = *b*, slope of the curve for K=-0.5… -1.5 cm^{-1}

$2HB_f$ = *c*, hysteresis of bending moment for K=0.5… 1.5 cm^{-1}

$2HB_b$ = *d*, hysteresis of bending moment for K=-0.5… -1.5 cm^{-1}

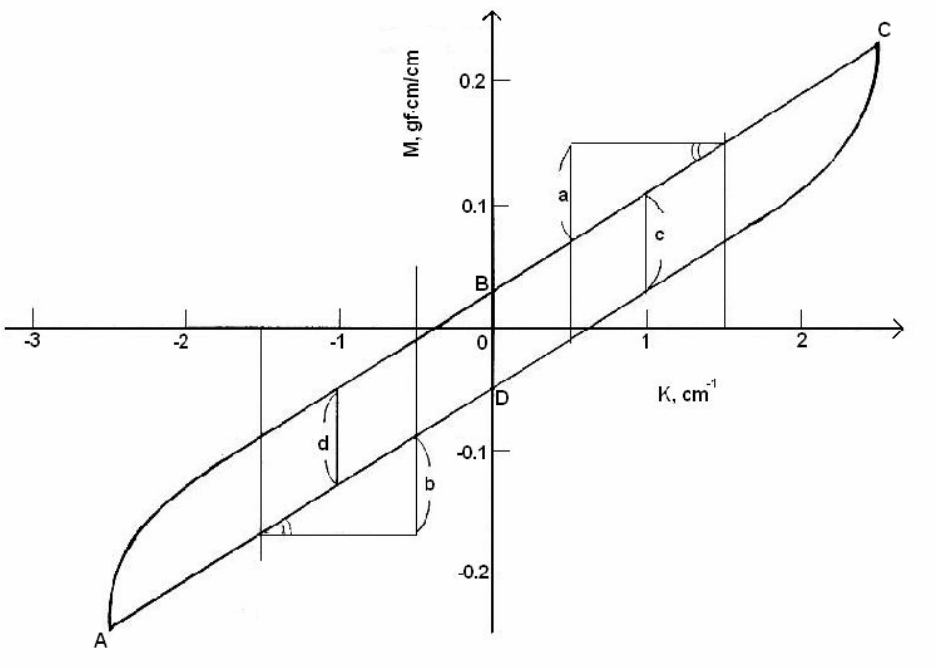

Figure VII-7: Moment – curvature curve resulted from the pure bending test.

KES-FB3 for compression test (Anonymous)

This instrument is designed to measure the compression properties of fabrics, rubber, film and leather with high accuracy and sensitivity. The specimen is placed on the plate and the compression plunger, driven by the motor, compresses the specimen with the rate 20 microns/sec. The displacement of the plunger is detected by a potentiometer. The compression force is detected by a transducer. A preset value (50 gf/cm^2) is defined for the output voltage of the compress ional load, to reverse the driving motor direction. The area of the compression plate of the plunger is 2 cm^2.

Figure VII-8: The instrument KES-FB3.

The compression load – thickness of the specimen curve is illustrated in the Figure VII-9. The characteristic values are:

$LC=\frac{WC}{WOC}$, Linearity of load – specimen thickness curve

$WC=\int_{T_m}^{T_0} P\,dT$, Compression energy

$RC=WC'/WC$, Compression resilience

where:

T_0, thickness of the specimen at pressure 0.5 gf/cm^2

T_m, thickness of the specimen at pressure 50 gf/cm^2

$WOC = P_m\,(T_0 - T_m)/2$

$WC' = \int_{T_m}^{T_0} P'\,dT$, recovering energy per unit area

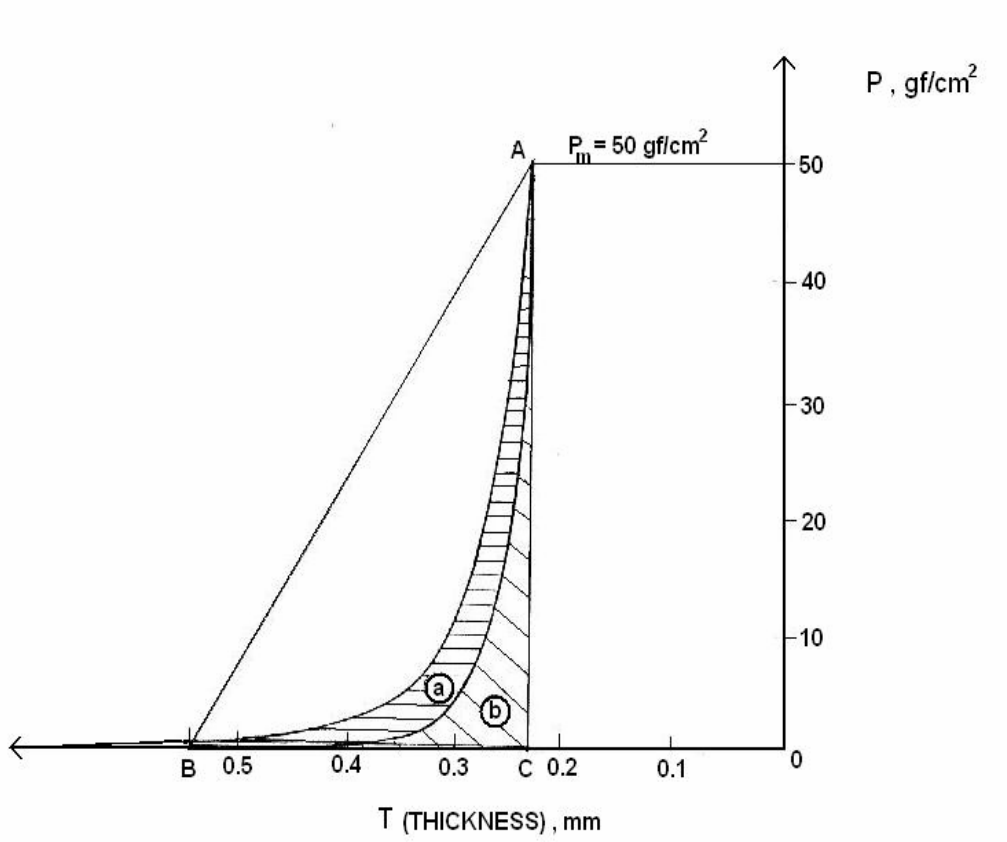

Figure VII-9: Compression load – specimen thickness curve resulted from the compression test.

KES-FB4 for surface friction and roughness measurement (Anonymous)

The specimen is clamped at both ends and an even constant tension (20 gf/cm) is applied in one end using a weight. One end of the specimen is fixed on the winding drum (chuck A) and the other end is held by the chuck B (with weight). The winding drum rotates at a speed 1 mm/sec by the motor, moving the specimen. When the displacement of the specimen reaches the maximum value of 3 cm, the motor reverses and the return motion is executed at equal speed. The moving distance of the specimen is detected by a potentiometer as the displacement output voltage. The friction conductor directly connected to the frictional force transducer is placed on the sample surface under the compression force of 50 gf. The frictional force transducer is a steel ring deflection type with a linear differential transformer. The conductor box for the roughness measurement is lowered (by loosing the handle) and it is fixed in a position that the conductor touches the fabric surface with a constant normal force 10 g. A transducer detects the vertical movements of the conductor caused by the roughness of the sample surface. The friction and roughness curves are recorded by the forward and backward process in three integrators. The curves resulting from the current instruments are illustrated in the Figure VII-11.

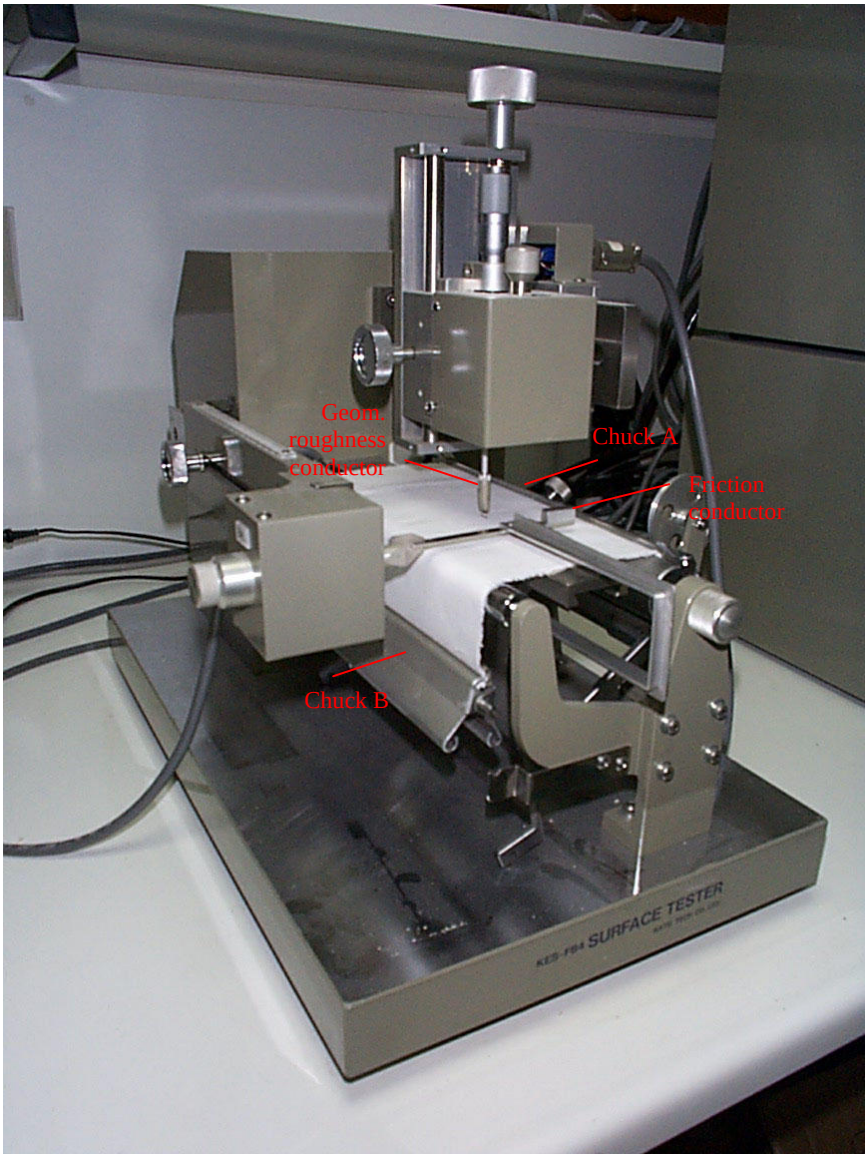

Figure VII-10: The instrument KES-FB4.

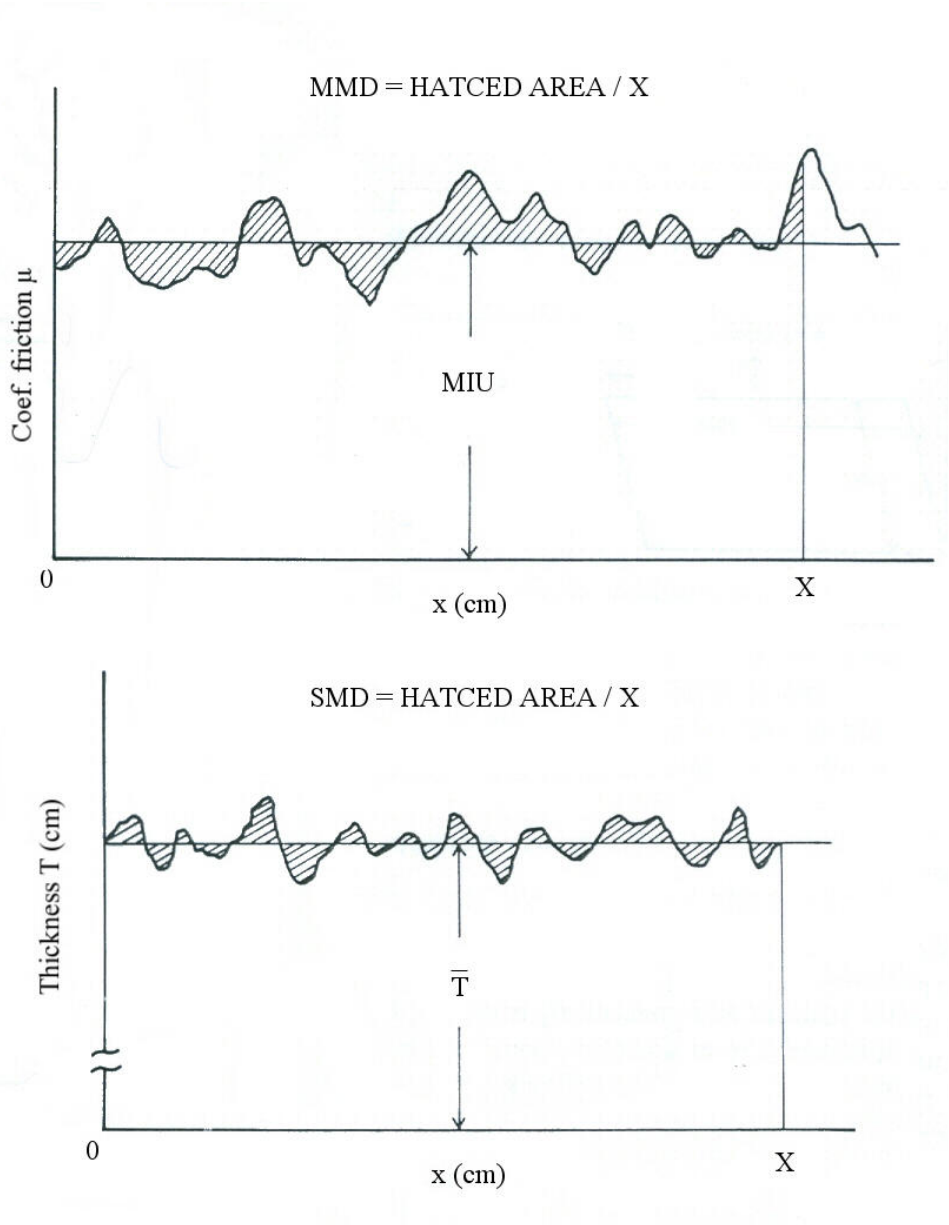

Figure VII-11: Resultant curve of surface friction (up) and surface roughness (down).

The characteristic values are:

$MIU = \frac{1}{X}\int_0^X \mu \, dx$, mean value of the coefficient of friction

$MMD = \frac{1}{X}\int_0^X \left|\mu - \bar{\mu}\right| dx$, mean deviation of coefficient of friction

$SMD = \frac{1}{X}\int_0^X \left|T - \bar{T}\right| dx$, mean deviation of surface roughness

where:

μ, frictional force / compression force

x, displacement of the conductor on the surface of specimen

X, 2 cm maximum scan length of the conductor

T, thickness of the specimen at position x

$\overline{T}$, mean value of T

The characteristics values measured in the KES-FB and their units are summarized in the Table VII-1.

Table VII-1: Parameters measured by the KES-F Instruments

Instrument	Test	Parameter	Description	Units
KES-FB1	Tensile	*LT*	Linearity	-
		WT	Tensile energy per unit area	gf cm/cm²
		RT	Tensile Resilience	%
	Shear	*G*	Shear stiffness	gf/cm degree
		2HG	Hysteresis at shear angle φ=0.5 degree	gf/cm
		2HG5	Hysteresis at shear angle φ=5 degree	gf/cm
KES-FB2	Bending	*B*	Bending rigidity per unit length	gf cm²/cm
		2HB	Hysteresis of bending moment per unit length	gf cm/cm
KES-FB3	Compression	*LC*	Linearity	-
		WC	Compression Energy	gf cm/cm²
		RC	Compression resilience	%
		T	Thickness of the specimen at 0.5 gf/cm²	mm
KES-FB4	Friction and roughness	*MIU*	Coefficient of steel/fabric friction	-
		MMD	Mean deviation of MIU	-
		SMD	Geometrical roughness	micron

Appendix VIII: Experimental data of samples drape

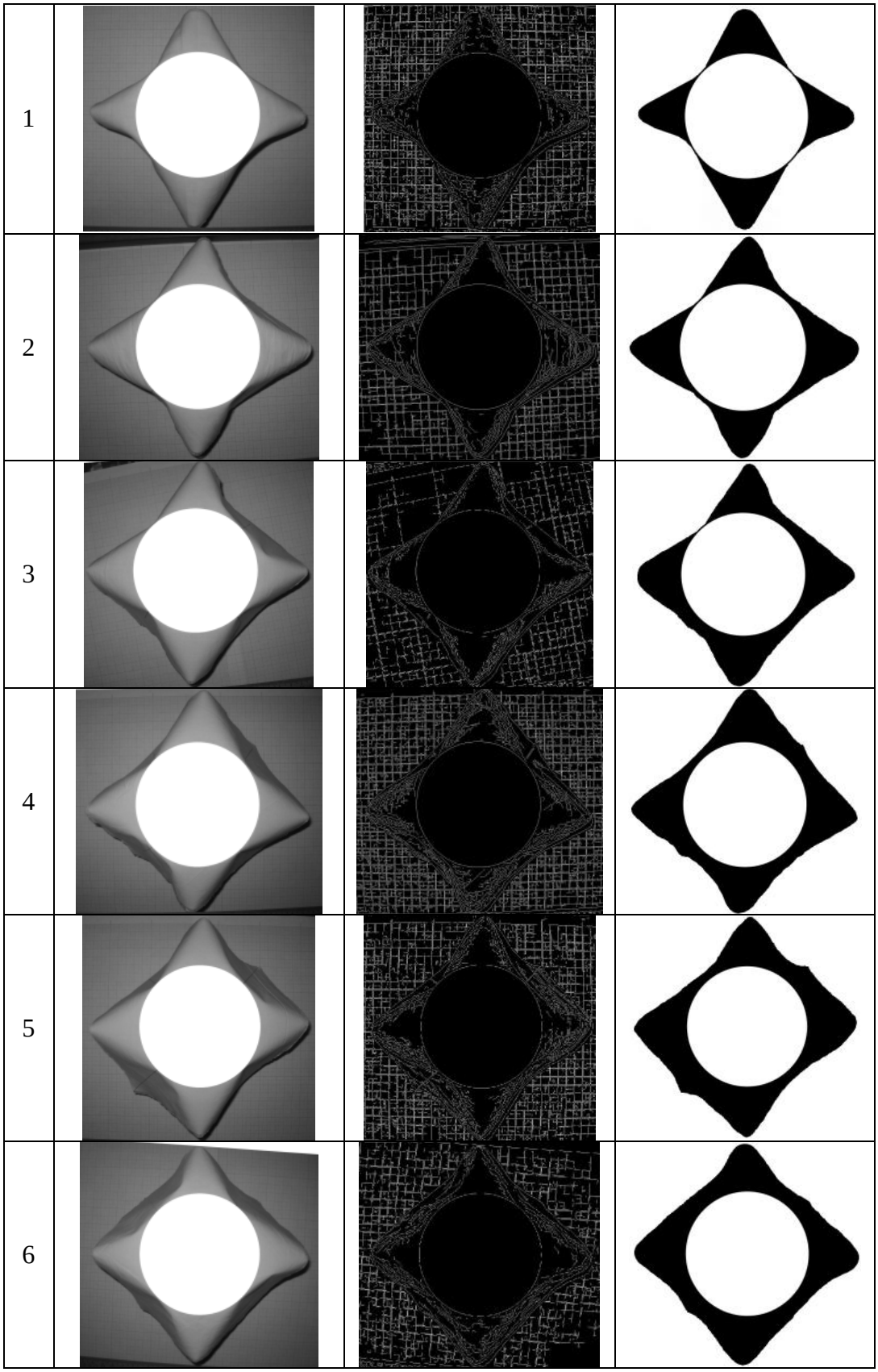

Figure VIII-1: Image process for the calculation of the drape coefficient (samples 1-6).

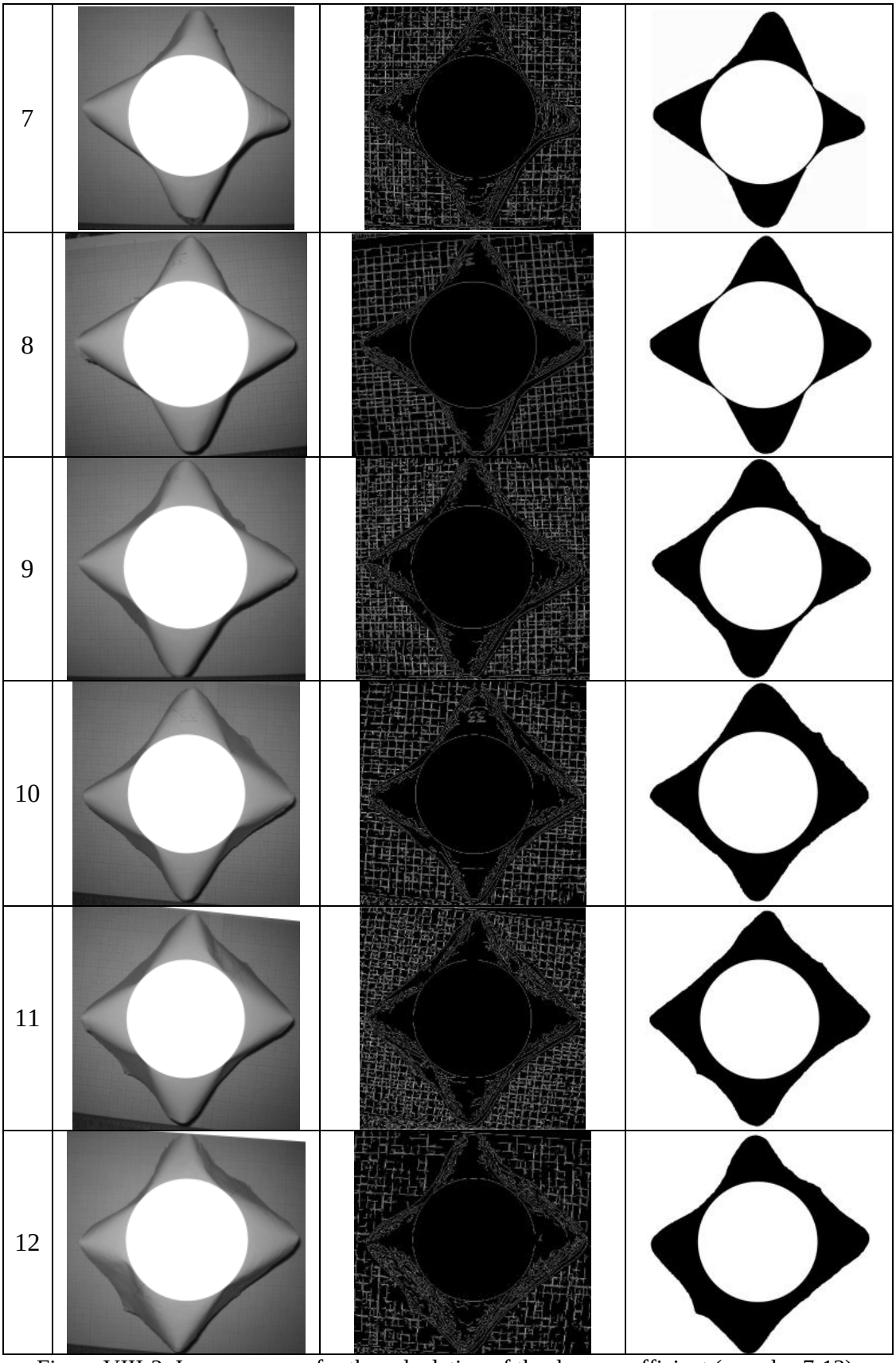

Figure VIII-2: Image process for the calculation of the drape coefficient (samples 7-12).

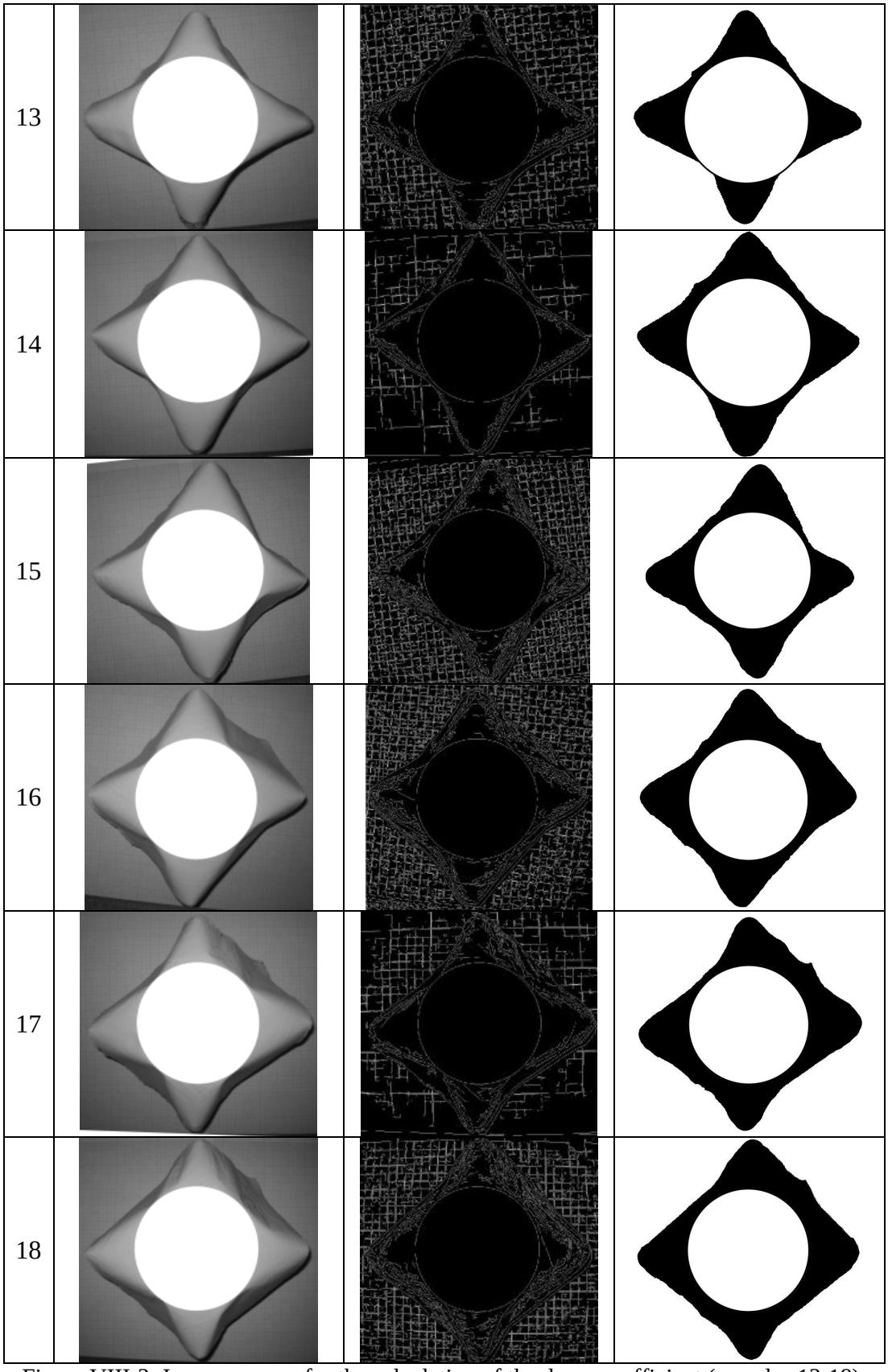

Figure VIII-3: Image process for the calculation of the drape coefficient (samples 13-18).

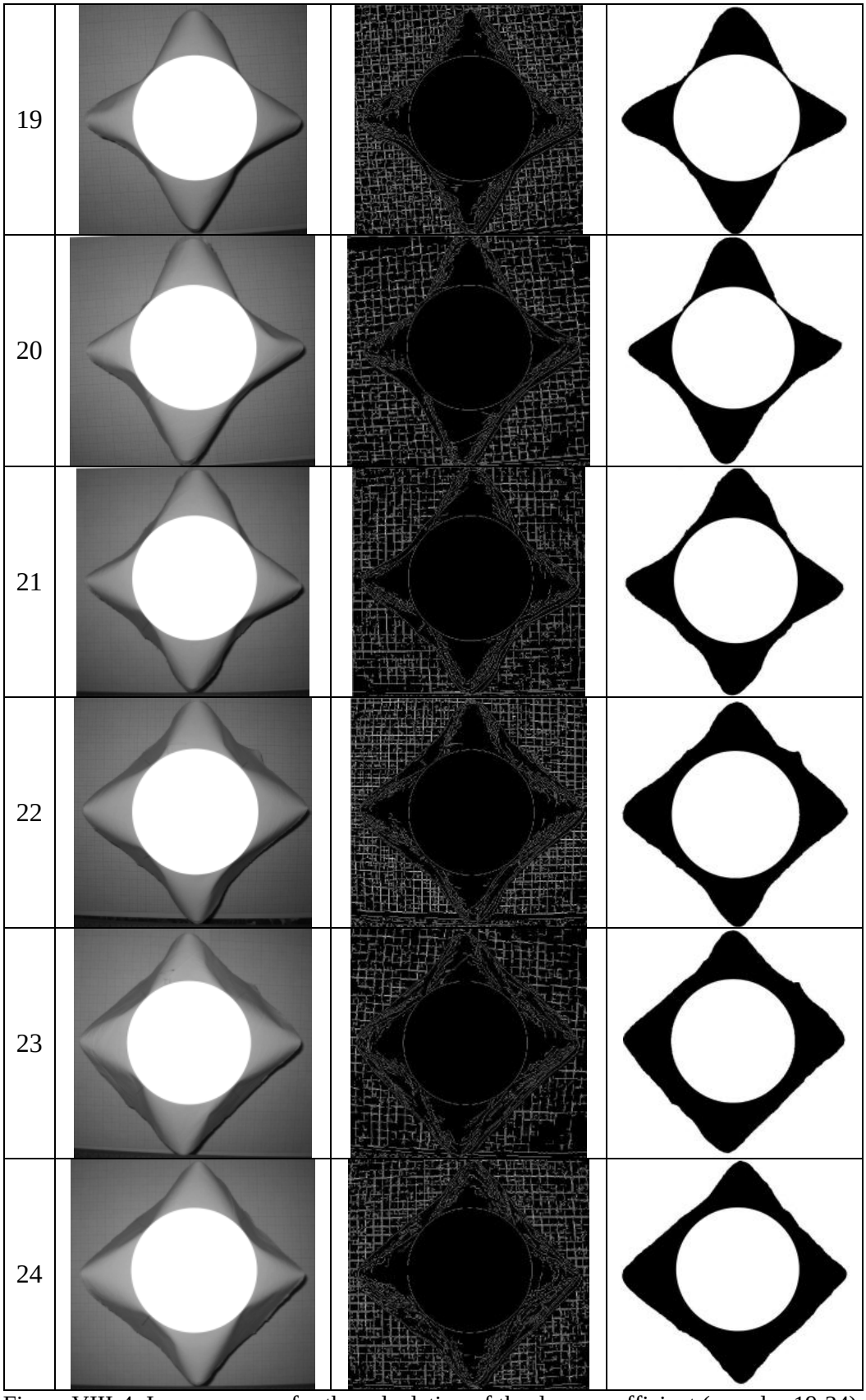

Figure VIII-4: Image process for the calculation of the drape coefficient (samples 19-24).

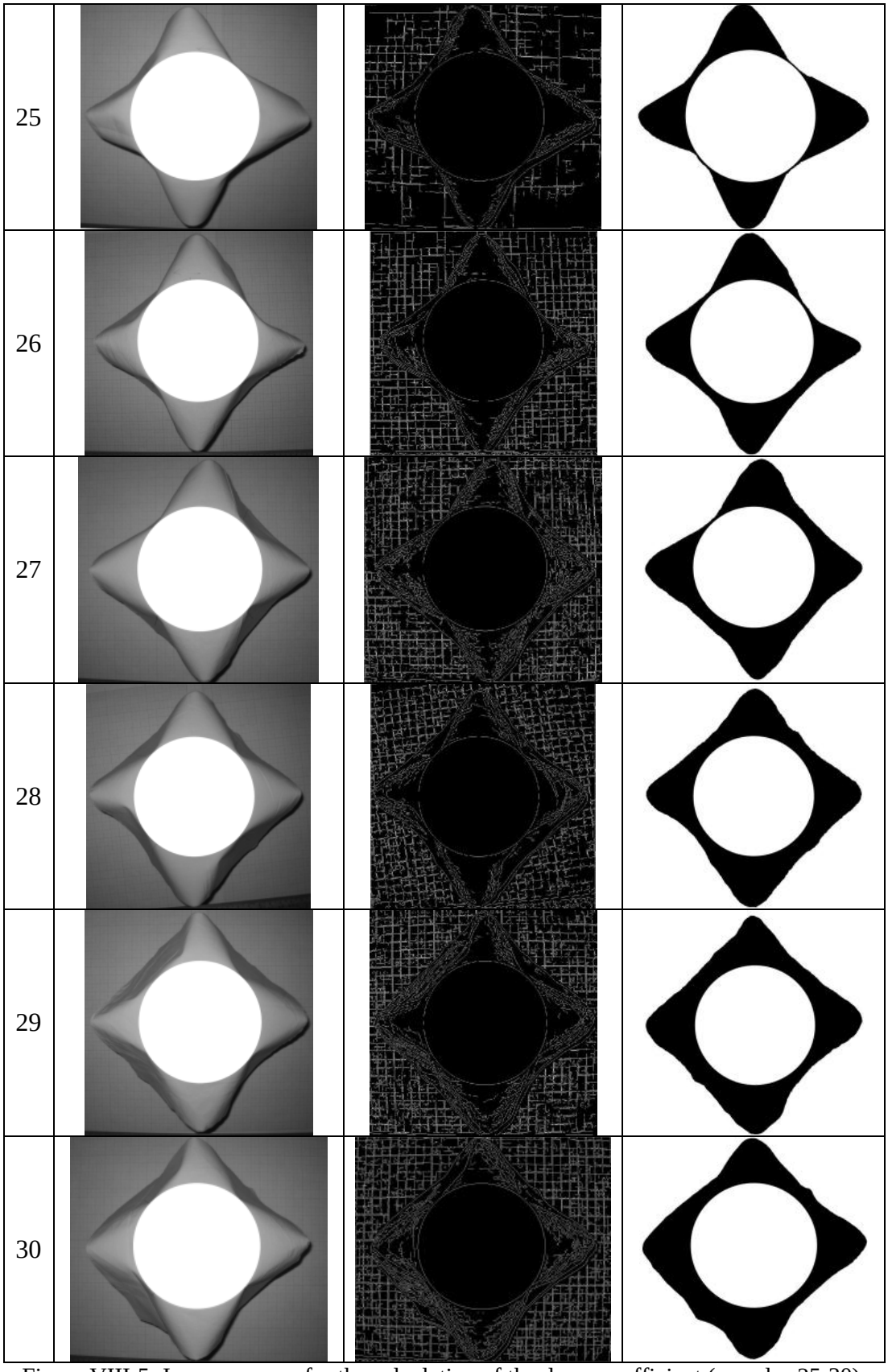

Figure VIII-5: Image process for the calculation of the drape coefficient (samples 25-30).

Publications

International Journals

Vassiliadis, S., Kallivretaki, A. & Provatidis, C. 2010, "Mechanical modelling of multifilament twisted yarns", *Fibers and Polymers*, vol. 11, no. 1, pp. 89-96.

Vassiliadis S., Kallivretaki A., Psilla N., Provatidis Ch., Mecit D., Roye A. 2009, "Numerical Modelling of the Compressional Behaviour of Warp-knitted Spacer Fabrics", *FIBRES & TEXTILES in Eastern Europe*, vol. 17, no. 5 (76) pp. 56-61.

Kallivretaki, A., Vassiliadis, S., Blaga, M. & Provatidis, C. 2007a, "Finite element modelling of the warp knitted structure", *Research Journal of Textile and Apparel*, vol. 11, no. 4, pp. 40-47.

Vassiliadis, S., Kallivretaki, A. & Provatidis, C. 2007a, "Mechanical Simulation of Plain Weft Knitted Fabrics", *International Journal of Clothing Science and Technology* , vol. 19 no. 2, pp. 109-130.

Vassiliadis, S.G., Kallivretaki, A.E. & Provatidis, C.G. 2007b, "Geometrical modelling of plain weft knitted fabrics", *Indian Journal of Fibre and Textile Research*, vol. 32, no. 1, pp. 62-71.

International Conferences

Provatidis, C., Kallivretaki, A. & Vassiliadis, S. 2009, "Fabric Drape using FEM", *2nd South East European Conference on Computational Mechanics*, Rhodes, Greece.

Kallivretaki, A., Vassiliadis, S. & Provatidis, C. 2009, "Mechanical Modelling of Woven Fabrics using a Homogenization Method", *2nd South East European Conference on Computational Mechanics*, Rhodes, Greece.

Vassiliadis, S., Kallivretaki, A., Frantzeskakis, P. & Provatidis, C. 2009, "Macromechanical Modelling of Woven Fabrics", *AUTEX 2009, World Textile Conference*, Çesme, Izmir, Turkey (***Royal TenCate Award***)

Vassiliadis, S., Kallivretaki, A. & Provatidis, C. 2009, "Problems and limitations on the Numerical Modelling of Textiles", *AUTEX 2009, World Textile Conference*, Çesme, Izmir, Turkey.

Kallivretaki, A., Vassiliadis, S. & Provatidis, C. 2008, "Computational Modeling of Fibrous Assemblies", *International Conference of Applied Research in Textiles*, CIRAT-3, Sousse, Tunisia.

Vassiliadis, S., Kallivretaki, A., Grancaric, A.M., Giannakis, S. & Provatidis C. 2008, "Computational modelling of twill and satin woven structure", *Autex 2008 - World Textile Conference*, Biella, Italy.

Vassiliadis, S., Kallivretaki, A., Kavagia, X., Provatidis, C., Mecit, D. and Roye, A. 2008, "Computational Modelling of Spacer Fabrics", *Autex 2008 - World Textile Conference*, Biella, Italy.

Kallivretaki, A., Blaga, M., Vassiliadis, S. & Provatidis, C. 2007, "On the effects of the boundary conditions in the computational textile mechanical", *International Conference on Intelligent Textiles and Mass Customisation*, Casablanca, Morocco.

Blaga, M., Kallivretaki, A., Vassiliadis, S. & Provatidis, C. 2007, "On the numerical modelling of weft knitted structures", *The XIIIth Romanian Textile and Leather Conference – CORTEP 2007*, Iasi, Romania.

Vassiliadis, S., Kallivretaki, A. & Provatidis, C. 2007c, "Contact Phenomena in the Knitted Fabrics Modelling", *7th World Textile Conference AUTEX*, Tampere, Finland.

Kallivretaki, A., Vassiliadis, S., Blaga, M. & Provatidis, C. 2007b, "Micromechanical Modelling of Warp Knitted Fabrics", *7th World Textile Conference AUTEX*, Tampere, Finland.

Kallivretaki A., Vassiliadis S., Blaga M. & Provatidis Ch. 2007c, "Finite Element Modelling of The Warp Knitted Structures", *Workshop: Modelling and Simulation in the Textile Industry (ISC' 2007)*, Delft, The Netherlands.

Vassiliadis, S., Kallivretaki, A. & Provatidis, C. 2006a, "Geometrical Representation of the Interlock Knitted Structure in Numerical Modelling", *Proceedings of the 33rd Aachen Textile Conference*, Aachen, Germany.

Vassiliadis, S., Kallivretaki, A. & Provatidis, C. 2006b, "Mechanical modelling of rib 1×1 knitted fabric", *37th International Symposium on Novelties in Textiles, Ljubljana, Slovenia*.

Vassiliadis, S., Kallivretaki, A. & Provatidis, C. 2006c, "Computational mechanical modeling as a textile design tool", *1st International Instabul Textile and Textile Machinery Congress*, Instabul, Turkey.

Literature

*The Karl Mayer guide to technical textiles*2000.

*ACI Committee 440, 440R-96: State of the art Report on Fiber Reinforced Plastic Reinforcement for Concrete Structures*1996, American Concrete Institute, Detroit, Michigan.

*ACI Committee 533, 533R-93: Guide for Precast Concrete Wall Panels*1993, American Concrete Institute.

Manual for Compression Tester KES-FB-3, a, KATO TECH CO., LTD., Kyoto 601 Japan.

Manual for pure Bending Tester KES-FB-2, b, KATO TECH CO., LTD., Kyoto 601 Japan.

"Manual for Surface Tester KES-FB-4", c, .

Manual for Tensile and Shear Tester KES-FB-1, d, KATO TECH CO., LTD., Kyoto 601 Japan.

Abbott, G.M., Grosberg, P. & Leaf, G.V.A. 1973, "The elastic resistance to bending of plain-woven fabrics", *Journal of the Textile Institute*, vol. 64, no. 3, pp. 346-362.

Abbott, G.M., Grossberg, P. & Leaf, G.A.V. 1971, "The mechanical properties of woven fabrics, part VII: hysteresis and bending of woven fabrics", *Textile Research Journal*, vol. 41, pp. 3455.

Allison, G.L. 1958, "Warp knitting calculation made easy", *Skinner's Silk Rayon Rec*, vol. 3, pp. 281-285.

Amirbayat, J. & Hearle, J.W.S. 1989, "The anatomy of buckling of textile fabrics: Drape and conformability of dimensionless groups", *Journal of the Textile Institute*, vol. 80, pp. 51-70.

Ascough, J., Bez, H.E. & Bricis, A.M. 1996, "A simple beam element, large displacement model for the finite element simulation of cloth drape", *Journal of the Textile Institute*, vol. 87, no. 1, pp. 152-165.

Backer, S. 1952, "The mechanics of bent yarns", *Textile Research Journal*, vol. 22, no. 5, pp. 668-681.

Badel, P., Vidal-Sallé, E., Maire, E. & Boisse, P. 2008, "Simulation and tomography analysis of textile composite reinforcement deformation at the mesoscopic scale", *Composites Science and Technology*, vol. 68, no. 12, pp. 2433-2440.

Barndt, H., Fortess, F., Wiener, M. & Furniss, J.C. 1990, "The use of KES and FAST Instruments: In Predicting Processability of Fabrics in Sewing", *International Journal of Clothing Science and Technology*, vol. 2, no. 3.

Batra, S.K. 1973, "Normal Force between Twisted Filaments - 1. Fibre-Wound-on -Cylinder Model - Analytical Treatment", *Journal of the Textile Institute*, vol. 64, no. 4, pp. 209-222.

Batra, S.K., Tayebi, A. & Backer, S. 1973, "Normal Force Between Twisted Filaments - 2. Experimental Verification", *Journal of the Textile Institute*, vol. 64, no. 6, pp. 363-373.

Behre, B. 1961, "Mechanical properties of textile fabrics, part I: Shearing", *Textile Research Journal*, vol. 31, no. 2, pp. 87-99.

Bishop, D.P. 2003, "Objective measurement of fabric properties" in *Fabrics: Sensory and Mechanical properties* Textile Progress, , pp. 27.

Bogdanovich, A.E. 2006, "Multi-scale modeling, stress and failure analyses of 3-D woven composites", *Journal of Materials Science*, vol. 41, no. 20, pp. 6547-6590.

Breen, D.E., House, D.H. & Wozny, M.J. 1994, "Predicting the drape of woven cloth using interacting particles", *Computer Graphics*, , no. 4, pp. 365-372.

Bruer, S.M., Powell, N. & Smith, G. 2005, "Three-dimensionally knit spacer fabrics: A review of production techniques and applications", *Journal of Textile and Apparel, Technology and Management*, vol. 4, no. 4, pp. 85-113.

Cartraud, P. & Messager, T. 2006, "Computational homogenization of periodic beam-like structures", *International Journal of Solids and Structures,* vol. 43, no. 3-4, pp. 686-696.

Carvelli, V., Corazza, C. & Poggi, C. 2008, "Mechanical modelling of monofilament technical textiles", *Computational Materials Science,* vol. 42, no. 4, pp. 679-691.

Cassidy, T., Cassidy, C., Cassie, S. & Arkison, M. 1991, "The Stiffness of Knitted Fabrics:: A New Approach to the Measurement of Bending, Part 1: Development", *International Journal of Clothing Science and Technology,* vol. 3, no. 5.

Chamberlain, J. 1926, "Hosiery yarns and fabrics", *City of Leicester College of technology,* vol. Vol.II, pp. 107.

Chen, B. & Govindaraj, M. 1995, "Physically based model of fabric drape using flexible shell theory", *Textile Research Journal,* vol. 65, no. 6, pp. 324-330.

Choi, J. & Tamma, K.K. 2001, "Woven fabric composites, Part I: Predictions of homogenized elastic properties and micromechanical damage analysis", *Int. J. Numer. Meth. Eng,* vol. 50, pp. 2285-2298.

Choi, K.F. & Tandon, S.K. 2006, "An energy model of yarn bending", *Journal of the Textile Institute,* vol. 97, no. 1, pp. 49-56.

Chu, C.C., Cummings, C.L. & Teixeira, N.A. 1950, "Mechanics of elastic performance of textile materials part V: A study of the factors affecting the drape of fabrics - The development of drape meter", *Textile Research Journal,* vol. 20, no. 8, pp. 539-548.

Collier, J.R., Collier, B.J., O'Toole, G. & Sargand, S.M. 1991, "Drape prediction by means of finite-element analysis", *Journal of the Textile Institute,* vol. 82, no. 1, pp. 96-107.

Cox, B. & Flanagan, G. 1997, *Handbook of Analytical Methods for Textile Composites.*

Cusick, G.E. 1968, "The measurement of fabric drape", *Journal of the Textile Institute,* vol. 59, pp. 253-260.

Dahlberg, B. 1961, "Mechanical properties of textile fabrics Part II: Buckling", *Textile Research Journal,* vol. 31, no. 2, pp. 94-99.

Dalidovici, A.S. 1940, *Basic Knitting,* .

Dastoor, P.H., Ghosh, T.K., Batra, S.K. & Hersh, S.P. 1994, "Computer-assisted structural design of industrial woven fabrics part III: modelling of fabric uniaxial/biaxial load-deformation", *Journal of the Textile Institute,* vol. 85, no. 2, pp. 135-137.

de Araújo, M., Fangueiro, R. & Hong, H. 2004, "Modelling and simulation of the mechanical behaviour of weft-knitted fabrics for technical applications. Part IV: 3D FEA model with a mesh of tetrahedric elements", *Autex Research Journal,* vol. 4, no. 2, pp. 72-80.

Demboski, G. & Bogoeva-Gaseva, G. 2005, "Textile Structures for technical textiles, II Part: Types and features of textile assemblies", *Bulletin of the Chemists and Technologists of Macedonia,* vol. 24, no. 1, pp. 77-86.

Demiroz, A. 2005, "Prediction of Large Deformation Behavior of Fabric Using Galerkin Finite Element Method", *Textile Research Journal,* vol. 75, pp. 662-669.

Demiroz, A. & Dias, T. 2000a, "A study of the graphical representation of plain-knitted structures part I: Stitch model for the graphical representation of plain-knitted structures", *Journal of the Textile Institute Part 1: Fibre Science and Textile Technology,* vol. 91, no. 1 PART 4, pp. 463-480.

Demiroz, A. & Dias, T. 2000b, "A study of the graphical representation of plain-knitted structures part II: Experimental studies and computer generation of plain-knitted structures", *Journal of the Textile Institute Part 1: Fibre Science and Textile Technology,* vol. 91, no. 1 PART 4, pp. 481-492.

Freeston, W.D., Platt, M.M. & Schoppee, M.M. 1967, "Mechanics of elastic performance of textile materials. XVIII. Stress-strain response of fabrics under two-demensional loading", *Textile Research Journal,* vol. 37, pp. 11.

Freeston, W.D. & Schoppee, M.M. 1975, "Geometry of Bent Continuous-Filament Yarns", *Textile Research Journal,* vol. 45, no. 12, pp. 835-852.

Gan, L., Ly, N.G. & Steven, G.P. 1995, "A study of fabric deformation using nonlinear finite elements", *Textile Research Journal,* vol. 65, no. 11, pp. 660-668.

Ganssauge, D., Lehmann, K.-. & Augenadel, A. 1998, "How do fabric attributes influence the handle characteristics of a fabric?", *Melliand International, ,* no. 2, pp. 103-106.

Gaucher, M.L., King, M.W. & Johnston, B. 1983, "Predicting the Drape Coefficient of Knitted Fabrics.", *Textile Research Journal,* vol. 53, no. 5, pp. 297-303.

Gegauff, C. 1907, "Strength and Elasticity of Cotton Threads", *Bull Soc Ind Mulhouse,* vol. 77, pp. 153-176.

Ghosh, T.K., Batra, S.K. & Barker, R.L. 1990, "Bending behaviour of plain-woven fabrics Part III. The case of bilinear thread-bending behaviour and the effect of fabric set", *Journal of the Textile Institute,* vol. 81, no. 3, pp. 272-287.

Göktepe, F., Lawrence, C.A. & Leaf, G.A.V. 2000, "Deformation of a single helix under simultaneous application of extension, compression, and bending", *Textile Research Journal,* vol. 70, no. 6, pp. 508-518.

Goktepe, O. 2001, "Use of non-uniform rational b-splines for three-dimensional computer simulation of warp knitted structures", *Turkish Journal of Engineering and Environmental Sciences,* vol. 25, no. 4, pp. 369-378.

Goktepe, O. & Harlock, S.C. 2002, "Three-dimensional computer modeling of warp knitted structures", *Textile Research Journal,* vol. 72, no. 3, pp. 266-272.

Gray, S. 1998, "In virtual fashion", *IEEE Spectrum,* vol. 35, no. 2, pp. 18-25.

Grosberg, P. 1966, "The mechanical properties of woven fabrics, Part II: The bending of woven fabrics", *Textile Research Journal,* vol. 36, no. 3, pp. 205-211.

Grosberg, P. 1964, "The geometrical properties of simple warp-knit fabrics", *J Textile Inst,* vol. 55, pp. T18-T30.

Grosberg, P. & Kedia, S. 1966, "The Mechanical Properties of Woven Fabrics, Part I: The Initial Load Extension Modulus of Woven Fabrics", *Textile Research Journal,* vol. 36, no. 1, pp. 71-79.

Haiqing, M. & Yanling, C. 2000, "Comparison of the fabric mechanical properties measured by the KES-F and FAST systems", *J. Dong Hua Univ,* vol. 17, no. 2, pp. 81-84.

Hearle, J.W.S. 2006, "Engineering design of textiles", *Indian Journal of Fibre and Textile Research,* vol. 31, no. 1, pp. 134-141.

Hearle, J.W.S. 2004, "The challenge of changing from empirical craft to engineering design", *International Journal of Clothing Science and Technology,* vol. 16, no. 1/2.

Hearle, J.W.S., El-Behery, H.M.A.E. & Thakur, V.M. 1959, "The mechanics of twisted yarns: Tensile properties of continuous-filament yarns", *Journal of the Textile Institute,* vol. 50, pp. T83-T111.

Hegger, J. & Voss, S. 2008, "Investigations on the bearing behaviour and application potential of textile reinforced concrete", *Engineering Structures,* vol. 30, no. 7, pp. 2050-2056.

Hepworth, B. 1978, "The biaxial load-extension behaviour model of plain weft knittin - Part I", *Journal of the Textile Institute,* vol. 69, pp. 101-107.

Holler, S., Butenweg, C., Noh, S.-. & Meskouris, K. 2004, "Computational model of textile-reinforced concrete structures", *Computers and Structures,* vol. 82, no. 23-26, pp. 1971-1979.

Hollister, S.J., Fyhrie, D.P., Jepsen, K.J. & Goldstein, S.A. 1991, "Application of homogenization theory to the study of trabecular bone mechanics", *Journal of Biomechanics,* vol. 24, no. 9, pp. 825-839.

Holmberg, S., Persson, K. & Petersson, H. 1999, "Nonlinear mechanical behaviour and analysis of wood and fibre materials", *Computers and Structures*, vol. 72, no. 4, pp. 459-480.

Hsieh, Y-. "Fibers" in *Kirk-Othmer Encyclopedia of Chemical Technology* John Wiley & Sons.

Hu, J. 2008, *3D fibrous assemblies - Proberties, applications and modelling of 3D textile structures*, Woodhead Publishing Limited; The Textile Institute.

Hu, J. & Chan, Y-. 1998, "Effect of fabric mechanical properties on drape", *Textile Research Journal*, vol. 68, no. 1, pp. 57-64.

Hu, J., Chen, S-. & Teng, J.G. 2000, "Numerical drape behavior of circular fabric sheets over circular pedestals", *Textile Research Journal*, vol. 70, no. 7, pp. 593-603.

Hu, J.L. & Teng, J.G. 1996, "Computational fabric mechanics: Present status and future trends", *Finite Elements in Analysis and Design*, vol. 21, no. 4, pp. 225-237.

Huang, N.C. 1979a, "Finite Biaxial Extension of Completely Set Plain Woven Fabrics", *Journal of Applied Mechanics, Transactions ASME*, vol. 46, no. 3, pp. 651-655.

Huang, N.C. 1979b, "Finite biaxial extension of partially set plain woven fabrics", *International Journal of Solids and Structures*, vol. 15, no. 8, pp. 615-623.

Hübsch, P.F., Knox, J., Jones, M.L. & Middleton, J. 1996, "Global and local behaviour of the stress field at the base of an orthodontic bracket", *Computer Methods in Biomechanics and Biomechanical Engineering*, , pp. 361-369.

Kang, T.J. & Yu, W.R. 1995, "Drape simulation of woven fabric by using the finite-element method", *Journal of the Textile Institute*, vol. 86, no. 4, pp. 635-648.

Kavagia, C. 2008, *Μηχανική ανάλυση τριδιάστατου υφάσματος με χρήση της μεθόδου των πεπερασμένων στοιχείων*, National Technical Univercity of Athens.

Kawabata, S. 1989a, "Knitted fabrics" in *Textile Structural Composites, Composite Materials Series 3*, eds. T.W. Chou & F.K. Ko, Elsevier Science Publishers, Amsterdam, pp. 99-116.

Kawabata, S. 1989b, "Nonlinear mechanics of woven and knitted materials, in textile structural composites", *Composite Materials Series*, vol. 3.

Kawabata, S. 1980, *The standardization and analysis of hand evaluation (2nd edition)*, The Textile Machinery Society of Japan edn, Osaka Science & Technology Center BLd., 8-4, Utsubo-1-chome, Nishi-ku, Osaka 550 Japan.

Kawabata, S. & Niwa, M. 1998, "Clothing engineering based on objective measurement technology", *International Journal of Clothing Science and Technology*, vol. 10, no. 3-4, pp. 263-272.

Kawabata, S., Niwa, M., Ito, K. & Nitta, M. 1990, *Recent progress in the application of objective measurement to clothing manufacture*.

Kawabata, S., Niwa, M. & Kawai, H. 1973, "Finite-Deformation Theory of Plain-Weave Fabrics - 1. The Biaxial-Deformation Theory.", *Journal of the Textile Institute*, vol. 64, no. 1, pp. 21-46.

Kawabata, S., Niwa, M. & Yamashita, Y. 2002, "Recent developments in the evaluation technology of fiber and textiles, towards the engineered design of textile performance", *Journal of Applied Polymer Science*, vol. 83, pp. 687-702.

Keefe, M., Edwards, D.C. & Yang, J. 1992, "Solid modeling of yarn and fiber assemblies", *Journal of the Textile Institute*, vol. 83, no. 2, pp. 185-196.

Kemp, A. 1958, "An extension of Peirce's cloth geometry to the treatment of non-circular threads", *Journal of the Textile Institute*, vol. 49, no. 1, pp. T44-T48.

Kim, D.H. 1995, *Composite Structures for Civil and Architectural Engineering*, .

Komori, T. 2001, "A generalized micromechanics of continuous-filament yarns part I: Underlying formalism", *Textile Research Journal*, vol. 71, no. 10, pp. 898-904.

Konopasek, M. 1980a, "Classical elastica theory and its generalizations" in *Mechanics of flexible fibre assemblies, Nato Advanced Study Institutes Series, Series E: Applied Science - No. 38*, eds. J.W.S. Hearle, J.J. Thwaites & J. Amirbaya, Sijthoff & Noordhoff, USA, pp. 255-274.

Konopasek, M. 1980b, "Computational aspects of large deflection analysis of slender bodies" in *Mechanics of flexible fibre assemblies, Nato Advanced Study Institutes Series, Series E: Applied Science - No. 38*, eds. J.W.S. Hearle, J.J. Thwaites & J. Amirbaya, Sijthoff & Noordhoff, USA, pp. 275-292.

Konopasek, M. 1980c, "Textile application of slender body mechanics" in *Mechanics of flexible fibre assemblies, Nato Advanced Study Institutes Series, Series E: Applied Science - No. 38*, eds. J.W.S. Hearle, J.J. Thwaites & J. Amirbaya, Sijthoff & Noordhoff, USA, pp. 293-310.

Korlinski, W. 1981, "Podstawy dziewiarstwa", *Podstawy Dziewiarstwa*, .

Leaf, G.A.V. 1979a, "Bending Behaviour of a Helical Filament - 1. The Rigidity of The Helix.", *Journal of the Textile Institute*, vol. 70, no. 8, pp. 323-329.

Leaf, G.A.V. 1979b, "Bending Behaviour of a Helical Filament - 2. CurvatureE, Twist and Strain Energy", *Journal of the Textile Institute*, vol. 70, no. 8, pp. 330-336.

Leaf, G.A.V. 1979c, "Woven fabric tensile mechanics", , pp. 143.

Leaf, G.A.V. & Glaskin, A. 1955, "The geometry of a plain knitted loop", *Journal of the Textile Institute*, vol. 45, pp. T587-T605.

Lee, J.S., Pande, G.N., Middleton, J. & Kralj, B. 1996, "Numerical modelling of brick masonry panels subject to lateral loadings", *Computers and Structures*, vol. 61, no. 4, pp. 735-745.

Lindberg, J., Behre, B. & Dahlberg, B. 1961, "Mechanical properties of textile fabrics, Part III: Shearing and buckling of various commercial fabrics", *Textile Research Journal*, vol. 31, no. 2, pp. 99-122.

Liu, T., Choi, K.F. & Li, Y. 2007, "Mechanical modeling of singles yarn", *Textile Research Journal*, vol. 77, no. 3, pp. 123-130.

Lloyd, D.W., Mete, F. & Hussain, K. 1996, "An approach to the theoretical mechanics of static drape", *International Journal of Clothing Science and Technology*, vol. 8, no. 3, pp. 43-58.

Lo, W.M., Hu, J.L. & Li, L.K. 2002, "Modeling a fabric drape profile", *Textile Research Journal*, vol. 72, no. 5, pp. 454-463.

Lomov, S.V., Gusakov, A.V., Huysmans, G., Prodromou, A. & Verpoest, I. 2000, "Textile geometry preprocessor for meso-mechanical models of woven composites", *Composites Science and Technology*, vol. 60, no. 11, pp. 2083-2095.

Lomov, S.V., Huysmans, G., Luo, Y., Parnas, R.S., Prodromou, A., Verpoest, I. & Phelan, F.R. 2004, "Textile Composites: Modelling Strategies", *Composites: Part A*, .

Lomov, S.V., Huysmans, G., Luo, Y., Parnas, R.S., Prodromou, A., Verpoest, I. & Phelan, F.R. 2001, "Textile composites: Modelling strategies", *Composites - Part A: Applied Science and Manufacturing*, vol. 32, no. 10, pp. 1379-1394.

Lomov, S.V., Ivanov, D.S., Verpoest, I., Zako, M., Kurashiki, T., Nakai, H. & Hirosawa, S. 2007, "Meso-FE modelling of textile composites: Road map, data flow and algorithms", *Composites Science and Technology*, vol. 67, no. 9, pp. 1870-1891.

McRory, B.M., McCraith, J.R. & McNamara, A.B. 1975, "The biaxial load-extension properties of plain weft-knitted fabrics: A theoretical analysis", *Textile Research Journal*, vol. 45, pp. 746-760.

Mecit, D. 2005, *Development and defining of a characterization method for 3D spacer fabrics considering concrete applications*, Institut für Textiltechnik.

Mecit, D. & Roye, A. 2006, "Defining and Applying a Test Method for Spacer Fabrics used in Concrete Applications", .

Minazio, P.G. 1995, "FAST - Fabric assurance by simple testing", *International Journal of Clothing Science and Technology*, vol. 7, no. 2-3, pp. 43-48.

Morooka, H. & Niwa, M. 1976, "Relation between drape coefficients and mechanical properties of fabrics", *Journal of Textile Machinery Society in Japan*, vol. 22, no. 3, pp. 67-73.

Munden, D.L. 1969, "Structural Mechanics of fibers, yarns and fabrics" in , ed. P. Grosberg, Wiley-Interscience, USA, pp. 420.

Munden, D.L. 1959, "The geometry and dimensional properties of plain-knit fabrics", *Journal of the Textile Institute*, vol. 50, no. 7, pp. T448-T471.

Munro, W.A., Carnaby, G.A., Carr, A.J. & Moss, P.J. 1997a, "Some Textile Applications of Finite-element Analysis. Part I: Finite Elements for Aligned Fibre Assemblies", *Journal of the Textile Institute*, vol. 88, no. 4, pp. 325-338.

Munro, W.A., Carnaby, G.A., Carr, A.J. & Moss, P.J. 1997b, "Some Textile Applications of Finite-element Analysis. Part II: Finite Elements for Yarn Mechanics", *Journal of the Textile Institute*, vol. 88, no. 4, pp. 339-351.

Ng, S.-., Tse, P.-. & Lau, K.-. 1998, "Numerical and experimental determination of in-plane elastic properties of 2/2 twill weave fabric composites", *Composites Part B: Engineering*, vol. 29, no. 6, pp. 735-744.

Niwa, M. & Seto, F. 1986, "Relationship between drapeability and mechanical properties of fabrics", *Textile Machinery Society in Japan*, vol. 39, no. 11, pp. 161-168.

Okur, A. & Cihan, T. 2002, "Prediction of fabric drape coefficients from FAST data", *Textile Asia*, vol. 33, no. 7, pp. 28-31.

Olofsson, B. 1964a, "A general model of a fabric as a geometric-mechanical structure", *Journal of the Textile Institute*, vol. 55, no. 11, pp. T541-T557.

Olofsson, B. 1964b, "The Setting of Wool Fabrics - A Theoretical Study", *Textile Research Journal*, vol. 20.

Önder, E. & Bacer, G. 1996, "A comprehensive stress and breakage analysis of staple fiber yarns Part I: Stress analysis of a staple yarn based on a yarn geometry of conical helix fiber paths", *Textile Research Journal*, vol. 66, no. 9, pp. 562-575.

Park, J.-. & Oh, A.-. 2006, "Bending rigidity of yarns", *Textile Research Journal*, vol. 76, no. 6, pp. 478-485.

PavlinicÂ, D.Z. & GerÅ¡ak, J. 2003, "Investigations of the relation between fabric mechanical properties and behaviour", *International Journal of Clothing Science and Technology*, vol. 15, no. 3/4.

Peirce, F.T. 1947, "Geometrical Principles Applicable to the Design of Functional Fabrics", *Textile Research Journal*, vol. 17, no. 3, pp. 123-147.

Peirce, F.T. 1937, "The geometry of cloth structure", *Journal of the Textile Institute*, vol. 28, no. 3.

Peirce, F.T. 1930, "The handle of cloth as a measurable quantity", *Journal of the Textile Institute*, vol. 21, no. 9, pp. T377-T416.

Platt, M.M. 1950, "Mechanics of elastic performance of textile materials, III: Some aspects of stress analysis of textile structures-continuous-filament yarns", *Textile Research Journal*, vol. 20, no. 1, pp. 1-15.

Platt, M.M., Klein, W.G. & Hamburger, W.J. 1959, "Mechanics of elastic performance of textiles materials, part XIV: Some aspects of bending rigidity of single yarns", *Textile Research Journal*, vol. 29, pp. 611.

Postle, J.R. & Postle, R. 1996, "Modelling fabric deformation as a nonlinear dynamical system using Bäcklund Transformations", *International Journal of Clothing Science and Technology*, vol. 8, no. 3, pp. 22-42.

Postle, R. & Munden, D.L. 1967, "Analysis of the dry-relaxed knitted loop configuration, part 2: Three dimensional analysis", *Journal of the Textile Institute*, vol. 58, no. 8, pp. 352-365.

Provatidis, C.G. & Vassiliadis, S.G. 2004, "On the performance of the geometrical models of fabrics for use in computational mechanical analysis", *International Journal of Clothing Science and Technology*, vol. 16, no. 5.

Provatidis, C.G., Vassiliadis, S.G. & Anastasiadou, E.A. 2005, "Contact mechanics in two-dimensional finite element modelling of fabrics", *International Journal of Clothing Science and Technology*, vol. 17, no. 1.

Provatidis, C. & Vassiliadis, S. 2002, "On the numerical estimation of the mechanical behaviour of fabrics", *2nd AUTEX World Textile Conference*, pp. 88.

Raz, S. 2000, *The Karl Mayer Guide to Technical Textiles*.

Raz, S. 1987, *Warp knitting production*, Veglar Melliand Textilberichte GmbH, Heidelberg.

Release 11.0 Documentation for ANSYS a, *14.174. CONTA174 3D 8-node surface-to-surface contact*.

Release 11.0 Documentation for ANSYS b, *14.52. CONTAC52, 3-D Point-to-Point Contact*.

Roye, A. & Gries, T. 2007, "3-D Textiles for Advanced Cement Based Matrix Reinforcement", *Journal of Industrial Textiles*, vol. 37, no. 2, pp. 163-173.

Sacco, E. 2009, "A nonlinear homogenization procedure for periodic masonry", *European Journal of Mechanics, A/Solids*, vol. 28, no. 2, pp. 209-222.

Shanahan, W.J., Lloyd, D.W. & Hearle, J.W.S. 1978, "Characterizing the elastic behaviour of textile fabrics in complex deformation", *Textile Research Journal*, vol. 48, pp. 495-505.

Shanahan, W.J. & Postle, R. 1970, "A theoretical analysis of the tensile properties of plain-knitted fabrics, Part I: the load extension curve for fabric extension parallel to the courses", *Textile Research Journal*, vol. 40, pp. 200-212.

Shinn, W.E. 1955, "An engineering approach to Jersey fabric construction", *Textile Research Journal*, vol. 25, no. 3, pp. 270-277.

Shishoo, R.L. 1990, *Relation between fabric mechanical properties and garment design and tailorability*.

Stump, D.M. & Fraser, W.B. 1996, "A simpified model of fabric drape based on ring theory", *Textile Research Journal*, vol. 66, no. 8, pp. 506-514.

Stylios, G., Wan, T.R. & Powell, N.J. 1995, "Modeling the dynamic drape of fabrics on synthetic humans, a physical, lumped-parameter model", *Int. J. Clothing Sci. Technol.*, vol. 7, no. 5, pp. 10-25.

Stylios, G.K. 2005, "New measurement technologies for textiles and clothing", *International Journal of Clothing Science and Technology*, vol. 17, no. 3-4, pp. 135-149.

Stylios, G.K. 2003, "The concept of fabric automated measurement and optimisation system for textiles and clothing", *4th IMCEP*, , pp. 1-6.

Stylios, G.K., Wan, T.R. & Powell, N.J. 1996, "Modelling the dynamic drape of garments on synthetic humans in a virtual fashion show", *International Journal of Clothing Science and Technology*, vol. 8, no. 3, pp. 95-112.

Stylios, G.K. & Zhu, R. 1997, "The Characterisation of the Static and Dynamic Drape of Fabrics", *Journal of the Textile Institute*, vol. 88, no. 4, pp. 465-475.

Sze, K.Y. & Liu, X.H. 2007, "Fabric drape simulation by solid-shell finite element method", *Finite Elements in Analysis and Design*, vol. 43, no. 11-12, pp. 819-838.

Takano, N., Uetsuji, Y., Kashiwagi, Y. & Zako, M. 1999, "Hierarchical modelling of textile composite materials and structures by the homogenization method", *Modelling and Simulation in Materials Science and Engineering*, vol. 7, no. 2, pp. 207-231.

Tarfaoui, M. & Akesbi, S. 2001, "Numerical study of the mechanical behaviour of textile structures", *International Journal of Clothing Science and Technology*, vol. 13, no. 3-4, pp. 166-175.

Toney, M.M. 2000, "Computer modeling of fibrous structures", *Journal of the Textile Institute*, vol. 91, no. 3, pp. 133-139.

Triantafillou, T.C. 1998, "Shear strengthening of reinforced concrete beams using epoxy-bonded FRP composites", *ACI Structural Journal*, vol. 95, no. 2, pp. 107-115.

Vassiliadis, S., Gurkan, P., Kallivretaki, A. & Provatidis, C. 2005, "Fabric hand: An important quality of the textile fabrics", *2nd International Scientic Conference in Information Technology and Quality*, Spetses,Greece .

Vékássy, A. 1960, *Konfekcioipar*, .

Verpoest, I. & Lomov, S.V. 2005, "Virtual textile composites software WiseTex: Integration with micro-mechanical, permeability and structural analysis", *Composites Science and Technology*, vol. 65, no. 15-16 SPEC. ISS., pp. 2563-2574.

Yick, K.-., Cheng, K.P.S., Dhingra, R.C. & How, Y.L. 1996, "Comparison of mechanical properties of shirting materials measured on the KES-F and FAST instruments", *Textile Research Journal*, vol. 66, no. 10, pp. 622-633.

ΕΘΝΙΚΟ ΜΕΤΣΟΒΙΟ ΠΟΛΥΤΕΧΝΕΙΟ
ΣΧΟΛΗ ΜΗΧΑΝΟΛΟΓΩΝ ΜΗΧΑΝΙΚΩΝ
ΤΟΜΕΑΣ ΜΗΧΑΝΟΛΟΓΙΚΩΝ ΚΑΤΑΣΚΕΥΩΝ ΚΑΙ ΑΥΤΟΜΑΤΟΥ ΕΛΕΓΧΟΥ

Περίληψη της Διατριβής στην Ελληνική Γλώσσα

ΤΡΙΔΙΑΣΤΑΤΑ ΜΙΚΡΟΜΗΧΑΝΙΚΑ ΜΟΝΤΕΛΑ ΥΦΑΣΜΑΤΩΝ

Αργυρώ Καλλιβρετάκη

Τριμελής συμβουλευτική επιτροπή:
Καθηγητής Χρ. Προβατίδης
Αν. Καθηγητής Ι. Αντωνιάδης
Επ. Καθηγητής Σ. Διπλάρης

Επταμελής εξεταστική επιτροπή:
Καθηγητής Χρ. Προβατίδης
Καθηγητής Δ. Μανωλάκος
Καθηγητής Γ. Τσαμασφύρος
Αν. Καθηγητής Ι. Αντωνιάδης
Αν. Καθηγητής Ν. Τσούβαλης
Επ. Καθηγητής Σ. Διπλάρης
Επ. Καθηγητής Σ. Βασιλειάδης

Μάιος 2010
Αθήνα

Πίνακας Περιεχομένων

Κατάλογος Σχημάτων

Κατάλογος Πινάκων

Κεφάλαιο 1
Εισαγωγή στη Μηχανική Ανάλυση των Κ/Υ Δομών

Abstract

Ο κλωστοϋφαντουργικός (κ/υ) τομέας παρουσιάζει αξιοσημείωτη καθυστέρηση στην υιοθέτηση μιας ολοκληρωμένης υπολογιστικής διαδικασίας σχεδιασμού των προϊόντων. Παρά τις μακροχρόνιες προσπάθειες της ερευνητικής κοινότητας για την ανάπτυξη μιας αξιόπιστης μεθοδολογίας για την πρόβλεψη της μηχανικής συμπεριφοράς των κ/υ δομών, η σχεδιαστική τους διαδικασία βασίζεται κυρίως σε παραδοσιακές μεθόδους όπως την μέθοδο δοκιμής – σφάλματος. Διεξήχθησαν εμπεριστατωμένες αναλυτικές έρευνες για την μελέτη των μηχανικών ιδιοτήτων των κ/υ δομών. Η αδυναμία των μεθόδων αυτών οφειλόταν κυρίως στην θεώρηση απλοποιητικών παραδοχών για την μείωση της πολυπλοκότητας και του υπολογιστικού κόστους. Η εξέλιξη των υπολογιστικών προγραμμάτων και η προκύπτουσα υπολογιστική ισχύς έστρεψε το ενδιαφέρον των ερευνητών σε αριθμητικές προσεγγίσεις. Τα προηγμένα υπολογιστικά εργαλεία μηχανικής ανάλυσης αποδεικνύονται σταδιακά κατάλληλα για την προσομοίωση σύνθετων καταπονήσεων γεωμετριών δομών πολλαπλών επαφών, όπως οι κ/υ δομές. Το πρώτο κεφάλαιο εστιάζει στην βιβλιογραφική επισκόπηση των μεθόδων που έχουν αναπτυχθεί για την μηχανική ανάλυση των κ/υ δομών, παρουσιάζοντας την εξελικτική πορεία των σχετικών ερευνών, τις προοπτικές και τους περιορισμούς. Επιπλέον προτείνεται μια ολοκληρωμένη διαδικασία σχεδιασμού των κ/υ δομών βασισμένη σε περιβάλλον CAE. Η προτεινόμενη διαδικασία βασίζεται στην υποδιαίρεση της σε τρία στάδια μοντελοποίησης που αντιστοιχούν στα επίπεδα της δομικής ιεραρχίας των κ/υ δομών: την μικρομηχανική μοντελοποίηση των νημάτων, την μεσομηχανική μοντελοποίηση της δομικής μονάδας του υφάσματος και την μακρομηχανική μοντελοποίηση του υφάσματος.

1.1 Εισαγωγή

Η κλωστοϋφαντουργική (κ/υ) βιομηχανία, σε αντίθεση με τους άλλους βιομηχανικούς τομείς, υστερεί στην ανάπτυξη κατάλληλων εργαλείων CAD και CAE για την μηχανική ανάλυση των κ/υ προϊόντων. Πιθανός λόγος είναι η αποκλειστική χρήση των κ/υ προϊόντων σε απλές εφαρμογές ένδυσης, για χιλιάδες χρόνια, που εξασθένησε την σημασία της μηχανικής ανάλυσης και σχεδίασης. Αξιοσημείωτο είναι ότι επειδή ο αισθητικός σχεδιασμός επικράτησε καθ' όλη την διάρκεια της χρήσης των κ/υ προϊόντων, έχουν αναπτυχθεί ανάλογα υπολογιστικά εργαλεία. Μερικά απ' αυτά είναι: *Textronics CAD/CAM*, *Optitex 2D/3D CAD*, *DesignScope Victor*, *Grafixoft*, *Evolution Textile Design Software*, *JacqCAD MASTERS*, *Lectra*, *Textile Vision* and *Triadem*. Η χρήση τους βέβαια ποικίλει. Κάποια ειδικεύονται στην οπτικοποίηση των κ/υ σχεδίων σε δύο διαστάσεις, άλλα κάνοντας χρήση προηγμένων

αλγορίθμων παρέχουν την τριδιάστατη απεικόνιση υφαντών δομών. Επίσης κάποια προσφέρουν ολοκληρωμένες λύσεις από την (οπτική) σχεδίαση ενός προϊόντος στην διαδικασία παραγωγής.

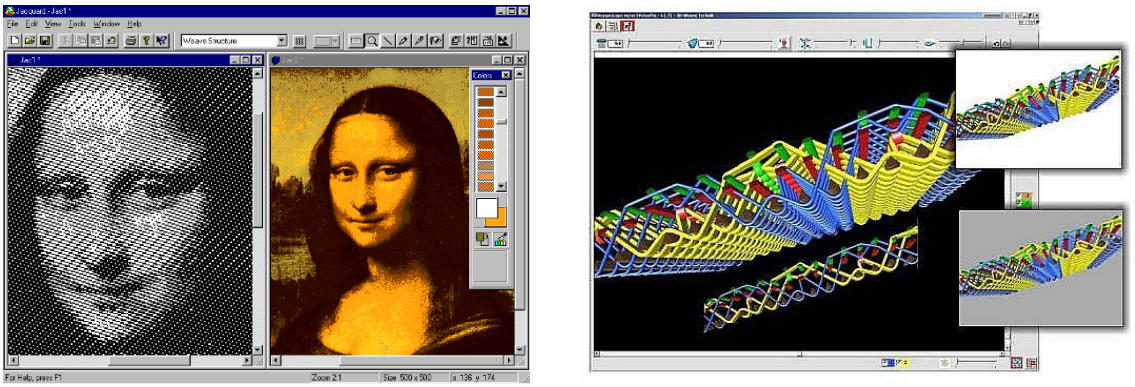

Σχήμα 1-1: Σχέδιο Jacquard (*Grafixoft*) και 3Δ ύφανση (*DesignScope Victor*)

Ωστόσο, η ανάπτυξη της κ/υ βιομηχανίας και η πρόσφατη δυναμική επέκτασή της σε προηγμένες τεχνικές εφαρμογές μετέτρεψε τον σχεδιασμό των κ/υ προϊόντων σε σύνθετη μηχανική μελέτη. Έτσι η απόδοση των κ/υ προϊόντων καθορίζεται από τις μηχανικές, θερμικές, ηλεκτρικές ιδιότητες και χαρακτηριστικά άνεσης και αισθητικής. Η παρούσα διατριβή εστιάζει μόνο στην μηχανική μελέτη, όμως η μεθοδολογία που αναπτύσσεται μπορεί να επεκταθεί και σε άλλα πεδία της μηχανικής.

1.2 Εισαγωγή στις κ/υ δομές

Μια σύντομη εισαγωγή στα κ/υ προϊόντα είναι απαραίτητη για την κατανόηση των δομικών χαρακτηριστικών τους θεωρώντας την ιεραρχία παραγωγής τους, ίνα – νήμα – ύφασμα. Επιπλέον εισάγονται θεμελιώδεις έννοιες που καθορίζουν την μηχανική συμπεριφορά των δομών αυτών.

1.2.1 Ίνα

Ως ίνα ορίζεται το εύκαμπτο, μακροσκοπικά ομογενές σώμα που παρουσιάζει υψηλή αναλογία μήκους/πάχος. Οι ίνες αποτελούν την πρώτη ύλη για την παραγωγή των κ/υ δομών. Οι μηχανικές, φυσικές και χημικές ιδιότητες των ινών διαφέρουν ουσιαστικά εξαρτώμενες από το υλικό και την δομή τους. Αποτέλεσμα αυτού είναι το μεγάλο εύρος των εφαρμογών τους στην κ/υ και κατασκευαστική βιομηχανία. Οι κ/υ ίνες ταξινομούνται συνήθως σύμφωνα με την προέλευσή τους. Οι περισσότερες από τις τεχνητές ίνες, π.χ. αναγεννημένες και συνθετικές, παράγονται σε συνεχή μορφή (συνεχείς ίνες). Συχνά όμως επιθυμείται η λήψη τους σε πεπερασμένα μήκη. Σ’ αυτή τη περίπτωση, χιλιάδες συνεχείς ίνες συλλέγονται σε μορφή δέσμης παράλληλων ινών που ονομάζεται tow. Στη συνέχεια η δέσμη των ινών

μετατρέπεται με απλό κόψιμο σε ασυνεχείς ίνες πεπερασμένου μήκους, το οποίο καθορίζεται από το σύστημα που θα χρησιμοποιηθεί για την νηματοποίηση. Οι ασυνεχείς ίνες μπορεί να είναι είτε φυσικές ίνες, όπως από βαμβάκι ή μαλλί, είτε από συνθετικές ίνες.

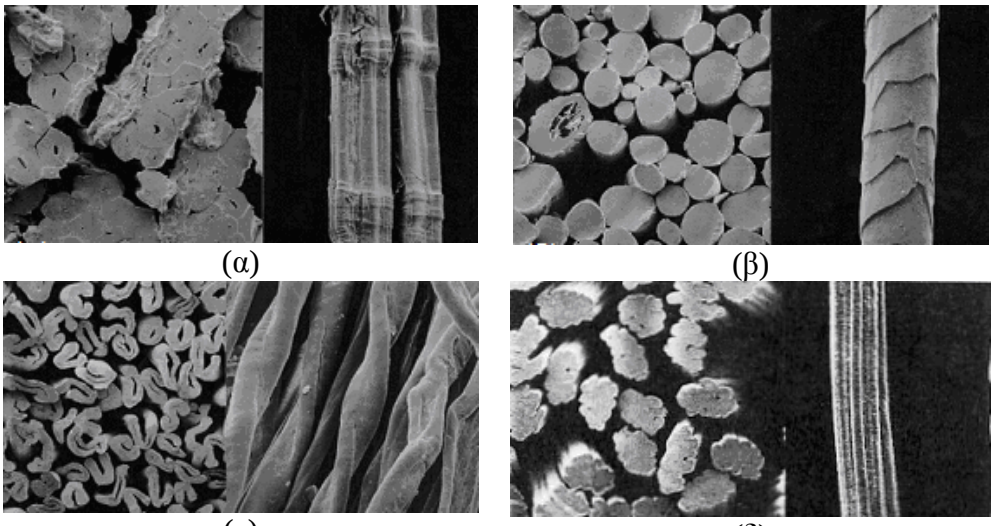

Σχήμα 1-2: Ίνες από (α) λινάρι, (β) μαλλί, (γ) βαμβάκι, (δ) βισκόζη.

1.2.2 Νήμα

Γενικά, ο τρόπος με τον οποίο μεταποιούνται σε νήματα καθορίζεται σε μεγάλο βαθμό από τον λόγο μήκους/πάχος των νημάτων. Έχουν αναπτυχθεί διάφορες μέθοδοι νηματοποίησης που ευθυγραμμίζουν και στη συνέχεια προσδίδουν συνοχή και στρίψεις στις ίνες των νημάτων. Η νηματοποίηση τυπικά απαιτεί ίνες υψηλού λόγου διαστάσεων, δηλαδή 1000 ή μεγαλύτερο. Βασικά χαρακτηριστικά για την διάκριση των νημάτων είναι:

Νήματα Συνεχών ή ασυνεχών ινών (πεπερασμένου μήκους)

Μονοϊνικά ή πολυινικά νήματα

Στριμμένα ή επίπεδα (δέσμη ινών)

Μονόκλωνα ή δίκλωνα ή πολύκλωνα νήματα.

Τα κ/υ νήματα παράγονται από ασυνεχείς ίνες (staple) με συνδυασμό διαδικασιών που αναφέρεται ως μέθοδος νηματοποίησης. Μετά την προκαταρκτική ευθυγράμμιση των ινών, οι ίνες συγκρατούνται μεταξύ τους με πρόσδοση στρίψεων για την διαμόρφωση του κλωστοποιημένου νήματος με ομοιόμορφο και συνεχές μήκος. Κ/υ νήματα παράγονται επίσης από συνεχείς συνθετικές ίνες (filaments). Ένας αριθμός συνεχών ινών συγκεντρώνεται σε δέσμη ινών, στην οποία προσδίδεται χαμηλός αριθμός στρίψεων για την απόδοση συνοχής, και παράγεται το πολυινικό νήμα (multifilament). Έχουν αναπτυχθεί διάφορες μέθοδοι για την αλλαγή των χαρακτηριστικών υφής (τεξτουράρισμα) των νημάτων συνεχών ινών. Μεμονωμένες συνεχείς ίνες που παρουσιάζουν μεγάλη διατομή χρησιμοποιούνται σε κάποιες εφαρμογές ως μονοϊνικά νήματα.

Σχήμα 1-3: Επίπεδο νήμα (δεξιά) και στριμμένο πολυινικό νήμα (αριστερά).

1.2.3 Διδιάστατα υφάσματα

Διδιάστατα υφαντά υφάσματα

Η ύφανση αποτελεί τον ευρύτερα χρησιμοποιούμενο μηχανισμό παραγωγής υφασμάτων που απαντάται στα διδιάστατα υφάσματα. Οι τυπικές δομές υφαντών αποτελούνται από δύο σειρές νημάτων που αλληλοπλέκονται. Τα νήματα που συναντώνται κατά το μήκος του υφάσματος αποτελούν τα στημόνια, ενώ τα νήματα που συναντώνται κατά το πλάτος του υφάσματος από ούγια σε ούγια καλούνται υφάδια. Τα στημόνια και τα υφάδια αλληλοπλέκονται σε γωνία 90°. Ο αριθμός των στημονιών και των υφαδιών ανά μονάδα μήκους αποτελούν αντίστοιχα την πυκνότητα στημονιού και υφαδιού. Ο τρόπος με τον οποίο αλληλοπλέκονται τα στημόνια και τα υφάδια ονομάζεται σχέδιο ύφανσης. Στο Σχήμα 1-4 παρουσιάζονται τα βασικά σχέδια ύφανσης διδιάστατων υφαντών υφασμάτων.

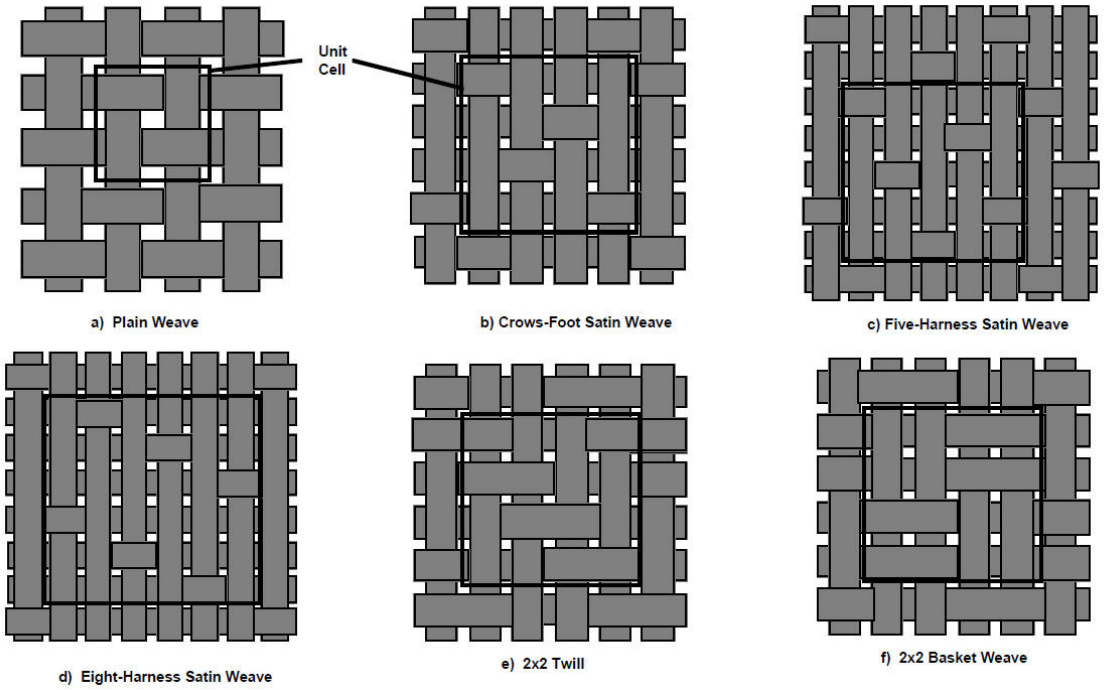

Σχήμα 1-4: Βασικά σχέδια ύφανσης διδιάστατων υφαντών υφασμάτων (Cox, Flanagan 1997).

Τριαξονικά υφαντά υφάσματα

Το τριαξονικό υφαντό ύφασμα (Σχήμα 1-5) παράγεται από τρία συστήματα νημάτων: ένα σύστημα για το υφάδι και δύο συστήματα για το στημόνι. Επειδή αυτά τα υφάσματα παρουσιάζουν τρεις στρώσεις υλικού σε κάθε σημείο έχουν υψηλότερη αντοχή από τα ορθογώνια υφαντά υφάσματα που παράγονται από τα ίδια στοιχεία. Στην τυπική δομή τριαξονικού υφαντού τα στημόνια υφαίνονται σε γωνία 60° και παρουσιάζουν υψηλή αντίσταση σε διάτμηση.

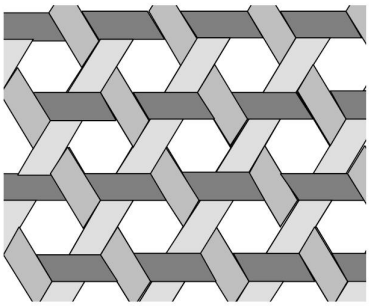

Σχήμα 1-5: Τυπική δομή τριαξονικού υφαντού.

Διδιάστατα πλεκτά υφάσματα

Τα πλεκτά υφάσματα είναι κ/υ δομές που σχηματίζονται από την βασική δομική μονάδα που ονομάζεται θηλιά. Υπάρχουν δύο βασικές τεχνικές για την παραγωγή πλεκτών υφασμάτων: η πλεκτική υφαδιού και η πλεκτική στημονιού.

Πλεκτά υφαδιού

Το χαρακτηριστικό των πλεκτών υφαδιού είναι ότι οι θηλιές μιας σειράς του υφάσματος σχηματίζονται από το ίδιο νήμα, δηλαδή οι θηλιές διαμορφώνονται κατά το πλάτος του υφάσματος (Hu 2008). Η απλούστερη δομή πλεκτού υφαδιού παράγεται από μια σειρά βελονών της πλεκτομηχανής και ονομάζεται απλό πλεκτό ή single jersey. Οι τυπικές δομές πλεκτών υφαδιού παρουσιάζονται στο Σχήμα 1-6.

Πλεκτά στημονιού

Στην τεχνική στημονιού κάθε θηλιά του υφάσματος διαμορφώνεται από ξεχωριστό νήμα, το στημόνι, που εισάγεται κυρίως κατά το μήκος του υφάσματος. Το πιο χαρακτηριστικό σημείο, λοιπόν, των πλεκτών στημονιού (Σχήμα 1-7) είναι ότι οι διπλανές θηλιές μιας σειράς του υφάσματος δεν παράγονται από το ίδιο νήμα. Ενώ η πλεκτική υφαδιού χρησιμοποιείται ευρέως στην βιομηχανία ένδυσης, η πλεκτική στημονιού είναι ουσιαστικά συνδεδεμένη με στην κατασκευή δομών για τεχνικές εφαρμογές. Ιδιαίτερο ενδιαφέρον για τεχνικές εφαρμογές

παρουσιάζουν τα στημονοπλεκτά με παρεμβαλλόμενα υφάδια (Hu 2008, Demboski, Bogoeva-Gaseva 2005).

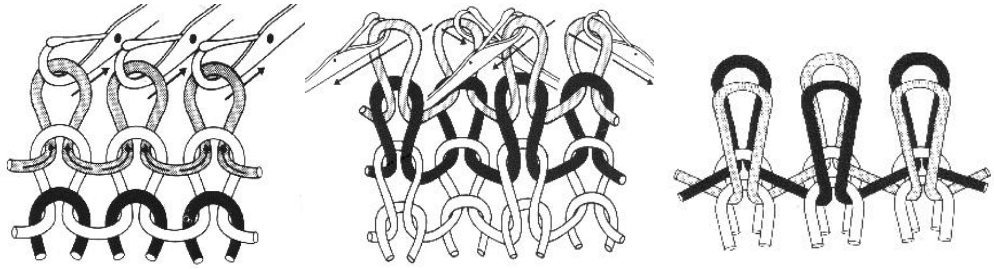

(α) (β) (γ)

Σχήμα 1-6: Δομές πλεκτών υφαδιού, (α) απλό πλεκτό, (β) ριμπ 1x1, (γ) ίντερλοκ.

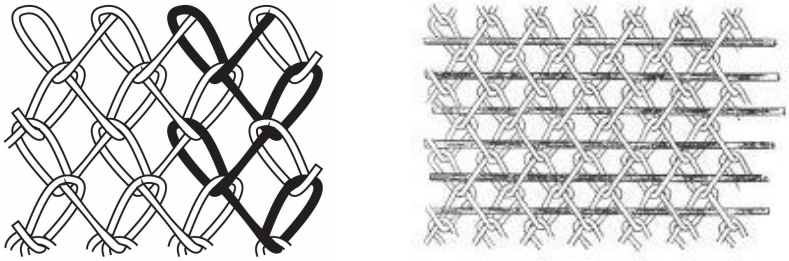

(α) (β)

Σχήμα 1-7: (α) Τυπική δομή στημονοπλεκτού (β) στημονοπλεκτό με παρεμβαλλόμενα υφάδια.

Διδιάστατα μη-υφάνσιμα υφάσματα

Τα μη-υφάνσιμα υφάσματα (Σχήμα 1-8) είναι κ/υ δομές των οποίων τα δομικά στοιχεία (ίνες) συνδέονται μεταξύ τους με μηχανικές, θερμικές ή χημικές διεργασίες. Συνιστούν επιφάνειες τύπου ελάσματος ή δικτύου με προσανατολισμένες ίνες ή τυχαία διατεταγμένες, εγκολλημένες από συγκόλληση, βελόνιασμα ή ραφή. Χρησιμοποιούνται φυσικές ή τεχνητές ίνες, ασυνεχείς ή συνεχείς. Κατασκευάζονται για να παρέχουν συγκεκριμένες ιδιότητες όπως απορροφητικότητα, υγροαπωθητικότητα, ανθεκτικότητα, ελαστικότητα, απαλότητα, αντοχή, επιβραδυντικότητα φλόγας, φιλτράρισμα, βακτηριακή προστασία κ.α. (Hu 2008).

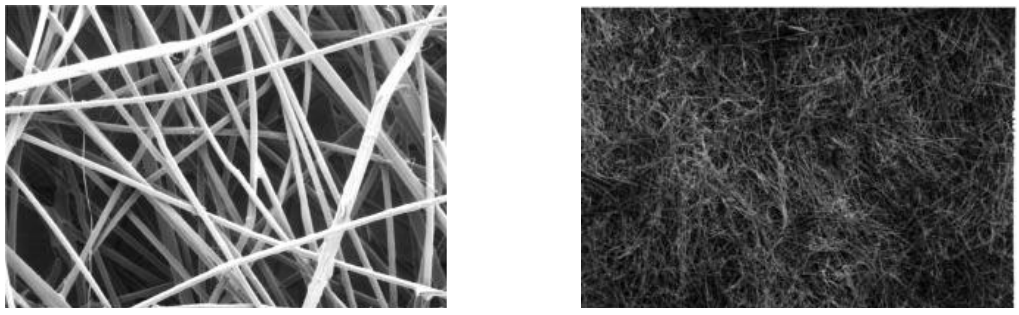

Σχήμα 1-8: Μη-υφάνσιμα υφάσματα (Hsieh).

1.2.4 Τριδιάστατα υφάσματα

Οι τριδιάστατες δομές υφαντών ή πλεκτών αποτελούν γεωμετρίες στις οποίες τα νήματα που κείτονται στο επίπεδο και στην εγκάρσια διεύθυνση συνδέονται για την διαμόρφωση μιας ενιαίας δομής με δομική μονάδα συγκρίσιμων διαστάσεων στις τρεις ορθογώνιες διευθύνσεις. Οι 3Δ κ/υ δομές προσφέρουν ιδιαίτερες ιδιότητες, όπως αντίσταση σε διαστρωματική διάτμηση, μηχανική και θερμική σταθερότητα κατά μήκος των τρισορθογώνιων αξόνων. Η ενιαία δομή τους, όταν χρησιμοποιείται ως ενίσχυση σε σύνθετα υλικά, βελτιώνει την δυσκαμψία και αντοχή στην εγκάρσια διεύθυνση και εμποδίζει τον διαχωρισμό των επίπεδων στρωμάτων, σε αντίθεση με τις διδιάστατες δομές. Λόγω των ιδιοτήτων αυτών καθώς και την παραγωγή τους κοντά στο τελικό προϊόν (near-net-shape), λαμβάνουν ιδιαίτερη προσοχή τα τελευταία χρόνια στην τεχνολογία των σύνθετων προϊόντων. (Hu 2008)

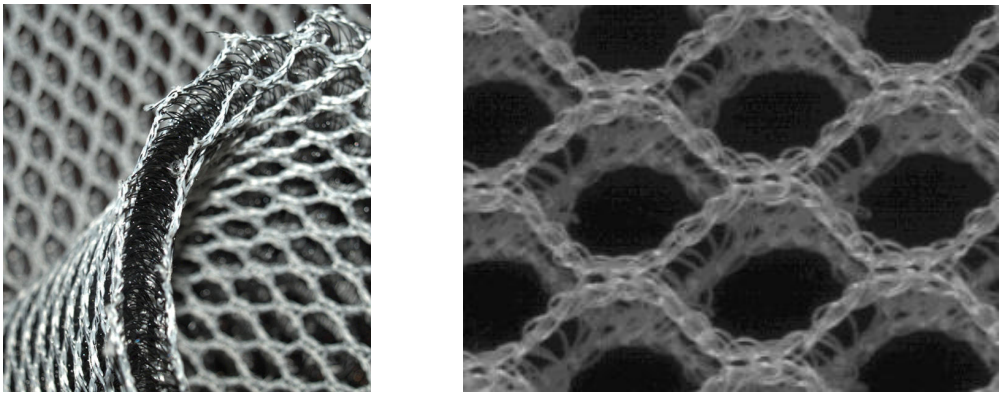

Σχήμα 1-9: Τριδιάστατες δομές στημονοπλεκτών.

1.2.5 Τεχνικές Εφαρμογές των κ/υ δομών

Τα σημαντικά πλεονεκτήματα της διαδικασία παραγωγής κ/υ προϊόντων όσον αφορά την ποικιλία των χρησιμοποιούμενων ινών (πρώτη ύλη), διαστάσεις, μορφή και δομή ήταν καθοριστικά για την εξάπλωση τους σε τεχνικές εφαρμογές. Σήμερα υπάρχει πληθώρα νέων εφαρμογών των ινωδών δομών σε πολλούς βιομηχανικούς και κατασκευαστικούς τομείς, που συνοψίζονται στα ακόλουθα:

Οικοδομικός τομέας: σύνθετα πλαίσια, διασταλτές δομές, πρόστεγα

Δημόσια έργα: σταθεροποίηση εδάφους, αποστράγγιση

Αεροπορική βιομηχανία: έλικες από σύνθετα υλικά, πλαίσια αεροσκάφους από σύνθετα, αλεξίπτωτα

Ναυπηγική: κύτος από ινώδη σύνθετα, επένδυση hovercraft, σκοινιά

Χερσαίες μεταφορές: ζώνες ασφαλείας, ύφασμα επισώτρων, φίλτρα αέρος, αερόσακοι, καλύμματα καθισμάτων

Συσκευασία: περιτυλίγματα, δίχτυα

Ασφάλεια: στολές, αλεξίσφαιρα, υφάσματα παραλλαγής

Αθλητισμός και ελεύθερος χρόνος: προστατευτικός εξοπλισμός, διαπνέοντα αδιάβροχα.

Ιατρική: χειρουργικά ράμματα, αντιβακτηριακοί επίδεσμοι, ενδύματα παρακολούθησης κυκλοφορικού

Η νέα έννοια της μηχανικής των κ/υ δομών γεννήθηκε κατά την ανάπτυξη των τεχνικών υφασμάτων ως φυσική εξέλιξη της μεθόδου δοκιμής – σφάλματος. Τα εμπορικά διαθέσιμα υφάσματα απέτυχαν σε πολλές περιπτώσεις να ικανοποιήσουν τις προδιαγραφές που τέθηκαν από τους κατασκευαστές οπότε οι μηχανικοί των κ/υ δομών κλήθηκαν να δημιουργήσουν εντελώς νέες δομές (Raz 2000).

1.2.6 Η μηχανική συμπεριφορά των κ/υ δομών

Η γεωμετρική πολυπλοκότητα των νημάτων και κατ' επέκταση των υφασμάτων αποτελεί βασικό εμπόδιο για την ακριβή αναπαράσταση των κ/υ δομών με τα διαθέσιμα υπολογιστικά μέσα. Η γεωμετρική πολυπλοκότητα έχει σαν αποτέλεσμα την σύνθετη παραμόρφωση των κ/υ δομών ακόμα και στις περιπτώσεις απλής φόρτισης. Για παράδειγμα, η παραμόρφωση ενός κλωσμένου νήματος από εφελκυστικό φορτίο αντιστοιχεί στην υπέρθεση κάμψης, εφελκυσμού και συμπίεσης των ελικοειδώς διαμορφωμένων ινών που το συνιστούν. Στον μηχανισμό παραμόρφωσης περιλαμβάνονται ακόμη φαινόμενα επαφής, όπως ανάπτυξη τριβής, ολίσθηση και πλάτυνση των διατομών των ινών, που αυξάνουν την πολυπλοκότητα της ανάλυσης. Ανάλογα, η μηχανική ανάλυση της ακτινικής συμπίεσης και της αξονικής κάμψης του νήματος αντιστοιχούν σε σύνθετες καταπονήσεις. Δεδομένου ότι η παραμόρφωση του υφάσματος προκύπτει από την υπέρθεση του εφελκυσμού και της κάμψης των νημάτων που το συνιστούν καθώς και των αλληλεπιδράσεων αυτών στις επιφάνειες επαφής, η αναμενόμενη πολυπλοκότητα της μηχανικής ανάλυσης είναι προφανώς πολύ υψηλή.

1.3 Μηχανική μοντελοποίηση των κ/υ δομών

1.3.1 Ταξινόμηση των προσεγγίσεων μοντελοποίησης

Το υψηλό επίπεδο δομικής πολυπλοκότητας που προκύπτει από την ιεραρχία ίνα – νήμα – ύφασμα επιφέρει σημαντικές δυσκολίες στην μοντελοποίηση και την μηχανική ανάλυση των κ/υ προϊόντων. Ενδεικτική είναι η απόκλιση που παρουσιάζουν οι διαστάσεις τυπικού μεγέθους υφάσματος (10^{-1} έως 10^{0} m) και των δομικών στοιχείων που το συνιστούν (διάμετρος ίνας, 10^{-5} m). Επομένως η ρεαλιστική απεικόνιση της δομής του υφάσματος, σε επίπεδο απεικόνισης των ινών, για την μακρομηχανική ανάλυση είναι υπολογιστικά αδύνατη. Η δομική ιδιαιτερότητα των υφασμάτων (ίνες και νήματα που συγκρατούνται κυρίως από δυνάμεις τριβής) επιφέρει την αυξημένη ευκαμψία τους. Έτσι η μακρομηχανική συμπεριφορά των υφασμάτων χαρακτηρίζεται από μεγάλες μετατοπίσεις των συνιστωσών ινών ακόμα και σε καταστάσεις χαμηλής φόρτισης.

Η κ/υ κοινότητα αντιμετώπισε την πολυπλοκότητα που συναντάται στην μοντελοποίηση και μηχανική ανάλυση των κ/υ δομών λόγω της δομικής ιεραρχίας υιοθετώντας ανάλογη ιεραρχία στην διαδικασία μοντελοποίησης (Takano et al. 1999, Lomov et al. 2004, Bogdanovich 2006). Μ' αυτόν τον τρόπο αναπτύχθηκαν τρία επίπεδα μοντελοποίησης: η μικρομηχανική μοντελοποίηση των νημάτων, η μεσομηχανική μοντελοποίηση της δομικής μονάδας του υφάσματος και η μακρομηχανική μοντελοποίηση ευρύτερου τμήματος του υφάσματος.

Τις τελευταίες δεκαετίες, διάφορες μέθοδοι υιοθετήθηκαν για την μηχανική ανάλυση των κ/υ δομών. Μια βασική ταξινόμηση, σύμφωνα με την εφαρμοζόμενη μέθοδο, διακρίνει τις αναλυτικές και αριθμητικές ή υπολογιστικές μεθόδους. Προφανώς η επικρατούσα προσέγγιση μηχανικής ανάλυσης στο ευρύτερο πεδίο κατασκευών αποτελούσε την βάση για την υιοθέτηση αντίστοιχων προσεγγίσεων στον κ/υ τομέα.

1.3.2 Αξιολόγηση των αναλυτικών μεθόδων

Η βιβλιογραφική επισκόπηση των αναλυτικών μεθόδων που εφαρμόστηκαν στην μηχανική ανάλυση των κ/υ δομών κατέδειξε την απουσία μιας επιτυχημένης ολοκληρωμένης μεθόδου που θα διασφάλιζε στην πρόβλεψη της μηχανικής συμπεριφοράς του υφάσματος σε μακροσκοπικό επίπεδο από την γνώση των χαρακτηριστικών των ινών και της δομής του υφάσματος. Βασικό μειονέκτημα των αναλυτικών μεθόδων αποτελούν οι πολλαπλές απλοποιητικές παραδοχές που θεωρούνται με σκοπό την μείωση του υπολογιστικού κόστους αλλά επιφέρουν σημαντική μείωση στην ρεαλιστικότητα των αποτελεσμάτων. Για παράδειγμα, η διδιάστατη θεώρηση των μεσομηχανικών μοντέλων των υφασμάτων μειώνει σημαντικά την αξιοπιστία των αποτελεσμάτων. Επιπλέον οι αναλυτικές μέθοδοι στερούνται καθολικότητας και ευελιξίας όσον αφορά το πεδίο εφαρμογής τους. Έτσι μια προσέγγιση που πιθανόν εφαρμόζεται σε συγκεκριμένο πρόβλημα ανάλυσης των κ/υ δομών να αδυνατεί να εφαρμοστεί σε κάποιο άλλο. Ιδιαίτερα στην περίπτωση της μακρομηχανικής ανάλυσης που η υπό εξέταση δομή μπορεί να ποικίλει σε σχήμα και διαστάσεις και η παραμορφωμένη δομή προκύπτει από τριδιάστατη ανάλυση με κάμψη σε πολλά επίπεδα και μεγάλες μετατοπίσεις, είναι αδύνατο να προσεγγιστεί επαρκώς από αναλυτικές μεθόδους.

Ωστόσο η επισκόπηση των αναλυτικών μεθόδων είναι ιδιαίτερα διαφωτιστική για την κατανόηση του μηχανισμού παραμόρφωσης των κ/υ δομών σε μικρο-, μεσο- και μακροσκοπικό επίπεδο. Εξάλλου πολλές από τις παραδοχές που λαμβάνονται στα υπολογιστικά μηχανικά μοντέλα των κ/υ δομών αντλήθηκαν από τις αναλυτικές προσεγγίσεις.

1.3.3 Αξιολόγηση των υπολογιστικών προσεγγίσεων

Η υιοθέτηση υπολογιστικών μεθόδων στην μηχανική των κ/υ δομών φαίνεται καθοριστική για την αντιμετώπιση αντικειμενικών δυσκολιών όπως είναι η τριδιάστατη γεωμετρική

απεικόνιση, οι σύνθετες παραμορφώσεις, οι ιδιαίτερες ιδιότητες των υλικών, τα φαινόμενα επαφής και η ανάλυση μεγάλων μετατοπίσεων.

Τα τελευταία χρόνια έχουν σημειωθεί σημαντικά βήματα στην υιοθέτηση υπολογιστικών μοντέλων για την μηχανική ανάλυση των κ/υ δομών. Έτσι έχουν αναπτυχθεί μοντέλα που εστιάζουν στην μικρο-, μεσο- ή μακρο-μηχανική ανάλυση χωριστά. Ιδιαίτερα στο τελευταίο πεδίο έχουν σημειωθεί πολύ ακριβής προσεγγίσεις που επιτυγχάνουν ρεαλιστική απεικόνιση της σύνθετης παραμόρφωσης του υφάσματος (drape) όταν είναι γνωστές (από εργαστηριακές μετρήσεις) οι μηχανικές του ιδιότητες. Επίσης σε μεσομηχανικό επίπεδο έχουν διεξαχθεί έρευνες που εστιάζουν κυρίως στην μηχανική ανάλυση της δομικής μονάδας σύνθετων υλικών σε επίπεδη φόρτιση.

Η αδυναμία που συναντάται στις υπάρχουσες υπολογιστικές μεθόδους αφορά την συνεργασία των διακριτών επιπέδων μοντελοποίησης με σκοπό την ανάπτυξη μιας ολοκληρωμένης μεθόδου σχεδιασμού των κ/υ προϊόντων. Έτσι η μοντελοποίηση της δομής σε μεσοσκοπικό επίπεδο πρέπει να ενσωματώνει την μικροσκοπική απόκριση των νημάτων. Ενώ η μοντελοποίηση της δομής σε μακροσκοπικό επίπεδο πρέπει να ενσωματώνει την μεσοσκοπική απόκριση των δομικών μονάδων και κατ' επέκταση την μικροσκοπική απόκριση των νημάτων. Η σύνδεση επομένως των επιμέρους επιπέδων μηχανικής ανάλυσης είναι δυνατή με κατάλληλη ανάπτυξη των μοντέλων.

1.4 Μια ολοκληρωμένη διαδικασία σχεδιασμού των κ/υ δομών

Η πολυπλοκότητα που συναντάται στην μοντελοποίηση και μηχανική ανάλυση των κ/υ δομών λόγω της δομικής ιεραρχίας αντιμετωπίζεται υιοθετώντας ανάλογη ιεραρχία στην διαδικασία μοντελοποίησης. Μ' αυτόν τον τρόπο αναπτύχθηκαν τρία επίπεδα μοντελοποίησης: η μικρομηχανική μοντελοποίηση των νημάτων, η μεσομηχανική μοντελοποίηση της δομικής μονάδας του υφάσματος και η μακρομηχανική μοντελοποίηση ευρύτερου τμήματος του υφάσματος. Για την μηχανική ανάλυση σε κάθε επίπεδο εφαρμόζεται η μέθοδος των Πεπερασμένων Στοιχείων.

Η μικρομηχανική μοντελοποίηση εστιάζει στην μελέτη των νημάτων στο μικροσκοπικό επίπεδο (επίπεδο ίνας). Για την ανάπτυξη του μηχανικού μοντέλου πολυινικού στριμμένου νήματος θεωρούνται οι ελαστικές και διαστατικές ιδιότητες των ινών και η δομή του ιδανικού νήματος. Σκοπός του τρέχοντος σταδίου είναι ο υπολογισμός των φαινόμενων ιδιοτήτων του νήματος, κυρίως του αξονικού μέτρου ελαστικότητας και της δυσκαμψίας. Για τον υπολογισμό τους πραγματοποιείται η προσομοίωση των αντίστοιχων δοκιμών.

Η μεσομηχανική μοντελοποίηση εστιάζει στην μελέτη των μηχανικών ιδιοτήτων της δομικής μονάδας του υφάσματος. Στο τρέχον στάδιο μοντελοποίησης παραλείπεται η απεικόνιση των ινών που συνιστούν τα νήματα για την μείωση του υπολογιστικού κόστους και τα νήματα μοντελοποιούνται ως ομογενείς δομές (οι φαινόμενες ιδιότητες τους υπολογίστηκαν στο πρώτο στάδιο). Επομένως η επιτυχής απόδοση των ιδιοτήτων στα μοντελοποιημένα νήματα αποτελεί βασικό παράγοντα για την αξιοπιστία των μεσομηχανικών μοντέλων. Σκοπός της

μεσομηχανικής ανάλυσης είναι ο υπολογισμός της φαινόμενης συμπεριφοράς της δομικής μονάδας του υφάσματος σε εφελκυσμό, διάτμηση και κάμψη από την προσομοίωση των αντίστοιχων δοκιμών.

Η μακρομηχανική ανάλυση εστιάζει στην μηχανική συμπεριφορά μεγάλου τμήματος του υφάσματος σε σύνθετες καταπονήσεις. Για την μείωση του υπολογιστικού κόστους η απεικόνιση της δομικής μονάδας του υφάσματος παραλείπεται και η διακριτή δομή του υφάσματος αντικαθίσταται από συνεχές μοντέλο. Προφανώς η απόδοση των φαινόμενων ιδιοτήτων του διακριτού μοντέλου στο ισοδύναμο συνεχές μοντέλο (μέθοδος ομογενοποίησης) είναι καθοριστική για την αξιοπιστία της μακρομηχανικής ανάλυσης.

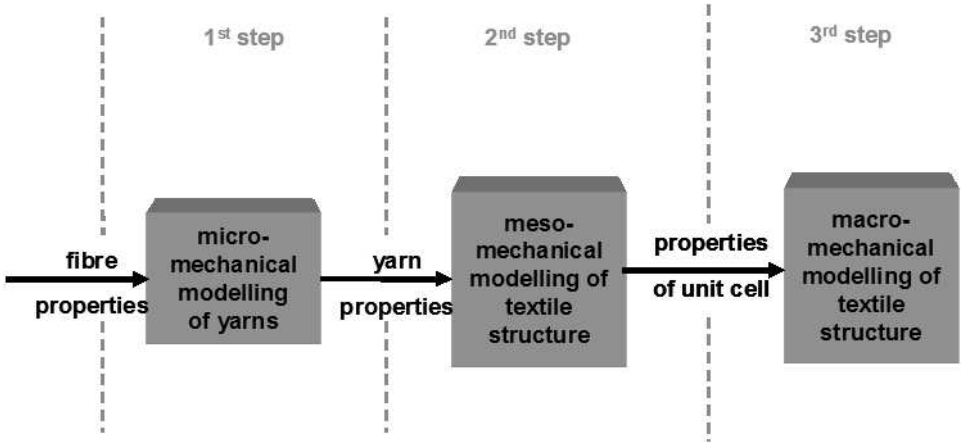

Σχήμα 1-10: Σχηματική απεικόνιση της ολοκληρωμένης διαδικασίας μηχανική ανάλυσης των κ/υ δομών.

Κεφάλαιο 2
Μικρομηχανική Μοντελοποίηση των Νημάτων

Περίληψη

Το δεύτερο κεφάλαιο εστιάζει στο στάδιο της μικρομηχανικής μοντελοποίησης. Μελετήθηκαν σε μικροκλίμακα (σε επίπεδο ίνας) νήματα τυπικής δομής τα οποία συνιστούν το δομικό στοιχείο για την παραγωγή των κ/υ προϊόντων. Για την ανάπτυξη του μηχανικού μοντέλου πολυινικού στριμμένου νήματος θεωρήθηκαν οι ελαστικές και διαστατικές ιδιότητες των ινών και η δομή του ιδανικού νήματος. Για την μοντελοποίηση και μηχανική ανάλυση εφαρμόστηκε η μέθοδος των πεπερασμένων στοιχείων (ΠΣ) με στοιχεία δοκών συζευγμένη με προηγμένους αλγορίθμους επίλυσης για την πρόβλεψη μεγάλων παραμορφώσεων. Η ευχρηστία της προτεινόμενης μεθόδου στην γεωμετρική απεικόνιση και την ανάπτυξη του πλέγματος την καθιστούν κατάλληλη για την αντιμετώπιση των δυσκολιών που απορρέουν από την υψηλή δομική πολυπλοκότητα των μοντέλων των νημάτων (π.χ. νήμα 100 ινών). Σκοπός του τρέχοντος σταδίου είναι ο υπολογισμός των φαινόμενων ιδιοτήτων του νήματος, κυρίως του αξονικού μέτρου ελαστικότητας και της δυσκαμψίας. Για τον υπολογισμό τους πραγματοποιείται η προσομοίωση των αντίστοιχων δοκιμών. Για την αξιολόγηση της προτεινόμενης μεθόδου παράχθηκε εργαστηριακά μια σειρά νημάτων από 2 μέχρι 1200 ίνες, τα οποία υποβλήθηκαν σε δοκιμές εφελκυσμού και κάμψης. Από την σύγκριση των πειραματικών και υπολογιστικών δεδομένων επιβεβαιώθηκε η αξιοπιστία της μοντελοποίησης. Επιπλέον ακολούθησε παραμετρική ανάλυση του μοντέλου του νήματος που αποτυπώνει την επίδραση των κύριων δομικών χαρακτηριστικών των νημάτων στο φαινόμενο μέτρο ελαστικότητας και την δυσκαμψία του νήματος.

2.1 Προτεινόμενη μηχανική μοντελοποίηση πολυινικών στριμμένων νημάτων

Η μηχανική μοντελοποίηση βασίστηκε στην ιδανική δομή του νήματος. Θεωρήθηκε κυκλική εγκάρσια διατομή για την απεικόνιση του νήματος και των ινών που το συνιστούν. Κάθε ίνα ακολουθεί ομοιόμορφη ελικοειδή διαδρομή σταθερής απόστασης από τον κεντρικό άξονα του νήματος. Η απόσταση των διπλανών ινών (ακτινικά και περιφερειακά) μηδενίζεται για την διαμόρφωση της πυκνής διάταξης που φαίνεται στο Σχήμα 2-1.

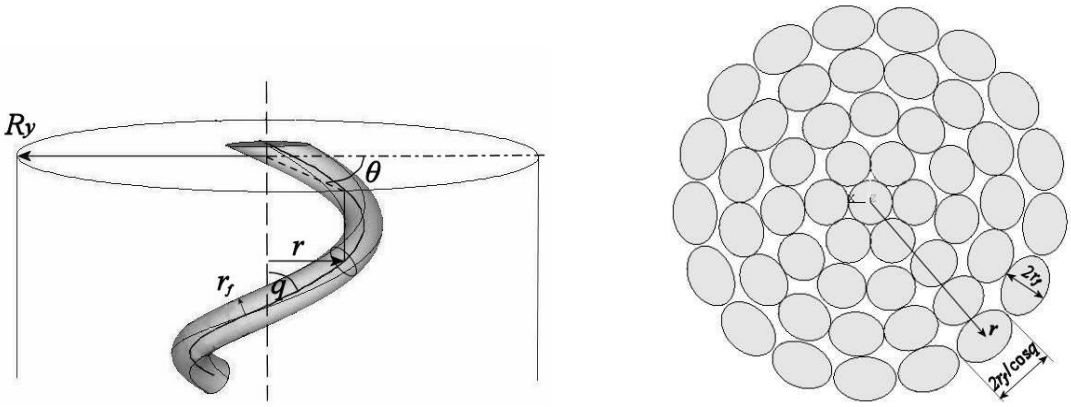

Σχήμα 2-1: Ελικοειδής διαμόρφωση της ίνας στην δομή του νήματος (αριστερά), Εγκάρσια διατομή του πολυινικού στριμμένου νήματος (δεξιά).

Οι δομικές παράμετροι είναι οι ακόλουθες:

r_f : ακτίνα ίνας

t : στροφές έλικας ανά μονάδα μήκους (στρίψη νήματος)

sp : μήκος βήματος της έλικας

r : απόσταση μεταξύ άξονα τυχαίας ίνας και του άξονα του νήματος

R_y : ακτίνα του νήματος

q : γωνία έλικας σε απόσταση r από τον άξονα του νήματος

θ : περιστροφική γωνία έλικας σε απόσταση r από τον άξονα του νήματος

nul : αριθμός των στρώσεων ινών εξωτερικά της κεντρικής ίνας

N : συνολικός αριθμός ινών

Οι βασικές γεωμετρικές σχέσεις που περιγράφουν την ιδανική δομή του νήματος είναι οι εξής:

$$sp=1/t \qquad \text{(Εξ. 2-1)}$$

$$q=\text{atan}(2\pi\cdot r\cdot t) \qquad \text{(Εξ. 2-2)}$$

$$R_y=r_f\cdot(2nul+1) \qquad \text{(Εξ. 2-3)}$$

$$LF(\text{i})=\text{LINT}(2\pi\cdot\text{i}\cdot\cos q) \qquad \text{(Εξ. 2-4)}$$

όπου LF(i) ο αριθμός των ινών που συνιστούν την i στρώση (i=0,1,..,nul) και η συνάρτηση LINT προσεγγίζει στον μικρότερο ακέραιο αριθμό.

Τα μηχανικά χαρακτηριστικά είναι τα εξής:

E : μέτρο ελαστικότητας της ευθύγραμμης ίνας

G : μέτρο διάτμησης της ευθύγραμμης ίνας

E_{eff} : δρώσα τιμή του μέτρου ελαστικότητας του νήματος

B_y: καμπτική δυσκαμψία του νήματος

Για την μηχανική ανάλυση στριμμένων πολυινικών νημάτων εφαρμόστηκε η Μέθοδος των Πεπερασμένων Στοιχείων (ΜΠΣ) με ΠΣ δοκού. Η μοντελοποίηση με ΠΣ δοκού θεωρείται κατάλληλη για τον υπολογισμό των παραμορφώσεων του νήματος δεδομένου ότι επικρατούν η επιμήκυνση και η κάμψη των συνιστωσών ινών. Επιπλέον η μοντελοποίηση με στοιχεία δοκού παρουσιάζει αναμφίβολα πλεονεκτήματα. Όσον αφορά την φάση μοντελοποίησης και πλεγματοποίησης, πρόκειται για εξαιρετικά ταχεία μέθοδο εφόσον απαιτείται μόνο ο καθορισμός των κεντρικών αξόνων των ινών. Ο καθορισμός της ροπής αδράνειας της διατομής της δοκού ως παράμετρο σχεδίασης επιτρέπει την ανάλυση ιδιαίτερων διατομών (ανοιχτές, κοίλες, ακανόνιστης μορφής). Σχετικά με το υπολογιστικό κόστος, τα αναπτυσσόμενα μοντέλα απαιτούν σχετικά χαμηλή υπολογιστική ισχύ, αφού αντιστοιχούν σε σύστημα με μικρό αριθμό βαθμών ελευθερίας (ΒΕ). Για παράδειγμα, μηχανική ανάλυση ενός μοντέλου πολυινικού νήματος 100 ινών και μήκους ίσο με την δομική μονάδα (μια πλήρη περιστροφή της έλικας) απαιτεί 3200 ΠΣ, 3300 κόμβους και 19800 ΒΕ. Στο Σχήμα 2-2 παρουσιάζονται τα πλεγματοποιημένα μοντέλα για νήματα 2, 4, 8, 12, 50 και 1200 ινών. Για την μοντελοποίηση θεωρείται μη-γραμμικό ελαστικό υλικό που αντιστοιχεί την καμπύλη τάσης – παραμόρφωσης του εφελκυσμού των ινών.

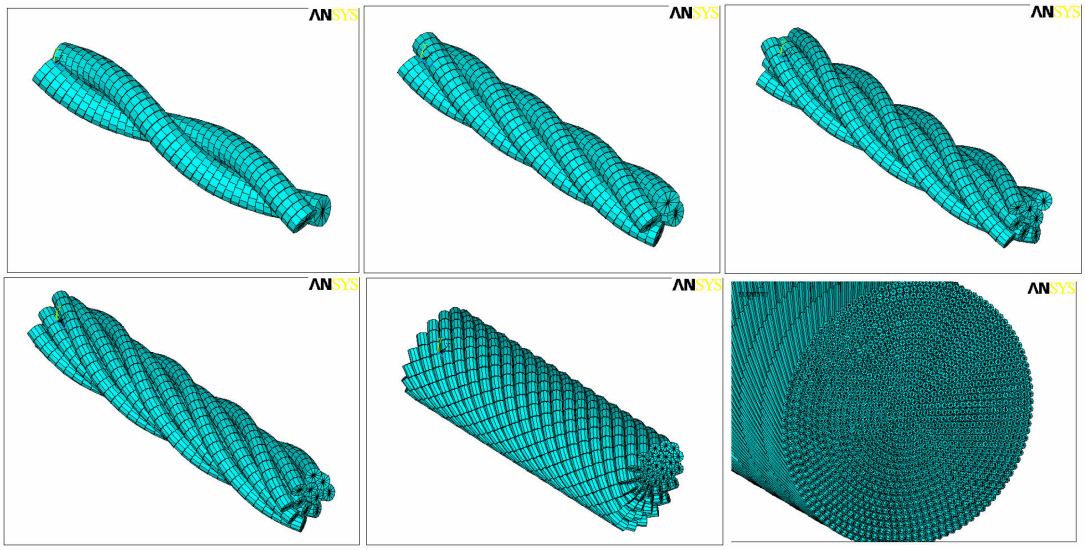

Σχήμα 2-2: Πλεγματοποιημένα μοντέλα για νήματα 2, 4, 8, 12, 50 και 1200 ινών.

Για την ανάπτυξη των μοντέλων των νημάτων που αποτελούνται από 50 και 1200 ίνες, σχεδιάζεται ο άξονας της ευθύγραμμης κεντρικής ίνας και περιφερειακά αναπτύσσονται οι άξονες των εξωτερικών στρώσεων ινών. Η ακτίνα της έλικας για την στρώση i δίνεται από:

$$r(i)=r(i-1)+2r_f \qquad \text{(Εξ. 2-5)}$$

Προφανώς η παρούσα προσέγγιση δεν μπορεί να εφαρμοστεί σε νήματα μικρού αριθμού ινών. Έτσι η ακτίνα της έλικας είναι $r= r_f$ για την περίπτωση του νήματος 2 ινών, ενώ για τις

περιπτώσεις των νημάτων 4, 8 and 12 ινών, που αποτελούνται από 1, 2 και 3 στρώσεις οι ακτίνες είναι:

$$r(1)= r_f/\cos(\pi/4) \quad \text{(Εξ. 2-6)}$$

$$r(2)= r_f(1+\sqrt{3}) \quad \text{(Εξ. 2-7)}$$

$$r(3)= r(1)+r_f \quad \text{(Εξ. 2-8)}$$

Η μοντελοποίηση των νημάτων και η προσομοίωση των δοκιμών εφελκυσμού και κάμψης διεξήχθησαν κάνοντας χρήση του εμπορικού πακέτου ANSYS. Οι προσομοιωμένες παραμορφώσεις έχουν μη-γραμμικό χαρακτήρα λόγω του μη-γραμμικού υλικού και της ανάπτυξης μεγάλων παραμορφώσεων. Για τον λόγο αυτό εφαρμόστηκε ο αλγόριθμος Newton-Raphson για την επίτευξη ταχείας σύγκλισης κατά την επίλυση. Βασικό πλεονέκτημα του αλγορίθμου αποτελεί η ενημέρωση του μητρώου δυσκαμψίας σε κάθε βήμα επανάληψης. Ο έλεγχος του αριθμού επαναλήψεων είναι σημαντικός για την σύγκλιση της διαδικασίας επίλυσης απαιτώντας κατά το δυνατόν χαμηλότερο χρόνο CPU. Η μείωση του αριθμού επαναλήψεων επιτυγχάνεται με ενεργοποίηση δύο επιλογών. Η επιλογή predictor εξάγει την λύση των βαθμών ελευθερίας (BE) χρησιμοποιώντας το προηγούμενο ιστορικό προκειμένου να επιτευχθεί καλύτερη εκτίμηση του επόμενου κύκλου επίλυσης. Η επιλογή line search αποσκοπεί στην βελτίωση της επίλυσης με Newton-Raphson διαβαθμίζοντας το διάνυσμα λύσης με μια αριθμητική τιμή γνωστή ως παράμετρος line search.

2.2 Αναλυτική προσέγγιση

Η προτεινόμενη μέθοδος μοντελοποίησης συγκρίθηκε με την αναλυτική προσέγγιση των Park και Oh (Park, Oh 2006) για την πρόβλεψη της καμπτικής δυσκαμψίας του στριμμένου πολυινικού νήματος. Η επιλογή της δεδομένης αναλυτικής προσέγγισης βασίστηκε σε συγκεκριμένα κριτήρια. Καταρχήν πρόκειται για πρόσφατα παρουσιαζόμενη μέθοδο που εφαρμόζει ρεαλιστικές παραδοχές και διεξοδική μηχανική ανάλυση. Ακόμα παρουσιάζει ευελιξία στην εφαρμογή της όσον αφορά το υλικό των ινών και την δομή του νήματος. Επιπλέον οι ερευνητές σύγκριναν την υπολογιζόμενη τιμή της αδιάστατης καμπτικής δυσκαμψίας με αντίστοιχες τιμές που προέκυψαν από τις αναλυτικές προσεγγίσεις των Zurek, Platt και Owens. Η αδιάστατη καμπτική δυσκαμψία ορίστηκε ως $B_y \cdot \frac{4}{E\pi R_y^4}$ (θεωρώντας την καμπτική δυσκαμψία του ομογενούς νήματος). Τα τέσσερα μοντέλα παρουσίασαν όμοια τάση σχετικά με τις ιδιότητες του υλικού (θεωρήθηκε ο λόγος $K=E/G$) και η στρίψη του νήματος. Η αδιάστατη καμπτική δυσκαμψία υπολογίστηκε για μεγάλο εύρος ιδιοτήτων υλικού και στρίψη νήματος μεταξύ των τιμών 0.25 και 1. Στην πράξη οι καμπύλες που προέκυψαν από την προσέγγιση των Park και Oh αντιστοιχούν σε ενδιάμεση συμπεριφορά. Οπότε η προσέγγισή τους επιλέχθηκε ως αντιπροσωπευτική των αναλυτικών μεθόδων.

Κατά την μέθοδό τους το μέτρο ελαστικότητας E_f μιας ίνας που είναι ενσωματωμένη στην δομή του νήματος είναι:

$$E_f = \frac{E\cos^2 q}{\cos^2 q + \frac{E}{G}\sin^2 q} = \frac{E}{1+K\tan^2 q} \qquad \text{(Εξ. 2-9)}$$

Η ροπή αδράνειας μιας ελικοειδώς διαμορφωμένης ίνας ως προς τον άξονα του νήματος είναι:

$$I_f = (r\sin\theta)^2 \frac{\pi r_f^2}{\cos q} \qquad \text{(Εξ. 2-10)}$$

Έτσι η καμπτική δυσκαμψία μιας ίνας B_f θεωρήθηκε:

$$B_f = E_f I_f = \frac{E(r\sin\theta)^2 \pi r_f^2}{(1+K\tan^2 q)\cos q} \qquad \text{(Εξ. 2-11)}$$

Η καμπτική δυσκαμψία του νήματος υπολογίστηκε ίση με το άθροισμα των καμπτικών δυσκαμψιών των συνιστωσών ινών. Για την απλοποίηση των υπολογισμών προτάθηκε επιπλέον η ολοκλήρωση που δίνεται στην Εξ. 2-12, η οποία εφαρμόζεται όταν η διάμετρος του νήματος είναι πολύ μεγαλύτερη από την διάμετρο των ινών.

$$B_y = \sum B_f = \int_{\theta=0}^{\theta=2\pi}\int_{r=0}^{r=R} \frac{E\pi r_f^2 \cos q (r\sin\theta)^2 r}{\pi r_f^2 \cos q(1+K\tan^2 q)} dr\cdot d\theta = \\ = \frac{E\pi R^4}{4}\cdot\frac{2}{K^2\tan^2 Q}\cdot\left\{K + \frac{1}{\tan^2 Q}\ln\left(\frac{1}{1+K\tan^2 Q}\right)\right\} \qquad \text{(Εξ. 2-12)}$$

όπου $\tan Q = 2\pi R_y t$. Αξιοσημείωτο είναι ότι η καμπτική δυσκαμψία του νήματος προκύπτει ανεξάρτητη από τον αριθμό και την ακτίνα των ινών.

2.3 Πειραματικά δεδομένα

Για την αξιολόγηση της ρεαλιστικότητας της προτεινόμενη μεθόδου παράχθηκε μια σειρά πολυινικών στριμμένων νημάτων από συνεχείς ίνες που επιλέχθηκαν από την αγορά. Τα ονομαστικά χαρακτηριστικά των συνεχών ινών (διάμετρος, βάρος και αντοχή) επιβεβαιώθηκαν πειραματικά και διεξήχθησαν πρόσθετες μετρήσεις. Η χαλάρωση και ο κλιματισμός των ινών προηγήθηκε των μετρήσεων ώστε να απομακρυνθούν οι παραμένουσες παραμορφώσεις που οφείλονται στην μεγάλης διάρκειας συσκευασία των ινών. Για καθεμία από τις επιλεγμένες ίνες πραγματοποιήθηκε η μέτρηση της διαμέτρου, της γραμμικής πυκνότητας καθώς και η ελαστική καμπύλη σε πλήθος 10 δοκιμίων. Οι φυσικές ιδιότητες των ινών δίνονται στον πίνακα που ακολουθεί.

Πίνακας 2-1: Φυσικές ιδιότητες των ινών που συνιστούν τα νήματα.

Διάμετρος (μm)	Γραμμική πυκνότητα (Tex)	Πυκνότητα (kg/mm³)
170	29.5	5.763E-09
110	10.5	1.048E-08
20	0.37	5.455E-08

Για τον ορισμό του υλικού στα υπολογιστικά μοντέλα η μη-γραμμική ελαστικότητα των ινών που προέκυψε από την μέτρηση των 10 δοκιμίων προσεγγίστηκε από τις πολυγραμμικές καμπύλες που παρουσιάζονται στο Σχήμα 2-3.

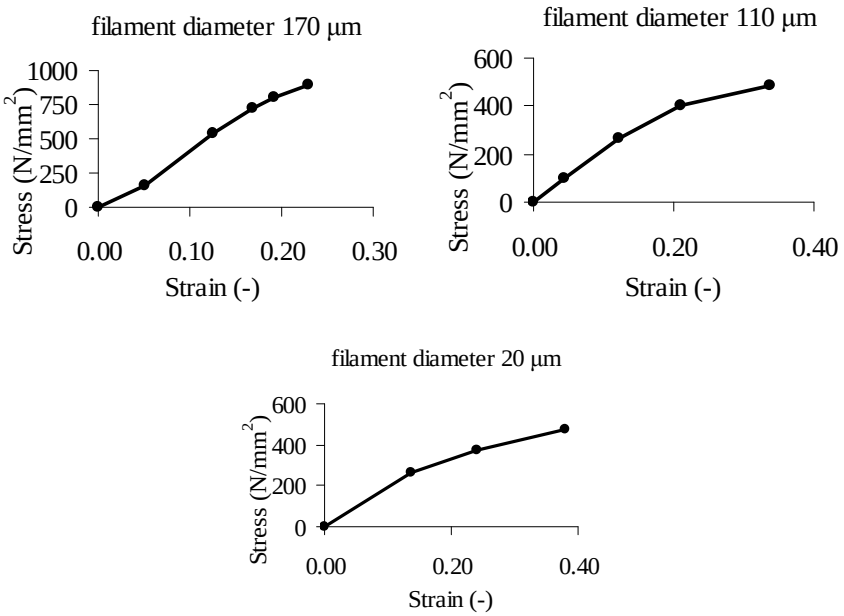

Σχήμα 2-3: Πολύ-γραμμική ελαστική καμπύλη των ινών που συνιστούν τα νήματα.

Για την παραγωγή των δειγμάτων, αυξάνοντας τον αριθμό των ινών του νήματος η διάμετρος των ινών μειωνόταν για ευκολότερο χειρισμό των δειγμάτων. Διευκόλυνε κυρίως την παραγωγή (σταθεροποίηση) και μέτρηση (μετρήσιμο βέλος κάμψης). Παράχθηκαν λοιπόν τρεις σειρές νημάτων: νήματα από 2, 4, 8, 12 ίνες διαμέτρου 170 μm, νήματα από 50 ίνες διαμέτρου 110 μm και νήματα από 1200 ίνες διαμέτρου 20 μm. Η εισαγωγή των στρίψεων επιτεύχθηκε με τη συσκευή Twist Tester D314 της Zweigle. Μετά την εισαγωγή των στρίψεων τα δείγματα απομακρύνθηκαν προσεκτικά από την συσκευή και προσδέθηκαν σε πίνακα ώστε να διατηρήσουν τις στρίψεις τους και να υποβληθούν σε θερμοφιξάρισμα για την σταθεροποίησή τους. Για κάθε συνδυασμό αριθμού ινών – διάμετρο ινών εισήχθησαν δύο πυκνότητες στρίψεων. Η ονοματολογία των δειγμάτων αντιστοιχεί σε: διάμετρο ίνας (μm) / αριθμός ινών / πυκνότητα στρίψης νήματος (στροφές/mm). Για κάθε νήμα παράχθηκαν 10 δοκίμια για την μέτρηση των μηχανικών ιδιοτήτων τους. Για τον υπολογισμό της γραμμικής

πυκνότητας των νημάτων χρησιμοποιήθηκαν τα υπολογιστικά μοντέλα. Η συσκευή Tensile Tester της Zweigle χρησιμοποιήθηκε για τον εφελκυσμό των δειγμάτων ενώ η καμπτική δυσκαμψία μετρήθηκε σύμφωνα με την αρχή του προβόλου.

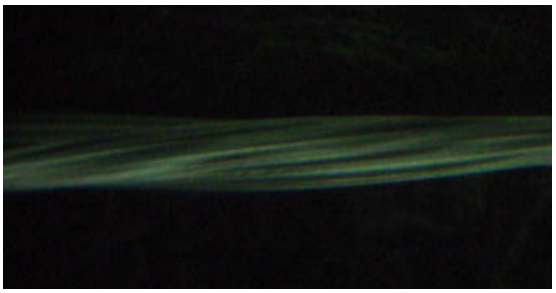

Νήμα 8 ινών

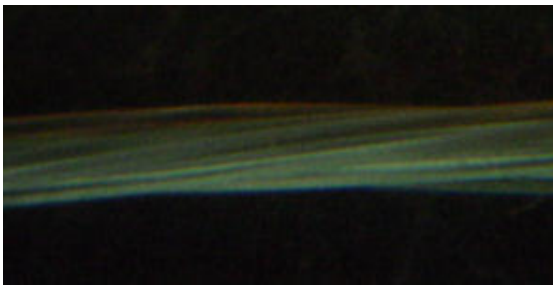

Νήμα 12 ινών

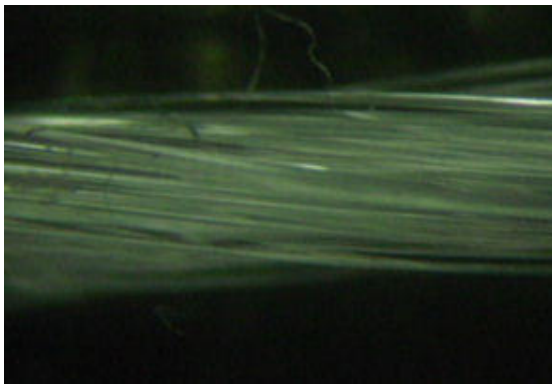

Νήμα 50 ινών

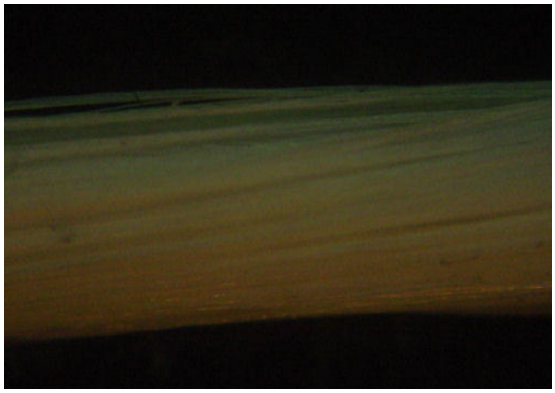

Νήμα 1200 ινών

Σχήμα 2-4: Μικροσκοπική απεικόνιση των νημάτων.

2.4 Αποτελέσματα

2.4.1 Αξιολόγηση των προσεγγίσεων

Η αναλυτική και υπολογιστική προσέγγιση υιοθετήθηκαν για τον υπολογισμό του μέτρου ελαστικότητας και της καμπτικής δυσκαμψίας των νημάτων. Παρόλο που η προσέγγιση των Park και Oh εστιάζει στον υπολογισμό της καμπτικής δυσκαμψίας των νημάτων, είναι δυνατός ο υπολογισμός του μέτρου ελαστικότητας των νημάτων από το μέτρο ελαστικότητας των ελικοειδών νημάτων E_{fi} (i=1…N) θεωρώντας την δρώσα διατομή των ινών (A_i) και του νήματος ($A_{eff} = \sum_{i=1}^{N} A_i = \sum_{i=1}^{N} \frac{\pi r_f^2}{\cos q_i}$).

$$E_{eff} = \frac{\sum_{i=1}^{N} E_{fi} A_i}{A_{eff}} \qquad \text{(Εξ. 2-13)}$$

Για την αναλυτική προσέγγιση θεωρήθηκε η μέση τιμή του μέτρου ελαστικότητας των ινών, δεδομένου ότι η υπολογιστική πολυπλοκότητα αποκλείει την χρήση μη γραμμικών ιδιοτήτων.

Το υπολογιστικό και αναλυτικό μοντέλο προσεγγίζουν ικανοποιητικά την πειραματική καμπύλη του εφελκυσμού των νημάτων (Σχήμα 2-5). Το υπολογιστικό μοντέλο βέβαια προκύπτει πιο ρεαλιστικό λόγω της θεώρησης των μη-γραμμικών ιδιοτήτων των ινών.

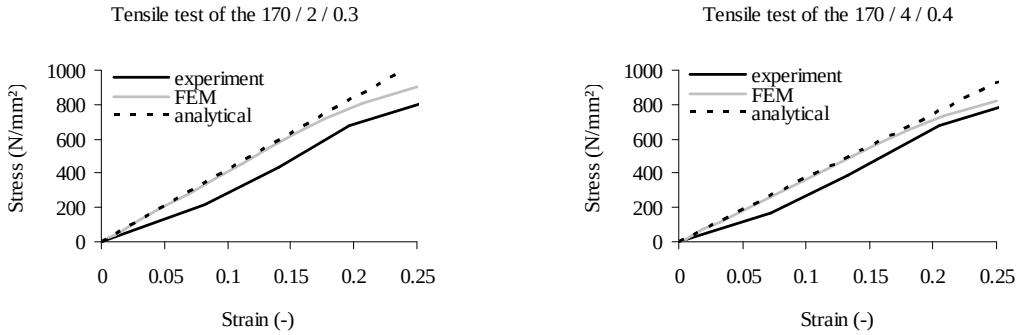

Σχήμα 2-5: Καμπύλες εφελκυσμού των νημάτων που προέκυψαν από το πείραμα και τα μοντέλα.

Η Εξ. 2-12 που προτάθηκε από του Park και Oh χρησιμοποιήθηκε για τον αναλυτικό υπολογισμό της καμπτικής δυσκαμψίας των νημάτων. Η ολοκλήρωση εφαρμόστηκε στα νήματα των 1200 ινών, ενώ η άθροιση εφαρμόστηκε στα νήματα των 2 έως 50 ινών. Η τιμή της καμπτικής δυσκαμψίας όπως προέκυψε από τα μοντέλα, αναλυτικό και υπολογιστικό, και το πείραμα δίνονται στον Πίνακας 2-2. Ικανοποιητική είναι η προσέγγιση των πειραματικών τιμών από το υπολογιστικό μοντέλο. Στην πραγματικότητα η απόκλιση κυμαίνεται μεταξύ των τιμών -28 και +36 %. Οι περιοχή των τιμών της απόκλισης περιορίζει την πιθανότητα ενός συστηματικού σφάλματος που οφείλεται στις θεωρούμενες παραδοχές ή την μέθοδο ανάλυσης. Θα μπορούσε μάλλον να αποδοθεί σε εργαστηριακά σφάλματα κατά την παραγωγή των δειγμάτων και την μέτρησή τους.

Αντίθετα, η αναλυτική προσέγγιση παρουσιάζει σημαντική απόκλιση από τα πειραματικά αποτελέσματα. Είναι ενδιαφέρον ότι για αυξανόμενο αριθμό ινών αυξάνεται η απόκλιση των αναλυτικών αποτελεσμάτων. Ο λόγος των τιμών της καμπτικής δυσκαμψίας που προκύπτει από την αναλυτική προσέγγιση και το πείραμα (*Ban*/*Bexp*) είναι ενδεικτικός για την αποτίμηση της απόκλισης. Επομένως η αναλυτική προσέγγιση είναι επαρκής για την πρόβλεψη της ελαστικής συμπεριφοράς των νημάτων αλλά ανεπαρκής στην καμπτική συμπεριφορά. Προφανώς το σφάλμα εισέρχεται στην παραδοχή της Εξ. 2-11 ($B_f=E_f \cdot I_f$), αφού τα E_f έχουν οριστεί επαρκώς. Πράγματι η Εξ. 2-11 είναι έγκυρη όταν ισχύουν κάποιες συνθήκες όπως η συνέχεια και η ομογένεια των δομών, η σταθερή διατομή της δοκού και η καθετότητα των διατομών στην καμπτόμενη δοκό.

Πίνακας 2-2: Τιμές καμπτικής δυσκαμψίας των νημάτων από το πείραμα και τα μοντέλα.

	Πείραμα	Αναλυτική προσεγ.		ΜΠΣ	
Δομή νήματος	*Bexp* (N·mm²)	*Ban* (N·mm²)	ratio *Ban*/*Bexp*	*Bc* (N·mm²)	ratio *Bc*/*Bexp*
170 / 2 / 0.3	0.233	1.012	4.34	0.261	1.12
171 / 2 / 0.5	0.225	0.931	4.14	0.251	1.12
170 / 4 / 0.2	0.507	2.035	4.02	0.525	1.04
170 / 4 / 0.4	0.454	1.800	3.96	0.498	1.10
170 / 8 / 0.1	0.797	9.726	12.20	1.056	1.33
170 / 8 / 0.15	0.938	9.319	9.93	1.043	1.11
170 / 12 / 0.1	1.157	21.351	18.45	1.576	1.36
170 / 12 / 0.15	1.490	20.103	13.49	1.548	1.04
110 / 50 / 0.1	0.594	48.557	81.68	0.594	1.00
110 / 50 / 0.16	0.611	46.860	76.65	0.591	0.97
20 / 1200 / 0.1	0.025	38.866	1552.94	0.018	0.72
20 / 1200 / 0.16	0.024	33.662	1385.28	0.018	0.72

2.4.2 Παραμετρική ανάλυση με εφαρμογή της ΜΠΣ

Η προτεινόμενη υπολογιστική μέθοδος εφαρμόστηκε για την μελέτη της επίδρασης της δομής του νήματος στην καμπτική δυσκαμψία του. Για τον σκοπό αυτό αναπτύχθηκε και αναλύθηκε μια σειρά μοντέλων μεταβάλλοντας της τιμή της ακτίνας των συνιστωσών ινών (r_f) , της πυκνότητας στρίψεων (t) και του αριθμού των ινών (N). Το γινόμενο $t \cdot r_f$ θεωρήθηκε καθοριστικό για την ανάλυση δεδομένου ότι για σταθερές τιμές του και σταθερό αριθμό ινών οι αναπτυσσόμενες δομές των νημάτων είναι όμοιες (ανάλογες διαστάσεις). Προφανώς οι όμοιες δομές αντιστοιχούν σε ανάλογη μηχανική συμπεριφορά. Η τιμή του γινομένου $t \cdot r_f$ κυμάνθηκε μεταξύ των τιμών 0 και 0.5, λόγω γεωμετρικών περιορισμών ($0 < 1/t < 2r_f$). Το άθροισμα των τιμών της καμπτικής δυσκαμψίας των συνιστωσών ινών στην ευθύγραμμη διάταξή τους ($B_{fs} = N\frac{E\pi r_f^4}{4}$) θεωρήθηκε ως ποσότητα αναφοράς για τον υπολογισμό της αδιάστατης καμπτικής δυσκαμψίας του νήματος B_y/B_{fs}. Η επίδραση του γινομένου $t \cdot r_f$ στην αδιάστατη καμπτική δυσκαμψία του νήματος B_y/B_{fs} παρουσιάζεται στο Σχήμα 2-6. Οι καμπύλες που δίνονται εφαρμόζονται για νήματα των οποίων οι ίνες παρουσιάζουν γραμμικά ελαστική συμπεριφορά και λόγο Poisson ίσο με 0.3, είναι ωστόσο ενδεικτικές και για άλλες ιδιότητες υλικού.

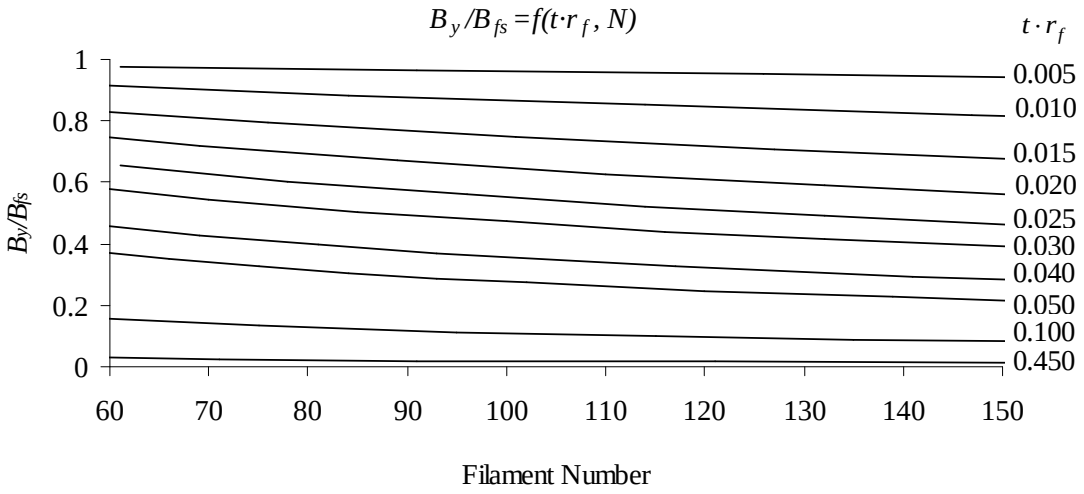

Σχήμα 2-6: Επίδραση του γινομένου $t \cdot r_f$ στην αδιάστατη δυσκαμψία του νήματος B_y/B_{fs} που παράγεται από ίνες γραμμικά ελαστικού υλικού.

Το διάγραμμα που δίνεται στο Σχήμα 2-6 αποδίδει ποσοτικά την επίδραση των χαρακτηριστικών (r_f, t, N, E) του νήματος στην καμπτική δυσκαμψία του. Έτσι η αδιάστατη δυσκαμψία του νήματος αυξάνεται όταν αυξάνεται ο αριθμός των ινών και όταν αυξάνεται το γινόμενο $t \cdot r_f$. Συγκεκριμένα προέκυψαν τα ακόλουθα συμπεράσματα:

- Μείωση του επιπέδου στρίψεων ενός νήματος, που παράγεται από ίνες συγκεκριμένου υλικού και σταθερού αριθμού και διαμέτρου, προκαλεί αύξηση της καμπτικής δυσκαμψίας του νήματος. Το άνω όριο φυσικά είναι η τιμή B_{fs} (άθροισμα των τιμών των καμπτικών δυσκαμψιών των ευθυγραμμισμένων ινών) χωρίς στρίψεις.
- Η αύξηση τα διαμέτρου των ινών για συγκεκριμένο νήμα, συγκεκριμένου υλικού, σταθερού αριθμού ινών και επιπέδου στρίψεων, αυξάνει την καμπτική δυσκαμψία του νήματος. Όπως αναφέρθηκε παραπάνω η αδιάστατη καμπτική δυσκαμψία μειώνεται σε αυτή την περίπτωση, ενώ η τιμή B_{fs} αυξάνεται ως συνάρτηση $4^{ης}$ δύναμης του r_f. Δεδομένου ότι ο ρυθμός μείωσης του B_y/B_{fs} είναι πολύ χαμηλός συγκριτικά με τον ρυθμό αύξησης B_{fs}, η καμπτική δυσκαμψία του νήματος αυξάνεται.
- Η αύξηση του αριθμού των ινών επιφέρει μείωση του B_y/B_{fs} και αύξηση του B_{fs}. Δεδομένου ότι ο ρυθμός μείωσης του B_y/B_{fs} είναι πολύ χαμηλός συγκριτικά με τον ρυθμό του B_{fs}, η καμπτική δυσκαμψία του νήματος αυξάνεται.

2.5 Συμπεράσματα

Για την μηχανική ανάλυση του πολυινικού στριμμένου νήματος προτάθηκε μια υπολογιστική προσέγγιση βασισμένη στην ΜΠΣ με στοιχεία δοκού. Η προτεινόμενη προσέγγιση παρουσιάζει σημαντικά πλεονεκτήματα στην μοντελοποίηση και την ανάλυση. Όσον αφορά την γεωμετρική απεικόνιση και τις ιδιότητες υλικού, προσφέρει ταχύτατο και ευέλικτο

σχεδιασμό. Επιπλέον η υιοθέτηση του αλγορίθμου επίλυσης Newton-Raphson υποστηρίζει την μη-γραμμική ανάλυση μεγάλων μετατοπίσεων. Η αξιολόγηση της ρεαλιστικότητας προτεινόμενης μεθόδου βασίστηκε σε πειραματικά δεδομένα. Παράχθηκε μια σειρά πολυινικών στριμμένων νημάτων από 2 έως 1200 ίνες, τα οποία υποβλήθηκαν σε δοκιμή εφελκυσμού και κάμψης. Η σύγκριση των πειραματικών τιμών των μηχανικών παραμέτρων των νημάτων και των αντίστοιχων τιμών που προέκυψαν από την προσομοίωση επιβεβαίωσαν την ρεαλιστικότητα της μεθόδου. Επιπλέον η προτεινόμενη μέθοδος εφαρμόστηκε για την παραμετρική ανάλυση της μηχανική συμπεριφοράς των νημάτων. Η επίδραση των χαρακτηριστικών των νημάτων (δομικές παράμετροι και μέτρο ελαστικότητας) παρουσιάστηκε ποσοτικά σε διάγραμμα.

Κεφάλαιο 3
Μεσομηχανική Μοντελοποίηση Υφασμάτων

Abstract

Στο τρίτο κεφάλαιο παρουσιάζεται το στάδιο της μεσομηχανικής μοντελοποίησης που εστιάζει στην μελέτη των μηχανικών ιδιοτήτων της δομικής μονάδας του υφάσματος. Στο τρέχον στάδιο μοντελοποίησης παραλήφθηκε η απεικόνιση των ινών που συνιστούν τα νήματα για την μείωση του υπολογιστικού κόστους και τα νήματα μοντελοποιήθηκαν ως ομογενείς δομές (οι φαινόμενες ιδιότητες τους υπολογίστηκαν στο πρώτο στάδιο). Επομένως η επιτυχής απόδοση των ιδιοτήτων στα μοντελοποιημένα νήματα αποτελεί βασικό παράγοντα για την αξιοπιστία των μεσομηχανικών μοντέλων. Επιπλέον η αλληλεπίδραση των νημάτων που συνιστούν την δομή του υφάσματος είναι καθοριστική για την δομική σταθερότητα του υφάσματος κατά την υποβολή του σε μηχανικά φορτία. Τρεις προσεγγίσεις, η μοντελοποίηση με ογκικά ΠΣ, ΠΣ κελύφους και ΠΣ δοκού, αναπτύχθηκαν για την μεσομηχανική ανάλυση της δομικής μονάδας του απλού υφαντού. Από την σύγκριση των προσεγγίσεων, η μοντελοποίηση με ΠΣ κελύφους αποδείχθηκε καταλληλότερη με πολλά σημεία υπεροχής, κυριότερο των οποίων είναι η επιτυχής απόδοση των φαινόμενων ιδιοτήτων στα ομογενοποιημένα νήματα. Σκοπός της μεσομηχανικής ανάλυσης είναι ο υπολογισμός της φαινόμενης συμπεριφοράς της δομικής μονάδας του υφάσματος σε εφελκυσμό, διάτμηση και κάμψη από την προσομοίωση των αντίστοιχων δοκιμών. Μελετήθηκε επίσης η γεωμετρία των βασικότερων δομών υφαντών και πλεκτών υφασμάτων και αναπτύχθηκαν τα αντίστοιχα μοντέλα. Ιδιαίτερα για τα μοντέλα των πλεκτών υφασμάτων από βαμβακερά νήματα αναπτύχθηκε μεθοδολογία σχεδιασμού που στηρίζεται στο ελάχιστο μήκος νήματος θηλιάς και επιβεβαιώθηκε από εργαστηριακά αποτελέσματα.

3.1 Γεωμετρική απεικόνιση της δομής των υφασμάτων

3.1.1 Γεωμετρική απεικόνιση υφαντών δομών

Έχουν διεξαχθεί αρκετές έρευνες που εστίασαν στην γεωμετρική απεικόνιση της δομής του απλού υφαντού. Τα επικρατέστερα αναλυτικά μοντέλα αντιστοιχούν στις πρωτοποριακές έρευνες του Peirce (Peirce 1937), Kawabata (Kawabata 1989), Leaf (Leaf 1979) και Kemp (Kemp 1958). Σήμερα τα αρχικά διδιάστατα αναλυτικά μοντέλα της δομής των υφαντών έχουν εξελιχθεί σε προηγμένα τριδιάστατα υπολογιστικά μοντέλα που περιγράφονται από καμπύλες splines και επιφάνειες NURBS.

3.1.2 Γεωμετρική απεικόνιση πλεκτών δομών υφαδιού

Για τον καθορισμό των γεωμετρικών χαρακτηριστικών τυπικών δομών υφαδοπλεκτών που παράγονται από βαμβακερά νήματα αναπτύχθηκε μια επαναληπτική μέθοδος. Η γενικότητα της προτεινόμενης μεθόδου επιβεβαιώθηκε με την εφαρμογή της σε τρεις δομές πλεκτού, απλό πλεκτό, ριμπ 1×1 και ίντερλοκ. Συνοπτικά η προτεινόμενη γεωμετρική απεικόνιση συνίσταται στην ανάπτυξη των πιθανών γεωμετρικών δομών θεωρώντας τις βασικές σχεδιαστικές παραμέτρους και τελική επιλογή του επικρατέστερου μοντέλου. Το μοντέλο που αντιστοιχεί στο μικρότερο μήκος θηλιάς θεωρείται το μοντέλο ελάχιστης ελαστικής ενέργειας και τελικά επιλέγεται ως το επικρατέστερο. Η παραδοχή αυτή αξιολογήθηκε με μηχανική ανάλυση των πιθανών μοντέλων και η προτεινόμενη μέθοδος αξιολογήθηκε από εργαστηριακά αποτελέσματα.

Απεικόνιση των 3Δ μοντέλων

Οι παράμετροι σχεδίασης της προτεινόμενης μεθόδου αντιστοιχούν στις βασικές δομικές παραμέτρους των πλεκτών δομών: απόσταση σειρών (*c*) απόσταση στηλών (*w*) και πάχος (φαινόμενη διάμετρος) του νήματος (*D*). Οι βασικές παράμετροι και μια (*t*, για το απλό πλεκτό και ριμπ 1×1) ή δύο (*t* και *dh*, για ίντερλοκ) δευτερεύουσες παράμετροι επαρκούν για την ανάπτυξη του μοντέλου (πλήρως ορισμένη γεωμετρία). Το πεδίο τιμών των δευτερευουσών παραμέτρων προκύπτει από τους γεωμετρικούς περιορισμούς της δομικής μονάδας. Τα υπόλοιπα γεωμετρικά χαρακτηριστικά που απαιτούνται για τον πλήρη καθορισμό της δομής προκύπτουν αναλυτικά από τις γεωμετρικές σχέσεις. Η αναπτυσσόμενη γεωμετρία βασίστηκε στην παραδοχή του ιδανικά ελαστικού νήματος. Έτσι τα νήματα απεικονίζονται ως ομογενείς κύλινδροι σταθερής διαμέτρου που παρουσιάζουν σημειακή επαφή μεταξύ τους. Στο Σχήμα 3-1 παρουσιάζονται τα γεωμετρικά μοντέλα της δομικής μονάδας του απλού πλεκτού, του ριμπ 1×1 και του ίντερλοκ. Έχουν σημειωθεί επίσης οι κύριες και δευτερεύουσες παράμετροι.

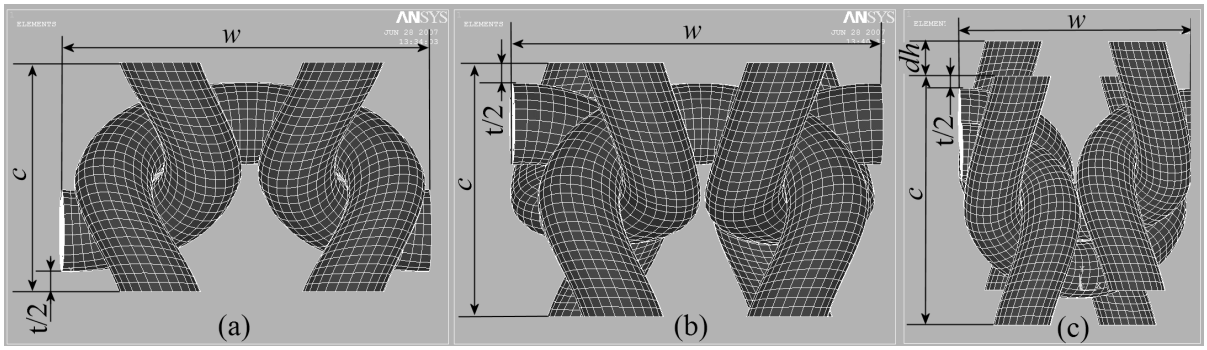

Σχήμα 3-1: Μοντέλα της δομικής μονάδας (α) απλού πλεκτού , (β) ριμπ 1×1, (γ) ίντερλοκ.

Για την επιλογή του τελικού μοντέλου ακολουθείται μια επαναληπτική υπολογιστική διαδικασία, η οποία συνίσταται στην ανάπτυξη διαφόρων μοντέλων για τις σταθερές τιμές

των κυρίων παραμέτρων και επιλεγόμενες τιμές από το πεδίο τιμών των δευτερευουσών παραμέτρων. Η τιμή της δευτερεύουσας παραμέτρου αυξάνεται βηματικά και για κάθε τιμή που λαμβάνει σχεδιάζεται ο κεντρικός άξονας των νημάτων της δομικής μονάδας και υπολογίζεται το μήκος θηλιάς. Τελικά επιλέγεται το μοντέλο που αντιστοιχεί στο μικρότερο μήκος θηλιάς. Η προτεινόμενη μέθοδος βασίζεται στην θεώρηση της ελαχιστοποίησης της ελαστικής ενέργειας των νημάτων που συνιστούν το ύφασμα που έχει υποστεί χαλάρωση. Θεωρήθηκε λοιπόν ότι κατά την χαλάρωση των υφασμάτων απομακρύνονται από τα νήματα οι παραμένουσες τάσεις (εφελκυστικές) που αναπτύσσονται κατά το πλέξιμο τον δειγμάτων. Η απομάκρυνση των τάσεων συνοδεύεται από την αφαίρεση των εφελκυστικών παραμορφώσεων και ολίσθηση μεταξύ των ινών η οποία οδηγεί σε μείωση που συνολικού μήκος του νήματος αλλά και μετακίνηση των νημάτων για τον σχηματισμό δομών χαμηλότερης ενέργειας.

Υπόθεση ελάχιστης ελαστικής ενέργειας

Η υπόθεση που εφαρμόστηκε για την επιλογή της δομής που αντιστοιχεί στην ελάχιστη ελαστική ενέργεια αποτμήθηκε με την μηχανική ανάλυση των αναπτυσσόμενων δομών. Εξετάστηκε επομένως η σύνδεση του μοντέλου ελάχιστης ενέργειας με το μοντέλο ελάχιστου μήκους θηλιάς. Η αξιολόγηση βασίστηκε στην σύγκριση της ενέργειας που απορροφάται από διάφορες δομές για ίδια παραμόρφωση της δομικής μονάδας. Η προσομοίωση του διαξονικού εφελκυσμού της δομικής μονάδας σε σταθερή παραμόρφωση διεξήχθη για τα επιλεγμένα μοντέλα στο λογισμικό πακέτο ANSYS. Η δομή που απορροφά την υψηλότερη ενέργεια αντιστοιχεί στην δομή ελάχιστης ελαστικής ενέργειας. Για τη προσομοίωση εφαρμόστηκε η ΜΠΣ με ογκικά ΠΣ και φαινόμενα επαφής. Τα νήματα μοντελοποιήθηκαν ως ομογενείς κύλινδροι με εγκάρσια ισότροπες ελαστικές ιδιότητες. Ο ορισμός εγκάρσια ισότροπων ιδιοτήτων εξυπηρετεί την διαφορετική ελαστική συμπεριφορά του νήματος κατά την αξονική και την ακτινική διεύθυνση. Ο ορισμός των οριακών συνθηκών διασφαλίζει δύο απαιτήσεις. Η πρώτη είναι η συμμετρική παραμόρφωση που οφείλεται στην συμμετρία της δομής. Η συνέχεια των παραμορφωμένων δομικών μονάδων που απορρέει από την γειτνίαση τους (περιοδική δομή) επιβάλλεται από την δεύτερη απαίτηση.

Τα μοντέλα που επιλέχθηκαν για την προσομοίωση αναπτύχθηκαν από τις δεδομένες τιμές των κύριων παραμέτρων και τις επιλεγμένες τιμές των δευτερευουσών παραμέτρων που δίνονται στο Σχήμα 3-2. Ο Πίνακας 3-1 παρουσιάζει την απορροφώμενη ενέργεια κατά τον διαξονικό εφελκυσμό για κάθε μοντέλο δομικής μονάδας. Το υψηλότερο ποσό ενέργειας απορροφάται σε κάθε περίπτωση από το μοντέλο ελάχιστου μήκους θηλιάς.

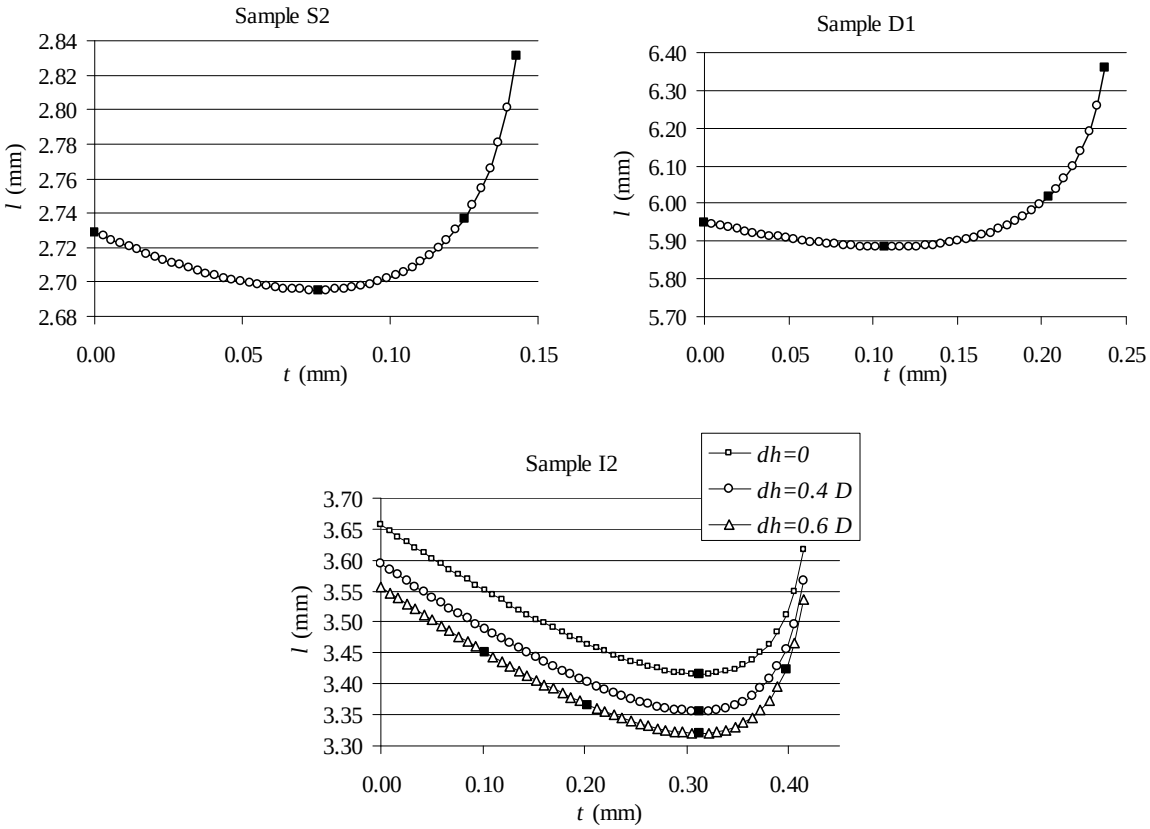

Σχήμα 3-2: Μοντέλα πλεκτών υφαδιού που επιλέχθηκαν για την προσομοίωση του διαξονικού εφελκυσμού.

Πίνακας 3-1: Ενέργεια που απορροφάται κατά τον διαξονικό εφελκυσμό της δομικής μονάδας των επιλεγμένων δομών.

	Μοντέλο	*l* (mm)	Ενέργεια (N/mm)
S2	S2_1	2.729	1.79E-04
	S2_2	**2.695**	**9.37E-04**
	S2_3	2.737	7.98E-04
	S2_4	2.832	3.38E-04
D1	D1_1	5.950	1.98E-04
	D1_2	**5.884**	**8.56E-04**
	D1_3	6.016	6.55E-04
	D1_4	6.361	4.17E-04
I2	I2_1	3.415	1.54E-03
	I2_2	3.355	1.77E-03
	I2_3	**3.321**	**1.96E-03**
	I2_4	3.452	1.40E-03
	I2_5	3.366	6.73E-04
	I2_6	3.423	9.41E-04

Η προτεινόμενη μέθοδος ανάπτυξης των μοντέλων, στη συνέχεια, εφαρμόστηκε σε 12 δείγματα πλεκτών (3 δείγματα ανά δομή) που παρήχθησαν από βαμβακερά νήματα. Οι δομικές παράμετροι των δειγμάτων δίνονται στον Πίνακας 3-2. Η αποτίμηση της μεθόδου βασίστηκε στη σύγκριση των τιμών του μήκους θηλιάς που προέκυψε από εργαστηριακή μέτρηση από τις αντίστοιχες τιμές των υπολογιστικών μοντέλων. Η μέση τιμή του απόλυτου σφάλματος αποτελεί ένδειξη της ακρίβειας των γεωμετρικών μοντέλων.

Πίνακας 3-2: Αξιολόγηση της προτεινόμενης μεσομηχανικής μοντελοποίησης πλεκτών υφαδιού.

δείγμα	τύπος υφάσματος	1/*c* (σειρές /cm)	1/*w* (στήλες /cm)	*C*×*W* (θηλιές /cm²)	*d* (mm)	μετρού-μενο μήκος θηλιάς (mm)	υπολογι-σμένο μήκος θηλιάς (mm)	Απόλυτη τιμή σφάλματος (%)
S1	απλό πλεκτό	16.29	10.35	168.6	0.241	3.473	3.288	5.33
S2		19.40	11.98	232.4	0.185	2.795	2.695	3.58
S3		20.30	14.01	284.4	0.177	2.634	2.503	4.97
D1	ριμπ 1×1	14.65	10.00	146.5	0.220	5.824	5.885	1.05
D2		16.32	11.00	179.6	0.227	5.742	5.680	1.08
D3		19.02	10.60	201.6	0.236	5.690	5.505	3.25
I1	ίντερλοκ	10.42	13.60	141.7	0.183	3.904	3.671	5.99
I2		12.65	13.60	172.0	0.184	3.368	3.321	1.42
I3		15.05	14.80	222.7	0.168	3.121	2.852	8.65
				Μέση τιμή απόλυτου σφάλματος:				3.93

3.2 Μεσομηχανικό μοντέλο του απλού υφαντού

Τρεις προσεγγίσεις, η μοντελοποίηση με ογκικά ΠΣ, ΠΣ κελύφους και ΠΣ δοκού, διερευνήθηκαν ως προς την εφαρμογή τους στην μεσομηχανική ανάλυση του υφάσματος. Οι τρεις προσεγγίσεις αξιολογήθηκαν όσον αφορά την απόδοση των ιδιοτήτων στα μοντελοποιημένα νήματα, την εφαρμογή των οριακών συνθηκών (ΒC), το υπολογιστικό κόστος, την επίτευξη σύγκλισης στην διαδικασία επίλυσης και την ρεαλιστικότητα των αποτελεσμάτων. Η αξιολόγηση των προσεγγίσεων βασίστηκε στην προσομοίωση της δομικής μονάδας σε εφελκυστική παραμόρφωση. Για την μελέτη επιλέχτηκε η απλή ύφανση δεδομένου ότι αντιστοιχεί στην απλούστερη δομή. Ο εφελκυσμός του υφαντού έγκειται στην υπέρθεση παραμόρφωσης εφελκυσμού και κάμψης των συνιστώντων νημάτων καθώς και συμπίεση και ολίσθηση μεταξύ αυτών. Έτσι η εφελκυστική παραμόρφωση της δομικής μονάδας αποτελεί αντιπροσωπευτική δοκιμή για την αξιολόγηση των εφαρμοζόμενων προσεγγίσεων, αφού συνθέτει διαφορετικές παραμορφώσεις νημάτων. Η μοντελοποίηση και προσομοίωση των δοκιμών διεξήχθησαν κάνοντας χρήση του εμπορικού πακέτου ANSYS.

Τα νήματα που συνιστούν την δομή του υπό εξέταση υφαντού θεωρήθηκαν να ακολουθούν την ιδανική δομή του νήματος. Λαμβάνοντας υπόψη τα χαρακτηριστικά των συνεχών ινών και την δομή του πολυινικού στριμμένου νήματος που δίνονται στον Πίνακας 3-3, είναι δυνατός ο υπολογισμός των ιδιοτήτων των νημάτων από την μικρομηχανική ανάλυση αυτών. Το φαινόμενο μέτρο ελαστικότητας και η καμπτική δυσκαμψία του νήματος θεωρήθηκαν επαρκή για την απόδοση της μηχανικής συμπεριφοράς των νημάτων.

Πίνακας 3-3: Δομικές και μηχανικές ιδιότητες των νημάτων που συνιστούν τα υπό εξέταση υφάσματα.

Χαρακτηριστικά νήματος		Ιδιότητες νημάτων που προέκυψαν από την μικρομηχανική μοντελοποίηση	
	Αριθμός ινών	E_{app} (N/mm^2)	B_y (N·mm^2)
R_y=1 mm, E=5000 N/mm^2, ν=0.3, t=0.1 turns/mm	1	5000	3927
	2	2075	454
	12	2454	113
	85	2649	20

Οι παράμετροι που δίνονται στον Πίνακας 3-3 είναι:

R_y : φαινόμενη ακτίνα του νήματος (mm)

E : μέτρο ελαστικότητας των συνεχών ινών (N/mm^2)

ν : λόγος Poisson των συνεχών ινών (-)

t : στρίψη του νήματος (στρίψεις/mm)

E_{app} : φαινόμενο μέτρο ελαστικότητας του νήματος (N/mm^2)

B_y : καμπτική δυσκαμψία του νήματος (N·mm^2)

Τα πλεονεκτήματα και οι αδυναμίες των υπό εξέταση μεθόδων μοντελοποίησης κατά την εφαρμογή τους στην μεσομηχανική ανάλυση κ/υ δομών παρουσιάζονται με + και ─ αντίστοιχα στον Πίνακας 3-4.

Πίνακας 3-4: Πλεονεκτήματα και αδυναμίες των υπό εξέταση μεθόδων μοντελοποίησης για την εφαρμογή τους στην μεσομηχανική ανάλυση.

Ειδικά χαρακτηριστικά	Μέθοδος Μοντελοποίησης			
	Ογκικά ΠΣ	ΠΣ κελύφους	ΠΣ δοκού + Link (στα σημεία επαφής)	ΠΣ δοκού + επαφή σημείο-προς-σημείο
Ορισμός μηχανικών ιδιοτήτων				
Ανεξάρτητος ορισμός των ελαστικών και καμπτικών ιδιοτήτων	–	–	+	+
Ανισοτροπική ελαστικότητα (ορθοτροπική, εγκάρσια ισοτροπική)	+	+	–	–
Μη-γραμμική ελαστικότητα (διγραμμική, πολύ-γραμμική)	+	+	+	+
Πλαστικότητα, Ιξωδοελαστικότητα	+	+	+	+
Φαινόμενα επαφής				
Δυνάμεις συμπίεσης μεταξύ των νημάτων	+	+	+	+
Ολίσθηση μεταξύ των νημάτων	+	+	–	+
Πλάτυνση των νημάτων	+	+	–	–
Υπολογιστικό κόστος (1 δομική μονάδα)				
Πλήθος ΠΣ	25920	1712	80	80
Πλήθος κόμβων	29524	4660	84	84
Πλήθος ΒΕ	88572	27960	504	504
Εύκολη εφαρμογή φόρτισης και ΒC	–	–	+	+
Μη-γραμμική επίλυση	+	+	+	+
Επίτευξη σύγκλισης				
Δοκιμή εφελκυσμού	+	–	+	+
Δοκιμή διάτμησης	αυξημένος αριθμός ΒC		Δεν εφαρμό-ζεται	+
Δοκιμή κάμψης	Υπέρογκο πλήθος ΒΕ		+	+
Δοκιμή συμπίεσης	αυξημένος αριθμός ΒC		+	+
Ρεαλιστικότητα παραμορφωμένων μοντέλων	+	–	+	+

Η μοντελοποίηση με ογκικά ΠΣ αποτελεί την ευρέως χρησιμοποιούμενη μέθοδο για την μεσομηχανική ανάλυση των κ/υ δομών. Τα πλεονεκτήματα της μεθόδου σχετίζονται με την εφαρμογή προηγμένων αλγόριθμων επαφής που διατίθενται για τα ογκικά μοντέλα ΠΣ. Έτσι ο υπολογισμός της μεταβαλλόμενης κατάστασης επαφής από απουσία επαφής σε επαφή

(ολίσθηση και προσκόλληση) και της παραμόρφωσης του ζεύγους επαφής λόγω της αναπτυσσόμενης πίεσης (πλάτυνση των διατομών των νημάτων) αυξάνει την ακρίβεια της ανάλυσης. Η λεπτομερής επίλυση της επαφής, ωστόσο, συνεπάγεται υψηλό υπολογιστικό κόστος και εμφάνιση δυσκολιών σύγκλισης κατά την επίλυση. Η μοντελοποίηση με ογκικά ΠΣ μιας δομικής μονάδας απλού υφαντού αντιστοιχεί σε υψηλό υπολογιστικό κόστος, 88572 ΒΕ. Η κυριότερη όμως αδυναμία της μεθόδου έγκειται στην απόδοση των ιδιοτήτων στα μοντελοποιημένα νήματα, δεδομένου ότι είναι αδύνατος ο ανεξάρτητος ορισμός των ελαστικών και καμπτικών χαρακτηριστικών τους.

Η μοντελοποίηση με ΠΣ κελύφους εφαρμόστηκε για την αντιμετώπιση των αδυναμιών που προκύπτουν από την προαναφερθείσα μοντελοποίηση. Η μοντελοποίηση με ΠΣ κελύφους είναι επαρκής στην ανάλυση επαφών, δεδομένου ότι διαθέτει προηγμένους αλγορίθμους επαφής. Επιπλέον παρουσιάζει χαμηλότερο υπολογιστικό κόστος (27960 ΒΕ) συγκρίνοντας με τα ογκικά μοντέλα, αφού απαιτείται μια στρώση ΠΣ περιφερειακά στην διατομή του μοντελοποιημένου νήματος. Ωστόσο κατά την διαδικασία επίλυσης παρουσιάστηκαν δυσεπίλυτες δυσκολίες σύγκλισης, οι οποίες πιθανόν οφείλονται στην δημιουργία πτυχώσεων στα τοιχώματα των μοντέλων. Στην πραγματικότητα η ανάπτυξη των πτυχώσεων και η αυξημένη πλάτυνση των διατομών των νημάτων που παρατηρήθηκε στα μοντέλα είναι μη-ρεαλιστική και οφείλεται στην ανεπιτυχή απόδοση των μηχανικών ιδιοτήτων των νημάτων στα μοντελοποιημένα νήματα. Για το λόγο αυτό η παρούσα μέθοδος μοντελοποίησης απορρίφθηκε ολοκληρωτικά.

Η μοντελοποίηση με ΠΣ δοκού προέκυψε επαρκής για αρκετούς λόγους. Αρχικά η προσφερόμενη δυνατότητα για ξεχωριστό ορισμό του μέτρου ελαστικότητας (E_{app}) και της καμπτικής δυσκαμψίας (B_y) είναι εξαιρετικά προνομιακός για την απόδοση των μηχανικών ιδιοτήτων στα μοντελοποιημένα νήματα. Ουσιαστικά πρόκειται για τον ανεξάρτητο ορισμό της επιφάνειας και της ροπής αδράνειας της διατομής των μοντελοποιημένων νημάτων. Δεύτερον οι κύριες παραμορφώσεις των νημάτων (εφελκυσμός και κάμψη), που απορρέουν από την φόρτιση των υφασμάτων, προβλέπονται επαρκώς από τα ΠΣ δοκού. Επιπλέον πρόκειται για ταχύτατα εφαρμοζόμενη μέθοδο, όσον αφορά την σχεδίαση, την πλεγματοποίηση και την μηχανική ανάλυση με εξαιρετικά χαμηλό υπολογιστικό κόστος (504 ΒΕ). Η αδυναμία της μεθόδου οφείλεται στις απλοποιήσεις για τον υπολογισμό των αλληλεπιδράσεων των νημάτων. Παρόλο που υπολογίζεται η κάθετη και εφαπτόμενη (τριβή) συνιστώσα της δύναμης λόγω επαφής, η πλάτυνση των διατομών παραλείπεται.

Η μοντελοποίηση με ΠΣ δοκού και ογκικά ΠΣ εφαρμόστηκαν για την προσομοίωση της εφελκυστικής παραμόρφωσης της δομικής μονάδας απλού υφαντού. Θεωρήθηκαν τα χαρακτηριστικά των νημάτων που δόθηκαν στον Πίνακας 3-3 και οι ιδιότητες που υπολογίστηκαν από την μικρομηχανική ανάλυση. Στην μοντελοποίηση με ΠΣ δοκού εισήχθησαν το φαινόμενο μέτρο ελαστικότητας (E_{app}), το εμβαδό και η ροπή αδράνειας της διατομής ($I=B_y/E_{app}$). Στην μοντελοποίηση με ογκικά ΠΣ ορίζονται το μέτρο ελαστικότητας και το εμβαδό διατομής των νημάτων. Γι’ αυτό εξετάστηκαν δύο περιπτώσεις. Στην πρώτη περίπτωση προσδόθηκε το φαινόμενο μέτρο ελαστικότητας στα νήματα. Στην δεύτερη

περίπτωση το μέτρο ελαστικότητας [$E_{b1} = 4B_y/(\pi R_y^4) < E_{app}$] υπολογίστηκε θεωρώντας την καμπτική δυσκαμψία των νημάτων και την ομογενή δομή του μοντελοποιημένου νήματος. Οι δύο περιπτώσεις συμπίπτουν όταν πρόκειται για μονοϊνικό νήμα ισότροπου υλικού.

Τα αποτελέσματα των δύο μεθόδων μοντελοποίησης δίνονται στον Πίνακας 3-5. Στην περίπτωση του μονοϊνικού νήματος οι διαφορετικές προσεγγίσεις παρουσιάζουν συμφωνία στα αποτελέσματα. Η αξιοπιστία της μοντελοποίησης με ογκικά ΠΣ ήταν αναμενόμενη σ' αυτήν την περίπτωση δεδομένου ότι προσδόθηκαν τα ακριβή μηχανικά χαρακτηριστικά στα νήματα. Η επιτυχία της μοντελοποίησης με ΠΣ δοκού στην περίπτωση του μονοϊνικού νήματος επιβεβαιώνει την αξιοπιστία της μεθόδου παρά τις απλοποιημένες συνθήκες επαφής. Επομένως η μοναδική αδυναμία που παρουσιάζει η μοντελοποίηση με ΠΣ δοκού έχει ασθενή επίδραση στην ακρίβεια των αποτελεσμάτων.

Η απόκλιση του υπολογιζόμενου μέτρου ελαστικότητας από τις δύο μεθόδους αυξήθηκε αυξάνοντας το πλήθος των ινών που συνιστούν τα νήματα. Η απόδοση των ιδιοτήτων των πολυινικών νημάτων εφαρμόζοντας την μοντελοποίηση με ΠΣ όγκου προέκυψε ανεπαρκής δεδομένου ότι θεωρήθηκε η ελαστική ή καμπτική συμπεριφορά των νημάτων για τον υπολογισμό των ιδιοτήτων τους.

Συμπερασματικά, η μοντελοποίηση με ΠΣ δοκού αποδείχθηκε αξιόπιστη για την μεσομηχανική μοντελοποίηση των κ/υ δομών αφού επιτυγχάνει την υπέρθεση της παραμόρφωσης εφελκυσμού, κάμψης και συμπίεσης των νημάτων κατά την φόρτιση της δομικής μονάδας.

Πίνακας 3-5: Φαινόμενες ελαστικές ιδιότητες της δομικής μονάδας του απλού υφαντού από την μοντελοποίηση με ΠΣ δοκού και ογκικά ΠΣ.

Χαρακτηριστικά νήματος		ιδιότητες δομικής μονάδας			
			ΠΣ δοκού	Ογκικά ΠΣ	
Ry=1 mm, *E*=5000 N/mm^2, *ν*=0.3, *t*=0.1 turns/mm	αριθμός ινών	density=2.5 threads/cm	μέτρο ελαστικότητας (N/νήμα)	μέτρο ελαστικότητας (N/νήμα) με E_{app}	μέτρο ελαστικότητας (N/νήμα) με E_b
	1		7015	6959	6959
	2		1698	2910	806
	12		829	3418	200
	85		217	3698	36

3.3 Μοντελοποίηση των υφαντών δομών με ΠΣ δοκού

Η μοντελοποίηση με ΠΣ δοκού εφαρμόστηκε για την μηχανική ανάλυση της δομικής μονάδας βασικών υφαντών δομών. Επιλέχτηκαν η απλή ύφανση, ύφανση basket, 2/2 twill και 5-satin. Η μηχανική ανάλυση αποσκοπεί στον υπολογισμό των φαινόμενων μηχανικών ιδιοτήτων των δομικών μονάδων για την χρησιμοποίησή τους στην μακρομηχανική ανάλυση (που αναπτύσσεται στο επόμενο κεφάλαιο). Έτσι προσομοιώθηκαν οι δοκιμές εφελκυσμού και διάτμησης κατά το στημόνι και το υφάδι για τον υπολογισμό των αντίστοιχων ιδιοτήτων. Υπολογίστηκε επίσης η καμπτική δυσκαμψία των δομών κατά την κατεύθυνση του υφαδιού και του στημονιού από την προσομοίωση της δοκιμής κάμψης. Για την προσομοίωση της δοκιμής κάμψης απαιτήθηκαν περισσότερες από μια δομικές μονάδες για τον περιορισμό της επίδρασης της στήριξης. Η μοντελοποίηση και προσομοίωση των δοκιμών διεξήχθησαν κάνοντας χρήση του εμπορικού πακέτου ANSYS.

Για τον ορισμό των οριακών συνθηκών (BC) και των περιορισμών (CE) ελήφθησαν υπόψη η συμμετρία και περιοδικότητα των δομικών μονάδων. Η καμπύλη φορτίου – μετατόπισης λαμβάνεται από την εφαρμοζόμενη μετατόπιση και τις αναπτυσσόμενες αντιδράσεις. Το μοντέλο με ΠΣ δοκού, το θεωρούμενο Καρτεσιανό σύστημα συντεταγμένων και η ονομασία των κόμβων για την περιγραφή των CE δίνονται στα αντίστοιχα σχήματα. Η διεύθυνση στημονιού και υφαδιού αντιστοιχεί στον άξονα Z και X. Οι BC, CE και η φόρτιση που εφαρμόζονται για τις προσομοιώσεις δίνονται στους αντίστοιχους πίνακες, όπου με UW(Ni) συμβολίζεται η μετατόπιση του κόμβου Ni κατά τον W άξονα, (W=X,Y,Z). Η ονομασία των κόμβων Ni δίνεται στα σχήματα των μοντέλων. Έτσι στους Πίνακας 3-6, Πίνακας 3-7 και Πίνακας 3-8 δίνονται οι BC και CE για την προσομοίωση του εφελκυσμού, της διάτμησης και της κάμψης αντίστοιχα.

Τα στοιχεία επαφής (point-to-point contact) που αναπτύσσονται σε κάθε δομική μονάδα απεικονίζονται με τους κεντρικούς άξονες των ΠΣ δοκών. Τα στοιχεία επαφής δημιουργούνται μεταξύ των κόμβων των συνορευόντων νημάτων χρησιμοποιώντας μια επαναληπτική διαδικασία που υπολογίζει τη απόσταση των κόμβων. Το διαφορετικό χρώμα που αποδίδεται στην απεικόνιση των στοιχείων επαφής (κόκκινο ή γαλάζιο) δηλώνει τις διαφορετικά ορισμένη αρχική συνθήκη. Οι χρησιμοποιούμενες αρχικές συνθήκες είναι οι εξής:

- όταν, απόσταση κόμβων ≤ διάμετρος νήματος

START=1, το διάκενο είναι αρχικά κλειστό και δεν υπάρχει ολίσθηση (κόκκινα στοιχεία),

- όταν, διάμετρος νήματος < απόσταση κόμβων < 1.2× διάμετρος νήματος

START=3, το διάκενο είναι αρχικά ανοιχτό (γαλάζια στοιχεία).

Δομή απλού υφαντού

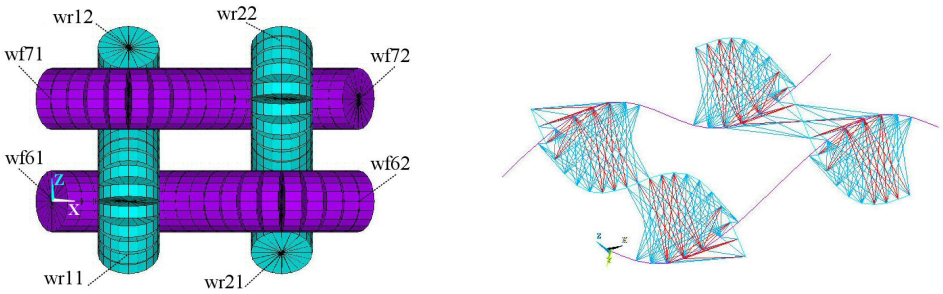

Σχήμα 3-3: Μοντέλο ΠΣ δοκού της δομική μονάδας του απλού υφαντού, ρεαλιστική απεικόνιση (αριστερά), κεντρικοί άξονες και στοιχεία επαφής (δεξιά). [BC εφελκυσμός: Πίνακας 3-6, i=1~2, j=6~7], [BC διάτμηση: Πίνακας 3-7, i=1~2, j=6~7]

Πίνακας 3-6: BC, CE και μετατοπίσεις που εφαρμόζονται για την προσομοίωση της δομικής μονάδας του υφαντού σε εφελκυσμό. {UW(Ni): μετατόπιση του κόμβου Ni κατά τον άξονα W, (W=X,Y,Z)}

Δοκιμή Εφελκυσμού	
Κατά το στημόνι	Κατά το υφάδι
UY(wr i1,wr i2, wf j1,wf j2)=0, i=1…5, j=6…10	UY(wr i1,wr i2, wf j1,wf j2)=0, i=1…5, j=6…10
UZ(wr i1)=-u , i=1…5 UZ(wr i2)=u , i=1…5	UX(wf i1)=-u , i=6…10 UX(wf i2)=u , i=6…10
UX(wf j1)=equal, UX(wf j2)=equal, j=6…10	UZ(wr i1)=equal, UZ(wr i2)=equal, i=1…5
UX(wf j1)=-UX(wf j2), j=6...10	UZ(wr i1)=-UZ(wr i2), i=1…5

Πίνακας 3-7: BC, CE και μετατοπίσεις που εφαρμόζονται για την προσομοίωση της δομικής μονάδας του υφαντού σε διάτμηση.

Δοκιμή διάτμησης	
Κατά το στημόνι	Κατά το υφάδι
UY(wr i1,wr i2, wf j1,wf j2)=0, i=1…5, j=6…10	UY(wr i1,wr i2, wf j1,wf j2)=0, i=1…5, j=6…10
UZ(wf i1)=u UZ(wf i2)=-u	UX(wr i1)=u , i=1…5 UX(wr i1)=-u , i=1…5
UX(wf j1)=equal, UX(wf j2)=equal, j=6…10	UZ(wr i1)=equal, UZ(wr i2)=equal, i=1…5
UX(wf j1)=-UX(wf j2), j=6...10	UZ(wr i1)=-UZ(wr i2), i=1…5
UZ(wr i1)=UZ(wr i2), i=1…5 UX(wr i1)=UX(wr i2), i=1…5	UZ(wf j1)=UZ(wf j2), j=6...10 UX(wf j1)=UX(wf j2), j=6...10

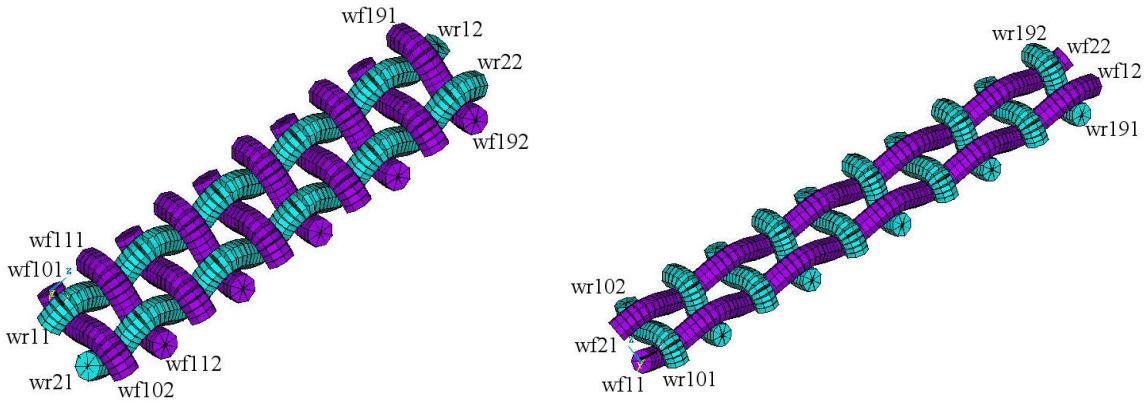

Σχήμα 3-4: Πλέγμα 5 δομικών μονάδων κατά το στημόνι (αριστερά), κατά το υφάδι (δεξιά) της δομής απλού υφαντού. [BC κάμψη κατά στημόνι: Πίνακας 3-8, i=1…2, j=10…19], [BC κάμψη κατά υφάδι: Πίνακας 3-8, j=1…2, i=10…19]

Πίνακας 3-8: BC, CE και μετατοπίσεις που εφαρμόζονται για την προσομοίωση του μοντέλου του υφαντού (5 δομικές μονάδες κατά το στημόνι η το υφάδι) σε δοκιμή κάμψης.

Δοκιμή κάμψης	
Κατά το στημόνι	Κατά το υφάδι
wr i1,i=1…5 fully supported	wf j1, j=1…5 fully supported
UY(wr i2)=u, i=1…5	UY(wf j2)=u, j=1…5
UZ(wf j1)=UZ(wf j2), j=10…34 UY(wf j1)=UY(wf j2), j=10…34	UX(wr i1)=UX(wr i2), i=10…34 UY(wr i1)=UY(wr i2), i=10…34

Δομή Basket

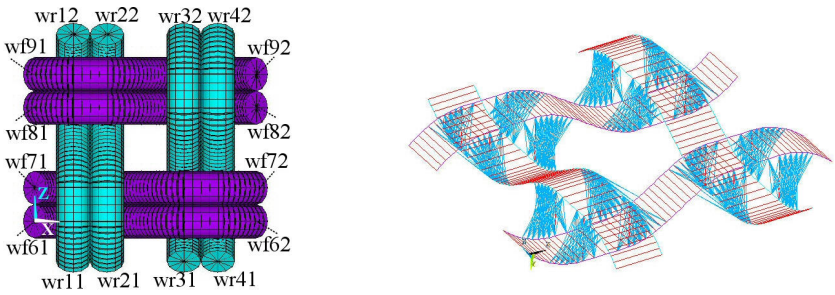

Σχήμα 3-5: Μοντέλο ΠΣ δοκού της δομική μονάδας του basket, ρεαλιστική απεικόνιση (αριστερά), κεντρικοί άξονες και στοιχεία επαφής (δεξιά). [BC εφελκυσμός: Πίνακας 3-6, i=1…4, j=6…9], [BC διάτμηση: Πίνακας 3-7, i=1…4, j=6…9]

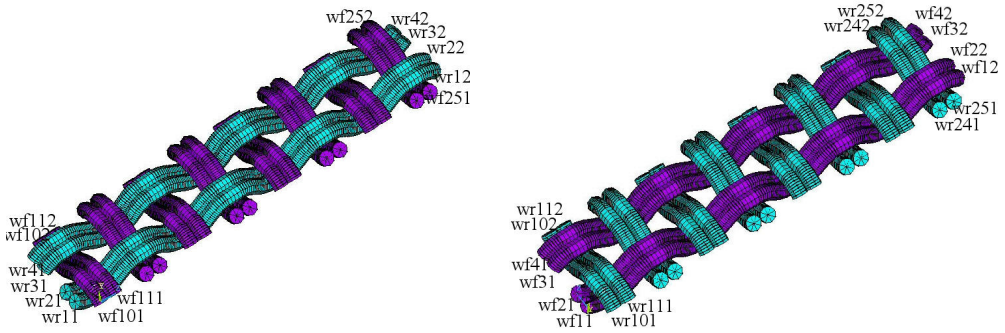

Σχήμα 3-6: Πλέγμα 5 δομικών μονάδων κατά το στημόνι (αριστερά), κατά το υφάδι (δεξιά) της δομής basket. [BC κάμψη κατά στημόνι: Πίνακας 3-8, i=1…4, j=10…25], [BC κάμψη κατά υφάδι: Πίνακας 3-8, j=1…4, i=10…25]

Δομή Twill

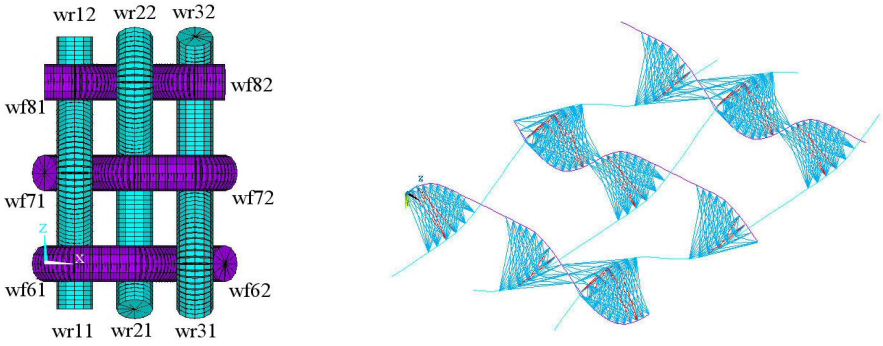

Σχήμα 3-7: Μοντέλο ΠΣ δοκού της δομική μονάδας του twill, ρεαλιστική απεικόνιση (αριστερά), κεντρικοί άξονες και στοιχεία επαφής (δεξιά). [BC εφελκυσμός: Πίνακας 3-6, i=1…3, j=6…8], [BC διάτμηση: Πίνακας 3-7, i=1…3, j=6…8]

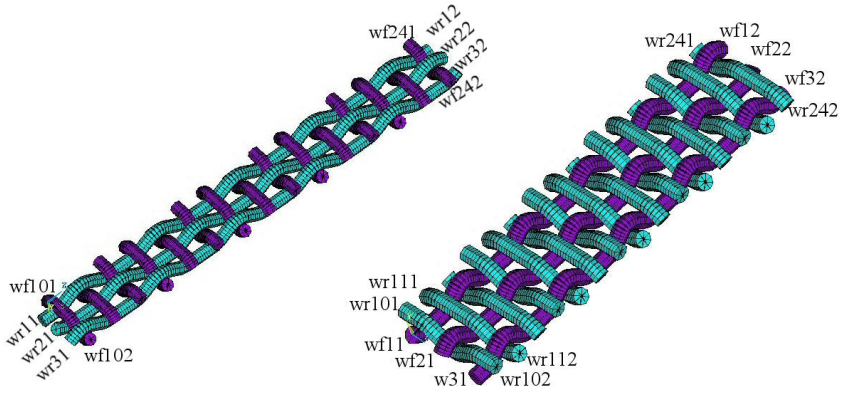

Σχήμα 3-8: Πλέγμα 5 δομικών μονάδων κατά το στημόνι (αριστερά), κατά το υφάδι (δεξιά) της δομής twill. [BC κάμψη κατά στημόνι: Πίνακας 3-8, i=1…3, j=10…24], [BC κάμψη κατά υφάδι: Πίνακας 3-8, j=1…3, i=10…24]

Δομή Satin

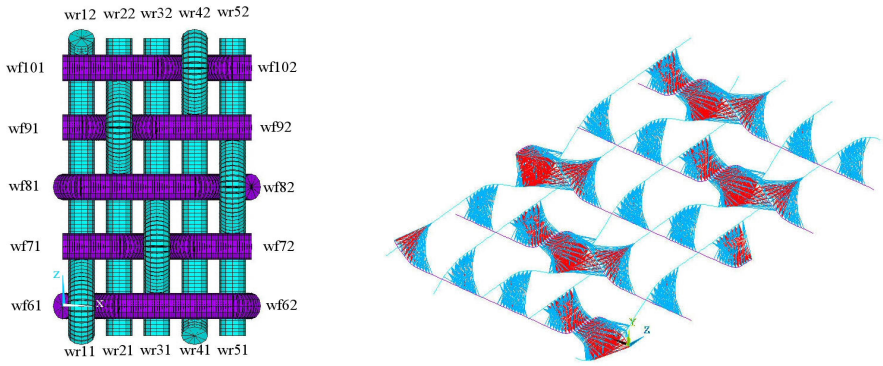

Σχήμα 3-9: Μοντέλο ΠΣ δοκού της δομική μονάδας του satin, ρεαλιστική απεικόνιση (αριστερά), κεντρικοί άξονες και στοιχεία επαφής (δεξιά). [BC εφελκυσμός: Πίνακας 3-6, i=1…5, j=6…10], [BC διάτμηση: Πίνακας 3-7, i=1…5, j=6…10]

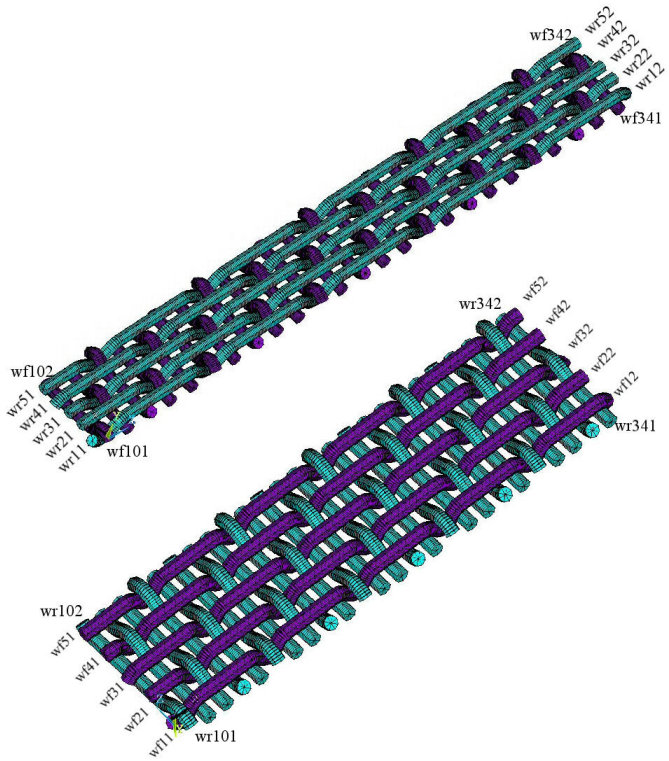

Σχήμα 3-10: Πλέγμα 5 δομικών μονάδων κατά το στημόνι (αριστερά), κατά το υφάδι (δεξιά) της δομής satin. [BC κάμψη κατά στημόνι: Πίνακας 3-8, i=1…5, j=10…34], [BC κάμψη κατά υφάδι: Πίνακας 3-8, j=1…5, i=10…34]

3.4 Μοντελοποίηση πλεκτών δομών με ΠΣ δοκού

Η μοντελοποίηση με ΠΣ δοκού εφαρμόστηκε για την μηχανική ανάλυση της δομικής μονάδας βασικών πλεκτών δομών. Επιλέχτηκαν η απλή πλέξη, πλέξη ριμπ 1×1, και ίντερλοκ. Προσομοιώθηκαν οι δοκιμές εφελκυσμού και διάτμησης κατά τη σειρά και τη στήλη για τον υπολογισμό των αντίστοιχων ιδιοτήτων. Υπολογίστηκε επίσης η καμπτική δυσκαμψία των δομών κατά την κατεύθυνση της σειράς και της στήλης από την προσομοίωση της δοκιμής κάμψης. Η μοντελοποίηση και προσομοίωση των δοκιμών διεξήχθησαν κάνοντας χρήση του εμπορικού πακέτου ANSYS.

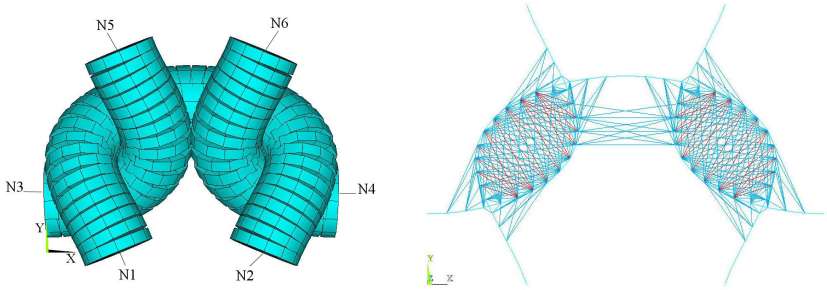

Σχήμα 3-11: Μοντέλο ΠΣ δοκού της δομική μονάδας του απλού πλεκτού, ρεαλιστική απεικόνιση (αριστερά), κεντρικοί άξονες και στοιχεία επαφής (δεξιά).

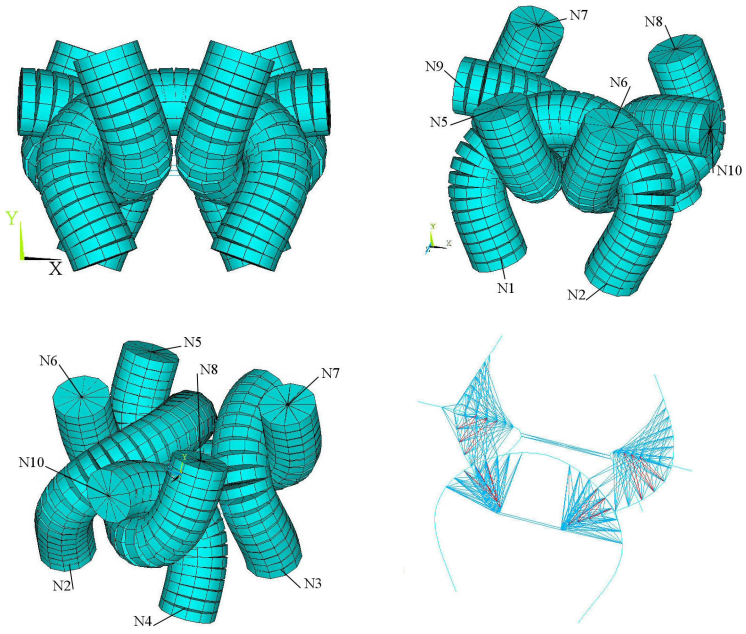

Σχήμα 3-12: Μοντέλο ΠΣ δοκού της δομική μονάδας του ριμπ 1×1, ρεαλιστική απεικόνιση, κεντρικοί άξονες και στοιχεία επαφής.

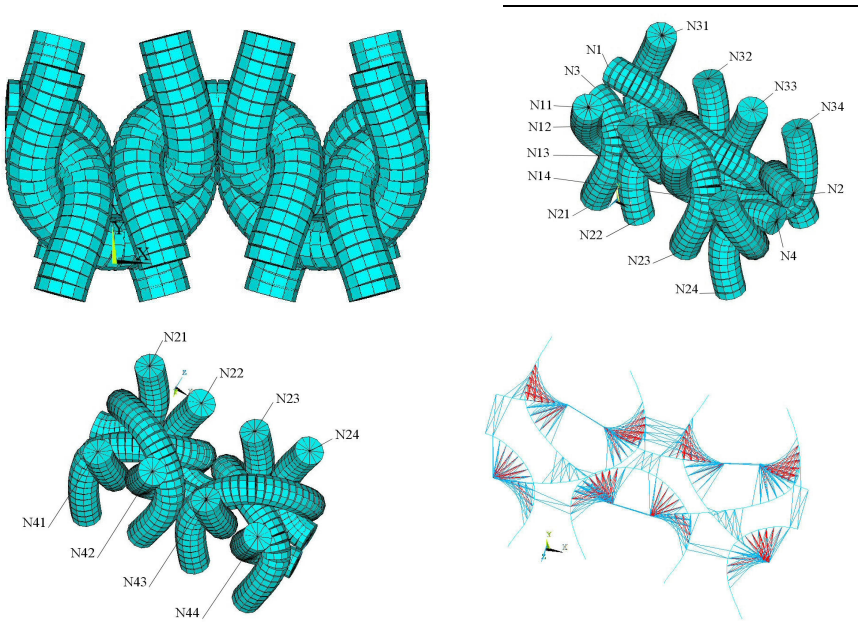

Σχήμα 3-13: Μοντέλο ΠΣ δοκού της δομική μονάδας του ίντερλοκ, ρεαλιστική απεικόνιση, κεντρικοί άξονες και στοιχεία επαφής.

3.5 Συμπεράσματα

Οι τυπικές δομές υφαντών και πλεκτών μελετήθηκαν για την ανάπτυξη των αντίστοιχων γεωμετρικών μοντέλων προκειμένου να χρησιμοποιηθούν στην μεσομηχανική ανάλυση των δομών. Βασική αρχή του παρόντος σταδίου μοντελοποίησης είναι η απεικόνιση των νημάτων ως ομογενείς δομές. Η ασυμπίεστη μορφή των νημάτων θεωρήθηκε για την μοντελοποίηση της δομικής μονάδας στην απαραμόρφωτη κατάσταση. Μ' αυτόν τον τρόπο η διατομή των νημάτων, κάθετα στον άξονα του νήματος, θεωρήθηκε κυκλική σε όλο το μήκος του νήματος. Υπό αυτές τις συνθήκες, η γεωμετρική μοντελοποίηση της δομής του υφάσματος ορίζεται πλήρως από την τριδιάστατη απεικόνιση του κεντρικού άξονα των νημάτων και τον ορισμό της διατομής τους. Τα προηγμένα αριθμητικά σχεδιαστικά εργαλεία που παρέχονται από τα σύγχρονα λογισμικά CAD επιτρέπουν ταχύτατη και εύκολη γεωμετρική απεικόνιση πολύπλοκων δομών.

Ιδιαίτερη μελέτη διεξάχθηκε για την γεωμετρική μοντελοποίηση των πλεκτών δομών. Προτάθηκε μια επαναληπτική μέθοδος για τον υπολογισμό τον γεωμετρικών χαρακτηριστικών τυπικών πλεκτών δομών που παράγονται από βαμβακερά νήματα. Συνοπτικά η προτεινόμενη γεωμετρική απεικόνιση συνίσταται στην ανάπτυξη των πιθανών γεωμετρικών δομών και τελική επιλογή του μοντέλου που αντιστοιχεί στο μικρότερο μήκος θηλιάς. Η αξιολόγηση της αξιοπιστίας της μεθόδου βασίστηκε στη σύγκριση των τιμών του μήκους θηλιάς που προέκυψε από εργαστηριακή μέτρηση από τις αντίστοιχες τιμές των υπολογιστικών μοντέλων.

Τρεις προσεγγίσεις, η μοντελοποίηση με ογκικά ΠΣ, ΠΣ κελύφους και ΠΣ δοκού, διερευνήθηκαν ως προς την εφαρμογή τους στην μεσομηχανική ανάλυση του υφάσματος. Οι τρεις προσεγγίσεις αξιολογήθηκαν όσον αφορά την απόδοση των ιδιοτήτων στα

μοντελοποιημένα νήματα, την εφαρμογή των οριακών συνθηκών (ΒC), το υπολογιστικό κόστος, την επίτευξη σύγκλισης στην διαδικασία επίλυσης και την ρεαλιστικότητα των αποτελεσμάτων. Η μοντελοποίηση με ΠΣ δοκού αποδείχθηκε η καταλληλότερη για την μεσομηχανική μοντελοποίηση των κ/υ δομών αφού επιτυγχάνει την υπέρθεση της παραμόρφωσης εφελκυσμού, κάμψης και συμπίεσης των νημάτων κατά την φόρτιση της δομικής μονάδας.

Η μοντελοποίηση με ΠΣ δοκού εφαρμόστηκε για την μηχανική ανάλυση της δομικής μονάδας τυπικών υφαντών και πλεκτών δομών. Μελετήθηκε η εφαρμογή των οριακών συνθηκών για την προσομοίωση της δομικής μονάδας σε δοκιμές εφελκυσμού, διάτμησης και κάμψης.

Κεφάλαιο 4
Μακρομηχανική Μοντελοποίηση Υφασμάτων

Περίληψη

Στο τέταρτο κεφάλαιο παρουσιάζεται η μακρομηχανική μοντελοποίηση των κ/υ δομών. Η μακρομηχανική ανάλυση εστιάζει στην μηχανική συμπεριφορά μεγάλου τμήματος του υφάσματος σε σύνθετες καταπονήσεις. Για την μείωση του υπολογιστικού κόστους η απεικόνιση της δομικής μονάδας του υφάσματος παραλείπεται και η διακριτή δομή του υφάσματος αντικαθίσταται από συνεχές μοντέλο. Προφανώς η απόδοση των φαινόμενων ιδιοτήτων του διακριτού μοντέλου στο ισοδύναμο συνεχές μοντέλο (μέθοδος ομογενοποίησης) είναι καθοριστική για την αξιοπιστία της μακρομηχανικής ανάλυσης. Αναπτύχθηκαν τρεις προσεγγίσεις που βασίστηκαν σε ΠΣ κελύφους ή όγκου-κελύφους (solid-shell) για την ανάπτυξη συνεχούς μοντέλου ΠΣ που παρουσιάζει ισοδύναμη μηχανική συμπεριφορά με την διακριτή δομή του απλού υφαντού. Η αξιοπιστία των μακρομηχανικών μοντέλων εκτιμήθηκε από πειραματικά αποτελέσματα που ελήφθησαν από βιβλιογραφικές πηγές. Συγκεκριμένα για την υπολογιστική πρόβλεψη της μακρομηχανικής συμπεριφοράς αναπτύχθηκε το μεσομηχανικό μοντέλο της δομικής μονάδας, υπολογίστηκαν οι φαινόμενες ιδιότητες, εφαρμόστηκαν οι μέθοδοι ομογενοποίησης και η προσομοίωση των μηχανικών καταπονήσεων στο συνεχές μακρομηχανικό μοντέλο. Αποτελεί επομένως επιβεβαίωση της ορθότητας των σταδίων μεσο- και μακρο-μηχανικής μοντελοποίησης.

4.1 Εφαρμογή της μεθόδου ομογενοποίησης στη δομή του απλού υφαντού

Η προτεινόμενη μέθοδος ομογενοποίησης εφαρμόστηκε για την μακρομηχανική ανάλυση του απλού υφαντού. Οι παραδοχές μοντελοποίησης και η μηχανική ανάλυση της δομικής μονάδας για τον υπολογισμό των φαινόμενων ιδιοτήτων παρουσιάστηκαν στο προηγούμενο κεφάλαιο. Από την δοκιμή εφελκυσμού, διάτμησης και κάμψης υπολογίζονται οι μηχανικές παράμετροι.

Ονοματολογία:

p_1	: απόσταση στημονιών της ύφανσης (mm)
p_2	: απόσταση υφαδιών της ύφανσης (mm)
B_{rp}	: καμπτική δυσκαμψία 5 δομικών μονάδων τοποθετημένες κατά το στημόνι, καμπτική ροπή γύρω από το υφάδι (N·mm²/νήμα)
B_{ft}	: καμπτική δυσκαμψία 5 δομικών μονάδων τοποθετημένες κατά το υφάδι,

καμπτική ροπή γύρω από το στημόνι (N·mm²/νήμα)

E_{rp} : μέτρο ελαστικότητας της δομικής μονάδας κατά το στημόνι (N/νήμα)

E_{ft} : μέτρο ελαστικότητας της δομικής μονάδας κατά το υφάδι (N/νήμα)

G_{rp} : μέτρο διάτμησης της δομικής μονάδας κατά το στημόνι (N/νήμα)

G_{ft} : μέτρο διάτμησης της δομικής μονάδας κατά το υφάδι (N/νήμα)

ν_{rp} : λόγος Poisson της δομικής μονάδας κατά το στημόνι

ν_{ft} : λόγος Poisson της δομικής μονάδας κατά το υφάδι

E_{iz} : elastic modulus of the layer *i* along *Z* - warp (N/mm^2)

E_{ix} : elastic modulus of the layer *i* along *X* - weft (N/mm^2)

G_{ixz} : μέτρο διάτμησης *XZ* του στρώματος *i* (N/mm^2)

G_{izx} : μέτρο διάτμησης *ZX* του στρώματος *i* (N/mm^2)

ν_{ixz} : λόγος Poisson *XZ* του στρώματος *i* (N/mm^2)

ν_{izx} : λόγος Poisson *ZX* του στρώματος *i* (N/mm^2)

th_i : πάχος του στρώματος *i*

i (δείκτης) : *M*, 1, 2 για μονοστρωματικό, στρώμα 1, στρώμα 2 αντιστοίχως

Επομένως το συνεχές μοντέλο πάχους th_M και μηχανικών παραμέτρων E_{Mx}, E_{Mz}, G_{Mxz}, G_{Mzx}, ν_{Mxz}, ν_{Mzx} πρέπει να ικανοποιεί το σύστημα εξισώσεων:

$$E_{Mz} = E_{rp} /(p_1 \cdot th_M) \quad \text{(Εξ. 4-1)}$$

$$E_{Mx} = E_{ft} /(p_2 \cdot th_M) \quad \text{(Εξ. 4-2)}$$

$$E_{Mz} = 12 \cdot B_{rp} /(p_1 \cdot th_M^3) \quad \text{(Εξ. 4-3)}$$

$$E_{Mx} = 12 \cdot B_{ft} /(p_2 \cdot th_M^3) \quad \text{(Εξ. 4-4)}$$

$$G_{Mxz} = \frac{G_{rp}}{th_M \cdot p_2} \quad \text{(Εξ. 4-5)}$$

$$G_{Mzx} = \frac{G_{ft}}{th_M \cdot p_1} \quad \text{(Εξ. 4-6)}$$

$$\nu_{Mxz} = \nu_{ft} \quad \text{(Εξ. 4-7)}$$

$$\nu_{Mzx} = \nu_{rp} \quad \text{(Εξ. 4-8)}$$

Το σύστημα των εξισώσεων 4-1, 4-2, 4-3, 4-4 (4 εξισώσεις – 3 άγνωστοι: E_{Mx}, E_{Mz}, th_M) έχει μοναδική λύση όταν ικανοποιείται η Εξ. 4-9, η οποία αντιστοιχεί στην παραδοχή συμμετρικής δομής υφαντού (ίδιο στημόνι και υφάδι σε διαστάσεις και ιδιότητες, ίσες πυκνότητες στημονιών και υφαδιών).

$$B_{rp} / B_{ft} = E_{rp} / E_{ft} \quad \text{(Εξ. 4-9)}$$

Οι διαφορετικές ελαστικές ιδιότητες της δομής του υφαντού κατά το στημόνι και το υφάδι (που εξαρτώνται από τις ιδιότητες των νημάτων και τις πυκνότητες στημονιών και υφαδιών) αποκλείουν την ανάπτυξη μιας συνεχούς ομογενούς δομής ισοδύναμης συμπεριφοράς. Εφαρμόστηκαν διάφορες μέθοδοι για την ανάπτυξη μοντέλου τύπου ελάσματος που να παρουσιάζει ισοδύναμη συμπεριφορά με την ασύμμετρη υφαντή δομή:

α. Μοντέλο από δύο πλέγματα με ΠΣ κελύφους, με συμπίπτοντες κόμβους, που παρουσιάζουν διαφορετικό είδος δυσκαμψίας (ελαστική – καμπτική).

β. Μοντέλο από δύο πλέγματα με ΠΣ κελύφους, με συμπίπτοντες κόμβους, από διαφορετικό υλικό.

γ. Μοντέλο τριών στρωμάτων συμμετρικής διατομής (πλεγματοποίηση με ΠΣ κελύφους, ογκικά ΠΣ ή όγκου-κελύφους ΠΣ).

Για κάθε πλέγμα θεωρήθηκε ορθοτροπικό υλικό ώστε να είναι δυνατός ο ορισμός διαφορετικών ελαστικών ιδιοτήτων κατά την διεύθυνση του στημονιού και του υφαδιού.

4.1.1 Δύο πλέγματα με ΠΣ κελύφους διαφορετικής δυσκαμψίας

Στην πρώτη προσέγγιση χρησιμοποιήθηκαν δύο πλέγματα με ΠΣ κελύφους με συμπίπτοντες κόμβους. Κάθε πλέγμα ξεχωριστά υποστηρίζει την ελαστική και καμπτική συμπεριφορά της δομής. Έτσι το πρώτο πλέγμα (στρώμα 1) παρέχει την ελαστική δυσκαμψία της δομής (ικανοποιώντας τις Εξ. 4-1, 4-2) ενώ το δεύτερο πλέγμα (στρώμα 2) παρέχει την καμπτική δυσκαμψία της δομής (ικανοποιώντας τις Εξ. 4-3, 4-3). Συνεπώς οι μηχανικές παράμετροι E_{Mx}, E_{Mz} που εμφανίζονται στις εξισώσεις της παραμόρφωσης εφελκυσμού και κάμψης λαμβάνουν ανεξάρτητες τιμές (M=1, 2) και το σύστημα των εξισώσεων 4-1, 4-2, 4-3, 4-4 έχει άπειρες λύσεις (4 εξισώσεις – 6 άγνωστοι: E_{1x}, E_{1z}, th_1, E_{2x}, E_{2z}, th_2). Δίνοντας τιμές στα πάχη, οι μηχανικές παράμετροι υπολογίζονται μονοσήμαντα από την επίλυση του συστήματος.

Για κάθε πλέγμα θεωρήθηκε ορθοτροπικό υλικό ώστε να είναι δυνατός ο ορισμός διαφορετικών ελαστικών ιδιοτήτων κατά την διεύθυνση του στημονιού και του υφαδιού. Το παρόν συνεχές μοντέλο παρουσιάζει ισοδύναμη συμπεριφορά σε εφελκυσμό και κάμψη με το διακριτό μοντέλο. Μειονέκτημα της παρούσας προσέγγισης είναι η αποτυχία ανάλυσης σε μεγάλες παραμορφώσεις, οι οποίες είναι βασικές για την μακρομηχανική ανάλυση των εύκαμπτων κ/υ δομών.

4.1.2 Δύο πλέγματα με ΠΣ κελύφους διαφορετικού υλικού

Η δεύτερη προσέγγιση αποτελεί εξέλιξη της πρώτης αποσκοπώντας στην ανάπτυξη του ισοδύναμου μοντέλου που υποστηρίζει επιπλέον την μη-γραμμική ανάλυση μεγάλων παραμορφώσεων. Η παρούσα προσέγγιση συνίσταται στην γένεση δύο πλεγμάτων με ΠΣ κελύφους με συμπίπτοντες κόμβους που παρουσιάζουν διαφορετικές ιδιότητες. Σ’ αυτήν την περίπτωση και τα δύο πλέγματα παρουσιάζουν ελαστική και καμπτική δυσκαμψία. Βασική

απαίτηση για την επιτυχία της προσέγγισης είναι η υπέρθεση των πλεγμάτων να παρουσιάζει ισοδύναμη συμπεριφορά με την διακριτή δομή. Οι ιδιότητες υλικού των πλεγμάτων προκύπτουν από την επίλυση του συστήματος των εξισώσεων:

$$E_{1z} \cdot th_1 + E_{2z} \cdot th_2 = E_{rp} / p_1 \quad \text{(Εξ. 4-10)}$$

$$E_{1x} \cdot th_1 + E_{2x} \cdot th_2 = E_{ft} / p_2 \quad \text{(Εξ. 4-11)}$$

$$E_{1z.} \cdot p_1 \cdot th_1^3 /12 + E_{2z.} \cdot p_1 \cdot th_2^3 /12 = B_{rp} \quad \text{(Εξ. 4-12)}$$

$$E_{1x.} \cdot p_2 \cdot th_1^3 /12 + E_{2x.} \cdot p_2 \cdot th_2^3 /12 = B_{ft} \quad \text{(Εξ. 4-13)}$$

$$G_{1xz} \cdot th_1 + G_{2xz} \cdot th_2 = G_{rp} / p_2 \quad \text{(Εξ. 4-14)}$$

$$G_{1zx} \cdot th_1 + G_{2zx} \cdot th_2 = G_{ft} / p_1 \quad \text{(Εξ. 4-15)}$$

$$\nu_{1xz} = \nu_{2xz} = \nu_{ft} \quad \text{(Εξ. 4-16)}$$

$$\nu_{1zx} = \nu_{2zx} = \nu_{rp} \quad \text{(Εξ. 4-17)}$$

Το σύστημα των εξισώσεων 4-10, 4-11, 4-12, 4-13 έχει άπειρες λύσεις (4 εξισώσεις – 6 άγνωστοι: E_{1x}, E_{1z}, th_1, E_{2x}, E_{2z}, th_2). Δίνοντας τιμές στα πάχη, οι μηχανικές παράμετροι υπολογίζονται μονοσήμαντα από τις εξισώσεις που ακολουθούν.

ΕΠΙΛΥΣΗ ΤΟΥ ΣΥΣΤΗΜΑΤΟΣ

ορίζονται τα th_1, th_2

$$E_{2z} = \left(12 \cdot B_{rp} - th_1^2 \cdot E_{rp}\right) / \left(p_1 \cdot th_2^3 - p_1 \cdot th_1^2 \cdot th_2\right) \quad \text{(Εξ. 4-18)}$$

$$E_{1z} = \frac{1}{th_1}\left(\frac{E_{rp}}{p_1} - E_{2z} \cdot th_2\right) \quad \text{(Εξ. 4-19)}$$

$$E_{2x} = \left(12 \cdot B_{ft} - th_1^2 \cdot E_{ft}\right) / \left(p_2 \cdot th_2^3 - p_2 \cdot th_1^2 \cdot th_2\right) \quad \text{(Εξ. 4-20)}$$

$$E_{1x} = \frac{1}{th_1}\left(\frac{E_{ft}}{p_2} - E_{2x} \cdot th_2\right) \quad \text{(Εξ. 4-21)}$$

Η δυνατότητα μη-γραμμικής ανάλυσης που προσφέρεται από την παρούσα προσέγγιση είναι απαραίτητη για την μακρομηχανική ανάλυση των παραμορφώσεων των υφασμάτων.

4.1.3 3-στρωματική συνεχής δομή (πλέγμα από ΠΣ κελύφους ή όγκου-κελύφους)

Η 3-στρωματική δομή αποτελείται από δύο ορθοτροπικά υλικά και συμμετρική διατομή. Δηλαδή τα εξωτερικά στρώματα παρουσιάζουν ίδιο πάχος και ιδιότητες. Θεωρώντας E_{1x}, E_{1z}, G_{1xz}, G_{1zx}, ν_{1xz}, ν_{1zx} οι μηχανικές ιδιότητες και th_1 το πάχος των εξωτερικών στρωμάτων και E_{2x}, E_{2z}, G_{2xz}, G_{2zx}, ν_{2xz}, ν_{2zx} οι μηχανικές ιδιότητες και th_2 το πάχος του εσωτερικού στρώματος, οι ισοδύναμες ιδιότητες ικανοποιούν το επόμενο σύστημα εξισώσεων:

$$2E_{1z}\cdot th_1 + E_{2z}\cdot th_2 = E_{rp}/p_1 \quad \text{(Εξ. 4-22)}$$

$$2E_{1x}\cdot th_1 + E_{2xt}\cdot th_2 = E_{ft}/p_2 \quad \text{(Εξ. 4-23)}$$

$$2E_{1z}\left(\frac{th_1^{\,3}}{12} + th_1\cdot\frac{(th_1+th_2)^2}{4}\right) + E_{2z}\frac{th_2^{\,3}}{12} = B_{rp}/p_1 \quad \text{(Εξ. 4-24)}$$

$$2E_{1x}\left(\frac{th_1^{\,3}}{12} + th_1\cdot\frac{(th_1+th_2)^2}{4}\right) + E_{2x}\frac{th_2^{\,3}}{12} = B_{ft}/p_2 \quad \text{(Εξ. 4-25)}$$

$$2G_{1xz}\cdot th_1 + G_{2xz}\cdot th_2 = G_{rp}/p_2 \quad \text{(Εξ. 4-26)}$$

$$2G_{1zx}\cdot th_1 + G_{2zx}\cdot th_2 = G_{ft}/p_1 \quad \text{(Εξ. 4-27)}$$

$$\nu_{1xz} = \nu_{2xz} = \nu_{ft} \quad \text{(Εξ. 4-28)}$$

$$\nu_{1zx} = \nu_{2zx} = \nu_{rp} \quad \text{(Εξ. 4-29)}$$

Το σύστημα των εξισώσεων (4-22, 4-23, 4-24, 4-25) έχει άπειρες λύσεις (4 εξισώσεις – 6 άγνωστοι: E_{1x}, E_{1z}, th_1, E_{2x}, E_{2z}, th_2). Δίνοντας τιμές στα πάχη, οι μηχανικές παράμετροι υπολογίζονται μονοσήμαντα από τις εξισώσεις που ακολουθούν.

ΕΠΙΛΥΣΗ ΤΟΥ ΣΥΣΤΗΜΑΤΟΣ

ορίζονται τα th_1, th_2

$$C_A = \frac{th_1^3}{12} + \frac{1}{4}th_1(th_1+th_2)^2 \quad \text{(Εξ. 4-30)}$$

$$C_B = \frac{th_2^3}{12} \quad \text{(Εξ. 4-31)}$$

$$E_{1z} = \frac{1}{2th_1}\left(\frac{E_{rp}}{p_1} - E_{2z}\cdot th_2\right) \quad \text{(Εξ. 4-32)}$$

$$E_{2z} = \frac{C_A\cdot E_{rp} - th_1\cdot B_{rp}}{p_1\left(C_A\cdot th_2 - C_B\cdot th_1\right)} \quad \text{(Εξ. 4-33)}$$

$$E_{1x} = \frac{1}{2th_1}\left(\frac{E_{ft}}{p_2} - E_{2x}\cdot th_2\right) \quad \text{(Εξ. 4-34)}$$

$$E_{2x} = \frac{C_A\cdot E_{ft} - th_1\cdot B_{ft}}{p_2\left(C_A\cdot th_2 - C_B\cdot th_1\right)} \quad \text{(Εξ. 4-35)}$$

4.2 Πειραματική αξιολόγηση της μεθόδου ομογενοποίησης

4.2.1 Περίπτωση 1: Μακρομηχανική ανάλυση της δοκιμής κάμψης

Η αξιοπιστία της προτεινόμενης μεθόδου ομογενοποίησης αξιολογήθηκε κάνοντας χρήση πειραματικών δεδομένων που προέκυψαν από την βιβλιογραφία (Ghosh, Batra & Barker 1990). Επιλέχθηκε μια σειρά δειγμάτων απλού υφαντού που παράχθηκαν από μονοϊνικά

νήματα. Οι ιδιότητες των νημάτων (υλικό, διάμετρος και καμπτική δυσκαμψία) και τα δομικά χαρακτηριστικά των δειγμάτων (πυκνότητα στημονιών και υφαδιών) δόθηκαν από τους συγγραφείς (Πίνακας 4-1). Οι ερευνητές επιπλέον μέτρησαν την καμπτική συμπεριφορά των δειγμάτων στην πειραματική διάταξη Kawabata Evaluation System for fabrics (KES-F). Οι καμπτικές ιδιότητες των δειγμάτων (μακρομηχανική συμπεριφορά) δίνονται στον Πίνακας 4-6.

Πίνακας 4-1: Ιδιότητες των εξεταζόμενων δειγμάτων.

Δείγμα	Απόσταση		Ιδιότητες νημάτων			
	Στημονιών (p_1,mm)	Υφαδιών (p_2,mm)	Είδος	Διάμετρος (D, mm)	Καμπτική δυσκαμψία (B, N·mm²)	Μέτρο ελαστικότητας* (E, N/mm²)
MF2	0.5181	0.5917	nylon 6	0.1975	0.0902	1208.0
MF3	0.5181	0.4975				
MF4	0.4098	0.4167	nylon 6.6	0.1450	0.0363	1672.2
MF5	0.4878	0.4831				
MF6	0.4098	0.4237				

*Το μέτρο ελαστικότητας των ινών Nylon υπολογίστηκε από $E=64\cdot B/(\pi\cdot D^4)$.

Για τον υπολογισμό των φαινόμενων μηχανικών ιδιοτήτων της δομικής μονάδας των δειγμάτων εφαρμόστηκε η μεσομηχανική μοντελοποίηση. Οι φαινόμενες ελαστικές ιδιότητες και ο λόγος Poisson υπολογίστηκαν από τη μη-γραμμική ανάλυση της δομικής μονάδας σε εφελκυσμό για παραμόρφωση 0.1. Τα φαινόμενα μέτρα διάτμησης υπολογίστηκαν από την μη-γραμμική ανάλυση της δομικής μονάδας για γωνία διάτμησης 0.1 ακτίνια. Η καμπτική δυσκαμψία υπολογίστηκε από γραμμική ανάλυση της δοκιμής κάμψης σε μοντέλο 5 δομικών μονάδων και βέλος κάμψης ίσο με το 5 % του μήκους του μοντέλου. Οι τιμές που προέκυψαν δίνονται στον Πίνακας 4-2.

Πίνακας 4-2: Αποτελέσματα από την μεσομηχανική ανάλυση της δομικής μονάδας.

Δείγμα	Μέτρο ελαστικότητας (N/νήμα)		Λόγος Poisson	
	στημόνι (E_{rp})	υφάδι (E_{ft})	στημόνι (ν_{rp})	υφάδι (ν_{ft})
MF2	22.4	19.0	0.288	0.311
MF3	19.8	20.9	0.256	0.238
MF4	15.7	15.3	0.321	0.325
MF5	16.3	16.5	0.369	0.373
MF6	15.9	15.2	0.324	0.326
Δείγμα	Καμπτική δυσκαμψία (N·mm²/νήμα)		Μέτρο διάτμησης (N/νήμα)	
	στημόνι (B_{rp})	υφάδι (B_{ft})	στημόνι G_{rp})	υφάδι (G_{ft})
MF2	8.47E-02	8.33E-02	0.365	0.268
MF3	8.27E-02	8.33E-02	0.319	0.356
MF4	3.39E-02	3.28E-02	0.202	0.196
MF5	3.45E-02	3.45E-02	0.102	0.105
MF6	3.40E-02	3.38E-02	0.183	0.169

Οι μηχανικές ιδιότητες των συνεχών μοντέλων υπολογίστηκαν από την επίλυση του αντίστοιχου συστήματος εξισώσεων δίνοντας τιμές στα πάχη.

Πίνακας 4-3: Ιδιότητες των πλεγμάτων με ΠΣ κελύφους με διαφορετική δυσκαμψία.

Δείγμα	Πλέγμα ΠΣ κελύφους με ελαστική δυσκαμψία				Πλέγμα ΠΣ κελύφους με καμπτική δυσκαμψία			
	th_1 (mm)	E_{1x} (N/mm^2)	E_{1z} (N/mm^2)	G_{1xz} (N/mm^2)	th_2 (mm)	E_{2x} (N/mm^2)	E_{2z} (N/mm^2)	G_{2xz} (N/mm^2)
MF2	0.2	160.6	216.2	3.09	0.2	211.1	245.3	2.58
MF3	0.2	209.7	191.0	3.21	0.2	251.0	239.5	3.44
MF4	0.2	184.1	191.3	2.42	0.2	118.1	124.1	2.39
MF5	0.2	170.3	167.2	1.06	0.2	107.1	106.0	1.08
MF6	0.2	179.9	193.7	2.16	0.2	119.8	124.3	2.07

Πίνακας 4-4: Ιδιότητες των πλεγμάτων με ΠΣ κελύφους διαφορετικού υλικού.

Δείγμα	πλέγμα 1				πλέγμα 2			
	th_1 (mm)	E_{1x} (N/mm^2)	E_{1z} (N/mm^2)	G_{1xz} (N/mm^2)	th_2 (mm)	E_{2x} (N/mm^2)	E_{2z} (N/mm^2)	G_{2xz} (N/mm^2)
MF2	0.14	63.5	142.9	1.60	0.26	84.9	89.3	1.51
MF3	0.14	125.8	99.0	1.60	0.26	95.0	93.6	1.61
MF4	0.15	108.1	117.7	1.60	0.17	106.8	121.2	1.43
MF5	0.15	127.4	123.3	0.70	0.17	83.4	87.9	0.63
MF6	0.15	111.5	129.8	1.30	0.17	136.4	113.3	1.39

Πίνακας 4-5: Ιδιότητες του 3-στρωματικού πλέγματος με ΠΣ κελύφους.

Δείγμα	Εξωτερικά στρώματα				Εσωτερικό στρώμα			
	th_1 (mm)	E_{1x} (N/mm^2)	E_{1z} (N/mm^2)	G_{1xz} (N/mm^2)	th_2 (mm)	E_{2x} (N/mm^2)	E_{2z} (N/mm^2)	G_{2xz} (N/mm^2)
MF2	0.07	160.5	182.4	2.80	0.08	120.6	221.2	2.82
MF3	0.07	188.3	180.9	2.90	0.08	194.8	160.8	2.95
MF4	0.04	230.8	243.4	3.00	0.08	229.4	234.8	3.05
MF5	0.04	208.0	206.3	1.30	0.08	217.6	211.6	1.35
MF6	0.04	236.9	243.1	2.70	0.08	212.9	241.0	2.69

Η μακρομηχανική ανάλυση της δοκιμής κάμψης του υφάσματος προσομοιώθηκε όπως διεξάγεται στην διάταξη KES-F. Σύμφωνα με την δοκιμή, δείγμα διαστάσεων 20 × 1 cm υποβάλλεται σε παραμόρφωση κάμψης κατά την μικρή διάσταση. Το δείγμα συγκρατείται μεταξύ ενός σταθερού κι ενός κινούμενου βραχίονα και κάμπτεται με σταθερό ρυθμό καμπυλότητας K από -2.5 έως 2.5 cm^{-1}. Το ίχνος του κινούμενου βραχίονα στο οριζόντιο επίπεδο x-y περιγράφεται από τις Εξ. 4-36, 4-37. Κατά την δοκιμή καταγράφεται η ροπή κάμψης.

$$x = (1 - \cos K) / K \qquad \text{(Εξ. 4-36)}$$

$$y = \sin K / K \qquad \text{(Εξ. 4-37)}$$

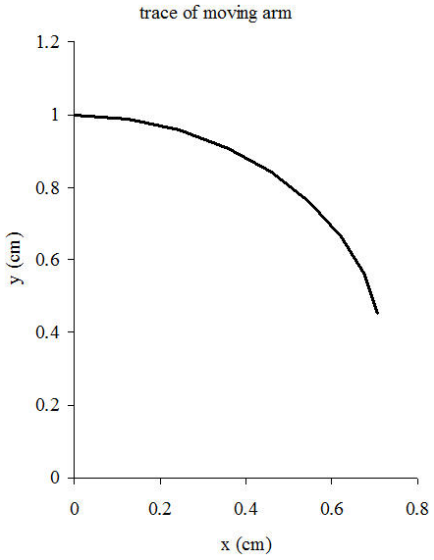

Σχήμα 4-1: Ίχνος του κινούμενου βραχίονα στο οριζόντιο επίπεδο *x*-*y*.

Η προσομοίωση της μακρομηχανικής κάμψης των συνεχών δομών εκτελέστηκε στο λογισμικό ANSYS. Για την μοντελοποίηση θεωρήθηκαν οι πραγματικές διαστάσεις της δρώσας επιφάνειας (20×1 cm) των δειγμάτων. Για την πλεγματοποίηση του μοντέλου χρησιμοποιήθηκαν ΠΣ κελύφους (SHELL63) για το μοντέλο δύο πλεγμάτων διαφορετικού υλικού και ΠΣ κελύφους με στρώματα (SHELL91) για το 3-στρωματικό συνεχές μοντέλο. Στην μια άκρη του μοντέλου εφαρμόστηκαν οριακές συνθήκες πάκτωσης ενώ στο άλλο άκρο εφαρμόστηκε μετατόπιση σύμφωνα με την τροχιά του κινούμενου βραχίονα. Για την επίλυση επιλέχτηκε μη-γραμμική ανάλυση μεγάλων παραμορφώσεων. Στο Σχήμα 4-2 παρουσιάζονται τα παραμορφωμένα μοντέλα σε διάφορες φάσεις κατά την εφαρμογή της μετατόπισης. Υπολογίστηκαν οι καμπύλες ροπής – καμπυλότητας και η καμπτική δυσκαμψία μεταξύ των καμπυλοτήτων 0.5 και 1.5 cm^{-1}.

Η καμπτική δυσκαμψία που προέκυψε από την πειραματική δοκιμή των δειγμάτων δίνεται στον Πίνακας 4-6. Οι αντίστοιχες υπολογιστικές τιμές από την μακρομηχανική ανάλυση και η απόκλιση από τις πειραματικές δίνονται στον Πίνακας 4-7 και Πίνακας 4-8. Οι χαμηλές τιμές της απόκλισης επιβεβαιώνουν την αξιοπιστία της προτεινόμενης μεθόδου ομογενοποίησης για τον υπολογισμό της καμπτικής συμπεριφοράς του υφάσματος.

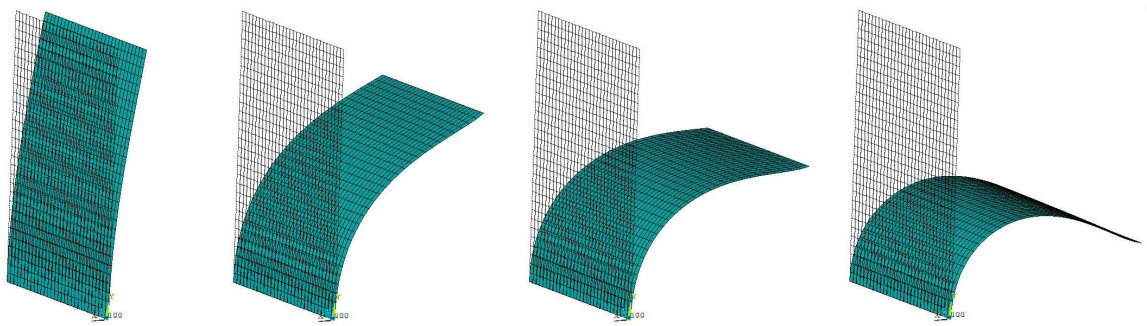

Σχήμα 4-2: Παραμορφωμένο μοντέλο από την δοκιμή κάμψης.

Πίνακας 4-6: Πειραματικά δεδομένα από την δοκιμή κάμψης των δειγμάτων.

Δείγμα	Πειραματική τιμή της καμπτικής δυσκαμψίας (gf·cm²/νήμα)		(N·mm²/νήμα)	
	Στημόνι	Υφάδι	Στημόνι	Υφάδι
MF2	0.112	0.121	0.1098	0.1187
MF3	0.115	0.118	0.1128	0.1157
MF4	0.049	0.050	0.0481	0.0490
MF5	0.043	0.045	0.0422	0.0441
MF6	0.046	0.048	0.0451	0.0471

Πίνακας 4-7: Τιμή της καμπτικής δυσκαμψίας από την μακρομηχανική ανάλυση με δύο πλέγματα με ΠΣ κελύφους διαφορετικού υλικού και απόκλιση από τις πειραματικές τιμές.

Δείγμα	Δύο πλέγματα ΠΣ κελύφους διαφορετικού υλικού Καμπτική δυσκαμψία (N·mm²/νήμα)		Απόκλιση (%)	
	Στημόνι	Υφάδι	Στημόνι	Υφάδι
MF2	0.1044	0.1198	5.17	-0.94
MF3	0.1121	0.1084	0.56	6.73
MF4	0.0448	0.0447	7.35	9.58
MF5	0.0461	0.0458	-8.61	-3.72
MF6	0.0445	0.0459	1.32	2.55

Πίνακας 4-8: Τιμή της καμπτικής δυσκαμψίας από την μακρομηχανική ανάλυση με 3-στρωματικό πλέγμα με ΠΣ κελύφους και απόκλιση από τις πειραματικές τιμές.

Δείγμα	3-στρωματικό πλέγμα Καμπτική δυσκαμψία (N·mm²/νήμα)		Απόκλιση (%)	
	Στημόνι	Υφάδι	Στημόνι	Υφάδι
MF2	0.1105	0.1188	-0.62	-0.14
MF3	0.1090	0.1185	3.43	-2.35
MF4	0.0460	0.0451	4.39	8.63
MF5	0.0473	0.0477	-10.81	-7.39
MF6	0.0465	0.0464	-2.93	1.34

4.2.2 Περίπτωση 2: Μακρομηχανική ανάλυση της δοκιμής εφελκυσμού και διάτμησης

Η προτεινόμενη μέθοδος ομογενοποίησης εφαρμόστηκε επιπλέον για την μακρομηχανική ανάλυση του υφάσματος σε εφελκυσμό και διάτμηση. Η αξιοπιστία της μεθόδου εκτιμήθηκε κάνοντας χρήση πειραματικών δεδομένων που ελήφθησαν από την βιβλιογραφία (Carvelli, Corazza & Poggi 2008). Στην δεδομένη βιβλιογραφική πηγή μελετήθηκε τεχνικό ύφασμα δομής απλού υφαντού που παράχθηκε από μονοϊνικά νήματα. Τα δομικά και μηχανικά χαρακτηριστικά των πολυεστερικών ινών δόθηκαν από τους ερευνητές. Επιπλέον μετρήθηκε η μηχανική συμπεριφορά του δείγματος σε εφελκυσμό και διάτμηση.

Για την μεσομηχανική μοντελοποίηση της δομής θεωρήθηκαν τα χαρακτηριστικά των νημάτων και η δομή του υφάσματος. Για το στημόνι και το υφάδι θεωρήθηκε η ονομαστική τιμή της διαμέτρου των νημάτων D_f = 0.034 mm. Θεωρήθηκαν επίσης τα μέτρα ελαστικότητας E_{warp} = 3800 N/mm² και E_{weft} = 4400 N/mm² για το στημόνι και το υφάδι αντίστοιχα και λόγος Poisson ν=0.2.

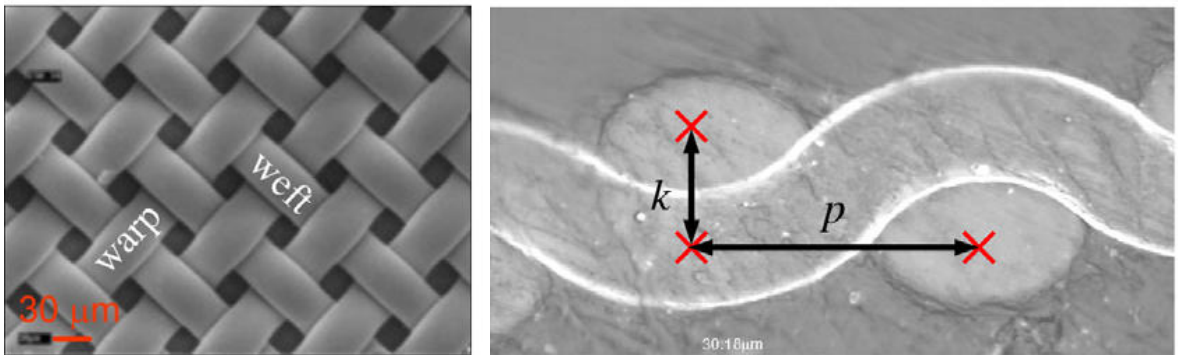

Figure 4-3: Εμπρόσθια όψη και τομή του δείγματος Α. Πηγή: (Carvelli, Corazza & Poggi 2008).

Οι ονομαστικές πυκνότητες στημονιών και υφαδιών (150 νήματα / cm) θεωρήθηκαν για το μεσομηχανικό μοντέλο, οπότε οι αποστάσεις στημονιών και υφαδιών έλαβαν την τιμή p_1=p_2=0.067 mm. Ο συντελεστή τριβής, 0.112, μεταξύ των νημάτων (μετρήθηκε από τον Carvelli) εισάχθηκε στο μοντέλο.

Για την εφαρμογή της επαφής point-to-point θεωρήθηκαν η κάθετη δυσκαμψία KN=2 και η δυσκαμψία προσκόλλησης KS=2. Από την μεσομηχανική ανάλυση υπολογίστηκαν: B_{rp} = 2.17E-04 N·mm²/νήμα, B_{ft} = 2.51E-04 N·mm²/νήμα, E_{rp} = 1.47 N/νήμα, E_{ft} = 1.57 N/νήμα, G_{rp} = 0.076 N/νήμα, G_{ft} = 0.076 N/νήμα, ν_{rp} = 0.166, ν_{ft} = 0.155.

Για την ανάπτυξη του συνεχούς μακρομηχανικού μοντέλου εφαρμόστηκε η μέθοδος ομογενοποίησης με δύο πλέγματα ΠΣ κελύφους από διαφορετικό υλικό. Τα μηχανικά χαρακτηριστικά του συνεχούς μοντέλου προέκυψαν: t_1 = 0.03 mm, t_2 = 0.05 mm, E_{1z} = 334.9 N/mm², E_{1x} = 380.8 N/mm², E_{2z} = 238.8 N/mm², E_{2x} = 300.1 N/mm², G_{1xz} = 14 N/mm², G_{2xz} = 14.19 N/mm², ν_{1xz} = ν_{2xz} = 0.155, ν_{1zx} = ν_{2zx} = 0.166.

Ο μονοαξονικός εφελκυσμός κατά την διεύθυνση του στημονιού και του υφαδιού διεξάχθηκε από τους Carvelli *et al.* Σύμφωνα με το πρότυπο ASTM D 5035-95. Κόπηκαν από το δείγμα ορθογώνιες ταινίες παράλληλα στα νήματα, 50 mm πλάτους και 300 mm μήκους. Κατά την δοκιμή καταγράφηκε η εφελκυστική δύναμη και η παραμόρφωση. Επιπλέον κόπηκαν δοκίμια με τα νήματα προσανατολισμένα ±45º από την διεύθυνση φόρτισης. Στην περίπτωση αυτή καταγράφηκε το φορτίο και η διατμητική παραμόρφωση.

Η προσομοίωση των πειραματικών δοκιμών διεξάχθηκε χρησιμοποιώντας τα μακρομηχανικά μοντέλα. Οι καμπύλες που προέκυψαν από την προσομοίωση συγκρίθηκαν με τις αντίστοιχες πειραματικές καμπύλες (Σχήμα 4-5, Σχήμα 4-6, Σχήμα 4-7). Το συνεχές μοντέλο, αρχικά όρια και παραμορφωμένη κατάσταση, που προέκυψε από την προσομοίωση του μονοαξονικού εφελκυσμού με τα νήματα προσανατολισμένα στις ±45º δίνεται στο Σχήμα 4-4. Η ασύμμετρη παραμόρφωση που προκύπτει αναδεικνύει την σημασία της μακρομηχανικής μοντελοποίησης.

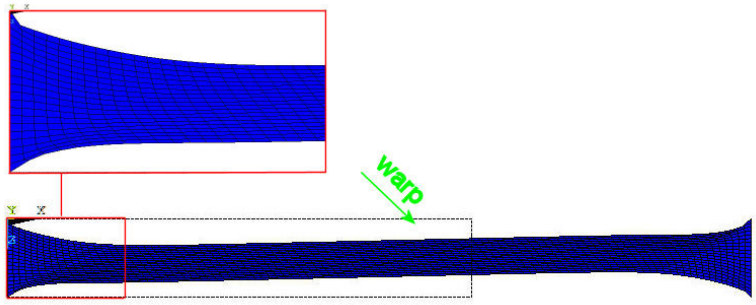

Σχήμα 4-4: Παραμορφωμένο μοντέλο από την προσομοίωση της δοκιμής εφελκυσμού του δείγματος με τα νήματα προσανατολισμένα στις ±45º.

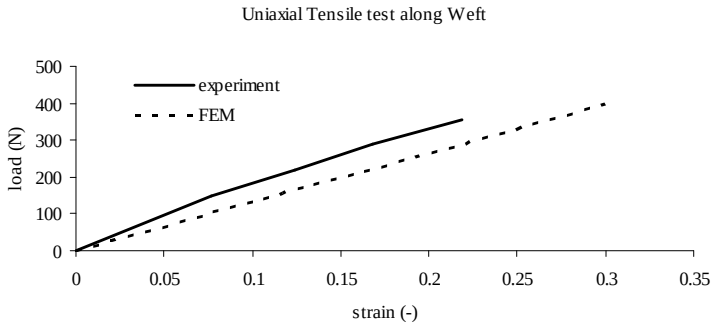

Σχήμα 4-5: Πειραματική και υπολογιστική καμπύλη φορτίου – παραμόρφωσης από τον μονοαξονικό εφελκυσμό του δείγματος κατά την διεύθυνση του υφαδιού.

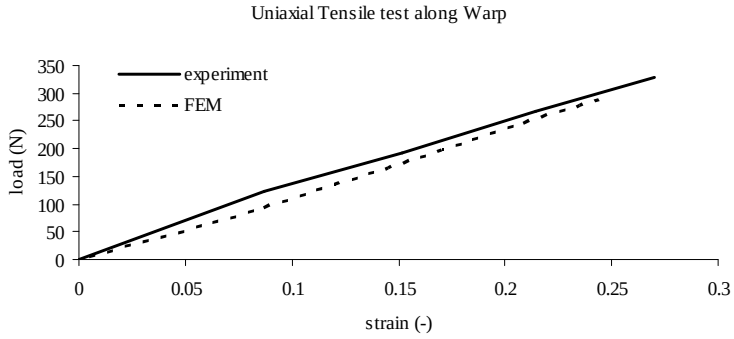

Σχήμα 4-6: Πειραματική και υπολογιστική καμπύλη φορτίου – παραμόρφωσης από τον μονοαξονικό εφελκυσμό του δείγματος κατά την διεύθυνση του στημονιού.

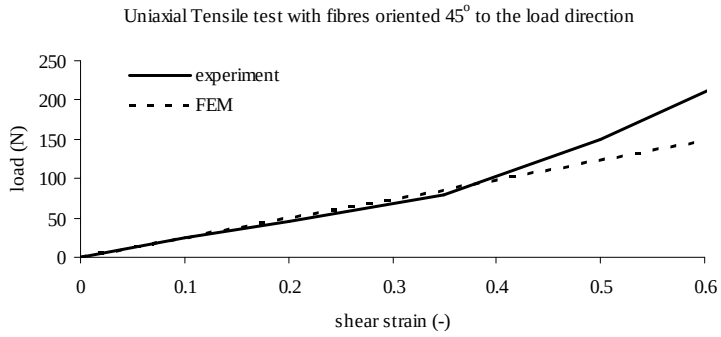

Σχήμα 4-7: Πειραματική και υπολογιστική καμπύλη φορτίου – διατμητικής παραμόρφωσης από τον μονοαξονικό εφελκυσμό του δείγματος με τα νήματα προσανατολισμένα στις ±45º.

Η επαρκής προσέγγιση των πειραματικών καμπυλών από τις υπολογιστικές επιβεβαιώνει την αξιοπιστία του μακρομηχανικού μοντέλου στην εφελκυστική και διατμητική παραμόρφωση. Η μικρή απόκλιση που παρουσιάζεται στον μονοαξονικό εφελκυσμό κατά την διεύθυνση των νημάτων οφείλεται πιθανόν στις θεωρούμενες παραδοχές (κυκλική διατομή των νημάτων, ονομαστική διάμετρος, ονομαστική πυκνότητα νημάτων, γραμμική ελαστικότητα). Ενδιαφέρον παρουσιάζει η τρίτη δοκιμή, της οποίας η πειραματική καμπύλη παρουσιάζει σημείο καμπής και η κλίση της καμπύλης αυξάνεται. Αυτό πιθανόν οφείλεται στην πλάτυνση των νημάτων και την αύξηση των δυνάμεων τριβής ή την προσέγγιση των διπλανών νημάτων και την ανάπτυξη επιπρόσθετων δυνάμεων συμπίεσης. Ο μηχανισμός αυτός δεν προβλέφθηκε από το προτεινόμενο μοντέλο δεδομένου ότι το μέτρο διάτμησης ορίστηκε γραμμικά.

4.3 Συμπεράσματα

Η ομογενοποίηση αποτελεί αξιόπιστη μέθοδο για την μακρομηχανική ανάλυση περιοδικών δομών. Ο ακριβής υπολογισμός των φαινόμενων ιδιοτήτων της δομικής μονάδας και η επαρκής απόδοση τους στο συνεχές μοντέλο είναι καθοριστικής σημασίας για την αξιοπιστία

του μακρομηχανικού μοντέλου. Προτάθηκαν τρεις μέθοδοι για την ανάπτυξη ισοδύναμου συνεχούς μοντέλου για την μακρομηχανική ανάλυση του απλού υφαντού ασύμμετρης δομής. Στην πρώτη προσέγγιση χρησιμοποιήθηκε μοντέλο από δύο πλέγματα με ΠΣ κελύφους, με συμπίπτοντες κόμβους, που παρουσιάζουν διαφορετικό είδος δυσκαμψίας (ελαστική – καμπτική). Στην δεύτερη προσέγγιση αναπτύχθηκε μοντέλο από δύο πλέγματα με ΠΣ κελύφους, με συμπίπτοντες κόμβους, από διαφορετικό υλικό. Η τρίτη προσέγγιση βασίστηκε σε μοντέλο τριών στρωμάτων συμμετρικής διατομής (πλεγματοποίηση με ΠΣ κελύφους, ογκικά ΠΣ ή όγκου-κελύφους ΠΣ). Η πρώτη αποτελεί την πιο αδύνατη των προσεγγίσεων δεδομένου ότι δεν υποστηρίζει μη-γραμμική ανάλυση μεγάλων παραμορφώσεων οπότε δεν μπορεί να εφαρμοστεί για την μακρομηχανική ανάλυση κ/υ δομών. Η αξιοπιστία των προτεινόμενων μεθόδων αξιολογήθηκε κάνοντας χρήση πειραματικών δεδομένων. Τα χρησιμοποιούμενα πειραματικά δεδομένα ελήφθησαν από βιβλιογραφικές πηγές, αφού η παραγωγή και μέτρηση των επιθυμητών δειγμάτων ήταν αδύνατες με τους διαθέσιμους πόρους. Τα μακρομηχανικά μοντέλα χρησιμοποιήθηκαν σε δύο ξεχωριστές περιπτώσεις για τον υπολογισμό της συμπεριφοράς εφελκυσμό, διάτμηση και κάμψη. Η επαρκής προσέγγιση των πειραματικών τιμών από τις υπολογιστικές επιβεβαιώνει την αξιοπιστία της μοντελοποίησης.

Κεφάλαιο 5
Προσομοίωση Σύνθετων Καταπονήσεων

Περίληψη

Το πέμπτο κεφάλαιο της διατριβής εστιάζει στην προσομοίωση του πεσίματος του υφάσματος υπό την επίδραση του βάρους του σε βάθρο στήριξης (drape test). Πρόκειται για ιδιαίτερα σύνθετη καταπόνηση δεδομένου ότι το ύφασμα κάμπτεται σε πολλά επίπεδα σχηματίζοντας πτυχώσεις. Η δυνατότητα των υφασμάτων να κάμπτονται σε πολλά επίπεδα επιτρέπει την διαμόρφωση τους σε μήτρες και την παραγωγή σύνθετων κομματιών πολύπλοκων σχημάτων. Η δοκιμή drape αποτελεί μη-γραμμικό πρόβλημα που διέπεται από μεγάλες μετατοπίσεις και στροφές. Η μέθοδος ομογενοποίησης με συνεχή δομή τριών στρωμάτων αποδείχτηκε κατάλληλη για την προσομοίωση της δοκιμής drape. Για την μοντελοποίηση χρησιμοποιήθηκαν τα 8-κομβικά solid-shell ΠΣ με 3 βαθμούς ελευθερίας ανά κόμβο. Η αξιοπιστία της προσομοίωσης αξιολογήθηκε πειραματικά.

5.1 Πειραματικά δεδομένα

Η μακρομηχανική μοντελοποίηση υιοθετήθηκε για την προσομοίωση του υφάσματος σε σύνθετη παραμορφωσιακή κατάσταση. Η αξιοπιστία της μοντελοποίησης εκτιμήθηκε πειραματικά, εφαρμοζόμενη σε μια σειρά 30 δειγμάτων υφαντών υφασμάτων. Τα δείγματα παράχθηκαν με σταθερά χαρακτηριστικά και μια μεταβλητή δομική παράμετρο. Τα στημόνια και τα υφάδια αποτελούν βαμβακερά νήματα 50 Ne και 40 Ne αντίστοιχα. Κάθε ομάδα 6 δειγμάτων παράχθηκε διατηρώντας σταθερή την πυκνότητα στημονιού και μεταβάλλοντας την πυκνότητα υφαδιού. Δεδομένου ότι δεν είναι γνωστά τα χαρακτηριστικά των νημάτων, δεν είναι δυνατή η μεσομηχανική ανάλυση για τον υπολογισμό των φαινομένων ιδιοτήτων της δομικής μονάδας των δειγμάτων. Γι' αυτό τα φαινόμενα χαρακτηριστικά της δομής που θα χρησιμοποιηθούν για την μέθοδο ομογενοποίησης υπολογίστηκαν στην πειραματική διάταξη KES-F. Τα δομικά χαρακτηριστικά της δομικής μονάδας και οι φαινόμενες μηχανικές ιδιότητες δίνονται στον Πίνακας 5-1.

Πίνακας 5-1: Δομικά χαρακτηριστικά των δειγμάτων και φαινόμενες ιδιότητες της δομικής μονάδας.

Δείγμα No	Απόσταση νημάτων (mm)		Επιφανειακή πυκνότητα (Kg/mm^2)	Καμπτική δυσκαμψία ($N \cdot mm^2$/νήμα)		Μέτρο διάτμησης (N/νήμα)		Μέτρο ελαστικότητας (N/νήμα)	
	υφάδι [p2]	στημόνι [p1]		υφάδι [Bft]	στημόνι [Brp]	υφάδι [Gft]	στημόνι [Grp]	υφάδι [Eft]	στημόνι [Erp]
1	0.500	0.185	1.02E-07	7.01E-04	7.65E-04	0.0052	0.0166	0.410	0.184
2	0.400	0.185	1.12E-07	1.03E-03	8.34E-04	0.0111	0.0250	0.333	0.147
3	0.333	0.185	1.22E-07	1.14E-03	9.77E-04	0.0211	0.0384	0.336	0.152
4	0.286	0.185	1.31E-07	1.34E-03	9.17E-04	0.0274	0.0414	0.338	0.127
5	0.250	0.185	1.41E-07	1.62E-03	1.05E-03	0.0379	0.0488	0.310	0.137
6	0.222	0.185	1.52E-07	1.66E-03	1.07E-03	0.0448	0.0532	0.255	0.134
7	0.500	0.175	1.07E-07	8.68E-04	6.83E-04	0.0049	0.0169	0.534	0.137
8	0.400	0.175	1.12E-07	1.15E-03	7.74E-04	0.0109	0.0265	0.482	0.150
9	0.333	0.175	1.25E-07	1.30E-03	9.70E-04	0.0191	0.0369	0.468	0.139
10	0.286	0.175	1.36E-07	1.41E-03	8.60E-04	0.0294	0.0458	0.429	0.126
11	0.250	0.175	1.43E-07	1.71E-03	1.26E-03	0.0413	0.0582	0.433	0.139
12	0.222	0.175	1.53E-07	1.84E-03	1.10E-03	0.0428	0.0553	0.322	0.120
13	0.500	0.167	1.11E-07	8.43E-04	7.19E-04	0.0056	0.0200	0.559	0.138
14	0.400	0.167	1.20E-07	1.05E-03	7.78E-04	0.0124	0.0317	0.499	0.127
15	0.333	0.167	1.33E-07	1.30E-03	7.42E-04	0.0208	0.0401	0.424	0.112
16	0.286	0.167	1.42E-07	1.26E-03	8.06E-04	0.0319	0.0515	0.420	0.121
17	0.250	0.167	1.48E-07	2.03E-03	9.61E-04	0.0393	0.0594	0.402	0.117
18	0.238	0.167	1.56E-07	1.93E-03	1.07E-03	0.0381	0.0527	0.347	0.115
19	0.500	0.159	1.13E-07	1.03E-03	7.86E-04	0.0057	0.0200	0.606	0.150
20	0.400	0.159	1.25E-07	8.24E-04	6.93E-04	0.0107	0.0286	0.570	0.116
21	0.333	0.159	1.33E-07	1.38E-03	8.00E-04	0.0211	0.0410	0.527	0.123
22	0.286	0.159	1.46E-07	1.38E-03	7.89E-04	0.0281	0.0488	0.463	0.115
23	0.250	0.159	1.57E-07	1.48E-03	1.08E-03	0.0363	0.0554	0.383	0.109
24	0.238	0.159	1.60E-07	2.26E-03	1.14E-03	0.0405	0.0563	0.406	0.108
25	0.500	0.152	1.16E-07	9.95E-04	7.25E-04	0.0056	0.0208	0.774	0.142
26	0.400	0.152	1.28E-07	1.05E-03	7.15E-04	0.0116	0.0326	0.543	0.116
27	0.333	0.152	1.39E-07	1.23E-03	7.79E-04	0.0222	0.0442	0.610	0.106
28	0.286	0.152	1.46E-07	1.43E-03	9.45E-04	0.0310	0.0562	0.508	0.130
29	0.250	0.152	1.57E-07	1.51E-03	1.01E-03	0.0384	0.0620	0.529	0.130
30	0.238	0.152	1.60E-07	1.77E-03	9.20E-04	0.0422	0.0605	0.543	0.129

Για την δοκιμή drape κόπηκαν τετραγωνικά δείγματα παράλληλα στα νήματα με διαστάσεις 200×200 mm. Στη συνέχεια τα δείγματα τοποθετήθηκαν σε κυκλικό βάθρο διαμέτρου 107 mm και καταγράφηκε η κάτοψη των παραμορφωμένων δειγμάτων. Ακολούθησε η επεξεργασία εικόνας για τον υπολογισμό του συντελεστή drape. Ως συντελεστής drape ορίστηκε το ποσοστό του εμβαδού της προβολής του παραμορφωμένου υφάσματος στο οριζόντιο επίπεδο αφαιρώντας το εμβαδό του βάθρου διαιρούμενου με το εμβαδό του υφάσματος αφαιρώντας το εμβαδό του βάθρου:

$$\mathrm{DC}(\%) = \frac{\textit{προβολή παραμ. υφάσματος στο οριζόντιο επίπεδο}\,(mm^2) - 0.25 \cdot \pi \cdot 107^2}{200 \cdot 200 - 0.25 \cdot \pi \cdot 107^2} \cdot 100 \qquad \text{(Εξ. 5-1)}$$

Η ανίχνευση των συνόρων των εικόνων και ο υπολογισμός των εμβαδών διεξήχθησαν στο λογισμικό Matlab. Η επεξεργασία εικόνας ενός δείγματος παρουσιάζεται στο Σχήμα 5-1.

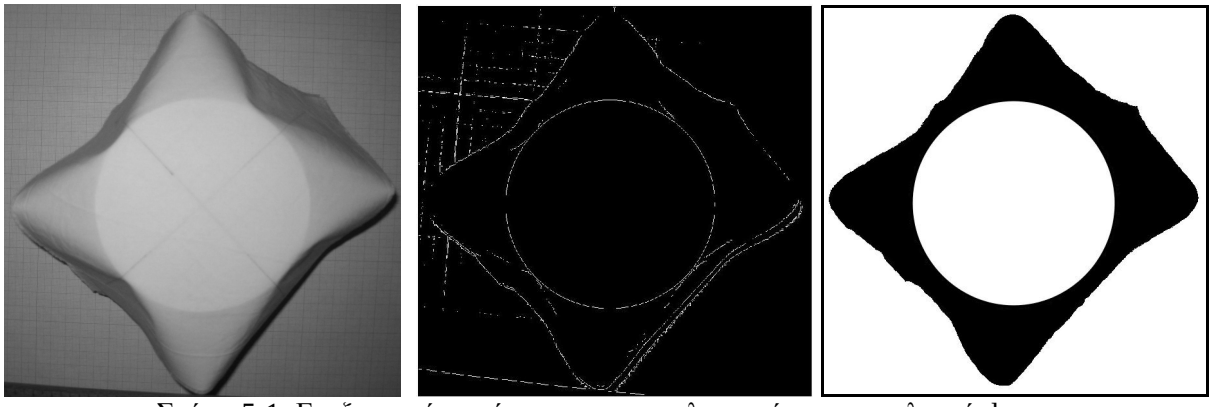

Σχήμα 5-1: Επεξεργασία εικόνας για τον υπολογισμό του συντελεστή drape.

5.2 Μακρομηχανική ανάλυση της δοκιμής drape

Η προσομοίωση της δοκιμής drape διεξάχθηκε στο λογισμικό ANSYS. Για την ανάπτυξη του ισοδύναμου συνεχούς μοντέλου υιοθετήθηκε η ομογενοποίηση με το μοντέλο των τριών στρωμάτων. Οι μηχανικές ιδιότητες των ισοδύναμων μοντέλων που χρησιμοποιήθηκαν για την μακρομηχανική ανάλυση των 30 δειγμάτων δίνονται στον Πίνακας 5-2. Για την προσομοίωση χρησιμοποιήθηκαν πολυστρωματικά ΠΣ όγκου-κελύφους (solsh190) που αποτελούνται από 8 κόμβους με 3 ΒΕ (μεταφορικούς) ανά κόμβο. Για την απόδοση των μηχανικών ιδιοτήτων στο συνεχές μοντέλο θεωρήθηκε ορθοτροπικό υλικό. Τους κύριους άξονες της ορθοτροπικής ελαστικότητας συνιστούν η διεύθυνση στημονιού, υφαδιού και του πάχους του υφάσματος.

Πίνακας 5-2: Φαινόμενες ιδιότητες συνεχών μοντέλων.

Δείγμα No	Πάχος στρώματος		Πυκνότητα (kg/mm^3)	Ελαστικές ιδιότητες εξωτερικών στρωμάτων			Ελαστικές ιδιότητες εσωτερικών στρωμάτων		
	t_1 (mm)	t_2 (mm)		E_{1z}	E_{1x}	G_{1xz}	E_{2z}	E_{2x}	G_{2xz}
1	0.1	0.1	3.38E-07	1.65	0.36	0.11	6.61	7.48	0.11
2	0.1	0.1	3.74E-07	1.92	0.94	0.21	4.11	6.43	0.20
3	0.1	0.1	4.06E-07	2.30	1.29	0.38	3.61	7.51	0.39
4	0.1	0.1	4.35E-07	2.19	1.85	0.48	2.46	8.12	0.49
5	0.1	0.1	4.70E-07	2.53	2.73	0.65	2.32	6.96	0.65
6	0.1	0.1	5.05E-07	2.60	3.26	0.80	2.04	4.96	0.79
7	0.1	0.1	3.56E-07	1.62	0.42	0.11	4.58	9.84	0.11
8	0.1	0.1	3.75E-07	1.85	0.94	0.22	4.86	10.17	0.22
9	0.1	0.1	4.17E-07	2.44	1.36	0.37	3.04	11.33	0.37
10	0.1	0.1	4.53E-07	2.15	1.84	0.53	2.90	11.33	0.54
11	0.1	0.1	4.75E-07	3.27	2.69	0.78	1.37	11.95	0.77
12	0.1	0.1	5.11E-07	2.84	3.54	0.83	1.15	7.40	0.83
13	0.1	0.1	3.70E-07	1.81	0.38	0.13	4.65	10.42	0.13
14	0.1	0.1	4.00E-07	2.02	0.79	0.26	3.58	10.89	0.27
15	0.1	0.1	4.44E-07	1.95	1.43	0.40	2.83	9.85	0.40
16	0.1	0.1	4.74E-07	2.12	1.59	0.60	3.00	11.50	0.60
17	0.1	0.1	4.94E-07	2.59	3.38	0.79	1.85	9.31	0.80
18	0.1	0.1	5.19E-07	2.92	3.44	0.74	1.04	7.68	0.74
19	0.1	0.1	3.78E-07	2.08	0.53	0.13	5.27	11.06	0.13
20	0.1	0.1	4.17E-07	1.88	0.44	0.24	3.53	13.39	0.24
21	0.1	0.1	4.42E-07	2.20	1.41	0.41	3.37	12.99	0.41
22	0.1	0.1	4.87E-07	2.18	1.74	0.57	2.89	12.70	0.57
23	0.1	0.1	5.25E-07	3.11	2.33	0.74	0.64	10.67	0.74
24	0.1	0.1	5.32E-07	3.31	4.04	0.79	0.18	8.96	0.79
25	0.1	0.1	3.88E-07	2.00	0.35	0.14	5.39	14.77	0.14
26	0.1	0.1	4.28E-07	2.04	0.75	0.27	3.56	12.09	0.27
27	0.1	0.1	4.63E-07	2.28	1.08	0.44	2.45	16.15	0.44
28	0.1	0.1	4.88E-07	2.76	1.76	0.65	3.04	14.26	0.67
29	0.1	0.1	5.23E-07	2.96	2.14	0.83	2.63	16.85	0.83
30	0.1	0.1	5.34E-07	2.68	2.76	0.85	3.12	17.30	0.85

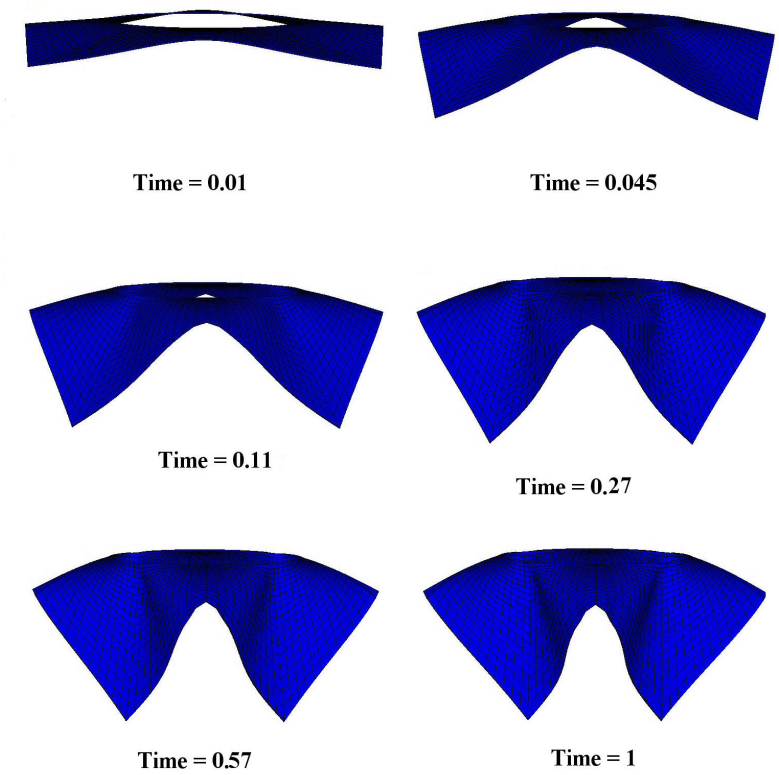

Σχήμα 5-2: Παραμορφωμένο μοντέλο του υφάσματος κατά την προσομοίωση της δοκιμής drape.

Γεωμετρικά τα μοντέλα αντιστοιχούν σε τετραγωνικές επιφάνειες με τις διαστάσεις του υφάσματος (200×200 mm) ενώ η κυκλική επιφάνεια που σχηματίζει το βάθρο έχει αφαιρεθεί. Το τμήμα του υφάσματος που στηρίζεται στην επιφάνεια του βάθρου αφαιρέθηκε από το μοντέλο για μείωση του υπολογιστικού κόστους και αντικαταστάθηκε από εφαρμογή περιορισμών στους κόμβους της περιφέρειας του κύκλου. Συγκεκριμένα οι περιορισμοί ορίστηκαν στους κατώτερους κόμβους των ΠΣ όγκου-κελύφους ώστε η εφαρμοζόμενη στήριξη να αντιστοιχεί σε απλή άρθρωση. Η εφαρμογή του φορτιού συνίσταται στον ορισμό της φαινόμενης πυκνότητας (ανηγμένη τιμή στο πάχος του φάσματος) και της επιτάχυνσης της βαρύτητας (9.807 m/sec²). Δηλαδή το μοντέλο υπόκειται σε σύνθετη παραμόρφωση (κάμψη σε πολλά επίπεδα) υπό συνθήκες χαμηλής φόρτισης (ίδιον βάρος). Πρόκειται για μη-γραμμικό πρόβλημα που παρουσιάζει μεγάλες μετατοπίσεις και περιστροφές. Για την διασφάλιση της σύγκλισης επιβλήθηκαν επιπρόσθετοι περιορισμοί σε 4 κόμβους του ανώτερου συνόρου της περιφέρειας του κύκλου. Οι κόμβοι αυτοί αντιστοιχούν στις γωνίες 0, 90, 180, 270 μοίρες της κυκλικής περιφέρειας. Χρησιμοποιήθηκε ο αλγόριθμος Newton-Raphson για την μη-γραμμική επίλυση μεγάλων παραμορφώσεων. Βασικό πλεονέκτημα του αλγορίθμου αποτελεί η ενημέρωση του μητρώου δυσκαμψίας σε κάθε βήμα επανάληψης. Ο έλεγχος του αριθμού επαναλήψεων είναι σημαντικός για την σύγκλιση της διαδικασίας επίλυσης απαιτώντας κατά το δυνατόν χαμηλότερο χρόνο CPU. Η μείωση του αριθμού επαναλήψεων επιτυγχάνεται με ενεργοποίηση δύο επιλογών. Η επιλογή predictor εξάγει την λύση των βαθμών ελευθερίας (BE) χρησιμοποιώντας το προηγούμενο ιστορικό προκειμένου να επιτευχθεί καλύτερη εκτίμηση του επόμενου κύκλου επίλυσης. Η επιλογή line search

αποσκοπεί στην βελτίωση της επίλυσης με Newton-Raphson διαβαθμίζοντας το διάνυσμα λύσης με μια αριθμητική τιμή γνωστή ως παράμετρος line search. Στο Σχήμα 5-2 παρουσιάζονται 6 στιγμιότυπα από την παραμόρφωση δείγματος κατά την δοκιμή drape.

5.3 Αξιολόγηση του μακρομηχανικού μοντέλου

Η αξιολόγηση της ρεαλιστικότητας του μακρομηχανικού μοντέλου στην δοκιμή drape βασίστηκε στα πειραματικά δεδομένα. Για την σύγκριση της υπολογιστικά προβλεπόμενης και πειραματικής απόδοσης του υφάσματος χρησιμοποιήθηκε ο συντελεστής drape (DC) όπως ορίστηκε στην Εξ. 5-1. Οι συντελεστές drape υπολογιζόμενοι από την προσομοίωση και το πείραμα δίνονται στον Πίνακας 5-3. Η μικρή απόκλιση που παρουσιάζεται μεταξύ των υπολογιστικών και πειραματικών τιμών επιβεβαιώνει την αξιοπιστία της υπολογιστικής μεθόδου.

Πίνακας 5-3: Συντελεστής Drape από την προσομοίωση και το πείραμα.

Δείγμα No	Συντελεστής Drape (%)		Απόκλιση (%)
	ΜΠΣ	Πείραμα	
1	24.2	20.6	17.7
2	26.1	24.0	9.1
3	29.6	26.5	11.7
4	31.0	30.3	2.1
5	34.7	34.3	1.0
6	35.1	32.9	6.6
7	23.9	21.5	11.5
8	26.2	22.3	17.3
9	29.8	27.1	9.9
10	31.3	31.4	-0.2
11	37.4	33.0	13.2
12	36.0	34.2	5.2
13	24.2	22.4	7.8
14	26.1	26.3	-0.6
15	28.1	28.8	-2.3
16	30.2	33.3	-9.5
17	36.2	34.4	5.1
18	35.4	35.2	0.4
19	24.7	23.9	3.7
20	24.7	25.5	-2.9
21	29.1	26.6	9.6
22	29.4	29.9	-1.4
23	33.6	35.0	-3.9
24	37.2	34.0	9.5
25	24.4	22.3	9.2
26	25.6	25.0	2.2
27	28.7	29.7	-3.2
28	32.3	32.3	0.3
29	34.5	34.1	1.2
30	35.8	32.6	9.7

5.4 Συμπεράσματα

Η δυνατότητα των υφασμάτων να κάμπτονται σε πολλά επίπεδα είναι ουσιαστική για την μηχανική τους συμπεριφορά και την εισαγωγή τους σε τεχνικές εφαρμογές. Η υιοθέτηση της ΜΠΣ για την μακρομηχανική ανάλυση του υφάσματος σε δοκιμή drape φέρει σημαντικές δυσκολίες. Καθοριστική είναι η απόδοση των ιδιοτήτων στο ισοδύναμο συνεχές μοντέλο. Επιπλέον πρόκειται για έντονα μη-γραμμικό πρόβλημα που διέπεται από μεγάλες μετατοπίσεις και περιστροφές. Στην προτεινόμενη προσέγγιση εφαρμόστηκε η μέθοδος ομογενοποίησης με ισοδύναμο μοντέλο τριών στρωμάτων. Για την ανάπτυξη του πλέγματος χρησιμοποιήθηκαν ΠΣ όγκου-κελύφους με μεταφορικούς ΒΕ. Έτσι αντιμετωπίστηκαν οι δυσκολίες που ανακύπτουν από τον υπολογισμό των στροφικών ΒΕ των κόμβων. Η αξιοπιστία της προτεινόμενης υπολογιστικής μεθόδου εκτιμήθηκε με πειραματικές μετρήσεις. Ο σχηματισμός του υφάσματος κατά την υποβολή του σε δοκιμή drape αποτυπώθηκε από την πειραματική δοκιμή και την αντίστοιχη προσομοίωση. Στη συνέχεια με επεξεργασία εικόνας υπολογίστηκε ο συντελεστής drape και για τις δύο περιπτώσεις. Η μικρή απόκλιση μεταξύ των πειραματικών και των υπολογιστικών τιμών επιβεβαιώνει την αξιοπιστία της προτεινόμενης υπολογιστικής μεθόδου.

Κεφάλαιο 6
Τεχνική Εφαρμογή: Συμπίεση Τριδιάστατων Υφασμάτων

Περίληψη

Στο έκτο κεφάλαιο επιχειρείται η εφαρμογή της προτεινόμενης μεθόδου μοντελοποίησης για την μελέτη της συμπεριφοράς τριδιάστατης κ/υ δομής σε δοκιμή συμπίεσης. Πρόκειται για στημονοπλεκτά υφάσματα με σημαντικό πάχος που παρουσιάζουν υψηλή αντίσταση σε συμπίεση και χρησιμοποιούνται σε οικοδομικές κατασκευές ως δομές ενίσχυσης σκυροδέματος για την παραγωγή πλαισίων τοίχου, επένδυση οροφής κ.α. Η αντίσταση του υφάσματος σε συμπίεση αποτελεί πλεονέκτημα για την παραγωγή του σύνθετου υλικού (εύκολη ενσωμάτωση του σκυροδέματος στην κ/υ δομή) και την λειτουργικότητά του. Παράχθηκαν τα μεσομηχανικά μοντέλα των στρωμάτων της δομής από τα οποία υπολογίστηκαν οι φαινόμενες ιδιότητες. Στη συνέχεια το μακρομηχανικό μοντέλο υποβλήθηκε σε δοκιμή συμπίεσης προσομοιώνοντας την πειραματική δοκιμή.

6.1 Πειραματικά δεδομένα

Τα τριδιάστατα στημονοπλεκτά που μελετώνται παράχθηκαν σε μηχανή Raschel τύπου HDR 6-7 DPLM, Karl Mayer Textilmaschinenfabrik GmbH, Obertshausen, που τροποποιήθηκε ιδιαίτερα στο ITA, RWTH Aachen University της Γερμανίας (Roye 2007) για παραγωγή 3Δ υφασμάτων για ενίσχυση σκυροδέματος. Πρόκειται για μια κατηγορία 3Δ στημονοπλεκτών που συνιστώνται από δύο εξωτερικά στρώματα και το εσωτερικό στρώμα που κατά κύριο λόγο καθορίζει την απόσταση των εξωτερικών στρωμάτων (warp knitted spacer fabrics). Τα εξωτερικά στρώματα παρουσιάζουν την μορφή δικτύου που φαίνεται στο Σχήμα 6-2. Το εσωτερικό στρώμα φέρει μονοϊνικά νήματα κατά την διεύθυνση του πάχους του, τα οποία προσδίδουν στο ύφασμα αντίσταση σε συμπίεση. Η δομή των υπό εξέταση στημονοπλεκτών είναι κατάλληλη για την ενίσχυση σκυροδέματος, αφού η ενσωμάτωσή του επιτυγχάνεται εύκολα με διείσδυση του σκυροδέματος πλευρικά στο ύφασμα μέσα από την δικτυακή μορφή των εξωτερικών στρωμάτων, ενώ η αντίσταση του εσωτερικού στρώματος σε συμπίεση επιτρέπει την διατήρηση του πάχους του υφάσματος.

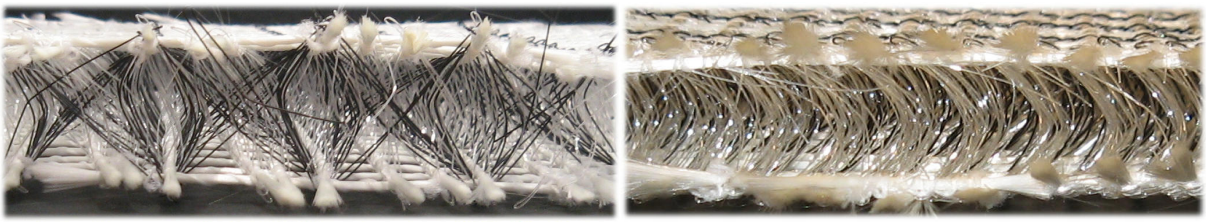

Σχήμα 6-1: Τομή του 3Δ στημονοπλεκτού στις δύο βασικές διευθύνσεις.

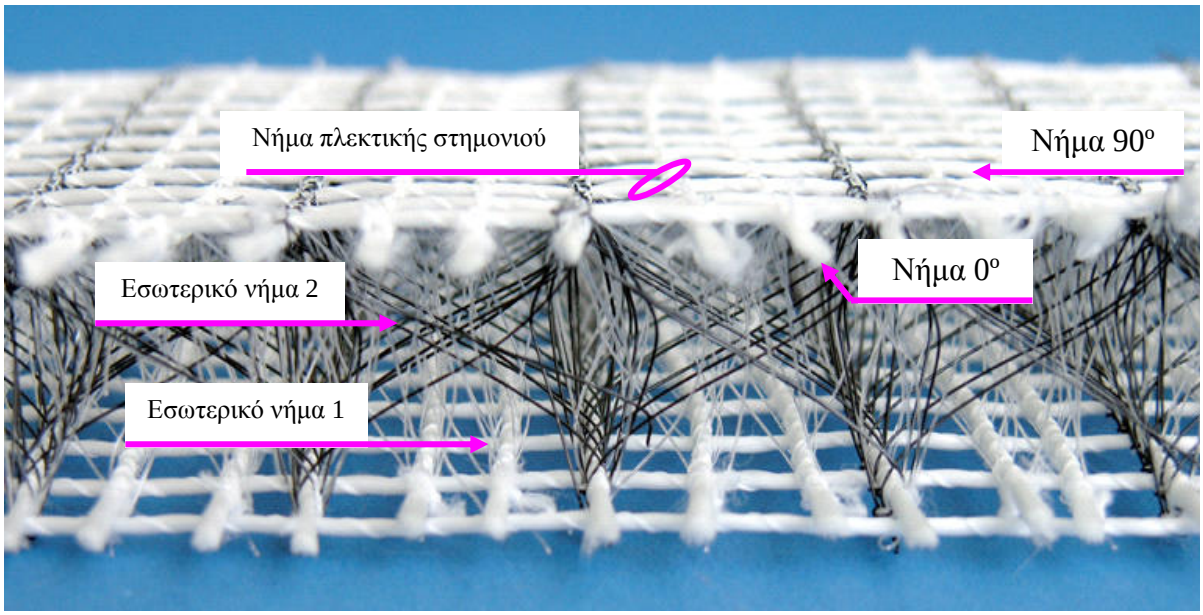

Σχήμα 6-2: Δομικά στοιχεία του 3Δ στημονοπλεκτού.

Πίνακας 6-1: Ιδιότητες των δομικών στοιχείων του 3Δ στημονοπλεκτού (X: Δεν χρησιμοποιείται, N/A: Δεν εφαρμόζεται)

Δομικό στοιχείο	Περιγραφή	Ελαστική συμπεριφορά	E (N/mm²)	ν	B (N·mm²)	σ (όριο διαρροής N/mm²)
Νήμα πλεκτικής στημονιού	16 tex πολυινικό νήμα συνεχών ινών PP	X	X	X	X	X
Νήμα 0º	2400 tex AR-Glass επίπεδο νήμα	Γραμμικά ελαστική	72000	0.3	24	N/A
Νήμα 90º	2400 tex AR-Glass επίπεδο νήμα τυλιγμένο με PA στριμμένο νήμα	Γραμμικά ελαστική	72000	0.3	24	N/A
Εσωτερικό νήμα 1	0,25 mm PES μονοϊνικό (λευκό)	Διγραμμικά ελαστική	E1=4876 E2=2252	0.3	0.94	167.2
Εσωτερικό νήμα 2	0,30 mm PES μονοϊνικό (μαύρο)	Διγραμμικά ελαστική	E1=5141 E2=1792	0.3	2.04	151.7

Οι ιδιότητες των δομικών στοιχείων που συνθέτουν τα 3Δ στημονοπλεκτά δίνονται στον Πίνακας 6-1. Τα νήματα 0º και 90º αντιστοιχούν στα παρεμβαλλόμενα στημόνια και υφάδια των εξωτερικών στρωμάτων. Τα εσωτερικά νήματα συνδέουν τα εξωτερικά στρώματα σχηματίζοντας το εσωτερικό στρώμα. Τα νήματα πλεκτικής στημονιού επιτελούν το δέσιμο της δομής μέσω της πλεκτικής διαδικασίας (Σχήμα 6-2). Η σειρά των εξεταζόμενων δειγμάτων έχει παραχθεί διατηρώντας σταθερά τα υλικά και τα σχέδια που χρησιμοποιούνται για το νήμα πλεκτικής στημονιού, τα παρεμβαλλόμενα νήματα 0° και 90° και το εσωτερικό νήμα 1, ενώ μεταβάλλεται το σχέδιο του εσωτερικού νήματος 2. Η απόσταση των παρεμβαλλόμενων στημονιών και υφαδιών ορίστηκε στα 8 mm. Το αρχικό πάχος του 3Δ στημονοπλεκτού ορίστηκε στα 25 mm. Οι τομές των δειγμάτων που εξετάζονται παρουσιάζονται στο Σχήμα 6-3.

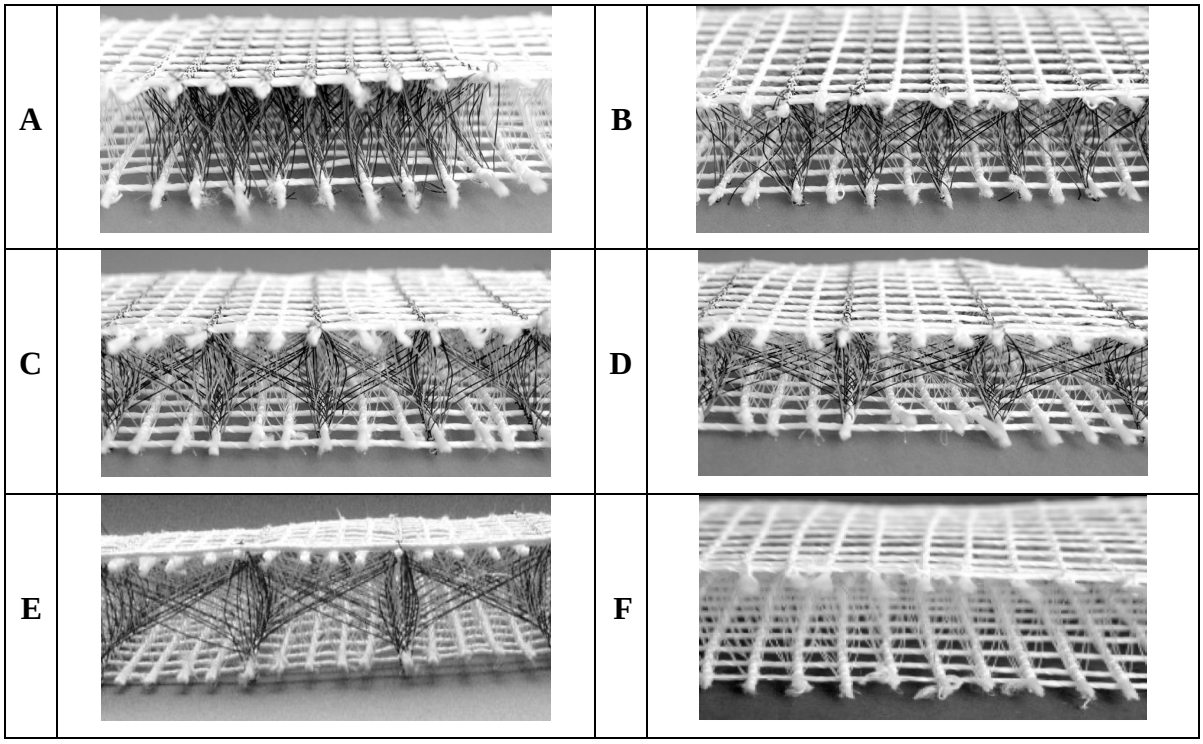

Σχήμα 6-3: Σειρά δειγμάτων 3Δ στημονοπλεκτών που εξετάζονται.

Το μέτρο ελαστικότητας των νημάτων μετρήθηκε στην συσκευή TEXTECHNO. Η καμπτική δυσκαμψία των εσωτερικών νημάτων (μονοϊνικά νήματα) υπολογίστηκε από την μηχανική. Η καμπτική δυσκαμψία των υαλονημάτων (πολυινικά νήματα) μετρήθηκε πειραματικά.

Η δοκιμή συμπίεσης των δειγμάτων διεξάχθηκε στην συσκευή Zwick/Roell 2.5. Τα δείγματα κόβονται σε κυκλικές επιφάνειες διαμέτρου 200 mm. Κατά την δοκιμή το κυκλικό έμβολο πίεσης διαμέτρου 50 mm κινείται με σταθερή ταχύτητα ως προς το δείγμα εισάγοντας την μετατόπιση συμπίεσης.

6.2 Μοντελοποίηση και προσομοίωση

Για την προσομοίωση της δοκιμής συμπίεσης των 3Δ στημονοπλεκτών υιοθετήθηκαν δυο επίπεδα μοντελοποίησης. Σε κάθε επίπεδο εφαρμόστηκε η ΜΠΣ με ΠΣ δοκού, κελύφους και ογκικά ΠΣ ανάλογα με τις απαιτήσεις της προσομοίωσης. Το πρώτο επίπεδο μοντελοποίησης αντιστοιχεί στην μεσομηχανική ανάλυση του εσωτερικού και των εξωτερικών στρωμάτων ξεχωριστά για τον υπολογισμό των φαινόμενων μηχανικών ιδιοτήτων. Στο δεύτερο επίπεδο μοντελοποίησης παράγεται το μακρομηχανικό μοντέλο που θα χρησιμοποιηθεί για την προσομοίωση της δοκιμής συμπίεσης των δειγμάτων. Για την ανάπτυξη του ισοδύναμου μακρομηχανικού μοντέλου θεωρήθηκαν οι φαινόμενες ιδιότητες του εσωτερικού στρώματος σε συμπίεση και του εξωτερικού στρώματος σε κάμψη και εφελκυσμό, δεδομένου ότι οι θεωρούμενες παραμορφώσεις συνθέτουν την παραμόρφωση που παρουσιάζει το δείγμα που υποβάλλεται σε συμπίεση. Η μοντελοποίηση και προσομοίωση πραγματοποιήθηκαν στο λογισμικό ANSYS.

6.2.1 Μεσομηχανική μοντελοποίηση του εσωτερικού στρώματος

Η μεσομηχανική μοντελοποίηση του εσωτερικού στρώματος διεξάχθηκε για τον υπολογισμό τον φαινόμενων ιδιοτήτων της δομικής του μονάδας θεωρώντας την δομή του στρώματος και τις ιδιότητες των συνιστώντων νημάτων (Πίνακας 6-1). Δεδομένου ότι η δοκιμή συμπίεσης του δείγματος επιφέρει συμπίεση στο εσωτερικό στρώμα, το εσωτερικό στρώμα μελετάται ως προς την αντίστοιχη δοκιμή. Για την μοντελοποίηση των εσωτερικών νημάτων θεωρήθηκαν δύο βασικές παραδοχές. Πρώτον, τα εσωτερικά νήματα θεωρήθηκαν εγκόλλητα στα παρεμβαλλόμενα στημόνια των εξωτερικών στρωμάτων. Η επίδραση των παραλειπόμενων θηλιών των εσωτερικών νημάτων (γύρω από τα νήματα 0^o των εξωτερικών στρωμάτων) και του παραλειπόμενου νήματος πλεκτικής στημονιού διασφαλίστηκε θέτοντας κατάλληλους περιορισμούς στους αντίστοιχους κόμβους. Δεύτερον, το μήκος των εσωτερικών νημάτων θεωρήθηκε ίσο με αυτό που αποκτούν αν αποτελούνται από ευθύγραμμα τμήματα και το πάχος του στημονοπλεκτού κατέχει την αρχική τιμή του.

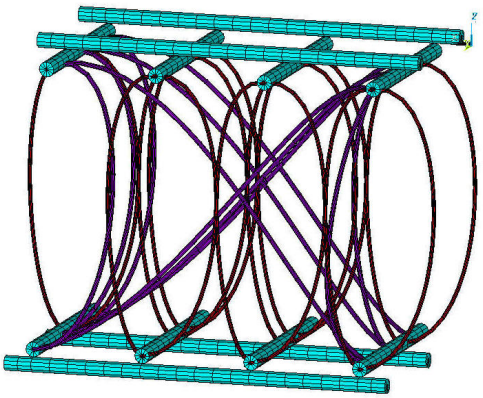

Σχήμα 6-4: Διακριτό μοντέλο της δομικής μονάδας (δείγμα C).

Για την προσομοίωση της δομικής μονάδας του εσωτερικού στρώματος σε συμπίεση εφαρμόστηκε η ΜΠΣ με ΠΣ δοκού. Η μοντελοποίηση με στοιχεία δοκού θεωρείται κατάλληλη για την προσομοίωση δεδομένου ότι η κάμψη των εσωτερικών νημάτων κυριαρχεί στην παραμόρφωση του εσωτερικού στρώματος σε συμπίεση. Για την προσομοίωση οι κόμβοι της κατώτερης εξωτερικής επιφάνειας δεσμεύτηκαν σε μηδενική μετατόπιση ενώ στους κόμβους της ανώτερης εξωτερικής επιφάνειας εφαρμόστηκε κατακόρυφη μετατόπιση, μειώνοντας την απόσταση των δυο επιφανειών. Οι κόμβοι στα σημεία της ένωσης των εσωτερικών νημάτων με τα εξωτερικά στρώματα δεσμεύτηκαν σε μηδενική περιστροφή (γύρω από τα στημόνια και τα υφάδια) προκειμένου να αποφευχθεί η διείσδυση των εσωτερικών νημάτων στα εξωτερικά στρώματα (Σχήμα 6-5). Ο αλγόριθμος Newton-Raphson υιοθετήθηκε για την μη-γραμμική επίλυση του προβλήματος μεγάλων παραμορφώσεων.

Στο Σχήμα 6-6 παρουσιάζεται το παραμορφωμένο μοντέλο της δομικής μονάδας του εσωτερικού στρώματος του δείγματος C σε συμπίεση. Από την προσομοίωση υπολογίστηκαν οι αντιδράσεις που αναπτύχθηκαν λόγω της επιβολής της κατακόρυφης μετατόπισης. Η καμπύλη φορτίου – μετατόπισης που προέκυψε από την προσομοίωση μετατράπηκε σε καμπύλη τάσης (φορτίο / φαινόμενη επιφάνεια εφαρμογής) – παραμόρφωση (μετατόπιση / πάχος εσωτερικού στρώματος) θεωρώντας τις φαινόμενες διαστάσεις της δομικής μονάδας. Μ’ αυτόν τον τρόπο η αντίσταση της δομικής μονάδας του εσωτερικού στρώματος σε συμπίεση ανάχθηκε στο μέτρο ελαστικότητας του συνεχούς μοντέλου του εσωτερικού στρώματος. Χρησιμοποιήθηκαν, λοιπόν, πολυγραμμικές καμπύλες για τον ορισμό της ελαστικότητας του εσωτερικού στρώματος των δειγμάτων.

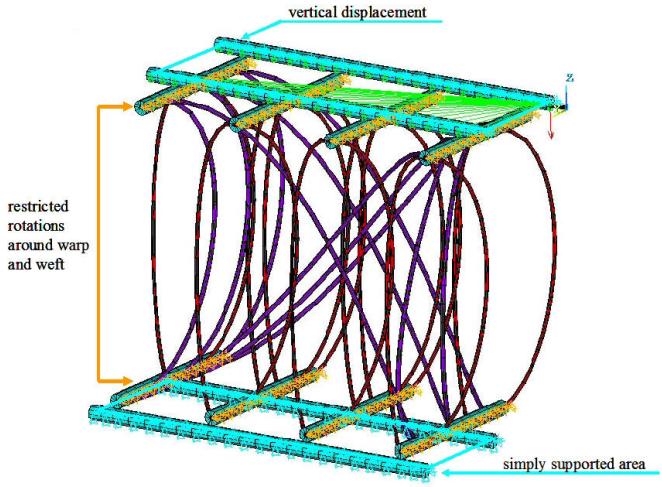

Σχήμα 6-5: Οριακές συνθήκες για την συμπίεση της δομικής μονάδας (δείγμα C).

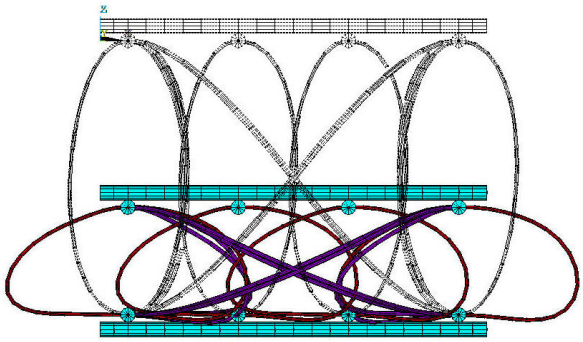

Σχήμα 6-6: Παραμορφωμένο μοντέλο δομικής μονάδας (δείγμα C).

6.2.2 Μεσομηχανική μοντελοποίηση του εξωτερικού στρώματος

Η μεσομηχανική μοντελοποίηση των εξωτερικών στρωμάτων διεξάχθηκε για τον υπολογισμό των μηχανικών ιδιοτήτων τους λαμβάνοντας υπόψη τα δομικά και μηχανικά χαρακτηριστικά των συνιστώντων νημάτων. Η δοκιμή του 3Δ υφάσματος σε συμπίεση εισάγει σύνθετη παραμόρφωση στα εξωτερικά στρώματα, κυρίως κάμψης. Για την αντικατάσταση του διακριτού μοντέλου του εξωτερικού στρώματος από ισοδύναμο συνεχές απαιτήθηκε ο υπολογισμός της καμπτικής δυσκαμψίας και του μέτρου ελαστικότητας (στο επίπεδο του στρώματος) του εξωτερικού στρώματος. Για την προσομοίωση των αντίστοιχων δοκιμών υιοθετήθηκε η ΜΠΣ με στοιχεία δοκού. Δεδομένου ότι η δομή του εξωτερικού στρώματος παρουσιάζει συμμετρία ως προς την διεύθυνση στημονιού και υφαδιού, αρκεί η δοκιμή σε μια διεύθυνση. Από την μεσομηχανική ανάλυση προέκυψαν τα χαρακτηριστικά του ισοδύναμου συνεχούς στρώματος (t_o=0.0671 mm, E_o=124031 N/mm² and B_o=624 N·mm²). Στα Σχήμα 6-7και Σχήμα 6-8 παρουσιάζονται τα παραμορφωμένα μοντέλα του εξωτερικού στρώματος σε εφελκυσμό και κάμψη.

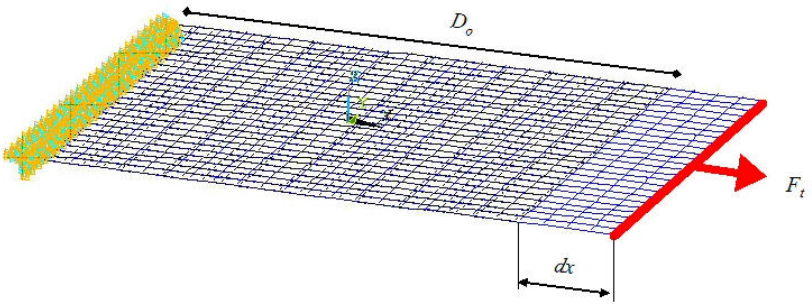

Σχήμα 6-7: Παραμόρφωση εξωτερικού στρώματος από εφελκυσμό.

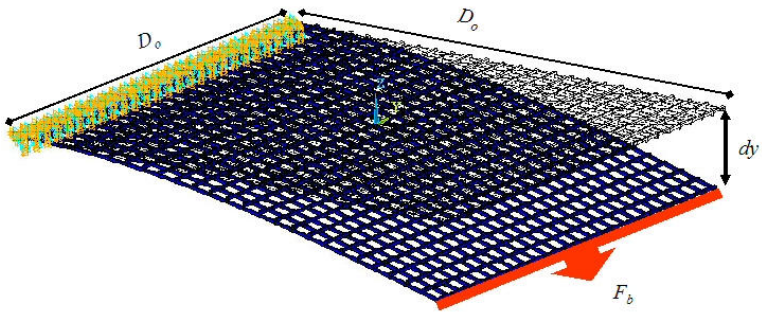

Σχήμα 6-8: Παραμόρφωση εξωτερικού στρώματος από κάμψη.

6.2.3 Μακρομηχανική μοντελοποίηση του συνολικού δείγματος

Για την προσομοίωση της σύνθετης παραμόρφωσης του συνολικού δείγματος όταν υποβάλλεται σε δοκιμή συμπίεσης παράχθηκε το μακρομηχανικό μοντέλο στο οποίο εισήχθησαν οι ισοδύναμες ιδιότητες των στρωμάτων. Το μακρομηχανικό μοντέλο αποτελείται από έναν εσωτερικό όγκο και δύο επιστρωμένες επιφάνειες που αντιστοιχούν στο εσωτερικό και τα εξωτερικά στρώματα αντίστοιχα. Ο όγκος και οι εξωτερικές επιφάνειες πλεγματοποιήθηκαν με ογκικά ΠΣ και ΠΣ κελύφους αντίστοιχα. Το πάχος του όγκου καθορίστηκε από το πάχος του εσωτερικού στρώματος. Ενώ η ελαστικότητά του καθορίστηκε από τις πολυγραμμικές καμπύλες τάσης – παραμόρφωσης που υπολογίστηκαν από την μεσομηχανική ανάλυση του εσωτερικού στρώματος. Το υλικό του όγκου θεωρήθηκε ισοτροπικό. Αντίθετα ορθοτροπικό υλικό με γραμμική ελαστικότητα θεωρήθηκε για την μοντελοποίηση του υλικού των εξωτερικών πλεγμάτων με ΠΣ κελύφους. Το πάχος των ΠΣ κελύφους (t_o) και το μέτρο ελαστικότητας (E_o) του συνεχούς μοντέλου των εξωτερικών επιφανειών υπολογίστηκαν από την μεσομηχανική ανάλυση του εξωτερικού στρώματος. Για την προσομοίωση του συνολικού δείγματος στη δοκιμή συμπίεσης εφαρμόστηκαν οριακές συνθήκες που αντιστοιχούν σε απλή στήριξη της κατώτερης επιφάνειας και επιβολή φορτίου σε περιοχή της ανώτερης επιφάνειας. Για την εφαρμογή του φορτίου επιλέχθηκε περιοχή κόμβων που αντιστοιχούν στην επιφάνεια του εμβόλου πίεσης, οι οποίοι δεσμεύτηκαν με ίση κατακόρυφη μετατόπιση. Για την μηχανική ανάλυση εφαρμόστηκε μη γραμμική επίλυση. Το μακρομηχανικό μοντέλο στην απαραμόρφωτη και παραμορφωμένη κατάσταση (σε τομή) παρουσιάζεται στο Σχήμα 6-9. Οι καμπύλες φορτίου – μετατόπισης που προέκυψαν από την προσομοίωση των μακρομηχανικών μοντέλων σε συμπίεση και οι αντίστοιχες πειραματικές καμπύλες των δειγμάτων δίνονται στο Σχήμα 6-10.

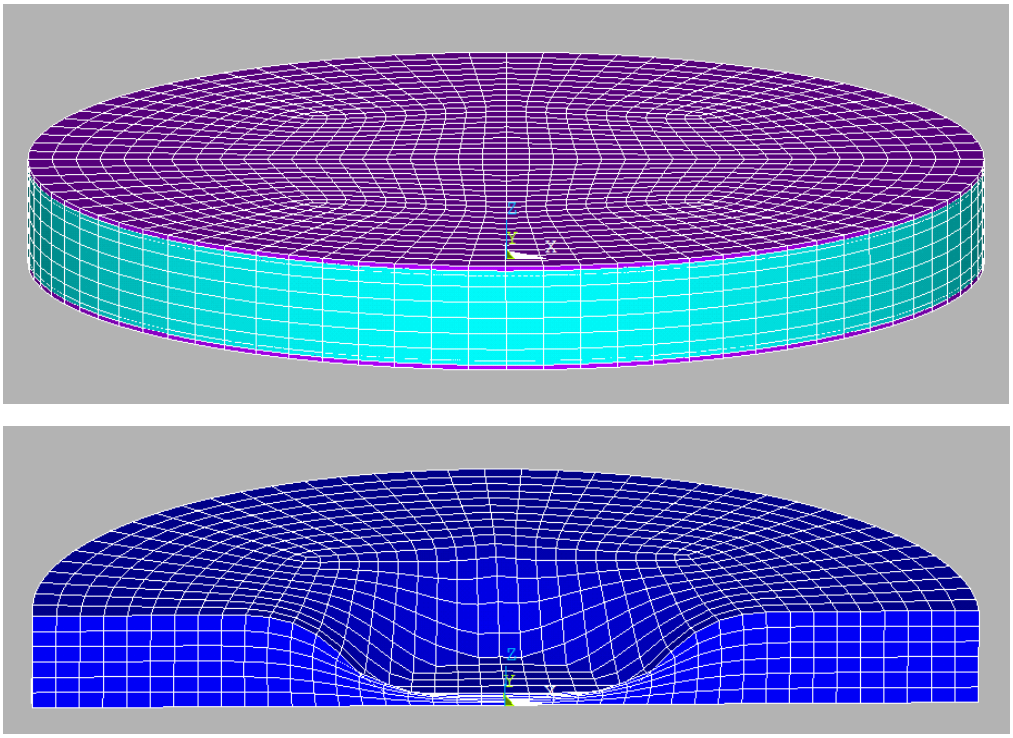

Σχήμα 6-9: Μακρομηχανικό μοντέλο στην απαραμόρφωτη και παραμορφωμένη κατάσταση.

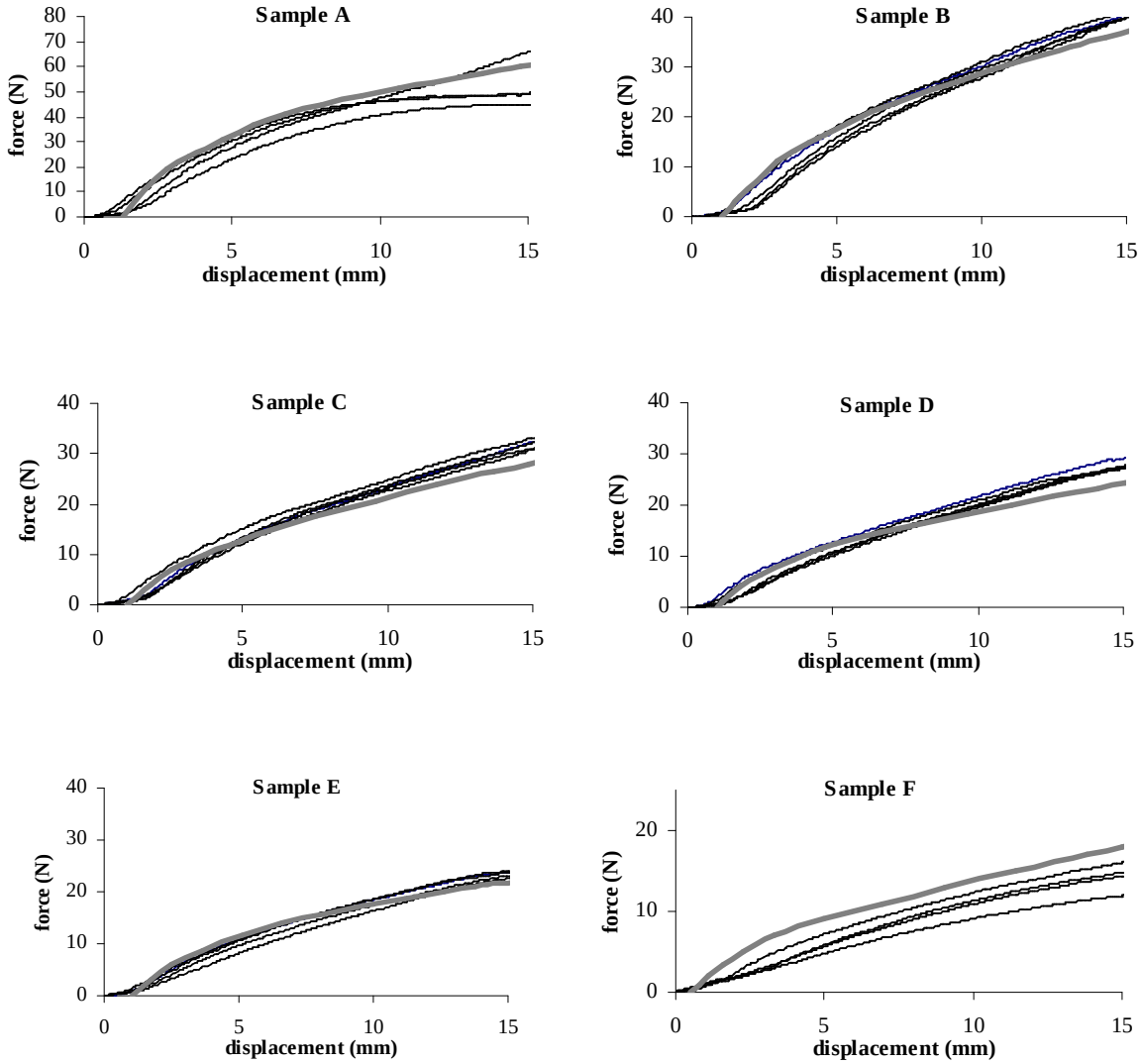

Σχήμα 6-10: Καμπύλες φορτιού – μετατόπισης της δοκιμής των δειγμάτων σε συμπίεση όπως προέκυψαν από το πείραμα (μαύρο) και την προσομοίωση (γκρι).

6.3 Αποτελέσματα

Η ικανοποιητική προσέγγιση των πειραματικών καμπυλών φορτίου – μετατόπισης της δοκιμής συμπίεσης από τις αντίστοιχες υπολογιστικές (Σχήμα 6-10) επιβεβαιώνει την ρεαλιστικότητα της προτεινόμενης μεθόδου μοντελοποίησης. Στη συνέχεια η προτεινόμενη μέθοδος εφαρμόστηκε για την ανάλυση της επίδρασης των δομικών και φυσικών παραμέτρων του 3Δ στημονοπλεκτού στην αντίστασή του σε συμπίεση. Το σχέδιο πλέξης του εσωτερικού νήματος 2 καθώς και οι μηχανικές ιδιότητες των νημάτων που συνθέτουν το εσωτερικό και τα εξωτερικά στρώματα θεωρήθηκαν ουσιαστικά για την αντίσταση του συγκεκριμένου τύπου στημονοπλεκτών σε συμπίεση. Στην πράξη, η επίδραση του σχεδίου πλέξης του εσωτερικού νήματος 2 προκύπτει από την σύγκριση των καμπυλών φορτίου –

μετατόπισης των δειγμάτων που εξετάστηκαν (A, B, C, D, E, F). Οι υπολογιστικές καμπύλες παρουσιάζονται σε κοινό διάγραμμα στο Σχήμα 6-11. Είναι προφανές ότι το αραιό σχέδιο πλέξης του εσωτερικού νήματος 2 οδηγεί σε χαμηλή αντίσταση σε συμπίεση. Σημαντική είναι η απόκλιση της αντίστασης σε συμπίεση που παρουσιάζουν τα σχέδια A και B. Επιπλέον τα δείγματα με τα σχέδια C, D, E παρουσιάζουν περίπου ίση αντίσταση σε συμπίεση. Το δείγμα F αντιστοιχεί στη δομή που παράχθηκε χωρίς το εσωτερικό νήμα 2.

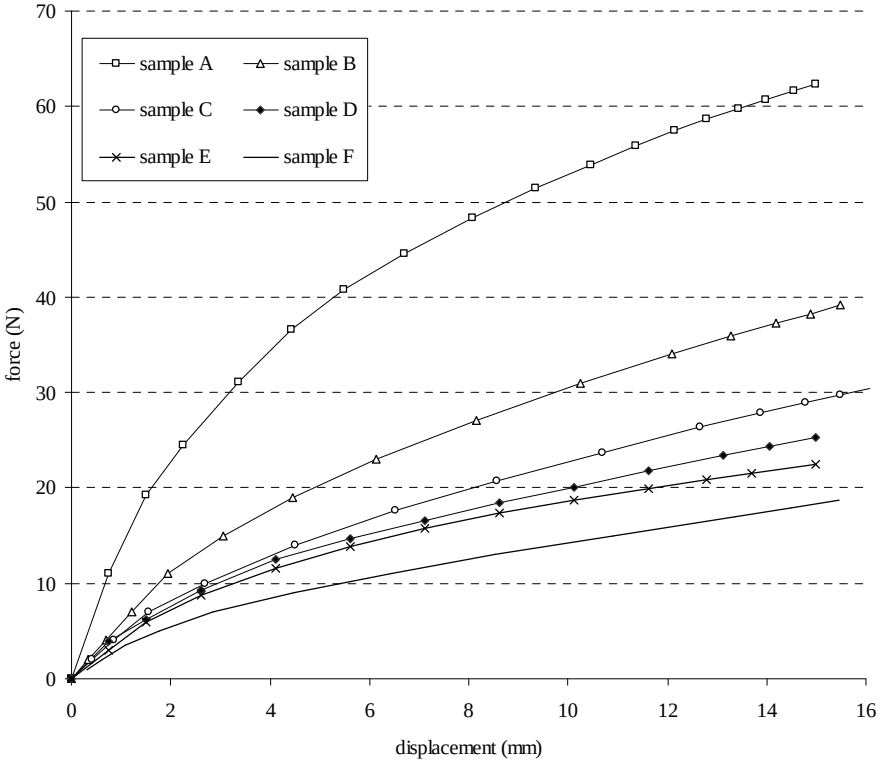

Σχήμα 6-11: Υπολογιστικές καμπύλες φορτίου – μετατόπισης από την δοκιμή συμπίεσης των δειγμάτων.

Στη συνέχεια μελετήθηκε η επίδραση των μηχανικών ιδιοτήτων των νημάτων που συνθέτουν το εσωτερικό και τα εξωτερικά στρώματα στην αντίσταση του 3Δ υφάσματος σε συμπίεση. Για την παραμετρική ανάλυση θεωρήθηκε η δομή του δείγματος F. Για τα νήματα θεωρήθηκαν γραμμικά ελαστικές ιδιότητες, χωρίς βλάβη της γενικότητας. Δεδομένου ότι η παραμόρφωση λόγω κάμψης των συνιστώντων νημάτων επικρατεί στην παραμορφωσιακή διαδικασία κατά την συμπίεση του 3Δ υφάσματος, η καμπτική δυσκαμψία των νημάτων αποτέλεσε την παράμετρο της ανάλυσης. Έτσι θεωρήθηκαν 10 τιμές για την καμπτική δυσκαμψία των υαλονημάτων (Bg=24 N·mm², 0.1·Bg, 0.5·Bg, 2·Bg, 5·Bg, 10·Bg, 15·Bg, 20·Bg, 25·Bg, 30·Bg)και του εσωτερικού νήματος 1 (Bs=0.94 N·mm², 0.1·Bs, 0.5·Bs, 2·Bs, 5·Bs,10·Bs, 15·Bs, 20·Bs, 25·Bs, 30·Bs)Η μεταβολή της τιμής της καμπτικής ακαμψίας των νημάτων επιτυγχάνεται μεταβάλλοντας το μέτρο ελαστικότητας ή την ροπή αδράνειας της διατομής των νημάτων. Αναπτύχθηκαν λοιπόν δύο ομάδες μοντέλων για την παραμετρική

ανάλυση. Η πρώτη αντιστοιχεί σε σταθερή τιμή της καμπτικής δυσκαμψίας των υαλονημάτων των εξωτερικών στρωμάτων (Bg) και μεταβλητή τιμή της καμπτικής δυσκαμψίας των εσωτερικών νημάτων. Η δεύτερη ομάδα αντιστοιχεί σε σταθερή τιμή της καμπτικής δυσκαμψίας των εσωτερικών νημάτων (Bs) και μεταβλητή τιμή της καμπτικής δυσκαμψίας των υαλονημάτων. Οι καμπύλες φορτίου – μετατόπισης από την προσομοίωση της δοκιμής κάμψης για τις δυο ομάδες μοντέλων παρουσιάζεται στο Σχήμα 6-12.

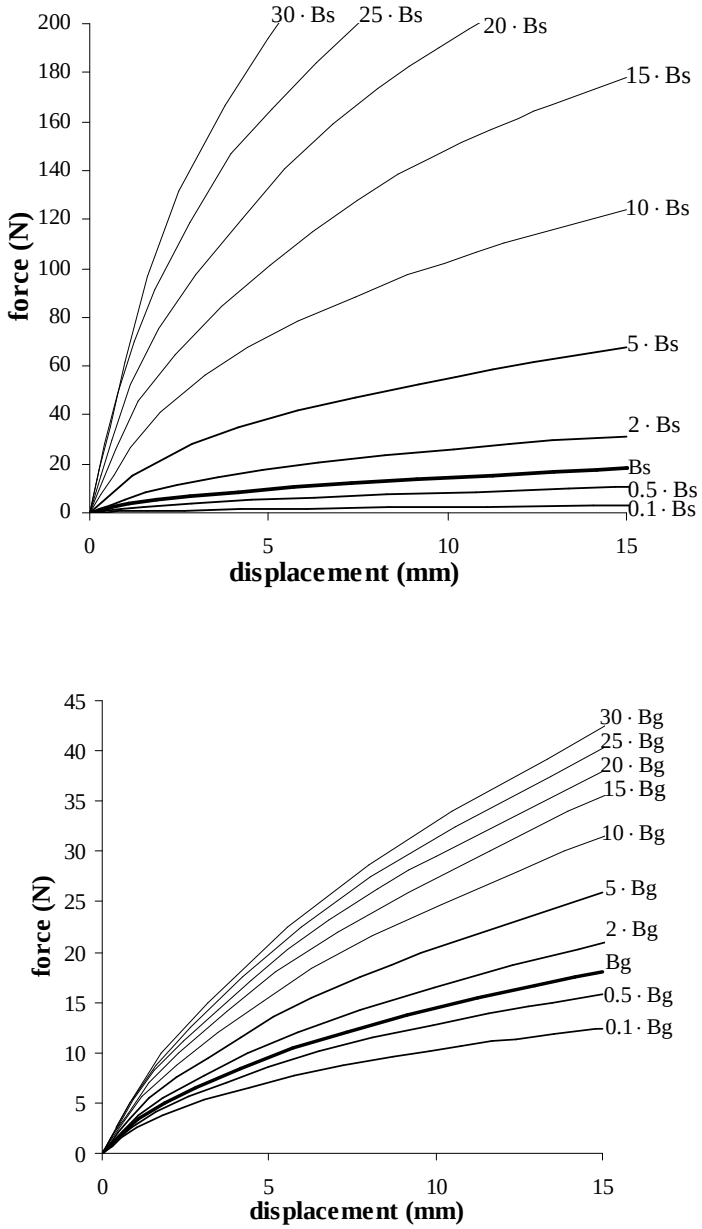

Σχήμα 6-12: Υπολογιστικές καμπύλες φορτίου – μετατόπισης από την δοκιμή συμπίεσης του δείγματος F για μεταβαλλόμενη τιμή της καμπτικής δυσκαμψίας των νημάτων του εσωτερικού στρώματος (άνω) και των εξωτερικών στρωμάτων (κάτω).

Οι καμπύλες φορτίου – μετατόπισης που παρουσιάζονται στο Σχήμα 6-12 παρέχουν την ποιοτική εκτίμηση της επίδρασης της καμπτική δυσκαμψίας των νημάτων που συνθέτουν το εσωτερικό και τα εξωτερικά στρώματα. Είναι προφανές ότι αύξηση της καμπτικής δυσκαμψίας των νημάτων επιφέρει αύξηση της αντίστασης του δείγματος σε συμπίεση. Από την σύγκριση των δύο διαγραμμάτων προκύπτει ότι η επίδραση της καμπτικής δυσκαμψίας των εσωτερικών νημάτων είναι υψηλότερη από των υαλονημάτων. Η καμπύλη του μοντέλου που αντιστοιχεί στις βασικές τιμές Bg και Bs παρουσιάζεται και στα δύο διαγράμματα με πιο έντονη γραμμή. Για την ποσοτική σύγκριση της επίδρασης της καμπτικής δυσκαμψίας των εσωτερικών νημάτων και υαλονημάτων στην αντίσταση των δειγμάτων σε συμπίεση υπολογίστηκε η ενέργεια που απορροφάται για σταθερή εκτροπή συμπίεσης (10 mm). Η απορροφώμενη ενέργεια αντιστοιχεί στο εμβαδόν που σχηματίζεται από την καμπύλη φορτίου – μετατόπισης και τον άξονα της μετατόπισης μέχρι την επιλεγμένη τιμή της μετατόπισης (10 mm). Η απορροφώμενη ενέργεια συναρτήσει της καμπτικής δυσκαμψίας των νημάτων δίνεται στο Σχήμα 6-13. Συνεπώς ο δεκαπλασιασμός της τιμής της καμπτικής δυσκαμψίας των εσωτερικών νημάτων συνεπάγεται αύξηση στην απορροφώμενη ενέργεια 6 – 7.6 φορές ενώ ο δεκαπλασιασμός της τιμής της καμπτικής δυσκαμψίας των υαλονημάτων συνεπάγεται αύξηση στην απορροφώμενη ενέργεια 1.3 – 1.7 φορές.

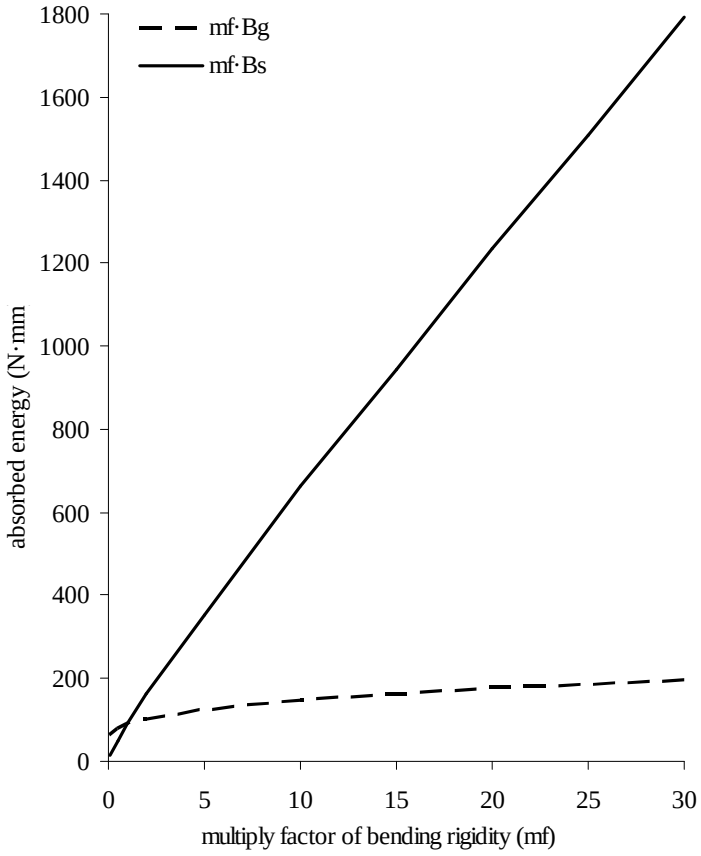

Σχήμα 6-13: Επίδραση της καμπτικής δυσκαμψίας των νημάτων στην ενέργεια που απορροφάται για συμπίεση κατά 10 mm.

6.4 Συμπεράσματα

Η προτεινόμενη μέθοδος μοντελοποίησης των κ/υ δομών εφαρμόστηκε σε τριδιάστατα υφάσματα τεχνικής εφαρμογής. Η εφαρμογή αφορά 3Δ στημονοπλεκτά με εσωτερικό διάκενο τα οποία χρησιμοποιούνται για την ενίσχυση σκυροδέματος. Μελετήθηκε η αντίσταση του υφάσματος σε συμπίεση, δεδομένου ότι είναι ουσιαστική για την παραγωγή της σύνθετης δομής. Η προτεινόμενη μέθοδος αποτελείται από δύο στάδια μηχανικής ανάλυσης στο μεσο- και μακρομηχανικό επίπεδο. Εφαρμόστηκε η ΜΠΣ με ΠΣ δοκού, κελύφους και ογκικά ΠΣ. Η μεσομηχανική ανάλυση διεξάχθηκε στο εσωτερικό στρώμα του υφάσματος για τον υπολογισμό της συμπεριφοράς του σε συμπίεση και στο εξωτερικό στρώμα για τον υπολογισμό της συμπεριφοράς του σε κάμψη. Οι φαινόμενες ιδιότητες που υπολογίστηκαν χρησιμοποιήθηκαν για την παραγωγή του ισοδύναμου μακρομηχανικού μοντέλου για την προσομοίωση του συνολικού υφάσματος σε συμπίεση.

Η αξιοπιστία της προτεινόμενης μεθόδου μοντελοποίησης εκτιμήθηκε συγκρίνοντας τα αποτελέσματα της προσομοίωσης με τα πειραματικά αποτελέσματα έξι δειγμάτων. Η ικανοποιητική προσέγγιση των πειραματικών καμπυλών φορτίου – μετατόπισης της δοκιμής συμπίεσης των δειγμάτων από τις αντίστοιχες υπολογιστικές καμπύλες επιβεβαίωσαν την εγκυρότητα της μεθόδου μοντελοποίησης. Στη συνέχεια ακολούθησε η παραμετρική ανάλυση της δομής για την εκτίμηση της επίδρασης των δομικών και μηχανικών παραμέτρων στην αντίσταση σε συμπίεση. Εξετάστηκε η επίδραση του σχεδίου πλέξης του εσωτερικού νήματος 2 καθώς και η επίδραση της καμπτικής δυσκαμψίας των εσωτερικών νημάτων και υαλονημάτων.

Αποδείχτηκε εξάλλου ότι η προτεινόμενη μέθοδος μοντελοποίησης συνιστώμενη από τα επιμέρους επίπεδα μικρο-, μεσο- και μακρομηχανικής ανάλυσης μπορεί να εφαρμοστεί και σε μη-συμβατικά κ/υ προϊόντα αν τροποποιηθεί κατάλληλα.

Συμπεράσματα και προτάσεις για περαιτέρω έρευνα

Η διδακτορική διατριβή στοχεύει στην ανάπτυξη μιας ολοκληρωμένης διαδικασίας μηχανολογικής σχεδίασης των κλωστοϋφαντουργικών προϊόντων. Προτάθηκε μια συστηματική προσέγγιση που ενοποιεί όλα τα στάδια της μοντελοποίησης των κ/υ δομών εφαρμόζοντας την Μέθοδο των Πεπερασμένων Στοιχείων. Η ιεραρχία παραγωγής των κ/υ δομών (ίνα – νήμα – ύφασμα) θεωρήθηκε για την υποδιαίρεση της διαδικασίας σχεδιασμού στα αντίστοιχα στάδια μοντελοποίησης. Μ' αυτόν τον τρόπο αναπτύχθηκαν τρία επίπεδα μοντελοποίησης: η μικρομηχανική μοντελοποίηση των νημάτων, η μεσομηχανική μοντελοποίηση της δομικής μονάδας του υφάσματος και η μακρομηχανική μοντελοποίηση ευρύτερου τμήματος του υφάσματος. Το κύριο επίτευγμα της προτεινόμενης διαδικασίας σχεδιασμού συναντάται στην προοδευτική μετάβαση μεταξύ των επιπέδων μοντελοποίησης, δηλαδή την απόδοση των ιδιοτήτων του νήματος στο μεσομηχανικό μοντέλο και την απόδοση των ιδιοτήτων της δομικής μονάδας στο μακρομηχανικό μοντέλο. Ο ορισμός των βασικών μηχανικών παραμέτρων του διακριτού μοντέλου και η ανάπτυξη του ισοδύναμου συνεχούς μοντέλου συνιστούν τις γενικές αρχές για κάθε μεταβατική φάση μεταξύ των επιπέδων μοντελοποίησης. Έτσι η προτεινόμενη διαδικασία σχεδιασμού αντιμετώπισε την βασική αδυναμία που παρουσιάζουν οι υπάρχουσες προσεγγίσεις μοντελοποίησης. Η ολοκληρωμένη διαδικασία σχεδιασμού επιτρέπει την προσομοίωση του υφάσματος σε σύνθετες καταπονήσεις, όπως η δοκιμή drape, όταν είναι γνωστές οι ιδιότητες των ινών, η δομή του νήματος και το σχέδιο του υφάσματος.

Εκτός της επιτυχούς ενοποίησης των σταδίων μοντελοποίησης, σημαντικά βήματα σημειώθηκαν και στα επιμέρους στάδια. Όσον αφορά το στάδιο της μικρομηχανικής μοντελοποίησης, για την ανάλυση των πολυινικών στριμμένων νημάτων προτάθηκε η ΜΠΣ χρησιμοποιώντας ΠΣ δοκού. Η προτεινόμενη προσέγγιση παρουσιάζει σημαντικά πλεονεκτήματα στην μοντελοποίηση και την ανάλυση. Έτσι προσφέρει ταχύτατο και ευέλικτο σχεδιασμό σχετικά με την γεωμετρική απεικόνιση και τις ιδιότητες υλικού. Επιπλέον η χαμηλή υπολογιστική ισχύς που απαιτείται αποτελεί σημαντικό πλεονέκτημα για την μελέτη των πολυινικών ινών. Η αξιολόγηση της ρεαλιστικότητας προτεινόμενης μεθόδου βασίστηκε σε πειραματικά δεδομένα. Τέλος η προτεινόμενη μέθοδος εφαρμόστηκε για την παραμετρική ανάλυση της μηχανική συμπεριφοράς των νημάτων. Η επίδραση των χαρακτηριστικών των νημάτων (δομικές παράμετροι και μέτρο ελαστικότητας) παρουσιάστηκε ποσοτικά σε διάγραμμα.

Τρεις προσεγγίσεις, η μοντελοποίηση με ογκικά ΠΣ, με ΠΣ κελύφους και με ΠΣ δοκού, διερευνήθηκαν ως προς την εφαρμογή τους στην μεσομηχανική ανάλυση του υφάσματος. Οι τρεις προσεγγίσεις αξιολογήθηκαν όσον αφορά την απόδοση των ιδιοτήτων στα μοντελοποιημένα νήματα, την εφαρμογή των οριακών συνθηκών, το υπολογιστικό κόστος, την επίτευξη σύγκλισης στην διαδικασία επίλυσης και την ρεαλιστικότητα των αποτελεσμάτων. Η μοντελοποίηση με ΠΣ δοκού αποδείχτηκε πλεονεκτικότερη σε αρκετά σημεία. Βασικό σημείο είναι η επιτυχής απόδοση των ιδιοτήτων των νημάτων λαμβάνοντας υπόψη την συμπεριφορά του νήματος σε εφελκυσμό και σε κάμψη. Αξιοσημείωτο είναι ότι οι υπάρχουσες προσεγγίσεις μεσομηχανικής μοντελοποίησης παραλείπουν τον υπολογισμό της τιμής της καμπτικής δυσκαμψίας του νήματος και την απόδοση της στο μοντελοποιημένο νήμα.

Η επαρκής απόδοση των φαινόμενων ιδιοτήτων της δομικής μονάδας της διακριτής δομής, που υπολογίστηκαν στο μεσομηχανικό στάδιο, στο συνεχές μοντέλο του υφάσματος αποτελεί καθοριστικό παράγοντα για την αξιοπιστία του σταδίου μακρομηχανικής μοντελοποίησης. Στην προτεινόμενη προσέγγιση για τον υπολογισμό των φαινόμενων ιδιοτήτων της δομικής μονάδας του υφάσματος θεωρήθηκε η μηχανική συμπεριφορά της δομικής μονάδας σε εφελκυσμό, διάτμηση και κάμψη κατά την διεύθυνση του στημονιού και του υφαδιού. Προτάθηκαν τρεις μέθοδοι για την ανάπτυξη ισοδύναμου συνεχούς μοντέλου για την μακρομηχανική ανάλυση του απλού υφαντού ασύμμετρης δομής. Η αξιοπιστία των προτεινόμενων μεθόδων αποδείχτηκε συγκρίνοντας με πειραματικά δεδομένα που προέκυψαν από την δοκιμή εφελκυσμού, διάτμησης και κάμψης των υφασμάτων. Τα χρησιμοποιούμενα πειραματικά δεδομένα ελήφθησαν από βιβλιογραφικές πηγές. Επιπλέον η μέθοδος της μακρομηχανικής μοντελοποίησης με ισοδύναμο μοντέλο τριών στρωμάτων εφαρμόστηκε για την προσομοίωση του υφάσματος σε συνθέτη μηχανική καταπόνηση πολλαπλών επιπέδων κάμψης (δοκιμή Drape). Για την ανάπτυξη του πλέγματος χρησιμοποιήθηκαν ΠΣ όγκου-κελύφους με μεταφορικούς ΒΕ. Έτσι αντιμετωπίστηκαν οι δυσκολίες που ανακύπτουν από τον υπολογισμό των στροφικών ΒΕ των κόμβων. Η αξιοπιστία της προτεινόμενης υπολογιστικής μεθόδου εκτιμήθηκε με πειραματικές μετρήσεις.

Η προτεινόμενη μέθοδος μοντελοποίησης των κ/υ δομών τροποποιήθηκε κατάλληλα για να εφαρμοστεί σε τριδιάστατα υφάσματα τεχνικής εφαρμογής. Η εφαρμογή αφορά 3Δ στημονοπλεκτά με εσωτερικό διάκενο τα οποία χρησιμοποιούνται για την ενίσχυση σκυροδέματος. Το μεσομηχανικό στάδιο μοντελοποίησης εφαρμόστηκε χωριστά για τον υπολογισμό των φαινόμενων ιδιοτήτων του εσωτερικού και των εξωτερικών στρωμάτων. Οι φαινόμενες ιδιότητες που υπολογίστηκαν χρησιμοποιήθηκαν για την παραγωγή του ισοδύναμου μακρομηχανικού μοντέλου για την προσομοίωση του συνολικού υφάσματος σε συμπίεση. Οι δρώσες φαινόμενες ιδιότητες των στρωμάτων, που συμβάλλουν στην δοκιμή συμπίεσης του υφάσματος, υπολογίστηκαν από τις αντίστοιχες δοκιμές. Το μικρομηχανικό μοντέλο της υπό εξέταση δομής χρησιμοποιήθηκε για την προσομοίωση της δοκιμής συμπίεσης. Η αξιοπιστία της προτεινόμενης μεθόδου μοντελοποίησης εκτιμήθηκε συγκρίνοντας τα αποτελέσματα της προσομοίωσης με τα πειραματικά αποτελέσματα έξι δειγμάτων.

Η προτεινόμενη διαδικασία σχεδίασης εστίασε στην στατική μηχανική ανάλυση των κ/υ δομών σε συνθήκες χαμηλής φόρτισης. Έτσι οι φαινόμενες ιδιότητες της δομικής μονάδας υπολογίστηκαν για χαμηλά φορτία και θεωρήθηκε γραμμική ελαστικότητα για το ισοδύναμο μακρομηχανικό μοντέλο. Τα μακρομηχανικά μοντέλα που αναπτύχθηκαν, λοιπόν, προβλέπουν ικανοποιητικά την μηχανική συμπεριφορά των υφασμάτων σε σύνθετες καταπονήσεις μεγάλων μετατοπίσεων και περιστροφών περιλαμβάνοντας κάμψη σε πολλά επίπεδα, όπως η δοκιμή drape ή η διαμόρφωση σε καμπύλο κέλυφος. Είναι επίσης επαρκή για τον υπολογισμό της συμπεριφοράς του υφάσματος σε δοκιμή εφελκυσμού και διάτμησης σχετικά μικρών παραμορφώσεων (εξαρτάται από την δομή). Στην πράξη αυξάνοντας το εφαρμοζόμενο φορτίο η συμπεριφορά του υφάσματος γίνεται έντονα μη-γραμμική λόγω της πλάτυνσης των νημάτων στα σημεία επαφής, της αύξησης της πίεσης συμπίεσης και της τριβής καθώς και της μείωσης της επιφάνειας διατομής του νήματος. Συνεπώς το γραμμικά ελαστικό μακρομηχανικό μοντέλο αδυνατεί να προβλέψει την προαναφερθείσα μη-γραμμική συμπεριφορά. Κάποιες κ/υ δομές μάλιστα, κυρίως πλεκτές, παρουσιάζουν έντονα μη-γραμμική συμπεριφορά ακόμα και σε συνθήκες χαμηλής φόρτισης λόγω των γεωμετρικών μεταβολών κατά την παραμόρφωση. Επομένως η εισαγωγή της μη-γραμμικής συμπεριφοράς της διακριτής δομής στο μακρομηχανικό μοντέλο θα έπρεπε να αποτελέσει το επόμενο βήμα της έρευνας.

Επιπλέον ο καθορισμός της διατμητικής συμπεριφοράς του υφάσματος (στο επίπεδο του υφάσματος) απαιτεί δυο μέτρα διάτμησης αφού το ύφασμα ασύμμετρης δομής παρουσιάζει διαφορετικές ιδιότητες διάτμησης κατά το στημόνι και το υφάδι. Στο προτεινόμενο μακρομηχανικό μοντέλο χρησιμοποιήθηκε η μέση τιμή των δύο μέτρων διάτμησης αφού ορίστηκαν ιδιότητες ορθοτροπικού υλικού. Η θεώρηση αυτή πιθανόν συνδέεται με τις συμμετρικές μορφές που λαμβάνει το μακρομηχανικό μοντέλο όταν υποβάλλεται σε δοκιμή drape. Η προκύπτουσα συμμετρία δεν είναι ρεαλιστική. Επομένως για περαιτέρω βελτίωση του μακρομηχανικού μοντέλου θα έπρεπε να θεωρηθούν δύο μέτρα διάτμησης κατά το επίπεδο του υφάσματος.

Στην πραγματικότητα ο σχεδιασμός των κ/υ δομών συνιστά ένα απεριόριστο πεδίο όσον αφορά τα υλικά, τις δομές και τις εφαρμογές. Στην παρούσα διατριβή παρουσιάστηκαν οι βασικές αρχές για την ανάπτυξη μιας ολοκληρωμένης διαδικασίας σχεδιασμού των κ/υ δομών εστιάζοντας σε συγκεκριμένο εύρος δομών και εφαρμογών. Για την διεύρυνση επομένως της προτεινόμενης διαδικασίας σχεδιασμού σε ευρύτερο πεδίο απαιτείται όγκος εργασιών που θα επεκταθεί στις εξεταζόμενες δομές (νήματα ασυνεχών ινών, 3Δ υφάσματα, σύνθετα υλικά), στις ιδιότητες υλικών (πλαστικότητα, ιξωδοελαστικότητα), και το είδος ανάλυσης (δυναμική ανάλυση).